From azobenzene glycosylation to multistate photoswitching: new approaches for the synthesis of photochromic glycoconjugates and glycomacrocycles

Dissertation

zur Erlangung des Doktorgrades
der Mathematisch-Naturwissenschaftlichen Fakultät
der Christian-Albrechts-Universität zu Kiel
vorgelegt von

Jonathan Berry

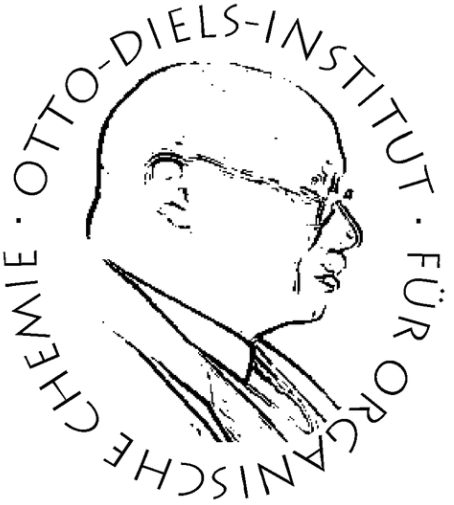

Otto-Diels institute für Organische Chemie

Kiel, 2023

“J´suis bien planqué sur ma planète,

comme Dieu derrière le mur de Planck.“

Dooz Kawa

Referentin: Pr. Dr. Thisbe K. Lindhorst

Korefferent: Pr. Dr. Manuel van Gemmeren

Tag der mündlichen Prüfung: 01.06.2023

Zum Druck genehmigt:

Die vorliegende Arbeit wurde unter Anleitung von
Prof. Dr. Thisbe K. Lindhorst
am Otto Diels Institut für Organische Chemie
der Christian-Albrechts Universität zu Kiel
im Zeitraum von
Januar 2018 bis Dezember 2022 angefertigt.

Hiermit erkläre ich, Jonathan Berry, dass ich die vorliegende Arbeit selbstständig und nur unter Verwendung der angegebenen Quellen und Hilfsmittel angefertigt habe. Inhalt und Form dieser Arbeit sind eigenständig erarbeitet und verfasst worden. Die Arbeit ist unter Einhaltung der Regeln guter wissenschaftlicher Praxis der Deutschen Forschungsgemeinschaft entstanden. Weder die gesamte Arbeit noch Teile davon sind an anderer Stelle im Rahmen eines Prüfungsverfahrens eingereicht worden. Dies ist mein erster Promotionsversuch. Mir wurde kein akademischer Grad entzogen.

Kiel, den

Jonathan Berry

Teile dieser Arbeit wurden bereits veröffentlicht:

- J. Berry, G. Despras and T. K. Lindhorst, *"Sulfur and Azobenzenes, a Profitable Liaison: Straightforward Synthesis of Photoswitchable Thioglycosides with Tunable Properties", Chem. Eur. J.*, **2022**, 28, e202200354. (DOI: 10.1002/chem.202200354).

- J. Berry, G. Despras and M. Kurfiřt, *"2,3,4-Tri-O-Benzoyl-6-O-(Tert-Butyldiphenylsilyl)-1-Thio-β-D-Glucopyranose",* in P. Kosma, T. M. Wrodnigg and A. Stütz (Eds.), *Carbohydrate Chemistry: Proven Synthetic Methods*, Volume 5 (1st ed.), CRC Press, Boca Raton, Chapter 31, **2021**.

- J. Berry, G. Despras and T. K. Lindhorst, "*A compatibility study on the glycosylation of 4,4´-dihydroxyazobenzene", RSC Adv.*, **2020**, 10, 17432-17437. (DOI: 10.1039/D0RA02435J).

Abstract

Azobenzene-based glycoconjugates (ABGs) are a class of photochromic carbohydrate derivatives that were first used in the early 2000s to probe carbohydrate-protein interactions. Owing to the photochemical *E*/*Z* isomerization of the azobenzene switch, the physico-chemical and biological properties of ABGs may be altered with light, opening new horizons in many domains, especially glycosciences.

Lately, the azobenzene moiety was embedded in carbohydrate-based macrocycles, resulting in photoresponsive glycophanes with unique properties. Notably, these compounds demonstrated intriguing chiroptical switching, due to a chirality transfer from the carbohydrates to the photoswitch, a restricted conformational freedom and light-controlled water-solubility.

In continuation of this research, a methodological investigation allowed the development of new synthetic pathways towards azo-based linear and cyclic glycoconjugates. A thorough investigation of the glycosylation of 4,4´-dihydroxyazobenzene allowed to delineate the scope and limitations of this reaction. The obtained ABGs were subsequently used as macrocycle precursors, and cyclized through a highly efficient thiourea-bridging reaction between an ABG with two isothiocyanate functions and different diamines. Four new photoresponsive glycophanes based on the dialkoxyazobenzene photochrome were synthesized. Their photoswitching behaviour was assessed, and especially their thermal isomerization properties were scrutinized.

Besides, a highly efficient palladium-catalyzed thioarylation of halogenated azo-derivatives with glycosyl thiols allowed the generation of novel ABGs, which photochromic properties could be modulated *via* oxidation of the bridging sulfur atoms. Importantly, one-pot procedures were developed for the heterogeneous *bis*-functionalization of azobenzenes. Finally, this reaction was used in the synthesis of macrocyclic glycoazobenzene dyads incorporating two different photochromes, which demonstrated multistate switching. Very interestingly, one of these macrocyclic dyads could be selectively switched in the four possible isomeric states with light only. Such derivatives may be of great interest in many applications, and their unprecedented switching properties might draw a lot of attention.

Kurzzusammenfassung

Azobenzol-basierte Glykokonjugate (ABGs) sind eine Klasse von photochromen Kohlenhydratderivaten, die erstmals in den frühen 2000er Jahren zur Untersuchung von Kohlenhydrat-Protein-Wechselwirkungen eingesetzt wurden. Aufgrund der photochemischen E/Z-Isomerisierung des Azobenzolschalters können die physikalisch-chemischen und biologischen Eigenschaften von ABGs durch Licht verändert werden, was in vielen Bereichen, insbesondere in den Glykowissenschaften, neue Horizonte eröffnet.

Kürzlich wurde der Azobenzol-Anteil in Makrozyklen auf Kohlenhydratbasis eingebettet, was zu lichtempfindlichen Glycophanen mit einzigartigen Eigenschaften führte. Insbesondere zeigten diese Verbindungen eine faszinierende chiroptische Schaltung, die auf einen Chiralitätstransfer von den Kohlenhydraten auf den Photoschalter, eine eingeschränkte Konformationsfreiheit und eine lichtgesteuerte Wasserlöslichkeit zurückzuführen ist.

In Fortsetzung dieser Forschung ermöglichte eine methodische Untersuchung die Entwicklung neuer Synthesewege für lineare und zyklische Glykokonjugate auf Azobasis. Eine gründliche Untersuchung der Glykosylierung von 4,4'-Dihydroxyazobenzol ermöglichte es, den Umfang und die Grenzen dieser Reaktion abzugrenzen. Die erhaltenen ABGs wurden anschließend als Makrozyklusvorläufer verwendet und durch eine hocheffiziente Thioharnstoff-Brückenreaktion zwischen einem ABG mit zwei Isothiocyanatfunktionen und verschiedenen Diaminen cyclisiert. Vier neue photoresponsive Glycophane auf der Basis des Dialkoxyazobenzol-Photochroms wurden synthetisiert. Ihr Photoswitching-Verhalten wurde bewertet und insbesondere ihre thermischen Isomerisierungseigenschaften untersucht.

Durch eine hocheffiziente Palladium-katalysierte Thioarylierung von halogenierten Azo-Derivaten mit Glycosylthiolen konnten neuartige ABGs hergestellt werden, deren photochrome Eigenschaften durch Oxidation der verbrückenden Schwefelatome moduliert werden können. Wichtig ist, dass ein Eintopfverfahren für die heterogene Bis-Funktionalisierung von Azobenzolen entwickelt wurde. Schließlich wurde diese Reaktion für die Synthese von makrozyklischen Glykoazobenzol-Dyaden mit zwei verschiedenen Chromophoren verwendet, die eine Multistate-Schaltung zeigten. Sehr interessant ist, dass einer dieser makrozyklischen Dyaden nur mit Licht selektiv in die vier möglichen isomeren Zustände geschaltet werden konnte. Solche Derivate könnten für viele Anwendungen von großem Interesse sein, und ihre beispiellosen Schalteigenschaften könnten viel Aufmerksamkeit erregen.

Table of contents

1. Introduction

1.1. General introduction

At all times, Humans have been fascinated by geometric shapes. From religion to science, from art to philosophy, geometric figures have always been a source of inspiration, sometimes merging different concepts or disciplines into one picture. For example, the Nazca geoglyphs in Peru are a spectacular example of the symbiosis of art and spirituality by the use of lines and curves to depict geometric shapes or sometimes, animals, considered as deities. Another very concrete example is the "Vitruvian Man" by Leonardo da Vinci. This sketch, representing a man in two superimposed positions with his arms and legs apart, and concomitantly embedded in a circle and a square, makes a symbolic connection between religion, science, art and philosophy.

Of all geometric shapes and figures, the circle is probably one of the most captivating. Symbol of perfection, the circle was associated by ancient Greeks, notably from the Pythagorean school, to God, and gave rise to the geocentric interpretation of the universe as a sphere, where the objects (planets, stars), supposedly of divine essence, must be spheres. This symbolism of geometrical figures was also largely developed by Plato, who associated an element (air, water, fire, earth and ether) to regular polyhedrons (platonic solids). This theory was later reinterpreted by Johannes Kepler as he was trying to find relationships between the five planets known at his time, and from this research emerged the discovery of Kepler´s solids, and the observation that planetary orbits are not circles but ellipses. The circle is a symbol present in all cultures, across all times, as attested by the large number of circular rituals (circumambulatio around a church, a sacred tree, the Ka´aba…) or objects and symbols (rosette, dome, yin-yang, mandala, ensō, Aztec calendar…). Finally, the symbolism of geometric shapes reached a peak with the hermetic doctrine promoted by alchemists, where the circle is widely represented.

Etymologically, the word circle comes from the ancient greek κύκλος (kúklos), which also gave the word cycle. Besides its purely geometric meaning, the word cycle gave a spatiotemporal dimension to the circle, as it defines a sequence of phenomena happening in a determinate order that repeat periodically. One of the most well-known symbol for the cycle is the uroboros, a picture representing a snake or a dragon biting its own tail. In Nature, there is a plethora of cyclic events that sometimes gave by extension units of time, such as the revolution of planets around their star (a year on earth), the earth rotation on its axis (a day), the water cycle, the cell cycle, the Calvin cycle etc... Interestingly, the mathematic description of periodic movements is done thanks to trigonometry, which derives from the application of Pythagoras' theorem in a circle. In chemistry, a cycle defines a carbon containing chain of 3 to 11 atoms that is bound by its extremities (Figure 1.1). If the chain is solely comprised of carbons, it is referred to as cycloalkane, and if the chain contains other atoms (O, N, P, S, Se…) it is then called a heterocycle. Cyclic molecules have additional intrinsic properties compared to their linear counterparts, and they are essential for life as they compose in majority the DNA and RNA (nucleobases, carbohydrates), as well as under the form of aminoacids (proline, tryptophane, tyrosine, histidine, phenylalanine), or as very important biologic regulators such as cyclic adenosine monophosphate (cAMP).

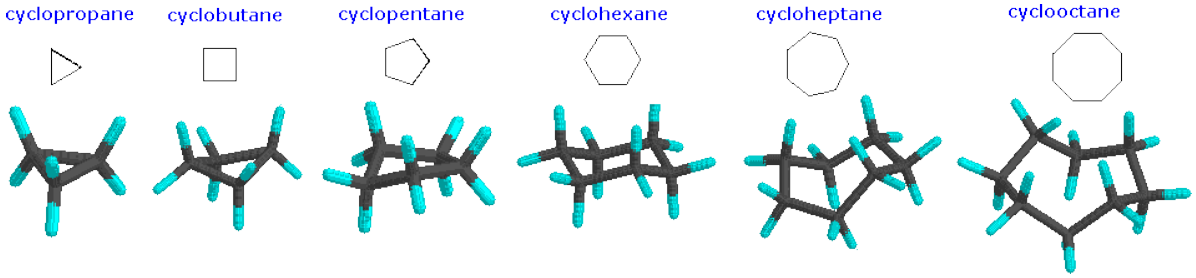

Figure 1.1. Schematic representation of cycloalkanes and their 3D representation in sticks.

There can be cyclic molecules with more than 11 atoms in the cycle, but they are then referred to as macrocycles. Macrocycles are generally defined as cyclic molecules containing 12 or more intracyclic atoms. These molecules have caught the attention of chemists for several reasons such as their elegant ring shape, the challenge represented by their synthesis, and their unique physicochemical properties. In fact, owing to their cyclic structures, macrocycles, compared to their linear counterparts, have a high propensity to be symmetrical, are excellent building blocks with low dispersity and display outstanding host-guest properties. In this thesis, we will focus on macrocycles, and most especially, on photoswitchable glycomacrocycles.

1.2. From natural bioactive macrocycles to glycomacrocycles

1.2.1. Naturally occurring bioactive macrocycles

Many naturally occurring macrocycles are pharmacologically active and used as therapeutics for numerous indications (antibiotic, antifungal, immunosuppressive/antitumor agents…). However, there is one motif which is essential for life: the tetrapyrroles (Figure 1.2). Porphyrins (Figure 1.2a) are aromatic macroheterocycles composed of 4 pyrrole subunits linked on their *alpha* carbons to a methine group. Porphyrins and related derivatives can accommodate metal ions in the cavity formed by the cycle *via* coordination of the nitrogen atoms, forming colorful metalloporphyrins that are called "the pigments of life". Notably, certain iron porphyrins constitute the family of haem (Figure 1.2b), an essential cofactor of metalloproteines responsible for the transport (haemoglobin), the storage (myoglobin), and the metabolism of dioxygen (cytochrome c oxidase). By reduction of one pyrrole to an azoline, a partially unsaturated porphyrin called chlorine is obtained, which is the basis for the chlorophyll pigments family (Figure 1.2c), responsible for the photosynthesis.[1] Finally, a tetrapyrrole structurally close to the porphyrin but lacking one methine group, the corrin, is the basis for the cobalamin, a very complex vitamin, essential for the brain functioning and cell metabolism (Figure 1.2d), which was first synthesized in 1972 by Woodward and Eschenmoser.[2]

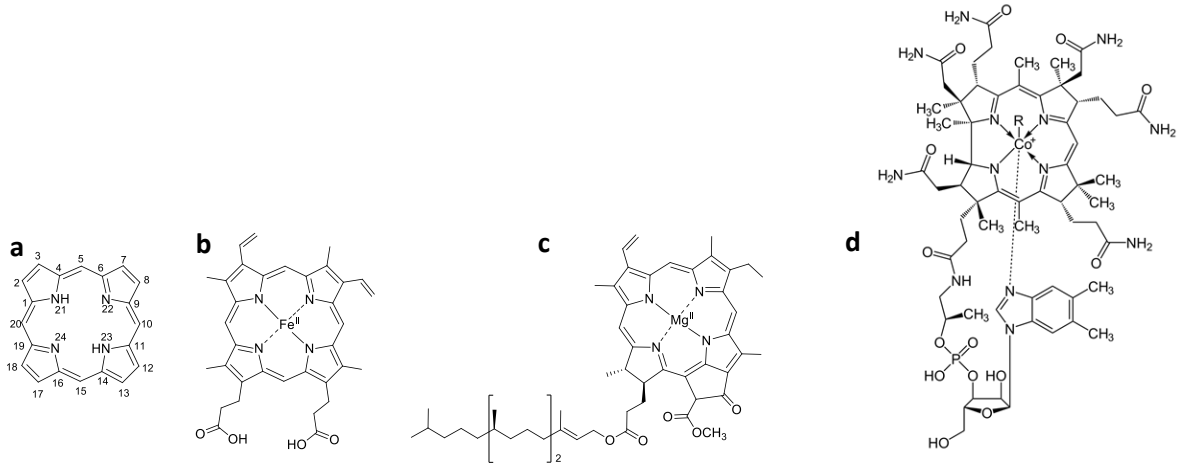

Figure 1.2. Chemical structures of porphyrin (a), haem b (b), chlorophyll a (c) and vitamin B_{12} (d).

Macrocycles represent a small proportion of the current marketed drugs and they are almost exclusively obtained or derived from natural sources (mainly microorganisms).[3] Different classes of macrocyclic therapeutics can be identified depending on their structure and biological activity.[4] The most well-known class is probably the macrolide antibiotics family (Figure 1.3), of which erythromycin (Figure 1.3a) was the first one to be used as anti-infective agent in 1952. Macrolides are glycosylated 12-, 14- and 16- membered macrolactone rings, generally biosynthesized by polyketide synthases.

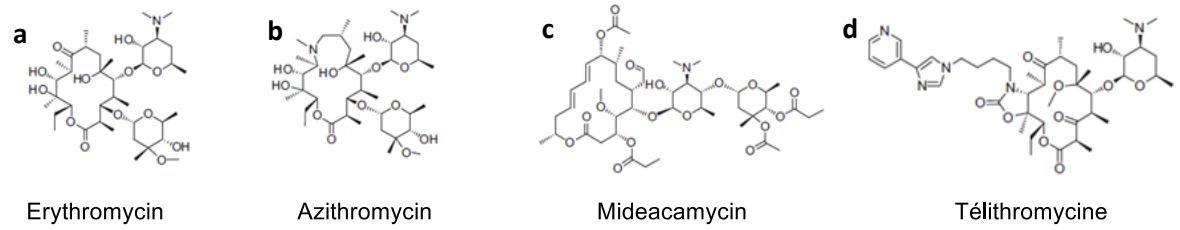

Figure 1.3. Chemical structures of 14-membered (a), 15-membered (b) and 16-membered (c) macrolides, and a 14-membered ketolide (d).

Macrolides are broad spectrum antibiotics used in case of allergies or resistance to penicillin for treating mainly respiratory tract diseases, skin and soft tissues infections, and also some sexually transmissible infections. They disrupt the bacterial protein synthesis by fixation to the ribosomal RNA, therefore preventing translocation and elongation.[5] However, their use is challenging due to limited knowledge on their ADMET properties, as well as numerous possible interactions with other substances.[6] Moreover, the ketolides, which are semisynthetic macrolides based on the erythromycin core, were developed to treat macrolide resistant respiratory tract infections.[7]

Cyclic peptides are another important class of bioactive macrocycles (Figure 1.4). About 30 of the current marketed macrocyclic drugs fall into this category, that comprises different subgroups such as: the disulfide bridged subclass (argipressin), the glycopeptide subclass (vancomycin, teicoplanin), the lipopeptide class (daptomycin), amongst others.[6] Although most of these molecules have an anti-infective activity, they may also have other indications as immunosuppressant (cyclosporin A) or in cancer therapy (actinomycin D).

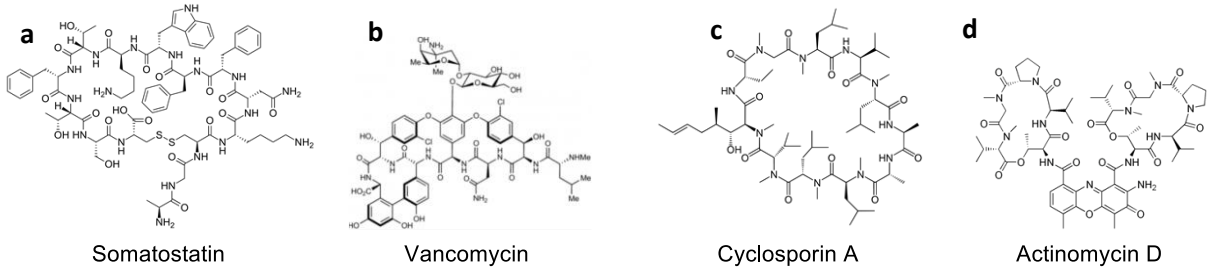

Figure 1.4. Chemical structures of a disulfide bridged peptide hormone (a), a tricyclic glycopeptide antibiotic (b), an immunosuppressive homodetic cyclopeptide (c) and a chemotherapeutic depsipeptide (d).

Some cyclic peptides such as calcitonin, oxytocin, somatostatin (Figure 1.4a) or vasopressin, are naturally occurring hormones and are used as therapeutics or biochemical tools. They form rigid structures *via* the connection of cysteine residues resulting in cyclisation. For example, somatostatin may be used for treating acromegaly, however the use of synthetic lanreotide is favored due to a longer duration of action.[8]

Antibiotic cyclic peptides such as vancomycin (Figure 1.4b) represent a successful development in combating antibioresistance. It allowed the treatment of β-lactamine resistant gram positive bacterial infections such as methicillin-resistant *Staphylococcus aureus* (MRSA) or penicillin-resistant *Streptococcus pneumoniae* (PRSP).[9] However, its spectrum of action is limited to gram positive bacteria, and its low oral bioavailability and relative toxicity only allow to use it in last resort. Despite a careful prescription, vancomycin resistant strains started to appear, which prompted the development of new vancomycin derivatives. This led in 2017, to the discovery of a vancomycin related drug 25,000 times more potent than the parent molecule.[10]

Cyclosporin A (Figure 1.4c) is the sole marketed cyclic peptide drug that can be administered orally.[6] Due to its immunosuppressant activity, it allowed great developments in the field of organ transplantation to prevent rejection.[11] Finally, actinomycin D (Figure 1.4d), which was isolated by

Waksman and Woodruff in 1940, is the first antibiotic which demonstrated anticancer activity. It was shown to bind to oncogenic promoter G-quadruplex, thus repressing gene expression.[12]

In order to close this non exhaustive section on naturally occurring bioactive macrocycles, must be cited some more examples: the polyene antifungals such as amphotericin B, the avermectine related antiparasitics such as ivermectin, the rifampin related antibiotics, the tubulin binders such as epothilone B, and the α-ketohomopropyl amides imunomodulators such as tacrolimus.[4] Some other natural macrocyles such as terpenenoids (lepidozene, casbene, humulene…), curare, and mycotoxins were also not covered despite their captivating structures and properties. Cyclodextrins on another hand, despite their natural origin will be discussed in the next part, as they have paved the way to supramolecular chemistry.

1.2.2. Supramolecular chemistry and the development of synthetic macrocycles.

Supramolecular chemistry (Figure 1.5) was defined by Jean-Marie Lehn in the 1980´s as follows:[13]

'' 'Chemistry beyond the molecule', bearing on the organized entities of higher complexity that result from the association of two or more chemical species held together by intermolecular forces. Its development requires the use of all resources of molecular chemistry combined with the designed manipulation of non-covalent interactions so as to form supramolecular entities, supermolecules possessing features as well defined as those of molecules themselves.''

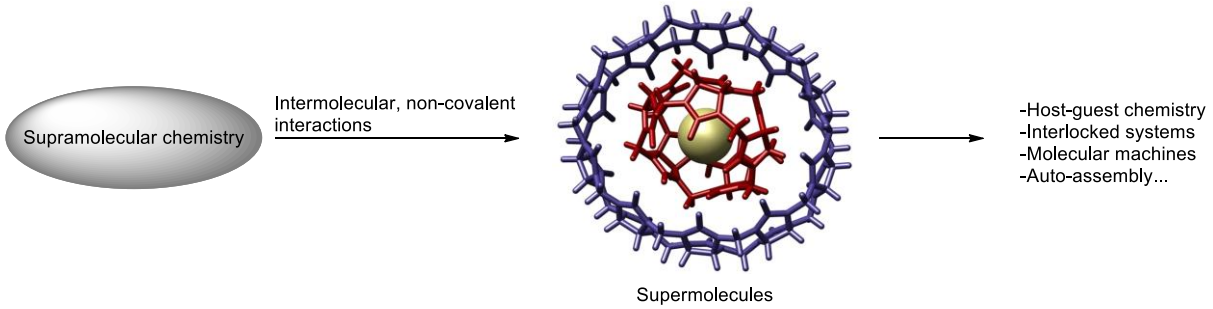

Figure 1.5. Schematic depiction of the concept of supramolecular chemistry.

Thus, supermolecules are the result of the cooperative and additive interactions between different chemical entities through non covalent interactions such as hydrogen bonding, hydrophobic, electrostatic and van der Waals interactions, as well as metal coordination.[14] This new field of chemistry led to the development of different branches such as self-assembly (helicates, foldamers…), interlocked systems (catenanes, rotaxanes, molecular knots…) and host guest chemistry (molecular recognition). Since the discovery of crown ethers by Pedersen in the 1960´s,[15] the field of host-guest chemistry has constantly grown, and the diversity and complexity of macrocyclic host molecules have boomed over the past fifty years. For the most prominent macrocyclic hosts must be cited the cucurbit[n]urils, the calixaromatics (calixarenes, pillararenes…) and other cyclophanes, π-conjugated macrocycles and molecular triangles amongst others.[16]

Host-guest chemistry, although older than the concept itself, is one branch of supramolecular chemistry based on the capacity of macrocycles to encapsulate other chemical entities inside their cavity. Two concepts were critical to the development of this field: the involvement of intermolecular forces, first postulated by van der Waals in 1873,[17] and the lock-and-key model of enzyme-substrate interactions introduced by Emil Fischer in the 1890´s[18] and further extended by Paul Ehrlich.[19] Thus, the host acts as a receptor that may accommodate a substrate (the guest), through a molecular recognition process, resulting in the formation of an inclusion complex.

Depending on their structure, host molecules may be classified in different categories: torus shaped hosts or corrands[20] (porphyrins, crown ethers…), container shaped hosts or cavitands[21] (cyclodextrins, cucurbiturils, calixarenes…) and three dimensional hosts otherwise called molecular cages or carcerands[22] (cryptands, cryptophanes, metal organic frameworks…). Also based on the structure and physicochemical features of the hosts, different types of guests may be included: ions (mostly cations, but also in a lesser extent anions) or neutral organic molecules. Due to their inherent chirality, highly functionalized nature and biocompatibility, carbohydrates-based macrocycles have emerged as very interesting macrocyclic structures with outstanding properties.

1.2.3. Glycomacrocycles: Carbohydrate-based macrocycles

Glycomacrocycles have attracted a great interest in the past 50 years due to their natural existence, their unique properties, their structural complexity, and the challenges associated with their synthesis.[23] Resin glycosides[24] and ellagitannins[25] for instance, are plant metabolites that have been extensively studied for their biological activity, and their synthesis led to significant methodological developments.[26] Besides their polyfunctional nature and stereoisomeric diversity, carbohydrates are inherently chiral, which makes them particularly attractive for the elaboration of enantioselective receptors for chiral amines and aminoacids, or chiral catalysts.[27] Sugar-based crown ethers and cryptands have therefore been extensively used in asymmetric catalysis,[28] or in supramolecular chemistry.[29] Another very interesting class of sugar-based macrocycles is the one of cyclodextrins, which were the first class of glycomacrocyclic hosts to be investigated, and dominated the field of host-guest chemistry until now.[30]

Cyclodextrins (CDs) are cyclic oligomers of D-(+)-glucopyranose units linked *via* α-1,4-glycosidic bonds. They were first prepared in the 1890´s by A. Villiers, by degradation of potato starch with the butyric ferment *Bacillus amylobacter* (*Clostridium butyricum*).[31] Although they were discovered 130 years ago, the industrial application of CDs really started in the 1980´s with their utilization in pharmaceutical and food industry.[32] This was made possible by the industrial production of the three "native" CDs, namely α-, β- and γ-CDs. These differ from one another by the number of glucopyranose units forming the macrocycle: respectively 6, 7 and 8 (Figure 1.6a). CDs form bucket shaped molecules (truncated cones), with the smaller rim formed by the primary hydroxyl groups, and the larger one by the secondary side (Figure 1.6b). Due to this orientation of the numerous hydrophilic OH groups, making them water soluble, the interior of CDs´cavity is fairly hydrophobic, allowing for the complexation of a wide range of neutral organic molecules and other non-polar guests.

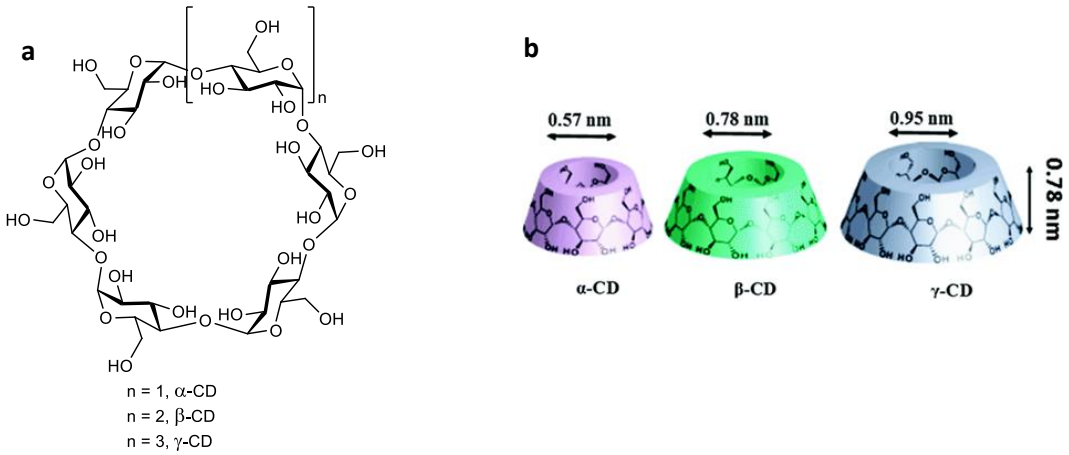

Figure 1.6. Chemical structure of native CDs (a) and their schematic representation (b).

The first documented example of a host-guest inclusion complex can be attributed to the Austrian microbiologist F. Schardinger, who reported in 1903 on the formation of adducts between CDs and molecular iodine.[33] By the time, only α- and β-CDs were known and their structure was not yet

elucidated. As a result, although CD-I_2 complexes were reported, the nature of the host-guest inclusion phenomenon was not understood. It was not until 1948 that the γ-CD was discovered, and that the cyclic and hollow structure of CDs was experimentally demonstrated by K. Freudenberg and his doctoral student F. Cramer.[34] Later on, the groups of F. Cramer and D. French further explored and understood CDs, investigating on their structure, aqueous conformation and the hydrophobic nature of the cavity.[35] In 1967, Cramer published a very important seminal article, in which he reported on a study of inclusion complexes of different types of spectroscopically active organic molecules (nitrophenols and azo dyes), with α-CD in aqueous solutions. This paper is important as it represents the first report of the enhancement of fluorescence intensity of a guest fluorophore by complexation to a CD.[36] It showed that α-CD produced a 2-fold increase of the fluorescence of 1,8-anilinonaphtalene sulfonate (1,8-ANS), whereas β- and γ-CDs induced a 10-fold increase. Figure 1.7 shows a photograph of the fluorescence enhancement of 1,8-ANS by complexation with hydroxypropyl-β-CD, a chemically modified CD with improved host properties compared with the native β-CD.[37] As can be seen from this picture, in addition to a tremendous increase in intensity, there is a blueshift of the $\lambda_{F,max}$. Nowadays, fluorescence spectroscopy has become a common technique to study host-guest inclusion systems,[38] and is the basis for fluorescence-based trace detection analytical methods.[39]

Figure 1.7. A visual illustration of the large fluorescence enhancement of a guest molecule which can be obtained by CD-host inclusion: the fluorescence of a 5.0×10^{-4} M solution of 1,8-ANS under UV-A irradiation in the absence (left) and presence (right) of 20 mM HP-β-CD.

CDs have found widespread applications as molecular hosts due to their biocompatibility, relative ease of chemical modification and thus tunable solubility, as well as their commercial availability. Moreover, although different methods were developed for their preparation, CDs are mostly produced by the action of specific enzymes on starch, which is a relatively green and inexpensive process and accounts for their commercial attractiveness.[40] CDs are now being used in many areas of everyday life such as food industry (slow release of flavors, removal of unpleasant odors…),[41] pharmaceutical and cosmetic industry (drug stabilization, solubilization and delivery, deodorant…).[42] One striking example of the use of modified cyclodextrins in medicine is the utilization of Sugammadex, a γ-CD with propionyl thioether groups on the primary positions, which effects the reversal of neuromuscular blockade induced by rocuronium and vecuronium in general anesthesia.[43] CDs have also been extensively used in analytical sciences,[44] separation sciences (GC, HPLC, TLC, chiral separation…)[45] or as molecular sensors.[46] Due to the wide variety of CD derivatives (in cavity size, charge and substituents - thousands of derivatives), the number of guest compounds suitable for complexation is immense. This, coupled to their low toxicity and high versatility, explains why these molecules have dominated the field of host-guest chemistry until now.

In addition to CDs, glycophanes (Figure 1.8) have also been used as tools to probe carbohydrate-carbohydrate interactions as well as carbohydrate-arene interactions and the hydrophobic effect.[47] The term glycophane was coined by C. S. Wilcox in 1988, as the structure obtained was a hybrid between a cyclophane and a cyclodextrin, a carbohydrate based cyclophane with a chiral hydrophobic cavity.[48] In order to study their complexation behavior in water, cyclophanes generally needed to

possess several charged groups such as ammonium or carboxylate.[49] The introduction of carbohydrates in the macrocyclic structure of cyclophanes is associated with many advantages. First, carbohydrates are readily accessible from natural sources, and their stereoisomeric diversity allows the construction of a large variety of macrocycles. Second, the multifunctionality of carbohydrates allows to enlarge the structure diversity by offering multiple possible linkages through the different positions of the sugar ring. In addition, substitution of the hydroxyl groups allows the modulation of the physicochemical properties such as solubility, hydrophilic/lipophilic balance, biodisponibility etc. Third, carbohydrates tend to form furanoid or pyranoid cycles, which imposes geometric constraints, a feature that can be exploited for the design of conformationally restricted macrocycles. Finally, the chiral nature of carbohydrates endows glycomacrocycles with chiral cavities, a property that can be exploited in the fields of asymmetric catalysis or chiral recognition for instance. Therefore, the introduction of carbohydrates in cyclophanes allowed the synthesis of neutral, chiral, and water soluble macrocyclic host molecules.

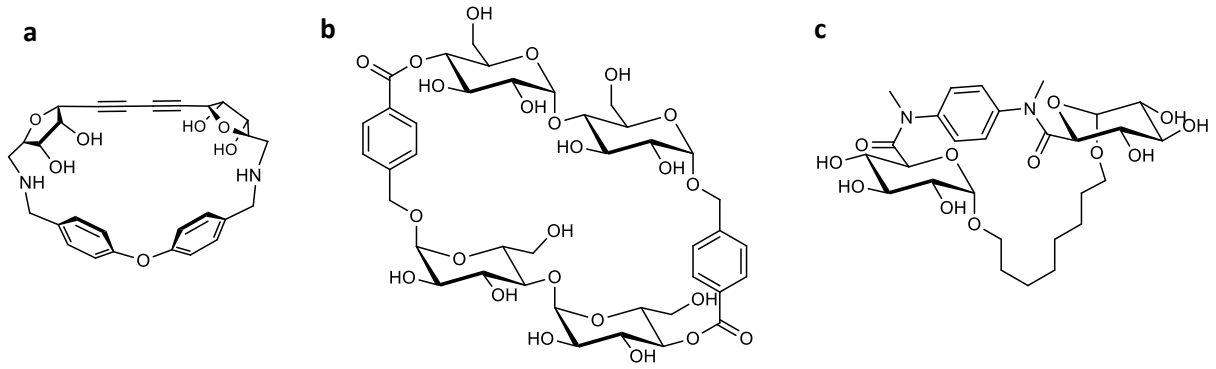

Figure 1.8. Examples of neutral water soluble symmetrical (a,[48] b[47c]) and asymmetrical (c[50]) glycophanes.

Following the successful synthesis of several glycophanes and the elaboration of synthetic routes to access them,[47,51] the group of S. Penadés investigated the binding behavior of a dimeric trehalose based glycophane obtained by nucleophilic substitution of trehalose-6,6´-ditriflate with 2,7-dihydroxynaphtalene.[51d] They showed that the host formed stable complexes with electron-deficient aromatic guests like di- or trinitrophenols in aqueous methanol (1:1).[52] This glycophane also exhibited chiral discrimination toward racemic 2,4-dinitrophenyl amino acid derivatives with enantioselectivity up to 40%. In addition, a stereospecific carbohydrate-carbohydrate interaction was demonstrated with 4-nitrophenyl glycosides, resulting in α-selectivity, and thorough analysis showed that hydrophobic forces between the carbohydrate surfaces were mainly responsible for the stability of the association. Further investigations were realized in water with different glycophanes and showed similar trends.[47c,53] Later on, in the 2000´s, P. V. Murphy and colleagues synthesized glycophanes by coupling of alkenyl and akynyl glucuronic acids with 1,4-phenylene and 1,4-xylene diamines, and subsequent cyclisation *via* ring closing metathesis.[50,54] These compounds showed reversal of quenching of the emissions of 1,8-ANS, similar to β-cyclodextrin, suggesting the formation of an inclusion complex. Furthermore, it was shown that these new glycophanes have potential as scaffolds for the development of peptidomimetics or glycoclusters.[55]

In the last decades, glycomacrocycles emerged as very interesting compounds with multifaceted properties, which can be used as supramolecular chiral hosts, scaffolds, or for the investigation of fundamental molecular forces, and the exploration of these compounds promises interesting discoveries. Concomitantly to the rapid development of macrocycles, scientists were increasingly interested in altering their properties with external stimuli such as light. This can be accomplished by embedding photoresponsive moieties, namely photoswitches, into the macrocyclic structure.

1.3. Photoresponsive compounds

1.3.1. Photochromism

Photochromism is defined as the reversible color change of a compound upon light irradiation. The first documented report on photochromism dates back to 1867, when Fritzsche observed the bleaching of an orange solution of tetracene upon exposure to daylight, and the regeneration of the color when kept in the dark.[56] Later on, in 1899, Markwald reported on the reversible coloring of otherwise colorless 2,3,4,4-tetrachloronaphthalen-1(4H)-one in the solid state upon light exposure.[57] The phenomenon was first coined "phototropy", but due to potential confusion with the biological phenomenon of phototropism, Hirshberg proposed the term photochromism in the 1950´s.[58] Although the interest in photochromic molecules was steady since the first studies, the development of analytical methods during the 1960´s (UV-Vis, IR, NMR, X-Ray) favored the maturation of the field, which then only kept growing until now.

Thanks to a better understanding of the phenomenon, a more accurate definition of photochromism could be given: "it is a reversible transformation of a chemical species in one or both directions by absorption of electromagnetic radiation between two forms, A and B, having different absorption spectra". When the difference of λ_{max} between A and B is sufficiently large, a color change occurs, but it is not perceptible to the human eye for all photochromic compounds. When $\lambda_{max}(B) > \lambda_{max}(A)$, the phenomenon is referred to as positive photochromism (Figure 1.9), as opposed to negative or inverse photochromism when $\lambda_{max}(A) > \lambda_{max}(B)$. Most photochromic compounds undergo unimolecular reactions, but in some cases, bimolecular processes may be observed as in the case of tetracene which dimerizes (in the absence of dioxygen) *via* a photochemical cycloaddition. The reverse reaction may occur thermally (Photochromism of type *T*), photochemically (Photochromism of type *P*), or both in most cases.[59]

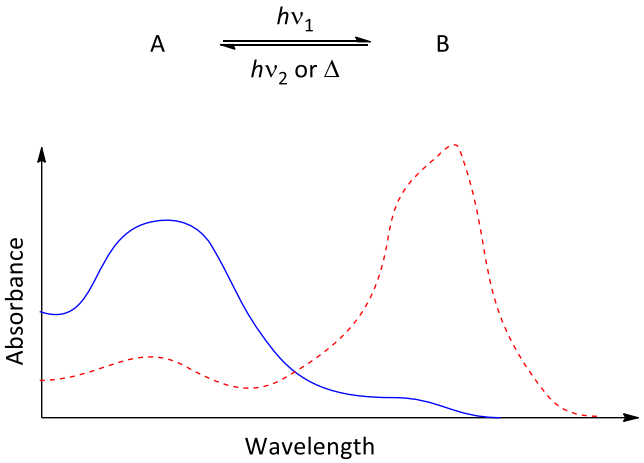

Figure 1.9. Schematic representation of positive photochromism with the change of UV-Vis spectrum when a species A (solid blue line) is photochemically converted into a metastable species B (dotted red line).

When the less energetic form A of a photochromic compound is irradiated, a metastable isomer B is produced by means of a photochemical reaction. The most encountered processes involved are pericyclic reactions, *cis-trans* isomerisations, intramolecular proton and group transfers, dissociation reactions and electron transfers. Therefore, the presence of insaturations and conjugated π-systems is a common feature of most photochromic organic molecules. Such compounds are characterized by their UV-vis spectra, but also by different variables accounting for their photochromic properties. The quantum yield determines the efficiency of the photochemical reaction regarding the amount of light absorbed. The fatigue resistance refers to the number of reactions in both directions that can be achieved before loss of reversibility, by photo-oxidation or other irreversible side reactions produced

by light. All photochromic materials are eventually prone to fatigue, though at different rates depending on their structure and the measurement conditions. The photostationary state (PSS) is a steady state reached under photoirradiation at a given wavelength, in which the composition of the system is fixed. Because the spectra of each isomeric form often overlap, it is rather difficult to obtain quantitative photoconversion in both directions. For thermoreversible systems, the half-life is the time necessary for half of the metastable isomer to be converted into the ground state at a given temperature. In addition, some physicochemical properties may vary upon isomerization such as the geometry, polarity, solubility, electric conductivity, chirality, etc… In solution, several other parameters may influence the photochromic properties of a given compound such as the solvent polarity and viscosity (solvatochromism), the pH (acidochromism), the presence of salts (ionochromism). Moreover, some photochromic substances may respond to other stimuli such as mechanical force (mechanochromism) or electric current (electrochromism) for example.[60]

A plethora of photochromic molecules have been studied to date, including inorganic and organic compounds. Many inorganic substances display photochromic properties, often with a better fatigue resistance than organic molecules. Several metal oxides were found to be photochromic when contaminated with other metals. For example, the rutile polymorph of titanium oxide is photochromic when contaminated with iron, chromium, copper, nickel and manganese, whereas the anatase form does not exhibit any photochromism with the same impurities.[61] Silver halides have been long used in the manufacture of photochromic lenses that darken when exposed to sunlight and fade in the dark within minutes. In addition, zinc, copper and mercury compounds are also often photochromic.

The variety of organic photochromic molecules is very large. Carbon-nitrogen double bond containing molecules often give rise to *E*/*Z* photo-isomerization processes such as anils, hydrazones, osazones or semicarbazones.[61] Conjugated carbon-carbon double bonds are also very prone to be photochromic. The most well-known example is found in nature and is an essential component for the vision of vertebrates: the retinal (Figure 1.10). This diterpenoid resulting from the oxidative cleavage of β-carotene contains 5 conjugated carbon-carbon double bonds terminated by an aldehyde. The 11-*cis*-retinal is embedded in a protein called opsin, and absorption of photons in the visible range causes the *cis*-*trans* isomerization of one double bond, forming the all-*trans*-retinal. This structure modification causes a mechanical stimulus to the protein which is converted into a chemical signal sent to the brain, indicating that light is detected. Then the 11-*cis*-retinal is recovered *via* the action of a retinoid isomerohydrolase and other enzymes, and the cycle starts again.[62]

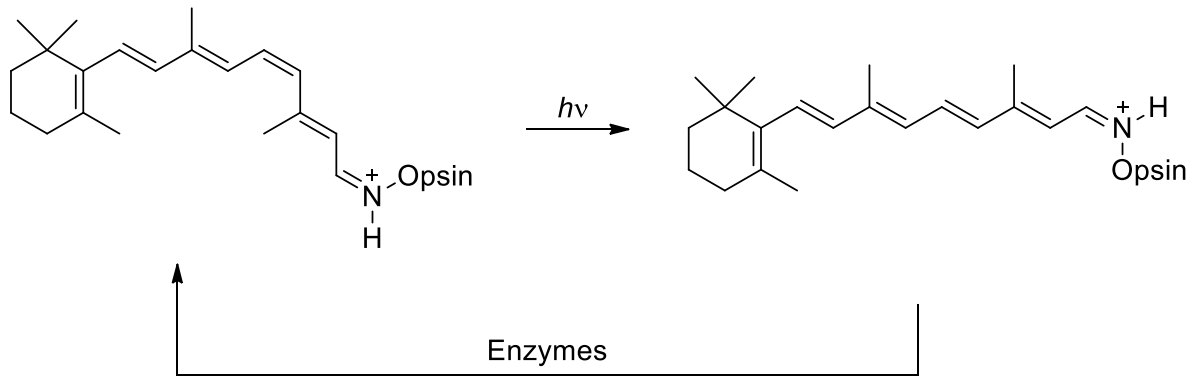

Figure 1.10. Photo-isomerization of 11-*cis*-retinal

Among organic photochromic molecules, a substantial amount has gained increasing attention due to their favorable photochromic properties. Indeed, some compounds were showing high resistance to fatigue, high photo-conversion efficiency, high thermal stability and highly tunable properties allowing them to be used as molecular switches controlled by light: photoswitches.

1.3.2. Photoswitches

The reversible changes induced by light on the molecular scale by the action of photoswitches (Figure 1.11), results in interesting macroscopic effects. Indeed, upon photoisomerization, those compounds are able to alter their properties, and transmit these changes to the materials or molecules in which they are embedded.[63] In that regard, light appears as an excellent stimulus for controlling macroscopic properties, as it is non-invasive, does not cause contamination, may be non-destructive in biological applications, and offers a high degree of spatiotemporal resolution.[64] Due to a high versatility in terms of structures, physicochemical properties and geometry, photoswitches were used in countless applications, ranging from material sciences[65] to biosciences[66] or pharmacology.[67] Each photoswitch have specificities that can address different purposes. For example, in order to operate large geometry changes for the photocontrol of biomolecules, azobenzene might be the best suited, while spiropyrans would be better for multi-stimuli responsive systems, due to the important difference in polarity between the open merocyanine and the closed spiropyran form. In this part, the properties and developments of the main classes of photoswitches are briefly reviewed, before going into the details of the azobenzene class.

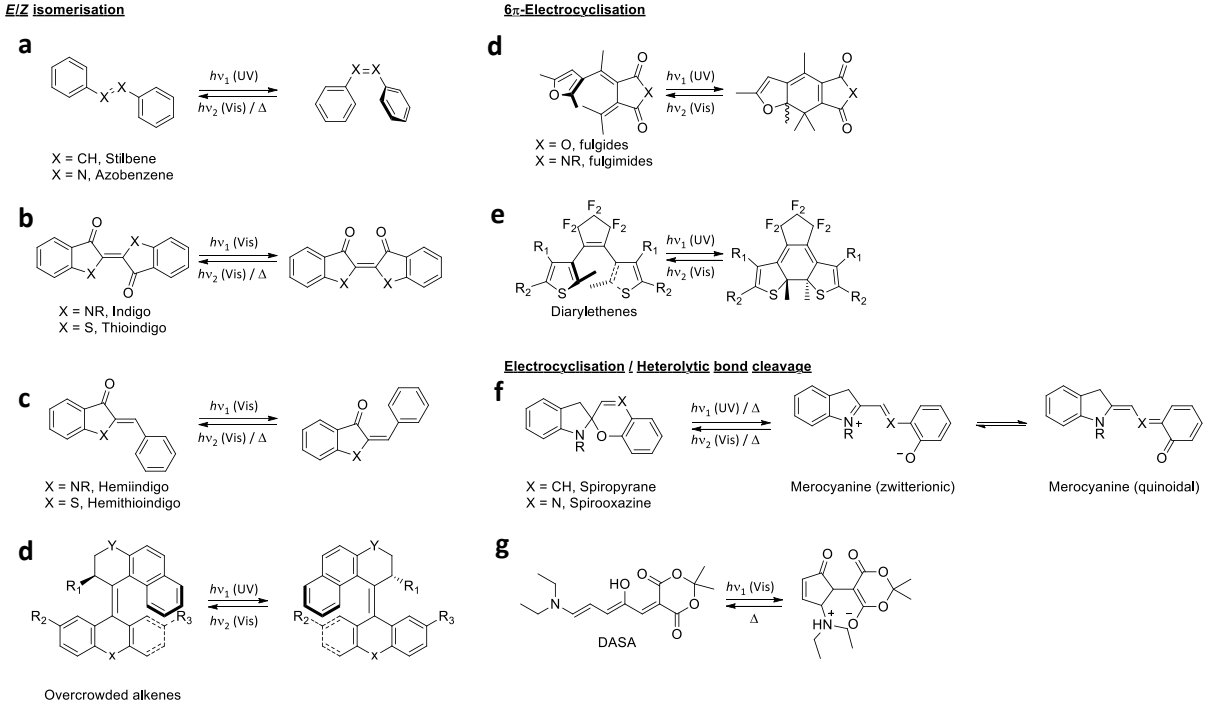

Figure 1.11. Main classes of photoswitches

As mentioned above, carbon-carbon double bonds may undergo E/Z isomerization with light.[68] Indeed, unconjugated alkenes are limited by a high activation energy (λ_{max} = 180 nm), which is only moderately altered by substitution. Conjugation of the double bond to π-systems significantly decreases the free enthalpy of activation, resulting in a bathochromic shift of the corresponding absorption band, allowing for the isomerization to occur at higher wavelengths. Therefore, stilbene (Figure 1.11a, X = CH), the simplest compound of the diarylethenes family, may be switched to the metastable *cis* form by irradiation with light of typically 310 nm, while the reverse reaction occurs under 280 nm irradiation.[69] Stilbene thus exhibits negative photochromism, with high thermal stability of the *cis*-isomer, which renders the *cis-trans* thermal isomerization generally negligible at room temperature. It has been investigated since the 1960´s as a model for understanding the isomerization mechanism in polyenes, and despite an apparent simplicity, the topic has been subject to debate until recently.[68,70] As photoswitches, stilbenes present some advantages such as a large amplitude geometry modification, high thermal stability, easy separation of both isomers, and very fast isomerization

kinetics. However, the need for damaging UV-light, a large overlap of each isomer´s absorption bands affecting the photoconversion in both direction, and the possibility for an irreversible oxidative 6π-electrocyclisation of the *cis*-isomer have limited the range of applications of stilbenes.[71] Indeed, chemical engineering may address these limitations, while improving the properties of stilbene derivatives as shown by the emergence of stiff stilbenes,[72] dithienylcyclopentenes[73] and overcrowded alkenes.[74]

Indigoid dyes have a multi-millennial history as highly colored organic pigments used to dye textiles.[75] Because of a relative scarcity of blue pigments in history, indigo became a highly valuable trading commodity that prompted the development of synthetic procedures towards its industrial fabrication in the 19th century.[76] Indigo (Figure 1.11b, X = NH) does not exhibit photochromism and is one of the most stable organic dye, due to a very fast and efficient excited state proton transfer (ESPT), which prevents degradation reactions to occur and quickly regenerates the initial *trans* state.[77] However, substitution of the N-H protons with alkyl, aryl or acetyl groups allows the generation of the metastable *cis* isomer upon visible light irradiation.[78] Alternatively, replacement of the NR group in indigo by a sulfur atom yields a thioindigo photoswitch (Figure 1.11b, X = S), that cannot undergo ESPT. This also comes with a decreased steric bulk around the central double bond, allowing both isomers to be planar, therefore providing with a nearly 180 ° wide movement of the substituents *ortho* to the thiophenone ring.[79] One of the main advantage of indigoid photoswitches is the fact that they have red-shifted absorption bands allowing photoisomerization to occur in both directions with visible light, rendering them particularly attractive for biological applications.[78] However, the insufficient band separation between each isomer affects the photoconversion yields so that it is generally difficult to reach more than 80% conversion at the PSS.[79,80] These limitations were overcome with the development of hemiindigoid photoswitches (Figure 1.11c) which are hybrid photoswitches with an indigo or thioindigo part coupled with a stilbene part.[78,81] Importantly, an iminothioindoxyl photoswitch based on thioindigo and azobenzene was recently described, showing favorable photochromic properties and improved water solubility.[82] Despite their long history, indigoid photoswitches re-gained considerable attention in the past years and the range of their applicability is constantly growing.[78]

Overcrowded alkenes (Figure 1.11d) are stilbene-based photoswitches with aromatic polycycles arranged in a way that generates atropisomerism[83] due to steric constraints. These compounds, discovered and developed by Ben Feringa, are chiroptical photoswitches.[84] Upon light irradiation of the less energetic *trans* atropisomer (P or M), a unidirectional rotation around the central double bond produces a PSS rich of the *cis* isomer in an unstable helical conformation (P or M). Due to the stereogenic center in the vicinity of the double bond (Figure 1.11d, C-R_1), a thermal equilibration of the unstable *cis* atropisomer yields the least energetic *cis* product. Irradiation with a different wavelength produces selectively the most energetic *trans* isomer, which ultimately converts thermally to the least energetic initial state. In addition, these molecules exhibit enantioselective and diastereoselective switching upon circularly polarized light irradiation.[85] Their unique properties make them particularly well suited for being applied as molecular machines,[86] but also as chirochromic catalysts[87] for instance.

Fulgides (Figure 1.11e) were first synthesized by Stobbe in the beginning of the 20th century,[88] but as most photochromic compounds, the mechanism of their color change was understood later in the 1960´s.[89] Early fulgide derivatives were thermally reversible and sensitive to photobleaching due to thermal 6π-electrocyclic ring opening, and detrimental hydrogen rearrangements followed by dehydrogenative aromatization.[90] In the 70´s, the first thermally irreversible fulgide was synthesized, and since then, they have rapidly gained a variety of properties through structural modifications. In particular, the nature of the aromatic ring (furane, indole, thiophene…), the size of the alkyl

substituents on both methylene carbons, and modifications of the succinic anhydride moiety (fulgimides, fulgenates, fulgenolides…), led to a large diversity of photochromic fulgide derivatives with different properties.[90,91] Fulgides were found to be particularly well suited for application in optical recording memory,[90,92] though they were also successfully applied to the switching of functions like fluorescence[93] or biological activity.[94] However, *E*/*Z* photoisomerisation of the aryl bearing methylene group contributes to decreasing the quantum yield of electrocyclisation, and because of the anhydride moiety, fulgides tend to be less fatigue resistant than fulgimides or dithienylethenes, as they tend to react with nucleophiles such as water or amines.

Based on a theoretical study of the cyclisation of different diarylethenes (Figure 1.11f) in 1988, the team of M. Irie predicted that replacing the phenyl rings of stilbenes by thiophene moieties would give a thermally irreversible photochromic system, that would undergo reversible 6π-electrocyclisation upon light irradiation.[95] This was explained by the fact that heteroaryl groups such as furane or thiophene have a lower aromatic stabilization energy than phenyl groups. Therefore, in the same year, the first thermally irreversible dithienylethenes were synthesized and studied.[96] It was found that the presence of methyl groups on the positions where the cyclisation occurs is critical to prevent hydrogen rearrangements and aromatization. On another hand, blocking the *E*/*Z* isomerization by incorporating the C=C double bond in a cycle was also found to improve the efficiency of the switch.[97] In the following years, Irie studied diarylethenes extensively and found that besides being thermally irreversible, diarylethenes were highly fatigue resistant, and were showing excellent photoconversion due to large changes in the absorption spectra of the open and closed forms.[98] Nowadays, diarylethenes have become one of the most popular photoswitch with azobenzenes and spiropyrans. Their range of applications spans from the design of memory devices,[98,99] multiresponsive agents,[100] to transition metal coordination[101] and self-assembled systems.[102]

Spiropyrans (Figure 1.11g, X = CH) and spirooxazines (Figure 1.11g, X = N) are some of the most versatile photoswitches. Besides their ability to switch between a colorless closed spiropyran form, and a colored open merocyanine form under light irradiation, these compounds also exhibit thermochromism, acidochromism, electrochromism and mechanochromism.[59,103] The thermochromism of spiropyrans was extensively studied in the 1960´s, and some general trends were established.[104] For example, dibenzospiropyran is not thermochromic, whereas the benzonaphtospiropyran and the indolinobenzospiropyran are.[104,105] This shows that polarization of the spiro center and stabilization of the open form through resonance are important parameters. In addition, depending on the substitution of the aromatic rings and the nature of the heterocycle, the merocyanine can be found either in a zwitterionic form or a quinoidal form. This renders merocyanines sensitive to pH, solvent polarity and electric potential, making spiropyrans multiresponsive switches. Due to their versatility, spiropyrans have found widespread applications in the design of dynamic materials,[106] rewritable data storage,[107] optical devices,[108] amongst others.[109]

Finally, Donor-acceptor Stenhouse adducts (DASAs, Figure 1.11h) are one of the latest class of photoswitches, that were investigated by the group of J. Read de Alaniz in the 2010´s.[110] These photoswitches, of which the name was chosen in recognition of John Stenhouse (1809-1880),[111] result from the condensation of furfural with a dicarboxylic active methylene compound such as Meldrum´s acid, followed by opening of the furane ring by an amine through a series of rearrangements similar to the Piancatelli rearrangement.[110a,112] This results in a highly colored triene with an electron donating moiety on one side and an electron withdrawing moiety on the other side, forming a so called “push-pull” system. This substitution pattern combined with the conjugation of the double bonds produces a large bathochromic shift of the main transition of the triene open form to wavelengths above 500 nm, allowing photoswitching with visible light and near infrared (NIR) light.[113] Depending on the nature of both the donor and acceptor moieties, the band may be further red shifted making DASAs promising

photoswitches for biological applications.[114] Another interesting feature of DASAs is their photochemical irreversibility (type *T* photochromism), and their applicability in wavelength selective addressing of different photoswitches.[115] DASAs were so far applied successfully in liquid crystalline systems,[116] in polymers and on surfaces,[117] or in drug delivery for example.[118] A major drawback of DASAs however, is that in aqueous environment, the closed zwitterionic isomer is greatly favored, which prevents the thermal return to the neutral open form, thus limiting the range of their applications.[119]

Besides these photoswitches that could be only briefly presented, the class of azobenzenes has dominated the field of photochromic compounds, and their properties will be presented in detail.

1.3.3. Azobenzene photoswitches

1.3.3.1. Photochromic properties of azobenzene photoswitches

Azobenzene (AB, Figure 1.11a, X = N) is the most prominently used photoswitch due to its simple structure, synthetic accessibility, as well as robust and efficient photochromism.[120] This compound consisting of a diazene (HN=NH) with phenyl groups instead of hydrogen atoms, was first prepared industrially in the middle of the 19th century by Nobel, and independently by Griess who discovered the diazotization of anilines and their coupling to electron rich aromatic compounds.[121] The first report on the *trans-cis* isomerization of AB dates back to 1937 when Hartley isolated the *cis* isomer thanks to its higher polarity.[122] Since then, an immense quantity of azo derivatives was synthesized, producing highly colored molecules that are light resistant and can exhibit a wide variety of tones, accounting for their extensive use in dye industry (60-70% of total production).[123]

AB can be found in two configurational isomeric states: a stable *trans* form with C_{2h} symmetry, and a metastable *cis* form with C_2 symmetry (Figure 1.12a). In the *trans* form, AB is planar[124] and has no dipolar moment. In the *cis* form however, the structure is bent and more polar, and steric repulsions constrain it to adopt a certain conformation. The CNNC dihedral angle is distorted to a value of 8 °, due to steric hindrance between the phenyl rings as well as electronic repulsion of the nitrogen lone pairs.[125] This feature gives rise to helicity, and hints that azobenzene could exhibit chiroptical properties when coupled to chiral molecules. On another hand, the NNCC dihedral angles are about 53 °,[125] which means that the phenyl rings are no longer coplanar with the N=N double bond, disrupting the conjugation in the molecule. The end to end distance between the two para positions is also greatly affected upon photoisomerization, leading to a nearly 4 Å wide movement. Conversion from *trans* to *cis* is achieved through irradiation with UV-light (313 nm),[126] mechanical stress[127] or electrostatic stimulation.[128] The reverse reaction occurs either thermally or photochemically, by irradiation in the visible range (436 nm).[120a]

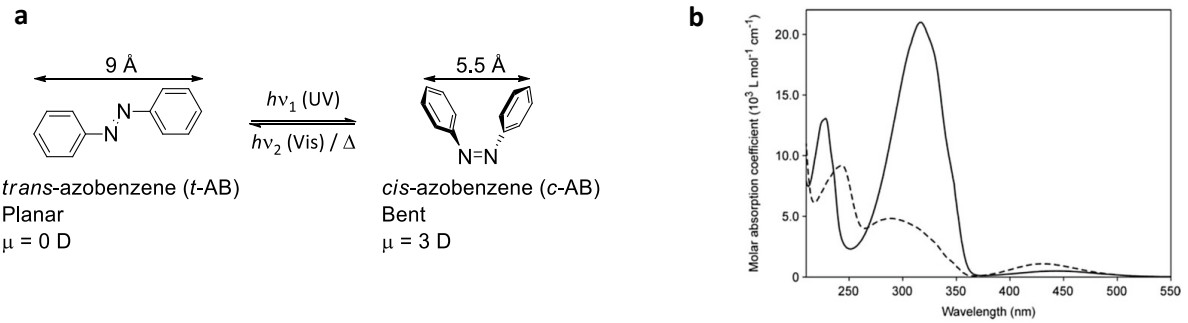

Figure 1.12. Isomerization of azobenzene (a) and UV-vis spectra (b) of the *trans* (full line) and *cis* (dashed line) isomers in acetonitrile at RT.

The UV-Vis spectrum of *t*-AB is characterized by three absorption bands in the UV-Vis region (Figure 1.12b). The least energetic one, located in the visible part of the spectrum (λ_{max} ~ 440 nm, ε ~ 500 L.mol^{-1}.cm^{-1}), corresponds to the symmetry forbidden n→π* transition.[129] In *cis*-AB, this band becomes allowed, therefore it is more intense (λ_{max} ~ 430 nm, ε ~ 1500 L.mol^{-1}.cm^{-1}), and slightly blue shifted due to an increased conjugation of the nitrogen lone pairs with the benzene rings. Irradiation at those wavelengths results in the excitation of the molecule to the first singlet state ($S_1 \leftarrow S_0$), and leads to isomerization.[130] The second and most intense band matches the allowed π→π* transition of the N=N double bond. It occurs in the UV region of the spectrum with *t*-AB absorbing at ~ 320 nm and *c*-AB at ~ 280 nm. The larger intensity of the band in *t*-AB and the hypsochromic shift observed for *c*-AB are explained by the non-planar conformation of the metastable isomer, which reduces the extent of conjugation in the molecule. This transition excites AB to the second singlet state ($S_2 \leftarrow S_0$) also resulting in isomerization,[130] according to a mechanism that will be discussed below. The third transition, corresponding to the π→π* transition of the benzene rings, undergoes only a slight bathochromic and hypochromic shift upon isomerization, and is less relevant in the photochemistry of AB as it is too energetic.

The isomerization mechanism of AB was long debated, due to multiple possible pathways.[131] It is now generally accepted that AB may isomerize according to four different mechanisms: rotation, inversion, concerted inversion and inversion-assisted rotation (Scheme 1.1).[120a]

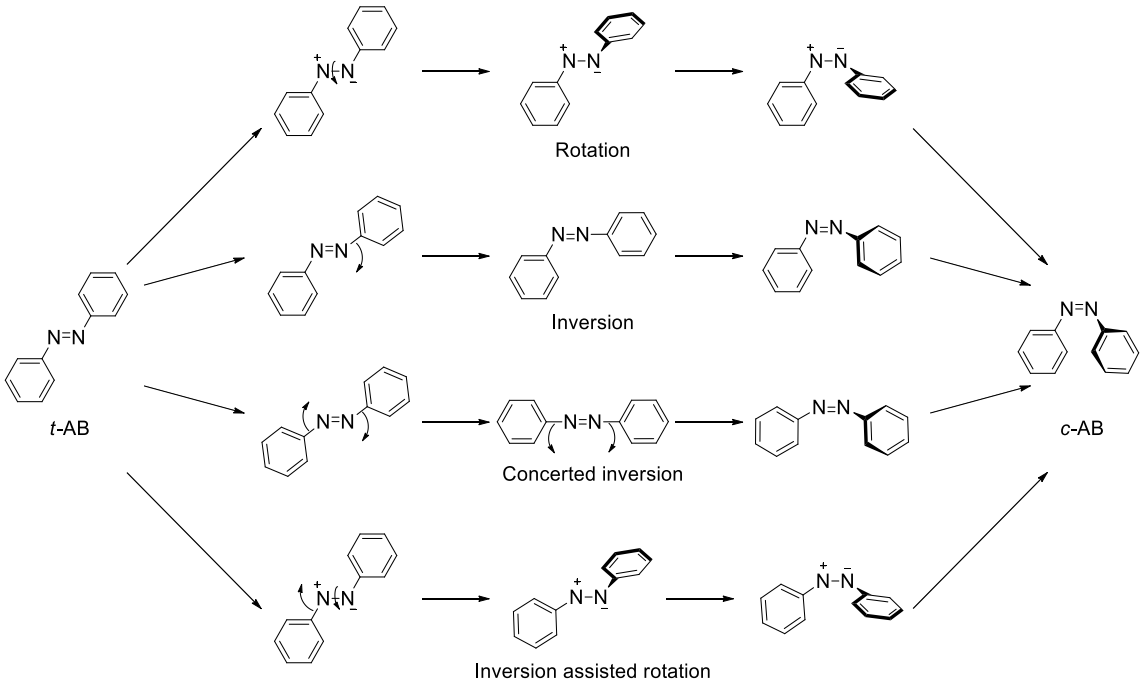

Scheme 1.1. Proposed mechanisms for the *trans*→*cis* isomerization of azobenzene.

In the rotational pathway, the N=N π-bond is cleaved, leading to a transition state allowing free rotation along the N–N axis, with an energy minimum for θ_{CNNC} = 90 °. Torsion of the CNNC dihedral angle generates *c*-AB while the CNN and NNC angles stay unaffected.[132] The inversion mechanism proceeds *via* the augmentation of one NNC bond angle to 180 °, leading to a planar transition state with one *sp* hybridized nitrogen atom.[133] The concerted inversion pathway involves an apolar linear transition state with both NNC bond angles equating 180 °.[134] Finally, the inversion-assisted rotation is a multidimensional pathway where both CNNC and NNC angles are affected simultaneously,[131,135] resembling a hula-twist motion.[136] Each of those transition states may relax either to the *cis* or the *trans* product, therefore predicting photostationary states consisting of both isomers. The preferred isomerization pathway depends on the wavelength of irradiation ($S_1 \leftarrow S_0$ or $S_2 \leftarrow S_0$ excitation),[135a] the

viscosity and polarity of the solvent,[137] and is strongly influenced by the nature of substituents on the benzene rings.[120a] Therefore, *t*-AB was found to isomerize predominantly *via* rotation following $S_1 \leftarrow S_0$ excitation in hexane, whereas concerted inversion is favored in a more viscous CCl_4/ethanol mixture.[138] In contrast, *t*-AB isomerizes *via* inversion following $S_2 \leftarrow S_0$ excitation in hexane.[139] Additionally, in many cases, multiple isomerization pathways may occur simultaneously, which accounts for some experimental observations that do not fit a unique isomerization mechanism.[140]

Such differences in the isomerization pathway after $S_1 \leftarrow S_0$ or $S_2 \leftarrow S_0$ excitation results in a wavelength-dependent photochemistry of AB: the quantum yield following $n \rightarrow \pi^*$ excitation is two-fold higher than following $\pi \rightarrow \pi^*$, which violates Kasha´s rule. In 2018, Nenov *et al.* demonstrated that the violation of Kasha´s rule is due to a high energy unreactive planar intermediate only accessible after $\pi \rightarrow \pi^*$ excitation, which regenerates the *trans* ground state.[141] A model of the excited-state pathways was used to quantify the percentages of photoproducts generated. It showed that $n \rightarrow \pi^*$ excitation produced 24% of *cis* whereas $\pi \rightarrow \pi^*$ excitation produced only 12% of *cis*, while the rest of decay events were regenerating the *trans* ground state, in agreement with the factor of two between each quantum yield.[135a] The quantum yield of photoisomerization may be inscreased by blocking some isomerization pathways through conformational strain. Azobenzenophanes and diazocines for example, are rotation-restricted azobenzene derivatives with improved quantum yields.[142] However, the torsional pathway is not always fully blocked, and the preferred pathway was shown to be inversion-assisted-torsion.[136,143]

The substitution of the benzene rings has a drastic influence on the photochromic properties of AB derivatives. In the 1990´s, Rau classified AB derivatives into three main categories depending on the relative energy of their $n \rightarrow \pi^*$ and $\pi \rightarrow \pi^*$ transitions (Figure 1.13).[144] The first class called azobenzenes (ABn), have similar spectra than that of the parent AB, with well separated transitions. In the aminoazobenzene type (aAB), electron donating substituents cause a red-shift of the $\pi \rightarrow \pi^*$ transition without affecting the S_1 energy level, causing both transitions to be nearly degenerate, and therefore to overlap. The pseudo-stilbenes (pSB) include the protonated AB (pAB) and push-pull azobenzenes (ppAB), for which the $\pi \rightarrow \pi^*$ transition is so red-shifted that it becomes the lowest lying transition. The pseudo-stilbene name refers to the fact that a strong asymmetry in the electronic distribution favors the rotation mechanism over all other isomerization pathways, reminiscent of stilbene´s only torsional photoisomerization.

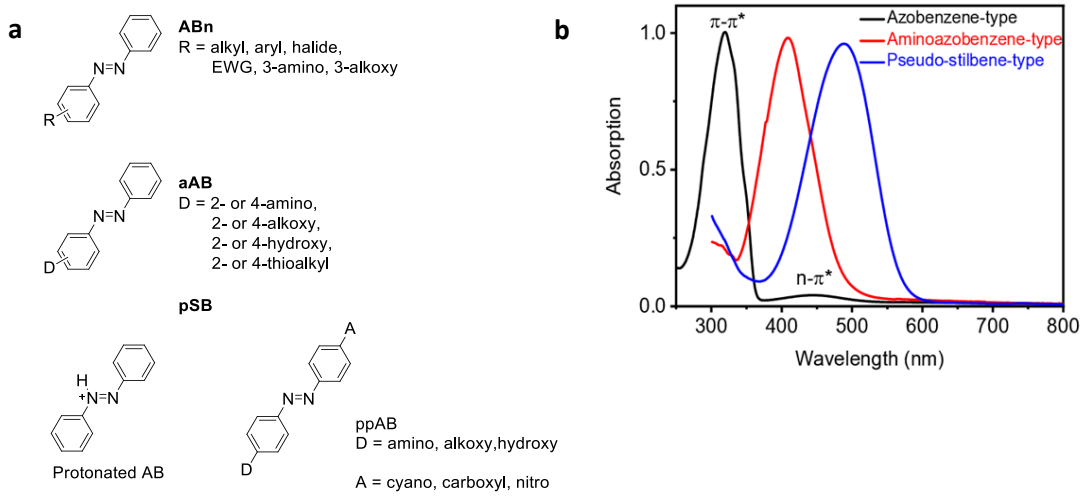

Figure 1.13. Types of substituted AB derivatives according to Rau´s classification (a), and UV-Vis spectra of each categories (b).

If ABn have similar quantum yields as the parent AB, they usually possess higher thermal relaxation rates, which depend on the temperature, polarity and viscosity of the medium.[120a,137] However, *cis*-

ABn have the higher thermal stability of all categories, ranging from hours to days at room temperature, and their relaxation usually occurs through inversion.[120a,145] The thermal relaxation of aAB is much faster than that of ABn, with half-lives ($t_{1/2}$) of seconds to minutes at room temperature,[146] while pSB show the shortest lived *Z*-form with half-lives ranging from picoseconds to seconds.[147] Hydroxy substituted AB have the peculiarity of showing enhanced thermal relaxation rates due to tautomerism between the azophenol form and a hydrazoquinone-like form, decreasing the double bond character of the central N=N bond. This renders the rotation about the N=N bond easier, and leads to a very fast recovery of the *trans* isomer.[148] Red-shifting of AB spectral bands would be favorable for applications in biological sciences[66a,149] or photopharmacology,[66b-67] however the subsequent drop in thermal stability may not always be desirable. Therefore, different strategies have been developed to decorrelate the addressability of AB derivatives and their thermal isomerization rate.[149]

The most prominent strategy for producing red-shifted AB derivatives (Figure 1.14) with extended half-lives lies on the rational design of suitably substituted compounds. As mentioned above, the push-pull substitution in *para* positions leads to a decreased thermal stability, therefore, endeavor has been directed to *ortho*-substitution.

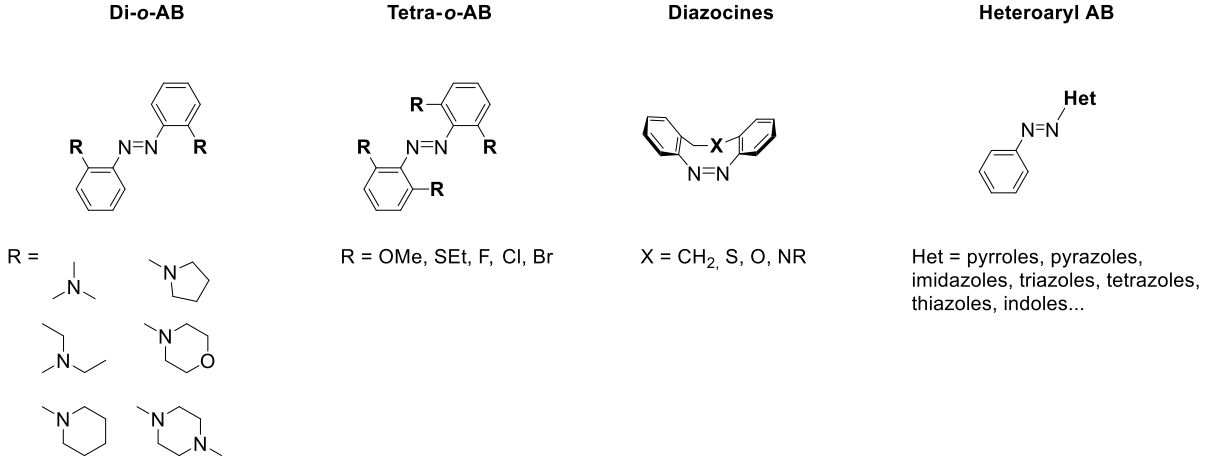

Figure 1.14. Examples of strategies used to red-shift and/or extend the half live of AB derivatives.

The group of Woolley pioneered in this field by first studying the influence of symmetric amino di-substitution, *ortho* to the azo bond.[150] A substantial red-shift of the main transitions was achieved, though medium amounts of *cis* were produced at the photostationary state, and half-lives were still in the range of seconds. Substitution of all *ortho* positions with methoxy groups showed more promising results.[151] The steric congestion caused by the substituents disrupted the planarity of the *trans* form, causing a hyperchromic effect on the n→π* band. Additionally, electrostatic interactions between the lone pairs of nitrogen and oxygen atoms caused a red-shift of the n→π* transition of the *trans* isomer, resulting in a 36 nm separation of the n→π* bands of *trans* and *cis* isomers. This resolution allowed to switch tetra-*o*-methoxy AB with visible light only ($\lambda_{E\rightarrow Z}$ = 530 nm; $\lambda_{Z\rightarrow E}$ = 460 nm), producing substantial amounts of *cis* (70%) and *trans* (80%) at the photostationary states, with good thermal stability ($t_{1/2}$ = 2 *d* in aqueous solution at room temperature). These compounds showed minimal photobleaching and pH stability for pH > 5, however they proved more sensitive to reducing conditions than the parent compound, which may not be optimal for biological applications. This limitation was addressed by replacing oxygen atoms with sulfur atoms, allowing for red-switching of a water soluble derivative, though at the expense of photoconversion and thermal stability.[152] More recently, a protonated AB derivative with fused dioxane rings in combination with methoxy substituents occupying all four *ortho* and two *meta* positions was reported. It showed near infrared (NIR) photoswitching with a half-life near 1 s under physiological conditions.[153]

In 2012, Hecht *et al*. reported on tetra-*o*-fluoro AB derivatives with extended half-lives and highly resolved n→π* bands.[154] Compared with methoxy groups, fluorine atoms are less bulky and more electron withdrawing. It causes less distortion of planarity in the *trans* state, and decreases repulsions between the nitrogen lone pairs in the *cis* state, resulting in the enhanced separation of n→π* bands up to 50 nm, and an increased thermal stability. Electron donating groups (EDG) in *para* positions were shown to decrease the band separation, while electron withdrawing groups (EWG) had the opposite effect. Excellent photoconversion was achieved in both directions with blue and green-light, with half-lives exceeding that of prior derivatives.[155] In the same lines, tetra-*o*-chloro and tetra-*o*-bromo AB derivatives showed similar properties, although with decreased band separation and thermal stability.[156] However, it was reported that irradiation in the tail of *trans* tetra-*o*-chloro AB n→π* band could produce significant amounts of *cis* at the PSS, allowing for the use of green to red-light to optically control biological systems.[157] Lately, di-*o*-fluoro-di-*o*-chloro AB derivatives demonstrated excellent thermal stability as well as efficient $E \rightarrow Z$ photoswitching with red-light (660 nm), despite slower switching kinetics at this wavelength.[158] Other mixed AB derivatives such as the fluoroamino series were also recently investigated and showed increased visible light absorptivity and good thermal stability.[159]

Diazocines are AB derivatives bridged on their *ortho* positions with an ethylene group. The bridge causes a cyclic strain on the N=N double bond that renders the *Z*-isomer thermodynamically favored, and induces a large separation (~ 100 nm) of the n→π* bands.[142c] Besides allowing selective switching of each isomer in the visible range, diazocines show good thermal stability, excellent photoconversions, high fatigue resistance and exceptionally high quantum yields.[142c,d] Hetero-diazocines containing oxygen or sulfur in the ethylenic bridge were found to have shorter and longer half-lives than the parent compound respectively, though with reduced $Z \rightarrow E$ photoconversion despite a greater band separation.[160] While *N*-acetyl hetero-diazocines showed efficient photoswitching in aqueous solution with blue and green-light,[161] $E \rightarrow Z$ photoisomerization of *N*-methyl derivatives was achieved with NIR-light.[161a] Interestingly, a sulfur containing nine membered cyclic AB derivative showed a reversed thermodynamic stability compared to the parent sulfur bridged diazocine, showing a ring size limit in terms of relative stability.[162] Comparison with a diazonine derivative (*Z*-isomer thermodynamically stable) also shows that the flexibility conferred by the sulfur atom is critical.[163]

Another emerging and particularly versatile class of AB derivatives is the one of arylazoheteroarenes.[164] After a first report by Majima *et al*. in 2003 on the photochromic behavior of nucleoside modified 2-(phenylazo)imidazoles, showing photoconversion over 90% in each direction,[165] Sinha *et al*. undertook a more detailed survey.[166] It revealed that 2- and 4-(phenylazo)imidazole derivatives behave substantially like the parent azobenzene, although with better photoconversion and quantum yields. A large separation of the π→π* bands of each isomer allows a near quantitative switching towards the *cis* form with UV-light (~ 360 nm), while the *trans* can be recovered with blue-light (~ 455 nm). However, those compounds show increased thermal relaxation rates compared with *cis*-AB, as a consequence of intermolecular H-transfer mediated tautomerism (Figure 1.15a), inducing the formation of a hydrazone form and reducing the rotation barrier.[166b] The extent of this tautomerism may be reduced by substitution of the imidazole-NH nitrogen, therefore preventing H-transfer. In addition, imidazole substituted in the 4- position have a longer $t_{1/2}$ than a 2-(phenylazo)imidazole, showing the impact of conjugation (Figure 1.15b) on the thermal stability.[167]

Later, Herges *et al*. prepared a series of 4- and 5-phenylazoimidazoles *via* addition of lithiated imidazole on phenyldiazonium, showing remarkably long half-lives, despite a low $Z \rightarrow E$ photoconversion.[168] The authors demonstrated that this new derivative was adopting an unusual configuration in the *cis* state, where the imidazole ring is coplanar and the phenyl ring orthogonal, relative to the CNNC plane. This reduces the conjugation in the *cis* state, and results in a better

separation of $\pi \rightarrow \pi^*$ transitions. In addition, they showed that in the case of 5-phenylazoimidazoles, the proton at C-4 is oriented in the deshielding range of the phenyl ring, therefore resulting in an upfield shift in NMR spectroscopy.

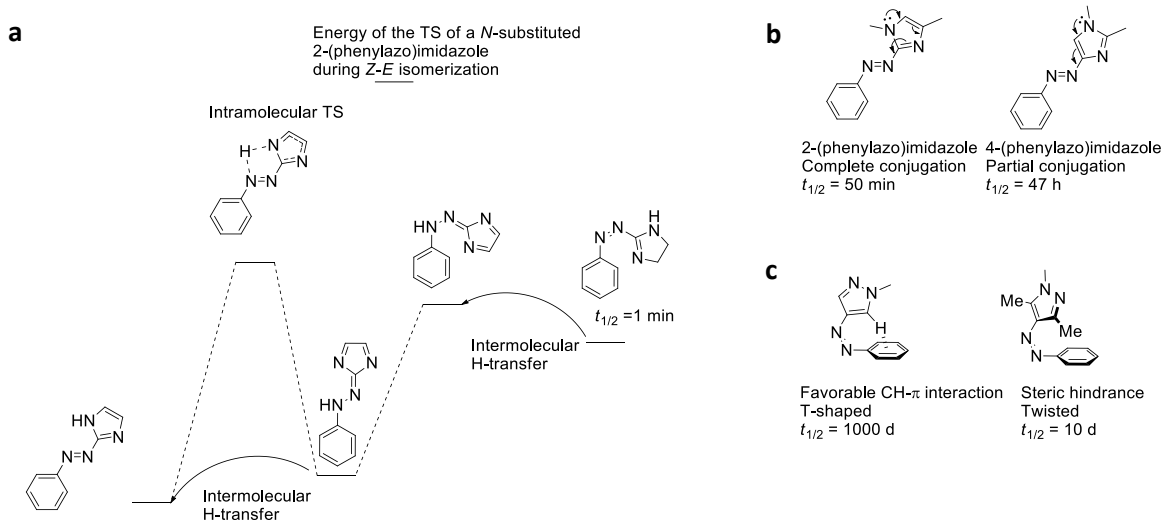

Figure 1.15. Dependence of the thermal stability of some heteroaryl AB derivatives on the type of heterocycle (a), the position of the azophenyl moiety on the heterocycle (b) and the substitution of the heterocycle (c).

In 2014, Fuchter *et al*. reported on phenylazopyrazoles with extremely long half-lives and quantitative photoswitching in both directions.[169] Due to the T-shaped conformation adopted by AB derivatives with 5-membered heterocycles (Figure 1.15c), a favorable CH-π interaction can be established in the *cis* form, resulting in a large stabilization of this isomer, with half-lives up to 1000 d at room temperature. Substitution of the "*ortho*" positions of the heterocycle produces a twisted conformation for the *Z* isomer. It decreases the half-life of the *Z* form and the separation of $\pi \rightarrow \pi^*$ bands, although it increases the absorption of the *cis* $n \rightarrow \pi^*$ transition, resulting in quantitative $Z \rightarrow E$ photoconversion, a property that was exclusively found in diazocines so far. Lately, a heteroaryl AB derivative combining a di-*o*-fluorophenyl and a pyrazole moiety was found to be the longest lived bistable azoarene photoswitch, with a half-life of 46 years.[170] Phenylazoheteroarenes revealed themselves being derivatives with highly tunable thermal stability (from picoseconds to years) and excellent addressability, making them promising targets for future AB photoswitches development.[147d,164-171]

1.3.3.2. Synthesis of azobenzene photoswitches

The long history of ABs and their extensive use has prompted the discovery of many synthetic methods towards their preparation, some of which are shown in Scheme 1.2.[172] Interestingly, one of the oldest methods, called diazo-coupling and discovered by Griess in 1858,[121b] is still extensively used today due to its efficiency and the use of an aqueous medium. Allowing access to symmetrical as well as non-symmetrical derivatives, this reaction is however limited to electron rich aromatic compounds (typically phenols or anilines), and gives poor yields for tetra-*o*-AB derivatives. Indeed, this reaction is an electrophilic aromatic substitution (S_EAr) of a phenyl ring with a diazonium salt, and is greatly influenced by the substitution pattern on each reactant, which limits the scope of substrates (Scheme 1.3a). For the addition step to occur, both steric and electronic parameters must be optimal, as the reaction may generally not happen at higher temperature than 10 °C, owing to the thermal instability of diazonium salts. This methodology is also highly pH-dependent, and works under slightly acidic conditions for anilines and around pH = 10 for phenols.

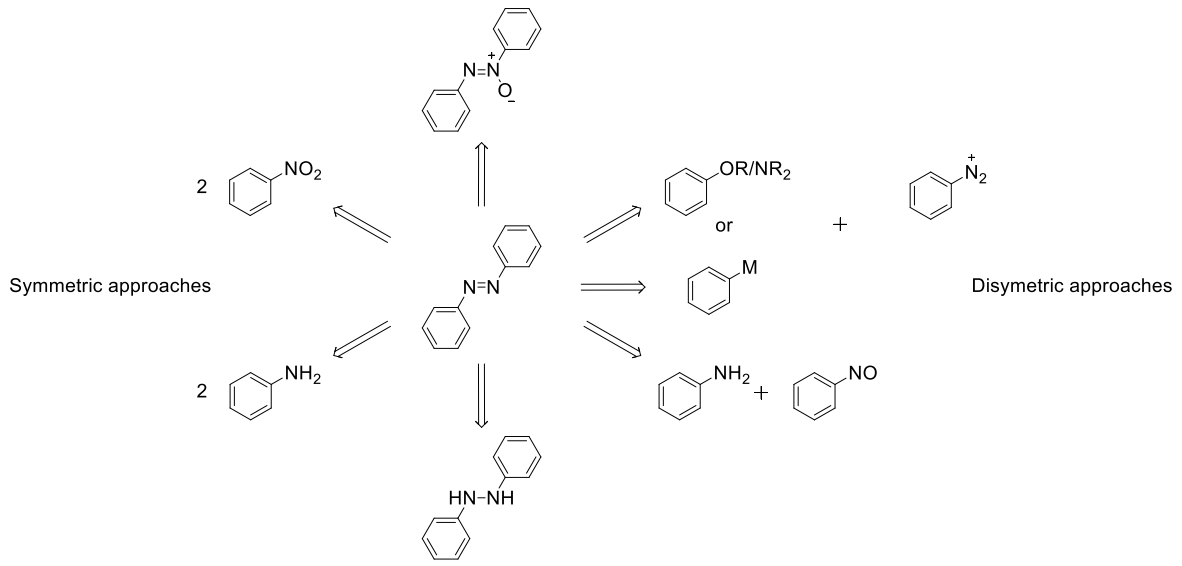

Scheme 1.2. Main retrosynthetic approaches towards AB derivatives.

An alternative is to use organometallic reagents to enhance the nucleophilicity of the aromatic group. Reaction between Grignard,[173] zinc[174] and tin[175] reagents with aryl diazonium salts have been reported, however the best yielding method may be the addition of organolithium species on aromatic diazoniums. This method was used by Herges *et al*. to synthesize arylazoimidazoles,[168] and was later shown to be highly efficient for the synthesis of tetra-*o*-substituted species, giving access to a wide variety of red shifted ABs in 40 to 90% (vs <30% for previous methods).[176]

The Baeyer-Mills reaction is another very common procedure used for the synthesis of ABs. First discovered by Baeyer in 1874, it was further explored by Mills in the end of the 19th century.[177] It proceeds *via* the condensation of an aniline with a nitrosoarene in acetic acid. The mechanism is similar to the condensation of an amine on a carbonyl leading to the imine. The nitrosoarene may be prepared by many methods,[178] but the most common is the oxidation of primary anilines with peroxides such as *m*-chloroperbenzoic acid (*m*CPBA). Recently, the use of Oxone® (*i.e.*, $2KHSO_5{\cdot}KHSO_4{\cdot}K_2SO_4$) in a biphasic system of CH_2Cl_2/H_2O became the method of choice to synthesize nitrosoarenes, as it secures a certain separation of the less water-soluble nitroso compound from the aniline precursor and the hydroxylamine intermediate, preventing undesirable condensation reactions.[179] The Baeyer-Mills reaction has a greater scope than the diazo-coupling reaction allowing the synthesis of AB derivatives with substitution patterns inaccessible with the S_EAr, however it is generally low yielding for tetra-*o*-substituted compounds.

When the aforementioned methods fail, one might also explore oxydoreductive methods to synthesize ABs. The reductive coupling of aromatic nitro compounds for example, provides symmetrical ABs with reducing agents such as $LiAlH_4$,[180] $Zn/Ba(OH)_2$,[181] glucose/NaOH,[182] or Mg/HCO_2HNEt_3,[183] amongst others.[172b] Some major problems with this method are that selective reduction to the nitroso (*e.g.* for unsymmetrical compounds) is challenging, and the reaction often affords mixtures of azoxybenzene and AB. In addition, the reducing agents are used in excess and their by-products are generally environmentally unfriendly. However it was for a while the method of choice for the preparation of diazocines.[181,182]

Alternatively, the oxidative coupling of aromatic amines may be used. A variety of reagents such as Ag_2O,[184] MnO_2,[185] HgO/I_2,[186] or $KMnO_4/CuSO_4$,[187] for example, afforded ABs in moderate to excellent yields. The latter reagent system, combining permanganate and metal sulfate, proved successful for the preparation of *o*-substituted derivatives, however it requires long reaction times and provides low yields.[152-155] A system employing Na_2WO_4/H_2O_2 oxidized the 2,6-dimethylaniline to the tetra-*o*-methyl

azo dioxide, which after reduction with Si_2Cl_6 gave tetra-*o*-methyl AB in 94 % overall yield, making this method potentially useful for the synthesis of congested azobenzenes.[188] Recently, a method using *N*-chlorosuccinimide (NCS) as oxidizing agent and 1,8-diazabicyclo[5.4.0]undec-7-ene (DBU) as a base was reported, yielding many AB derivatives in short times and good yields.[189] This method showed great efficacy to prepare symmetrical tetra-*o*-fluoro and perfluoro-AB derivatives in good yields.[189,190] Another advantage of the oxidation of anilines is that the nitroso derivative can be selectively formed, and used to prepare unsymmetrical compounds.[179] Also, recently, an improved preparation of cyclic AB derivatives using *m*CPBA allows access to diazocines in good yields from dianilines.[163] When over-oxidation or incomplete reduction occur, AB can also be prepared from azoxybenzene, either *via* the Wallach rearrangement producing hydroxy-substituted AB,[191] or by reduction using $Al/H_2NNH_2.H_2O$ in methanol,[192] AlI_3,[193] or $Cu(OTf)_2$[194] for example. In contrast, when over-reduction produces undesired arylhydrazine, the latter may be dehydrogenated using oxidants such as MnO_2,[195] $CuCl_2$[196] or $TiCl_3/HBr/H_2O_2$.[197]

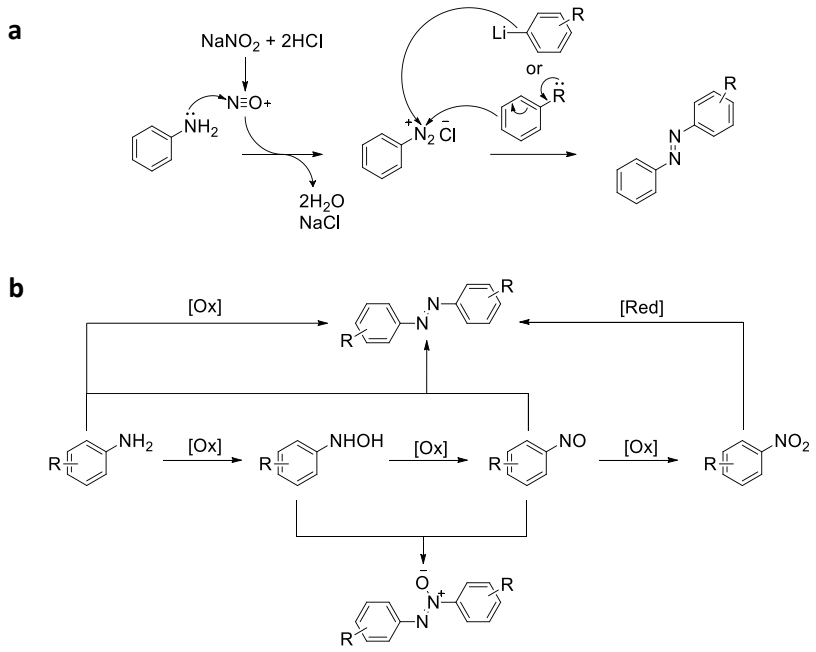

Scheme 1.3. Preparation of AB *via* diazotization of aniline and addition of different aromatic nucleophiles (a), or *via* oxydoreductive methods (b).

The preparation of functionalized AB dervivatives is important as it allows to equip ABs with functional groups in view of their incorporation into larger molecular architectures. This enlarges the range of applications of ABs, and enables to use them for the photocontrol of physico-chemical properties. Their synthesis may often be tedious, and usually requires prefunctionalization prior to the azo bond formation, which limits the possible synthetic modifications of the AB core. Moreover, the diazenyl group is naturally sensitive to oxidizing and reducing agents. To circumvent these limitations, metal assisted transformations have been investigated, and proved to be powerful methods towards various functionalized ABs.[198] The directing effect of the diazenyl group allows efficient C-H activation of the *ortho* positions, providing mono-,[199a] di-[199a] and tetra-*o*-halogenated[199b,c] products, as well as tetra-*o*-alkoxylated[199d] derivatives. However, *ortho* fluorination remains challenging, and efficient functionalization methods for tetra-*o*-fluoro derivatives are still lacking. Furthermore, C-H activation has allowed the formation of C-C, C-O, C-N, C-S, C-Se and C-Si bonds,[198b] and in some cases, *meta* alkylation and sulfonation was achieved.[200] (Pseudo)-halogenated ABs in *meta* or *para* positions were extensively used as electrophiles in metal catalyzed coupling with C-, O-, N- and P- nucleophile, and the examples where the AB was used as a nucleophile are rarer.[198a]

As shown in this section, ABs are very versatile photoswitches with almost limitless potential for applications, due to their highly modular properties, efficient photochromism and good synthetic accessibility. Therefore, fast relaxing AB derivatives addressable in the UV-vis range may be employed as real-time information-transmitting materials,[147] while the more thermally stable derivatives may be used in photomechanics,[201] as solar energy fuels[202] or in optical data storage[203] for instance. In the biomedical field, the need for thermal stability and/or red-shifted addressability is dictated by the application. Hence, when the activity of a photoswitchable biomolecule needs to be turned off as soon as the irradiation stops, the use of push-pull AB is the most suitable as it combines red-shifting of the excitation wavelength with enhanced thermal relaxation rates. In contrast, when the reversible photocontrol over a biological function with light is desired, a bistable switch with visible light addressability and high photoconversions is preferable.[67] ABs have also been introduced into many macrocyclic structures, offering the possibility to alter properties of macrocycles with light.

1.4. Azobenzene-containing macrocycles

The incorporation of AB into macrocyclic structures and the effect of isomerization on their intrinsic properties have been extensively studied.[204] It does not only allow to control the properties of the cycle (binding affinity, bioactivity, solubility…) with light, but also affects the performances of the photoswitch itself. In the past 40 years, a plethora of responsive macrocycles were synthesized, and restricting the research to the sole AB switch still gives several hundreds of results.[205] In this part, a particular focus was put on two aspects: the consequences of macrocyclization on the photochromism of AB, and the influence of isomerization on the properties of some selected macrocycles, and a few examples of applications are given.

Azobenzenophanes are cyclophanes containing at least one AB unit into the cyclic backbone (Figure 1.16). Early dithia-diaza-paracyclophanes (Figure 1.16a) were synthesized by Grützmacher and coll. by nucleophillic substitution of alkyl dithiols on the benzylic positions of a 4,4´-*bis*-(bromomethyl)-hydrazobenzene, that was locked in *cis* configuration *via* formation of a pyrazolidine-3,5-dione with dimethylmalonyl chloride.[206] The yields of cyclization were dependent on the alkyl chain length, with an optimum length of 6 carbon atoms, giving the expected product in a good yield of 55%. Reducing or increasing the chain length generally resulted in lower yields with the exception of butanedithiol giving a similar result.

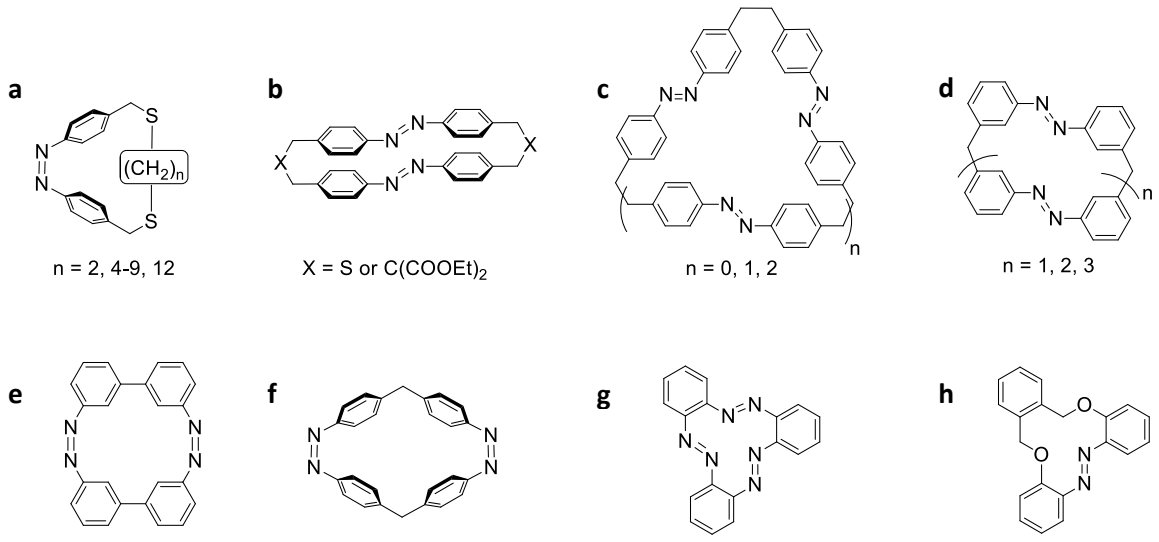

Figure 1.16. Structures of selected azobenzenophanes with varying number of azobenzene units.

The authors showed that the strain induced by the cyclization forced the AB moiety to adopt a *cis* configuration for chain lengths between 2 and 5 carbon atoms. This is the first example of inverted thermodynamic stability, where the *cis* form is the most stable isomer. However, these compounds were so strained that the *trans* isomer could not be generated photochemically nor thermally, and irradiation with UV or visible light led to decomposition. For C_6 and C_7 alkyl chains, a thermally equilibrated mixture of *cis* and *trans* isomers was observed, and UV irradiation generated quantitatively the *cis* isomer while visible light irradiation produced 50% of *trans* isomer (n = 6), or regenerated the initial mixture containing 78% of the *trans* isomer (n = 7). For chain length superior or equal to 8, the properties of the azobenzene moiety became closer to those of the linear *p*-azotoluene parent molecule, that is a photostationary state with around 90% *cis* after UV-light irradiation, and full recovery of the stable *trans* isomer under visible light irradiation.

Unfortunately, this study gave no information regarding the thermal stability of the metastable isomer, but given the trend observed, one might expect that the cyclic strain destabilizing the *trans* isomer might result in a longer lived *cis* isomer compared to linear AB. This was shown by Rau and colleagues who synthesized the first cyclo-*bis*-AB (Figure 1.16b), by nucleophilic substitution of 4,4´-*bis*-(bromomethyl)AB with disodium sulfide.[142] The obtained azobenzenophane with thioether linkages was found to isomerize sequentially to the *cis*/*trans* (*c,t*) form, and further to the *cis*/*cis* (*c,c*) form, upon UV irradiation. Furthermore, the authors showed that the (*c,c*) isomer is more stable than the parent *cis*-AB and the (*c,t*) isomer by a factor 1.5 and 1000 respectively at 25 °C. In addition, they found that the activation energy for the thermal (*c,t*) → (*t,t*) isomerization was 3 kcal.mol^{-1} inferior to that of the *cis* → *trans* relaxation of AB, while it was doubled for the (*c,c*) → (*c,t*) relaxation, reflecting a high steric strain in the structure of the (*c,t*) isomer. By replacing one of the sulfur atoms with an sp^3 carbon atom, the rigidity of the bridge was increased, and the stabilization of the (*c,c*) isomer as well.[207] This mixed azobenzenophane showed a thermal stability of the (*c,c*) isomer of more than a year at 25 °C, making it virtually thermally stable, whereas the (*c,t*) isomer had a half life of 14 min. As seen in the case of *ortho* bridged AB such as diazocine, diazonine, and the corresponding sulfur-containing analogues, sulfur atoms provide an important flexibility that can be used to tune the thermal stability of cyclic AB derivatives.[160-163] Finally, the finding that the quantum yields of isomerization were the same upon S_1 or S_2 excitation led Rau to hypothesize that the rotation pathway was blocked by cyclization, however this was contradicted in further studies.[143a,208]

In the same lines, Tamaoki and colleagues prepared *para*-oligoazobenzenophanes with two to four AB units linked in para positions with an ethylene linker (Figure 1.16c).[209] Surprisingly, reducing the length of the bridge did not result into a more stable (*c,c*)-AB dimer (Figure 1.16c, n = 0) compared with Rau´s azobenzenophanes, although the difference in stability between the (*c,c*) and the (*c,t*) isomers was increased. Indeed, the (*c,t*) isomer, with a half-life of 22 s, was 10000 times less stable than the (*c,c*) isomer at 25 °C, and also less stable than azobenzenophanes with C-S-C or C_3 linkers as it would be expected. However the (*c,c*) isomer had a similar stability as the parent *cis*-4,4´-dimethylAB, which is in contradiction with the observed trend that azobenzenophanes of increasing rigidity exhibit higher thermal stability of the all-*cis* isomer, but this compound seems to be an exception. In fact, a xanthene-based cyclo-*bis*-AB was synthesized, and besides producing a hinge with a butterfly motion, this extremely rigid 14-membered ring had a half life of 6.4 years at room temperature.[210a] Furthermore, the authors showed that, due to the million fold difference in thermal relaxation rates between the (*c,c*) and the (*c,t*) isomers, the rate of photoisomerization to the (*c,c*) isomer depends on the intensity of the light source.[209,210b] Another interesting effect of the cyclic strain is the distortion of the planarity of the CNNC dihedral angle (11 ° deviation from planarity), which causes spectral modifications of the AB dimer (Figure 1.16c, n = 0). This results into a significantly increased molar extinction coefficient for the n→π* band, while the one of the π →π* band is reduced. Increasing the number of AB units in the cycle results in a decreased cyclic strain, and the spectral properties of each AB unit become closer to

that of linear AB. In addition, the discrepancies between the thermal sabilities of the mixed isomers compared with the all-*cis* isomer are smaller. For exemple, the AB trimer (Figure 1.16c, n = 1) had thermal isomerization constants of 10.2, 1.2 and 22 μs^{-1} for the (*ZZZ*)→(*EZZ*), the (E*ZZ*)→(*EEZ*) and the (*EEZ*)→(*EEE*) relaxations respectively.[211] As can be seen, the (*EZZ*) is the most stable isomer, and its enrichment (up to 70%) by applying temperature raises the possibility of designing systems with more than two functional states.

Continuing their research on azobenzenophanes, Tamaoki and colleagues reported the crystal structures of all three possible isomers of a methylene-bridged *meta*-cyclo-*bis*-AB[212a,b] (Figure 1.16d, n = 1) and compared its thermal and photochemical isomerization properties with an open-chain dimer.[212c] In general, the quantum yields for the photochemical isomerization, and the activation energies for the thermal isomerization were higher in the cyclized form than in the linear form. They also prepared the first cyclic AB dimer with thermal *trans*→*cis* and photochemical *cis*→*trans* isomerization (Figure 1.16e).[213] This compound, which was most stable in the *c,c* form, could be converted to a long lived *t,t* isomer ($t_{1/2}$ = 20 days), while the (*c,t*) isomer was highly unstable ($t_{1/2}$ = 1 s) at 25 °C. Very interestingly, while *meta*- and *para*-azobenzenophanes have similar thermal relaxation properties, it was shown by Tauer *et al*. that AB dimers linked on their *ortho* positions with ethylene bridges had an opposite stability of the (*c,c*) and the (*c,t*) isomers, with half-lives of 5 days and 6 weeks respectively.[214]

More recently, Wegner *et al.* reported on the synthesis and spectroscopic characterization of a *para*-cyclo-*bis*-AB with methylene linkers (Figure 1.16f).[215] This compound, existing only in the *c,c* form did not produce any detectable accumulation of the (*c,t*) and (*t,t*) isomers upon irradiation. This is due to a very fast relaxation (8 ms) of the (*c,t*) isomer, preventing the formation of the (*t,t*) isomer, even under continuous irradiation. In contrast, the cyclo-*tris*-AB (Figure 1.16g) is completely inert to photo-isomerization, due to an ultrafast and complete dissipation of UV excitation as heat, making this compound a potential UV-absorber for sunscreens for example.[216] Lately, Wegner and colleagues demonstrated selective three state switching in a symmetrical azobenzenophane trimer with >70% relative concentration using irradiation or a combination of irradiation and heating, paving the way for effective multistate switching (Figure 1.17).[217] The authors showed that each state could be reversibly generated, regardless of the starting state, with excellent reversibility and repeatability. However, the synthesis of this azobenzenophane was impaired with a very low cyclization yield (3%).

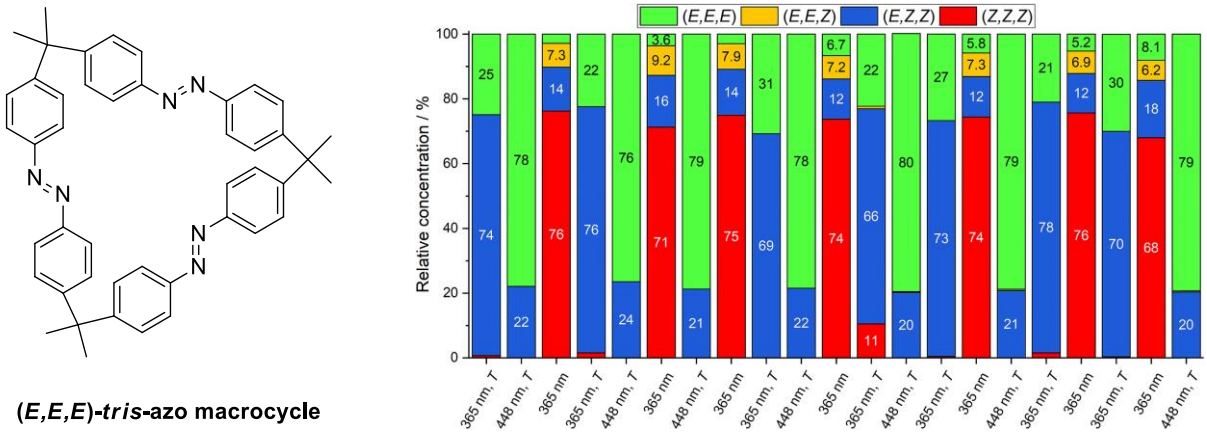

Figure 1.17. Selective three-state switching in a macrocyclic *para*-AB-trimer with dimethylmethane linkers. Reprinted with permission from reference 217.

Finally, an exceptionally stable medium sized azobenzenophane (Figure 1.16h) was reported lately by Staubitz *et al*., which was virtually bistable at 20 °C.[218a] A combination of the right ring size, flexibility and substitution pattern, confer to this macrocycle an excellent thermal stability, with no thermal reversion observed over a period of 120 days at 20 °C. Further substitution of the azobenzene *via*

Suzuki cross-coupling with electron-rich or electron-deficient aryl substituents allowed further tuning of the thermal stability of these derivatives.[218b]

Owing to the large geometrical change of the AB hinge upon isomerization, the shape of a macrocycle can be altered, and eventually its physicochemical properties may be modulated. The host properties of crown ethers could thus be switched on and off by light (Figure 1.18), due to a total lack of affinity of the *trans* isomer for alkali metal cations.[219]

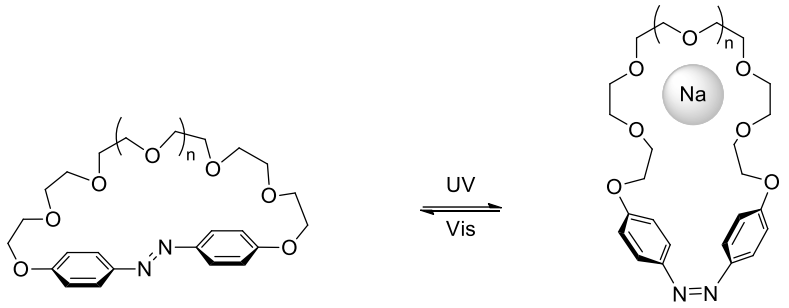

Figure 1.18. Photocontrol of the complexation ability of AB based crown ethers.

In the *trans* state, the ethylene glycol chain was forced in a linear arrangement that does not enable any complexation to occur, in contrast to a non-cyclic podand that still may adopt a circular arrangement due to its flexibility. By irradiation with UV-light (330<λ<380 nm), about 70% of the *cis* isomer was formed, allowing a more favorable arrangement of the polyether chain for complexation. Photoresponsive crown ethers with 7, 8 or 9 oxygen atoms had sodium, potassium or rubidium selectivity respectively, and the complexes had a longer thermal relaxation than the free hosts. Also, the *trans* isomer was quantitatively regenerated in two minutes with visible light (λ>460 nm).

The same authors reported on a water soluble [3,3](4,4´)azobenzenophane (Figure 1.16b, X = Me_2N^+) capable of binding disodium adipate in the (*c,c*) form but not in the (*t,t*) form.[220] It was elegantly synthesized *via* a phase transfer reaction in high dilution conditions, where a 4,4´-*bis*-(*N,N*-dimethyaminomethyl)AB substitutes a *bis*-(chloromethyl)AB in chloroform, furnishing a protonated azobenzene dyad that proceeds to cyclisation in a substrate-free water phase, therefore preventing oligomerization. Although the photoconversion to the metastable isomer was scarce (27%), a reduction of the thermal isomerization rate in the presence of disodium adipate indicated that complexation occurred. Monocationic or neutral guests were not complexed, and surprisingly neither did disodium terephthalate, presumably due to its shorter length compared to the adipate. Later on, the photocontrolled encapsulation of neutral and ionic aromatic guests was achieved with larger arene systems with embedded AB.[221] By using macrocycles with larger cavities, the aromatic guests could insert thermselves between two AB units, and were released upon isomerization. Lately, Huang and colleagues achieved the selective solid-liquid extraction of phenanthrene from a solid mixture containing anthracene, with an aqueous solution of the host.[222] The host was recovered by irradiation followed by centrifugation and relaxation, and after five cycles, the phenanthrene was obtained in an average 91% purity. Since the pioneering work of Shinkai and Manabe, the range of guests for photocontrolled encapsulation has considerably increased, and photoswitchable hosts show promises in various fields such as decontamination or biological target delivery for instance.[223]

Finally, macrocycles with embedded AB may undergo different intrinsic property modifications upon isomerization. For example, the fluorescence of an azobenzene-bridged perylene bisimide cyclophane was modulated with light.[224] In another register, the secondary structure of stapled peptides was altered photochemically, which modified their cell penetration,[225] or photoswitchable streptavidin ligands were discovered that cease binding after irradiation.[226]

AB-containing macrocycles found application in supramolecular chemistry (host-guest chemistry,[219-222] self-assembly,[227] interlocked systems[228]), as chiroptical switches,[229] or for molecular machines construction.[230] Also, the stabilization of the *cis* isomer *via* cyclization may have potential in the fields of solar-thermal energy storage,[231] or optical memory devices.[232] Surprisingly, despite their widespread application, ABs have only been recently and seldomly used in glycosciences, as compared to other domains of chemical sciences. The field of AB-based carbohydrate conjugates has emerged only about two decades ago, and has shown promises in glycomics and supramolecular chemistry.

1.5. From azobenzene glycoconjugates (ABGs) to glycoazobenzene macrocycles

Along with nucleobases,[233] amino acids[234] and lipids,[235] carbohydrates[236] are some of the earliest organic molecules formed on earth, and one class of building blocks essential for all life forms. This links carbohydrates to the very origin of life, as they constitute the backbone of all genetic information. Indeed, nucleic acids (RNA and DNA) have an oligomeric carbohydrate scaffold, where 5-membered cyclic carbohydrate monomers (pentose) are linked to one another *via* phosphate linkage of their 3- and 5- positions. The way these primordial molecules were synthesized is still unclear, although several hypotheses were formulated (RNA first or metabolism first),[237,238] and many lab experiments where the earth´s supposed prebiotic conditions were simulated, produced several of these molecules. If the Miller-Urey experiment[239] is one of the most famous test trying to understand prebiotic chemistry and explain the apparition of amino-acids, Butlerow[240] and Löb[241] sought to explain the formation of carbohydrates from fromaldehyde and CO_2/H_2O respectively (Scheme 1.4a). These two experiments show the importance of an intermediate, the glycolaldehyde, which can produce multiple carbohydrates through an autocatalytic process (Scheme 1.4b), by repetitive aldolizations and retroaldolizations.[242]

Besides their inestimable role in the apparition of life, carbohydrates have, in modern cell biology, several fundamental functions.[243] In addition to be building blocks for the synthesis of macromolecules (nucleic acids, cellulose, chitin…), they serve for energy production (glucose) and storage (glycogen, starch), allowing for the sparing of proteins as an energy source. Furthermore, carbohydrates are essential components of eukaryotic and some prokaryotic cells´ surface, in the form of complex glycoconjugates. Such glycoconjugates or glycans, form a coat on the surface of cells, named "glycocalyx" (Figure 1.19).[244]

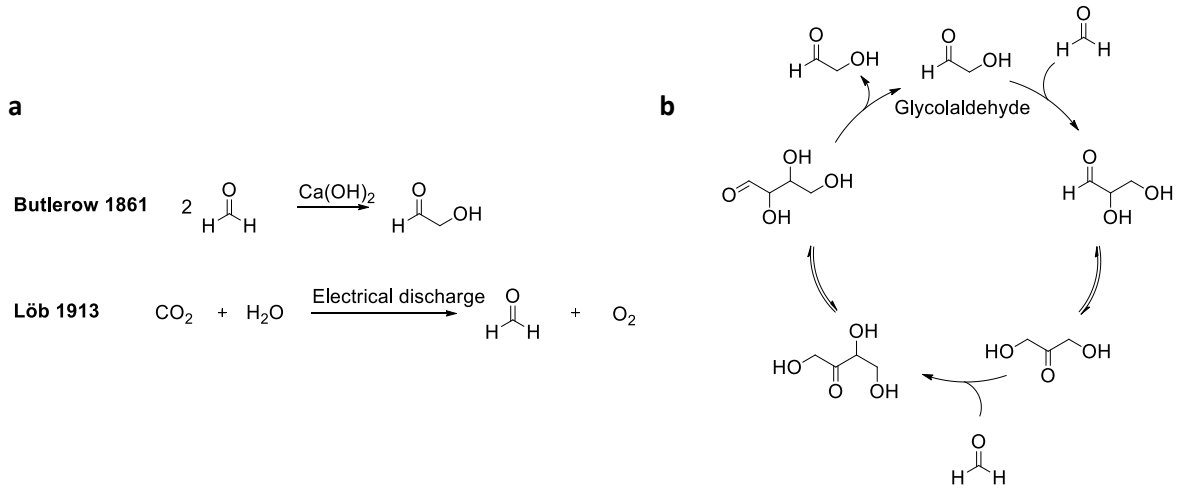

Scheme 1.4.: Potential explanation for the prebiotic synthesis of carbohydrates, *via* the formation of formaldehyde and glycolaldehyde (a), and the formose autocatalytic process (b).

It is mainly constituted of various complex polysaccharides attached to several backbone macromolecules such as proteins or lipids, forming proteoglycans, glycoproteins and glycolipids.[245] The glycocalyx plays a pivotal role in cell-cell communication and recognition,[246] immunity and signaling,[244,247] microbial adhesion[248] and pathophysiology[249] amongst others. The composition of the glycocalyx varies from cell to cell in the same organism, and also from an individual to another within the same species. Similar to the genome, the proteome, and the emerging microbiome, the glycome is the entire content of sugars, whether free or conjugated, of an organism. Otherwise known as the sugar code, the glycome is perhaps the most complex biological alphabet, due to an unsurpassed versatility in terms of possible structures. In fact, several parameters need to be taken into account such as the number of carbon atoms (pentoses, hexoses…), the nature of functional groups (hydroxy, deoxy-amino, acetylation, phosphorylation…), or the regio- and stereochemistry for instance. In order to read this code, Nature has developed tools in the form of lectins, which are proteins that bind carbohydrates in a very selective and affine manner.[250] Such proteins mediate the adhesion of microorganisms to animal cells, as in the case of commensal and symbiotic microbes forming the microbiome,[251] or that of pathogenic bacteria[252] and viruses.[253]

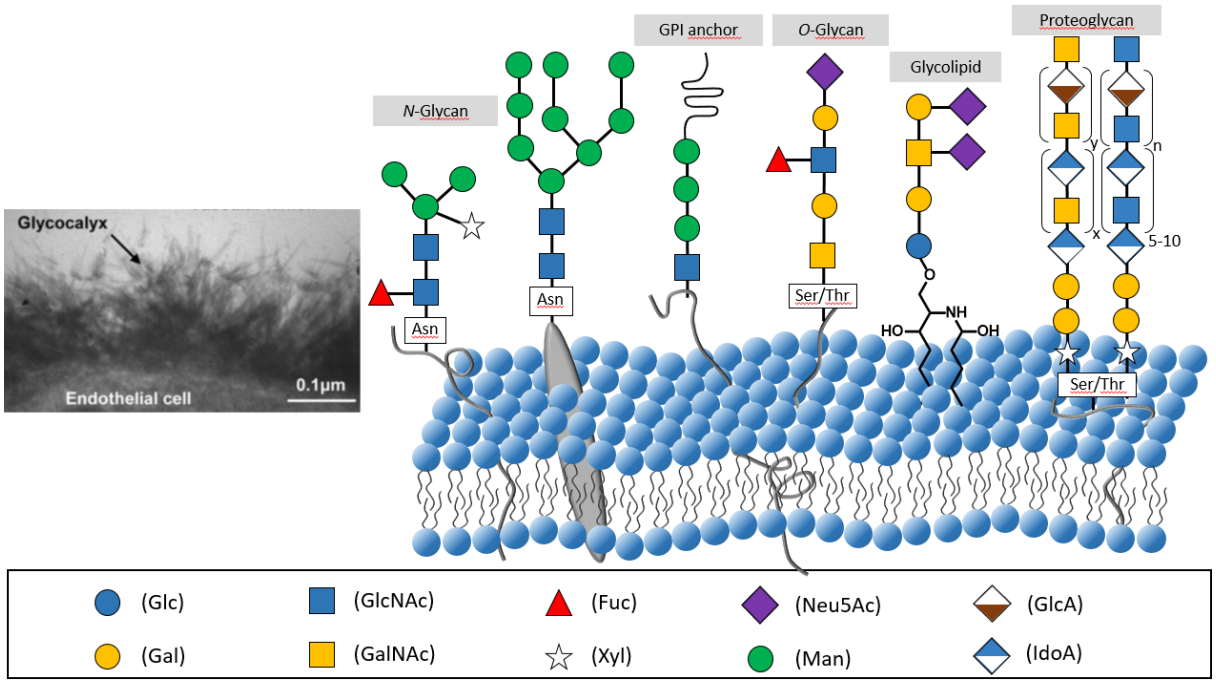

Figure 1.19. Electron micrograph of an endothelial cell (left) showing the glycocalyx.[254] Schematic illustration of a cellular membrane (right) with incorporated glycosylated proteins and lipids. The carbohydrates are represented according to the conventions suggested by the Consortium for Functional Glycomics (CFG)[255a] by using the following abbreviations: Asn (asparagine), Ser (serine), Thr (threonine), Glc (glucose), Gal (galactose), GlcNAc (*N*-acetylglucosamine), GalNAc (*N*-acetylgalactosamine), Fuc (fucose), Xyl (xylose), Neu5Ac (*N*-acetylneuraminic acid), Man (mannose), GlcA (glucuronic acid), IdoA (iduronic acid). Figure adapted with permission from the PhD thesis of Dr. Ole Jaeschke.[255b]

However, owing to a substantial heterogeneity and a large variety in terms of structural and conformational order, a clear picture of carbohydrate recognition is still lacking. Glycobiology has therefore emerged about 30 years ago,[256] in order to gain a better insight into the mechanisms through which cells interact *via* the mediation of carbohydrates. The investigation of interactions between lectins and carbohydrates has highlighted that besides the selective recognition of sugar epitopes, lectins could increase substantially the avidity towards their ligand through multivalency effects.[257] Multivalent glycoconjugates, also referred to as glycoclusters, have been helpful tools in the understanding of multivalency,[258] although it appeared that additional features such as carbohydrate orientation may play an important role in carbohydrate-lectin interactions.[259]

In order to address this issue, the idea to combine carbohydrates with azobenzene to alter the orientation of sugar ligands emerged.[260] Jayaraman and colleagues pioneered in this field and demonstrated in 2002 that the *Z* isomer of a bivalent β-D-lactose-azobenzene conjugate had a higher affinity with the plant lectin peanut agglutinin (PNA) than the *E* isomer.[261] Although both isomers exhibited a biphasic binding profile, suggesting a cooperative binding process, the binding constant for the second binding event was nearly 4-fold greater in the case of the *cis*-rich mixture than for the *trans* isomer. In a subsequent study, di-, tetra- and octavalent photoswitchable glycoclusters were synthesized *via* amidation of amine-tethered mono-and divalent mannoside and lactoside units (Scheme 1.5).[262]

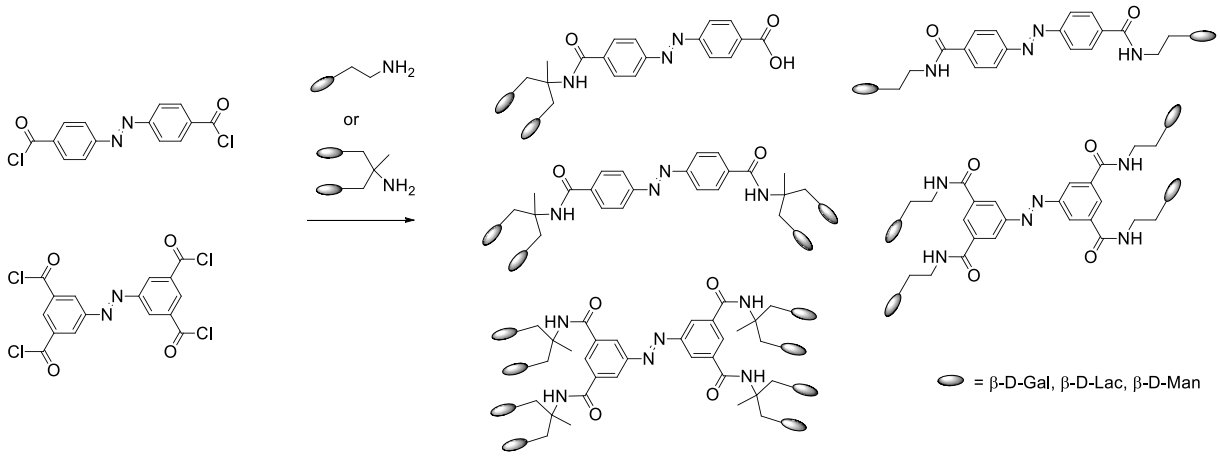

Scheme 1.5. First library of azobenzene glycoclusters synthesized by Jayaraman *et al*. to assess the effect of ligand orientation on the binding avidity of plant lectins PNA and ConA.

The authors showed that the binding thermodynamics of the dissymmetrical carboxylic acid derivatives were not altered by the isomeric state of the photoswitch, while their symmetrical bivalent counterpart exhibited enhanced affinity in the *cis* state. Furthermore, the tetravalent *p*-azobenzene-lactoside conjugate bind to PNA with a biphasic binding profile in the *cis* state only. The same effect was observed with tetravalent *p*-azobenzene-mannoside conjugate and Concavalin A (ConA). Therefore, the authors ascertained that in addition to the valency, the relative orientation and spatial distribution of clustered glycoligands have a marked influence on the supramolecular features of carbohydrate-lectin interactions.

Before 2010, the only reported AB glycoconjugates included amphiphilic AB glycosides investigated for their liquid crystaline properties,[263] and several cyclodextrin derivatives functionalized with an AB unit.[264] Two main synthetic strategies are commonly employed to attach AB to carbohydrates (Scheme 1.6). A direct approach like the one used by Jayaraman, where a fully formed AB derivative with suitable functional groups is reacted with a complementary motif. For example, AB dicarbonyl chloride reacts efficiently with amines, whereas a propargyl substituted AB may be engaged in a Huisgen 1,3-dipolar cycloaddition[265] with an azido functionalized carbohydrate.[266] When a more direct connection between the photoswitch and the glycoside is desired (i.e. without tether or linker), Williamson etherification,[267] glycosylation,[268] or the Mitsunobu reaction may be used.[269] Alternatively, in the indirect approach, a carbohydrate is first substituted with an aromatic aglycone suitably substituted to react with another aromatic partner to form the azo-bond. This approach involves reactions such as azo-coupling,[263a,270] Mills reaction,[268b] or reductive dimerization of aromatic nitro compounds.[268d] If the direct strategy is generally more straightforward, the indirect approach allows a more efficient preparation of unsymmetrical compounds, or synthetically challenging targets such as 1,2-*cis*-glycosides.

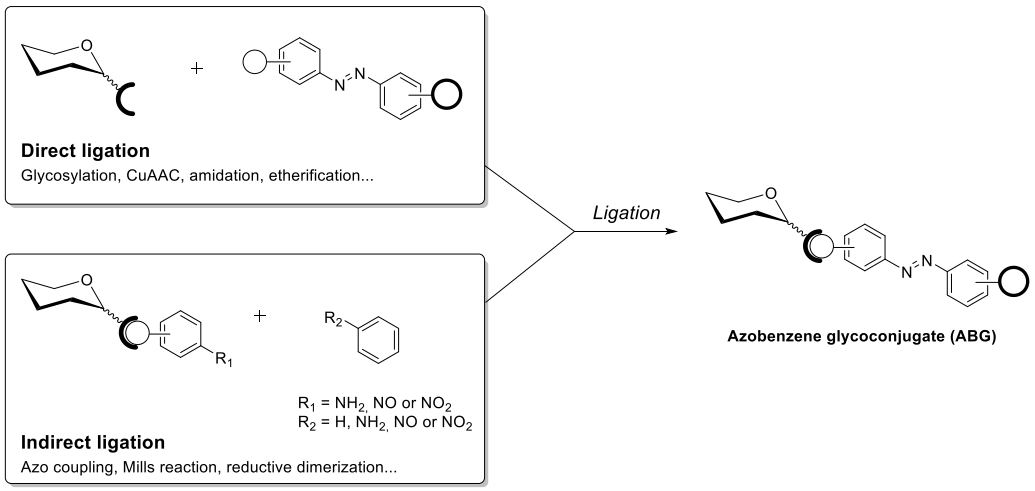

Scheme 1.6. Different synthetic approaches for the preparation of ABGs.

In 2012, the group of Pr. Lindhorst initiated a project aiming at synthesizing and characterizing different azobenzene glycoconjugates and to utilize them in different biochemical applications.[260] In an initial study, some mono-, di- and trivalent ABGs were synthesized by click chemistry[265b,266] and their photochromic behavior was investigated. It was shown that azobenzene bearing ether groups in both *para* positions have nearly quantitative $E \rightarrow Z$ photoconversion and good thermal stability (15-20 h), allowing independent evaluation of both isomers in biological assays. Furthermore, di- and trivalent glycoclusters bearing an AB glycoside on each branch produced mixtures of isomers upon irradiation, with a valency dependent decrease in photoconversion to the all-*cis* form. This is due to intramolecular quenching processes and stacking, showing that clustering ABs in a limited space may be detrimental to the photoswitching efficiency. Shortly thereafter, a systematic study of the photochromic properties of various AB glycosides was undertaken.[268b] The stereochemistry of the anomeric center (α or β), the nature of the attached hexoses (glucose or mannose), and the effect of an additional ester or carboxylic acid group on the AB core were investigated. It was shown that the anomeric configuration in monosubstituted ABGs has a substantial impact on the position of the $\pi \rightarrow \pi^*$ band and the thermal relaxation rate, and that the addition of a carboxyl- or methoxycarbonyl group significantly shortens the half-life (89 vs 2 and 5 h in the mannoside series). Furthermore, aggregation of carboxy-substituted derivatives was observed, which reduced the photoconversion yields (from >95% to 50-90%) and seemed to be dependent on both the C-1 and the C-2 configurations.

Given these favorable photochromic properties, in order to assess the bacterial adhesion of type 1 fimbriae of *Escherichia coli* bacteria, an AB-mannobioside was synthesized as a ligand for the bacterial lectin FimH.[268a] Interestingly, the photochromic mannobioside had blue shifted transitions, a similar $E \rightarrow Z$ photoconversion yield, and a doubled half-life, as compared with the parent AB-mannoside. Both isomeric states had similar inhibitory potency, although they were about 10 and 100 times higher than that of common inhibitors such as of *p*-nitrophenylmannoside and methylmannoside respectively. Thus, AB glycoconjugates obtained by direct glycosylation of a photochromic aglycone on a carbohydrate scaffold showed promises towards the investigation of specific lectin-carbohydrate interactions. Consequently, AB-mannosides were immobilized on gold surfaces in the form of self-assembled monolayers (SAMs),[268c,f] and the adhesion of type 1 fimbriated *E. coli* bacteria was measured before and after irradiation, showing a drop in bacterial adhesion by a factor of 5 upon reorientation of the ligands on the surface.[271] Following the same idea, bacterial adhesion could also be photocontrolled in the more complex environment of human cells.[270] This was achieved by metabolic oligosaccharide engineering of human microvascular endothelial cells variant 1 (HMEC-1), resulting in the incorporation of bioorthogonal azide functions on the surface glycans. Subsequent cycloaddition with a propargylated α-D-mannosyl-AB derivative completed the labelling of the cells. As

a consequence, the adhesivity of the cells was reversibly altered by irradiation with UV (365 nm) and green (488 nm) light (Figure 1.20). Interestingly, the effect was only observed when the outer regions of the cell surface were labelled. When inner regions were labelled with the photochromic mannoside ligand, no significant changes in bacterial adhesion were reported. Along the same lines, a photoswitchable trivalent mannoside cluster was recently bioorthogonally conjugated to the surface of HMEC-1 cells, and showed that bacterial adhesion was 50% higher in the *trans* state than in the *cis* state.[272] Whether a monovalent or a trivalent mannoside epitope is presented, and despite a greater flexibility of the ligands in the cluster, comparable reduction of adhesivity was observed upon $E \rightarrow Z$ isomerization, underlining again the importance of carbohydrate ligand orientation in the context of specific lectin-carbohydrate recognition.

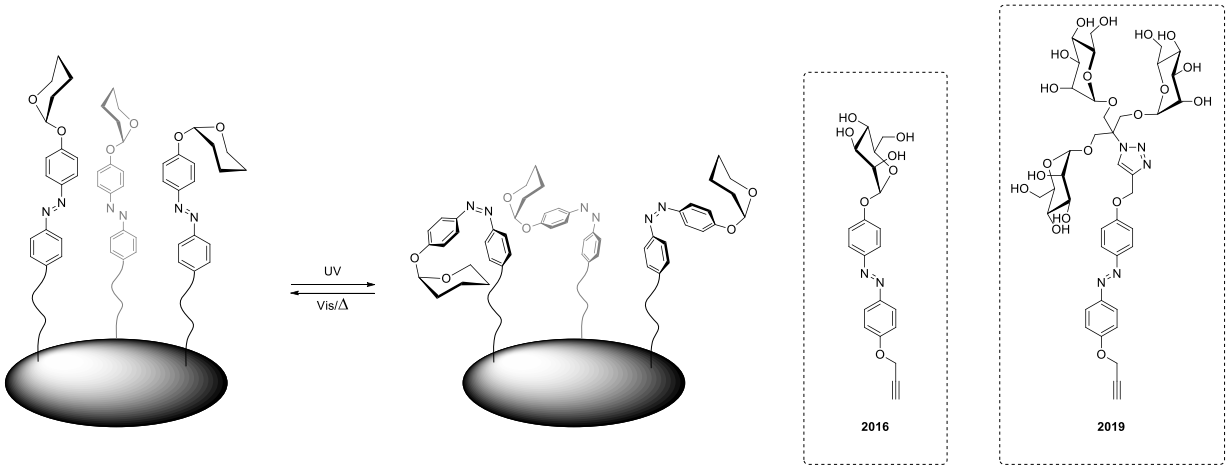

Figure 1.20. Schematic representation of the reversible photomodulation of carbohydrate orientation on a surface, and examples of bioorthogonal photochromic FimH ligands used for photoswitching the adhesivity of human cells.[239,241]

In another register, Lindhorst and colleagues synthesized ABGs as photosensitive cross-linkers for the modulation of the secondary structure and function of peptides. Based on the work of Woolley,[273] cysteine side chains are commonly used for linking photoswitching units to proteins by nucleophilic substitution of a typically chloro- or iodoacetylated linker. Such cross linking allowed the reversible photocontrol of the secondary structure of peptides (i.e. helical folding/unfolding), and therefore the modulation of their activity. Indeed, there must be a complementarity between the spacing of the cysteine residues and the size of the linker. For a *p,p´-bis*-(2-chloroacetamidoyl)-AB derivative for example, it was shown that the *trans* state stabilized α-helix conformation for a spacing of i,i+11, while switching to the *cis* state prevents formation of the secondary structure. In contrast, the α-helical fold is stabilized by the *cis* isomer when the linker is connected to residues i,i+4 or i,i+7. Hence, Lindhorst reported the synthesis of ABGs functionalized with chloroacetamide or allyl ether groups,[268d] for cross linking *via* nucleophilic substitution or thiol-ene click chemistry[274] respectively. These cross-linkers showed favorable photochromic properties and were successfully conjugated to protected cysteine, glutathione and a synthetic nonadecapeptide. Subsequently, heterobivalent ABG cross linkers with different biorthogonal functional groups were reported.[275]

Lately, Dr. Despras started, within the Lindhorst group, an independent research project and reported on novel glycoazobenzene macrocycles.[268e,269b] The use of carbohydrates in such molecular architectures is advantageous. Indeed, carbohydrates are biocompatible, have generally a good water solubility, and are decorated with multiple functional groups (alcohol, amino, carboxy groups) allowing for further modification of the corresponding macrocycle. In addition, the use of cyclic carbohydrates (furanose or pyranose) reduces the conformational flexibility of the molecule, resulting in macrocycles with a well-defined and stable shape. Furthermore, the inherent chirality of sugars may be transferred

to the AB, resulting in an induced helicity. Point chirality[276] as well as axial[229a,c,e-f] and planar chirality[277] have all been shown to induce helicity in AB-containing molecules, by favoring one stereoisomer over the other one.

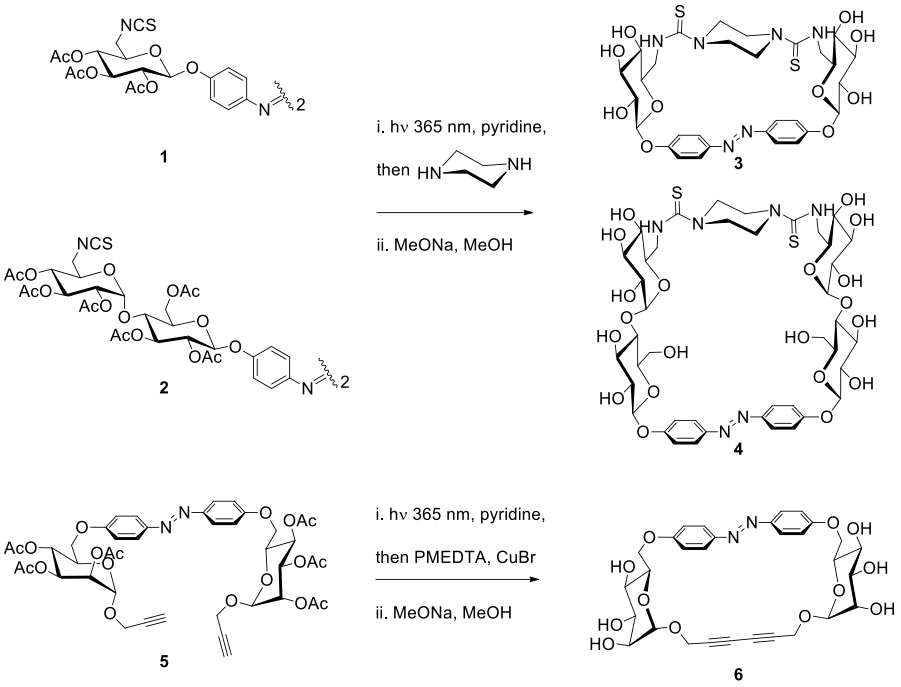

Scheme 1.7. Final steps of the synthesis of glycoazobenzene macrocycles according to Despras and coworkers.

Interestingly, despite a widespread use of AB and carbohydrates respectively in macrocyclic chemistry,[205,278] Despras´ macrocycles were the first examples of photoresponsive carbohydrate based macrocycles with an embedded AB. Macrocycles **3** and **4** were synthesized *via* glycosylation of azido functionalized D-glucosyl and D-maltosyl acetimidates with 4,4´-dihydroxyazobenzene (DHAB), yielding AB-*bis*-glycosides **1** and **2**. Azide reduction and isothiocyanate formation, followed by cyclisation with piperazine and subsequent deprotection afforded the desired compounds.[268e] Macrocycle **6** on the other hand, was synthesized by Mitsunobu reaction of propargyl-α-D-manoside with 4,4´-DHAB followed by acetylation, then Glaser-Hay coupling and Zemplen deacetylation (Scheme 1.7).[269b] Strikingly, for the cyclisation to occur, the open-chain substrates had to be pre-organized by isomerization to the *cis* state in order to bring the reactive ends closer to one another.

Macrocycles **3**, **4** and **6** exhibit comparable photochromic properties. All produced high contents of *cis* (>95%) when irradiated with UV-light (365 nm), and were thermally stable with half-lives of 6 h, 17 h and 114 h at 27 °C respectively. As could be expected, the thermal stability seems to be dependent on the cyclic strain, similarly to the *cis* to *trans* photoconversion yield. In fact, molecular modelling studies highlighted that the AB unit in **3** and **4** is no longer planar in the *trans* state, which results in increasing the intensity of its $n\rightarrow\pi^*$ band and reducing the photoconversion yields with blue-light to 53% and 63% respectively. In **6** however, the hyperchromic effect on the $n\rightarrow\pi^*$ band of the *E* isomer is less pronounced, which affords 88% of the *trans* isomer after green-light irradiation. A large amplitude shape modification upon switching was evidenced by significant shifts of some characteristic NMR signals, and modifications in the NOESY spectra. In addition, circular dichroism (CD) spectroscopy analysis showed that macrocycles **3**, **4**, and **6** all exhibit strong dichroic signals both in the *trans* and *cis* state. In the case of macrocycle **4**, the CD spectra of each isomer show a sign inversion upon switching, as confirmed by the measurement of specific optical rotatory power (*E*: $[\alpha]^{20}_D$ = +461; *Z*: $[\alpha]^{20}_D$ = -623; *c* = 0.054 in water). For macrocycles **3**, and **6**, significant changes in the CD spectra indicated a major change in chirality upon irradiation. The intensity of the dichroic signals suggests that a single helix (*P*

or *M*) is largely predominant in each isomeric form, hinting for a unidirectional switching process. In addition, the water solubility of macrocycle **6** was greatly altered upon isomerization, in such a way that a suspension of *trans*-**6** in water could be turned into a clear solution after irradiation and *vice versa*.

Along the same lines, the group of Xie reported on an AB-embedded macrolactone with a monosaccharide backbone.[279] A protected thio-α-D-mannopyranoside equipped with two adjacent bromoacetyl groups was cyclized under basic conditions with 2,2´-DHAB in moderate yields, affording an AB containing glycomacrolactone. The resulting macrocycle showed excellent $E \rightarrow Z$ and moderate $Z \rightarrow E$ photoconversion, strong dichroic signals, and a multistimuli-responsive gelation ability in cyclohexane. In a later report, Xie and colleagues described the synthesis and photochromism of three new AB-glycomacrolactones with the photoswitch linked to 2,3 or 4,6 positions of *gluco* and *manno* derivatives.[280] Remarkably, these compounds display a better thermal stability (37-72 d) than macrocycles **3**, **4** and **6**, presumably owing to the ring size and the difference between the *para* and *ortho* substitution. Lately, the same group used photochromic templates to stereoselectively synthesize larger AB-glycomacrolactones through intramolecular glycosylation.[281] Challenging 1,2-*cis* glycosylation was achieved with excellent stereoselectivity, regardless of the configuration of the switch, although the yields were lower in the *cis* state. Recently, Xie´s macrocycles were applied as dopants for photoresponsive cholesteric liquid crystals.[282]

The only other example of photoresponsive glycoazobenzene macrocycle was described by Jarosz and coworkers.[283] It consists in a sucrose-containing crown ether with an embedded azobenzene, showing cation complexation ability. This macrocycle formed stable complexes with alkali metals, with a higher affinity in the *cis* state, and a potassium selectivity. It displays equivalent photochromic properties as Xie´s macrolactones, that is, efficient photoisomerization and slow thermal relaxation (25 d). Notably the macrocyclisation step was high yielding due to templating effect with cesium ions. Glycoazobenzene macrocycles are an emerging class of photoswitchable chiral macrocyclic compounds, holding a lot of potential for various applications, and their investigation promises thrilling discoveries.

1.6. Motivations

The synthesis of glycoazobenzenophanes as described by Despras *et al.* lies on two critical steps: the glycoconjugation and the macrocyclization. Therefore, the first objective of this thesis was the optimization of the glycoconjugation. In order to have an efficient chirality transfer from the sugar to the azobenzene, they need to be ligated in the most direct way, precluding the use of ligation methods such as azide-alkyne cycloaddition, amide/ester or thiourea linkage. Therefore, a first thorough investigation on the glycosylation of 4,4´-dihydroxyazobenzene (DHAB) was undertaken, in order to assess the substrate scope of this reaction and find high yielding conditions. The results of this study constitute the chapter 2.

Then, an alternative glycoconjugation method was sought after, in order to develop a new approach for the functionalization of AB derivatives with carbohydrates, while conserving the shortest tether between both moieties. Therefore, a palladium-catalyzed *S*-arylation of glycosyl thiols with halogenated AB derivatives was investigated. With this method, the oxygen atoms bridging the sugar to the photoswitch would be replaced by sulfur. As an isostere of oxygen, sulfur was expected to have similar effects on the photochromic properties of the resulting molecules. Moreover, sulfur offers the possibility of oxidation to sulfoxide or sulfone, which would allow the modulation of the AB photochromism. The chapter 3 is hence dedicated to study of the Buchwald-Hartwig-Migita cross

coupling, the oxidation of the obtained glycoazobenzene sulfides, and the investigation of the sulfur oxidation state on the photochromic properties of the switch.

Then, with the open-chain precursors obtained after the glycosylation study, several macrocyclizations *via* intermolecular thiourea bridging were achieved with different diamines, providing access to four novel AB-glycophanes. The cyclization protocol was optimized and systematized, giving the desired macrocycles in very good yields.

On another hand, cyclization *via* Buchwald-Hartwig-Migita coupling was also investigated, and the construction of macrocycles with two different AB switches was achieved. In this approach, different AB chromophores were associated by pairs in a macrocyclic structure, in order to exploit their photochromic differences towards multistate photoswitchable macrocycles. By using carbohydrates as tethers between each AB unit, the possibility for chiroptical multistate switching was envisaged. In addition, carbohydrates are multifunctional scaffolds allowing further derivatization, or the facile incorporation of the synthesized macrocycle in larger molecular architectures. The 4th chapter therefore details the synthesis of four AB glycomacrocycles and three glycoazobenzene dyads.

Finally, the photochromic properties of the synthesized macrocycles were investigated and are detailed in chapter 5. First, the photochromic properties of the thiourea bridged macrocycles were assessed and compared with the previously reported macrocycles by Despras *et al.*, and their thermal isomerization was closely monitored. Secondly, the glycoazobenzene dyads were investigated, and their multistate switching as well as their thermal relaxation were analyzed.

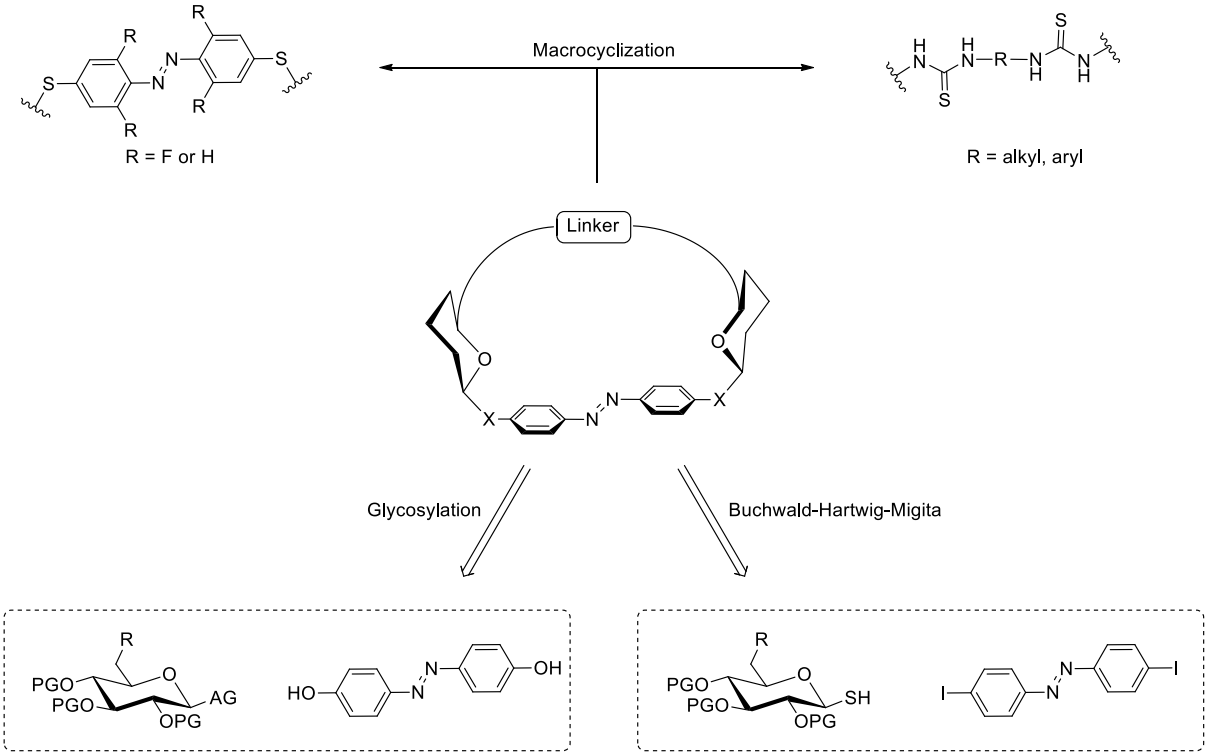

Scheme 1.8. General overview of the different synthetic strategies employed in this thesis for the construction of glycoazobenzene macrocycles. PG: protecting group; AG: activable group

2. Glycosylation of 4,4´-dihydroxyazobenzene (DHAB)

The glycosylation reaction, also known as glycosidation, is a complex and essential reaction in carbohydrate chemistry. It consists in the condensation of a nucleophile on the anomeric position of a reducing sugar, resulting in a glycoside. A glycoside is composed of a glycone moiety (the sugar), and an aglycone moiety (the nucleophile), linked together *via* a glycosidic bond. The aglycone may either be a non-carbohydrate moiety yielding glycoconjugates, or another mono- or oligosaccharide unit, providing di- or oligosaccharides respectively. The generic term "*glycoside*" usually refers to *O*-glycosides resulting from the condensation of an alcohol on a carbohydrate. Nonetheless, *N*-, *S*- and *C*-glycosides are also found in nature, and many other anomeric functionalities can be introduced chemically.[236a,284]

The Fischer glycosidation, by which an unprotected aldose hemiacetal may be transformed into a cyclic acetal by condensation of an alcoholic nucleophile, requires a large excess of the alcohol, and is only suitable for the synthesis of simple glycosides. When more complex aglycones are to be glycosylated, a different approach has to be taken. On the one hand, the anomeric position has to be activated by the introduction of a leaving group, which departure may be facilitated by the action of a suitable catalyst or promoter reagent. On the other hand, in order to avoid self-condensation of the donor, the other hydroxyl groups need to be protected. Therefore, a glycosylation proceeds as follows (Scheme 2.1): a suitably functionalized glycosyl donor is activated with a promoter (at best catalytically), providing a highly reactive electrophile, which can then be substituted by a partially protected acceptor nucleophile, following either a S_N1-like or a S_N2-like mechanism (*vide infra*).

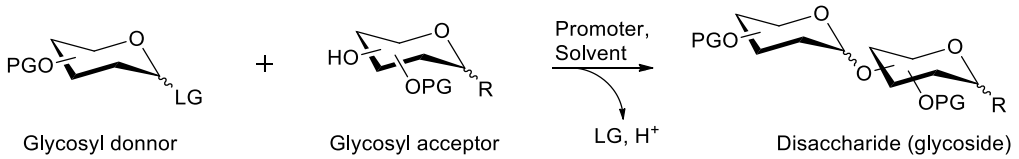

Scheme 2.1. General depiction of a glycosylation reaction between two monosaccharide units. LG: leaving group, PG: protecting group.

The mechanism of the glycosylation is best described as a continuum of mechanisms spanning from pure S_N1 with an intermediate oxocarbenium ion, to pure S_N2 with Walden inversion (Scheme 2.2).[285] The S_N1 or S_N2 character of the reaction depends on many factors such as: the nature of the leaving group and the promoter, the kind of ions generated by the activation, the anomeric stereochemistry of the donor, the nature of the solvent, the reactivity of the acceptor, the temperature, the conformation of the sugar, the type of substituents, *etc.* In general, in order to achieve high stereoselectivity, it is necessary to find conditions that favor an S_N2-like pathway. Pure S_N2 glycosylations may occur by reaction between strong nuceophiles (thiolates, azides, thiourea…) and electrophilic glycosyl halides without the need for a promoter, providing glycosides in a stereospecific fashion. For hydroxylated acceptors however, activation of the anomeric leaving group is generally required, and thus, the chances for a dissociative mechanism are higher. In apolar solvents, a tight ion pair may be formed, with the counterion shielding the face from which it just departed, resulting in an S_N2-like substitution. However, in polar solvents, or when the counterion is highly solvatable, the oxocarbenium ion is more naked, resulting in an S_N1-like pathway and a decreased stereoselectivity. It has been shown experimentally that both pathways are possible, through the generation and characterization of oxocarbenium ions as well as covalently bound intermediates such as α-triflates or α-nitrilium ions for example.[285b] In addition, it was shown that the nature and the orientation of substituents around the ring, as well as the conformation, have a strong influence on the stability of an intracyclic positive charge, and thus on the reactivity of glycosides.[286]

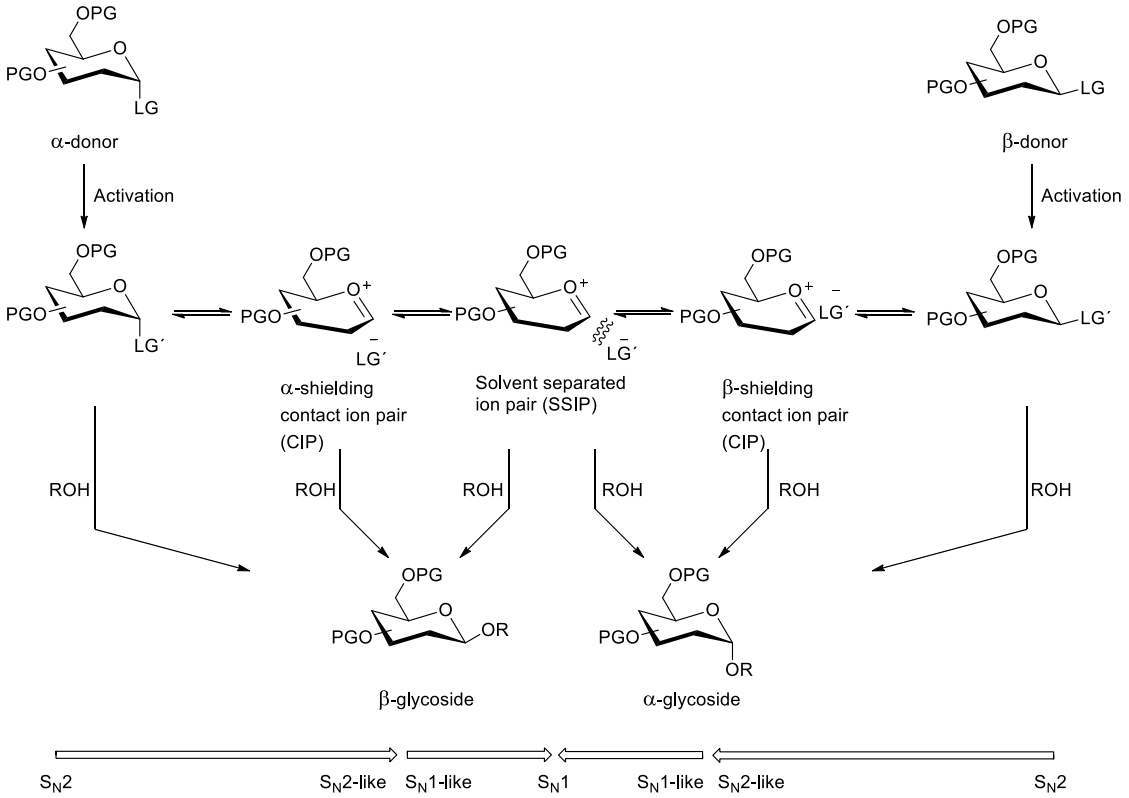

Scheme 2.2. General glycosylation mechanism.

The glycosylation reaction is stereoselective, and may be in some cases, regioselective and stereospecific. Indeed, a stereo-electronic effect called the anomeric effect, and consisting in a stabilization by negative hyperconjugation, favors the formation of glycosides with an axial aglycone, accounting for the stereoselectivity. The glycosylation of a polyhydroxylated acceptor may occur on different positions, depending on the relative reactivity of each group.[287] This parameter is usually controlled by suitable protection of the acceptor, leaving only the one functional group to be substituted free. In addition, the reaction is stereospecific when the mechanism involves a pure S_N2 pathway, or when participating protecting groups are present on the substituents of the donor. Participation of protecting groups may arise from the substituent neighboring the anomeric center (vicinal anchimeric assistance), as in the case of 1,2-trans glycosylation (Scheme 2.3a,b),[288] or from remote substituents (Scheme 2.3c,d).[289] These parameters determine the configuration of the anomeric center following the glycosylation, yielding α- or β-glycosides. In addition, the nature of the solvent, of the leaving group and the promoter, may also influence the stereochemical outcome of the reaction. Due to the large variety of effects that govern a glycosylation reaction, there can be no universal procedure to glycosylate every carbohydrate, a situation that was nicely summed up by Hans Paulsen:[290] "*Each oligosaccharide synthesis remains an independent problem which resolution requires considerable systematic research and a good deal of know-how.*" Therefore, it is hard to predict which glycosylation method is best suited to synthesize a specific glycoside, and the development of new methods for the stereoselective synthesis of oligosaccharides is a very active field in glycochemistry.[291]

The first example of glycosylation of *p*-hydroxyazobenzene dates back to 1947 when Hurd and Zellinski prepared acetylated phenylazophenyl glycosides.[292] The authors showed that Koenigs-Knorr glycosylation[293] employing acetylated glycosyl halides and silver oxide as promoter could afford AB glycosides in yields comprised between 20 and 40% with complete stereocontrol. In addition, the authors performed direct substitution of peracetylated glycosides in the presence of *p*-toluenesulfonic acid or zinc chloride at high temperature *via* a fusion method. This method gave similar yields as the Koenigs-Knorr method, though with lesser reproducibility and harsher conditions.

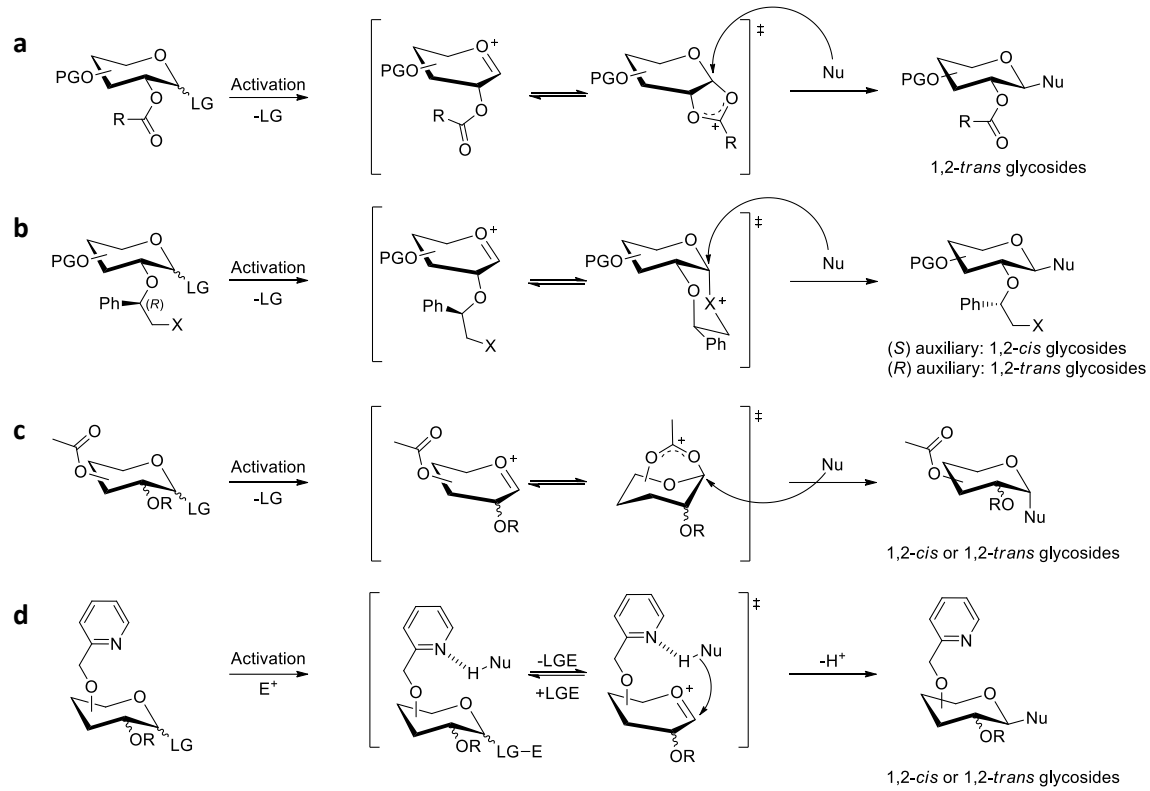

Scheme 2.3. Examples of neighboring and remote group participation in glycosylation reactions through vicinal anchimeric assistance by a 2-*O*-acyl group (a), vicinal assistance of a chiral nucleophilic auxiliary at O2 (b), remote acyl group participation (c) or by hydrogen bond mediated aglycon delivery (HAD) with remote participation of the picolinyl group (d).

Later, in the early 2010´s, Lindhorst employed the acetimidate method[294] to prepare AB glycosides. The glycosylation of 4–hydroxyazobenzene[268a,b] or *mono*-protected 4,4´-dihydroxyazobenzene[266b,268d,f] (DHAB) with glycosyl trichloroacetimidate gave the corresponding AB *mono*-glycosides in very good yields (70-90%). The reaction of glycosyl acetimidates with unprotected DHAB proved however more difficult, as it produced azobenzene *mono*- or *bis*-glycosides in 30-50% yield.[268b-e] This is likely due to a tautomerism between DHAB and a hydrazoquinone form, promoted by intermolecular hydrogen bonding, which contributes to increase the sp^2 character of the C-O bonds, and resulting in a decreased nucleophilicity of the hydroxyl groups in *para* positions (Figure 2.1).[295] In *ortho*-hydroxy-substituted compounds, the hydrogen bonding may occur intramolecularly, such as in the case of phenylazo-2-naphtols, which were found to exist mostly in the hydrazo form.[296] Consequently, *para* and *ortho* hydroxylated *cis*-ABs have very short half-lives[147] and are weak nucleophiles.

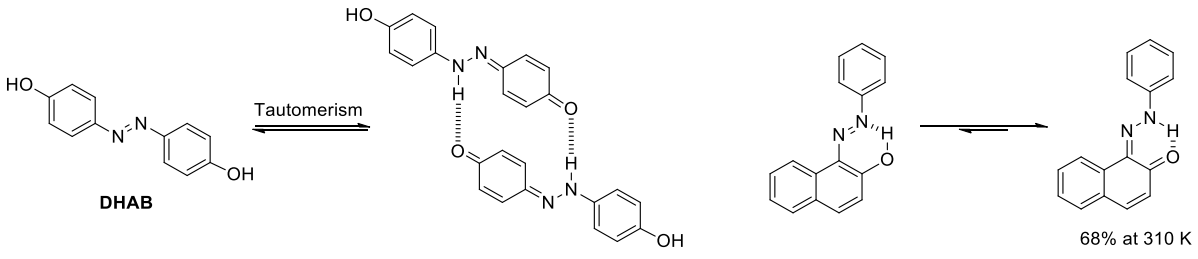

Figure 2.1. Tautomeric equilibrium between DHAB (left) or phenylazo-2-naphtol (right), and their hydrazoquinone tautomer, and involvement of intermolecular and intramolecular H-bonding respectively.

As the *bis*-glycosylation of DHAB is a crucial step in the preparation of photoresponsive glycomacrocycles,[268e] a part of this thesis was dedicated to finding efficient reaction conditions to improve the yield of the reaction and broaden the scope of AB *bis*-glycosides. The results, which were published,[297] are presented herein.

To do so, four common types of glucosyl donors (Figure 2.2) were investigated, namely glucosyl bromide, sulfoxide and acetimidate, as well as thioglucosides. In most cases, ester protecting groups were installed to ensure the stereoselective formation of 1,2-*trans* glycosides, however two donors were silylated to achieve so-called super-armed donors.[286e] Based on Fraser-Reid´s armed/disarmed concept,[298] super-armed donors are exceptionally reactive due to a conformational change imposed by the silyl groups. Indeed, owing to a vicinal clash overruling the 1,3-diaxial interactions, bulky silyl groups tend to drive the conformational equilibrium towards an axial rich conformation, which increases the electron density in the pyranose ring,[286a-d] and thus the reactivity of silylated donors. In addition, silyl ethers are less electron withdrawing than ester groups, which contributes to the overall reactivity enhancement. Particular focus was put on improving the yields of DHAB *bis*-glycosylation with 6-azido-6-deoxy functionalized donors, as they enable the incorporation of the glycoazobenzene motif into larger molecular architectures by simple ligation methods.

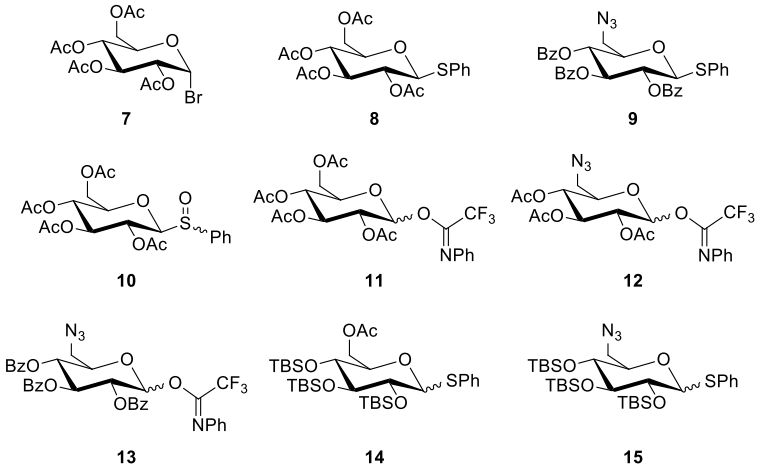

Figure 2.2. Structures of the glucosyl donors used in this study.

Donors **7**,[299a] **8**,[299b] **10**,[299c] **11**[299d] and **12,**[275,299d] were prepared starting from D-glucose according to known procedures. Donors **9** and **13** were prepared starting from levogulcosan **16** (Scheme 2.4). First, perbenzoylation with benzoyl chloride in pyridine afforded **17** in 92% yield. Then, a ring opening reaction of the protected 1,6-anhydroglucose **17** with (phenylthio)trimethylsilane (TMSSPh), in the presence of zinc iodide at 120 °C under microwave heating, provided thioglucoside **18** in 98% yield in a β-selective manner. Subsequently, Bose-Mitsunobu[300] mediated azidation of the free 6-hydroxyl in **18** afforded 6-azido-6-deoxy-thioglucoside **9** in 71% yield. Finally, hydrolysis of **9** promoted by trichlorocyanuric acid (TCCA) in wet acetone yielded the hemiacetal, which was then reacted with (*N*-phenyl)trifluoroacetimidoyl chloride under basic conditions to afford the glucosyl donor **13** in 76% yield over two steps.

For the preparation of silylated donors **14** and **15**, the persilylation of levoglucosan required an optimization (Table 2.1). The first attempt (Table 2.1, entry 1), performed by addition of TBSCl to a suspension of levoglucosan and imidazole in THF, afforded the desired persilylated product **19a** in a mediocre yield of 15%. The same reaction, catalyzed by DMAP in a CH_2Cl_2/pyridine mixture (8:1), gave only the 2,4-disilylated compound **19b** in 50% yield (Table 2.1, entry 2). This result is interesting as it allows the selective formation of **19b**, on which the 3-position may be differentiated, adding interesting functionalization possibilities. Then, the reaction was performed in pyridine in the presence of imidazole (Table 2.1, entry 3) to give **19a** in 38% yield. The best result (Table 2.1, entry 4) was achieved by addition of iodine to a mixture of TBSCl, levoglucosan and *N*-methyl-imidazole in pyridine, affording **19a** in 80% yield. In fact, Stawinski *et al.* showed that iodine could efficiently promote silylation reactions, by complexing the chloride counter ion of the activated silyl intermediate formed

by substitution of the chlorine of Me_2t-BuSiCl by the catalyst, making the imidazolium intermediate more naked and thus more reactive.[301]

Table 2.1. Optimisation of the persilylation conditions.

Entry	Me_2t-BuSiCl (eq.)	Cat. (eq.)	Additive (eq.)	Solvent	Temp.	Time	Yield (%) **19a** : **19b**
1	5	Imidazole (7)	–	THF	0 °C to rt	20 h	15 : ND
2	6	DMAP (1.6)	–	Pyr/DCM	0 °C to rt	72 h	– : 50
3	6	Imidazole (7)	–	Pyr	0 °C to rt	48 h	38 : ND
4	6	NMI (7)	I_2 (2.5)	Pyr	rt	20 h	80 : ND

In agreement with the higher reactivity of silylated glycosides compared with the acylated derivative **17**, the ring opening of **19a** proceeded smoothly at RT, yielding 96% of an anomeric mixture of **20** (α : β = 1 : 4). The primary alcohol function in **20** was then acetylated to afford the glucosyl donor **14** in 95% yield, and the targeted 6-azido-6-deoxy glucosyl donor **15** was obtained in 85% under Bose-Mitsunobu conditions.

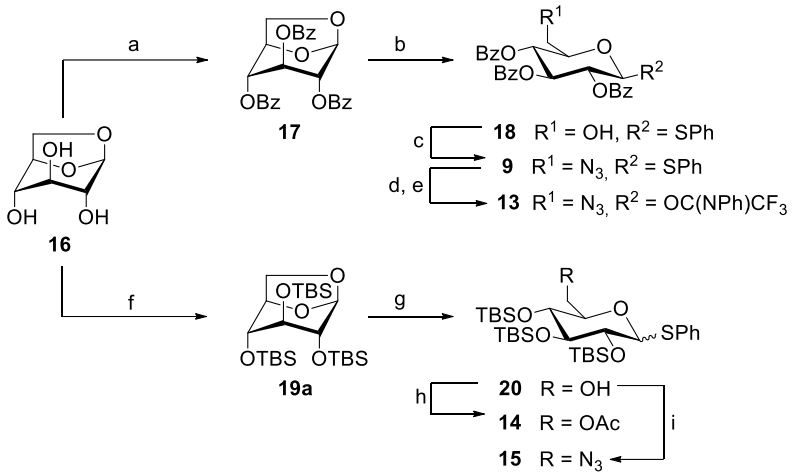

Scheme 2.4. Preparation of glucosyl donors **9** and **13–15**. Reagents and conditions: (a) BzCl (6 eq.), pyridine, rt, 92%; (b) ZnI_2 (4 eq.), TMSSPh (2.5 eq.), CH_2Cl_2, μW (150 W), 120 °C, 25 min, 98%; (c) PPh_3 (1.5 eq.), DIAD (2.5 eq.), DPPA (1.5 eq.), THF, −15 °C to rt, 71%; (d) TCCA (1 eq.), acetone/H_2O (9 : 1), rt; (e) $ClC(NPh)CF_3$ (1.5 eq.), Cs_2CO_3 (1.5 eq.), CH_2Cl_2, rt, 76% over 2 steps; (f) TBSCl (6 eq.), NMI (7 eq.), I_2 (2.5 eq.), pyridine, rt, 80%; (g) ZnI_2 (4 eq.), TMSSPh (2.5 eq.), CH_2Cl_2, rt, 96%; (h) Ac_2O (1.5 eq.), DMAP (0.2 eq.), pyridine, rt, 95%; (i) PPh_3 (1.5 eq.), DIAD (2.5 eq.), DPPA (1.5 eq.), THF, −15 °C to rt, 85%; DIAD = diisopropyl azodicarboxylate; DPPA = diphenylphosphorylazide; TCCA = trichlorocyanuric acid; TBSCl = *t*-butyldimethylchlorosilane; NMI = *N*-methylimidazole; TMSSPh = (phenylthio)trimethylsilane.

Then, with these nine glucosyl donors in hand, the *bis*-glycosylation of DHAB was investigated (Scheme 2.5). The results are presented in Table 2.2.

The glucosyl bromide **7** was evaluated first, as silver salts, which are used in Koenigs-Knorr glycosylation, are compatible with hydroxylated AB derivatives.[292] However, although silver carbonate and silver oxide efficiently activated the donor, the acceptor did not react, yielding after work up the hydrolyzed donor while DHAB was nearly fully recovered (Table 2.2, entry 1). Of the nine glucosyl donors, we chose to investigate thioglycosides particularly, because they present several great advantages. Indeed, thioglycosides are bench-stable, can be easily prepared in high yields, can be activated under mild conditions, and are compatible with a wide range of reaction conditions, allowing facile functionalization and protecting group manipulations. Unfortunately, when the acetyl-protected donor **8** was reacted under standard *N*-iodosuccinimide (NIS)/triflic acid (TfOH) activation,[302] complete donor hydrolysis was observed (Table 2.2, entry 2). When NIS was replaced by NBS (*N*-bromosuccinimide) a similar result was observed (Table 2.2, entry 3).

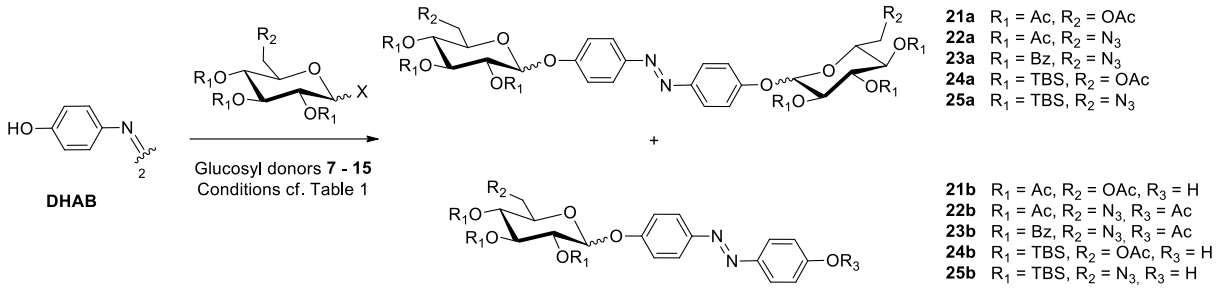

Scheme 2.5. Glycosylation of DHAB with different glycosyl donors. The desired *bis*-glycosylated products are numbered with "a", the *mono*-glycosylated by-products with "b".

Table 2.2. Glycosylation of DHAB under various conditions.[a]

Entry	Donor[b]	Promoter (eq/donor)	Base (eq/DHAB)	Solvent	Temp	*Bis*-glycoside, yield, α,β:β,β *Mono*-glycoside, yield, α:β
1	**7**	Ag_2CO_3 (1.1) or Ag_2O (2)	–	MeCN	rt	Donor hydrolysis
2	**8**	NIS/TfOH (1.5/0.05)	–	MeCN	0 °C	Donor hydrolysis Azo reduction
3	**8**	NBS/TfOH (1.5/0.1)	–	MeCN	rt	Donor hydrolysis
4[c]	**8**	I_2 (2.5)	–	MeCN	rt	Azo reduction
5	**9**	MeOTf (3.0)	DTBMP (2.2)	CH_2Cl_2	rt	Donor hydrolysis
6	**9**	DMTST (1.5)	DTBMP (2.2)	CH_2Cl_2	-30 °C	No activation
7	**10**[d]	Tf_2O (1.0)	DTBMP (3.0)	CH_2Cl_2	-78 °C	Donor hydrolysis
8	**11**	$BF_3{\cdot}OEt_2$ (1.1)	–	MeCN	rt	**21a**, 68%, 0:1 **21b**, not observed
9	**12**	$BF_3{\cdot}OEt_2$ (1.1)	–	MeCN	rt	**22a**, 48%, 0:1 **22b**, 14%, 0:1
10	**13**	$BF_3{\cdot}OEt_2$ (1.1)	–	MeCN	rt	**23a**, 38%, 0:1 **23b**, 25%, 0:1
11	**14**	MeOTf (3.0)	DTBMP (2.2)	CH_2Cl_2	rt	**24a**, 50%, 1:5 **24b**, 20%, 1:10
12	**14**	MeOTf (3.0)	DTBMP (2.2)	MeCN	rt	**24b**, 17%, 1:5
13	**14**	MeOTf (3.0)	DTBMP (2.2)	CH_2Cl_2/ [bmim][OTf] (10:1)	rt	**24a**, 7%, 1:6 **24b**, 31%, 1:12
14[e]	**14**	BSP/Tf_2O (2.2/2.2)	DTBMP (2.2)	CH_2Cl_2/ [bmim][OTf] (9:1)	-90 °C	**24a**, 18% 1:10 **24b**,12% 1:5
15	**15**	MeOTf (3.0)	DTBMP (2.2)	CH_2Cl_2	rt	**25a**, 10%, 1:4 **25b**, 14%, 1:8

[a] All reactions were performed under dry conditions with addition of 3 Å molecular sieves (MS) and with [DHAB] = 0.05 mol × L^{-1} unless otherwise stated. [b] 2.2 eq. of donor were used unless otherwise stated. [c] The azobenzene was used as a di-potassium salt. The salt was prepared by treatment of DHAB with *t*BuOK (2 eq) in MeCN and precipitated by addition of Et_2O. [d] 4 eq. of donor were used. [e] A solution of the acceptor was added to a mixture of donor and promoter; DTBMP = 2,6-di-*tert*-butyl-4-methylpyridine; DMTST = dimethyl(methylthio)sulfonium trifluoromethanesulfonate; [bmim][OTf] = 1-butyl-3-methylimidazolium trifluoromethanesulfonate; BSP = 1-benzenesulfinyl piperidine; NIS = *N*-iodosuccinimide; NBS = *N*-bromosuccinimide.

In both cases various DHAB-derived side products were formed, including the *N*-dehydro-*N*-iodohydrazoquinone intermediate **26**, which quickly rearranged after isolation to the *bis*-hydrazoquinone **27** (Scheme 2.6). These results indicate that, in addition to decreasing the nucleophilicity of oxygen atoms, the azo/hydrazo tautomerism renders the nitrogen atoms more nucleophilic, especially towards soft electrophiles such as iodonium-donating reagents. Thus, *N*-halogenation of the azo group competes with the activation of the donor and inhibits the reactivity of the acceptor. Interestingly, when the di-potassium salt of DHAB was used in an iodine promoted glycosylation with donor **8**, the product **27** was formed (Table 2.2, entry 4), while the treatment of protonated DHAB with iodine is ineffective.

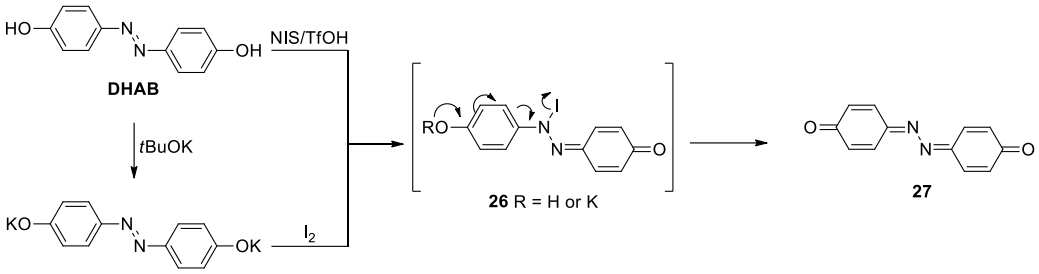

Scheme 2.6. Reduction of DHAB to the *bis*-hydrazoquinone **27** with NIS/TfOH. Only the dipotassium salt of DHAB may react with iodine to provide **27**.

As it was not possible to activate thioglycosides with halogenium-donating promoters, the benzoylated thioglucoside **9** was activated with methyl triflate (MeOTf)[303] or dimethyl(methylthio)sulfonium triflate (DMTST).[304] Bearing the azophenol/hydrazoquinone tautomerism in mind, it was assumed that acidic media may favor the formation of the hydrazoquinone tautomer. Therefore, the following glycosylation reactions were buffered with 2,6-di-*tert*-butyl-4-methylpyridine (DTBMP), which is known as an efficient non-nucleophilic proton scavenger. Unfortunately, glycosylation of DHAB with **9** under these conditions failed (Table 2.2, entries 5 and 6). While the glucosyl donor was hydrolyzed or remained unreacted, again a number of DHAB-derived by-products were formed, presumably including *O*-methylated derivatives. In addition to MeOTf and DMTST, several other promoters that were presumed to be compatible with DHAB, were screened with donor **9**. However, activations with Me_2S_2/Tf_2O,[305] $Cu(OTf)_2/h\nu$,[306] DDQ/$h\nu$[307] or Selectfluor/$BF_3.OEt_2$,[308] all failed to provide the desired glycosides.

The disappointing results with the acylated thioglycosides led us to consider the sulfoxide **10** as glucosyl donor. In fact, sulfoxides may be activated with equimolar amounts of Tf_2O at low temperature, providing a highly reactive triflate intermediate, which was shown to be effective for the glycosylation of unreactive alcohols.[309] This procedure allows a pre-activation of the donor, leaving no promoter in the reaction mixture, preventing side reactions with DHAB. Unfortunately, treatment of donor **10** with Tf_2O and DTBMP at -78 °C, followed by addition of a solution of DHAB, led after an hour, to a complete consumption of the donor, presumably transformed into the corresponding triflate, while the acceptor remained unreacted (Table 2.2, entry 7). Prolonging the reaction time while thawing to RT did not show any improvement, and the donor eventually hydrolyzed. Although Kahne *et al.* have described the successful glycosylation of sterically hindered and electronically deactivated phenols with sulfoxides, this method was not successful with DHAB, again underlining the limited reactivity of this azobenzene diol.

Next, the *O*-(glucosyl)-*N*-phenyltrifluoroacetimidate donors were assessed. The peracetylated donor **11** under BF_3-etherate activation afforded satisfyingly 68% of the desired *bis*-glycosylated compound **21a** as a single ββ-anomer (Table 2.2, entry 8), while the *mono*-glycosylated by-product **21b** was not observed. Encouraged by this result, the same treatment was applied to the 6-azido-6-deoxy-functionalized glucosyl donor **12** (Table 2.2, entry 9). This reaction yielded 48% of *bis*-glycoside **22a**

and 14% of *mono*-glycoside **22b** again with full β-selectivity, in agreement with previous reports where the yields of *bis*-glucosylation of DHAB were 32%[268d] and 52%.[268e] The benzoyl protected analogue of **12**, the acetimidate **13**, afforded under the same conditions, the pure ββ-anomer **23a** in 38% yield, along with 25% of the β-*mono*-glycoside **23b** (Table 2.2, entry 10). These result hint that the azido function in position 6 may play a detrimental role during the reaction, leading to lower yields. This was already observed for the glycosylation of *mono*-hydroxylated AB derivatives: reaction of 4-hydroxyazobenzene with a peracetylated glucosyl imidate gave 73% yield,[268b] while 4-hydroxy-4´-allyloxyazobenzene reacted with 2,3,4-*O*-acetyl-6-azido-6-deoxyglucosyl imidate in 39% only.[275] Yield reduction in presence of an azido group was also observed with different kinds of phenolic acceptors, yielding the products in low to moderate yields.[310]

Despite an effective activation, thioglycoside **8** failed to react with DHAB, contrarily to imidate **11**. Two factors may provide a plausible explanation for this difference in reactivity (Scheme 2.7): firstly, the phenylmethylsulfonium group might be a less good nucleofuge than the trifluoroacetimide group, therefore preventing the generation of the oxocarbenium ion. Indeed, while the generated methylphenylsulfide remains a potent nucleophile that can attack the positively charged C-1, the acetimide group rearranges to the less nucleophilic trifluoro-*N*-phenylacetamide.

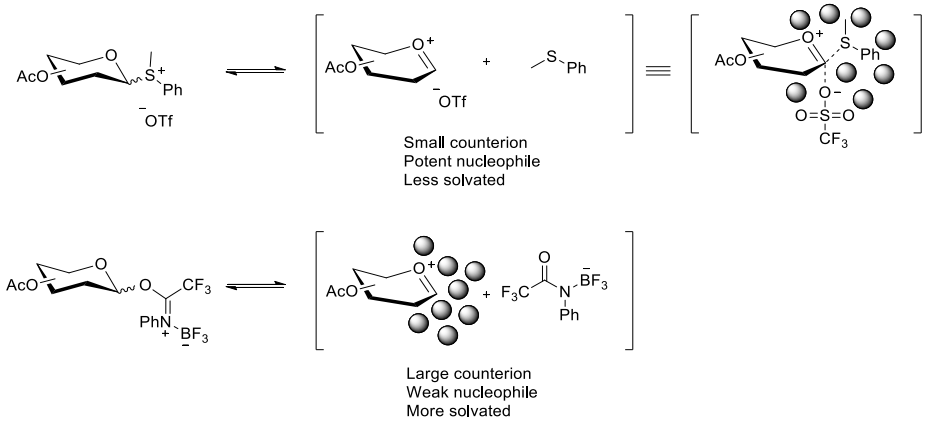

Scheme 2.7: Potential explanation for the reactivity difference between peracetylated thioglycosides and glycosyl imidates in the glycosylation with DHAB.

Secondly, the nature of the counter ion is also important. The triflate ion is a small and hard anion that might stay close to the positive center (S^+ or C^+), thus hindering the approach of the acceptor. In the contrary, the BF_3-acetamide complex is a large and diffuse anion that might be better solvated, leading to a more naked and thus more reactive oxocarbenium intermediate. In other words, the glycosylation with disarmed thioglycosides might involve intermediates that are more covalently bonded, implying an S_N2-like mechanism for which the DHAB might not be nucleophilic enough. The same reasoning may apply to glycosyl bromides, or sulfoxides. Hence, in order to glycosylate DHAB, one might want to find conditions that favor an S_N1-like mechanism.

Next, the conformationally armed thioglycosides **14** and **15** were evaluated. In view of the results obtained with the disarmed thioglucosides (Table 2.2, entries 2-6), MeOTf was chosen for the activation. Also, the reaction medium was buffered with DTBMP in order to avoid acid-mediated intermolecular silyl transfer. Gratifyingly, the reaction between DHAB and donor **14** (Table 2.2, entry 11), afforded under these conditions 50% of the *bis*-glycosylated product **24a** (αβ : ββ = 1 : 5), and 20% of *mono*-glycoside **24b** (α : β = 1 : 10), though as anomeric mixtures. DHAB is only partially soluble in CH_2Cl_2, hence **14** was employed under identical conditions in acetonitrile (Table 2.2, entry 12), in which the acceptor is more soluble. However, only *mono*-glycosylated compound **24b** was obtained in 17% yield, along with methylated DHAB derivatives.[311] This intriguing result hints that the low solubility of DHAB in CH_2Cl_2 favors glycosylation over methylation of the phenolic OH group, as well as *bis*-

glycosylation over *mono*-glycosylation. In addition, the reaction in acetonitrile was two-fold less β-selective than in CH_2Cl_2, a rather counterintuitive result, given that acetonitrile is known as a participating solvent favoring the formation of β-glycosides *via* an α-nitrilium intermediate.

Encouraged by this result, several buffering bases with different strength were assessed, in the hope of increasing the reactivity of the acceptor (*cf*. experimental section). Unfortunately, there was no improvement in anomeric selectivity, and the amount of methylated DHAB by-products increased with the strength of the base, thus reducing the yield of the desired *bis*-glycoside. Hence DTBMP appeared as the base of choice for conducting the *bis*-glycosylation of DHAB with armed silylated donors and avoid the undesired methylation of the acceptor. The use of the ionic liquid 1-butyl-3-methylimidazolium trifluoromethanesulfonate ([bmim][OTf]) as a co-solvent in CH_2Cl_2 was also examined.[312] This solvent mixture allows the complete dissolution of DHAB, and activation of donor **14** with MeOTf in presence of DTBMP (Table 2.2, entry 13) favored again the *mono*-glycoside **24b** (31%) with a good anomeric selectivity (α : β = 1 : 12), while **24a** was obtained in 7% yield. As observed for the reaction in acetonitrile, *O*-methylated derivatives of DHAB were formed. Interestingly, the promoter system 1-benzenesulfinyl piperidine (BSP)/Tf_2O[313] efficiently activated donor **14** without reacting with the DHAB acceptor (Table 2.2, entry 14). This reaction afforded **24a** in 18% yield (αβ : ββ = 1 : 10) and **24b** in 12% (α : β = 1 : 5). Finally, the 6-azido-functionalized donor **15** was assessed under the glycosylation conditions which were found optimal for the armed donor **14** (Table 2.2, entry 11). This reaction afforded the *bis*-glycoside **25a** in 10% yield (αβ : ββ = 1 : 4) and the *mono*-glycosylated compound **25b** in 14% yield (α : β = 1 : 8) (Table 2.2, entry 15). When the BSP/Tf_2O system was applied with donor **15** only hydrolysis was observed. As observed with the acylated donors **12** and **13**, the 6-azido group seems to have a detrimental effect on the glycosylation of DHAB.

This study highlighted five factors that influence the efficiency of glycosylation with DHAB. First, DHAB is a poorly reactive acceptor, because of a decreased nucleophilicity of the phenolic hydroxyl group as a consequence of a tautomeric equilibrium between the azophenol and the hydrazoquinone form. Second, this tautomerism also increases the nucleophilicity of the nitrogen atoms in the azo bond, preventing the use of halogenium donating thiophilic promoters, as *N*-halogenation occurs. Third, when MeOTf-promoted glycosylations require a buffered medium (*i.e.* for silylated donors), the choice of the base is critical to prevent competing *O*-methylation of DHAB. Fourth, the solubility of DHAB is an important parameter to avoid *O*-methylation and control the degree of DHAB glycosylation. The lower the solubility of DHAB, the higher the yield of *bis*-glycosylated product, and the less chances for *O*-methylation. Fifth, the presence of an azide in the position 6 of the donor seems to be detrimental, and generally results in decreased yields. Therefore, based on these observations, alternative strategies may be proposed to maximize the yields of AB-*bis*-glycosides with an azide function on the 6 position (Scheme 2.8).

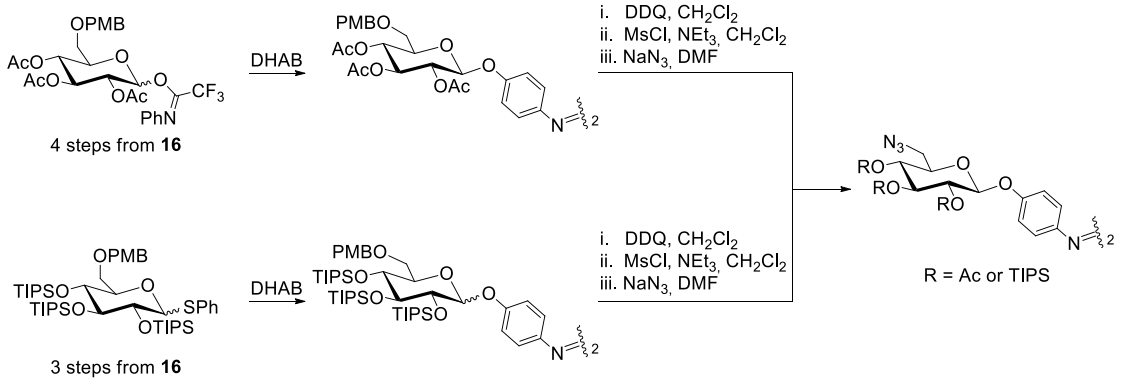

Scheme 2.8. Alternative synthesis pathways to optimize the generation of AB 6-azido-6-deoxy-glycosides

On the one hand, one could use a disarmed acetylated imidate donor with an orthogonal protecting group on the 6- position to achieve a good yielding glycosylation of DHAB with complete stereocontrol. Further deprotection and azidation would afford the 6-azido-6-deoxy-azobenzene glycosides. On the other hand, the use of silylated thioglycosides with larger groups than TBS in order to improve the stereoselectivity, and an orthogonal protecting group on the 6- position may be envisaged. The *p*-methoxybenzyl (PMB) group seems like a good candidate for orthogonal protection as it can be removed in mild oxidative conditions with dichlorodicyanobenzoquinone (DDQ), and could participate to enhance the reactivity of the donor.[314]

3. Palladium-catalyzed coupling of glycosyl thiols, and influence of sulfur oxidation on the photochromic properties of AB-glycoconjugates

In the context of photoswitchable glycomacrocycles synthesis, in order to best exploit the geometrical information transmission between the sugar and the AB hinge, a minimal flexibility is required, and thus, a direct connection between both moieties is necessary. To do so, the coupling of the AB moiety to the anomeric position of the carbohydrate *via* a glycosidic bond is the most obvious approach. As seen in the previous chapter, the glycosylation of DHAB is a challenging reaction, and might be even harder with more sophisticated AB derivatives such as diazocines or *o*-tetrasubstituted compounds. Inspired by the work of Messaoudi *et al.*,[315] it was envisaged to employ glycosyl thiols as nucleophiles in a palladium-catalyzed thioarylation (Buchwald-Hartwig-Migita) of halogenated AB derivatives (Scheme 3.1).

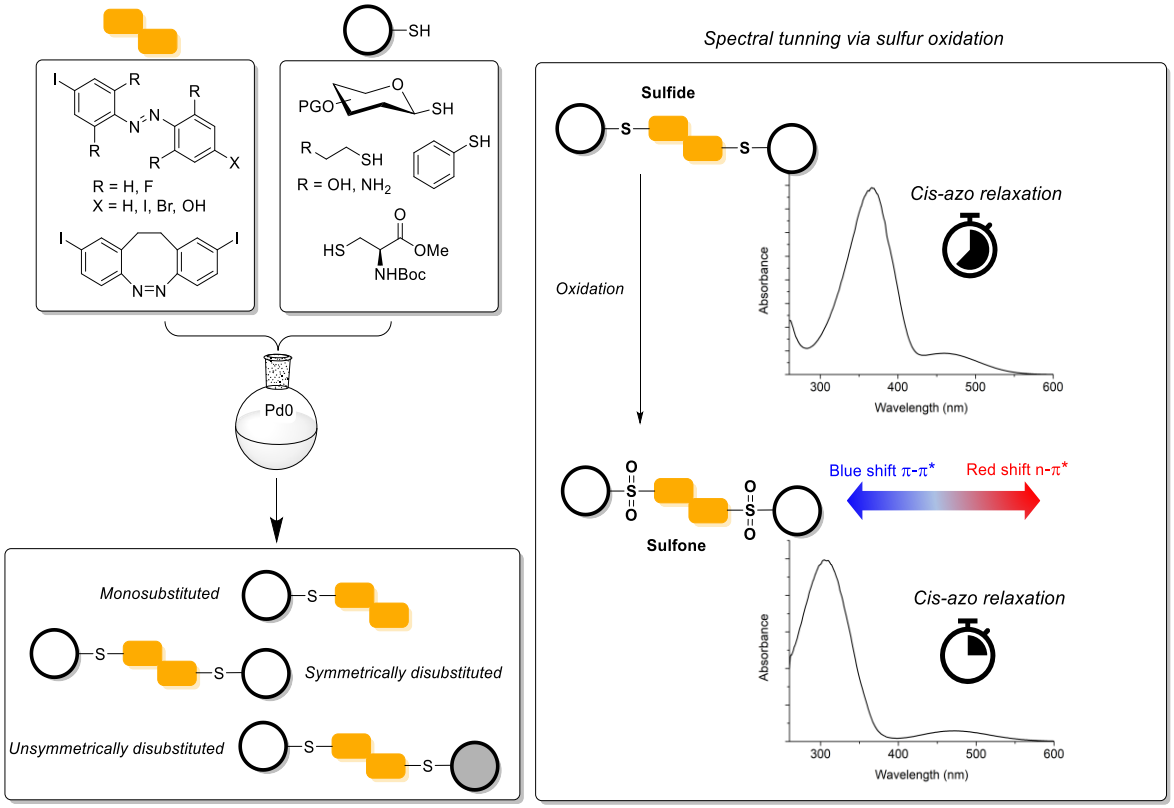

Scheme 3.1. General depiction of the palladium-catalyzed thioarylation of halogenated AB derivatives for the preparation of photoresponsive conjugates and subsequent oxidation of the sulfide bridges allowing the modulation of the photochromic properties.

The use of sulfur instead of oxygen for the glycosidic linkage presents several advantages. First, as sulfur and oxygen are isoelectronic, it was anticipated that AB conjugates with sulfide bridges in *para* positions would have similar photochromic properties than that of their *para*-oxygenated counterparts. Furthermore, the sulfur atoms can be oxidized to the respective sulfoxides or sulfones, resulting in a modified electron density within the AB unit, therefore allowing to modulate its photochromic properties. Second, glycosyl thiols are stable towards mutarotation, allowing a complete stereocontrol of the anomeric configuration. In addition, thiosaccharides are known to be resistant towards enzyme-catalyzed glycosidic bond cleavage.[316] Third, methods for the direct modification of *ortho*-substituted AB or diazocine derivatives are still limited,[198] which may lead to tedious synthetic sequences.[151-157,317] This new synthetic approach however, allows the facile and efficient derivatization of such derivatives, and provides molecules of which the photochromic properties may be further altered with simple one-step oxidation. The results of this study were also published.[190b]

3.1. *Bis*-functionalization of *p,p´*-diiodoazobenzene derivatives with glycosyl thiols

Since AB *bis*-glycosides are key intermediates in the synthesis of photoswitchable glycomacrocycles, we commenced our investigation by studying the coupling of *p,p'*-diiodoazobenzene derivatives with glycosyl thiols (Scheme 3.2). As electrophiles of the Buchwald-Hartwig-Migita cross-coupling, the azobenzene **28** was chosen as a reference, besides tetra-*ortho*-fluoroazobenzene **29** and diazocine **30**, which may be synthesized according to known procedures.[163,189] As nucleophiles, three differently substituted glucosyl thiols **31**–**33** were used, plus the thioglycoside **34** carrying a primary SH functional group.

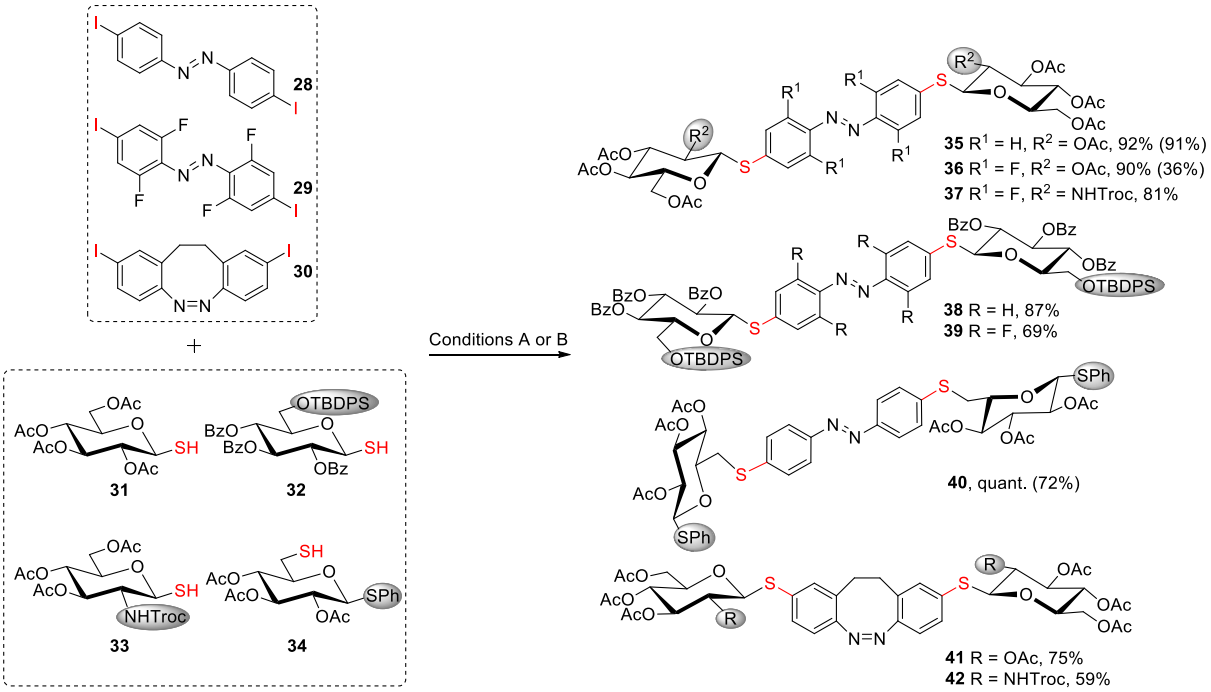

Scheme 3.2. Preparation of symmetrical azobenzene *bis*-thioglycosides via palladium catalyzed Buchwald-Hartwig-Migita cross coupling of various glycosyl thiols with diiodo-AB derivatives. Conditions A: $Pd(OAc)_2$ (10 mol%), Xantphos (5 mol%), thiol (3 eq), Et_3N (2 eq), 1,4-dioxane, 100 °C; Conditions B: Xantphos-PdG3 (2 mol%), thiol (2 eq), Et_3N (2 eq), THF, RT; The yields in brackets correspond to those obtained with conditions A. Compounds **41** and **42** were obtained with conditions B in 1,4-dioxane at 80 °C. TBDPS: *tert*-butyldiphenylsilyl; Troc: trichloroethoxycarbonyl.

In preliminary experiments, we compared the efficacy of two catalytic systems, $Pd(OAc)_2$/Xantphos (Conditions A) and the palladacycle precatalyst PdG3 elaborated by Buchwald,[318] with Xantphos as the ligand (Conditions B). We found comparable results for the reaction between thiol **31** and AB **28** (91% *vs* 92%), however lower yields were obtained with $Pd(OAc)_2$ in the case of reaction between **31** and **29** (36% *vs* 90%) or **34** and **28** (72% *vs* 100%). In addition, conditions B are generally applicable at RT, while the use of $Pd(OAc)_2$ requires higher temperatures.

Therefore, we focused on the use of Xantphos-PdG3 to obtain the cross-coupling products **35**–**42** at room temperature, in 5 to 20 min, with only 2 mol% of catalyst used. Under these conditions, AB-*bis*-glycosides **35**-**39** were obtained in yields ranging from 69 to 92%. The bulky 6-*O*-TBDPS group in **32** and the demanding NTroc protecting group in **33** only slightly impaired the yield with a 5-20% decrease. Sulfide functionality was also very well tolerated, as shown by the quantitative isolation of **40**. The reaction of diazocine diiodide **30** with thiols **31** and **33** required a higher temperature (80 °C), therefore 1,4-dioxane was used as the solvent to afford **41** and **42** in 75% and 59% yield respectively. Given these excellent results, the scope of the reaction was next explored, towards the synthesis of unsymmetrical AB-conjugates.

3.2. *Mono*-functionalization of unsymmetrical azobenzenes with different thiols

In order to delineate the scope of this thioarylation reaction with respect to the nature of the thiol substrate, the *mono*-functionalization of differently substituted *p*-iodoABs with various thiols was studied (Scheme 3.3). The *mono*-substituted AB **43** was used as a reference compound and reacted with the glucosyl thiol **31**, to afford the expected coupling product **50** within minutes in 90 % yield. The reaction of the AB derivative **44** with **31** gave product **51** in 87 % yield. To our delight, an excellent chemoselectivity was observed between iodine and bromine substituents in **44**, as reported by Messaoudi *et al.*,[315b] hence allowing for a subsequent substitution of the bromine atom. The reaction of 4-iodo-4´-hydroxy-AB **45** with **31** showed that hydroxyl group are also well tolerated on the electrophile, yielding 93% of the phenolic conjugate **52**, which could be further alkylated or glycosylated, for instance. Also, thiophenol smoothly reacted with **45** to afford product **53** in 86% yield, and aliphatic thiols bearing competitive hydroxy (**47**) or amino (**48**) groups, were coupled with **45**, providing products **54** and **55** in 81 % and 47 % yield, respectively. In the case of cysteamine **48** however, a higher temperature (70 °C) was required, and a lower yield was obtained due to incomplete conversion. This might be due to the amino group acting as an ancillary ligand of the cross-coupling catalyst and thus impairing the reaction. Importantly, no side-product was observed in the reaction of **48** and **45**, indicating that *N*-arylation did not occur. The *N*-boc protected cysteine methyl ester **49** was also readily coupled to **45**, though in a longer time, and gave product **56** in 68% yield. Very interestingly, when an excess (2 eq) of diiodide **29** was reacted with thiol **31** at 0 °C and under dilute conditions, the *mono*-substituted product **57** was isolated in 81% yield, while the *bis*-glycoside was obtained in 14 % yield. These conditions allow the sequential preparation of unsymmetrical tetra-*o*-fluoro-AB conjugates, starting from symmetrical derivative **29**.

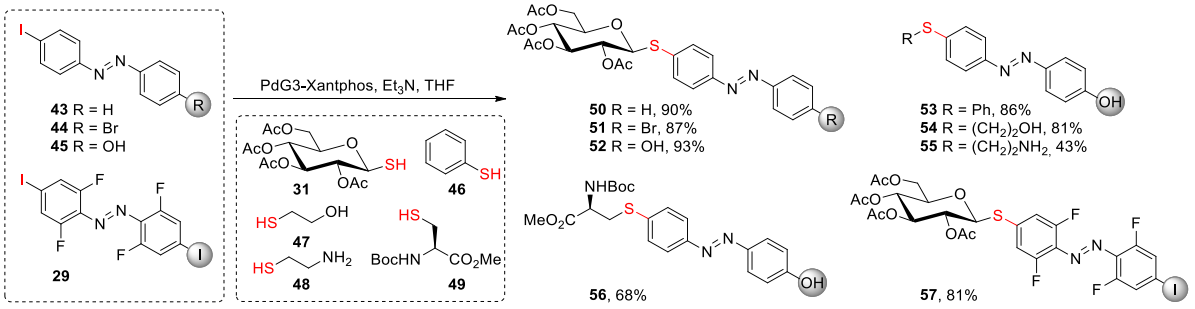

Scheme 3.3. *Mono*-functionalization of differently substituted *p*-iodoazobenzene derivatives with various thiols. Conditions for preparation of compounds **50**–**56**: the thiol (1–1.2 eq) and the azobenzene (1–1.2 eq) were stirred in THF in presence of PdG3-Xantphos (1–5 mol%) and Et_3N (1–1.4 eq) at RT except for **55** which was obtained after heating at 70 °C; conditions for the preparation of **57**: the thiol and an excess of the azobenzene (2 eq) were stirred at 0 °C in the presence of 1 mol% catalyst and Et_3N (1 eq).

Encouraged by these excellent results, the preparation of hetero-*bis*-azobenzene glycosides, *via* sequential and one-pot procedures was achieved.

3.3. Hetero-*bis*-functionalization *via* sequential and one pot procedures

The unsymmetrical azobenzene *mono*-thioglycosides **51** and **52** were engaged in either a cross coupling or a glycosylation reaction (Scheme 3.4). The bromide atom in **51** was substituted with thiol **32** under the *mono*-functionalization conditions, in 1,4-dioxane at 60 °C, affording product **58** in 73% yield. On the other hand, the phenolic acceptor **52** was reacted with the glycosyl thioimidate donor **59** (prepared in one step from thiol **31**),[319] under BF_3-etherate activation, to provide compound **60** in 65 % yield.

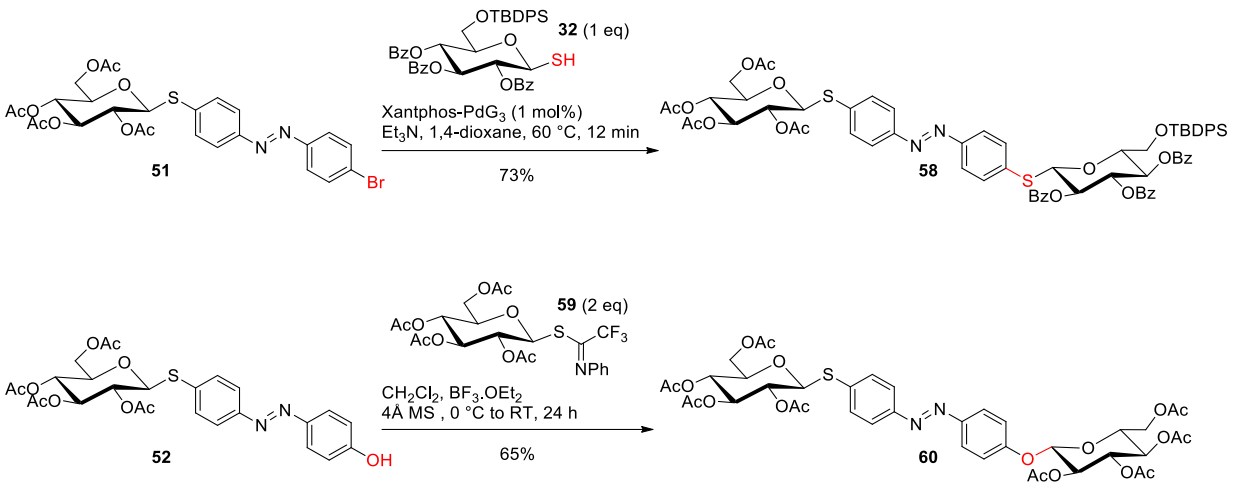

Scheme 3.4. Preparation of unsymmetrical azobenzene *bis*-glycoconjugates according to two sequential conjugation reactions (two sequential cross-coupling reactions or cross-coupling followed by glycosylation, respectively).

Having shown that both **51** and **52** may be further functionalized, one-pot procedures for the preparation of unsymmetrical AB *bis*-conjugates were established (Scheme 3.5).

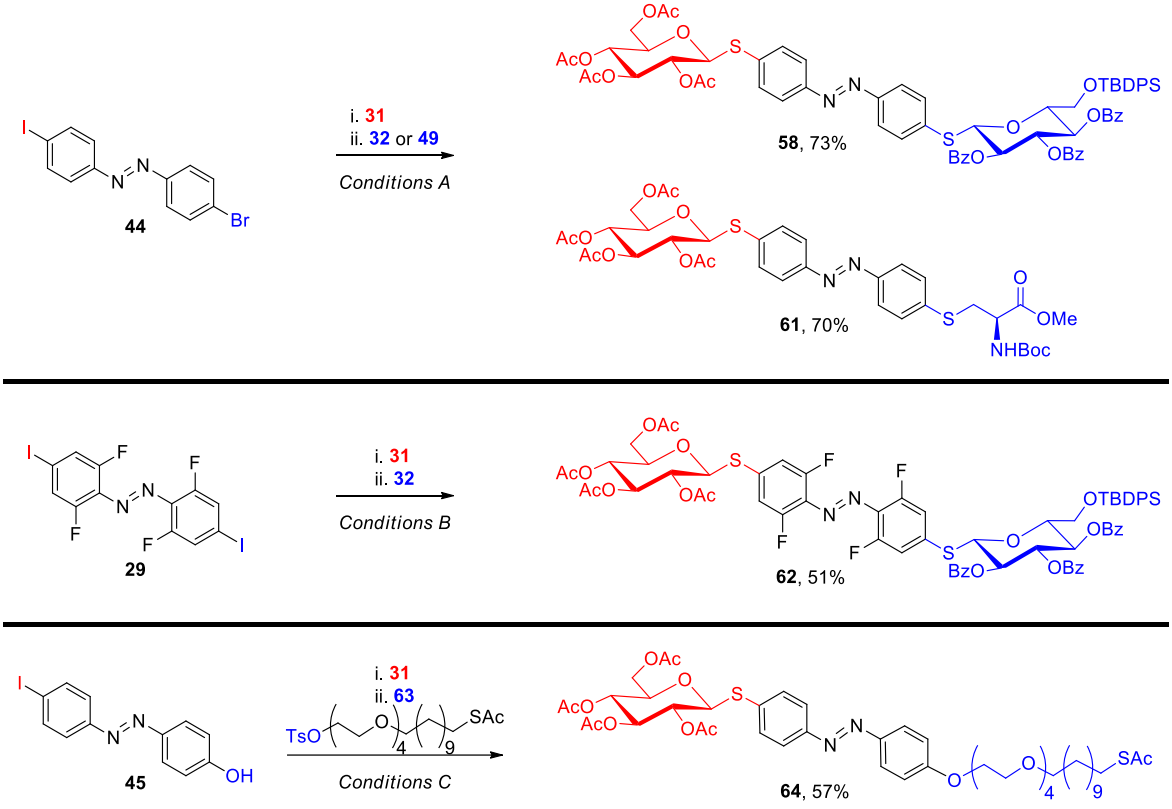

Scheme 3.5. Preparation of unsymmetrical AB hetero-*bis*-conjugates in a one-pot fashion. Pd^0: Xantphos-PdG3; *Conditions A*: A solution of thiol **31** (0.1 mol.L^{-1}, 1 mL, 1 eq) in 1,4-dioxane was added to AB **44** (0.1 mmol, 1 eq) and the catalyst (1 mol%) under nitrogen atmosphere, followed by Et_3N (1.5 eq), and the mixture was stirred at RT for 15 min. Then, thiol **32** (1.5 eq) or **49** (1.5 eq) were added with an additional load of catalyst (1 mol%) at RT. The mixture was heated to 60 °C, Et_3N (1.5 eq) was added, and the heating was continued for 30-60 min; *Conditions B*: To a solution of thiol **31** (1 eq), AB **29** (1 eq) and catalyst (1 mol%) in THF was added Et_3N (1 eq) at -10 °C. The reaction was stirred 1 h at this temperature and then thiol **32** (1.2) was added followed by another load of catalyst (1 mol%) and Et_3N (1 eq) and the reaction was then thawed to RT over 30 minutes; *Conditions C*: Thiol **31** was reacted with AB **45** according to the conditions described in part 3.2. Then the solvent was evaporated, and the resulting residue was dissolved in DMF and reacted with tosylate **63** (1.2 eq) in presence of potassium carbonate (3 eq) at 80 °C for 2 h.

Exploiting the sharp reactivity difference between the *p*-iodide and *p´*-bromide in **44**, two sequential cross couplings were achieved in a one pot manner with two different thiols. In order to ensure an efficient coupling in the second part of the reaction, we systematically added, with an excess of the second thiol, the same amount of catalyst as the initial load (1 mol%). Therefore, reaction of **44** with thiol **31** at RT, followed by addition of thiol **32** at 60 °C afforded product **59** in a very good yield of 73%. In the same way, **44** was successfully substituted with both **31** and the cysteine derivative **49**, to give conjugate **61** in 70% yield. Then, based on the efficacious preparation of *mono*-functionalized derivative **57**, a stoichiometric amount of **29** was reacted with **31** at -10 °C, followed by addition of excess thiol **32**, affording the desired compound **62** in a fair yield (51%), along with symmetrical by-products. Finally, AB **45** was coupled with thiol **31** at RT, and subsequent alkylation of the phenol with the tosylate **63** in DMF at 80 °C, yielded 57% of the conjugate **64**. This compound, bearing a thioacetate-terminated linker, would be suitable for the fabrication of glyco-SAMs on gold surface for instance.[268c,f]

Owing to an excellent chemoselectivity as well as a remarkable tolerance towards various functional groups, this approach opens new horizons towards the preparation of multifunctional AB derivatives. In addition to the use of a low catalyst load (1 mol%), the possibility of performing multiple steps in a one-pot fashion is an economical and straightforward way to modify AB derivatives. This also raises the possibility to use the Buchwald-Hatwig-Migita reaction for the incorporation of AB into sulfur-containing macrocycles, as an alternative to the nucleophilic substitution which was used previously.[206-208] Next, selected compounds were oxidized in order to obtain a library of symmetrical and unsymmetrical AB *mono*- and *bis*-glycosides to study the effect of the sulfur oxidation state on the photochromism of the synthesized AB glycoconjugates.

3.4. Oxidation of glycosidic sulfur atoms

Oxidation of the glycosidic sulfur is relevant because the modification of the electron density in the phenyl rings has a strong influence on the photochromic properties of AB switches. Through oxidation, the sulfide which is an electron donating group, can be transformed into the corresponding sulfoxide or sulfone, which are increasingly electron withdrawing. Such modification may influence both the $S_1 \leftarrow S_0$ and $S_2 \leftarrow S_0$ transitions. In the case of tetra-*o*-fluoro derivatives, it was shown that electron-withdrawing substituents increase the separation of the $n \rightarrow \pi^*$ bands of each isomer, resulting in better photoconversion in the visible range.[154] Additionally, a hypsochromic shift of the $\pi \rightarrow \pi^*$ transition and an alteration of the thermal stability of the *cis* isomer were expected in general.[320]

Meta-chloroperbenzoic acid (*m*CPBA) was used to oxidise sulfur bridges into sulfoxides or sulfones on a selection of previously synthesized azobenzene glycoconjugates (Scheme 3.6). Sulfoxidation was only realized for the *mono*-glycosides **50** and **65**, because the configuration of the newly formed stereogenic center is difficult to control, giving rise to diastereomeric mixtures, complicating the analyses in the case of *bis*-glycosides. Treatment of **50** with a slight excess of *m*CPBA (1.5 eq) in CH_2Cl_2, afforded sulfoxide and sulfone **66a** and **66b** in 43% and 53% respectively. Since the sulfoxide and the sulfone were easily separable by chromatography, they were both generated in a single reaction.

As alkylation or glycosylation of *para*-phenol is a good mean to prepare unsymmetrical conjugates, a model compound bearing a *para*-methoxy group was investigated. Therefore, compound **52** was methylated to obtain quantitatively **65**, which was subsequently oxidised, under the same conditions as **50**, to sulfoxide **67a** and sulfone **67b** in 48% and 49% yield respectively. Since compound **67b** was obtained as an α/β mixture which could not be resolved by chromatography, it was prepared independently at low temperature (see experimental section). Unsymmetrical mixed sulfone/sulfide derivatives were prepared in a two steps sequence starting from *mono*-glycosides **51** and **57**. First,

oxidation with *m*CPBA afforded sulfones **68** and **69** in 87% and 68% respectively, and subsequent cross coupling with thiol **31** at 70 °C gave compounds **70** (46%) and **71** (59%).

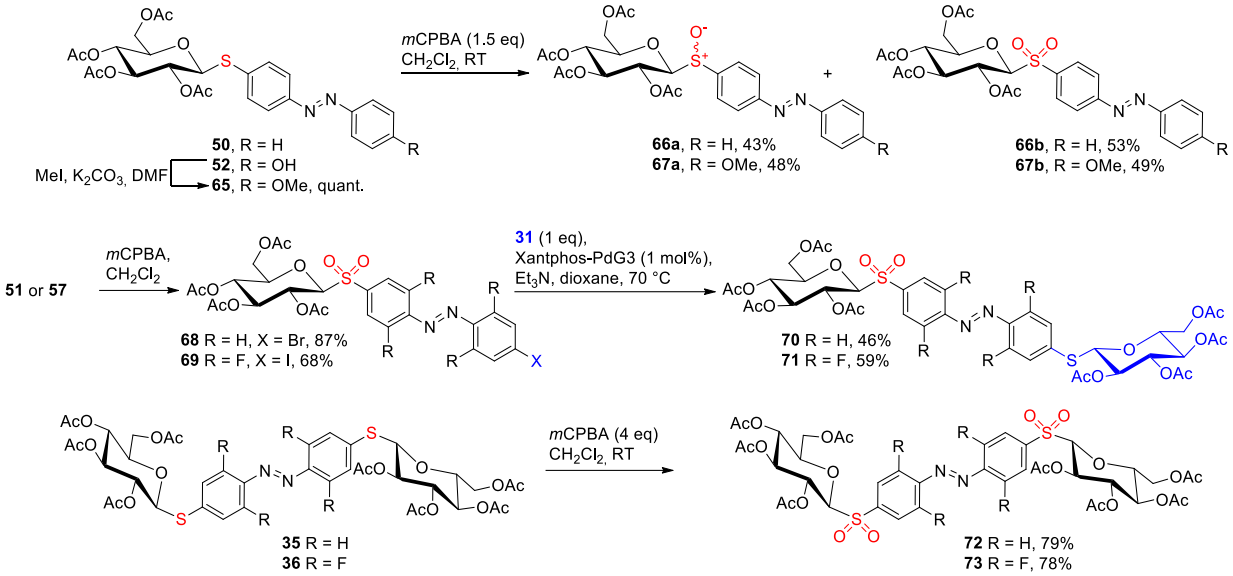

Scheme 3.6. *m*CPBA-mediated oxidations of the sulfur linkages to afford sulfoxides (**66a**, **67a**) or sulfone (**66b**, **67b**, **72**, **73**) derivatives. Mixed products bearing both sulfide and sulfone functions (**70**, **71**) were synthesized in a sequential fashion.

Finally, *bis*-glycosides **35** and **36** were completely oxidized to furnish the di-sulfone derivatives **72** and **73** in respective yields of 79% and 78%. Then, the photochromic properties of thirteen compounds (**35**, **36**, **41**, **50**, **65**, **66a**, **66b**, **67a**, **67b**, **70**, **71**, **72**, **73**) were investigated.

3.5. Photochromic properties of selected AB glycoconjugates

The selected molecules were divided in five subsets. The first one, comprised of the *mono*-glycosides **50**, **66a** and **66b** was chosen as a basis to evaluate the effect of *para* sulfur oxidation alone on the photochromic behavior of AB. The second one comprised of *p,p´*-di-substituted AB *mono*-glycosides **65**, **67a** and **67b** gives information about the effect of one additional electron donating group in *p´* position. Then, the subset of non-fluorinated *bis*-glucosides **35**, **70** and **72**, provides data on *p,p´*-di-substitution with symmetrical electron donation or withdrawing, and unsymmetrical electron distribution. The third subset was composed of the *o*-fluorinated *bis*-glucosides **36**, **71** and **73**, to study the effect of additional *ortho* substitution. The spectroscopic data of these four subsets are listed in Table 3.1, and Figure 3.1 shows the UV-vis spectra of each compound in the *trans* ground state and after irradiation at an appropriate wavelength in DMSO. Finally, the data corresponding to the diazocine *bis*-glucoside **41**, which makes its own subset, are listed in Table 3.3 and its spectra are shown in Figure 3.2.

Comparably to a previously studied β-D-glucoside analogue,[268b] *trans*-AB-thioglucoside **50** shows two absorption maxima at 351 nm (*vs* 347 nm for the *trans-O*-glucoside) and 441 nm (*vs* 439 nm for the *cis-O*-glucoside), corresponding to the π→π* and *n*→π* transitions respectively (Table 3.1, entry 1, Figure 3.1a). Upon oxidation of the sulfur atom to the corresponding sulfoxide and sulfone, a hypsochromic shift of the π→π* transitions of the *trans* isomer was observed, with a maximum shift of 24 nm in case of the sulfone derivative **66b** (Table 3.1, entries 2 and 3, Figure 3.1a). The *n*→π* bands however, underwent a slight red-shift resulting in a better separation of $S_1 \leftarrow S_0$ and $S_2 \leftarrow S_0$ transition bands. Irradiation at 365 nm produced PSS with high contents of *cis* (68-95%). However, due to a blue-shift of the *n*→π* band of the *cis* and the π→π* of the *trans* isomer after oxidation, the optimal window for the irradiation was also shifted (*i.e.* irradiation wavelength = λ_{max}), resulting in decreased photoconversions for sulfoxide and sulfone **66a** and **66b** after 365 nm irradiation.

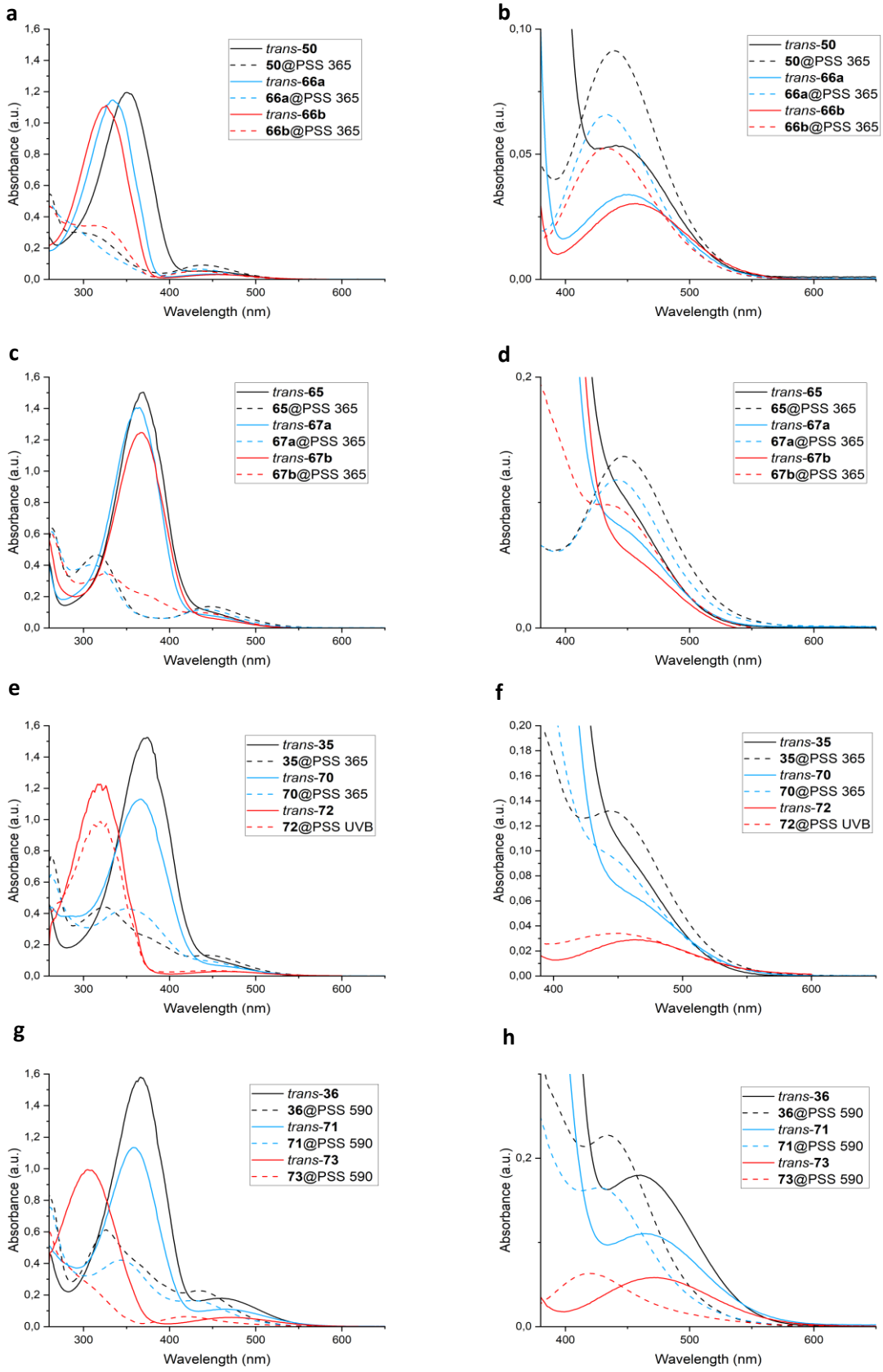

Figure 3.1. Overlays of absorption spectra and corresponding expansions in the area of the $n \rightarrow \pi^*$ transitions for compounds **50**, **66a**, and **66b** (a, b), **65**, **67a**, **67b** (c,d), **35**, **70**, and **72** (e, f), **36**, **71**, and **73** (g, h); solid lines: *trans* isomers, dashed lines: *cis*-rich PSS after irradiation for 2–20 min at an appropriate wavelength; spectra were recorded in DMSO (50 µM) at 25 °C.

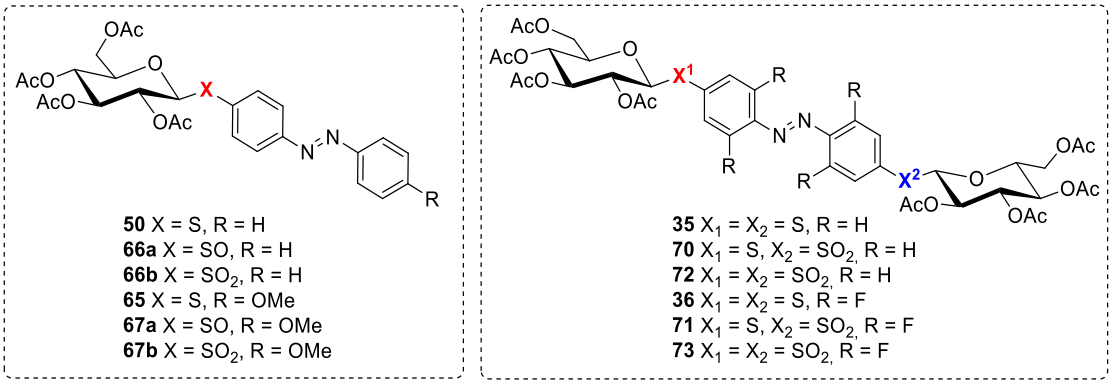

50 X = S, R = H
66a X = SO, R = H
66b X = SO_2, R = H
65 X = S, R = OMe
67a X = SO, R = OMe
67b X = SO_2, R = OMe

35 $X_1 = X_2$ = S, R = H
70 X_1 = S, $X_2 = SO_2$, R = H
72 $X_1 = X_2 = SO_2$, R = H
36 $X_1 = X_2$ = S, R = F
71 X_1 = S, $X_2 = SO_2$, R = F
73 $X_1 = X_2 = SO_2$, R = F

Table 3.1. Spectroscopic data of selected AB thioglycosides: maxima (λ_{max}) of π→π* and *n*→π* transitions of *trans* and *cis* isomers,[a] with the corresponding separation of the n→π* bands ($\Delta\lambda_{n\rightarrow\pi^*}$) in each isomeric state, composition of the photostationary state (PSS) mixtures at different wavelengths of irradiation[b] and half-lives of thermal relaxation.[c,d]

Entry	Compound	λ_{max} π→π* *trans* [nm]	λ_{max} *n*→π* *trans* [nm]	λ_{max} *n*→π* *cis* [nm]	$\Delta\lambda_{n\rightarrow\pi^*}$ [nm]	PSS 365 nm[b]	PSS 435 nm[b]	PSS 520 nm[b]	PSS 590 nm[e]	$t_{1/2}$ *cis*
1	**50**	351	441	439	2	5/95	78/22	-	-	10 h
2	**66a**	334	451	434	17	10/90	84/16	-	-	20 h
3	**66b**	327	453	432	21	32/68	87/13	-	-	2.1 h
4	**65**	370	ND	447	-	3/97	57/43	75/25	88/12[d]	2.6 h
5	**67a**	365	ND	441	-	3/97	67/33	78/28	85/15[d]	4.0 h
6	**67b**	368	ND	433	-	9/91	73/27	73/27	88/12[d]	31 min
7	**35**	374	ND	445	-	14/86	74/26	82/18	95/5[d]	3.0 h
8	**70**	366	ND	ND	-	31/69	86/14	80/20	86/14[d]	1.4 h
9	**72**	317	464	ND	-	-	-	-	-	-
10	**36**	369	460	433	27	20/80	80/20	30/70	16/84[d]	100 h
11	**71**	358	464	429	35	32/68	86/14	32/68	8/92[d]	93 h
12	**73**[f]	310	472	423	49	97/3	91/9	28/72	9/91[d]	31 min

[a] UV-Vis spectra were recorded in DMSO (50 µM) at 25°C; ND: not determined because of the overlap between the π→π* and n→π* transition bands; [b] composition at the PSS were measured by NMR (600 MHz, 300 K) in DMSO-d_6 (1 mM), after 2 min irradiation at the appropriate wavelength; mixtures at the PSS are given as %(trans)/%(cis); [c] the half-lives of cis isomers were measured by UV-Vis spectroscopy in DMSO (50 µM) at 40 °C; [d] For compounds **36** and **71**, thermal relaxation parameters were measured at 65, 70, 75 and 80 °C, then an Arrhenius plot provided the corresponding rate constant and half-life at 40 °C; [e] after 2 min irradiation with UV (365 nm) or green (520 nm) light, the sample was irradiated for 5-20 min with orange (590 nm) light; [f] PSS were measured by NMR (600 MHz, 300 K) in MeCN- d_3 (1 mM) after 2 min irradiation at the appropriate wavelength.

In contrast, the photoconversion for the *cis*→*trans* isomerization was improved upon oxidation. This is due to a concomitant blue shift of the *n*→π* band of the *cis* isomer and a red-shift of the *n*→π* band of the *trans*, resulting in a better separation (Figure 3.1b). However, the separation remains insufficient to achieve *trans*→*cis* isomerization with visible light. The thermal relaxation rate of the *cis* isomer was also strongly impacted by the oxidation state of the sulfur atom. The half-life of *cis*-**66b** (2.1 h) was found to be 5 times smaller than for **50** (10 h), while the half-life of the sulfoxide *cis*-**66a** (20 h) was two-fold higher (Table 3.1, entries 1-3). The increase of the half-life upon oxidation to the sulfoxide is somehow intriguing, and further studies on sulfenyl- and sulfinyl-AB derivatives are required to explain this behavior. Yet, enantiopure *ortho* and *meta*-substituted *p*-tolylsulfinyl-AB derivatives were shown to exhibit chiroptical properties and slow thermal relaxation, making glycosulfinyl-AB derivatives interesting to investigate further.[276]

Compared with *mono*-substituted AB-thioglucoside **50**, the π→π* band of *trans p´*-methoxy-AB-thioglucoside **65** was red-shifted by 19 nm, and the half-life the corresponding *cis* isomer was reduced (2.6 h *vs* 10 h), as expected from the addition of an opposite electron donating substituent in the *p´* position (Table 3.1, entry 4, Figure 3.1c). The *n*→π* of *cis*-**65** was also bathochromically shifted to a lesser extent (*Δλ* = 8 nm), which decreased the separation between the π→π* band of *trans* and the *n*→π* of the *cis* (*Δλ* = 77 nm). However, a nearly quantitative *E*→*Z* conversion was achieved after irradiation with 365 nm light, owing to the fact that the main transition of *trans*-**65** is more centered on the excitation wavelength, thus matching better the optimal irradiation window. In line with what was observed for compounds **50**, **66a** and **66b**, the oxidation to the sulfoxide and sulfone resulted in an increasing blue-shift of the *n*→π* band of the *cis* isomer (Table 3.1, entries 4-6, Figure 3.1d). However, the π→π* bands of *cis* and *trans*-**65** behaved differently. The π→π* band of sulfoxide **67a** was blue-shifted compared to **65** (*Δλ* = 5 nm), but in a lesser extent than **66a** compared to **50** (*Δλ* = 17 nm), and sulfone **67b** was red-shifted compared to **67a** (*Δλ* = 3 nm). The same effect was observed on the π→π* bands of the *cis* isomers of **65**, **67a** and **67b** (Figure 3.1c). This indicates that the augmentation of the polarization of the N=N double bond counterbalances the effect of electron depletion on the position of the π→π* bands. In other words, while the energy of the π orbital is reduced upon oxidation which increases the ππ* gap in **66b**, the higher polarization of the azo bond in **67b** increases its single bond character and thus decreases the energy of the π* orbital, hence reducing the energy difference between π and π* orbitals. This observation is in agreement with what would be expected from a push-pull substitution pattern. Compounds **65**, **67a** and **65b** all showed excellent photoconversion at 365 nm (>90%), however with the same propensity to decrease upon oxidation due to the blue-shift of the *cis* *n*→π* band. Moderate to good photoconversions (57-88%) were obtained after visible light irradiation up to 590 nm. Interestingly, at 590 nm, the kinetics of irradiation were slower, and longer irradiation times were required to reach the PSS. The use of light of low energy (i.e. orange-NIR) is beneficial for using azobenzene conjugates in biological studies. Although the molar extinction coefficient in the near red range is quite weak, such effective photoisomerization performed by addressing the tail of the *n*→π* band was already reported in case of *ortho*-substituted azobenzenes.[156b,321-322] This property might be interesting to exploit, because azobenzenes having different kinetics of irradiation at a given wavelength can then be switched in a selective manner (cf chapter 5). The half-life of compounds **65**, **67a** and **67b** followed the same trend as the *mono*-substituted AB conjugates, which is somehow surprising given that push-pull substitution is known for reducing the thermal stability of ABs in a higher extent than other substitution patterns (*vide infra*). Indeed, the reduced double bond character in **67b** compared to **66b**, which manifests by a red-shift of the π→π* band upon oxidation from sulfoxide to sulfone, a feature not observed in the *mono*-substituted series, would indicate that the half-life of metastable sulfone **67b** would be more strongly impacted than that of **66b** compared to the parent sulfides **50** and **65**. In contrast, oxidation from sulfide to sulfone results in both series in a 5-fold reduction of thermal stability of the *cis* isomer.

The *bis*-thioglucoside **35**, compared to **65**, showed a reduction of the gap between the π→π* and *n*→π* bands of the *trans* and *cis* isomers respectively (*Δλ* = 71 nm), which resulted expectedly in a reduced isomerization yield (86% *vs* 98%) after irradiation at 365 nm (Table 3.1, entry 7, Figure 3.1e). Interestingly, despite the red-shift of its π→π* band, *cis*-**35** had a longer half-life than **65** contrarily to what is usually observed. In fact, the red-shift of the π→π* band through substitution is generally associated with a reduction of the thermal stability. These effects might arise from the difference in electronegativity between the two chalcogen atoms, and a reduced orbital overlap between the sulfur lone pairs and the benzene ring (Figure 3.2a). In line with what was observed for **67b**, oxidation of one sulfur atom to give the mixed conjugate **70**, resulted in a slight hypsochromic shift (*Δλ* = 8 nm) of the *trans* π→π* and a reduced photoisomerization yield (69% *vs* 91% for **35**) at 365 nm (Table 3.1, entry 8, Figure 3.1e,f). Variations of the *n*→π* bands for compounds **35** and **70** cannot be properly observed

due to a strong overlap with the π→π* band. However, the trend observed so far seems to also apply in this case, and good to excellent *cis*→*trans* isomerization yields (74-95%) were obtained with visible light up to 590 nm. C*is*-**70** relaxed nearly twice as fast as *cis*-**35**, whereas the half-life of *cis*-**67b** was reduced by a factor 5 compared to *cis*-**65**. This, associated to the larger blue-shift of the *trans* π→π* band after oxidation (8 nm *vs* 2 nm), is in agreement with a reduction of the polarization of the N=N double bond, due to the lower overlap of the sulfur *p* orbitals with the benzene rings compared to oxygen. Oxidation of all sulfur atoms as in **72** (Table 3.1, entry 9, Figure 3.1e,f), caused a dramatic blue-shift of the π→π* of the *trans* isomer ($\Delta\lambda$ = 57 nm) compared to **35**, and a substantial red-shift of its *n*→π* (λ = 469 nm), as could be expected from the observation of **50** and **66b**. This compound was however unresponsive to UV-Vis light, and only scarce changes were observed after irradiation with UV-B (280-315 nm), in agreement with previous reports on *p,p´-bis*-sulfonamides.[323]

Tetra-*o*-fluorinated conjugates **36** and **71** exhibit similar properties as their non-fluorinated counterparts **35** and **70** (Table 3.1, entries 10 and 11, Figure 3.1g,h). A decrease of the gap between the π→π* of the *trans* and the *n*→π* of the *cis* affected the photoconversion of **36** at 365 nm compared to **35**. However, the increased separation between the *n*→π* of both isomers ($\Delta\lambda_{n\rightarrow\pi^*}$ = 27 nm and 35 nm for **36** and **71** respectively) allowed selective switching with visible light only, in agreement with previous reports.[154,321] Therefore, irradiation with green to orange-light effected the *trans*→*cis* isomerization in good yields (68% and 92%), while the reverse reaction was effected with 435 nm light (80% and 86%). As observed before, oxidation of one sulfur atom decreased the photoconversion of **71** at 365 nm compared to **36** (68% *vs* 80%), whereas the increased separation of the *n*→π* bands of each isomer in **71** afforded better *cis*→*trans* isomerization yields with visible light (86% *vs* 80% at 435 nm, 92% *vs* 84% at 590 nm). In addition, compared to non-fluorinated *bis*-glycosides, the direction of switching for **36** and **71** with green to orange-light was opposite, as a result of the large red-shift of the *trans n*→π*, which then passed beyond the *cis n*→π* (Figure 3.1f,h). The half-life of *cis*-**36** was also exceptionally improved compared to *cis*-**35** (100 h *vs* 3.0 h), and the mixed conjugate **71** was only slightly less stable than **36** (93 h). Interestingly, the influence of the push-pull substitution on the thermal stability was again reduced, presumably reflecting a lower polarizability of the N=N double bond due to the four fluorine atoms acting as electron sinks, and reducing the influence of *para* substituents. With the most blue-shifted π→π* band (λ = 310 nm) and the largest separation of its *n*→π* bands ($\Delta\lambda$ = 49 nm), disulfone **73** showed the best photoswitching performances (Table 3.1, entry 12, Figure 3.1g,h). Excellent photoconversions in both directions were obtained with light of 365, 435 and 590 nm (91-97%). With green-light however, **73** had similar conversions as **36** and **71**. Indeed, the more the excitation wavelength is close to the isobestic point between the respective *n*→π* bands of the *cis* and *trans* isomers, the less selective the switching. Strikingly, *cis*-**73** was found to relax over 190-fold faster than *cis*-**36** and as fast as **67b**.

Comparison of these newly synthesized AB glycoconjugates with previously studied sulfur containing ABs allows a qualitative interpretation of their photochromic behavior (Table 3.2). Compared to *p*-thiomethyl-AB and *p,p´*-dithiomethyl-AB, compounds **50** and **35** exhibit blue-shifted (≈ 10 nm) π→π* transitions for the *trans* isomer (Table 3.2, entries 1 and 2).[324] It was shown that tertiary thioalkyl substituents produce a substantial blue-shift of the main transition compared to primary and secondary thioalkyl groups (Table 3.2, entries 3-6). This is due to a conformational restriction favoring a geometry in which the C=C-S-CR_3 dihedral angle is close to 90 °, that is with the C-S-C plane orthogonal to the benzene ring.[325] This conformation prevents the lone pairs of the S atom from conjugation with the aromatic system, resulting in a more energetic π→π* transition. In contrast, primary and secondary thioalkyl groups can adopt a coplanar conformation, allowing interactions between the *p* orbitals of the sulfur and the benzene ring (Figure 3.2b). In AB-thioglycosides, the coplanar conformation should be possible, hence the observed blue-shift has presumably an electronic origin. Indeed, thioglycosides are thioacetals, and as such, the electronic density of the sulfur is

reduced compared to alkyl sulfides, owing to inductive effects as well as negative hyperconjugation (*i.e. exo*-anomeric effect).

Table 3.2. Spectroscopic data of previously studied sulfur containing *p*- and *p,p´*-substituted ABs: maxima (λ_{max}) of π→π* transition of the *trans* isomer, and half-lives of thermal relaxation.

Entry	*p*-	*p´*-	Solvent	λ_{max} (π→π*)	$t_{1/2}$ *cis* (*T* °C)	Ref.
1	SMe	H	EtOH	362	-	324
2	SMe	SMe	EtOH	380	-	324
3	SMe	HO_2C	[a]	385	0.42 h (60)	325
4	S(*i*-Pr)	HO_2C	[a]	388	0.58 h (60)	326
5	$SCH(i\text{-}Pr)_2$	HO_2C	[a]	394	0.59 h (60)	326
6	S(*t*-Bu)	HO_2C	[a]	343	-	326
7	O(*n*-Bu)	NO_2	$CHCl_3$	384	24 min (25)	327
8	SMe	NO_2	$CHCl_3$	406	-	327
9	$N(n\text{-}Bu)_2$	NO_2	DMSO	513	≈ 1.5 ms (25)[b]	328
10	$N(n\text{-}Bu)_2$	SO_2CH_3	DMSO	475	≈ 1 s[c]	328
11	$O(CH_2)_5P(O)OEt_2$	SO_2CH_3	EtOH	362	-	329

[a] The ABs in this study were conjugated to DNA strands to photo-regulate its hybridization. Solution conditions: 100 mM NaCl, 10 mM phosphate buffer pH = 7.0; [b] The half-life corresponds to that of *p*-diethylamino-*p´*-nitroAB in DMSO at 25 °C from ref. 330; [c] The half-life corresponds to a *p*-diethylamino-*p´*-sulfonyl(cyclohexyl)urea-AB from ref. 331.

An examination of push-pull substituted ABs with different acceptor and donor substituents also sheds some light on the effects of mixed O/SO_2 and S/SO_2 substitution patterns. It is striking that the sulfonyl group, despite being apparently a stronger electron-withdrawing group than a nitro or carboxylic acid group,[332] produces smaller bathochromic shifts of the π→π* transition (Table 3.2, entries 7 *vs* 11 and 9 *vs* 10, compound **67b** *vs* entry 7).

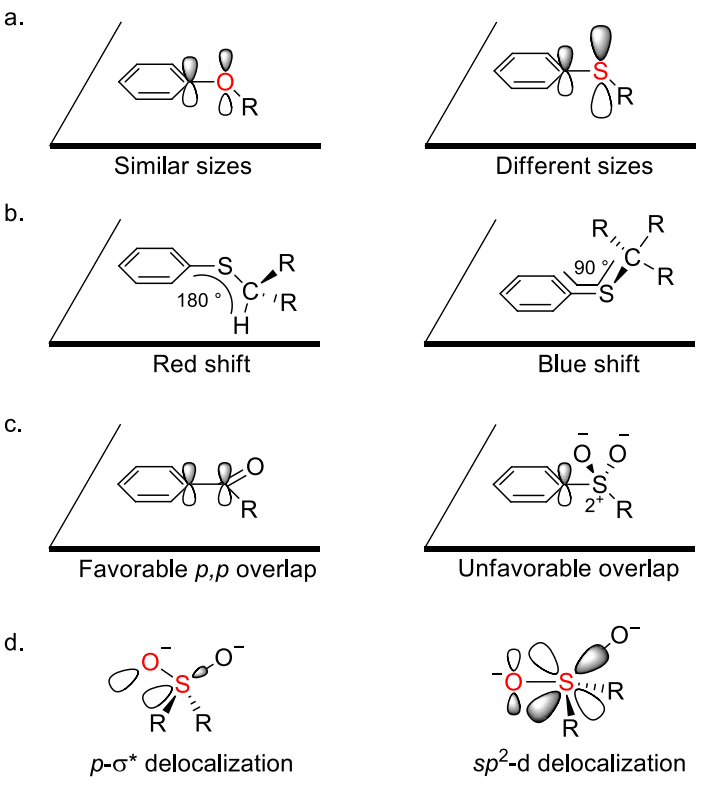

Figure 3.2. Representation of stereoelectronic effects in differently substituted aromatic systems, and in the sulfonyl group.

This is due to several factors regarding the electronic structure of the sulfonyl group and the possible stereoelectronic interactions it offers. First, the sulfonyl group is tetrahedral, which is not favorable for π conjugation (Figure 3.2c). Second, the S-O bonds are not double bonds, but rather coordinate covalent single $S^{+}\rightarrow O^{-}$ bonds.[333] This means that the double bond character of the S-O bond results from the sum of different stereoelectronic interactions such as *p–d* and sp^{x}*–d* delocalization, or negative hyperconjugation (Figure 3.2d). Indeed, the sulfonyl group possesses regions of highly positive potential in the extension of the σ S-O bond (*i.e.* σ* orbital), called σ-holes, which account for the efficient stabilization of vicinal negative charges through negative hyperconjugation.[334] Therefore, the sulfonyl group is an excellent stabilizer of negative charges in α position *via* stereoelectronic effects, but a poor mesomeric acceptor since it cannot establish *p–p* conjugation.[335] This is reminiscent of the studies on sulfonyl ylides,[336] where the adjacent carbanion was shown to keep an sp^3 hyrbidization.[337] As a consequence, in contrast to planar sp^2 hybridized groups such as nitro or carbonyl, the sulfonyl group cannot create a formal double bond with the *para* carbon of the benzene ring, which reduces the contribution of the zwitterionic hydrazoquinone form. This results in a reduced polarizability of the azo bond, thus a stronger double bond character, and hence a smaller red-shift of the π→π* transition and a longer half-life are observed.

Finally, the photochromism of the diazocine *bis*-glycoconjugate **41** was also assessed in DMSO. The representative absorption spectra are shown in Figure 3.3 and Table 3.3 lists the main photochromic features of **41**.

Table 3.3. Spectroscopic data of diazocine conjugate **41**: maxima (λ_{max}) of *n*→π* transitions of *trans* and *cis* isomers,[a] with the corresponding separation of the *n*→π* bands ($\Delta\lambda_{n\rightarrow\pi^*}$) in each isomeric state, composition of the photostationary state (PSS) mixtures at different wavelengths of irradiation[b] and half-life of thermal relaxation.[c]

λ_{max} *n*→π* *cis* [nm]	λ_{max} *n*→π* *trans* [nm]	$\Delta\lambda_{n\rightarrow\pi^*}$ [nm]	PSS 400 nm	PSS >500 nm[d]	$t_{1/2}$ *trans*
407	497	90	71:29	>1:99	22 min

[a] UV-Vis spectra were recorded in DMSO (50 µM) at 25 °C; [b] composition at the PSS were measured by NMR (600 MHz, 300 K) in DMSO-d6 (1 mM), after 2 min irradiation at the appropriate wavelength; mixtures at the PSS are given as %(trans)/%(cis); [c] the half-life of *trans*-**41** was measured by UV-Vis spectroscopy in DMSO (50 µM) at 40 °C; [d] irradiations at 520, 590, 630, 660 and 690 nm were achieved, leading to a quantitative recovery of *cis*-**17** in each case.

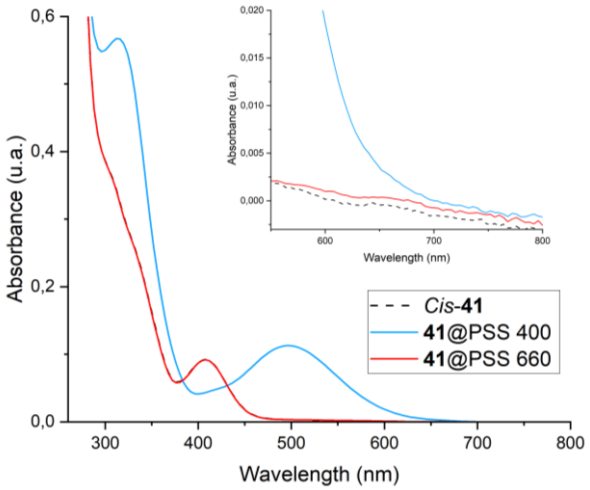

Figure 3.3. Representative absorption spectra in the area of the *n*→π* transitions for diazocine conjugate **41**; inset: expansion in the 600–800 nm area; dashed black line: ground state, blue line: PSS after 2 min irradiation at 400 nm, red line: PSS after 30 s irradiation at 660 nm; spectra were recorded in DMSO (100 µM) at 25 °C.

Irradiation at 400 nm produced a PSS contraining 71 % of the *trans* isomer while *cis*-**41** was quantitatively regenerated upon exposure to visible light (λ>500 nm), or *via* thermal relaxation with a

half-life of 22 min at 40 °C. Interestingly, the *trans*→*cis* photoisomerization process can also be achieved quantitatively with red-light (660 nm, Figure 3.3) and even with far red-light (690 nm), though longer irradiation time was necessary in the last case. Until now, only red-shifted diazocines containing a heteroatom in the bridge showed similar features.[160,161a] Hence, this new thioarylation approach allows the straightforward preparation of functional and red-light-switchable diazocines in only three steps.

3.6. Selective switching of AB-conjugates pairs in mixtures

Based on the photoisomerization results described above, two pairs of azo derivatives, **35**/**73** and **41**/**73** were investigated in orthogonal switching experiments. Orthogonal photoswitching is of great interest to control distinct parameters with the use of light only.[325,326,338] However, achieving full orthogonality (i.e. four state switching) with only azoderivatives is challenging due to overlaps between the absorption bands of the respective switches,[339] and systems solely fueled by light require fine-tuning of irradiation conditions.[338] Hence equimolar solutions of the two selected pairs were investigated by NMR spectroscopy, and their switching with light of three different wavelengths was assessed (Figure 3.4).

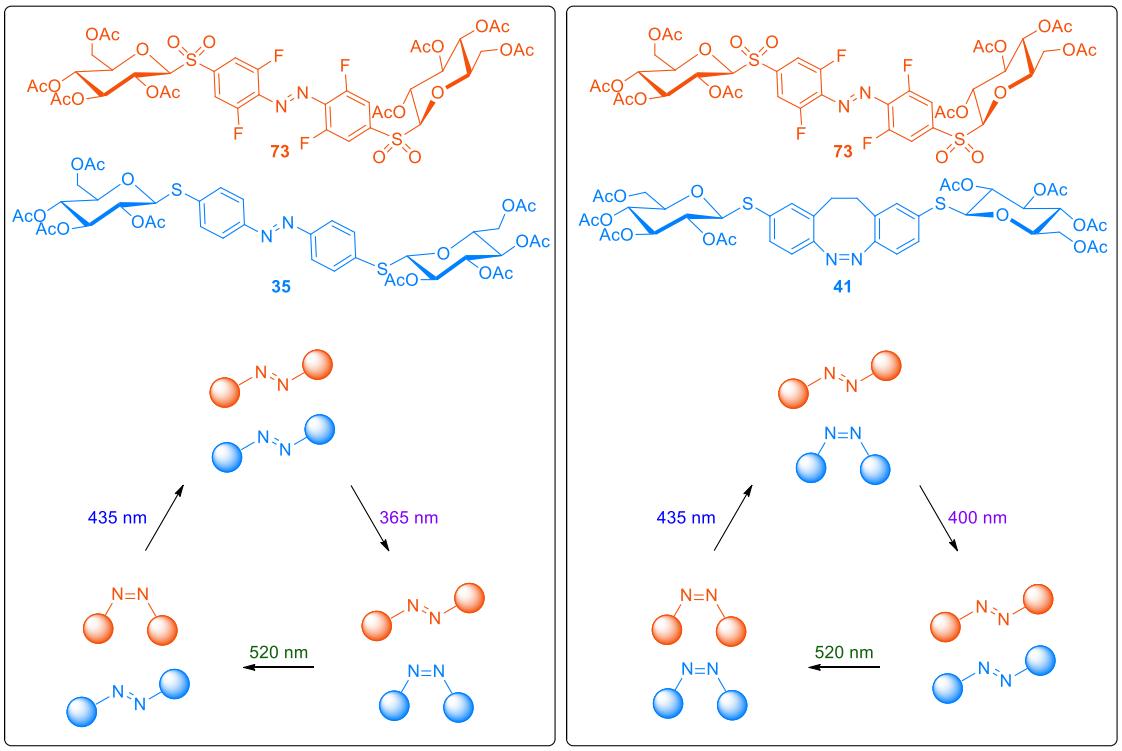

Figure 3.4. Orthogonal photoisomerization of azobenzene or diazocine glycoconjugates in solution mixtures with light of three distinct wavelengths. Two pairs of conjugates were investigated: **35**/**73** and **41**/**73**.

In case of the pair **35**/**73**, switching between *trans*/*trans*, *cis*/*trans*, and *trans*/*cis* states were expected, while the pair **41**/**73** would provide *cis*/*trans*, *trans*/*trans* and *cis*/*cis* states. By applying light in the near UV – green range, it was possible to reach PSS mixtures with over 70% of the major isomer for each of the two compounds (Table 3.4). The *trans*/*cis* ratios observed in each PSS were very similar to those measured with the single molecules, indicating that at the chosen concentration, the switching of one conjugate does not affect the performances of the other in a mixture. It is worthy to note that using the temperature as an additional stimulus is an efficient way to effect selective relaxation in mixtures with AB derivatives with different thermal stabilities.[211,217] For example, with the pair **36**/**73**, starting from the *trans*/*trans* ground state, irradiation at 590 nm would provide the *cis*/*cis* state. Then,

relaxation of **73** (200 fold quicker than **36**) would provide the *cis*/*trans* state. However, even in this case, the generation of the fourth *trans*/*cis* state seems challenging.

Table 3.4. Isomer ratios measured by ^{1}H NMR spectroscopy of equimolar mixtures of **35**/**73** and **35**/**41**, respectively, in d_3-MeCN (1 mM, 300 K), after irradiation with light of 365 nm, 400 nm, 435 nm or 520 nm.

Mixture	365 nm	400 nm	435 nm	520 nm
35 *trans*:*cis*	17:83	–	78:22	78:22
73 *trans*:*cis*	97:3	–	90:10	27:73
41 *trans*:*cis*	–	72:28	29:71	> 1:99
73 *trans*:*cis*	–	97:3	91:9	27:73

Another possibility would be the exploitation of the difference in photoisomerization kinetics. Indeed, using the tail of the *n*→π* band, different ABs have different kinetics depending on how red-shifted their transitions are. Therefore, a red-shifted AB derivative could be switched faster and therefore selectively, compared to a blue-shifted AB derivative in the orange-red-light range. For example, diazocine **41** was quantitatively switched to *cis* in less than 30 s at 590 nm while compound **73** needed between 15-25 min of irradiation at the same wavelength to reach the PSS. Therefore, with the pair **41**/**73**, the diazocine conjugate **41** could be selectively switched to *trans* and back to *cis* with light of 400 nm and 590 nm respectively, while **73** stayed mostly in *trans* (Figure 3.5). Unfortunately, no efficient trigger was found to generate the fourth *trans*/*cis* state.

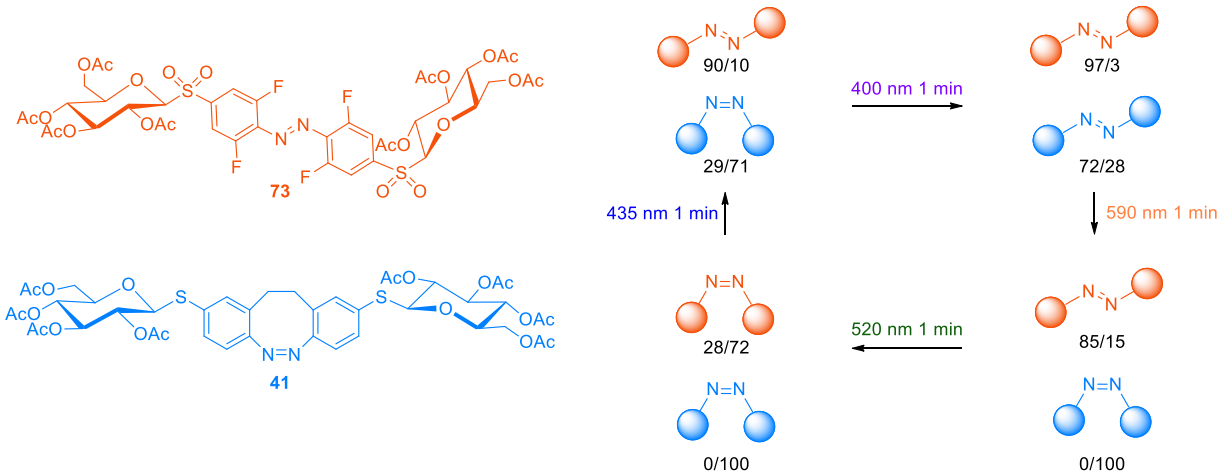

Figure 3.5. Selective switching of diazocine glycoconjugate **41** in the presence of azobenzene derivative **73**.

In conclusion, the palladium-catalyzed thioarylation of halogenated ABs is an efficient and straightforward method to produce functionalized AB-thioglycoconjugates, which photochromic properties may be further tuned by means of sulfur oxidation. Such tuning allowed the generation of different classes of ABs (aminoAB, push-pullAB, red-shifted AB, cyclic AB) with wide thermal stability range and efficient switching properties allowing selective switching in mixtures, with a certain degree of orthogonality. The scope of the reaction was demonstrated to be large in terms of thiol substrates and electrophiles. In addition, the chemoselectivity of the reaction allows hetero-functionalization in a sequential or in a one-pot manner with very good yields. Such versatility enables an easy and efficient modification of the azobenzene core in view of their incorporation in complex molecules that could be used in chemical, material, and biological sciences. In particular, this synthetic approach was successfully used in the synthesis of glycomacrocycles containing two different AB chromophores and capable of selective multistate photoswitching. This work will be described in the next section.

4. Synthesis of glycoazobenzenophanes

The synthesis of macrocycles has drawn a lot of attention in the past century. Indeed, due to their unique pharmaceutical properties,[340] naturally occurring macrocycles have been the targets of many total syntheses,[341] with the macrocyclisation being a critical step.[342] Different approaches may be considered for the cyclization of linear precursors (Figure 4.1). The most obvious one, and perhaps the most difficult, is the "head-to-tail" cyclization which is a unimolecular process where two complementary reactive ends of an open chain precursor react together to form the cycle. With this approach, the formation of large cycles (>12 intracyclic atoms) is rather challenging for several reasons. First, the longer the chain, the less likely the reactive ends are to find themselves in sufficient proximity for the reaction to occur, favoring the formation of linear and cyclic oligomers. In order to overcome this issue, high-dilution conditions are frequently used to favor the unimolecular process over bimolecular ones, however dilution is often impaired with long reaction times. For certain strained linear substrates, this strategy is simply not viable due to geometric constraints that do not allow the formation of monomeric macrocycles (*e.g.* shape persistent phenylene acetylene macrocycles).[343] Such challenges can be addressed by understanding and controlling the preorganization of the linear precursor.[343] One example is for instance the synthesis of crown ethers assisted *via* templation of the linear podand (*i.e.* the polyethylene glycol chain) around a metal cation, allowing the macrocyclization to occur without high-dilution techniques.[344,345] The bimolecular macrocyclization also confers more control on the molecular organization in view to improve the yield of annulation. In this approach, both fragments may be designed in a way that their lengths match, with restricted conformational freedom, so as to augment the probability of reaction between the reactive ends in a bimolecular fashion.

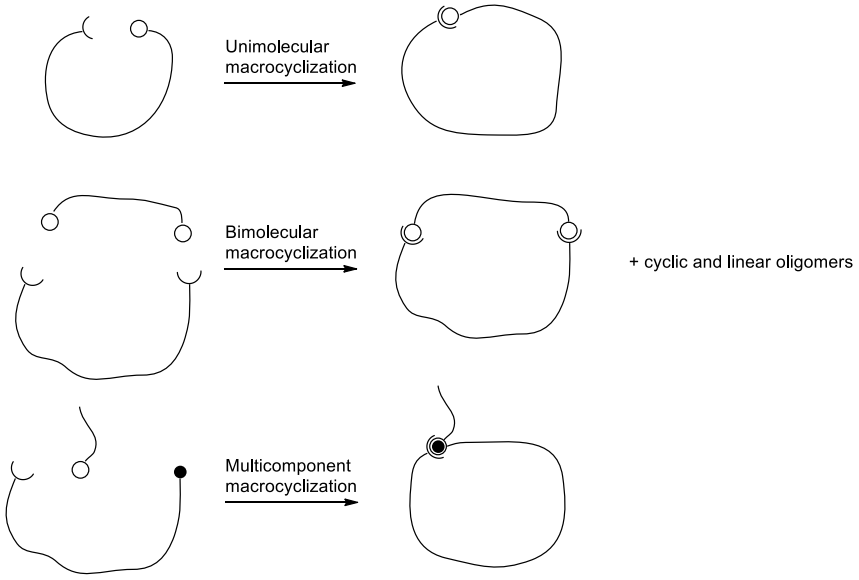

Figure 4.1. Different approaches towards the synthesis of macrocycles.

This approach was used by Despras *et al*. for the cyclization of AB-*bis*-glucoside and maltoside bearing isothiocyanate groups on the 6 and 6´ positions respectively, with piperazine, *via* thiourea ligation. The cyclization only occurred when the linear AB precursor was switched to the *cis* form, providing the desired macrocycles in 48 to 71% yield.[268e] This shows how important the configurational and conformational preorganization of the substrate is critical in the success of the cyclization, and controlling these parameters is essential in the synthesis of highly strained structures.[346] Another example is the chloride templated synthesis of sucrose-based thiourea bridged macrocycle by Jarosz *et al*., with an outstanding yield of 90%.[347] In this example, the ring closure which is the limiting step, was facilitated by the coordination of a chloride ion to the first formed thiourea function and the second unreacted amine, favoring a cyclic arrangement.

Multicomponent reactions (MCRs) are also powerful tools for the synthesis of macrocycles.[348] These reactions which involve more than two reactive partners, often proceed *via* coordinated transition states (hydrogen bonds, stereoelectronic interactions, metals…), and at low concentration, the preorganization of the reactive ends to form a cycle is facilitated. On another hand, MCRs have enabled the generation of high molecular diversity, and allow the incorporation of reactive handles or activable groups during the cyclisation step. Especially, multiple MCRs with bifunctional building blocks have allowed the synthesis of many macrocyclic peptoids incorporating biarylethers and steroids, generating a great diversity by using different amines in one-pot reactions.[347b] The most used MCRs for macrocycle synthesis are certainly the Ugi, the Passerini and the Mannich reactions.

Due to the prevalence of ester and amide bonds in naturally occurring macrocycles, macrolactonization and macrolactamizations have been extensively used, which led to considerable methodological developments.[349] However, a plethora of different reactions may be used, depending on the chosen retrosynthetic disconnections. Cyclization *via* C-C bond formation may be achieved efficiently by ring closing metathesis (RCM),[350] palladium catalyzed coupling[351] or using carbonyl-ylide chemistry.[352] C-X bonds are usually formed by nucleophilic substitution, acylation or palladium catalyzed arylation reactions.[342,349] Finally, annulations through click chemistry[353] or thiourea ligation[268e,347] have also shown excellent results.

The synthesis of azobenzenophanes especially, was achieved according to many different procedures depending on the type of bond formed in the final cyclization step.[204a] When the moiety linking the azo units contains heteroatoms, nucleophilic substitution,[142,206,279] condensation reactions,[354] or thiocarbonyl chemistry[268e,347] may be used. However, when aliphatic linkers are employed, the formation of the azo-bond as final cyclisation step might sometimes be the only viable option.[210] In a lesser extent, the diazo-coupling[355] or the palladium catalyzed *N*-arylations of arylhydrazines followed by oxidation[356] were also used to form azobenzenophanes. However, the synthesis of azobenzenophanes is frequently impaired with low yields,[204a] and the development of new synthetic methods to access them is important.

In this thesis, two different strategies were employed for the synthesis of azobenzene containing glycophanes. On the one hand, the thiourea bridging reaction was used with different diamines to explore the scope of the reaction, and to study the influence of the linking chain on the photochromic properties of the resulting macrocycles. On the other hand, the palladium-catalyzed thioarylation reaction discussed in Chapter 3 was exploited towards the fabrication of macrocyclic glycoazobenzene dyads, starting from AB-*bis*-thioglucosides with thiol groups at the primary positions. The results of these cyclizations are detailed herein.

4.1. Macrocyclization *via* thiourea bridging

As the bimolecular thiourea ligation showed good results for the synthesis of glycoazobenzenophanes **3** and **4**, this reaction was further investigated with different diamines (Scheme 4.1). The azide functions in the compound **22a**, obtained by glycosylation with DHAB, were converted to isothiocyanates by a Staudinger/azaWittig reaction.[357] This reaction is an efficient alternative to the use of toxic thiophosgene, allowing the one pot transformation of azides into isothiocyanates. Hence, treatment of **22a** with triphenylphosphine (PPh_3) and carbon disulfide (CS_2) in chloroform at room temperature afforded the desired compound **1** in 84% yield. Then, the obtained diisothiocyanates were engaged in macrocyclization reactions with C_2, C_3 and C_4 alkyl diamines as well as *p*-phenylenediamine. The results are summarized in Table 4.1.

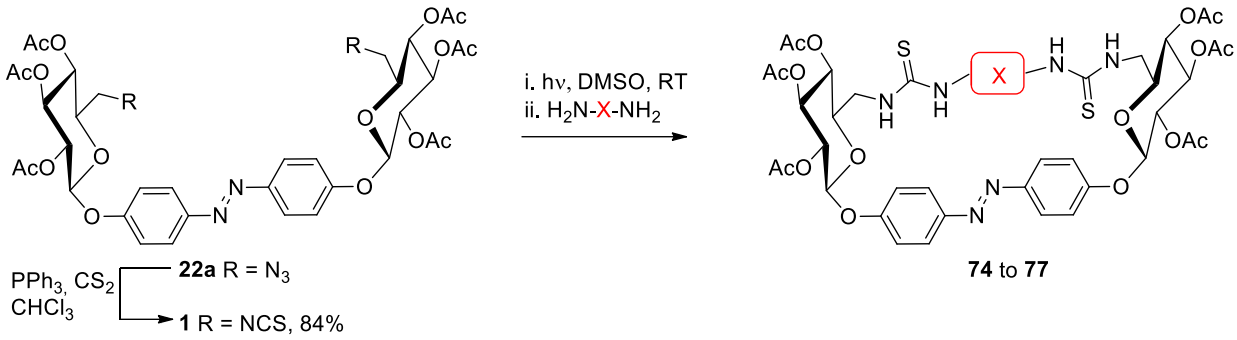

Scheme 4.1. Isothiocyanate formation and subsequent macrocyclization through thiourea ligation.

Table 4.1. Conditions for macrocyclization.[a]

Entry	X (diamine)	Concentration (mM)	Time	Product, yield
1	$(CH_2)_3$	1	1 h	**74**, 82%
2	$(CH_2)_3$	10	1 h	**74**, 69%
3	$(CH_2)_3$	50	1 h	**74**, 53%
4[b]	$(CH_2)_4$	5	1.5 h	**75**, 44%
5	$(CH_2)_4$	1	0.5 h	**75**, 71%
6	$(CH_2)_2$	1	0.5 h	**76**, 53%
7	1,4-C_6H_4	1	5 d	**77**, 56%

[a] All reactions were performed in DMSO at RT. The substrate was first dissolved in DMSO, and irradiated at 365 nm for 10 min. Then a 100 µM solution of the diamine (1.05 eq) was added over 15 min, and the reaction was stirred for the indicated time at RT. [b] A 40 µM solution of diamine was added over 30 min.

In their seminal report, Despras *et al.* performed the macrocyclization in pyridine with 1.05 eq of piperazine at 15 mM.[268e] Based on further practical experience from Dr. Despras, DMSO was chosen as an alternative solvent. Reaction of linear precursor **1** with propylene diamine at a concentration of 1 mM in DMSO provided after 1 h the macrocycle **74** in an excellent yield of 82% (Table 4.1, entry 1). Increasing the concentration to 10 or 50 mM reduced the yield to 69% and 53% respectively (Table 4.1, entries 2 and 3). When butylene diamine was used at a concentration of 5 mM, the desired compound **75** was obtained in 44% yield (Table 4.1, entry 4). In contrast, reaction at 1 mM afforded **75** in 71% yield after 30 min (Table 4.1, entry 5). With ethylene diamine at 1 mM, the macrocycle **76** was isolated in 53% yield (Table 4.1, entry 6). Finally, reaction with phenylene diamine was longer, as expected from a less nucleophilic aromatic diamine. The macrocycle **77** was however obtained in a good yield of 56% (Table 4.1, entry 7). The reaction with propylene diamine gave better yields than with ethylene or butylene diamine in the same conditions. This might reflect a correlation between the macrocyclization efficiency and the length and flexibility of the diamine, as observed in other similar cyclizations.[206] It is quite likely that beyond a certain length, the irradiation might become unnecessary, or even detrimental. The successful ligation with phenylene diamine is encouraging as it allows the incorporation of aromatic motifs in the cycle in view of future developments towards chiroptical molecular receptors.

The deprotection of the synthesized macrocycles **74**-**77** was achieved under Zemplen conditions, however it rendered them insoluble in any solvent but DMSO, and made their isolation very complicated. Only the macrocycle **77** could be isolated after deprotection in 33% yield. The photochromic properties of macrocycles **74**-**77**, which are detailed in Chapter 5, were hence investigated in the acetylated form. Encouraged by these results, glycoazobenzene dyads with different chromophores were synthesized with the intent to achieve selective multistate switching.

4.2. Macrocyclization *via* palladium-catalyzed thioarylation

Based on the study of the photochromic properties of sulfur containing AB-*bis*-glycosides in Chapter 3, it was envisaged to synthesize macrocycles with two AB moieties, connected at the 1 and 6 positions of glucose (Figure 4.2). At the anomeric position, an AB with CH_2 (DMAB) in *para* positions was chosen, and owing to the cyclization method, the AB in position 6 had thioether auxochromes (DSAB). This choice was made so as to have a maximum gap between the $\pi \rightarrow \pi^*$ bands of each chromophore, as well as different photoisomerization and relaxation kinetics, in order to affect each azobenzene in a selective manner. Also, this would allow to oxidize the sulfur bridges in **79** to sulfone to provide **80**, with a minimal effect on the photochromic performances of the DMAB (Figure 4.2). Hence, the switching of the tetrafluoroAB (TFAB) would be possible with visible light only, while the DMAB could be switched with UV-light.

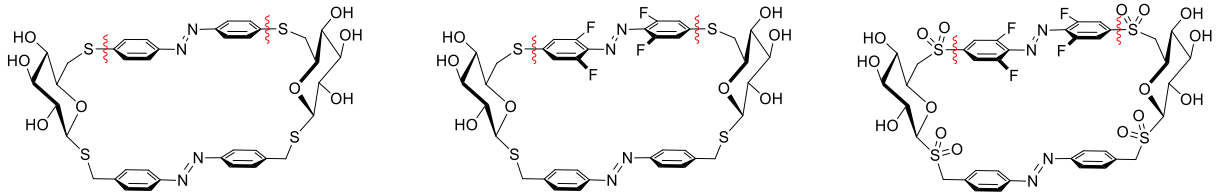

Figure 4.2. Structures of the targeted glycoazobenzenophane dyads **78**-**80**. The retrosynthetic disconnections for the macrocyclization step are shown, highlighting a common dithiol precursor for all cycles.

As shown in Figure 4.2, macrocycles **78**-**80** can all be obtained from a common dithiol precursor. A first synthesis of this compound was examined starting from levoglucosan **16** (Scheme 4.2). Perbenzoylation of **16** in pyridine afforded compound **17** in 95% yield, and subsequent ring opening with (phenylthio)trimethylsilane (TMSSPh) gave **18** in 97% yield. Then, iodine promoted silylation[301] with *tert*-butyldiphenylsilyl chloride (TBDPSCl) followed by bromination of the anomeric center with iodine monobromide (IBr) in dichloromethane afforded **81** in 89% yield over 2 steps. It is noteworthy that the bromide **81** was very stable (no signs of degradation after weeks on the bench), and could therefore be easily purified by column chromatography. Then, reaction with disodium sulfide nonahydrate ($Na_2S.9H_2O$) and carbon disulfide (CS_2) in DMF[358] provided thiol **82** in 73% yield. This very efficient sequence for the preparation of glycosyl thiols with the 6 position differentiated was found to be highly reproducible providing the desired thiol in 56-78% overall yield over 5 steps.[359] Then, the thiol **82** was reacted in presence of triethylamine (Et_3N) with 4,4´-*bis*(bromomethyl)azobenzene **83** in CH_2Cl_2 to give the AB-*bis*-glycoside **84** in 91% yield.

Deprotection of the TBDPS group using the usual TBAF/AcOH/THF conditions led to substantial benzoyl migration. Therefore, the deprotection was achieved in harsh acidic conditions, with acetyl chloride (AcCl) and triflic acid (TfOH) in a mixture MeOH/THF allowing the isolation of the diol **85** in 60% yield.[360] Alternatively, replacement of the TBDPS group by an acetyl group, and subsequent substitution with **83** and deprotection (AcCl in CH_2Cl_2/MeOH) afforded the desired diol **85** in 78% yield over 2 steps. Subsequent mesylation of **85** with mesyl chloride (MsCl) and Et_3N in CH_2Cl_2 gave compound **86** in 93% yield. Then, starting from the diol **85** or the dimesylate **86**, several conditions were explored to install the thiol function at the 6 position. The results are summarized in Table 4.2.

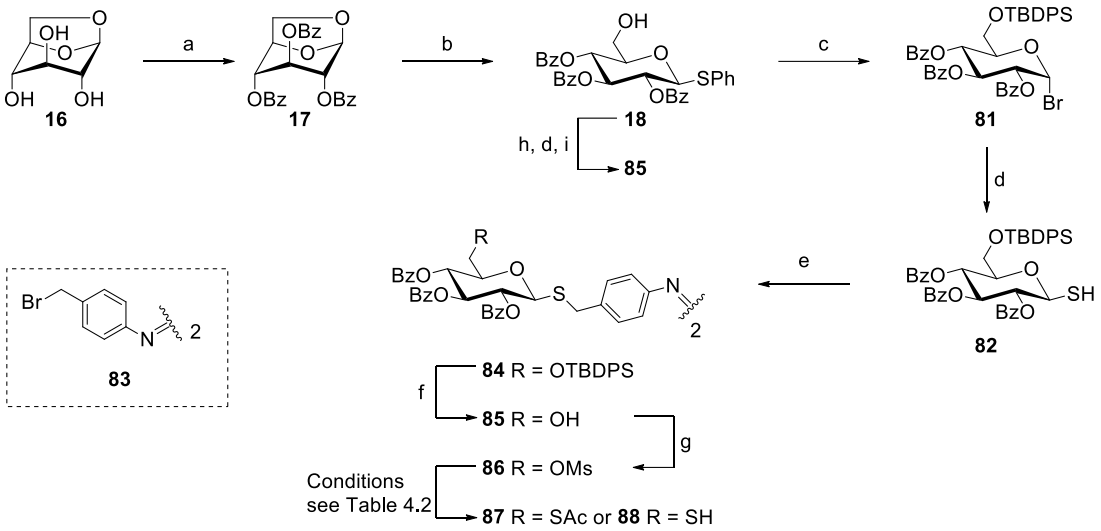

Scheme 4.2. Synthesis of a linear dithiol building block. Reagents and conditions: (a) BzCl (6 eq.), pyridine, 0°C to RT, 95%; (b) ZnI_2 (3 eq.), TMSSPh (2.5 eq.), 1,2-DCE, 85 °C, 97%; (c) TBDPSCl (1.05 eq.), NMI (1.05 eq.), I_2 (0.75 eq.), pyridine, RT then IBr (1.5 eq.), CH_2Cl_2, 0 °C, 89% over two steps; (d) $Na_2S.9H_2O$ (2 eq.), CS_2 (1.5 eq.), DMF, RT, 73%; (e) 4,4´-*bis*(bromomethyl)azobenzene **83** (1 eq.), Et_3N (2.1 eq.), CH_2Cl_2, RT, 91%; (f) AcCl (6 eq.), TfOH (2 eq.), THF/MeOH 1:1, RT, 60%; (g) MsCl (2.2 eq.), Et_3N (2.2 eq.), CH_2Cl_2, RT, 93%; (h) Ac_2O (1.5 eq.), pyridine, RT then IBr (1.5 eq.), CH_2Cl_2, RT, 90% over two steps; (i) **83** (0.5 eq.), Et_3N (2.2 eq.), CH_2Cl_2, RT then AcCl (2 eq.), MeOH/THF/ CH_2Cl_2 1:1:2, RT, 78% over two steps; TBDPSCl = *t*-butyldiphenylchlorosilane; NMI = *N*-methylimidazole; TMSSPh = (phenylthio)trimethylsilane.

First, very mild conditions were applied by reacting dimesylate **86** with Et_3N and thioacetic acid (AcSH) in CH_2Cl_2 (Table 4.2, entry 1), however nothing happened according to TLC analysis. Using potassium thioacetate (KSAc) in DMF gave the same result (Table 4.2, entry 2), and adding potassium iodide produced the desired compound **87** in 25% yield (Table 4.2, entry 3). Increasing the temperature to 70 °C only slightly improved the yield to 33% (Table 4.2, entry 4). Applying conditions for direct thiol formation[358] yielded the dithiol **88** in 30% yield, however this reaction was hardly reproducible and led to substantial degradation (Table 4.2, entry 5). Reaction of AcSH with diol **85** under Mitsunobu conditions did not show any improvement (Table 4.2, entry 6), thus the formation of a ditriflate derivative followed by substitution was envisaged. When the triflate was generated in pyridine (Table 4.2, entry 7), TLC analysis showed the formation of an apolar carbohydrate by-product that did not contain an AB moiety, and formation of a very polar AB derivative. This was rationalized as an intramolecular thioglycoside activation with substitution of the benzylic position by pyridine, yielding a 1,6-thioanhydroglucose derivative and a bipyridinium AB (Scheme 4.3). This is consistent with a study on the DAST mediated C1→C6 migration of anomeric thioaryl/alkyl groups,[361] however the products were not isolated so the hypothesis was not verified. Performing the triflation in CH_2Cl_2 in presence of a non-nucleophilic pyridine base (DTBMP) and subsequent addition of KSAc at RT (Table 4.2, entry 8) or AcSH/Et_3N at -78 °C (Table 4.2, entry 9) did not show any improvement. Given the difficulty of introducing a thiol function *via* nucleophilic substitution in presence of an anomeric thioalkyl group, this synthetic route was abandoned.

Instead it was decided to functionalize adequately the carbohydrate building block, to have the least modifications following the AB substitution (Scheme 4.4). Hence, the position 6 of D-glucose was selectively tosylated in pyridine, and then acetylated in the same pot. Subsequent substitution with potassium thioacetate (KSAc) in acetone provided compound **89** in 89% overall yield. Then, bromination with hydrobromic acid (HBr) followed by sulfidation afforded the thiol **90** in 71% yield. Then, substitution of **83** gave AB glycoconjugate **87´** in 90% yield, which was next *S*-deacetylated with dithiotreitol (DTT) to give the dithiol **88´** in 66% yield.

Table 4.2. Conditions for the introduction of the thiol function in position 6.

Entry	Compound	Conditions	Temperature	Product, yield
1	**86**	AcSH, Et_3N, CH_2Cl_2	RT	-
2	**86**	KSAc, DMF	RT	-
3	**86**	KSAc, KI, DMF	RT	**87**, 25%
4	**86**	KSAc, KI, DMF	70 °C	**87**, 33%
5	**86**	$Na_2S{\cdot}9H_2O$, CS_2, DMF	RT	**88**, 30%
6	**85**	AcSH, PPh_3, DIAD, THF	0 °C to RT	-
7	**85**	i. Tf_2O, pyr, CH_2Cl_2; ii. AcSH	RT	-
8	**85**	i. Tf_2O, DTBMP, CH_2Cl_2; ii. KSAc	RT	-
9	**85**	i. Tf_2O, DTBMP, CH_2Cl_2; ii. AcSH, Et_3N	-78 °C	-

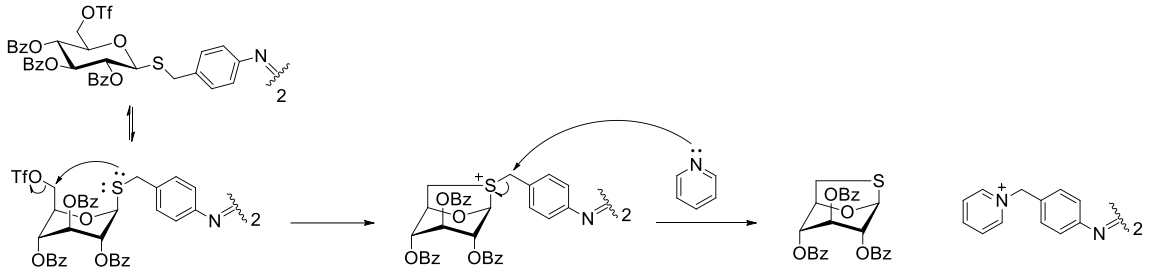

Scheme 4.3. Proposed mechanism explaining the formation of a very polar AB derivative and a colorless carbohydrate by-product.

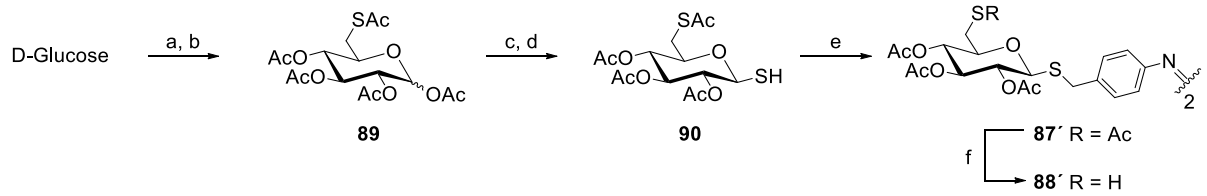

Scheme 4.4. Synthesis a linear dithiol building block from a prefunctionalized glycosyl thiol. Reagents and conditions: (a) TsCl (1.5 eq.), DMAP (0.2 eq.), pyridine, 0 °C to RT, then Ac_2O (10 eq.); (b) KSAc (2.5 eq.), acetone, reflux, 89% over 3 steps; (c) HBr/AcOH, Ac_2O, CH_2Cl_2, 0 °C to RT; (d) $Na_2S.9H_2O$ (2 eq.), CS_2 (1.5 eq.), DMF, RT, 71% over 2 steps; (e) **83** (0.5 eq.), Et_3N (2.2 eq.), CH_2Cl_2, RT, 91%; (f) DTT (6 eq.), Et_3N (1 eq.) DMA, RT, 66%; DTT = dithiothreitol; DMA = dimethylacetamide.

With the dithiol **88´** in hands, the conditions for the macrocyclization were screened and the results are summarized in table 4.3. In a first attempt, the dithiol **88´** was converted to the *cis* form, and reaction with *trans*-diiodoazobenzene **28** at 1 mM afforded satisfyingly the expected product **91**, although in a low yield of 12% (Table 4.3, entry 1). Due to the high dilution, this reaction seemed quite slow, thus the same reaction was performed at 10 mM, which improved the yield to 31% and reduced the reaction time considerably (Table 4.3, entry 2). Pre-irradiation of both substrates showed a great improvement, as the expected product was obtained in 58% yield, although at a concentration of 5 mM (Table 4.3, entry 3). Also, it seemed that mixing both substrates in an equimolar fashion was more efficient that the slow addition of one of the reactants. Therefore, the slow addition of an equimolar solution of dithiol **88´** and AB **28** to a solution of the catalyst and Et_3N was envisaged, but resulted in a slightly lower yield of 50% (Table 4.3, entry 4). Despite the lower concentration in this last reaction, which should favor the cyclization, it seemed that the slow addition was not necessary. Hence, the dithiol, the AB and the catalyst were premixed in the solvent, and the reaction was started by adding Et_3N, which afforded delightfully the expected product in very good yields of 67% at 5 mM and 70% at 2.5 mM (Table 4.3 entry 5 and 6). Increasing the temperature of the reaction decreased the yield to 47% (Table 4.3, entry 7). Interestingly, the yield was better when the substrates were not isomerized (Table 4.3, entry 3 *vs* 5 and 6). In contrast to the reaction of diisothiocyanate **1** with small diamines, both reaction partners have a similar size, and the pre-irradiation of the substrates here seems

unnecessary. With these optimized conditions, the macrocyclization with the diiodo-TFAB **29** was performed. Reaction of dithiol **88´** with **29** proceeded smoothly at 5 mM to afford the desired product **92** in 55% yield (Table 4.3, entry 8). Reducing the concentration or increasing the temperature did not result in any improvement (Table 4.3, entries 9 and 10).

Table 4.3. Conditions for the palladium-catalyzed macrocyclization.[a]

Entry	Azobenzene	Conc. (mM)	Method[b]	Time[c]	Product, yield
1[d]	**28**	1	A	20 h	**91**, 12%
2[d]	**28**	10	A[e]	15 min	**91**, 31%
3	**28**	5	B	30 min	**91**, 58%
4	**28**	2.5	C	5 min	**91**, 50%
5	**28**	5	D	1 h	**91**, 67%
6	**28**	2.5	D	1 h	**91**, 70%
7[f]	**28**	2.5	D	15 min	**91**, 47%
8	**29**	5	D	2 h	**92**, 55%
9	**29**	2.5	D	2 h	**92**, 47%
10[f]	**29**	2.5	D	15 min	**92**, 32%

[a] Cyclizations were performed in THF at RT with stoichiometric amounts of dithiol **88´**, AB and Et_3N, and 10 mol% of PdG_3-Xantphos; [b] **Method A**: A solution of dithiol **88´**, the catalyst and Et_3N was irradiated for 10 min at 365 nm before slowly adding the AB dissolved in THF (within 30 min); **Method B**: A solution of dithiol **88´** and the AB was irradiated for 10 min at 365 nm, then the catalyst and the Et_3N were added; **Method C**: To a solution of the catalyst and Et_3N was slowly added a pre-irradiated equimolar solution of the dithiol **88´** and the AB in THF(within 40 min); **Method D**: To a solution of dithiol **88´**, AB and the catalyst was added Et_3N; [c] Time after the addition; [d] 4 mol% of catalyst were used; [e] the dithiol was irradiated before addition of the catalyst and Et_3N; [f] The reaction was performed in 1,4-dioxane at 50 °C.

The macrocycles **91** and **92** were then deprotected under Zemplen conditions to afford **78** and **79** in 92% and 99% yield respectively (Scheme 4.5). Macrocycle **79** was then subjected to a late-stage oxidation with peroxytrifluoroacetic acid in trifluoroacetic acid (TFA).[362] The oxidation seemed to have worked, however NMR analysis showed a mixture of at least 2 products. It was assumed that over-oxidation of the DMAB in position 1 occurred, and this was confirmed by performing a *m*CPBA-mediated oxidation of AB-*bis*-conjugate **87´**. The reaction afforded a mixture in which the *N*-oxide was observed in mass spectrometry along with the expected AB-*bis*-sulfone. The synthesis of macrocycle **80** was therefore abandoned.

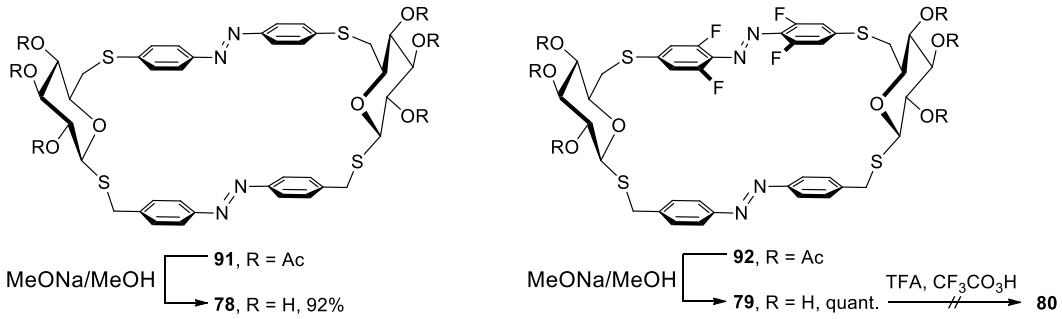

Scheme 4.5. Deprotection of macrocycles **91** and **92**, and attempted oxidation of **92**.

Encouraged by these results, the synthesis of a diazocine-containing macrocycle was achieved (Scheme 4.6) from diiododiazocine **30** (see Chapter 3). The thiol **90** was coupled to **30** in 75% yield, and subsequent *S*-deacetylation with DTT afforded the dithiol **94** in 37% yield. Then the macrocyclization was successfully achieved, affording macrocycle **95** in 26% yield. Given the results detailed in Table 4.3, *cis*-**94** was first irradiated at 405 nm to produce a *trans*-rich mixture prior to cyclization. The obtained macrocycle **95** was characterized in the acetylated form, given the small quantity (5 mg) obtained.

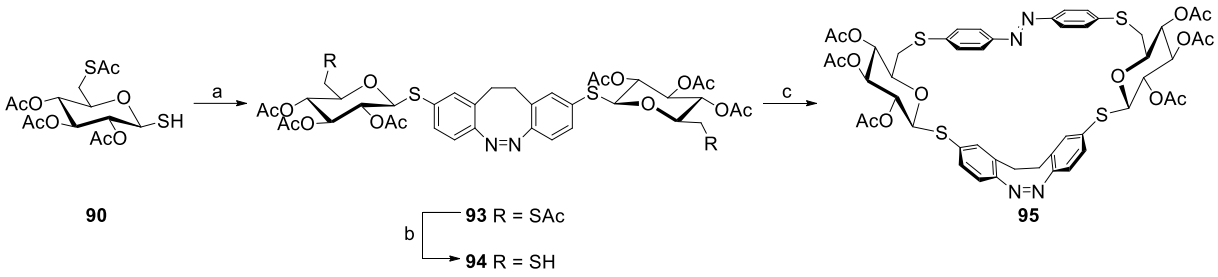

Scheme 4.6. Synthesis of a diazocine containing macrocycle. Reagents and conditions: (a) **29** (0.5 eq.), PdG_3-Xantphos (1 mol%), Et_3N (1eq.), 1,4-dioxane, 80 °C, 75%; (b) DTT, Et_3N, DMA, RT, 37%; (c) i. THF (2.5 mM), 405 nm, 10 min; ii. *p,p´*-diiodoazobenzene **28** (1 eq.), Et_3N (2 eq), PdG_3-Xantphos (10 mol%), RT, 20 min, 26%.

Furthermore, the synthesis of glycoazobenzenophane **79** was attempted starting from the thioarylation in position 6, followed by cyclization through the anomeric position (Scheme 4.6). This would allow to compare the efficacy of cyclization by nucleophilic substitution to the palladium catalyzed annulation. Also it would give access to a variety of different macrocyclic glycoazobenzene dyads in a modular way. Monomethoxytrityl (MMTr) protection was installed on the anomeric position, and subsequent *S*-deacetylation of the 6-position with hydrazine acetate in DMF afforded thiol **96** in 53% yield over two steps. Palladium catalyzed thioarylation with TFAB **29** gave the *bis*-glycoside **97** in 82% yield. Unfortunately, any attempt to cleave the trityl protecting groups produced complex mixtures resulting from migration of acetyl groups. The use of more stable benzoyl groups instead of acetyl groups led to the same result. This route was thus also abandoned.

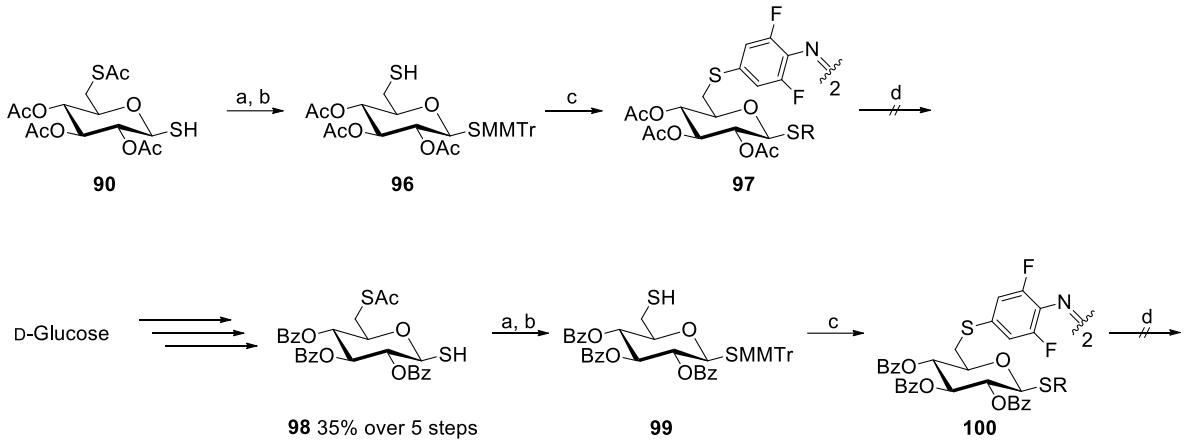

Scheme 4.7. Attempted synthesis of macrocycle **79** starting from the functionalization in position 6. Reagents and conditions: (a) MMTrCl (1.1 eq.), Et_3N (1.1 eq), CH_2Cl_2, RT, 75% from **90**, 83% from **98**; (b) $(H_2N)_2$.AcOH (1.05 eq.), DMF, RT, 70% for **96**, quant. for **99**; (c) *p,p´*-diiodoTFAB **29** (0.5 eq.), Et_3N (2 eq.), PdG_3-Xantphos (2 mol%), THF, RT, 82% for **97**, 97% for **100**; (d) TFA (0.8%), Et_3SiH (1%), CH_2Cl_2, 0 °C; MMTrCl : 4-methoxytrityl chloride.

Finally, three linear AB-*bis*-glycosides containing the same auxochromes as in macrocycles **78**, **79** and **95** were synthesized (Scheme 4.8). Added to the data obtained with diazocine *bis*-glycoside **41** previously studied, their photochromic behavior would provide a good basis of comparison for understanding the properties of the new glycoazobenzenophanes. Thus, the diol **85** obtained earlier was deprotected under Zemplen conditions to afford DMAB-*bis*-glycoside **101** in 73% yield. Then, the thiol **102** was first arylated with diiodoazobenzene **28** and deacetylated to give the DSAB-*bis*-glycoside **103** quantitatively over two steps. The same sequence was applied to **102** and **29** furnishing TFAB-*bis*-glycoside **104** in 75% overall yield.

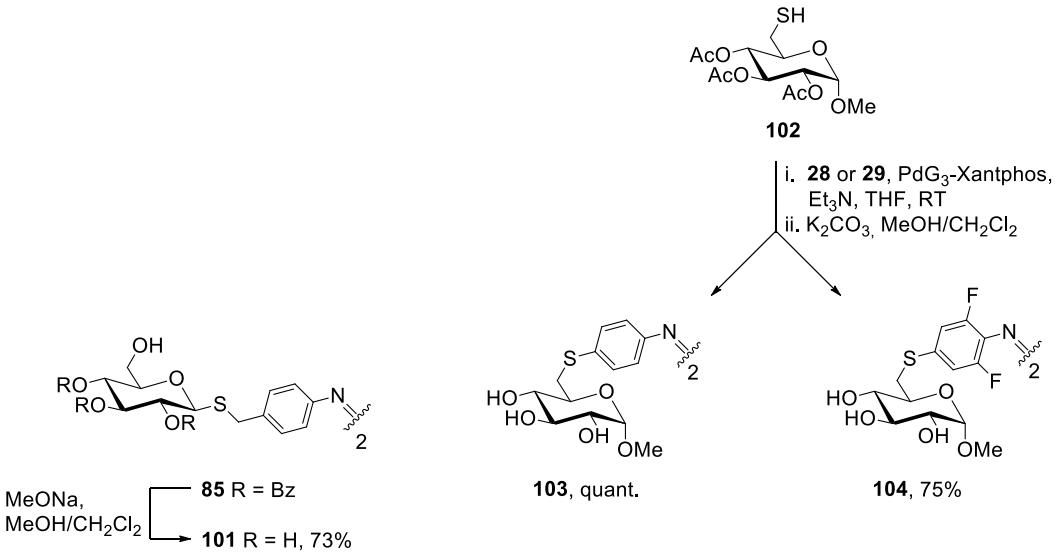

Scheme 4.8. Synthesis of linear AB-*bis*-glycosides **101**, **103** and **104**, based on the photochromes used in glycoazobenzenophanes **78**, **79** and **95**.

In this chapter was demonstrated the outstanding potential of thiourea ligation and palladium catalyzed thioarylation in the synthesis of glycoazobenzene macrocycles in good to excellent yields. Once again, the preorganization principle was exploited in order to achieve the most efficient macrocyclization reactions.[268e,344,346] Six new glycoazobenzenophanes with one or two responsive moieties were prepared. The synthesis of carbohydrate precursors to access them was optimized, and allowed the isolation of target molecules **78** and **79** in 27% and 21% overall yield in 7 steps starting from D-glucose. Finally, the photochromic properties of the synthesized macrocycles were assessed and will be discussed in the next chapter.

5. Photochromic properties of the synthesized AB glycophanes

As mentioned earlier, the introduction of azobenzene moieties into macrocyclic structures results in modifications of their properties. Spectral properties may be altered, as shown by the hyperchromic red-shift of the *trans* $n \rightarrow \pi^*$ and the hypochromic blue-shift of the $\pi \rightarrow \pi^*$ when the planarity of the diazo bond is reduced due to steric effects.[209] The thermostability may also be significantly altered, as shown by the influence of cyclization on the thermal isomerization rates,[142] or the inverted thermodynamic stability of *para*-azobenzenophanes linked with methylene groups,[215] in which the all-*cis* form is the most stable. This means that the relative energy of each isomer can be modified in order to reduce or increase the energy gap between them. Increasing the energy gap (ΔH) means stabilizing the *trans* form and destabilizing the *cis* form, and increasing the thermal relaxation rate means increasing the activation energy (*Ea*) by stabilizing the *cis* isomer and destabilizing the transition state. This approach makes azobenzenophanes interesting for energy storage for example. Indeed, by increasing the gap between the stable and the metastable states (ΔH), and by increasing the thermal stability of the metastable state, considerable amounts of energy could be stored in the chemical bonds of oligoazobenzenophanes, and then released as heat.[202]

In 2013, a theoretical study compared the storage capacities of *para*-methylene-azobenzenophanes with 2 to 6 AB units in the cycle (Figure 5.1).[231] Of course, due to the inverted thermodynamic stability in *p*-methylene-*bis*-azobenzenophanes, the ΔH between the all-*trans* and the all-*cis* form is negative. With 3 AB units, the stable form is the all-*trans*, and the energy stored per AB unit is nearly identic to that of isolated azobenzene. With 4 AB in the cycle, the energy stored in each photoswitch reaches a maximum of 0.97 eV, which is 65% superior to the energy accumulated in isolated AB. Upon increasing the number of AB moieties, the ΔH decreases again as a result of the reduction of the cyclic strain. This behavior is a direct evidence of the effect of the cyclic strain on the thermodynamic properties of azobenzenophanes.

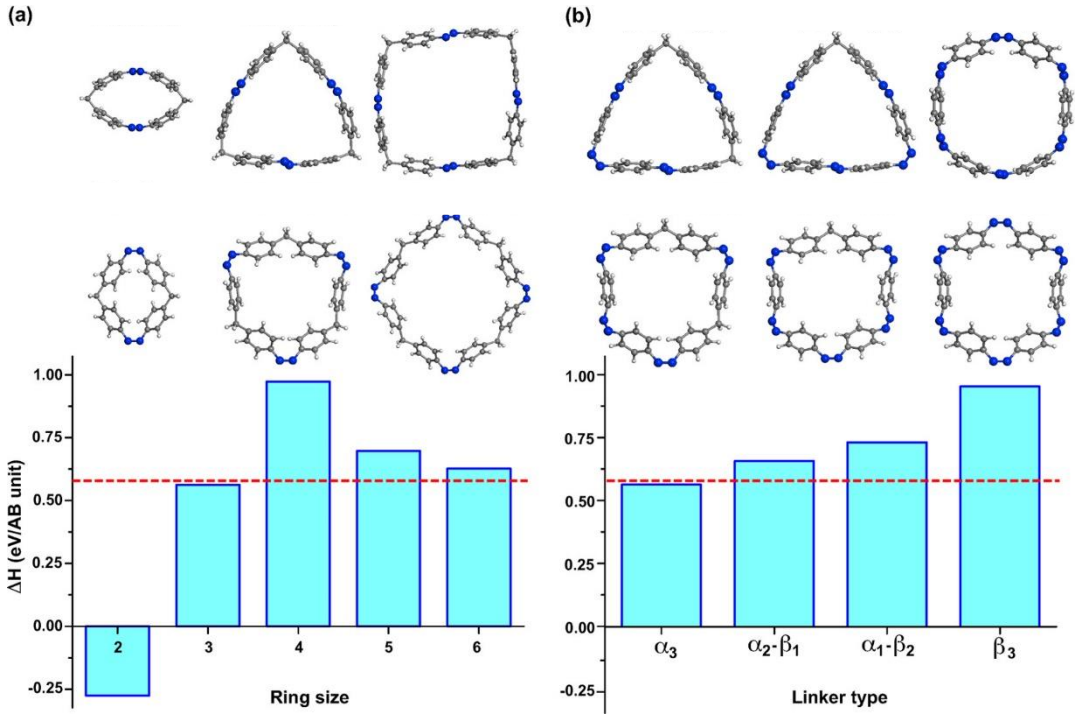

Figure 5.1. Variation of the energy stored per AB unit depending on number of embedded AB moieties (a), and effect of the linker molecule on the stored energy per AB unit in a *tris*-azobenzenophane (b). The red dotted line corresponds to the energy stored by isolated AB. The values were calculated in the gas phase from first-principles calculations. Figure adapted with permission from reference 231.

Indeed, with the *bis*-azobenzenophane, the CNNC torsion angle is so distorted from planarity that the overall energy of the all-*trans* becomes higher than that of the all-*cis* isomer by about 11 kcal.mol^{-1}. In the *tris*-azobenzenophane, the strain on the azo bond in the all-*trans* form is reduced, and in the all-*cis* form, the triangular shape allows the bend angles CNN and NNC to be close to those of isolated AB. Thus, with a slightly destabilized all-*trans* form and an all-*cis* free from additional steric distortions, the stored energy per AB unit is slightly lower than the isolated AB. In the *tetra*-azobenzenophane, each *trans* AB unit is fully planar, while the bend angles in the all-*cis* form are now obliged to tighten, due to the square arrangement of the cycle. This stabilization of the *trans* and destabilization of the *cis* AB units results in a higher energy difference between both forms. By further increasing the size of the cycle, these steric effects become less marked, and the stored energy tends to return to the value of isolated AB. Finally, by modifying the linker molecule from CH_2 to N_2 (to be understood as singly bound nitrogen atoms), the energy storage in the *tris*-azobenzenophane was increased again, as a result of the widening of the angles in the molecule. The more CH_2 groups were replaced, the higher the stored energy.

Therefore, the utilization of the *tetra*-azobenzenophane as solar-thermal fuel would allow the storage of up to 3.9 eV of energy in the all-*cis* form (Figure 5.2). However, no details about the thermal relaxation rate was given, which is an important feature to store energy over longer periods of time. But given the activation energies given, each metastable state seems to have a similar activation energy (between 0.93-1.04 eV), which should predict similar thermal relaxation rates. This is reminiscent of the studies by Tamaoki et al. who mentioned the homogenization of the relaxation rates of the metastable isomers upon reducing the cyclic strain.[211] Another important point is to actually ensure that this behavior would not be altered in the solid state or in the materials in which this molecule would be grafted for such application.

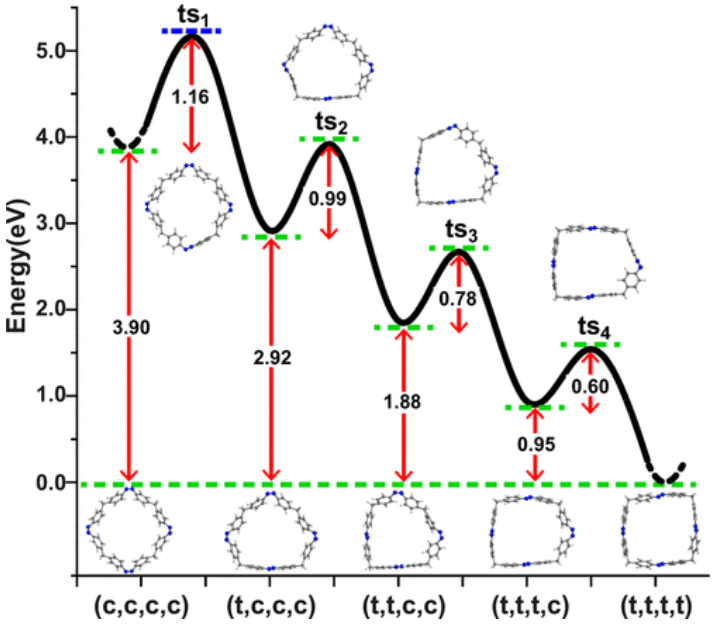

Figure 5.2. Computed parameters for the stepwise thermal relaxation of a methylene bridged *p*-tetra-azobenzenophane from the metastable all-*cis* form the stable all-*trans* form. Reprinted with permission from reference 231.

As shown by Despras and co-authors in their seminal paper, glycoazobenzene macrocycles possess intriguing chiroptical properties, however no information about the thermodynamic parameters was given. Therefore, with the newly synthesized azobenzene glycophanes **74**-**77**, a particular emphasis was put on the determination of the thermodynamic parameters, and their correlation with the nature and the length of the linking diamine. Unfortunately, close examination of the chiroptical behavior was

not possible due to technical restrictions, but will be the very next step in the investigation of these molecules.

In a second time, the synthesized glycoazobenzene dyads **78**, **79** and **95** were investigated for their potential multistate switching ability, and the studies were limited to their light sensitivity and isomeric steady state composition upon irradiation. Their thermal relaxation was also monitored to determine their relative stability, towards a potential exploitation of the temperature as an orthogonal stimulus. Finally, based on a personal interpretation of the results, examples of applications are proposed as a conclusion to this work.

5.1. Properties of AB-glycophanes 74-77

The photochromic properties of glycophanes **74**-**77** (Figure 5.3) were monitored in DMSO by UV-Vis spectroscopy at a concentration of 50 µM, and the ratios of *E* and *Z* isomers were determined at the PSS by NMR spectroscopy in DMSO-d_6 at 1 mM. The representative UV-Vis spectra of the *E* isomers, along with with the spectra after irradiation at 365 nm and 520 nm are shown in Figure 5.4, and the main photochromic features (λ_{max}, ε and $t_{1/2}$) of each compound are detailed in Table 5.1, and compared to the data of the previously reported AB-glycophane **105** by Despras and colleagues. For more commodity in the discussion, the new cycles were classified depending on the length and nature of the linking diamine (Figure 5.3). Thus compound **76** containing a flexible C_2 linker compares to **105** which has a rigid C_2 linker. **74** and **75**, with C_3 and C_4 linkers respectively, compare to **76** by the length of the linker. Finally, **77** with a C_4 rigid linker compares to **105** by the length, and to **75** by the rigidity of the tether.

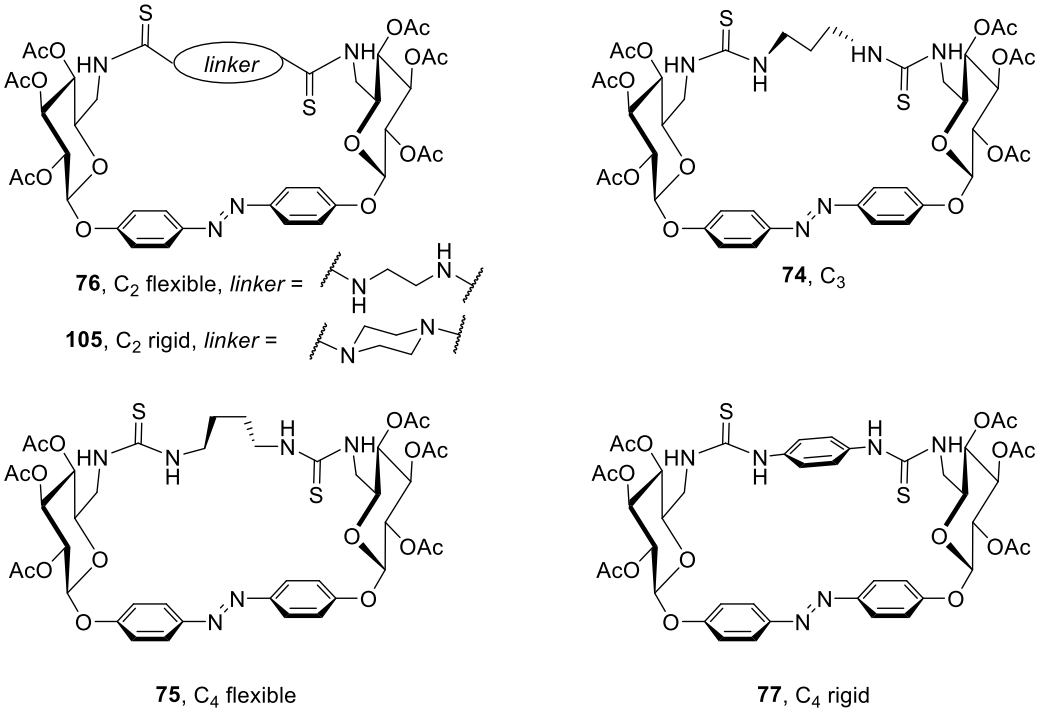

Figure 5.3. Structures of macrocycles **74**-**77**, and classification according to the linker´s nature.

Comparably to the previously reported macrocycle **105** (Table 5.1, entry 1) the *E* isomers of compounds **74**-**77** (Table 5.1, entries 2-5) have a main π→π* transition centered at 350 nm. Their n→π* bands are located at 443 nm for **76** and around 435 nm for **74**, **75** and **77**. Despite similar spectral features, **74**-**77** led to lower amounts of *cis* isomer (90-92%) in the PSS reached upon irradiation at 365 nm than for

105 (98%). The latter compound exhibits a better resolution, by 5-7 nm, between the π→π* bands of the respective *trans* and *cis* isomers, compared to **74**-**77**. On the other hand, the π→π* transition of *trans* isomer is slightly better resolved with the n→π* of the *cis* in **74**-**77**. A striking spectral modification is the strong hypochromic effect observed in **76** compared to **105**. Indeed, despite a greater flexibility of the linker in **76**, which should reduce the cyclic strain and thus increase the absorptivity, the extinction coefficients of **76** are about half those of **105**. This is also in contrast to what is observed when comparing **76** to **74** and **75**, or **75** to **77**.

Table 5.1. Photochromic parameters of AB-glycophanes **76**, **74**, **75**, **77** and **105.**

Entry	Compound	$\lambda_{\pi\rightarrow\pi^*}$ (nm) *trans / cis*	$\lambda_{n\rightarrow\pi^*}$ (nm) *trans / cis*	$\varepsilon_{\pi\rightarrow\pi^*}$ (L/mol/cm) *trans / cis*	$\varepsilon_{n\rightarrow\pi^*}$ (L/mol/cm) *trans / cis*	$t_{1,2}$ at 300 K (h)
1[a]	**105**	352 / 302	443 / 444	ND / ND	1184 / 2165	6.4
2	**76**	350 / 305	443 / 446	10225 / 3906	827 / 1092	37.8[b]
3	**74**	350 / 305	436 / 446	21568 / 7300	1626 / 2088	14.2[b]
4	**75**	350 / 307	435 / 448	24825 / 8013	1693 / 2468	9.2[b]
5	**77**	351 / ND	436 / 449	18771 / ND	1295 / 2207	5.4[b]

[a] Unpublished data provided by Dr. Despras; [b] Evolution of the absorbance at λ_{max} was monitored in DMSO at 50 µM by UV-Vis spectroscopy at 60, 65, 70 and 75 °C, then an Arrhenius plot provided the corresponding thermal parameters necessary to calculate the half-life at 27 °C. ND: not determined.

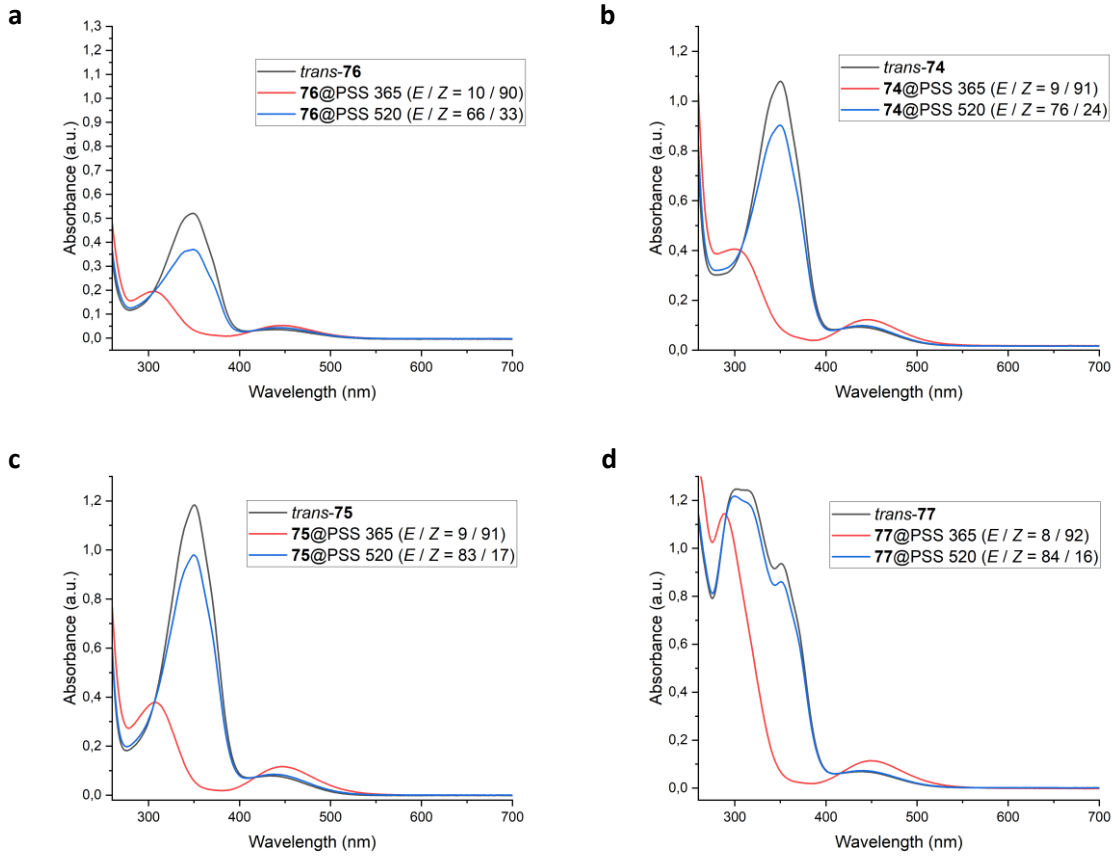

Figure 5.4. UV-Vis absorption spectra in DMSO (50 µM) at 25 °C of the four new AB-glycophanes **76** (a), **74** (b), **75** (c) and **77** (d), in the ground state (black line), and after irradiation at 365 nm (red line) and 520 nm (blue line). The PSS ratios, indicated in brackets, were measured by ^{1}H NMR (600 MHz, 300 K) in DMSO-d_6 (1 mM). Conditions for irradiation: 2 min irradiation of the sample with the indicated wavelength for both UV-Vis and NMR experiments. Photoisomerization of **105** under similar conditions provided *E*/*Z* ratios of 98/2 upon irradiation at 365 nm (unpublished data provided by Dr. Despras).

The process of photochemical back isomerization, which takes place in the visible range, depends on several parameters. Due to the overlap of the *trans* and *cis* n→π* bands, the quantum yields of isomerization for each transition, the molar extinction coefficients, and the band separation have to be considered. In the absence of values for the quantum yields, the observation of the variations of extinction coefficients and band separation gives a qualitative basis to explain the backswitching behavior upon visible light irradiation. Indeed, the photoconversions for the back reaction seem to correlate well with the evolution of the *trans* and *cis* n→π* bands. Upon increasing the linker size, and thus reducing the cyclic strain in **74**-**76**, all n→π* undergo a hyperchromic shift. However, the ratio of the extinction coefficients of the n→π* bands for the *trans* and *cis* isomers changes. In **76**, the ratio:

$$\frac{\varepsilon(\mathrm{n} \rightarrow \pi *, trans)}{\varepsilon(\mathrm{n} \rightarrow \pi *, cis)}$$

is equal to 0.75, and the photoconversion yield at 520 nm is 66%. In **74**, this ratio is higher, with a value of 0.78, which should indicate a reduced yield of back isomerization. However, the n→π* transitions of **74** are better separated compared to **76** ($\Delta\lambda$ = 10 nm *vs* 3 nm for **76**), which results in a slightly higher photoisomerization yield of 76% at 520 nm. For **75**, the band separation is the same as for **74**, but the ratio of extinction coefficients decreases to 0.69, and a photoisomerization yield of 83% was obtained. For compound **77**, the linker might be considered as a rigid C_4 unit. Comparing with **75** which has a flexible C_4 unit, a general hypochromic shift is observed on all bands, while the wavelengths of absorption are unchanged. The ratio of extinction coefficients decreases to a value of 0.59, resulting in a photoconversion of 84% at 520 nm. Compound **105** shows a ratio (0.55) close to the one measured for **77.** Although, the back photoisomerization with green-light has not been measured so far for **105**, it is interesting to note that **77** and **105** both have a rigid linker and a similar molar extinction coefficient ratio for the n→π* bands. Also, these results compare well with what was observed for macrocycles **3** and **4**. Although all the extinction coefficients were not measured, it can be graphically estimated that the more strained AB-glycophane **3** has a higher extinction coefficient ratio than **4**, which reflects in the same manner on the yields of back isomerization.[268e] Additionally, the back isomerization yields seem to be higher when using green-light rather than blue-light, which is likely due to the fact that the *cis* n→π* is generally red-shifted regarding the *trans* n→π*, and the contribution of the latter in the PSS decreases when increasing the irradiation wavelength. Therefore, the sensitivity of macrocycles **74**-**77** to orange and red-light was examined. First, the macrocycle **74** was assessed (Figure 5.5): starting from a mixture obtained after green-light irradiation (520 nm), the content of *trans* isomer could be enriched within 6 minutes of irradiation with orange (Figure 5.5a) or red-light (Figure 5.5b). Starting from a *cis*-rich mixture obtained after 365 nm irradiation, 15 minutes were necessary to reach a similar composition as the PSS at 520 nm (Figure 5.5c,d). Thus, a combination of green and red-light, applied successively, provides a mean to increase the photoconversion yields in a reasonable amount of time.

Because no significant difference was found between the effect of orange or red-light on the back isomerization of **74**, the same experiment was carried out for cycles **75**-**77** with red-light only (see experimental section). In analogy to the back switching behavior with green-light, the C_2 bridged macrocycle **76** was found to be the least responsive upon 625 nm irradiation, while the C_4 bridged compound **75** was more responsive than **74**. Strikingly, macrocycle **77** showed the fastest kinetics upon red-light irradiation, and excellent recovery of the ground state was achieved with only 4 to 15 min of illumination starting from the PSS 520 or the PSS 365 respectively. Because of the longer irradiation times necessary upon red-light illumination, the thermal $Z \rightarrow E$ isomerization process is not anymore negligible, and thus the system does not seem to reach a clear steady state when the irradiation is prolonged. Therefore, *trans*/*cis* ratios were measured by NMR for each compounds **74**-**77** after being irradiated systematically according to the following sequence: after 2 min irradiation at 520 nm, the

sample was irradiated at 625 nm for 10 min. The smallest photoconversion yield of 81% was reached by C_2-bridged **76**, which is significantly higher than the yield after green-light irradiation. C_3- and C_4-bridged **74** and **75** followed with 82% and 92% yield respectively. Finally, derivative **77** showed a 93% photoconversion.

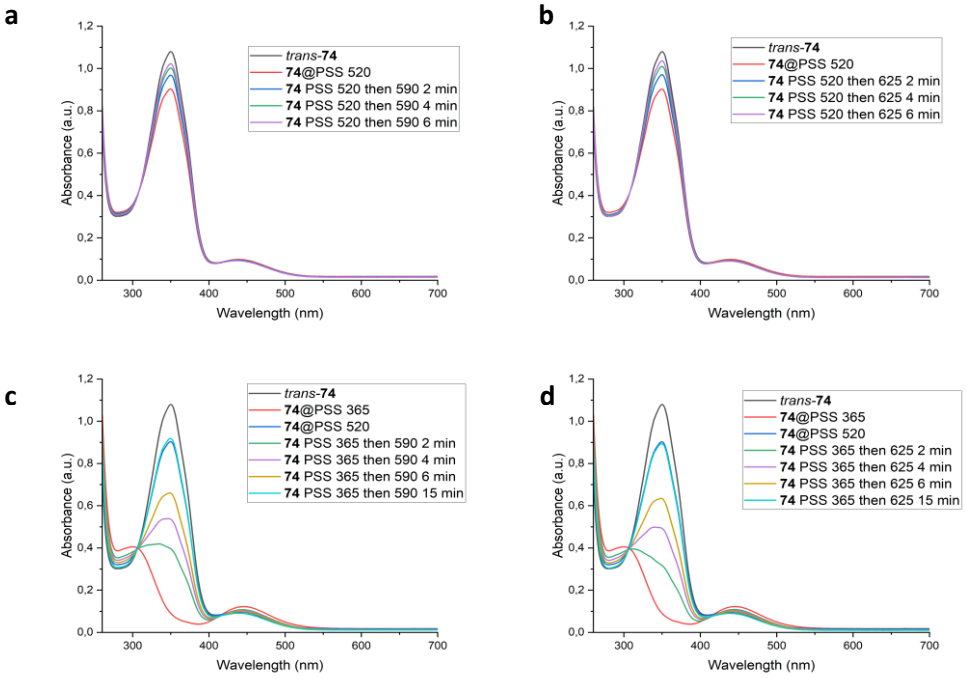

Figure 5.5. Evolution of the UV-vis spectra of macrocycle **74** in DMSO (50 µM) at 25 °C upon irradiation with orange (a, c) and red-light (b, d), starting from the PSS 520 (top) or the PSS 365 (bottom).

Following this study on the photoswitching behavior of macrocycles **74**-**77**, the thermal relaxation of their *cis* isomer was examined. To do so, the thermal back isomerization of each compound was monitored by UV-Vis spectroscopy in the same solvent and at the same concentration, at temperatures of 60, 65, 70 and 75 °C (Figure 5.6a,c,d,f). As the thermal relaxation is a first order reaction, the evolution of the absorbance at λ_{max} *versus* the time was plotted, and the data were fitted with an exponential growth law, which gave the thermal isomerization constants for each compound at each temperature. These constants were then converted into their natural logarithm, and plotted against the inverse of the temperature (Figure 5.6b,d,e,g). According to the Arrhenius equation:

$$k = Ae^{\frac{-Ea}{RT}} \quad (1)$$

the fitting of such a plot provides a straight line that has ln*A* as ordinate at the origin, and $\frac{-Ea}{RT}$ as slope. From these values, the relaxation constants can be calculated at any temperature for each compound. In a second time, the Eyring equation, in which k_b, h and R are Boltzmann´s, Planck´s and the gas constants respectively:

$$k = \frac{k_b T}{h} e^{\frac{\Delta S^{\neq}}{R}} e^{\frac{-\Delta H^{\neq}}{RT}} \quad (2)$$

was used (see experimental section) to extract the enthalpy of activation ($\Delta H^{\neq}$) and the entropy of activation ($\Delta S^{\neq}$). The free Gibbs energy of activation ($\Delta G^{\neq}$) was then calculated according to the formula:

$$\Delta G^{\neq} = \Delta H^{\neq} - T\Delta S^{\neq} \quad (3)$$

The obtained thermodynamic parameters are shown in Table 5.2.

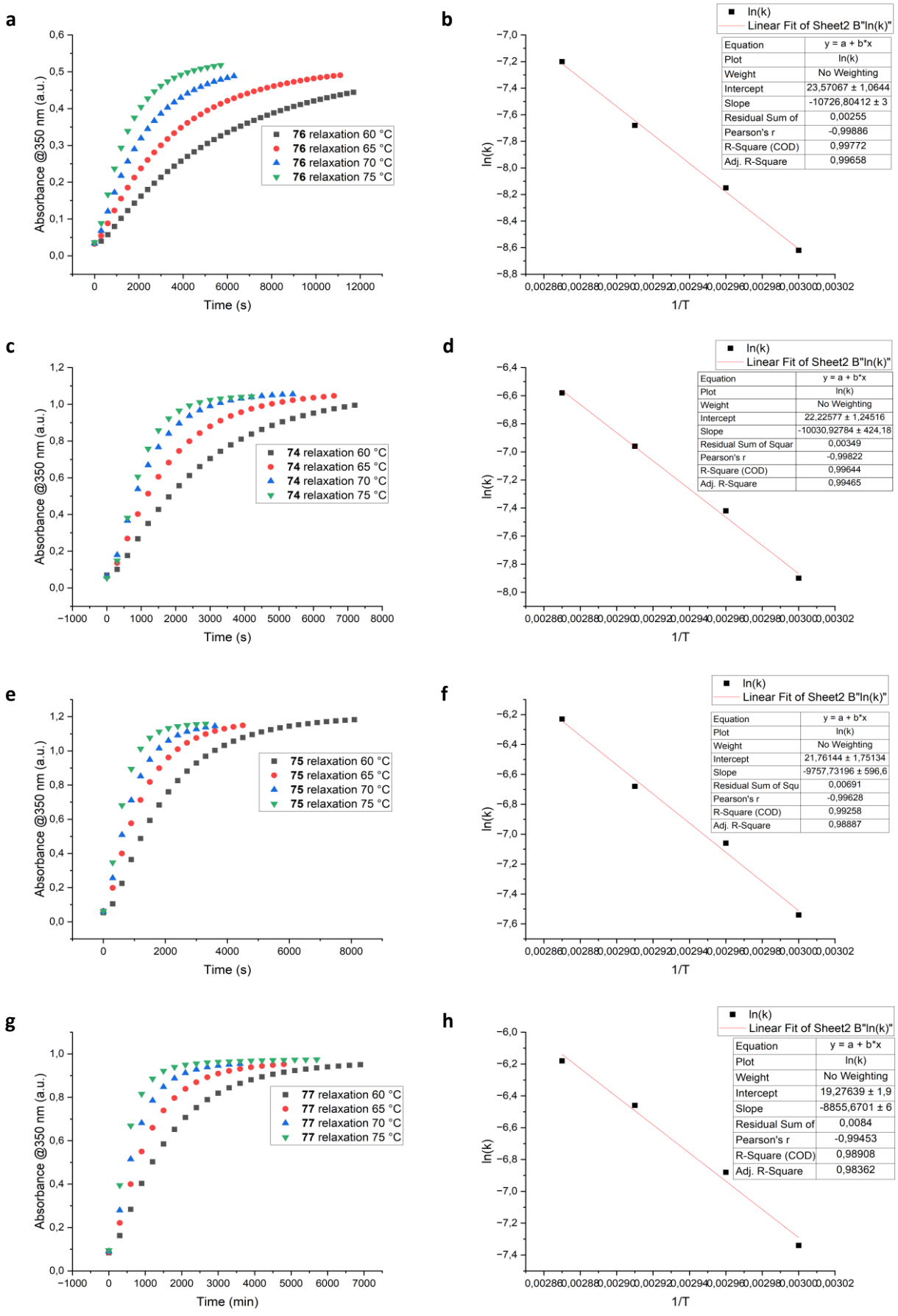

Figure 5.6. Evolution of the absorbance at λ_{max} in DMSO (50 µM) for compounds **74**-**77** at 60, 65, 70 and 75 °C (a, c, e, g), and corresponding Arrhenius plots (b, d, f, h).

Table 5.2. Activation parameters for the thermal isomerization of macrocycles **74**-**77**.

Entry	Compound	$k_{27\,°C}$ (s^{-1})	*Ea* (kcal.mol^{-1})	$\Delta H^{\neq}$ (kcal.mol^{-1})	$\Delta S^{\neq}$ (cal.mol^{-1}. K^{-1})	$\Delta G^{\neq}$ (kcal.mol^{-1})	$t_{1/2}$[a] (h)
1	**76**	5.1×10^{-6}	21.4	20.8	-13.9	24.9	37.8
2	**74**	1.4×10^{-5}	20.0	19.3	-16.7	24.3	14.2
3	**75**	2.1×10^{-5}	19.5	18.7	-17.9	24.1	9.2
4	**77**	3.6×10^{-5}	17.7	17.0	-22.5	23.8	5.4

[a] Calculated values for a temperature of 27 °C, from the resolution of the Arrhenius equation.

Because the activation energy *Ea* and the free enthalpy of activation $\Delta H^{\neq}$ are linked by the following equation:

$$Ea = \Delta H^{\neq} + RT \qquad (4)$$

and because the free Gibbs energy of activation is linked to $\Delta H^{\neq}$ by equation (3), it is logical that all these values follow the same evolution. Hence, the activation energy necessary for the thermal $Z \longrightarrow E$ isomerization process to occur tends to decrease upon increasing the chain length and the rigidity of the linker (Table 5.2, entries 1-4). In contrast, the entropic cost to reach the transition state increases with the size of the linker. The measured enthalpies of activation correlate well with the measured half-lives of the metastable isomers, such as, the higher the activation energy, the more stable the *cis* isomer. This shows that by reducing the length of the linker, the steric effects tend to stabilize the *cis* isomer, while the transition state is destabilized. Moreover, it is noteworthy that macrocycles **105** (rigid C_2 linker) and **77** (rigid C_4 linker) have similar thermal relaxation rates, which are significantly higher than **76** and **75** which have flexible C_2 and C_4 linker. This seems to indicate that the flexibility of the linker has more impact on the thermal stability than its length.

Interestingly, plotting the enthalpies of activation $\Delta H^{\neq}$ against the entropies of activation $\Delta S^{\neq}$ showed a linear relationship for compounds **74**-**77** (R^2 = 0.9889, see experimental section). However, compound **77** seemed slightly off the linearity, therefore the same plot was made for compounds **74**-**76**, and showed a correlation coefficient of 0.9998 (Figure 5.7a). Such a linear relationship indicates a compensation or isokinetic relationship.[363]

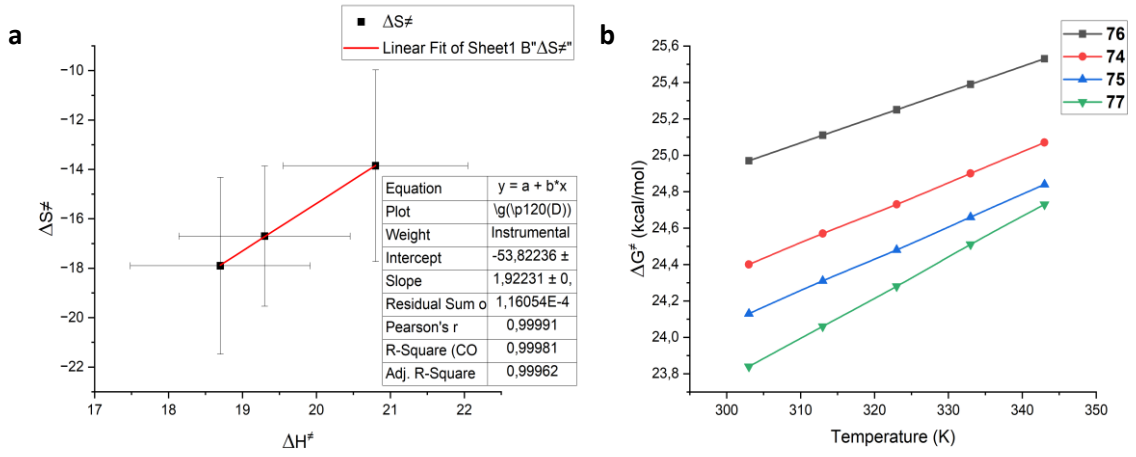

Figure 5.7. Enthalpy-entropy compensation plot for compounds **74**-**76** (a) and van´t Hoff plots for macrocycles **74**-**77** (b).

An isokinetic relationship means that, when considering different reactions, or the same reaction in different compounds, there exists a temperature at which the rate constants of each reaction are equal. In the context of thermal isomerization of ABs, this relationship is usually invoked when derivatives isomerize with the same mechanism. To verify if the compensation relationship is valid, a plot of $\Delta G^{\neq}$ *versus* the temperature can be made, and fitting of the data gives linear function equations

(Figure 5.7b). By calculating the intersections of each of these functions together, isokinetic temperatures are found, and the closer these values are to a unique temperature, the more the isokinetic relationship is true. The calculated isokinetic temperatures from the van´t Hoff plot were 579 °K for **74** and **76**, 570 °K for **74** and **75**, and 529 °K for **75** and **76**, which seems to confirm the compensation relationship. In contrast, macrocycle **77** has more spread isokinetic temperatures of 367, 403 and 440 °K with **75**, **74** and **76** respectively, which is in agreement with the deviation from linearity observed in the compensation plot.

This result would therefore indicate that *cis*-AB glycophanes **74**-**76** thermally isomerize through the same mechanism, while *cis*-**77** may proceed differently. Comparison with the thermodynamic parameters of **105** and elucidation of the isomerization mechanism would be interesting to fully understand the differences between all these compounds in view to rationally design new derivatives with tailored properties.

These data do not provide information about the quantity of energy stored upon isomerization, but the following hypothesis might stand: reducing the length of the linker would tend to destabilize the *trans* isomer while stabilizing the *cis* isomer, which would result in a lower amount of energy stored. This would need to be confirmed by computing the energy difference between the *trans* and the *cis* state of each compound. Of course, in application as solar energy fuels, the chiroptical properties of macrocycles **74**-**77** would not be exploited, but carbohydrates remain excellent scaffolds with interchangeable and multiple functionalities that could be used for introducing these macrocycles into larger architectures. Besides, the overall strategy of the synthesis, based on an efficient substitution of DHAB and a high yielding cyclization, might be adapted to other non-chiral substrates. Moreover, binding studies with macrocycles **3**, **4, 105** and **74**-**77** and several small chiral guests could reveal interesting chiroptical complexation behavior. Finally, by tailoring the linker moiety (*i.e.* the diamine used for the cyclization), one might imagine a chiral photoswitchable catalyst as shown in Figure 5.8.

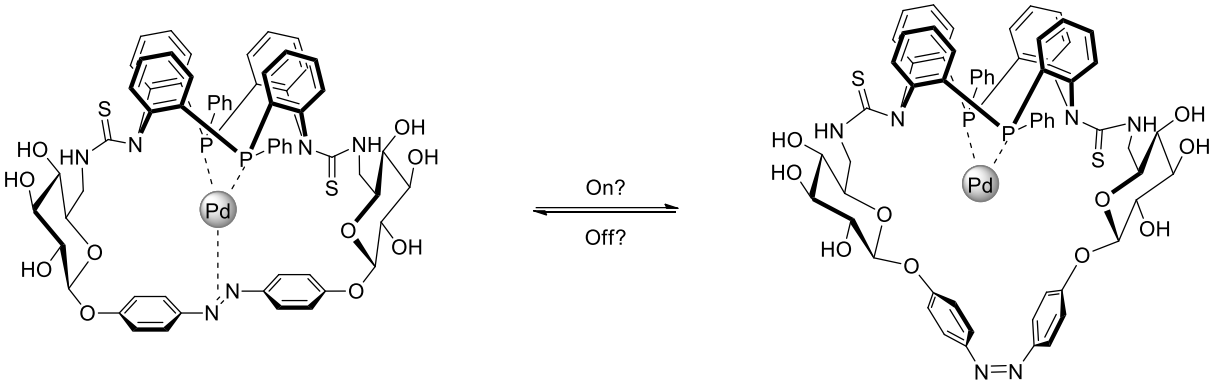

Figure 5.8. Example of a plausible chiral photoswitchable catalyst based on AB-glycophanes.

In the next section, a different approach was explored. The carbohydrate scaffold was designed in a way to embed two different AB chromophores in a macrocyclic structure, to form glycoazobenzenophanes. The novelty of this approach stands on the fact that AB derivatives with different substitution patterns were incorporated within the same macrocycle, in order to achieve multistate switching.

5.2. Properties of glycoazobenzenophanes 78, 79 and 95

5.2.1. Properties of linear derivatives 101, 103 and 104

Before starting the discussion on the properties of compounds **78**, **79** and **95**, a first analysis of the photochromism of linear derivatives **101** (DMAB), **103** (DSAB) and **104** (TFAB) is necessary. Their photoswitching behavior depending on the wavelength of irradiation was first explored by UV-Vis spectroscopy, and the ratio of photoisomerization products was measured by NMR for the most promising PSSs. Their structure is shown in Figure 5.9, and the evolution of their spectra is shown in Figure 5.10, and some characteristic parameters are listed in Table 5.3.

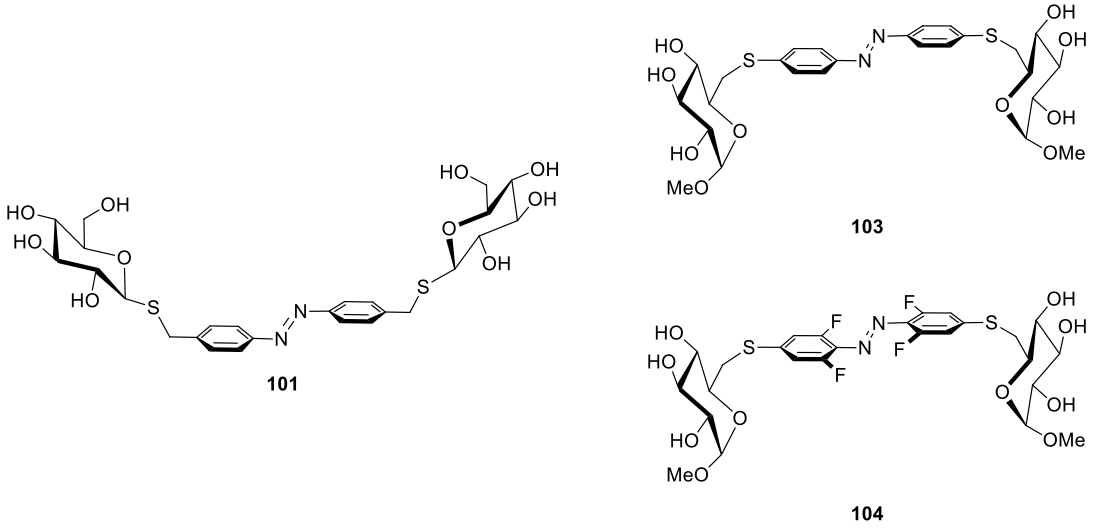

Figure 5.9. Structures of the AB-*bis*-glucosides **101**, **102** and **104**.

Table 5.3. Photochromic parameters for compounds **101**, **103** and **104**.

Entry	Compound	$\lambda_{\pi\rightarrow\pi^*}$ (nm) *trans* / *cis*	$\lambda_{n\rightarrow\pi^*}$ (nm) *trans* / *cis*	*E*/*Z* ratio after 625 nm[a]	$t_{1,2}$ at 323 K (h)
1	**101**	348 / 298	443 / 440	97/3	2.7
2	**103**	394 / 338	ND / 442	98/2	0.2
3	**104**	386 / 338	ND / ND	30/70	9.2

[a] The PSS ratio, were measured by ^{1}H NMR (600 MHz, 300 K) in DMSO-d_6 (1 mM). Conditions for irradiation: 2 min irradiation of the sample with 470 nm light, and then 10 min with 625 nm light for **103** and **104**, or 15 min for **101**.

The DMAB-*bis*-glycoside **101** (Table 5.3, entry 1) shows well resolved transitions in the *trans* state, with maximums of absorption at 348 and 440 nm for the *trans* π→π* and n→π* bands respectively (Figure 5.10a). A near quantitative photoconversion towards the *cis* isomer was obtained with 365 nm light, while blue-light (405-470 nm) efficiently regenerated the *trans* state with about 80% conversion. As observed previously, irradiation with orange or red-light efficiently triggered the isomerization and produced high contents of *trans* isomer in 30-50 min, starting from the mixture composition at the PSS 365 nm (Figure 5.10b). As also observed earlier, the time of irradiation could be reduced when starting from another mixture composition, and successive irradiation with 470 nm light (2 min) and 625 nm light (15 min) produced 97% of *trans* isomer as measured by NMR. Finally, the half-life of *cis*-**101**, measured at 50 °C, was found to be 2.7 h.

The DSAB-*bis*-glycoside **103** (Table 5.3, entry 2) exhibits a red-shifted π→π* transition compared to **101** ($\Delta\lambda$ = 46 nm), as could be expected from the modification of the nature of the *para*-substituents (CH_2 *vs* S). With a value of 394 nm, the position of the π→π* is, as expected, higher than that of AB-*bis*-glycoside **35** ($\Delta\lambda$ = 20 nm). As discussed previously, the difference resides in the fact that the

electronic density of sulfur at the anomeric position (thioacetal) is lower than that at the position 6 (thioether). Interestingly though, this value was also significantly higher ($\Delta\lambda$ = 14 nm) than that of the *bis*-dithiomethyl-AB discussed previously (Table 3.2, entry 2). Up to 90% *cis* was generated upon irradiation with 385 or 405 nm light (Figure 5.10c), while irradiation with 365 nm light produced only 68% of *cis* isomer. The back isomerization could be effected in 2 min with any light between 450 and 520 nm, with mediocre efficacy (Figure 5.10d). However, **103** was found very responsive to red-light, and the *trans* isomer seemed to be quantitatively regenerated after 10 min irradiation starting from a *cis*-rich PSS. And indeed, a photoconversion yield of 98% was measured after successive irradiation with blue and red-light. Moreover, the thermal relaxation rate of **103** was expectedly found faster than that of **101**, by a factor of 10.

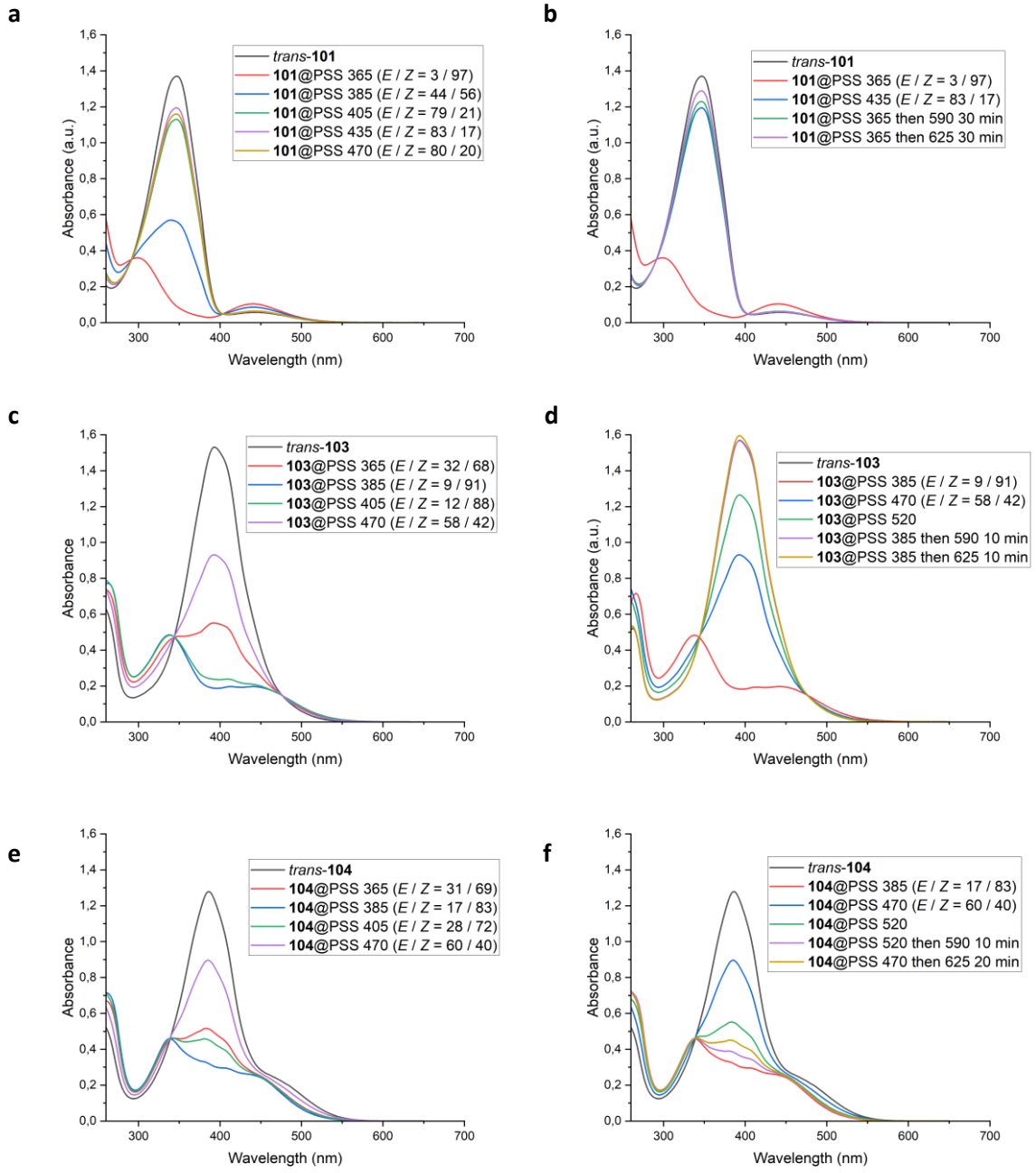

Figure 5.10. Evolution of the UV-vis spectra of compounds **101**, **103** and **104** in DMSO (50 µM) at 25 °C upon irradiation with UV to blue-light (a, c, e) and green to red-light (b, d, f). The PSS ratios, indicated in brackets, were measured by ^{1}H NMR (600 MHz, 300 K) in DMSO-d_6 (1 mM). Conditions for irradiation: 2 min irradiation, unless otherwise stated, of the sample with the indicated wavelength for both UV-Vis and NMR experiments.

The properties of TFAB-*bis*-glycoside **104** (Table 5.3, entry 3), which has a π→π* transition centered at 386 nm in the *trans* state, suffered from the red-shift of its π→π* compared to **36**. Indeed, tetra-*o*-fluoro derivatives, which photoswitching performances lie on the separation of the n→π* bands, require to have a blue-shifted π→π* to ensure the highest photoconversion yields. Here, because the π→π* band of **104** has a relatively low energy compared to **36** and other TFABs,[154,155,322] there is a larger overlap between the *cis* n→π* and the *trans* π→π*, impairing the photoconversion in both directions (Figure 5.10e). Thus, irradiation with 385 nm light produced 83% of *cis*, while not more than 60% of *trans* could be generated upon blue-light irradiation. As observed in **103**, the switching at 365 nm only produced about 70% of *cis*-**104**, whereas this wavelength was the best for **101**. This is due to the general red-shift of the π→π* bands of each isomer, which shifted the optimal irradiation window, as discussed earlier (Chapter 3). Therefore, irradiating **103** and **104** with 365 nm light results in exciting both *cis* and *trans* π→π* bands, which then reduces the photoconversion yield. Moreover, irradiation with orange or red-light, which gave better conversion than with UV-light for **36**, did not show any improvement for **104** (Figure 5.10f). As expected, *cis*-**104** was found to be the most stable derivative with a half-life of 9.2 h at 50 °C.

From these data, one can anticipate some properties of macrocyclic glycoazobenzene dyads composed of these chromophores. When using the DMAB and the DSAB chromophores (Figure 5.11, R = H), at least 3 states could be selectively enriched photochemically. A *Z*/*Z*-rich state could be produced with light between 365 and 385 nm, whereas an *E*/*Z*-rich state would be obtained upon irradiation with 405 nm light, and the *E*/*E* ground state regenerated with red-light. Secondly, due to the differences in thermal stability and photoisomerization kinetics with red-light, the *Z*/*E* state could probably be enriched thermally or photochemically starting from the *Z*/*Z* isomer. When using DMAB and TFAB (Figure 5.11, R = F), the same states could be photochemically generated, but the relative thermal stability would be inverted, and the *Z*/*E* state could not be selectively enriched neither photochemically nor thermally.

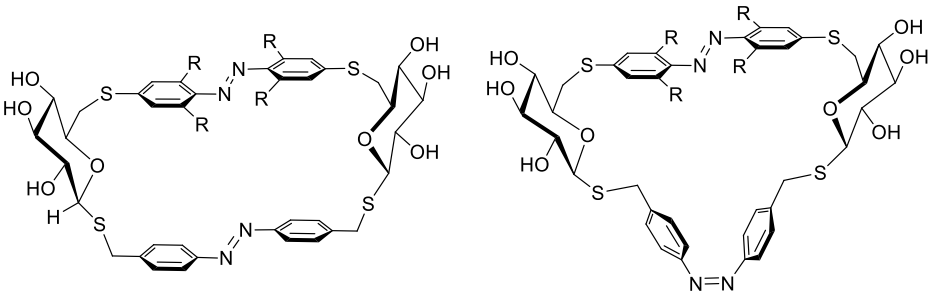

(*E*,*E*)-**78**, R = H
(*E*,*E*)-**79**, R = F

(*Z*,*E*)-**78**, R = H
(*Z*,*E*)-**79**, R = F

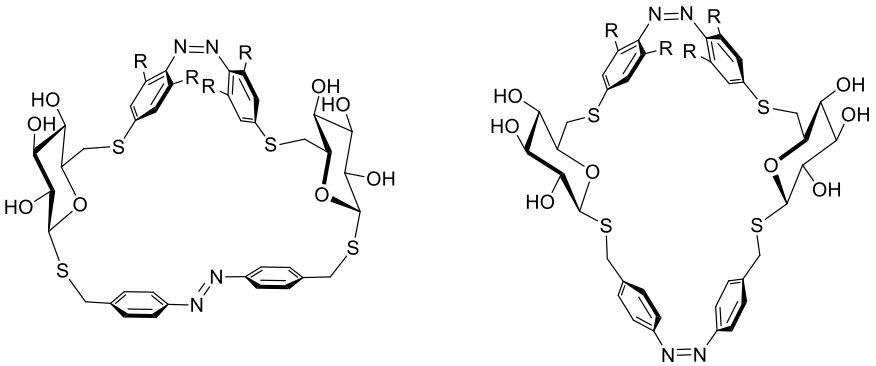

(*E*,*Z*)-**78**, R = H
(*E*,*Z*)-**79**, R = F

(*Z*,*Z*)-**78**, R = H
(*Z*,*Z*)-**79**, R = F

Figure 5.11. Structures of all possible isomers of **78** or **79**.

For more commodity, in the following discussion, the 4 possible isomers of azobenzenophanes **78**, **79** and **95** will be referred to as the (*E*,*E*), (*Z*,*E*), (*E*,*Z*) and (*Z*,*Z*), with the first letter corresponding to the AB moiety in position 1, and the second letter to the AB moiety in position 6 of the sugar.

5.2.2. Properties of glycoazobenzenophane 78

Following the isolation of azobenzenophane **78**, a first examination of its structure in the ground (*E*,*E*) state was realized by NMR spectroscopy. The shifts of the most characteristic signals (Figure 5.12) such as the aromatic protons of both AB units (H_{ortho}, H_{meta}), the CH_2 protons of the DMAB (CH_2a, CH_2b), the CH_2 protons of the sugar´s position 6 (H-6a, H-6b) and the anomeric protons (H-1), were compared with those of **101** and **103**. These changes are compiled in Table 5.4. Then, the photoswitching behavior of **78** was examined by UV-Vis (Figure 5.13) and NMR spectroscopy (Figure 5.14), and the isomeric composition at the most promising PSSs was determined by ^{1}H NMR (Table 5.5). In a third time, the thermal relaxation of **78** was monitored by NMR in order to determine the relative thermal stability of each isomer, and specific sequences of irradiation were determined for its selective multistate switching.

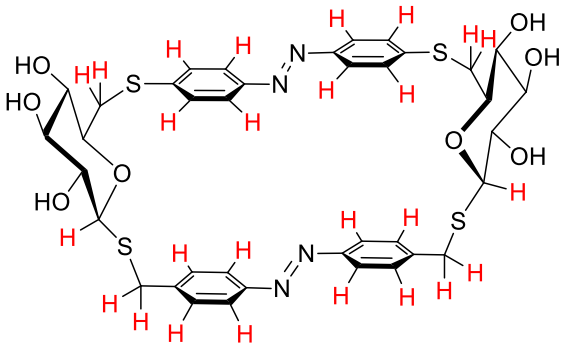

(*E*,*E*)-**78**

Figure 5.12. The red hydrogens shown in (*E*,*E*)-**78** are those used for comparison with the open chain derivatives **101** and **103**.

Table 5.4. Chemical shifts of characteristic signals of derivative (*E*,*E*)-**78** in comparison with **101** and **103**.[a]

Entry	Compound	DMAB		DSAB		CH_2 (DMAB)		H-6		H-1
		H_{ortho}	H_{meta}	H_{ortho}	H_{meta}	a	b	a	b	
1	**101**	7.83	7.56	-	-	4.05	3.87	-	-	4.03
2	**103**	-	-	7.81	7.50	-	-	3.53	3.07	-
3	**78**	7.14	7.08	7.99	7.54	3.93	3.74	3.91	2.99	3.64

[a] All spectra were recorded in DMSO-d_6 (600 MHz, 300 K) at 1 mM.

As can be seen, the aromatic protons of the DMAB unit in **78** got shielded compared to **101** (Table 5.4, entries 1 and 3), whereas those of the DSAB unit were deshielded compared to **103** (Table 5.4, entries 2 and 3). The CH_2 protons of the DMAB unit and the anomeric protons got also shielded upon cyclization, whereas the two H-6 protons were shifted in opposite directions, increasing the separation of both signals. These changes were accompanied by a red-shift of the π→π* bands of each azo unit. In fact, the UV-vis spectrum of *trans*-**78** (Figure 5.13a) shows one large absorption band (300-460 nm), with two maximums of absorption at 357 and 411 nm, presumably corresponding to the π→π* transitions of the DMAB and the DSAB units respectively. Compared to **101** and **103**, this represents a rather large shift of 9 and 17 nm, and contrasts with the spectral modifications observed in previously reported cyclic AB dimers compared to the parent linear AB.[142b,209] Upon irradiation with 365 nm light, the absorbance of both bands was reduced simultaneously, indicating the conversion of both AB units to the *cis* state, and favoring the (*Z*,*Z*) isomer. Irradiation with 385 or 405 nm light provoked an increase

of the absorbance at 357 nm, and a decrease at 411 nm, suggesting the back switch of the DMAB unit while the DSAB unit was further converted to *cis*, favoring the (*E*,*Z*) state. Then, irradiation with blue to green-light (435-520 nm) provoked the simultaneous absorbance increase of both bands, suggesting the regeneration of the (*E*,*E*) isomer. Finally, the susceptibility of **78** to red-light (Figure 5.13b) was assessed starting from the mixture containing supposedly the highest (*Z*,*Z*) and (*E*,*Z*) amounts, that means after reaching the PSS at 385 nm. Irradiation at 625 nm for 1.5 min resulted in a rapid augmentation of the absorbance at 411 nm, while the regeneration of the band at 357 nm needed 30 min.

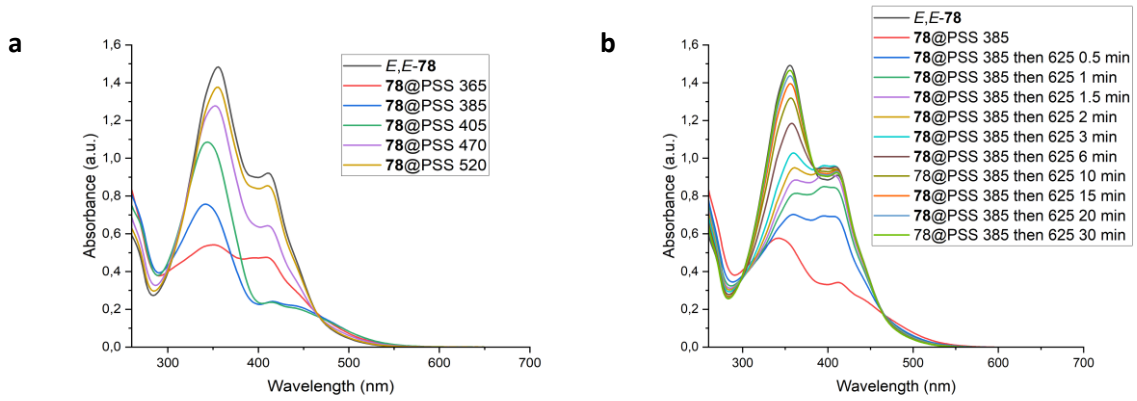

Figure 5.13. Evolution of the UV-Vis spectrum of azobenzenophane **78** in DMSO (50 µM) at 25 °C upon irradiation with UV to green-light (a), or with UV then red-light (b).

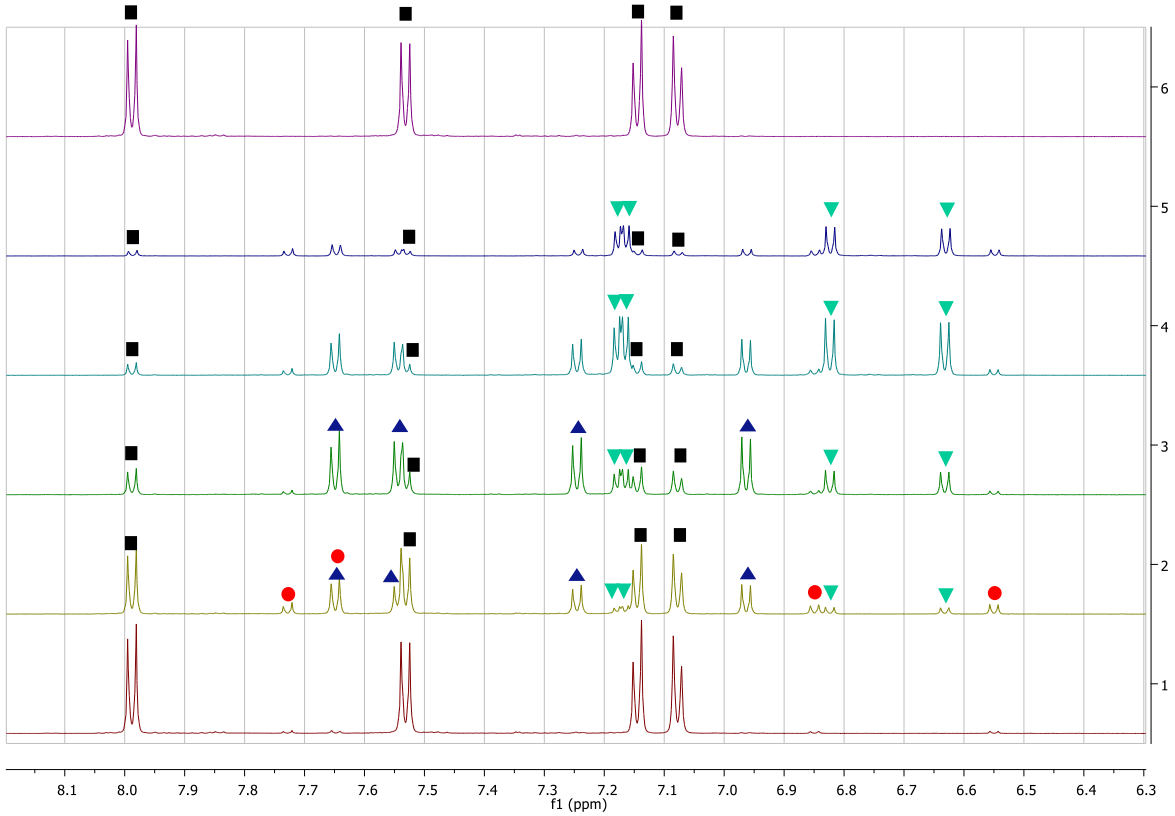

Figure 5.14. Expansion in the aromatic region of the ^{1}H NMR spectrum (600 MHz, 300 K) of **78** in DMSO-d_6 (1 mM) in the (*E*,*E*) state (violet), and evolution of the isomeric composition after irradiating 2 min at 365 nm (blue), 385 nm (turquoise), 405 nm (green), 470 nm (yellow) and 10 min with 625 nm light (red). The signals of each isomer were attributed by correlating the evolutions of the UV-Vis and NMR spectra in comparison with the data obtained for compounds **101** and **103**. ■: (*E*,*E*); ●: (*Z*,*E*); ▲: (*E*,*Z*); ▼: (*Z*,*Z*).

These data are in agreement with what was anticipated from the study of linear AB-*bis*-glycosides **101** and **103**. It also provided useful hints about the evolution of the mixture composition upon irradiation, which, combined to NMR analysis of the PSS composition (Figure 5.14), enabled the identification of each of the four isomers of **78**. In the thermodynamically stable (*E*,*E*) state, only four doublets are present in the aromatic region of the spectrum, as expected from two *p,p´*-disubstituted-ABs with different substitution patterns. Upon irradiation with 365 nm light, 15 doublets are observed, which means that, delightfully, the signals of each isomer are nearly all separated. A major isomer can be identified in this PSS mixture, presumably corresponding to the (*Z*,*Z*) state, which shows a doublet at 6.63 ppm that might be used for integration. Then, irradiation with 385 nm light enriched the mixture, supposedly with the (*E*,*Z*) isomer, which shows two exploitable signals at 7.25 and 6.96 ppm. By elimination, the signals at 7.73 and 6.55 ppm must correspond to those of the (*Z*,*E*) isomer, and the fact that these signals are always minor is in agreement with the prediction that the (*Z*,*E*) isomer could not be enriched by the use of only one stimulus.

Hence, the identification of the aromatic signals of each isomer allowed their quantification in every PSS mixture (Figure 5.15). The measured ratios are compiled in Table 5.5. As anticipated, irradiation with 365 nm light produced the highest content of (*Z*,*Z*) isomer, with a yield of 62%, while the other isomers were quite evenly distributed. At 385 nm, the (*Z*,*Z*) form was still the major photoproduct, although the content of (*E*,*Z*) isomer was more than doubled. Enrichment of the (*E*,*Z*) isomer up to 60% was achieved with 405 nm light, while the same amount of (*E*,*E*) was obtained with 470 nm light. Finally, nearly full recovery of the (*E*,*E*) state was achieved with 625 nm light.

Table 5.5. Isomeric composition after irradiation with different wavelengths.[a]

Isomer of 78	PSS 365 (%)[b]	PSS 385 (%)	PSS 405 (%)	PSS 470 (%)	PSS 625 (%)[c]
E,E	11	11	17	**59**	**97**
Z,E	14	5	2	9	3
E,Z	13	32	**60**	26	0
Z,Z	**62**	**51**	22	6	0

[a] The values in bold represent the major isomer in a given PSS mixture; [b] 6 min of irradiation were necessary to reach the PSS. [c] The measure was taken after successive irradiations of 2 min at 470 nm and 15 min with 625 nm light.

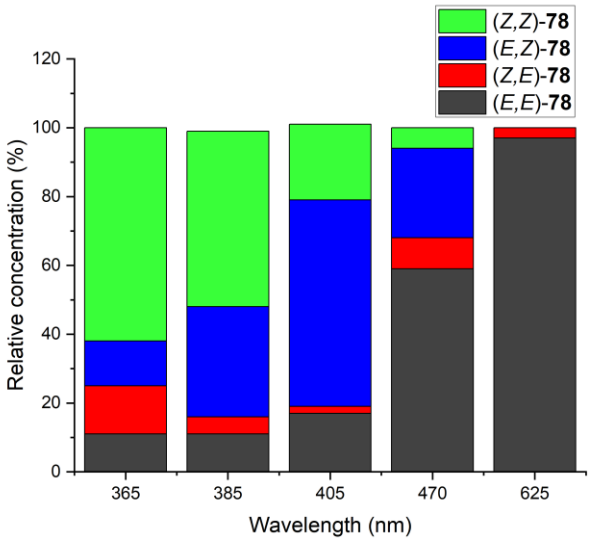

Figure 5.15. Isomeric composition after irradiation with light of different wavelengths, allowing the enrichment of 3 isomeric states.

The thermal relaxation from the (*Z*,*Z*) to the (*E*,*E*) isomer may theoretically proceed *via* two possible pathways, which are both composed of two consecutive first order reactions (Figure 5.16a). On the one hand, the (*Z*,*Z*) isomer may transform into the isomer (*Z*,*E*), which shall eventually regenerate the ground state. On the other hand, the second pathway involves the (*E*,*Z*) isomer as intermediary state, before complete reversion.

Given the half-lives measured for compounds **101** and **103**, and given that *p,p´*-azobenzenophanes are more stable in the (*Z*,*Z*) state than in the (*E*,*Z*) state, the following relationships may be assumed : $k_1 > k_2$, $k_4 > k_3$, $k_3 > k_2$ and $k_4 > k_1$. By following the evolution of the relative concentration of each isomer at 50 °C *via* NMR spectroscopy (Figure 5.16b), and by fitting the obtained data with the appropriate method (see experimental section), each rate constant was calculated. The obtained values are presented in Table 5.6.

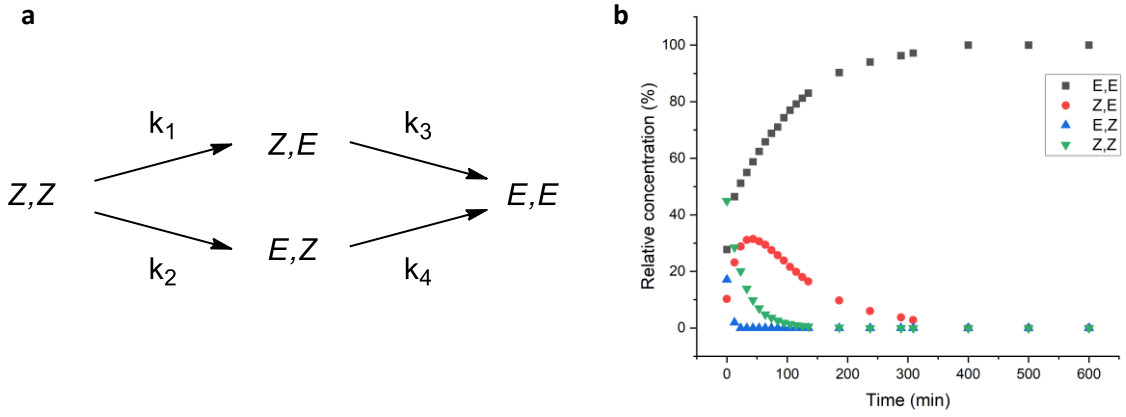

Figure 5.16. Schematic representation of the thermal relaxation process of (*Z*,*Z*)-**78** (a), and evolution of the relative concentration of each isomer with time (b), monitored by ^{1}H NMR (600 MHz) at 50 °C in DMSO-d_6 (1 mM).

Table 5.6. Thermal isomerization rate constants of **78** at 50 °C, and corresponding half-lives.

Entry	Reaction	Rate constant at 50 °C (min^{-1})	$t_{1/2}$ (min)
1	(*Z*,*Z*) → (*Z*,*E*)	$k_1 = 3.3 \times 10^{-2}$	21
2	(*Z*,*Z*) → (*E*,*Z*)	$k_2 = 2.2 \times 10^{-3}$	315
3	(*Z*,*E*) → (*E*,*E*)	$k_3 = 1.1 \times 10^{-2}$	63
4	(*E*,*Z*) → (*E*,*E*)	$k_4 = 2.0 \times 10^{-1}$	3.5

As could be expected, the least stable isomer corresponds to the (*E*,*Z*) state (Table 5.6, entry 4). In this state, the *cis*-DSAB, which is the least stable chromophore (Table 5.3, entry 2 *vs* 1), is subjected to a higher cyclic strain than in (*Z*,*Z*)-**78**, which results in a 3-fold shorter half-life than the linear reference **103**. Interestingly though, the half-life of (*Z*,*Z*)-**78** (Table 5.6, entry 1) is nearly twice as high as that of **103**. A similar effect is observed on the DMAB unit: in the (*Z*,*Z*) state, the thermal isomerization of the DMAB unit is slower than its open chain counterpart **101**, whereas in the (*Z*,*E*) state, it is faster (Table 5.6 entries 2 and 3 *vs* Table 5.3 entry 1). All these data fit very well with the behavior foreseen from the analysis of the linear parent molecules, which provides additional proofs of the correct identification of each isomers.

By considering all these data together, it was envisioned that cycles of irradiation with different wavelength could generate all four possible states (Scheme 5.1). Indeed, the (*E*,*Z*) state could not be enriched with any of the tested wavelengths, but as seen in Figure 5.13b, and as expected from the responsivity of **101** and **103** to red-light, one might generate this state by using a short (1-2 min) irradiation with 625 nm light, starting from the (*Z*,*Z*) state. Therefore, starting from the ground state,

irradiation at 365 nm produced 62% of (*Z*,*Z*). Subsequently, the (*Z*,*E*) state was enriched up to 49% with only 1 min of irradiation at 625 nm. Then irradiation with 405 nm light produced 60% of (*E*,*Z*), while the ground state was nearly quantitatively recovered upon 625 nm irradiation for 20 min (Scheme 5.1a).

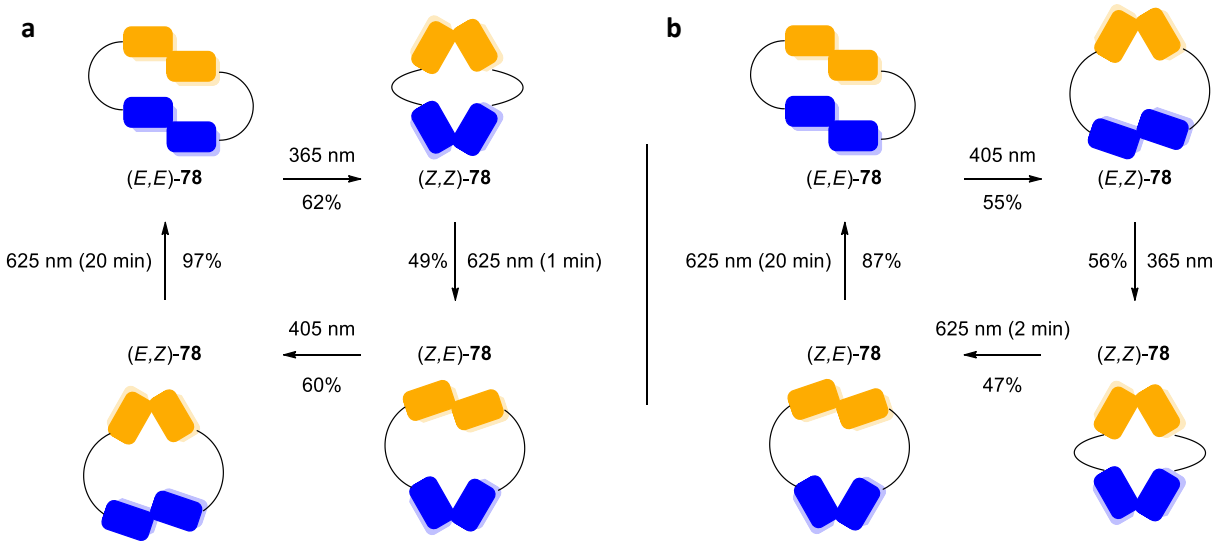

Scheme 5.1. Selective multistate switching of macrocycle **78**.

In a second sequence (Scheme 5.1b), each AB unit was addressed in an apparently more selective manner. Starting from the ground state, the DSAB unit was selectively isomerized with light of 405 nm, providing the (*E*,*Z*) state in 55% yield. Then, the DMAB unit was addressed with light of 365 nm yielding 56% of the (*Z*,*Z*) isomer. Subsequently, the DSAB unit was once again selectively addressed with red-light, which provided 47% of (*Z*,*E*) after 2 min of irradiation with 625 nm light, and 87% of the (*E*,*E*) were recovered when prolonging the irradiation for 20 min. The yield of the last step in this cycle was reduced compared with the first cycle, as consequence of the difference in responsivity with red-light between the DMAB and the DSAB units.

Stimulated by these results, the complexation of (*E*,*E*)-**78** with terephtalonitrile was attempted. This electron-deficient aromatic molecule, was recently shown to intercalate between the two azo units of a macrocyclic *bis*-azo-arene system in the (*E*,*E*) state, while being released upon isomerization .[221d] The size of the macrocycle involved in this study was however 8 atoms larger than **78**, and no sign of complexation was observed with **78**. Of course the size of the cavity is an important parameter in this process, but the orientation of each AB unit is also critical. For the complexation to occur, both AB units need to be stacked, and their plane orthogonal to the overall plane of the macrocycle. However, the DSAB unit of **78** is so red-shifted that the phenyl rings and the C-S-C linkage must be coplanar, and given the conformational restriction in **78**, it is likely that both AB units actually do not face each other.

Thus, glycoazobenzenophane **78** appears as a very interesting molecule, exhibiting multistate switching possibilities, and potentially many other features that were not yet investigated, such as chiroptical switching and complexation abilities for example. To the best of our knowledge, it is the first time that four-state switching is achieved with only two AB units in a macrocycle, and the concept of embedding two different chromophores in a macrocycle to achieve multistate switching was shown highly promising. Further studies on the chiroptical properties of this macrocycle and quantum yields measurements are ongoing. Following, the properties of the fluorinated AB macrocycle **79** were investigated in the same manner, and are described in the next section.

5.2.3. Properties of glycoazobenzenophane 79

As before, in a first time, the chemical shifts of characteristic signals were compared between the cyclized form **79** and the open chain compounds **101** and **104**. The changes are detailed in Table 5.7. Then the responsivity of macrocycle **79** to light of different wavelength was assessed (Figure 5.17), and NMR analysis in correlation with the evolutions observed in the UV-Vis spectra allowed the identification of each isomer (Figure 5.18). Then the isomeric composition was determined at different wavelengths (Figure 5.19), the ratios are shown in Table 5.8. Finally, the thermal relaxation of (*Z*,*Z*)-**79** was monitored by NMR and allowed the calculation of the thermal isomerization rate constants, giving the relative stability of each isomer.

Table 5.7. Chemical shifts of characteristic signals of derivatives **79** in comparison with **101** and **104**.[a]

Entry	Compound	DMAB		TFAB		CH_2 (DMAB)		H-6		H-1
		H_{ortho}	H_{meta}	H_{ortho}	H_{meta}	a	b	a	b	
1	**101**	7.83	7.56	-	-	4.05	3.87	-	-	4.03
2	**104**	-	-	-	7.31	-	-	3.55	3.09	-
3	**79**	7.35	7.20	-	7.36	3.93	3.75	3.81	3.11	3.82

[a] All spectra were recorded in DMSO-d_6 (600 MHz, 300 K) at 1 mM.

As observed for macrocycle **78**, the chemical shifts of the DMAB unit in **79** were all shielded, although in a lesser extent. Compared to **104**, the H-6 protons of **79** were deshielded, and their separation was increased. The anomeric proton was also slightly shifted upfield, as seen in **78**. The π→π* transitions were also red-shifted comparably to **78**, with maximums of absorption at 354 and 404 nm. In analogy to **78**, irradiation at 365 nm effected the simultaneous decrease of both bands indicating the conversion to the (*Z*,*Z*) isomer (Figure 5.17a). Then, using 385 or 405 nm reduced the absorbance at 404 nm while it was increased at 354 nm indicating the formation of the (*E*,*Z*) isomer. Blue-light irradiation (470 nm) then resulted in the increase of the absorbance of both bands, suggesting the regeneration of the (*E*,*E*) form. As observed in the other TFABs (**36**, **71**, **73** and **104**) studied in this thesis, the use of red-light provokes the *trans* → *cis* isomerization whereas it effects the opposite reaction in non-fluorinated ABs. Therefore, the use of this wavelength should promote the formation of the (*E*,*Z*) isomer. Unfortunately, the use of orange and red-light did not show any improvement compared to light of 405 nm in generating (*E*,*Z*)-**79** (Figure 5.17b).

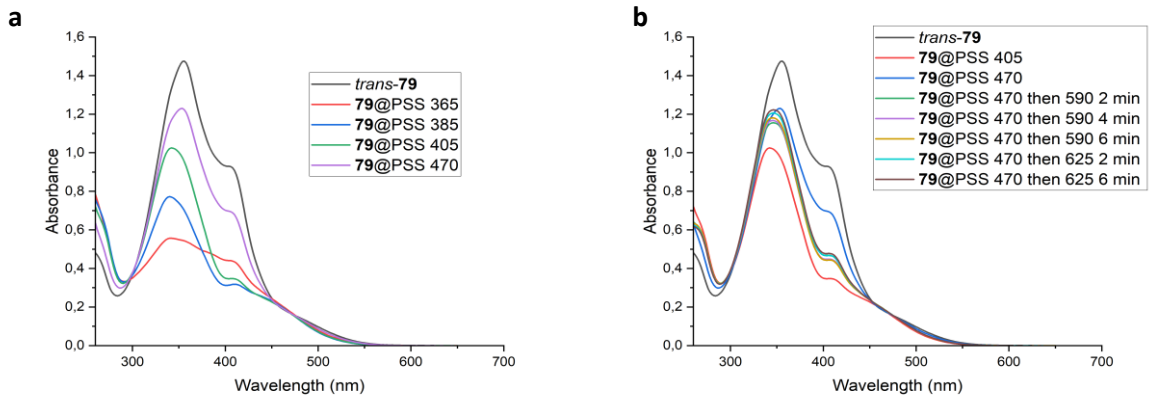

Figure 5.17. Evolution of the UV-Vis spectrum of azobenzenophane **79** in DMSO (50 µM) at 25 °C upon irradiation with UV to blue-light (a), or with blue and orange or red-light (b).

Then, careful analysis of the evolution of the ^{1}H spectra after irradiation with light of different wavelengths, correlated with the observed modifications of the UV-Vis spectra, and comparison with the linear molecules **101** and **104** allowed the identification of all isomers (Figure 5.18).

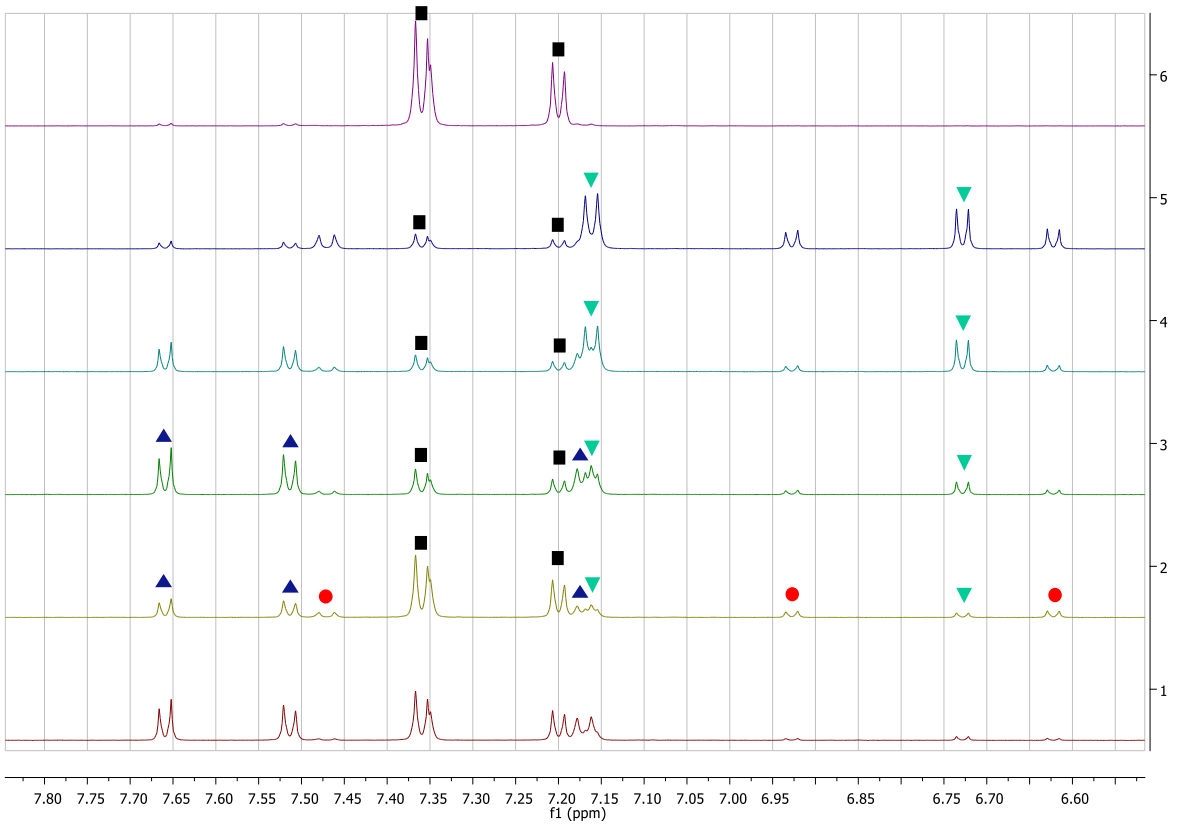

Figure 5.18. Expansion in the aromatic region of the ^{1}H NMR spectrum (600 MHz, 300 K) of **79** in DMSO-d_6 (1 mM) in the (*E*,*E*) state (violet), and evolution of the isomeric composition after irradiation 2 min at 365 nm (blue), 385 nm (turquoise), 405 nm (green), 470 nm (yellow) and 10 min with 625 nm (red). The signals of each isomer were attributed by correlating the evolutions of the UV-Vis and NMR spectra in comparison with the data obtained for compounds **101** and **104**. ■: (*E*,*E*); ●: (*Z*,*E*); ▲: (*E*,*Z*); ▼: (*Z*,*Z*).

In the ground state, only two signals are visible. The first one at 7.36 ppm comprises the protons of the TFAB unit overlapping with the *ortho* protons of the DMAB unit. At 7.20 ppm are located the *meta* protons of the DMAB unit, which are exploitable for integration. Then after irradiation at 365 nm, 9 signals are visible, meaning that 4 signals are overlapping, of which the one at 7.36 ppm. The major compound in this mixture was assumed to be the (*Z*,*Z*) isomer. This compound also showed only two signals instead of 3, so there must be an overlap again between the aromatic protons. Therefore, the signal at 6.73 ppm, which integrates for less than half the signal at 7.16 ppm, may be used for the integration. Then irradiation with 385 and 405 nm light led to the progressive augmentation of two peaks in the left part of the spectrum, presumably belonging to the (*E*,*Z*) isomer, and which seem both well resolved and exploitable. Also, the shape of the signal at 7.16 ppm changed, indicating that in addition to the peaks of the (*Z*,*Z*) isomer, there is also a peak of the (*E*,*Z*) form at this shift. Finally, by elimination, the peaks at 7.47, 6.93 and 6.62 can safely be attributed to the (*Z*,*E*) isomer. Interestingly, the cyclic strain in the mixed isomers improves the resolution between the signals of the TFAB and the DMAB units. Then, the proportions of each isomer were measured after reaching the PSSs with different wavelengths (Figure 5.19a, Table 5.8). The quantity of (*Z*,*Z*) in the PSS after irradiation at 365 nm was lower than for **78** (51% *vs* 62%), while the amount of (*Z*,*E*) was higher (25% *vs* 14%), as could be expected from the lower photoconversion observed for TFAB **104**. At 385 nm, the proportion of (*Z*,*Z*) diminished by 10% while the relative concentration of (*E*,*Z*) went up to 35%. At 405 nm, the (*E*,*Z*) became the major isomer with 55%, and the ground state was regenerated up to 59% upon 470 nm irradiation. Finally, at 625 nm, the mixture contained almost exclusively the (*E*,*E*) and the (*E*,*Z*) isomers, while the two other forms accounted for only 8%.

Table 5.8. Isomeric composition after irradiation with different wavelengths.[a]

Isomer of 79	PSS 365 (%)	PSS 385 (%)	PSS 405 (%)	PSS 470 (%)	PSS 625 (%)[b]
E,E	13	15	23	**59**	43
Z,E	25	8	6	9	3
E,Z	9	35	**55**	6	**49**
Z,Z	**52**	**42**	16	25	5

[a] The values in bold represent the major isomer in a given PSS mixture; [b] The measure was taken after successive irradiations of 2 min at 470 nm and 5 min with 625 nm light.

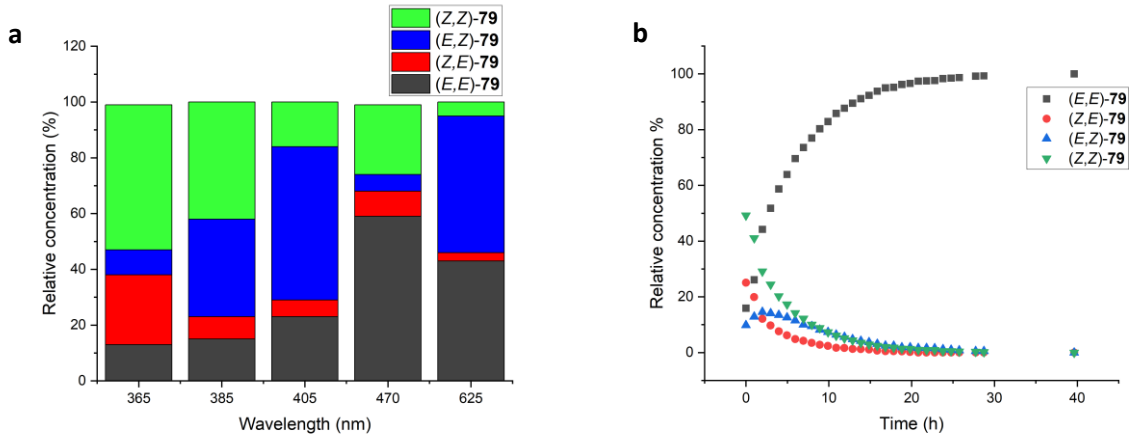

Figure 5.19. Isomeric composition after irradiation with light of different wavelengths, allowing the enrichment of 3 states (a), and evolution of the relative concentration of each isomer with time (b), monitored by ^{1}H NMR (600 MHz) at 50 °C in DMSO-d_6 (1 mM).

Finally, the thermal relaxation of macrocycle **79** was monitored by NMR at 50 °C starting from the PSS after irradiating with light of 365 nm (Figure 5.19b). Given that the relative thermal stability between the two azo units has been inverted compared to **78**, it was expected to see an inversion in the profiles of the (*E*,*Z*) and (*Z*,*E*) isomers. As can be seen, the enrichment of the (*Z*,*E*) isomer in this compound is impossible, neither photochemically nor thermally. Fitting of the profiles provided the thermal isomerization constants which are presented in Table 5.9. As observed before, the thermal stability of the DMAB unit was improved compared to the linear precursor **101** in the (*Z*,*Z*) form, and reduced in the (*Z*,*E*) isomer. Also, the (*Z*,*E*) → (*E*,*E*) reaction had higher rate constant than **78** by a factor 2.9. Surprisingly, the *cis*-TFAB unit was generally less stable in the cyclized form than in the open chain derivative **104**, with a drop of about a factor of 7.6 in the (*E*,*Z*) state, and of 1.3 for the (*Z*,*Z*) form.

Table 5.9. Thermal isomerization rate constants of **79** at 50 °C, and corresponding half-lives.

Entry	Reaction	Rate constant at 50 °C (min^{-1})	$t_{1/2}$ (min)
1	(*Z*,*Z*) → (*Z*,*E*)	$k_1 = 1.6 \times 10^{-3}$	433
2	(*Z*,*Z*) → (*E*,*Z*)	$k_2 = 1.8 \times 10^{-3}$	385
3	(*Z*,*E*) → (*E*,*E*)	$k_3 = 3.2 \times 10^{-2}$	22
4	(*E*,*Z*) → (*E*,*E*)	$k_4 = 9.5 \times 10^{-3}$	73

It is unfortunate that the properties of the TFAB unit were so much altered by the electron donation of the sulfur atoms. The red-shift issue of the π→π* transition in this compounds may either be solved by oxidation of the sulfur bridges, or by inserting a CH_2 group between the phenyl ring and the sulfur. This compound shows similar switching properties as macrocycle **78**, although with smaller photoconversion yields, and an improved thermal stability. If three-state switching was possible with

79, no efficient trigger was found for the enrichment of the fourth (*Z*,*E*) state. Finally, in the next part will be described some properties of the first thermodynamically stable (*Z*,*E*) *bis*-azobenzenophane.

5.2.4. Properties of glycoazobenzenophane 95

The investigation of macrocycle **95** (Figure 5.20) started with a careful analysis of its NMR spectrum in the ground state. Very interestingly, in deuterated chloroform ($CDCl_3$), nearly all signals were separated, in contrast with macrocycles **78** and **79**, for which the signals of both sugar moieties were identical. This is due to the ethylene bridge in the cyclic AB unit (CAB), which breaks the symmetry of the molecule. In fact, **78** and **79** are characterized by a C_2 rotational axis, passing through the middle of both N=N bonds. In **95**, this axis is no more existent, therefore the groups on each side of the azo units are no longer equivalent. This feature is also a good proof of the orientation of the carbohydrates within the macrocycle backbone. Previous modeling suggested that the sugar moieties had an opposite orientation on the macrocycle, by a 180 ° rotation, making that their hydroxyl groups were oriented either up or down, regarding the plane of the macrocycle.[268e] The observed separation of the signals for the CAB and the carbohydrate units in **95** would tend to confirm this orientation.

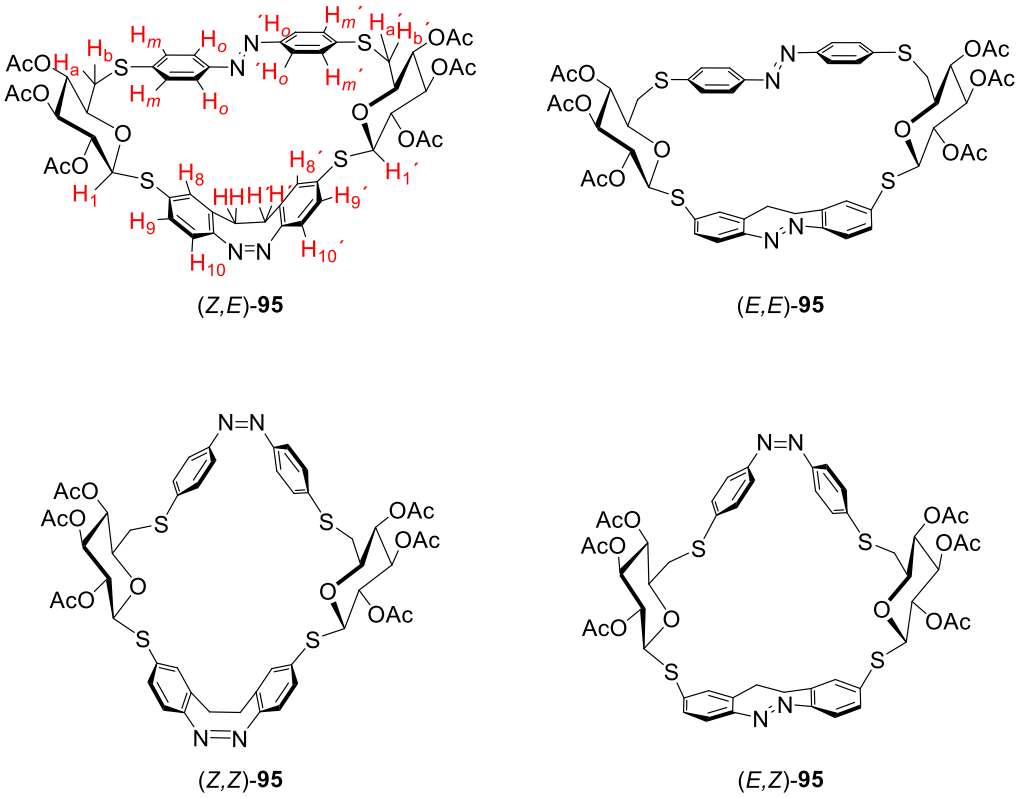

Figure 5.20. Structures of the four possible isomers of **95**. The red hydrogens shown in the (*Z*,*E*) structure are those used for comparison with the open chain derivatives **41** and **103**.

The chemical shifts of the protons of the diazocine and the anomeric protons between **95** and **41** were compared in $CDCl_3$ and those of the DSAB unit and the H-6 protons in **95** and **103** were compared in DMSO, and the values are compiled in Table 5.10. As can be seen, all the signals of the CAB unit were shifted upfield, presumably due to the shielding effect of the DSAB unit positioned on top of the CAB unit. Additionally, all signals for the CAB were separated, which was not observed in the linear counterpart **41**. Indeed, a certain separation of the H_9 was noticed in **41** and interpreted as being due to rotational isomerism, but the effect is much stronger in **95** as a consequence of the immobilization of the molecule in a conformationally restricted arrangement. The anomeric protons were also slightly shifted upfield and well separated. Interestingly, the H_{ortho} of the DSAB unit were nearly unaffected by

the cyclization, while the H_{meta} were slightly deshielded, which reduced the separation of both signals. The separation of the H-6 protons of the sugar was reduced however compared with **103**, which contrasts with what was observed for **78** and **79**, and probably reflects the difference in cyclic strain.

Table 5.10. Chemical shifts of characteristic signals of derivatives **95** in comparison with **41** and **103**.

Entry	Cpd.	CAB[a]					DSAB[b]		H_1[a]	H-6a[b]	H-6b[b]
		H_8	H_9	H_{10}	CH_2a	CH_2b	H_{ortho}	H_{meta}			
1	**41**	7.13	7.32, 7.37	6.80	2.97	2.76	-	-	4.65	-	-
2	**103**	-	-	-	-	-	7.81	7.50	-	3.53	3.07
3	**95**	6.56, 6.49	6.36, 6.14	6.10	2.73, 2.70	2.39, 2.32	7.83, 7.82	7.74	4.55, 4.41	3.45	3.30

[a] The values were measured in $CDCl_3$ (600 MHz, 300 K); [b] The values were measured in DMSO-d_6 (600 MHz, 300 K).

Then, the evolution of the UV-Vis spectrum of **95** in DMSO upon irradiation with different wavelengths was examined (Figure 5.21). As mentioned in chapter 3, irradiation with UV or blue-light should favor the (*E*,*Z*) state, while the ground state should be regenerated with green to red-light. Also, because the CAB has faster kinetics than the DSAB in the far red range, it should be possible to effect the selective back isomerization of the CAB unit by using a short irradiation with far red-light (>650 nm). The spectrum of **95** in the ground state is characterized by a single band centered at 393 nm, presumably corresponding to the π→π* transition of the DSAB unit. Interestingly, this transition has the same maximum of absorption as the linear compound **103**, in contrast with the red-shift observed in **78** and **79**.

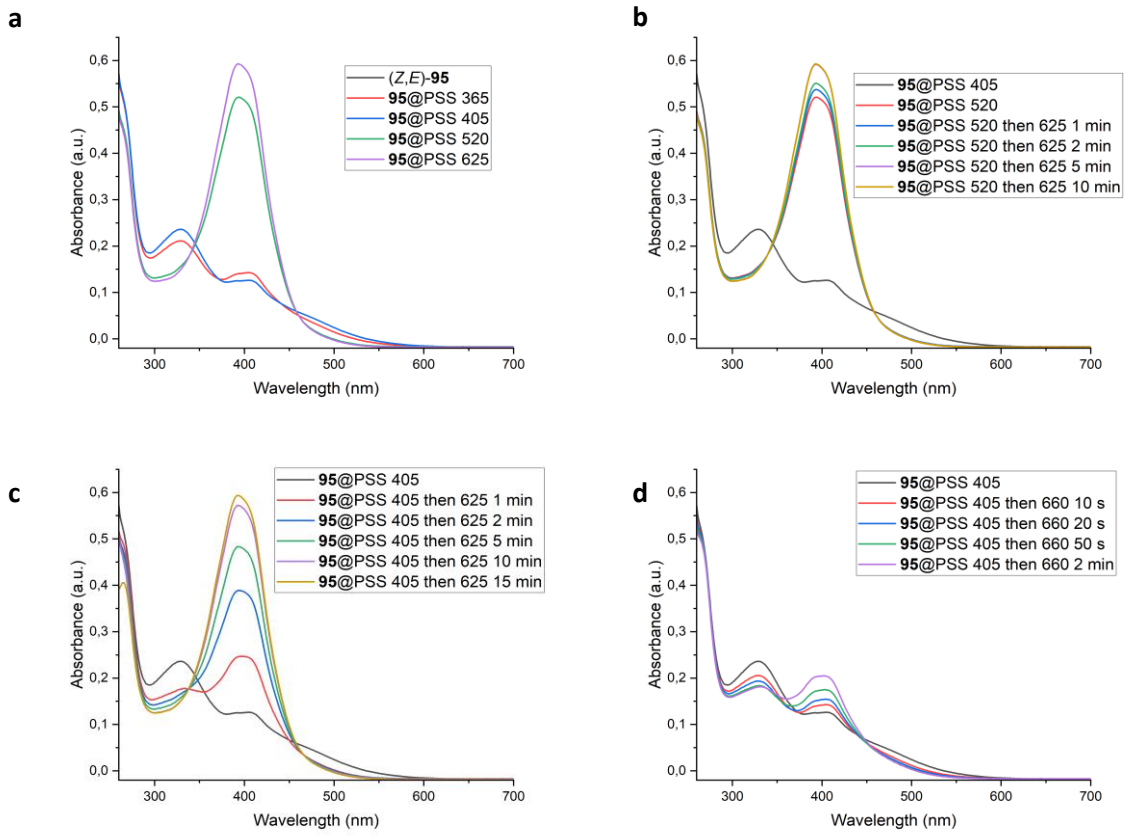

Figure 5.21. Evolution of the UV-Vis spectrum of azobenzenophane **95** in DMSO (50 µM) at 25 °C upon irradiation with UV to red-light (a), with green and red-light (b), with blue and red-light (c), or with blue and far-red-light (d).

Upon irradiation with UV-light, the absorbance at 393 nm was strongly reduced indicating the $E \rightarrow Z$ isomerization of the DSAB unit. A new band appearing at 332 nm and the increase of the absorbance between 458 and 600 nm indicate also the isomerization of the CAB unit, therefore predicting a (*E*,*Z*)-rich PSS. Upon irradiation at 405 nm, the conversion seemed slightly improved, while irradiation with light of 520 nm regenerated the (*Z*,*E*) ground state (Figure 5.21a).

From the PSS 520, irradiation with red-light for only 5 min quantitatively regenerated the ground state (Figure 5.21b), while it needed between 10 and 15 min when starting from the PSS 405 (Figure 5.21c). Finally, from the PSS 405 which should be rich in (*E*,*Z*) isomer, irradiation with far red-light (660 nm) should selectively isomerize the CAB unit favoring the (*Z*,*Z*) and (*Z*,*E*) isomers. Therefore, in less than a minute of irradiation, a rapid decrease of the absorbance at 332 and >458 nm occurred, until reaching what seemed to be a plateau, indicating the isomerization of the CAB unit. In contrast the absorbance at 393 nm only slightly increased gradually.

Then, the evolution of the NMR spectrum with 4 different wavelengths was monitored (Figure 5.22). Unfortunately, due to the separation of the signals of the diazocine, the aromatic part of the spectrum was unexploitable, however, the carbohydrate part showed that several signals were well resolved.

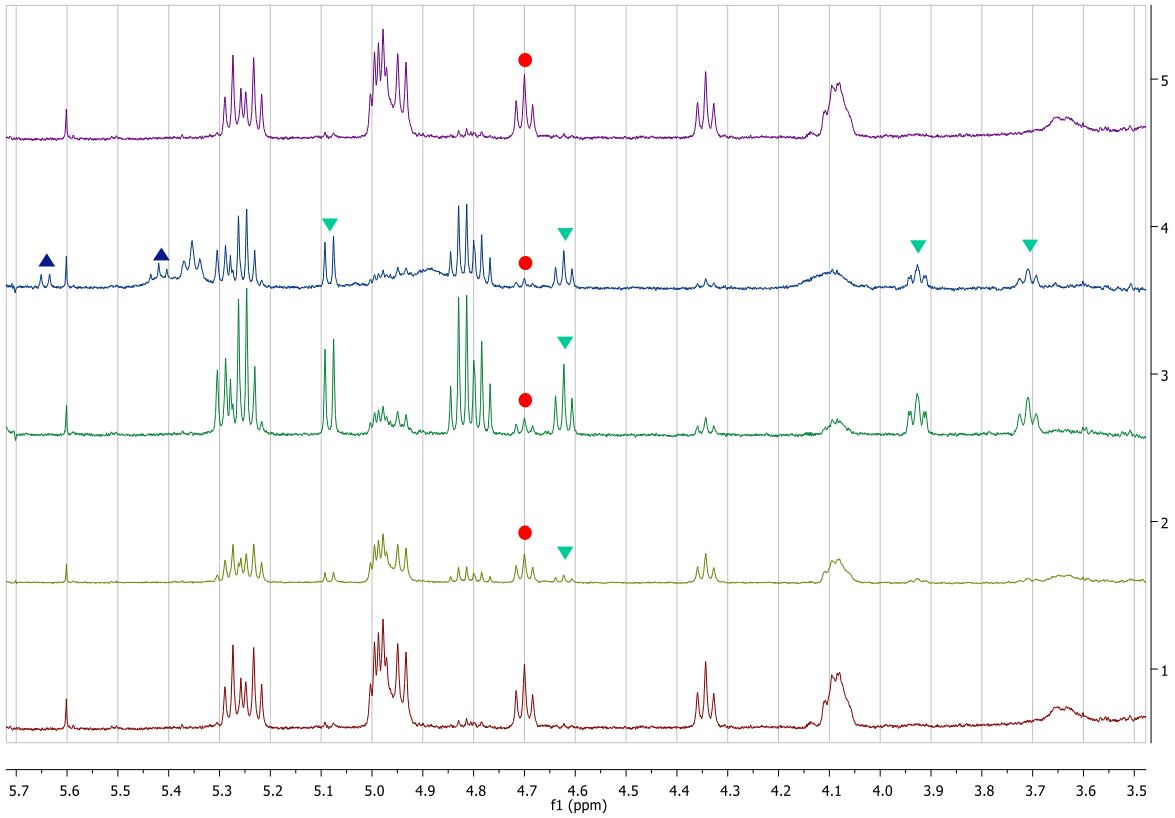

Figure 5.22. Expansion in the carbohydrate region of the ^{1}H NMR spectrum (600 MHz) of **95** in DMSO-d_6 (1 mM) at 300 K in the (*Z*,*E*) state (violet), and evolution of the isomeric composition after irradiation for 2 min at 405 nm (blue), then 30 s at 660 nm (green), 2 min at 520 nm (yellow), and 5 min at 625 nm (red). The signals of each isomer were attributed by correlating the evolutions of the UV-Vis and NMR spectra in comparison with the data obtained for compounds **41** and **103**, and by the identification of the (*E*,*E*) isomer (*vide infra*). At this stage, the identification of each species is uncertain.

Indeed, two triplets at 4.70 and 4.35 ppm corresponding to the H-2 seemed usable. Starting from the ground state, irradiation at 405 nm provoked the apparition of new sets of signals. On the one hand, four well resolved signals at 5.08, 4.62, 3.93 and 3.71 ppm, were all integrating for 1 proton, and thus seemed to belong to the same molecule. On the other hand, two smaller signals at 5.64 and 5.42 ppm seemed to indicate the presence of a third species. After irradiation for 30 s at 660 nm which should

selectively isomerize the CAB unit, the signals at 5.64 and 5.42 and 5.35 ppm disappeared, while those at 5.08, 4.62, 3.93 and 3.71 ppm increased, making this molecule largely predominant in the mixture. This would tend to indicate that the signals that disappeared corresponded to the (*E*,*Z*) form and that the newly formed compound was the (*Z*,*Z*) isomer. Then irradiation with green and red-light progressively regenerated the ground state. These data indicate the formation of at least 3 isomers, but one seems missing, presumably the (*E*,*E*). However, the (*E*,*Z*) isomer which was expected to be major upon irradiation at 405 nm was only minor. Hence, these results contrast with the observed evolution of the spectrum by UV/vis spectroscopy.

Fortunately, the last isomer was fortuitously generated during a manipulation error. During an irradiation experiment with 405 nm light, the NMR tube was too close to the irradiation source, and therefore was strongly heated while being irradiated. The obtained spectrum following this manipulation showed the presence of the last unidentified isomer, with a doublet at 5.59 ppm (Figure 5.23).

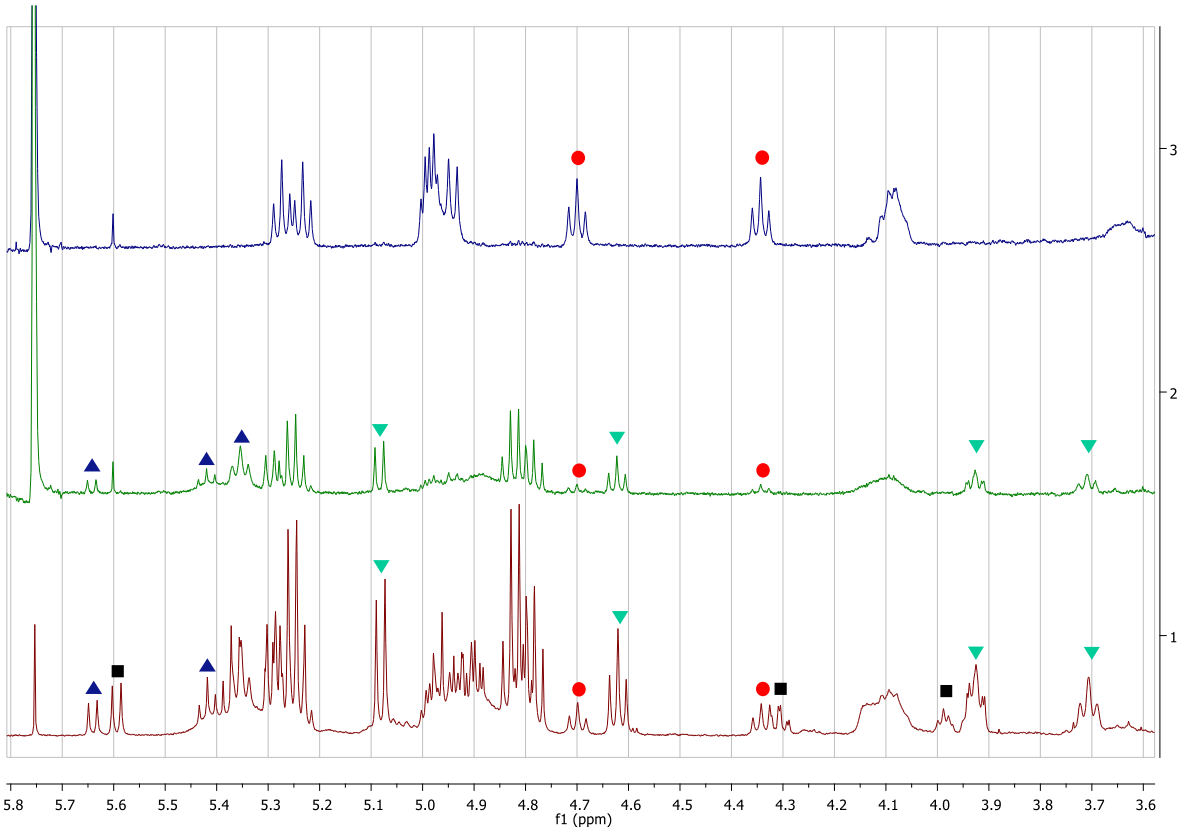

Figure 5.23. Expansion in the carbohydrate region of the ^{1}H NMR spectrum (600 MHz, 300 K) of **95** in DMSO-d_6 (1 mM) in the (*Z*,*E*) state (blue), and evolution of the isomeric composition after irradiation for 2 min at 405 nm without heating (green), or with heating (red). The signals of each isomer were attributed by correlating the evolutions of the UV-Vis and NMR spectra, in comparison with the data obtained for compounds **41** and **103**, and by the identification of the (*E*,*E*) isomer. ■: (*E*,*E*); ●: (*Z*,*E*); ▲: (*E*,*Z*); ▼: (*Z*,*Z*). Note: The peak at 5.6 ppm in the blue and green spectra is a satellite peak from residual CH_2Cl_2 in the sample. In the red spectrum this peak should have disappeared as the compound was further dried under vacuum prior to analysis.

Therefore, the identification was possible: at 405 nm, the PSS contained a majority of (*Z*,*Z*), along with small amounts of (*E*,*Z*) and (*Z*,*E*). When irradiating with 660 nm light, all the (*E*,*Z*) was converted to the (*Z*,*Z*), giving a mixture with only two isomers. Finally, it seems that the (*E*,*E*) isomer can be enriched upon heating, which indicates that in the (*E*,*Z*) form, the *cis*-DSAB would relax faster than the *trans* CAB. This identification correlates well with the fact that the most downfield shifted protons are one of the H-1 protons of the two isomers having the CAB in *trans*. This was confirmed by HSQC, which

showed 6 correlation peaks for the H-1 protons. The correlation peak for the doublet at 5.64 ppm was not observed, perhaps due to the low concentration of this isomer, and explaining the two missing correlation peaks. It is quite surprising that the quantity of (*E*,*Z*) after 405 nm irradiation was so small, but the generation of this isomer might require longer irradiation time, or a lamp of higher intensity.[209,210b]

Thanks to the good resolution of at least one peak per isomer, the isomeric composition after irradiation could be finally determined (Table 5.11). The (*Z*,*Z*) isomer was generally obtained after irradiation with UV or blue-light with yields of 70 and 62% respectively. The (*Z*,*Z*) could be enriched up to 75% by applying a combination of blue and far red-light, while the ground state was regenerated up to 81% with green-light and quantitatively in 5-15 min with red-light (625 nm).

Table 5.11. Isomeric composition after irradiation with different wavelengths.[a]

Isomer of 95	PSS 385 (%)	PSS 405 (%)	PSS 660 (%)[b]	PSS 520 (%)	PSS 625 (%)
E*,*E	0	0	0	0	0
Z*,*E	16	20	25	**81**	**>98**
E*,*Z	14	19	0	0	0
Z*,*Z	**70**	**62**	**75**	19	<2

[a] The values in bold represent the major isomer in a given PSS mixture; [b] The measure was taken after successive irradiations of 2 min at 405 nm and 30 s with 660 nm light.

In contrast with the previously studied glycoazobenzenophanes **78** and **79**, **95** is characterized by high photoconversion yields, and the fact that only the (*Z*,*Z*) can be enriched photochemically, although in theory the (*E*,*Z*) should be favored with UV and blue-light. Thermal relaxation studies would be necessary to see if the other isomers could be enriched thermally, and to study the relative stability of each isomer, unfortunately due to time constraints, this could not be achieved. The diazocine-containing macrocycle **95** is the very first example of *bis*-azobenzenophane thermodynamically stable in the (*Z*,*E*) state, and its investigation sadly had to be interrupted. Further studies should be realized to investigate the complexation and chiroptical properties of these new glycoazobenzenophanes, allowing to find an application for their use. Indeed, the multistate switching might be interesting for applications such as optical memory devices, but the inherent chirality of these cycles and the strong strain imposed by their structure might make them potentially very interesting as chiral dopants, as shown recently by Xie et al.[282]

6. Conclusion

In this thesis, the synthesis of glycoazobenzene macrocycles was scrutinized in order to find the highest yielding procedures towards the elaboration of photoresponsive glycoconjugates. First, the glycosylation of *p,p´*-dihydroxyazobenzene (DHAB) was thoroughly investigated. The limitations of this reaction regarding its scope and efficacy were delineated, and optimized reaction conditions were found that produce the desired glycoconjugates in 50-70% yield. Alternative synthesis pathways with different protecting group strategies were proposed to further increase the yield of glycosylation, and produce macrocycle precursors in a similar amount of steps. Such macrocycle precursors, possessing an azide function in the position 6 of the sugar, were prepared in 5 steps from D-glucose in an overall yield of 30%.

In a second time, another reaction was investigated for the glycoconjugation of carbohydrates to azobenzene. The palladium-catalyzed thioarylation of glycosyl thiols was used as an alternative to the glycosylation to functionalize AB derivatives by keeping the shortest linkage between the sugar and the photoswitch (*i.e.* a glycosidic bond). This reaction was shown to have a large scope of substrates, producing a large variety of AB-conjugates in very high yields, with excellent chemoselectivity between iodine and bromine. This chemoselectivity allowed the sequential hetero-difunctionalization of AB derivatives generating unsymmetrical derivatives. Importantly, one pot procedures for the difunctionalization of *p*-iodo-*p´*-bromoAB were established, producing unsymmetrical derivatives in one step in excellent yields (>70%). In addition, the use of the thioether group as a tether between the AB and the carbohydrate moieties allows the tuning of the photochromic properties of the switch by oxidation of the sulfur atoms. Such a modulation provides access to derivatives with a wide thermal stability range (0.5-100 h at 40°C), and showing excellent photoswitching properties with a wide addressability range. Notably, red-shifted derivatives addressable with visible light only were discovered, and 2 pairs of AB derivatives showing selective photoswitching properties were studied. In summary, this thioarylation method presents two main advantages compared with the glycosylation: a synthetic advantage in terms of efficacy and diversity of structures, and a photochromic advantage thanks to the modulation of the properties through oxidation.

Then, by using the macrocycle precursors obtained by glycosylation of DHAB, four new AB glycophanes were synthesized by means of an intermolecular thiourea bridging reaction between an AB-*bis*-glycoside bearing isothiocyanate functions and different diamines. An optimized procedure for the cyclization was elaborated, allowing access to four new AB glycomacrocycles **74**-**77** in 53-82% yield, and 14-21% overall yield starting from D-glucose. The main concept of the synthesis, lying on an efficient functionalization of DHAB (glycosylation, alkylation, Mitsunobu…), followed by a high yielding annulation reaction can be adapted to other non-carbohydrate-based materials, allowing an easy and effective access to a variety of AB macrocycles based on the dialkoxyAB chromophore.

Secondly, the nucleophilic substitution of glycosyl thiols was used to conjugate carbohydrates to a *p,p´*-dibromomethylAB (DMAB chromophore), and the thioarylation reaction was used in the annulation step for the fabrication of macrocyclic glycoazobenzene dyads. The conditions for the cyclization were optimized, providing access to two novel glycoazobenzenophanes **78** and **79** in 55-70% yield, and in 21-27% overall yield in 7 steps starting from D-glucose. These two macrocycles were designed so as to have a long-lived UV-light addressable DMAB unit in anomeric position of the glucose, and a red-shifted AB unit based on the *p,p´*-dithioAB chromophore (DSAB) or the *p,p´*-dithio-tetra-*o*-fluoro AB chromophore (TFAB). Finally, another macrocycle bearing a cyclic AB unit (CAB) in the anomeric position, and a DSAB unit in the position 6, was synthesized. It was cyclized under the optimized thioarylation conditions, although the desired macrocycle **95** was isolated in a lower yield.

In a final part, the photochromic properties of the synthesized macrocycles were investigated. The photoswitching behavior and the thermodynamic parameters of the four thiourea bridged macrocycles were analyzed, and compared with the previously reported macrocycle **105**. Their thermal relaxation behavior was examined, and the extraction of the thermodynamic parameters from Arrhenius and Eyring plots showed that their thermal stability was correlated with the length and rigidity of the linking diamine. A compensation relationship was evidenced between cycles **74**-**76**, suggesting a similar thermal isomerization mechanism, and the influence of the cyclic strain on the stability of the metastable state was paralleled with other studies on azobenzenophanes. Then, the properties of macrocycles **78**, **79** and **95** were examined. Macrocycle **78** showed unprecedented four-state switching with enrichments of each of the three possible metastable isomers up to 50-60%, and near quantitative back-switching with red-light. In contrast, the photoswitching properties of macrocycle **79** were slightly impaired compared to **78**, but its thermal stability was improved. Finally, only preliminary studies could be conducted with macrocycle **95**, but this new macrocycle seems also very interesting. It is the first azobenzenophane thermodynamically stable in the (*E*,*Z*) state, and shows high yielding two-state switching (75-100%) between the ground state and the (*Z*,*Z*) isomer. In addition, a separation of the proton signals of each sugars observed by NMR spectroscopy suggests a very specific orientation of the carbohydrates, and hints a potentially large chiroptical power.

In the end, azobenzene-containing glycomacrocycles are fascinating molecules showing multifaceted properties that should be investigated further. As shown, the cyclization has a strong impact on the photochromic properties, especially the thermal stability, and could be used as a mean to develop new AB derivatives with tailored characteristics. Notably the thiourea bridging reaction could be performed on different positions of the carbohydrates, for example on the position 2 by using glucosamine as a scaffold. It would provide access to a large variety of macrocycles of different shapes and conformational strain, from simple starting materials. Secondly, the chiroptical properties of such derivatives might be exploited in various fields such as chiral recognition and/or catalysis, or for the optical switching of cholesteric liquid crystals for instance. The addition of a second AB chromophore in the macrocycle was shown very promising for the design of multistate photoswitches. By optimizing the conformational freedom and the substitution of the different AB units, their properties may be finely tuned, so as to achieve orthogonal multistate switching. This behavior could be very interesting for the elaboration of optical logic gates, or optical memory devices, provided that the derivatives are sufficiently thermally stable. Furthermore, the multistate photoswitching could be exploited for the fine tuning of interactions, in a biological or a supramolecular context for instance, by using the carbohydrate scaffold to graft functional groups or biological ligands.

7. Experimental section

7.1. Materials and methods

All reactions were carried out under atmospheric conditions (unless otherwise stated). Moisture-sensitive reactions were carried out under a nitrogen atmosphere in flame-dried glassware.

Solvents and chemicals

All chemicals were purchased from ABCR, Acros, Alfa Aesar, Merck, Sigma-Aldrich or TCI, and used without further purification. For extractions and column chromatography, technical grade solvents were used, which were distilled before use. Dry solvents were either directly purchased from the manufacturer or dried by an Inert PureSolv MD5 solvent purification system.

Acetonitrile	over calcium hydride
Dichloromethane	over aluminum oxide
Methanol	over magnesium
Pyridine	over potassium hydroxide
THF	over aluminum oxide

Thin layer chromatography (TLC)

Analytical thin layer chromatography (TLC) was performed on silica gel plates (GF 254 Merck). Visualization was achieved by UV-light and/or by charring with 10 % sulfuric acid in ethanol, vanillin, or PPh_3/CH_3Ph and ninhydrin, followed by heat treatment at ca. 400 °C. (1.5 g ninhydrin and 15 mL acetic acid in 500 mL EtOH).

Flash chromatography

Flash chromatography was carried out on silica gel 60 (Merck, 230-400 mesh, particle size 0.040-0.063 mm) or by using an Interchim puriFlashR450 chromatography system with distilled solvents.

Nuclear magnetic resonance spectroscopy (NMR)

The ^{1}H and ^{13}C spectra were recorded on following spectrometers at 298 K:

Bruker AC 200	^{1}H NMR (200 MHz)	^{13}C NMR (50 MHz)
Bruker DRX 500	^{1}H NMR (500 MHz)	^{13}C NMR (126 MHz)
Bruker AV 600	^{1}H NMR (600 MHz)	^{13}C NMR (150 MHz)

Chemical shifts are referenced to the residual proton or the carbon signal of the used deuterated solvent.

$CDCl_3$	^{1}H 7.26 ppm (s)	^{13}C 77.2 ppm (t)
DMSO-d_6	^{1}H 2.50 ppm (quint)	^{13}C 39.5 ppm (sept)

Data are presented in the following format: chemical shift (δ) (multiplicity: s for singlet, d for doublet, dd for doublet of doublets, t for triplet, at for apparent triplet, bs for broad singlet, q for quartet, and m for multiplet; coupling constant in Hertz (Hz), integration, assignment). Full assignment of the signals was achieved by using 2D NMR techniques (^{1}H-^{1}H COSY, ^{1}H-^{13}C HSQC and ^{1}H-^{13}C HMBC). All NMR spectra of *trans*-isomer of azobenzene derivatives were recorded after samples were kept in the dark for at least 20 h at 40 °C for the non-fluorinated conjugates or at 60 °C for the fluorinated conjugates.

Mass spectrometry (MS)

ESI mass spectra were recorded on a Bruker Daltonics Esquire-LC instrument. EI mass spectra were recorded on a Jeol AccuTOF 4GCV instrument.

Infrared (IR) spectroscopy

IR spectra were recorded on a PerkinElmer FT-IR Paragon 1000 (ATR) spectrometer. The absorption bands are presented in cm^{-1}.

Optical rotations

Optical rotations were measured on a PerkinElmer 241 polarimeter (sodium D-line: 589 nm, cell length: 1 dm) in the indicated solvents. The specific rotation values $[\alpha]^{23}_{D}$ are given in [°.mL.g^{-1}.dm^{-1}] and the concentration *c* in [mol.mL^{-1}].

Irradiation experiments

For irradiation experiments, the samples were irradiated at the appropriate wavelength for 2 min (unless otherwise stated) at a distance of about 1-2 cm from the light source. Only for irradiation at with orange or red-light, were longer irradiation times required. Photo-irradiation was performed using either two UV LED (Nichia Corporation, emitting 365 nm light, with a FWMH of 10 nm and an intensity of 235 mW/cm² per LED, 1 LED; Nichia Corporation, emitting 385 nm light, with a FWMH of 9 nm and an intensity of 220 mW/cm² per LED, 1 LED), or a violet LED (in house built, emitting 405 nm light with a FMVH of 12 nm and an intensity of 190 mW/cm² per LED, 3 LED), or a blue LED (in house built, emitting 435 nm light, with a FWMH of 13 nm and an intensity of 130 mW/cm² per LED, 3 LEDs), or a green LED (Nichia Corporation, emitting 520 nm light, with a FWMH of 30 nm and an intensity of 190 mW/cm² per LED, 5 LEDs), or an orange LED (Osram, emitting 590 nm light, with a FWMH of 18 nm and an intensity of 130 mW/cm² per LED, 5 LEDs) or 3 red lamps (Sahlmann Photochemistry Solutions, emitting 630 or 660 nm light, with a FWMH of 20 nm and an intensity of 250 mW/cm² per LED, 3 LEDs ; and a light emitting at 690 nm with a FWMH of 29 nm and an intensity of 75 mW/cm² per LED, 3 LEDs).

7.2. Glycosylation of DHAB

7.2.1. Preparation of glycosyl donors

Donors **7**,[298a] **8**,[298b] **10**,[298c] **11**[298d] and **12**,[275,298d] were prepared starting from D-glucose according to known procedures.

1,6-anhydro-2,3,4-tri-O-((tert-butyldimethyl)silyl)-β-D-glucopyranose (19a).

To a mixture of levoglucosan (162 mg, 1.00 mmol) and N-methylimidazole (559 μL, 7.00 mmol, 7 eq) in dry pyridine (2.00 mL) was added Me_2t-BuSiCl (904 mg, 6.00 mmol, 6 eq). The mixture was stirred at RT for 30 min and then iodine (634 mg, 2.50 mmol, 2.5 eq) was added. The mixture was stirred for 24 h, and then was diluted in EtOAc. It was washed with satd. aq. $Na_2S_2O_3$ solution until the organic phase was colorless. Then it was washed with 1N HCl (3x), satd. aq. $NaHCO_3$ (1x) and brine (1x) before being dried over $MgSO_4$ and concentrated in *vacuo*. Column chromatography (cyclohexane:EtOAc 1:0 to 9:1) afforded the title compound **19a** (405 mg, 80%) as a white amorphous solid. The obtained analytical data are in agreement with reported literature.[364]

1,6-anhydro-2,4-di-O-((tert-butyldimethyl)silyl)-β-D-glucopyranose (19b).

To levoglucosan (200 mg, 1.23 mmol) in dry CH_2Cl_2 (17.0 mL) were added pyridine (4.20 mL, 51.7 mmol) and 4-dimethylaminopyridine (297 mg, 1.97 mmol, 1.6 eq). The resulting suspension was cooled to 0 °C, and Me_2t-BuSiCl (1.11 g, 7.38 mmol, 6 eq) was added as a solution in dry CH_2Cl_2 (17.0 mL). The mixture was stirred at 0 °C for 10 min, and then was allowed to stir at RT for 3 days. After that time, the solvent was removed in *vacuo*, and the resulting residue was triturated in toluene. The insoluble materials were filtered and the filtrate was concentrated. Column chromatography (cyclohexane:CH_2Cl_2:Et_2O 1:0:0 to 7:1.5:1.5) afforded the title compound **19b** (240 mg, 50%) as a white amorphous solid. The obtained analytical data are in agreement with reported literature.[364]

(6-azido-6-deoxy-2,3,4-tri-O-acetyl-α,β-D-glucopyranosyl)-1-(N-phenyl)-2,2,2-trifluoroacetimidate (12).

To a solution of 6-azido-6-deoxy-2,3,4-tri-O-acetyl-α,β-D-glucopyranose[275] (993 mg, 3.00 mmol) and cesium carbonate (1.47 g, 4.50 mmol, 1.5 eq) in dry CH_2Cl_2 (30.0 mL), was added 2,2,2-trifluoro-N-phenylacetimidoyl chloride (713 μL, 4.50 mmol, 1.5 eq) at RT. The mixture was stirred 1.5 h at RT, then it was diluted with CH_2Cl_2 and filtered through celite. The celite pad was washed with CH_2Cl_2 and the filtrate was concentrated in *vacuo*. Column chromatography (cyclohexane:EtOAc 8:2 to 7:3) afforded an anomeric mixture of the title compound **12** (1.35 g, 90%) as a white foam. **β-12** (major anomer): ^{1}H NMR (500 MHz, $CDCl_3$) δ = 7.32 (t, ^3J = 7.6 Hz, 2H, 2Ar-H_{ortho}), 7.14 (t, ^3J = 7.6 Hz, 1H, Ar-H_{para}), 6.86 (d, ^3J = 7.6 Hz, 2H, 2Ar-H_{meta}), 5.85 (bs, 1H, H-1), 5.26 (bs, 2H, H-2, H-3), 5.12-5.04 (m, 1H, H-4), 3.79 (bs, 1H, H-5), 3.41 (dd, $^2J_{6a,6b}$ = 13.6 Hz, $^3J_{6a,5}$ = 6.7 Hz, 1H, H-6a), 3.25 (dd, $^2J_{6b,6a}$ = 13.6 Hz, $^3J_{6b,5}$ = 2.6 Hz, 1H, H-6), 2.09 (s, 3H, CH_3CO), 2.04 (s, 3H, CH_3CO), 2.03 (s, 3H, CH_3CO) ppm; ^{13}C NMR (126 MHz, $CDCl_3$) δ = 170.3, 169.5, 169.1 (3C, $3CH_3CO$), 143.1 (Ar-C_{ipso}), 129.0 (2C, 2Ar-C_{ortho}), 124.8 (Ar-C_{para}), 119.4 (2Ar-C_{meta}), 74.5 (C-1), 72.5 (C-2), 70.7 (C-3), 70.2(C-4), 69.2 (C-5), 51.0 (C-6), 20.7, 20.6 (3C, $3CH_3CO$) ppm; ESI HRMS: m/z: calcd for $C_{20}H_{21}F_3O_8N_4 + Na^+$: 552.1204 [M + Na^+] found: 552.1208.

1,6-anhydro-2,3,4-tri-*O*-benzoyl-β-D-glucopyranose (17).

To a cold solution (0 °C) of levoglucosan (2.00 g, 12.3 mmol) in dry pyridine (20.0 mL) was added benzoyl chloride (8.57 mL, 73.8 mmol, 6 eq). The mixture was allowed to stir 1 h at RT, then water was added and the resulting suspension was extracted with CH_2Cl_2 (3x20 mL). The combined organic layers were successively washed with aq. 1N HCl (3x), satd. aq. $NaHCO_3$ (1x) and brine (1x). The organic phase was dried over $MgSO_4$, concentrated in *vacuo* and the remaining pyridine was co-evaporated with

toluene. The residue was then triturated with the minimum amount of toluene, filtered and washed three times with cold toluene, to afford **17** (5.36 g, 92%) as white crystals. The obtained analytical data are in agreement with reported literature.[365]

Phenyl 2,3,4-tri-*O*-benzoyl-1-thio-β-D-glucopyranoside (18).

To **17** (235 mg, 0.500 mmol) in CH_2Cl_2 (5 mL) were added zinc iodide (640 mg, 2.00 mmol, 4 eq) and trimethyl(phenylthio)silane (240 µL, 1.25 mmol, 2.5 eq). The mixture was stirred under micro-wave irradiation (200 W) at 120 °C for 25 min. The resulting suspension was filtered through celite, diluted with methanol and treated with Amberlite IR 120 H^+. The resin was filtered-off and the solvents removed in *vacuo*. The residue was purified by column chromatography (cyclohexane:EtOAc 9:1 to 7:3) to afford the title compound **18** (286 mg, 98%) as a white foam. The obtained analytical data are in agreement with reported literature.[366]

Phenyl-6-azido-6-deoxy-2,3,4-tri-*O*-benzoyl-1-thio-β-D-glucopyranoside (9).

To a solution of **18** (2.67 g, 4.57 mmol) in dry THF (23.0 mL) was added triphenylphosphine (1.80 g, 6.85 mmol, 1.5 eq). The solution was cooled to -15 °C and diisopropyl azodicarboxylate (2.25 mL, 11.4 mmol, 2.5 eq) was added dropwise. The mixture was stirred for 15 min at -15 °C. It was then allowed to warm to -5 °C. After formation of a precipitate, diphenylphosphoryl azide (1.48 mL, 6.85 mmol, 1.5 eq) was added dropwise. The mixture was then allowed to warm slowly to RT and stirred for 14 h. Then, the solvent was removed in *vacuo* and the residue was purified by column chromatography (cyclohexane:EtOAc 9:1 to 8:2) to afford the title compound **9** (1.99 g, 71%) as a white foam. The obtained analytical data are in agreement with reported literature.[367]

(6-azido-6-deoxy-2,3,4-tri-*O*-benzoyl-α,β-D-glucopyranosyl)-1-(*N*-phenyl)-2,2,2-trifluoroacetimidate (13).

To a solution of **9** (1.36 g, 2.24 mmol) in acetone:water (9:1, 67.0 mL) was added trichlorocyanuric acid (546 mg, 2.35 mmol, 1.05 eq) at RT. The mixture was stirred at RT for 30 min, and then the acetone was evaporated. The resulting residue was dissolved in CH_2Cl_2 and washed with satd. aq. $NaHCO_3$ (1x), brine (1x), and dried over $MgSO_4$. The solvent was evaporated in *vacuo* and the crude was purified by column chromatography (cyclohexane:EtOAc 9:1 to 7:3) to afford an α,β mixture of hemiacetals as a white foam. This mixture (978 mg, 1.94 mmol) was dissolved in dry CH_2Cl_2 (19.0 mL) and Cs_2CO_3 (1.11 g, 2.91 mmol, 1.5 eq) and 2,2,2-trifluoro-*N*-phenylacetimidoyl chloride (465 µL, 2.91 mmol, 1.5 eq) were added sequentially at RT. The mixture was stirred for 4 h, then diluted with CH_2Cl_2 and filtered through celite, and the filtrate concentrated. The crude residue was purified by column chromatography (cyclohexane:EtOAc 9:1 to 7:3) to afford an anomeric mixture of the title compound **13** (1.03 g, 76%) as a white foam. **β-13** (major anomer): ^{1}H NMR (500 MHz, $CDCl_3$) δ = 7.97 (d, J = 7.6 Hz, 2H, 2Ar-H), 7.92 (d, ^3J = 7.6 Hz, 2H, 2Ar-H), 7.85 (d, ^3J = 7.6 Hz, 2H, 2Ar-H), 7.58-7.51 (m, 2H, 2Ar-H), 7.46 (t, ^3J = 7.5 Hz, 1H, Ar-H), 7.44-7.36 (m, 4H, 4Ar-H), 7.34-7.28 (m, 4H, 4Ar-H), 7.13 (t, ^3J = 7.4 Hz, 1H, Ar-H), 6.81 (d, ^3J = 7.4 Hz, 2H, 2Ar-H), 6.22 (bs, 1H, H-1), 5.92 (bs, 1H, H-3), 5.76 (dd, $^3J_{1,2}$ = $^3J_{2,3}$ = 8.3 Hz, 1H, H-2), 5.57 (t, $^3J_{3,4}$ = $^3J_{4,5}$ = 9.4 Hz, 1H, H-4), 4.12 (bs, 1H, H-5), 3.59 (dd, $^2J_{6a,6b}$ = 13.1 Hz, $^3J_{6a,5}$ = 7.2 Hz, 1H, H-6a), 3.40 (dd, $^2J_{6b,6a}$ = 13.1 Hz, $^3J_{6b,5}$ = 2.6 Hz, 1H, H-6b) ppm; ^{13}C NMR (126 MHz, $CDCl_3$) δ = 165.6, 165.2, 164.8 (3C, 3 PhCO), 143.0, 133.8, 133.6, 133.5, 129.9, 129.8, 128.8, 128.6, 128.5,

128.4, 124.6, 119.3 (24 C, 24 Ar-C), 74.9 (C-5), 72.3 (2C, C-1, C-3), 70.7 (C-2), 69.6 (C-4), 51.1 (C-6) ppm; ESI HRMS: *m/z*: calcd for $C_{35}H_{27}F_3N_4O_8$ + Na^+: 711.1679 [M + Na^+] found: 711.1671.

Phenyl-2,3,4-tri-*O*-((*tert*-butyldimethyl)silyl)-1-thio-α,β-D-glucopyranoside (20).

To a mixture of **19a** (1.50 g, 2.97 mmol) and zinc iodide (3.80 g, 11.9 mmol, 4 eq) in dry CH_2Cl_2 (30.0 mL) was added trimethyl(phenylthio)silane (1.40 mL, 7.43 mmol, 2.5 eq) at RT. The mixture was stirred for 1.5 h at RT then it was filtered through celite. The filtrate was diluted with methanol (20.0 mL) and the solvents removed in *vacuo* (concentration of the crude mixture in presence of MeOH is sufficient for removing the 6-*O*-TMS groups). The crude was purified by column chromatography (cyclohexane:CH_2Cl_2:Et_2O 95:2.5:2.5 to 8:1:1) to afford **α-20** (350 mg, 19%) and **β-20** (1.42 g, 77%) as colorless syrups. For characterization purposes, both anomers were separated, but mixtures were used in the further steps. **α-20**: ^{1}H NMR (500 MHz, $CDCl_3$) δ = 7.53-7.49(m, 2H, 2Ar-H_{ortho}), 7.32-2.27 (m, 2H, 2Ar-H_{meta}), 7.25-7.20 (m, 1H, Ar-H_{para}), 5.58 (d, $^3J_{1,2}$ = 4.2 Hz, 1H, H-1), 4.20 (ddd, $^3J_{5,4}$ = 8.8 Hz, $^3J_{5,6a}$ = 6.0 Hz, $^3J_{5,6b}$ = 2.6 Hz, 1H, H-5), 4.08 (m, 1H, H-2), 3.86-3.79 (m, 2H, H-3, H-6a), 3.72 (d, $^3J_{4,3}$ = $^3J_{4,5}$ = 8.8 Hz, 1H, H-4), 3.60-3.53 (dd, $^2J_{6b,6a}$ = 11.5 Hz, $^3J_{6b,5}$ = 2.6 Hz, 1H, H-6b), 0.99 (s, 9H, $C(CH_3)_3$), 0.89 (s, 9H, $C(CH_3)_3$), 0.87 (s, 9H, $C(CH_3)_3$), 0.22 (s, 3H, CH_3), 0.14 (s, 3H, CH_3), 0.13 (s, 3H, CH_3), 0.11 (s, 3H, CH_3), 0.10 (s, 3H, CH_3), 0.09 (s, 3H, CH_3) ppm; ^{13}C NMR (126 MHz, $CDCl_3$) δ = 136.4 (Ar-C_{ipso}), 131.5 (2C, 2Ar-C_{ortho}), 129.0 (2C, 2Ar-C_{meta}), 126.9 (Ar-C_{para}), 87.4 (C-1), 76.4 (C-3), 73.6 (C-4), 73.5 (C-5), 72.9 (C-2), 63.2 (C-6), 26.2, 26.1, 25.9 (9C, 3 C($\underline{C}H_3)_3$), 18.4, 18.2, 18.0 (3C, 3$\underline{C}(CH_3)_3$), -3.5, -3.6, -3.9, -4.3, -4.9, -5.0 (6C, 6CH_3) ppm; ESI HRMS: *m/z*: calcd for $C_{30}H_{58}O_5SSi_3$ + Na^+: 637.3205 [M + Na^+] found: 637.3196; **β-20**: ^{1}H NMR (500 MHz, $CDCl_3$) δ = 7.48-7.44 (m, 2H, 2Ar-H_{ortho}), 7.31-7.26 (m, 2H, 2Ar-H_{meta}), 7.23-7.19 (m, 1H, Ar-H_{para}), 4.98 (d, $^3J_{1,2}$ = 6.4 Hz, 1H, H-1), 3.92,3.88 (m, 1H, H-5), 3.86-3.81 (m, 2H, H-2,H-3), 3.80-3.75 (m, 2H, H-2, H-6_a), 3.72 (dd, $^2J_{6b,6a}$ = 11.4 Hz, $^3J_{6b,5}$ = 3.7 Hz, 1H, H-6b), 2.31 (bs, 1H, OH), 0.92 (s, 9H, $C(CH_3)_3$), 0.89 (s, 9H, $C(CH_3)_3$), 0.88 (s, 9H, $C(CH_3)_3$) , 0.13 (s, 3H, CH_3), 0.11 (s, 6H, 2CH_3), 0.09 (s, 3H, CH_3), 0.08 (s, 3H, CH_3), 0.07 (s, 3H, CH_3) ppm; ^{13}C NMR (126 MHz, $CDCl_3$) δ = 135.7 (Ar-C_{ipso}), 130.4 (2C, 2Ar-C_{ortho}), 129.0 (2C, 2Ar-C_{meta}), 126.8 (Ar-C_{para}), 87.2 (C-1), 83.0 (C-5), 77.3 (C-3), 75.5 (C-2), 71.3 (C-4), 64.2 (C-6), 26.1, 26.0 (9C, 3C($\underline{C}H_3)_3$), 18.2, 18.1 (3C, 3$\underline{C}(CH_3)_3$), -4.1, -4.2, -4.3, -4.8 (6C, 6CH_3) ppm; ESI HRMS: *m/z*: calcd for $C_{30}H_{58}O_5SSi_3$ + Na^+: 637.3205 [M + Na^+] found: 637.3198.

Phenyl-6-*O*-acetyl-2,3,4-tri-*O*-((*tert*-butyldimethyl)silyl)-1-thio-α,β-D-glucopyranoside (14).

To **α,β-20** (420 mg, 683 µmol) in pyridine (6.8 mL) were added DMAP (16.4 mg, 137 µmol, 0.2 eq) and Ac_2O (970 µL, 1.02 mmol, 1.5 eq) at RT. The mixture was stirred for 2 h at RT, and the pyridine was co-evaporated with toluene. The remaining residue was dissolved in EtOAc, and washed with HCl 1N (3x), $NaHCO_3$ (1x) and brine (1x). The organic layer was dried over $MgSO_4$, filtered and concentrated in *vacuo*. The crude was purified by column chromatography (cyclohexane:EtOAc 95:5) to afford the title compound **14** (426 mg, 95%) as a colorless syrup. **α-14**: ^{1}H NMR (500 MHz, $CDCl_3$) δ = 7.57-7.54 (m, 2H, 2Ar-H_{ortho}), 7.29-7.24 (m, 2H, 2Ar-H_{meta}), 7.24-7.18 (m, 1H, Ar-H_{para}), 5.50 (d, $^3J_{1,2}$ = 4.3 Hz, 1H, H-1), 4.40-4.24 (m, 2H, H-5, H-6a), 4.15 (dd, $^2J_{6b,6a}$ = 11.8 Hz, $^3J_{6b,5}$ = 7.0 Hz, 1H, H-6b), 4.09-4.02 (m, 1H, H-2), 3.87-3.82 (m, 1H, H-3), 3.75-3.67 (m, 1H, H-4), 2.04 (s, 3H, CH_3CO), 0.99 (s, 9H, $C(CH_3)_3$), 0.89 (s, 9H, $C(CH_3)_3$), 0.87 (s, 9H, $C(CH_3)_3$), 0.22 (s, 3H, CH_3), 0.14 (s, 3H, CH_3), 0.12 (s, 3H, CH_3), 0.11 (s, 3H, CH_3), 0.09 (s, 3H, CH_3), 0.07 (s, 3H, CH_3) ppm; ^{13}C NMR (126 MHz, $CDCl_3$) δ = 171.1 ($CH_3\underline{C}O$), 136.2 (Ar-C_{ipso}), 132.1 (2Ar-C_{ortho}), 128.9 (2Ar-C_{meta}), 127.0 (Ar-C_{para}), 87.4 (C-1), 76.2 (C-3), 73.7 (C-4), 72.7 (C-2), 71.5 (C-5), 64.4 (C-6), 26.3, 26.1 (9C, 3C($\underline{C}H_3)_3$), 21.0 ($\underline{C}H_3CO$), 18.5, 18.2 (3C, 3$\underline{C}(CH_3)_3$), -3.4, -3.9, -4.1, -4.3, -4.9 (6C, 6

CH_3) ppm; ESI HRMS: *m/z*: calcd for $C_{32}H_{60}O_6SSi_3$ + Na^+: 679.3311 [M + Na^+] found: 679.3311; **β-14**: ^{1}H NMR (500 MHz, $CDCl_3$) δ = 7.50-7.46 (m, 2H, 2Ar-H_{ortho}), 7.30-7.24 (m, 2H, 2Ar-H_{meta}), 7.23-7.18 (m, 1H, Ar-H_{para}), 5.00 (d, $^3J_{1,2}$ = 7.0 Hz, 1H, H-1), 4.29 (dd, $^2J_{6a\text{-}6b}$ = 11.3 Hz, $^3J_{6a,5}$ = 7.2 Hz, 1H, H-6a), 4.23 (dd, $^2J_{6b\text{-}6a}$ = 11.3, $^3J_{6b,5}$ = 6.2 Hz, 1H, H-6b), 4.03-3.98 (m, 1H, H-5), 3.86-3.80 (m, 3H, H-2, H-3, H-4), 2.06 (s, 3H, CH_3CO), 0.91 (s, 9H, $C(CH_3)_3$), 0.89 (s, 9H, $C(CH_3)_3$), 0.88 (s, 9H, $C(CH_3)_3$), 0.11 (s, 3H, CH_3), 0.10 (s, 3H, CH_3), 0.09 (s, 3H, CH_3), 0.08 (s, 3H, CH_3), 0.08 (s, 6H, $2CH_3$) ppm; ^{13}C NMR (126 MHz, $CDCl_3$) δ = 170.8 ($CH_3\underline{C}O$), 135.7 (Ar-C_{ipso}), 130.5 (2C, 2Ar-C_{ortho}), 128.8 (2C, 2Ar-C_{meta}), 126.8 (Ar-C_{para}), 86.6 (C-1), 80.0 (C-5), 77.4 (C-2), 75.5 (C-3), 70.9 (C-4), 65.5 (C-6), 26.0, 25.9 (9C, $3C(\underline{C}H_3)_3$), 21.0 ($\underline{C}H_3CO$), 18.1, 18.0 (3C, $3\underline{C}(CH_3)_3$), -3.6, -4.0, -4.2, -4.4, -5.0 (6C, $6CH_3$) ppm; ESI HRMS: *m/z*: calcd for $C_{32}H_{60}O_6SSi_3$ + Na^+: 679.3311 [M + Na^+] found: 679.3311.

Phenyl-6-azido-6-deoxy-2,3,4-tri-*O*-((*tert*-butyldimethyl)silyl)-1-thio-α,β-D-glucopyranoside (15).

To **α,β-20** (1.12 g, 1.82 mmol) in dry THF (7.30 mL) was added triphenylphosphine (716 mg, 2.73 mmol, 1.5 eq) at RT. The mixture was cooled down to -15 °C, and diisopropylazodicarboxylate (896 μL, 4.55 mmol, 2.5 eq) was added. The temperature was allowed to raise to -5 °C over 30 min, and upon apparition of a precipitate, diphenylphosphorylazide (588 μL, 2.73 mmol, 1.5 eq) was added. The reaction was then stirred at RT for 16 h, then the solvent was removed in *vacuo*, and the resulting residue was purified by column chromatography (cyclohexane:CH_2Cl_2 1:0 to 9:1) to afford the title compound **15** (995 mg, 85%) as a colorless oil. For characterization purposes, both anomers were separated, but mixtures were used in the further steps. **α-15**: ^{1}H NMR (500 MHz, $CDCl_3$) δ = 7.56-7.52 (m, 2H, 2Ar-H_{ortho}), 7.31-7.26 (m, 2H, 2Ar-H_{meta}), 7.23-7.18 (m, 1H, Ar-H_{para}), 5.59 (d, $^3J_{1,2}$ = 4.2 Hz, 1H, H-1), 4.30 (ddd, $^3J_{5,4}$ = 9.0 Hz, $^3J_{5,6b}$ = 5.9 Hz, $^3J_{5,6a}$ = 2.6 Hz, 1H, H-5), 4.09 (m, 1H, H-2), 3.84 (d, $^3J_{3,2}$ = 3.6 Hz, 1H, H-3), 3.73 (d, $^3J_{4,5}$ = 9.0 Hz, 1H, H-4), 3.52 (dd, $^2J_{6a,6b}$ = 13.1 Hz, $^3J_{6a,5}$ = 2.6 Hz, 1H, H-6a), 3.22 (dd, $^2J_{6b,6a}$ = 13.1 Hz, $^3J_{6b,5}$ = 5.9 Hz, 1H, H-6b), 0.98 (s, 9H, $C(CH_3)_3$), 0.89 (s, 9H, $C(CH_3)_3$), 0.88 (s, 9H, $C(CH_3)_3$), 0.22 (s, 3H, CH_3), 0.14 (s, 6H, $2CH_3$), 0.12 (s, 3H, CH_3), 0.09 (s, 3H, CH_3), 0.09 (s, 3H, CH_3) ppm; ^{13}C NMR (126 MHz, $CDCl_3$) δ = 136.7 (Ar-C_{ipso}), 130.8 (2Ar-C_{ortho}), 128.9 (2Ar-C_{meta}), 126.5 (Ar-C_{para}), 87.2 (C-1), 76.3 (C-3), 74.6 (C-4), 73.0 (C-2), 72.8 (C-5), 52.5 (C-6), 26.2, 26.1, 25.9 (3C, $3C(\underline{C}H_3)_3$), 18.4, 18.1, 18.0 (3C, $3\underline{C}(CH_3)_3$), -3.4, -3.6, -3.8, -4.4, -4.9, -5.0 (6C, $6CH_3$) ppm; ESI HRMS: *m/z*: calcd for $C_{30}H_{57}O_4N_3Si_3$ + Na^+: 662.3270 [M + Na^+] found: 662.3262; **β-15**: ^{1}H NMR (500 MHz, $CDCl_3$) δ = 7.52-7.48 (m, 2H, 2Ar-H_{ortho}), 7.31-7.26 (m, 2H, 2Ar-H_{meta}), 7.24-7.19 (m, 1H, Ar-H_{para}), 5.01 (d, $^3J_{1,2}$ = 6.3 Hz, 1H, H-1), 3.94,3.89 (m, 1H, H-5), 3.88-3.84 (m, 1H, H-2), 3.84,3.82 (m, 1H, H-3), 3.78-3.74 (m, 1H, H-4), 3.56 (dd, $^2J_{6a,6b}$ = 12.5 Hz, $^3J_{6a,5}$ = 7.3 Hz, 1H, H-6a), 3.38 (dd, $^2J_{6b,6a}$ = 12.5 Hz, $^3J_{6b,5}$ = 5.9 Hz, 1H, H-6b), 0.92 (s, 9H, $C(CH_3)_3$), 0.89 (s, 9H, $C(CH_3)_3$), 0.88 (s, 9H, $C(CH_3)_3$), 0.13 (s, 3H, CH_3), 0.11 (s, 3H, CH_3), 0.10 (s, 3H, CH_3), 0.09 (s, 3H, CH_3), 0.08 (s, 3H, CH_3), 0.08 (s, 3H, CH_3) ppm; ^{13}C NMR (126 MHz, $CDCl_3$) δ = 135.5 (Ar-C_{ipso}), 130.8 (2Ar-C_{ortho}), 128.9 (2Ar-C_{meta}), 126.9 (Ar-C_{para}), 87.0 (C-1), 80.5 (C-5), 77.5 (C-3), 75.4 (C-2), 71.6 (C-4), 53.5 (C-6), 26.1, 26.0, 25.9 (3C, $3C(\underline{C}H_3)_3$), 18.2, 18.1, (3C, $3\underline{C}(CH_3)_3$), -4.1, -4.2, -4.3, -4.8 (6C, $6CH_3$) ppm; ESI HRMS: *m/z*: calcd for $C_{30}H_{57}O_4N_3Si_3$ + Na^+: 662.3270 [M + Na^+] found: 662.3262.

7.2.2. Glycosylations

Procedure A: $BF_3.OEt_2$ promoted glycosylation:

To a solution of DHAB (1 eq) and donor (2.2 eq) in dry MeCN (45 mM), was added freshly activated molecular sieves (10mg/mg acceptor). The mixture was stirred for 30 min at RT and $BF_3.OEt_2$ (1.1 eq)

was added. After stirring for 2 h at RT, the mixture was diluted with CH_2Cl_2, filtered through celite, and the filtrate washed with satd. aq. $NaHCO_3$. The aqueous phase was extracted with CH_2Cl_2, and the combined organic layers were dried over $MgSO_4$ and concentrated in *vacuo*. The residue was purified by column chromatography to afford *bis*- (**21a, 22a** or **23a**) and *mono*-glycosylated (**22b** or **23b**) compounds (see Table 2.2 for yields) respectively.

Procedure B: MeOTf promoted glycosylation:

To a suspension of DHAB (1 eq) and glycosyl donor (2.2-2.5 eq) in the appropriate dry solvent (see Table 2.2 for solvent and concentration) was added freshly activated molecular sieves (10mg/mg acceptor). The mixture was stirred at RT for 30 min and the base (see Table 2.2; 2.2 eq) was added. Then MeOTf (5.5-6.6 eq) was added and the reaction was stirred at RT until completion. The mixture was then diluted with CH_2Cl_2 and filtered through celite. The filtrate was subsequently washed with satd. aq. $NaHCO_3$ solution and brine. The aqueous phase was extracted with CH_2Cl_2, and the combined organic layers were dried over $MgSO_4$ and concentrated in *vacuo*. The resulting residue was purified by column chromatography to afford *bis*- (**24a** or **25a**) and *mono*-glycosylated (**24b** or **25b**) compounds (see Table 2.2 for yields) respectively.

Procedure C: BSP/Tf_2O promoted glycosylation:

To a solution of glycosyl donor (0.1 mmol), 2,6-di-*tert*-butyl-4-methylpyridine (0.11 mmol), 1-(phenylsulfinyl)piperidine (BSP) (0.1 mmol) and freshly activated molecular sieves (10mg/mg acceptor) in dry CH_2Cl_2 (0.5 mL) was added Tf_2O (0.1 mmol) at -90 °C. The mixture was stirred for 10 min at -90 °C and DHAB (45.0 µmol) was added as a solution in a 4:1 CH_2Cl_2/[bmim][OTf] mixture (0.5 mL). The mixture was stirred for 1 h between -90 °C and -40 °C then it was allowed to warm to RT and filtered through celite. The filtrate was washed with satd. aq. $NaHCO_3$, the aqueous phase was extracted with CH_2Cl_2, and the combined organic layers were dried over $MgSO_4$ and concentrated in *vacuo*. The residue was purified by column chromatography to afford *bis*- (**24a**) and *mono*-glycosylated (**24b**) compounds (see Table 2.2 for yields) respectively.

For symmetrical azobenzene *bis*-glycosides, assignments of NMR data for the azobenzene signals were reported as H_{ortho}, H_{meta}, C_{ipso}, C_{ortho}, C_{meta}, C_{para}, regarding to the position of the azo bond. In the case of unsymmetrical compounds (*mono*-glycosides or αβ isomers), the following numbering was used (Figure 7.2.1).

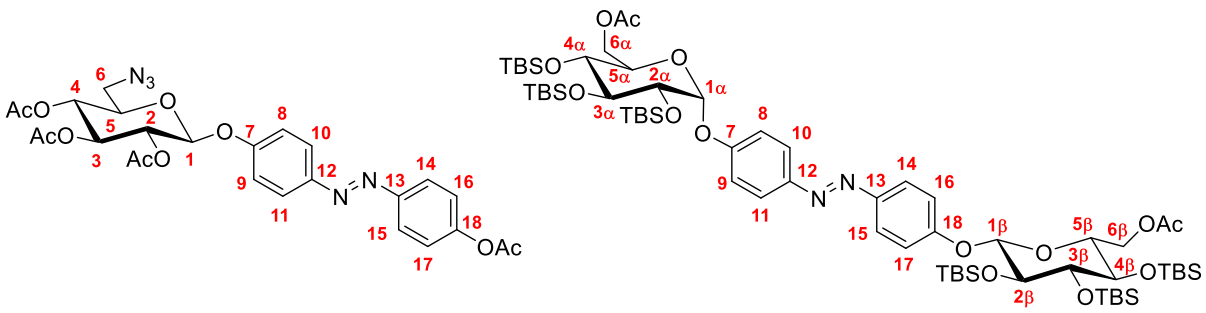

Figure 7.2.1. Numbering of unsymmetrical glycosides for assignment of NMR data.

Screening of a base in the glycosylation with silylated donor 14

Table 7.2.1. Screening of glycosylation conditions of DHAB with donor **14**.[a]

Entry	Donor[b]	Promotor (eq/donor)	Base (eq/DHAB)	Solvent	Temp.	*Bis*-glycoside, yield, αβ:ββ *Mono*-glycoside, yield, α:β
1[d]	**14**	MeOTf (2.5)	DBU (2.2)	DCM	rt	**24a**, 20%, 1:5 **24b**, 30%, 1:10
2[c, e]	**14**	MeOTf (2.5)	Cs_2CO_3 (2.2)	DCM	rt	**24a**, 27%, 1:5 **24b**, 21%, 1:10
3[c, e]	**14**	MeOTf (2.5)	*t*-BuOK (2.2)	DCM	rt	**24a**, 7%, 1:5 **24b**, 25%, 1:10
4	**14**	MeOTf (2.5)	Collidine (2.2)	DCM	rt	**24a**, 20%, 1:3 **24b**, 35%, 1:6

[a] All reactions were performed with [DHAB] = 0.05 mol.L^{-1} unless otherwise stated.

[b] 2.2 eq of donor were used in each glycosylation unless otherwise stated.

[c] 2.5 eq of donor were used

[d] [DHAB] = 0.03 mol.L^{-1}

[e] [DHAB] = 0.04 mol.L^{-1}

(*E*)-*p,p'-bis*-(2,3,4,6-tetra-*O*-acetyl-β-D-glucopyranosyloxy) azobenzene (21a).

General procedure A was applied to DHAB (10.0 mg, 45.0 µmol) and donor **11** (52.0 mg, 100 µmol, 2.2 eq). Reagents and conditions: boron trifluoride etherate (6.30 µL, 50.0 µmol, 1.1 eq), molecular sieves (100 mg), dry acetonitrile (1.00 mL, *c* = 45 mM). Column chromatography (cyclohexane:EtOAc 1:1) afforded the title compound **21a** (27.0 mg, 68%) as an orange foam. $[\alpha]^{20}_{D}$ = -22.3 (*c* = 0.5 in $CHCl_3$); ^{1}H NMR (500 MHz, $CDCl_3$) δ = 7.87 (d, ^3J = 9.0 Hz, 4H, 4Ar-H$_{ortho}$), 7.09 (d, ^3J = 9.0 Hz, 4H, 4Ar-H$_{meta}$), 5.35-5.28 (m, 4H, 2H-2, 2H-3), 5.21-5.16 (m, 4H, 2H-1, 2H-4), 4.30 (dd, $^2J_{6a,6b}$ = 12.3 Hz, $^3J_{6a,5}$ = 5.5 Hz, 2H, 2H-6a), 4.19 (dd, $^2J_{6b,6a}$ = 12.3 Hz, $^3J_{6b,5}$ = 2.3 Hz, 2H, 2H-6b), 3.92 (ddd, $^3J_{5,4}$ = 10.0 Hz, $^3J_{5,6a}$ = 5.5 Hz, $^3J_{5,6b}$ = 2.3 Hz, 2H, 2H-5), 2.08 (s, 3H, CH_3CO), 2.07 (s, 3H, CH_3CO), 2.06 (s, 3H, CH_3CO), 2.04 (s, 3H, CH_3CO) ppm; ^{13}C NMR (126 MHz, $CDCl_3$) δ = 170.7, 170.4, 169.5, 169.4 (8C, 8$CH_3\underline{C}O$), 158.8 (2C, 2Ar-C$_{para}$), 148.7 (2C, 2Ar-C$_{ipso}$), 124.5 (4C, 4Ar-C$_{ortho}$), 117.2 (4C, 4Ar-C$_{meta}$), 98.8 (C-1), 72.8 (C-2), 72.4 (C-5), 71.3 (C-3), 68.4 (C-4), 62.1 (C-6), 20.8, 20.7 (8C, 8$\underline{C}H_3CO$) ppm; ESI HRMS: *m/z*: calcd for $C_{40}H_{46}N_2O_{20}$ + H^+: 875.2717 [M + H^+] found: 875.2690.

(*E*)-*p,p'-bis*-(2,3,4-tri-*O*-acetyl-6-azido-6-deoxy-β-D-glucopyranosyloxy) azobenzene (22a).

General procedure A was applied to DHAB (193 mg, 900 µmol) and donor **12** (1.04 g, 2.00 mmol, 2.2 eq). Reagents and conditions: boron trifluoride etherate (126 µL, 1.00 mmol, 1.1 eq), molecular sieves (1.93 g), dry acetonitrile (20.0 mL, *c* = 45 mM). Column chromatography (cyclohexane:EtOAc 9:1 to 1:1) afforded the title compound **22a** (367 mg, 48%) as an orange foam as well as the *mono*-glycosylated compound. Since the latter was eluted in the same time as the hydrolysis products of the corresponding donor, acetylation of these fractions needed to be performed to isolate the pure compounds. Column chromatography (cyclohexane:EtOAc 9:1 to 7:3) afforded the *mono*-glycosylated compound **22b** (72.0 mg, 14%) as an orange foam. The obtained analytical data for **22a** are in agreement with reported literature.[275]

(*E*)-*p*-(2,3,4-tri-*O*-acetyl-6-azido-6-deoxy-β-D-glucopyranosyloxy)-*p´*-acetoxy azobenzene (22b).

$[\alpha]^{20}_D$ = -60.0 (*c* = 1 in $CHCl_3$); ^{1}H NMR (500 MHz, $CDCl_3$) δ = 7.94-7.89 (m, 4H, H-10, H-11, H-14, H-15), 7.24 (d, ^3J = 8.9 Hz, 2H, H-16, H-17), 7.13 (d, ^3J = 9.0 Hz, 2H, H-8, H-9), 5.35-5.27 (m, 2H, H-2, H-3), 5.20 (d, $^3J_{1,2}$ = 7.6 Hz, 1H, H-1), 5.12-5.06 (m, 1H, H-4), 3.83 (ddd, $^3J_{5,4}$ = 10 Hz, $^3J_{5,6a}$ = 7.3 Hz, $^3J_{5,6b}$ = 2.7 Hz, 1H, H-5), 3.45 (dd, $^2J_{6a,6b}$ = 13.3 Hz, $^3J_{6a,5}$ = 7.3 Hz, 1H, H-6a), 3.35 (dd, $^2J_{6b,6a}$ = 13.3 Hz, $^3J_{6b,5}$ = 2.7 Hz, 1H, H-6b), 2.33 (s, 3H, Ar-CH_3CO), 2.08 (s, 3H, CH_3CO), 2.07 (s, 3H, CH_3CO), 2.05 (s, 3H, CH_3CO) ppm; ^{13}C NMR (126 MHz, $CDCl_3$) δ = 170.3, 169.6, 169.4, 169.3 (4C, 4$CH_3\underline{C}O$), 158.9 (C-7), 152.6 (C-18), 150.34 (C-13), 148.7 (C-12), 124.8 (2C, C-14, C-15), 124.1 (2C, C-10, C-11), 122.3 (2C, C-16, C-17), 117.4 (2C, C-8, C-9), 98.8 (C-1), 73.8 (C-5), 72.6, 71.2 (C-2, C-3), 69.5 (C-4), 51.4 (C-6), 21.3 (Ar-$\underline{C}H_3CO$), 20.8, 20.7 (3C, $\underline{C}H_3CO$) ppm; ESI HRMS: *m/z*: calcd for $C_{26}H_{27}N_5O_{10}$ + H^+: 570.1831 [M + H^+] found: 570.1829.

(*E*)-*p,p'-bis*-(2,3,4-tri-*O*-benzoyl-6-azido-6-deoxy-β-D-glucopyranosyloxy) azobenzene (23a).

General procedure A was applied to DHAB (97.0 mg, 450 µmol) and donor **7** (690 mg, 1.00 mmol, 2,2 eq). Reagents and conditions: boron trifluoride etherate (63.0 µL, 500 µmol, 1.1 eq), molecular sieves (970 mg), acetonitrile (10.0 mL, *c* = 45 mM). Column chromatography (PhMe:EtOAc 9:1 to 8:2 to separate *mono*- from *bis*-glycosylated products; then cyclohexane:acetone 8:2) afforded the title compound **23a** (213 mg, 38 %) as an orange foam as well as the *mono*-glycosylated compound. Since the latter was eluted in the same time as the hydrolysis products of the corresponding donor, acetylation of these fractions needed to be performed to isolate the pure compound. Column chromatography (cyclohexane:EtOAc 8:2) afforded **23b** (85.0 mg, 25 %) as an orange foam. **23a**: $[\alpha]^{20}_D$ = +61.7 (*c* = 1 in $CHCl_3$); ^{1}H NMR (500 MHz, $CDCl_3$) δ = 7.98-7.92 (m, 8H, 8Ar-H_{Bz}), 7.87-7.83 (m, 8H, 4Ar-H_{Bz} + 4Ar-H_{ortho}), 7.56-7.49 (m, 4H, 4Ar-H_{Bz}), 7.47-7.42 (m, 2H, 2Ar-H_{Bz}), 7.41-7.35 (m, 8H, 8Ar-H_{Bz}), 7.33-7.28 (m, 4H, 4Ar-H_{Bz}), 7.14 (d, *J* = 9.1 Hz, 4H, 4Ar-H_{meta}), 6.00 (dd, $^3J_{3,2}$ = $^3J_{3,4}$ = 9.6 Hz, 2H, 2H-3), 5.81 (dd, $^3J_{2,3}$ = 9.6 Hz, $^3J_{2,1}$ = 7.8 Hz, 2H, 2H-2), 5.58 (dd, $^3J_{4,3}$ = $^3J_{4,5}$ = 9.6 Hz, 2H, 2H-4), 5.49 (d, $^3J_{1,2}$ = 7.8 Hz, 2H, 2H-1), 4.13 (ddd, $^3J_{5,4}$ = 9.6 Hz, $^3J_{5,6a}$ = 7.5 Hz, $^3J_{5,6b}$ = 2.6 Hz, 2H, 2H-5), 3.62 (dd, $^2J_{6a,6b}$ = 13.5 Hz, $^3J_{6a,5}$ = 7.5 Hz, 2H, 2H-6a), 3.48 (dd, $^2J_{6b,6a}$ = 13.5 Hz, $^3J_{6b,5}$ = 2.6 Hz, 2H, 2H-6b) ppm; ^{13}C NMR (126 MHz, $CDCl_3$) δ = 165.9, 165.5, 165.2 (6C, 6Ph$\underline{C}O$), 158.8 (2C, 2Ar-C_{para}), 148.8 (2C, 2Ar-C_{ipso}), 133.9, 133.6, 133.5 (6C, 6Ar-C_{Bz}), 130.0, 129.9 (12C, 12Ar-C_{Bz}), 129.1 (2C, 2Ar-C_{Bz}), 128.8, 128.7 (6C, 6Ar-C_{Bz}) 128.6 (6C, 6ArC_{Bz}) 128.5 (4C, 4Ar-C_{Bz}), 124.6 (4C, 4Ar-C_{ortho}), 117.6 (4C, 4Ar-C_{meta}), 99.5 (2C-1), 74.4 (2C-5), 72.6 (2C-3), 71.7 (2C-2), 70.2 (2C-4), 51.6 (2C-6) ppm; ESI HRMS: *m/z*: calcd for $C_{66}H_{52}O_{16}N_8$ + H^+: 1213.3574 [M + H^+] found: 1213.3579.

(*E*)-*p*-(2,3,4-tri-*O*-benzoyl-6-azido-6-deoxy-β-D-glucopyranosyloxy)-*p´*-acetoxy azobenzene (23b).

$[\alpha]^{20}_D$ = +20.2 (*c* = 1 in $CHCl_3$); ^{1}H NMR (500 MHz, $CDCl_3$) δ = 7.99-7.93 (m, 4H, 4Ar-H_{Bz}), 7.92 (d, ^3J = 9.0 Hz, 2H, H-14, H-15), 7.89 (d, ^3J = 9.0 Hz, 2H, H-10, H-11), 7.88-7.84 (m, 2H, 2Ar-H_{Bz}), 7.57-7.50 (m, 2H, 2Ar-H_{Bz}), 7.48-7.43 (m, 1H, Ar-H_{Bz}), 7.43-7.36 (m, 4H, 4Ar-H_{Bz}), 7.34-7.28 (m, 2H, 2Ar-H_{Bz}), 7.24 (d, ^3J = 9.0 Hz, 2H, H-16, H-17), 7.16 (d, ^3J = 9.0 Hz, 2H, H-8, H-9), 5.99 (dd, $^3J_{3,2}$ = $^3J_{3,4}$ = 9.6 Hz, 1H, H-3), 5.83 (dd, $^3J_{2,3}$ = 9.6 Hz, $^3J_{2,1}$ = 7.8 Hz, 1H, H-2), 5.59 (dd, $^3J_{4,3}$ = $^3J_{4,5}$ = 9.6 Hz, 1H, H-4), 5.50 (d, $^3J_{1,2}$ = 7.8 Hz, 1H, H-1), 4.14 (ddd, $^3J_{5,4}$ = 9.6 Hz, $^3J_{5,6a}$ = 7.5 Hz, $^3J_{5,6b}$ = 2.6 Hz, 1H, H-5), 3.62 (dd, $^2J_{6a,6b}$ = 13.5 Hz, $^3J_{6a,5}$ = 7.5 Hz, 1H, H-6a), 3.49 (dd, $^2J_{6b,\ 6a}$ = 13.5 Hz, $^3J_{6b,5}$ = 2.6 Hz, 1H, H-6b), 2.33 (s, 3H, CH_3CO) ppm; ^{13}C NMR (126 MHz, $CDCl_3$) δ = 169.3 ($CH_3\underline{C}O$), 165.9, 165.5, 165.2 (3C, 3Ph$\underline{C}O$), 159.0 (C-7), 152.6 (C-18),

150.3 (C-13), 148.8 (C-12), 133.9, 133.6, 133.5 (3C, 3Ar-C_{Bz}), 130.0, 130.0, 129.9 (6C, 6Ar-C_{Bz}), 129.1, 128.7, 128.7, 128.6, 128.6, 128.5 (9C, 9Ar-C_{Bz}), 124.8 (2C, C-11, C-10), 124.1 (2C, C-14, C-15), 122.3 (2C, C-16, C-17), 117.6 (2C, C-8, C-9), 99.5 (C-1), 74.4 (C-5), 72.6 (C-3), 71.7 (C-2), 70.2 (C-4), 51.6 (C-6), 21.3 ($\underline{C}H_3CO$) ppm; ESI HRMS: *m/z*: calcd for $C_{41}H_{35}O_{10}N_5 + H^+$: 756.2300 [M + H^+] found: 756.2297.

(*E*)-*p,p'-bis*-(2,3,4-tri-*O*-((*tert*-butyldimethyl)silyl)-6-*O*-acetyl-β-D-glucopyranosyloxy) azobenzene (ββ-24a).

Route 1. General procedure B was applied to DHAB (10.0 mg, 45.0 µmol) and donor **8** (66.0 mg, 100 µmol, 2.2 eq). Reagents and conditions: methyl trifluoromethanesulfonate (33.0 µL, 304 µmol, 6.6 eq), 2,6-di-*tert*-butyl-4-methylpyridine (20.0 mg, 100 µmol, 2.2 eq), molecular sieves (100 mg), dichloromethane (1.00 mL, *c* = 45 mM). Column chromatography (cyclohexane:CH_2Cl_2 1:1 to 0:1 then cyclohexane:EtOAc 7:3) afforded an αβ:ββ (1:5) anomeric mixture of the title compound **24a** (30 mg, 50 %) as well as an α:β (1:10) anomeric mixture of *mono*-glycosylated compound **24b** (7 mg, 20 %). **Route 2.** General procedure C was applied to DHAB (10.0 mg, 45.0 µmol) and donor **14** (66.0 mg, 100 µmol, 2.2 eq). Reagents and conditions: 1-(phenylsulfinyl)piperidine (21.0 mg, 100 µmol, 2.2 eq), trifluoromethansulfonic anhydride (17.0 µL, 100 µmol, 2.2 eq), 2,6-di-*tert*-butyl-4-methylpyridine (23 mg, 110 µmol, 2.5 eq), molecular sieves (100 mg), CH_2Cl_2:bmimOTf (9:1, 1.00 mL, *c* = 45 mM). Column chromatography (cyclohexane:CH_2Cl_2 1:1 to 0:1 then cyclohexane:EtOAc 7:3) afforded an αβ:ββ (1:10) anomeric mixture of the title compound **24a** (11 mg, 18 %) as well as an α:β (1:5) anomeric mixture of *mono*-glycosylated compound **24b** (7 mg, 20 %).

For a proper characterisation of the αβ anomer, the αβ,ββ mixture isolated after the glycosylation was enriched in αβ isomer after silica gel chromatography (see figures 7.6.25-7.6.28). **ββ-24a**: ^{1}H NMR (500 MHz, $CDCl_3$) δ = 7.87 (d, ^3J = 9.0 Hz 4H, 4Ar-H_{ortho}), 7.06 (d, ^3J = 9.0 Hz 4H, 4Ar-H_{meta}), 5.50 (d, $^3J_{1,2}$ = 6.0 Hz, 2H, 2H-1), 4.31 (dd, $^2J_{6a,6b}$ = 11.1 Hz, $^3J_{6a,5}$ = 7.3 Hz, 2H, 2H-6a), 4.26 (dd, $^2J_{6b,6a}$ = 11.1 Hz, $^3J_{6b,5}$ = 6.2 Hz, 2H, 2H-6b), 4.21-4.16 (m, 2H, 2H-5), 3.96 (d, $^3J_{2,1}$ = 6.0 Hz, 2H, 2H-2), 3.90-3.83 (m, 4H, 2H-3, 2H-4), 2.00 (s, 6H, $2CH_3CO$), 0.94 (s, 18H, $2C(CH_3)_3$), 0.92 (s, 18H, $2C(CH_3)_3$), 0.86 (s, 18H, $2C(CH_3)_3$), 0.18 (s, 6H, $2CH_3$), 0.16 (s, 6H, $2CH_3$), 0.13 (s, 6H, $2CH_3$), 0.12 (s, 6H, $2CH_3$), 0.12 (s, 6H, $2CH_3$), 0.02 (s, 6H, $2CH_3$) ppm; ^{13}C NMR (126 MHz, $CDCl_3$) δ = 170.7 (2C, $2CH_3\underline{C}O$), 159.1 (2C, 2Ar-C_{para}), 148.0 (2C, 2Ar-C_{ipso}), 124.4 (4C, 4Ar-C_{ortho}), 116.2 (4C, 4Ar-C_{meta}), 99.0 (2C-1), 79.0 (2C-5), 78.0 (2C-3), 76.5 (2C-2), 70.6 (2C-4), 65.1 (2C-6), 26.0, 25.9 (18C, $6C(\underline{C}H_3)_3$), 20.9 (2C, $2\underline{C}H_3CO$), 18.2, 18.1 (6C, $\underline{C}(CH_3)_3$), -4.0, -4.3, -4.4, -4.6, -4.7, -4.9 (12C, $12CH_3$) ppm; ESI HRMS: *m/z*: calcd for $C_{64}H_{118}N_2O_{14}Si_6 + H^+$: 1307.7271 [M + H^+] found: 1307.7257.

(*E*)-*p*-(2,3,4-tri-*O*-((*tert*-butyldimethyl)silyl)-6-*O*-acetyl-α-D-glucopyranosyloxy)-*p'*-(2,3,4-tri-*O*-((*tert*-butyldimethyl)silyl)-6-*O*-acetyl-β-D-glucopyranosyloxy) azobenzene (αβ-24a).

^{1}H NMR (500 MHz, $CDCl_3$) δ = 7.89-7.84 (m, 4H, 4Ar-H_{ortho}), 7.19 (d, ^3J = 9.0 Hz, 2H, H-8, H-9), 7.06 (d, ^3J = 9.0 Hz, 2H, H-16, H-17), 5.52 (d, $^3J_{1,2}$ = 3.5 Hz, 1H, H-1$_\alpha$), 5.50 (d, $^3J_{1,2}$ = 6.0 Hz, 1H, H-1$_\beta$), 4.34-4.24 (m, 4H, H-5$_\alpha$, H-6a$_\alpha$, H-6a$_\beta$, H-6b$_\beta$), 4.22-4.16 (m, 2H, H-6b$_\alpha$, H-5$_\beta$), 4.06-4.03 (m, 1H, H-2$_\alpha$), 3.99-3.93 (m, 2H, H-3$_\alpha$, H-2$_\beta$), 3.90-3.83 (m, 2H, H-3$_\beta$, H-4$_\beta$), 3.70-3.67 (m, 1H, H-4$_\alpha$), 2.0 (s, 3H, CH_3CO_β), 1.95 (s, 3H, CH_3CO_α), 0.96 (s, 9H, $C(CH_3)_3$), 0.93 (s, 9H, $C(CH_3)_3$), 0.92 (s, 9H, $C(CH_3)_3$), 0.92 (s, 9H, $C(CH_3)_3$), 0.89 (s, 9H, $C(CH_3)_3$), 0.86 (s, 9H, $C(CH_3)_3$), 0.20 (s, 3H, CH_3), 0.18 (s, 3H, CH_3), 0.16 (s, 3H, CH_3), 0.15 (s, 3H, CH_3), 0.14 (s, 3H, CH_3), 0.13 (s, 3H, CH_3), 0.12 (s, 3H, CH_3), 0.12 (s, 3H, CH_3), 0.11 (s, 3H, CH_3), 0.08 (s, 3H, CH_3),

0.02 (s, 3H, CH_3), 0.02 (s, 3H, CH_3) ppm; ^{13}C NMR (126 MHz, $CDCl_3$) δ = 171.0 ($CH_3\underline{C}O_\alpha$), 170.7 ($CH_3\underline{C}O_\beta$), 159.6 (C-7), 159.1 (C18), 148.0 (C-13), 147.9 (C-12), 124.4 (2C, C-14, C-15), 124.3 (2C, C-10, C-11), 117.1 (2C, C-8, C-9), 116.2 (2C, C-16, C-17), 99.0 (C-1_β), 94.9 (C-1_α), 79.2 (C-5_β), 78.0 (C-3_β), 76.6 (C-2_β), 76.0 (C-3_α), 73.1 (C-4_α), 72.8 (C-5_α), 71.6 (C-2_α), 70.6 (C-4_β), 65.1 (C-6_β), 64.0 (C-6_α), 26.1, (9C, 3C($\underline{C}H_3)_3$, α-side), 26.0, 25.9 (9C, 3C($\underline{C}H_3)_3$, β-side), 21.0 ($\underline{C}H_3CO$, α-side), 20.9 ($\underline{C}H_3CO$, β-side), 18.5, 18.2, 18.1 (6C, 6$\underline{C}(CH_3)_3$), -3.2, -3.7, -4.0, -4.1, -4.3, -4.4, -4.6, -4.7, -4.8, -4.9 (12C, CH_3) ppm; ESI HRMS: *m/z*: calcd for $C_{64}H_{118}N_2O_{14}Si_6 + H^+$: 1307.7271 [M + H^+] found: 1307.7257.

(*E*)-*p*-(2,3,4-tri-*O*-((*tert*-butyldimethyl)silyl)-6-*O*-acetyl-β-D-glucopyranosyloxy)-*p´*-hydroxy azobenzene (β-24b).

^{1}H NMR (500 MHz, $CDCl_3$) δ = 7.87-7.79 (m, 4H, H-10, H-11, H-14, H-15), 7.06 (d, ^3J = 9.1 Hz, 2H, H-8, H-9), 6.91 (d, ^3J = 9.1 Hz, 2H, H-16, H-17), 5.91 (bs, 1H, Ar-OH), 5.52 (d, $^3J_{1,2}$ = 6.0 Hz, 1H, H-1), 4.34 (dd, $^2J_{6a\text{-}6b}$ = 11.2 Hz, $^3J_{6a,5}$ = 7.5 Hz, 1H, H-6a), 4.28 (dd, $^2J_{6b\text{-}6a}$ = 11.2 Hz, $^3J_{6b,5}$ = 6.3 Hz, 1H, H-6b), 4.23,4.18 (m, 1H, H-5), 3.97 (d, $^3J_{2,1}$ = 6.0 Hz, 1H, H-2), 3.90 (d, $^3J_{3,4}$ = 3.3 Hz, 1H, H-3), 3.87 (d, $^3J_{4,3}$ = 3.3 Hz, 1H, H-4), 2.00 (s, 3H, CH_3CO), 0.94 (s, 9H, $C(CH_3)_3$), 0.93 (s, 9H, $C(CH_3)_3$), 0.86 (s, 9H, $C(CH_3)_3$), 0.18 (s, 3H, CH_3), 0.17 (s, 3H, CH_3), 0.13 (s, 3H, CH_3), 0.13 (s, 3H, CH_3), 0.12 (s, 3H, CH_3) 0.02 (s, 3H, CH_3) ppm; ^{13}C NMR (126 MHz, $CDCl_3$) δ = 171.1 ($CH_3\underline{C}O$), 159.0 (C-7), 158.3 (C-18), 147.9 (C-12), 147.2 (C-13), 124.8 (2C, C-14, C-15), 124.4 (2C, C-10, C-11), 116.2 (2C, C-8, C-9), 115.9 (2C, C-16, C-17), 98.9 (C-1), 78.9 (C-5), 77.9 (C-3), 76.4 (C-2), 70.6 (C-4), 65.2 (C-6), 26.0, 25.9 (9C, 3C($\underline{C}H_3)_3$), 20.9 ($\underline{C}H_3CO$), 18.2, 18.1 (3C, 3$\underline{C}(CH_3)_3$), -4.1, -4.3, -4.4, -4.6, -4.7, -4.9 (6C, 6CH_3) ppm; ESI HRMS: *m/z*: calcd for $C_{38}H_{64}O_8N_2Si_3 + H^+$: 761.4043 [M + H^+] found: 761.4017.

(*E*)-*p*-(2,3,4-tri-*O*-((*tert*-butyldimethyl)silyl)-6-*O*-acetyl-α-D-glucopyranosyloxy)-*p´*-hydroxy azobenzene (α-24b).

^{1}H NMR (500 MHz, $CDCl_3$) δ = 7.88-7.79 (m, 4H, 4Ar-H_{ortho}), 7.18 (d, ^3J = 9.0 Hz, 2H, H-8, H-9), 6.91 (d, ^3J = 9.0 Hz, 2H, H-16, H-17), 5.53 (d, $^3J_{1,2}$ = 3.7 Hz, 1H, H-1), 4.32-4.27 (m, 2H, H-5, H-6a), 4.25,4.21 (m, 1H, H-6b), 4.07-4.03 (m, 1H, H-2), 3.97-3.93 (m, 1H, H-3), 3.72,3.68 (m, 1H, H-4), 1.97 (s, 3H, CH_3CO), 0.96 (s, 9H, $C(CH_3)_3$), 0.93 (s, 9H, $C(CH_3)_3$), 0.90 (s, 9H, $C(CH_3)_3$), 0.20 (s, 3H, CH_3), 0.16 (s, 3H, CH_3), 0.14 (s, 3H, CH_3), 0.13 (s, 3H, CH_3), 0.12 (s, 3H, CH_3), 0.09 (s, 3H, CH_3) ppm; ESI HRMS: *m/z*: calcd for $C_{38}H_{64}O_8N_2Si_3 + H^+$: 761.4043 [M + H^+] found: 761.4017. Since the isolated amount of **α,β-24b** (α minor anomer) was too small, no proper ^{13}C-NMR characterization of the α species could be achieved.

(*E*)-p,p'-*bis*-(2,3,4-tri-*O*-((*tert*-butyldimethyl)silyl)-6-azido-6-deoxy-β-D-glucopyranosyloxy) azobenzene (ββ-25a).

General procedure B was applied to DHAB (21.0 mg, 97.0 µmol) and donor **15** (136 mg, 212 µmol, 2.2 eq). Reagents and conditions: methyl trifluoromethanesulfonate (70.0 µL, 636 µmol, 6.6 eq), 2,6-di-*tert*-butyl-4-methylpyridine (44.0 mg, 212 µmol, 2.2 eq), molecular sieves (210 mg), dichloromethane (2.12 mL, *c* = 45 mM). Column chromatography (cyclohexane:CH_2Cl_2 9.1 to 7:3 then cyclohexane:EtOAc 7:3) afforded an αβ:ββ (1:4) anomeric mixture of the title compound **25a** (13 mg, 10 %) as well as an α:β (1:8) anomeric mixture of *mono*-glycosylated compound **25b** (11 mg, 14 %). For a proper characterisation of the αβ anomer, the αβ,ββ mixture isolated after the glycosylation was enriched in αβ isomer after silica gel chromatography (see figures 7.6.33-7.6.35). **ββ-25a:** ^{1}H NMR (500 MHz, $CDCl_3$)

δ = 7.87 (d, ^{3}J = 9.0 Hz, 4H, 4Ar-H_{ortho}), 7.07 (d, ^{3}J = 9.0 Hz, 4H, 4Ar-H_{meta}), 5.50 (d, $^{3}J_{1,2}$ = 5.8 Hz, 2H, 2H-1), 4.11-4.05 (m, 2H, 2H-5), 3.96 (d, $^{3}J_{2,1}$ = 5.8 Hz, 2H, 2H-2), 3.89, (bs, 2H, 2H-3), 3.85 (bs, 2H, 2H-4), 3.61 (dd, $^{2}J_{6a\text{-}6b}$ = 12.2 Hz, $^{3}J_{6a,5}$ = 6.9 Hz, 2H, H-6a), 3.48 (dd, $^{2}J_{6b\text{-}6a}$ = 12.2 Hz, $^{3}J_{6b,5}$ = 7.4 Hz, 2H, H-6b), 0.94 (s, 18H, 2C$(CH_3)_3$), 0.92 (s, 18H, 2C$(CH_3)_3$), 0.86 (s, 18H, 2C$(CH_3)_3$), 0.18 (s, 3H, CH_3), 0.17 (s, 3H, CH_3), 0.14 (s, 3H, CH_3), 0.14 (s, 3H, CH_3), 0.12 (s, 3H, CH_3), 0.02 (s, 3H, CH_3) ppm; ^{13}C NMR (126 MHz, $CDCl_3$) δ = 159.0 (2C, 2Ar-C_{para}), 148.1 (2C, 2Ar-C_{ipso}), 124.5 (4C, 4Ar-C_{ortho}), 116.2 (4C, 4Ar-C_{meta}), 99.1 (2C-1), 79.8 (2C-5), 78.2 (2C-3), 76.5 (2C-2), 70.9 (2C-4), 53.2 (2C-6), 26.0, 25.9 (18C, C($\underline{C}H_3)_3$), 18.2, 18.1, 18.0 (6C, C($\underline{C}H_3)_3$), -4.1, -4.3, -4.5, -4.7, -4.8 (12C, CH_3) ppm; ESI HRMS: *m/z*: calcd for $C_{60}H_{112}O_{10}N_8Si_6$ + H^+: 1273.7190 [M + H^+] found: 1273.7193.

(*E*)-*p*-(2,3,4-tri-*O*-((*tert*-butyldimethyl)silyl)-6-azido-6-deoxy-α-D-glucopyranosyloxy)-*p'*-(2,3,4-tri-*O*-(*tert*-butyldimethyl)silyl)-6-azido-6-deoxy-β-D-glucopyranosyloxy) azobenzene (αβ-25a).

^{1}H NMR (500 MHz, $CDCl_3$) δ = 7.90-7.85 (m, 4H, 4Ar-H_{ortho}), 7.18 (d, ^{3}J = 9.1 Hz, 2H, H-8, H-9), 7.07 (d, ^{3}J = 9.0 Hz, 2H, H-16, H-17), 5.57 (d, $^{3}J_{1,2}$ = 3.5 Hz, 1H, H-1$_\alpha$), 5.50 (d, $^{3}J_{1,2}$ = 6.0 Hz, 1H, H-1$_\beta$), 4.36-4.32 (m, 1H, H-5$_\alpha$), 4.11-4.05 (m, 2H, H-5$_\beta$, H-2$_\alpha$), 3.96 (d, $^{3}J_{2,1}$ = 6.0 Hz, 1H, H-2$_\beta$), 3.94,3.91 (m, 1H, H-3$_\alpha$), 3.91-3.88 (m, 1H, H-3$_\beta$), 3.87-3.83 (m, 1H, H-4$_\beta$), 3.75 (m, 1H, H-4$_\alpha$), 3.61 (dd, $^{2}J_{6a,6b}$ 12.3 Hz, $^{3}J_{6a,5}$ = 6.9 Hz, 1H, H-6a$_\beta$), 3.52,3.45 (m, 2H, H-6b$_\beta$, H-6a$_\alpha$), 3.20 (dd, $^{2}J_{6a,6b}$ = 13.3 Hz, $^{3}J_{6a,5}$ = 5.5 Hz, 1H, H-6b$_\alpha$), 0.96 (s, 9H, C$(CH_3)_3$), 0.94 (s, 9H, C$(CH_3)_3$), 0.92 (s, 9H, C$(CH_3)_3$), 0.92 (s, 9H, C$(CH_3)_3$), 0.88 (s, 9H, C$(CH_3)_3$), 0.86 (s, 9H, C$(CH_3)_3$), 0.22 (s, 3H, CH_3), 0.18 (s, 3H, CH_3), 0.17 (s, 3H, CH_3), 0.16 (s, 3H, CH_3), 0.14 (s, 3H, CH_3), 0.14 (s, 3H, CH_3), 0.12 (s, 3H, CH_3), 0.12 (s, 3H, CH_3), 0.09 (s, 3H, CH_3), 0.07 (s, 3H, CH_3), 0.02 (s, 3H, CH_3), 0.02 (s, 3H, CH_3) ppm; ESI HRMS: *m/z*: calcd for $C_{60}H_{112}O_{10}N_8Si_6$ + H^+: 1273.7190 [M + H^+] found: 1273.7193; Since the isolated amount of **αβ**,**ββ-25a** (αβ minor isomer) was too small, no proper ^{13}C-NMR characterization of the α,β species by could be achieved.

(*E*)-*p*-(2,3,4-tri-*O*-((*tert*-butyldimethyl)silyl)-6-deoxy-6-azido-β-D-glucopyranosyloxy)-*p´*-hydroxy azobenzene (β-25b).

^{1}H NMR (500 MHz, $CDCl_3$) δ = 7.87 (d, ^{3}J = 9.0 Hz, 2H, H-10, H-11), 7.83 (d, ^{3}J = 8.9 Hz, 2H, H-14, H-15), 7.07 (d, ^{3}J = 9.0 Hz, 2H, H-8, H-9), 6.93 (d, ^{3}J = 8.9 Hz, 2H, H-16, H-17), 5.51 (d, $^{3}J_{1,2}$ = 5.9 Hz, 1H, H-1), 4.11-4.06 (m, 1H, H-5), 3.96 (t, $^{3}J_{2,1}$ = 5.9 Hz, 1H, H-2), 3.90-3.88 (m, 1H, H-3), 3.86-3.83 (m, 1H, H-4), 3.61 (dd, $^{2}J_{6a,6b}$ = 12.4 Hz, $^{3}J_{6a,5}$ = 6.9 Hz, 1H, H-6a), 3.48 (dd, $^{2}J_{6b,6a}$ = 12.4 Hz, $^{3}J_{6b,5}$ = 7.4 Hz, 1H, H-6b), 0.94 (s, 9H, C$(CH_3)_3$), 0.92 (s, 9H, C$(CH_3)_3$), 0.86 (s, 9H, C$(CH_3)_3$), 0.18 (s, 3H, CH_3), 0.17 (s, 3H, CH_3), 0.14 (s, 6H, 2CH_3), 0.12 (s, 3H, CH_3), 0.02 (s, 3H, CH_3) ppm; ^{13}C NMR (126 MHz, $CDCl_3$) δ = 159.0 (C-7), 158.0 (C-18), 148.0 (C-12), 147.4 (C-13), 124.8 (2C, C-14, C-15), 124.4 (2C, C-10, C-11), 116.2 (2C, C-8, C-9), 115.9 (2C, C-14, C-15), 99.1 (C-1), 79.8 (C-5), 78.2 (C-3), 76.5 (C-2), 70.9 (C-4), 53.2 (C-6), 26.0, 25.9 (9C, 3C($\underline{C}H_3)_3$), 18.2, 18.1, 18.0 (3C, 3$\underline{C}(CH_3)_3$), -4.1, -4.3, -4.5, -4.7, -4.8 (6C, 6CH_3) ppm; ESI HRMS: *m/z*: calcd for $C_{38}H_{61}O_6N_5Si_3$ – H^+: 742.3857 [M - H^+] found: 742.3861.

(*E*)-*p*-(2,3,4-tri-*O*-((*tert*-butyldimethyl)silyl)-6-deoxy-6-azido-α-D-glucopyranosyloxy)-*p´*-hydroxy azobenzene (α-25b).

^{1}H NMR (500 MHz, $CDCl_3$) δ = 7.89-7.81 (m, 4H, H-10, H-11, H-14, H-15), 7.18 (d, ^{3}J = 9.1 Hz, 2H, C-8, C-9), 6.93 (d, ^{3}J = 9.1 Hz, 2H, H-16, H-17), 5.57 (d, $^{3}J_{1,2}$ = 3.5 Hz, 1H, H-1), 4.34 (ddd, $^{3}J_{5,4}$ = 8.9 Hz, $^{3}J_{5,6b}$ = 5.5 Hz, $^{3}J_{5,6a}$ = 2.7 Hz, 1H, H-5), 4.11-4.07 (m, 1H, H-2), 3.94,3.91 (m, 1H, H-3), 3.75 (t, $^{3}J_{4,5}$ = 8.9 Hz, 1H,

H-4), 3.48 (dd, $^{2}J_{6a,6b}$ = 13.3 Hz, $^{3}J_{6a,5}$ = 2.7 Hz, 1H, H-6a), 3.21 (dd, $^{2}J_{6b,6a}$ = 13.3 Hz, $^{3}J_{6b,5}$ = 5.5 Hz, 1H, H-6b), 0.96 (s, 9H, C(CH_3)$_3$), 0.93 (s, 9H, C(CH_3)$_3$), 0.88 (s, 9H, C(CH_3)$_3$), 0.22 (s, 3H, CH_3), 0.16 (s, 3H, CH_3), 0.14 (s, 3H, CH_3), 0.12 (s, 3H, CH_3), 0.11 (s, 3H, CH_3), 0.09 (s, 3H, CH_3) ppm; ESI HRMS: *m/z*: calcd for $C_{38}H_{61}O_6N_5Si_3$ – H^+: 742.3857 [M - H^+] found: 742.3861; Since the isolated amount of **α,β-25b** (α minor anomer) was too small, no proper ^{13}C-NMR characterization of the α species by could be achieved.

7.2.3. Synthesis and characterization of methylated azobenzenes

To a suspension of DHAB (214 mg, 1.00 mmol) in acetonitrile (10 mL) were added diisopropylethylamine (0.348 mL, 2.00 mmol) and methyltrifluoromethanesulfonate (0.164 mL, 1.50 mmol) at RT. The mixture was stirred for 2 h at this temperature and then was concentrated and purified by column chromatography (cyclohexane-ethyl acetate) to afford 4,4´-dimethoxyazobenzene **S1** (34 mg, 11 %) and 4-hydroxy-4´-methoxyazobenzene **S2** (72.8 mg, 32 %).

***p,p´*-dimethoxyazobenzene (S1)**. ^{1}H NMR (500 MHz, $CDCl_3$) δ = 7.93-7.78 (m, 4H, 4-H_{ortho}), 7.05-6.87 (m, 4H, 4-H_{meta}), 3.89 (s, 6H, OMe) ppm; ^{13}C NMR (126 MHz, $CDCl_3$) δ = 161.7 (2C, Ar-C_{para}), 147.2 (2C, Ar-C_{ipso}), 124.5 (4C, Ar-C_{ortho}), 111.3 (4C, Ar-C_{meta}), 55.7 (2C, OCH_3) ppm; ESI HRMS: *m/z*: calcd for $C_{14}H_{14}O_2N_2$ + H^+: 243.1128 [M + H^+] found: 243.1124.

***p*-methoxy-*p´*-hydroxyazobenzene (S2)**. ^{1}H NMR (500 MHz, $CDCl_3$) δ = 7.90-7.80 (m, 4H, 4-H_{ortho}), 7.02-6.98 (m, 2H, 2-H_{meta}, OMe side), 6.94-6.90 (m, 2H, 2-H_{meta}, OH side), 5.51, (bs, 1H, OH), 3.88 (s, 3H, OMe) ppm; ^{13}C NMR (126 MHz, $CDCl_3$) δ = 161.8 (1Ar-C_{para}, OMe side), 157.9 (1Ar-C_{para}, OH side), 147.3 (1Ar-C_{ipso}, OH side), 147.1 (1Ar-C_{ipso}, OMe side), 124.7 (2C, 2Ar-C_{ortho}, OH side), 124.5 (2C, 2Ar-C_{ortho}, OMe side), 115.9 (2C, 2Ar-C_{meta}, OH side), 114.3 (2C, 2Ar-C_{meta}, OH side), 55.7 (OCH_3) ppm; ESI HRMS: *m/z*: calcd for $C_{13}H_{12}O_2N_2$ + H^+: 229.0972 [M + H^+] found: 229.0968.

7.2.4. Analytical proofs of the formation of *N*-dehydro-*N*-iodo-*p*-hydroxyphenylhydrazoquinone 26

DHAB, upon treatment with NIS/TfOH gave compound **26**, which after isolation underwent the following rearrangement:

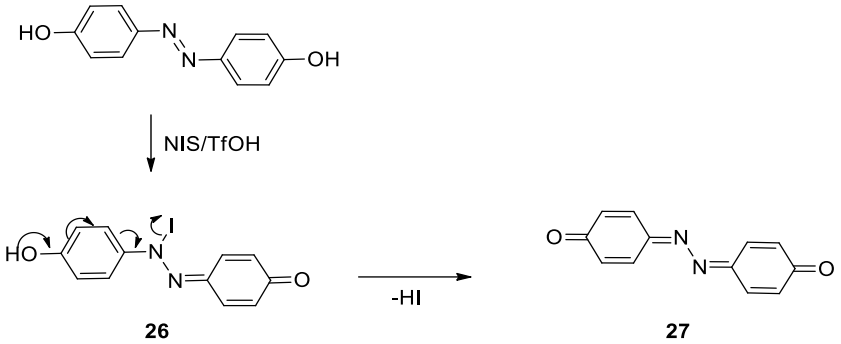

The following data are thus concerning compound **27**, however, the peak corresponding to **26** was observed in HRMS.

26: ESI HRMS: *m/z*: calcd for $C_{12}H_9IN_2O_2$ - H^+: 338.9636 [M - H^+] found: 338.9636

27: ESI HRMS: *m/z*: calcd for $C_{12}H_8N_2O_2$ + H^+: 213.0659 [M + H^+] found: 213.0663

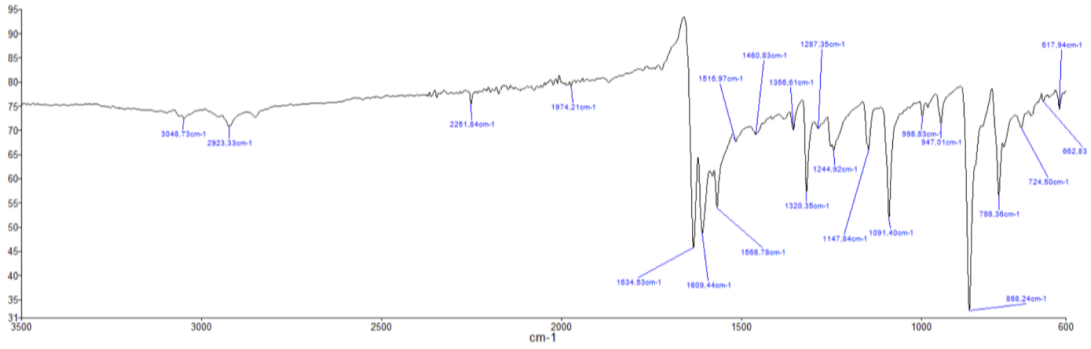

Figure 7.2.2. FTIR spectrum of **27**.

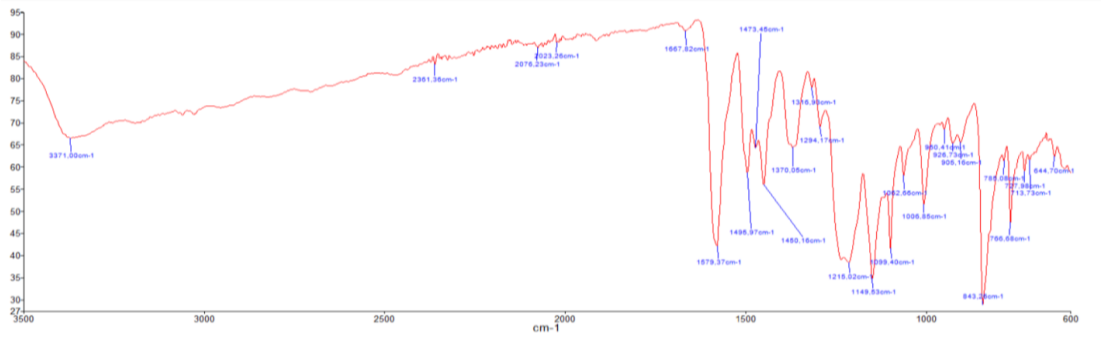

Figure 7.2.3. FTIR spectrum of **DHAB**.

7.3. Palladium-catalyzed thioarylation

Compounds **28**-**34**, **43**-**45** and **59** were synthesised according to known procedures.[163,189,319,358,359,368-370] Compounds **46**-**49** were commercially available and used without further purification.

For symmetrical azobenzene *bis*-glycosides, assignments of NMR data for the azobenzene signals were reported as H_{ortho}, H_{meta}, C_{ipso}, C_{ortho}, C_{meta}, C_{para}, regarding the position of the azo bond. In the case of unsymmetrical compounds as well as diazocine conjugates, the following numbering was used (Figure S1).

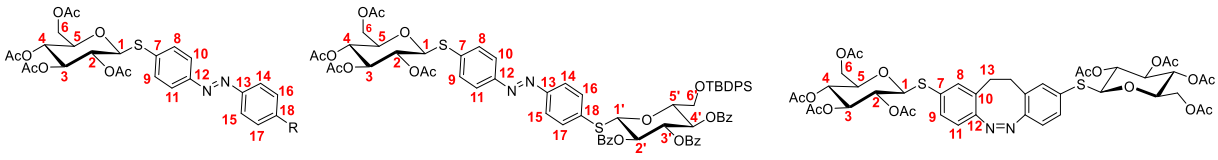

Figure 7.3.1. Numbering of unsymmetrical azobenzene glycoconjugates and diazocine glycoconjugates for assignment of NMR data.

7.3.1. Homo-*bis*-functionalization of *p,p´*-diiodoazobenzene derivatives with glycosyl thiols

General procedure A: In a flame-dried Schlenk tube were loaded the azo derivative (1eq), the thiol (3 eq), palladium acetate (10 mol%) and Xantphos (5 mol%), and vacuum was applied for 15 min. Meanwhile, dry 1,4-dioxane was degassed by bubbling nitrogen through. Then, the Schlenk tube was filled with a nitrogen atmosphere, and the solvent was added ([azo derivative] = 0.15 M), followed by Et_3N (2 eq). The tube was sealed with a screw cap and the reaction was stirred for 1 h at 100 °C. Then, the mixture was cooled to RT, and the resulting suspension was filtered through celite, the filter was rinsed with EtOAc, and the filtrate was concentrated *in vacuo*. Column chromatography afforded the pure desired compound.

General procedure B: In a flame dried round bottom flask were loaded the azo derivative (1 eq), the thiol (2 eq) and PdG3-Xantphos (2 mol%), and vacuum was applied for 15 min. Meanwhile the solvent (dry dioxane or dry THF) was degassed by bubbling nitrogen through. Then the flask was filled with a nitrogen atmosphere and the solvent was added ([azo derivative] = 0.05-0.3 M), followed by Et_3N (2 eq). The reaction was stirred at the appropriate temperature for the appropriate time (if heating is required, the flask may be equipped with a nitrogen flushed condenser). Then, the mixture was diluted in EtOAc, washed with aq. 1N HCl and brine, and the aqueous phase was extracted with EtOAc. The combined organic layers were dried over $MgSO_4$, filtered and concentrated *in vacuo*. Column chromatography afforded the pure desired compound.

(*E*)-4,4'-*bis*-(2,3,4,6-tetra-*O*-acetyl-1-thio-β-D-glucopyranosyl) azobenzene (35).

Route A: General procedure **A** was applied to 4,4´-di-iodoazobenzene **28** (49 mg, 112 µmol, 1.0 eq) with thiol **31** (2.0 eq) in 1,4-dioxane (0.700 mL) with $Pd(OAc)_2$ (10 mol%) and Xantphos (5 mol%) and Et_3N (2.0 eq); stirring at 100 °C for 1 h. Column chromatography (cyclohexane:EtOAc 4:1 to 1:1) afforded the title compound **35** (92 mg, 101 µmol) in 91% yield as a yellow solid. **Route B**: General procedure **B** was applied to 4,4´-di-iodoazobenzene **28** (65 mg, 150 µmol, 1.0 eq) with thiol **31** (2.0 eq) in THF (1.00 mL) with PdG3-Xantphos (2 mol%) and Et_3N (2.0 eq); stirring at RT for 15 min. Column chromatography (cyclohexane:EtOAc 4:1 to 1:1) afforded the title compound **35** (126 mg, 139 µmol)

in 93% yield as a yellow solid. $[\alpha]^{20}_D$ = -12.0 (*c* = 0.5 in $CHCl_3$); ^{1}H NMR (500 MHz, $CDCl_3$) δ = 7.88-7.84 (m, 4H, 4Ar-H_{ortho}), 7.64-7.59 (m, 4H, 4Ar-H_{meta}), 5.27 (at, $^3J_{3,2}$ = 9.3 Hz, $^3J_{3,4}$ = 9.4 Hz, 2H, H-3), 5.08 (at, $^3J_{4,5}$ = 10.1 Hz, $^3J_{4,3}$ = 9.4 Hz, 2H, H-4), 5.05 (dd, $^3J_{2\text{-}1}$ = 10.1 Hz, $^3J_{2,3}$ = 9.3 Hz, 2H, H-2), 4.82 (d, $^3J_{1,2}$ = 10.1 Hz, 2H, H-1), 4.26 (dd, $^2J_{6a,6b}$ = 12.3 Hz, $^3J_{6a,5}$ = 5.3 Hz, 2H, H-6a), 4.21 (dd, $^2J_{6b,6a}$ = 12.3 Hz, $^3J_{6b,5}$ = 2.5 Hz, 2H, H-6b), 3.79 (ddd, $^3J_{5,4}$ = 10.1 Hz, $^3J_{5,6a}$ = 5.3 Hz, $^3J_{5,6b}$ = 2.5 Hz, 2H, H-5), 2.11 (s, 3H, C(O)CH_3), 2.10 (s, 3H, C(O)CH_3), 2.04 (s, 3H, C(O)CH_3), 2.00 (s, 3H, C(O)CH_3) ppm ; ^{13}C NMR (126 MHz, $CDCl_3$) δ = 170.6, 170.2, 169.4, 169.3 (8C, 8$\underline{C}$(O)CH_3), 151.9 (2C, 2Ar-C_{ipso}), 135.9 (2C, 2Ar-C_{para}), 132.6 (4C, 4Ar-C_{meta}), 123.3 (4C, 4Ar-C_{ortho}), 85.3 (2C, C-1), 76.0 (2C, C-5), 73.9 (2C, C-3), 69.9 (2C, C-2), 68.2 (2C, C-4), 62.1 (2C, C-6), 20.8, 20.7, 20.6 (8C, 8C(O)$\underline{C}H_3$) ppm ; ESI HRMS: *m/z*: clcd for $C_{40}H_{40}N_2O_{18}S_2$ + H^+: 907.22598 [M+H^+] found: 907.22489.

(*E*)-2,2',6,6'-tetrafluoro-4,4'-*bis*-(2,3,4,6-tetra-*O*-acetyl-1-thio-β-D-glucopyranosyl) azobenzene (36).

Route A: General procedure **A** was applied to 2,2´,6,6´-tetrafluoro-4,4´-di-iodoazobenzene **29** (51 mg, 100 µmol, 1.0 eq) with thiol **31** (2.0 eq) in 1,4-dioxane (0.630 mL) with $Pd(OAc)_2$ (10 mol%) and Xantphos (5 mol%) and Et_3N (2.0 eq); stirring at 100 °C for 1 h. Column chromatography (cyclohexane:EtOAc 4:1 to 1:1) afforded the title compound **36** (35 mg, 36 µmol) in 36% yield as a red foam. **Route B**: General procedure **B** was applied to 2,2´,6,6´-tetrafluoro-4,4´-di-iodoazobenzene **29** (76 mg, 150 µmol, 1.0 eq) with thiol **31** (2.0 eq) in THF (3.00 mL) with PdG3-Xantphos (2 mol%) and Et_3N (2.0 eq); stirring at RT for 20 min. Column chromatography (cyclohexane:EtOAc 4:1 to 1:1) afforded the title compound **36** (132 mg, 135 µmol) in 90% yield as a red foam. $[\alpha]^{20}_D$ = +32.8 (*c* = 0.5 in DMSO); ^{1}H NMR (500 MHz, DMSO) δ = 7.42 (d, $^3J_{H,F}$ = 10.0 Hz, 4H, 4Ar-H_{meta}), 5.69 (d, $^3J_{1,2}$ = 10.1 Hz, 2H, 2H-1), 5.41 (dd, $^3J_{3,2}$ = 9.4 Hz, $^3J_{3,4}$ = 9.3 Hz, 2H, 2H-3), 5.04-4.97 (m, 4H, 2H-2, 2H-4), 4.29 (ddd, $^3J_{5,4}$ = 10.1 Hz, $^3J_{5,6a}$ = 5.5 Hz, $^3J_{5,6b}$ = 3.1 Hz, 2H, 2H-5), 4.17-4.09 (m, 4H, 2H-6a, 2H-6b), 2.05 (s, 6H, C(O)CH_3), 2.02 (s, 6H, C(O)CH_3), 1.97 (s, 6H, C(O)CH_3) ppm ; ^{13}C NMR (126 MHz, $CDCl_3$) δ = 169.8, 169.4, 169.2, 169.1 (8C, 8$\underline{C}$(O)CH_3), 154.6 (dd, $^1J_{C,F}$ = 261.5 Hz, $^3J_{C,F}$ = 4.9 Hz, 4C, 4Ar-C_{ortho}), 140.4 (t, $^3J_{C,F}$ = 11.5 Hz, 2C, 2Ar-C_{para}), 128.8 (t, $^2J_{C,F}$ = 9.6 Hz, 2C, 2Ar-C_{ipso}), 112.6, 112.4 (d, $^2J_{C,F}$ = 24.6 Hz, 4C, 4Ar-C_{meta}), 81.3 (2C, 2C-1), 74.5 (2C, 2C-5), 72.6 (2C, 2C-3), 69.0, 67.9 (4C, 2C-2, 2C-4), 62.0 (2C, 2C-6), 20.3, 20.2 (8C, 8C(O)$\underline{C}H_3$) ppm ; ESI HRMS: *m/z:* clcd for $C_{40}H_{42}F_4N_2O_{18}S_2$ + H^+ = 979.18829 [M+H^+] found: 979.18657.

(*E*)-2,2',6,6'-tetrafluoro-4,4'-*bis*-(3,4,6-tri-*O*-acetyl-2-deoxy-2-trichloroethoxycarbonylamino-1-thio-β-D-glucopyranosyl) azobenzene (37).

General procedure **B** was applied to 2,2´,6,6´-tetrafluoro-4,4´-di-iodoazobenzene **29** (50.5 mg, 100 µmol, 1.0 eq) with thiol **33** (2.2 eq) in THF (0.400 mL) with PdG3-Xantphos (5 mol%) and Et_3N (2.2 eq); stirring at RT for 10 min. Column chromatography (cyclohexane:EtOAc 9:1 to 1:1) afforded the title compound **37** (101 mg, 81 µmol) in 81% yield as a red solid. $[\alpha]^{20}_D$ = +39.8 (*c* = 0.5 in DMSO); ^{1}H NMR (500MHz, $CDCl_3$) δ = 8.23 (d, $^3J_{NH,2}$ = 9.6 Hz, 2H, 2NH), 7.43 (d, $^3J_{H,F}$ = 10.2 Hz, 4H, 4Ar-H_{meta}), 5.38 (d, $^3J_{1,2}$ = 10.4 Hz, 2H, 2H-1), 5.21 (t, *J* = 9.8 Hz, 2H, 2H-3), 4.98-4.87 (m, 4H, 2H-4, CH_2CCl_3), 4.76 (d, ^2J = 12.4 Hz, 2H, CH_2CCl_3), 4.24-4.17 (m, 2H, 2H-5), 4.16-4.09 (m, 4H, 2H-6a, 2H-6b), 3.85-3.73 (m, 2H, 2H-2), 2.02 (s, 6H, C(O)CH_3), 2.01 (s, 6H, C(O)CH_3), 1.93 (s, 6H, C(O)CH_3) ppm ; ^{13}C NMR (126MHz, $CDCl_3$) δ = 169.9, 169.4, 169.2 (6C, 6$\underline{C}$(O)CH_3), 154.6 (dd, $^1J_{C,F}$ = 261.6 Hz, $^3J_{C,F}$ = 4.8 Hz, 4C, 4Ar-C_{ortho}), 154.2 (2C, 2$\underline{C}$(O)OCH_2CCl_3), 141.0 (t, $^3J_{C,F}$ = 11.3 Hz, 2C, 2Ar-C_{para}), 128.6 (t, $^2J_{C,F}$ = 9.6 Hz, 2C, 2Ar-C_{ipso}), 112.3 (d, $^2J_{C,F}$ = 23.8 Hz, 4C, 4Ar-C_{meta}), 96.0 (2C, $CH_2\underline{C}Cl_3$), 82.8 (2C, 2C-1), 74.6 (2C, 2C-5), 73.3 (2C, $\underline{C}H_2CCl_3$) 73.0 (2C, 2C-3), 68.2 (2C, 2C-4), 61.9 (2C, 2C-6), 53.9 (2C, 2C-2), 20.3, 20.2 (6C, C(O)$\underline{C}H_3$) ppm ; ESI HRMS: *m/z*: clcd for $C_{42}H_{42}Cl_6N_4F_4O_{18}S_2$ + Na^+: 1262.98950 [M+Na^+] found: 1262.98932.

(*E*)-4,4'-*bis*-(2,3,4-tri-*O*-benzoyl-6-*O*-(*tert*-butyldiphenyl)silyl-1-thio-β-D-glucopyranosyl) azobenzene (38).

General procedure **B** was applied to 4,4´-di-iodoazobenzene **28** (65 mg, 150 µmol, 1.0 eq) with thiol **32** (2.0 eq) in THF (1.00 mL) with PdG3-Xantphos (2 mol%) and Et_3N (2.0 eq); stirring at RT for 5 min. Column chromatography (cyclohexane:EtOAc 1:0 to 3:2) afforded the title compound **38** (224 mg, 134 µmol) in 87% yield as an orange solid. $[\alpha]^{20}_D$ = +60.4 (*c* = 0.5 in $CHCl_3$); ^{1}H NMR (500 MHz, $CDCl_3$) δ = 8.00-7.96 (m, 4H, 4Ar-H), 7.88-7.78 (m, 12H, 8Ar-H, 4Ar-H_{ortho}), 7.74-7.70 (m, 4H, 4Ar-H), 7.69-7.65 (m, 4H, 4Ar-H_{meta}), 7.63-7.59 (m, 4H, 4Ar-H), 7.56-7.51 (m, 4H, 4Ar-H), 7.44-7.25 (m, 22H, 22Ar-H), 7.22-7.17 (m, 4H, 4Ar-H), 5.91 (at, $^3J_{3,4}$ = 9.6 Hz, $^3J_{3,2}$ = 9.4 Hz, 2H, 2H-3), 5.67 (at, $^3J_{4,5}$ = 9.9 Hz, $^3J_{4,3}$ = 9.6 Hz, 2H, 2H-4), 5.57 (at, $^3J_{2,1}$ = 10.0 Hz, $^3J_{2,3}$ = 9.4 Hz, 2H, 2H-2), 5.16 (d, $^3J_{1,2}$ = 10.0 Hz, 2H, 2H-1), 4.02-3.97 (m, 2H, 2H-5), 3.94-3.87 (m, 4H, 2H-6a, 2H-6b), 1.07 (s, 18H, C(CH_3)$_3$) ppm ; ^{13}C NMR (126 MHz, $CDCl_3$) δ = 166.0, 165.2, 165.1 (6C, 6<u>C</u>(O)Ph), 151.9 (2C, 2Ar-C_{ipso}), 136.8 (2C, 2Ar-C_{para}), 135.7, 135.8 (8C, 8Ar-C), 133.5, 133.4, 133.3 (6C, 6Ar-C), 133.0, 132.9 (4C, 4Ar-C), 132.3 (4C, 4Ar-C_{meta}), 130.0, 129.9, 129.8 (16C, 16Ar-C), 129.3, 129.2, 129.0 (6C, 6Ar-C), 128.6, 128.5, 128.4 (12C, 12Ar-C), 127.9, 127.8 (8C, 8Ar-C), 123.6 (4C, 4Ar-C_{ortho}), 86.0 (2C, 2C-1), 79.8 (2C, 2C-5), 74.7 (2C, 2C-3), 70.8 (2C, 2C-2), 68.9 (2C, 2C-4), 62.9 (2C, 2C-6), 26.8 (6C, 2C(<u>C</u>H_3)$_3$), 19.3 (2C, 2<u>C</u>(CH_3)$_3$) ppm ; ESI HRMS: *m/z:* clcd for $C_{98}H_{90}N_2O_{16}S_2Si_2$ + H^+: 1671.53431 [M+H^+] found: 1671.53445.

(*E*)-2,2',6,6'-tetrafluoro-4,4'-*bis*-(2,3,4-tri-*O*-benzoyl-6-*O*-(*tert*-butyldiphenyl)silyl-1-thio-β-D-glucopyranosyl) azobenzene (39).

General procedure **B** was applied to 2,2´,6,6´-tetrafluoro-4,4´-di-iodoazobenzene **29** (76 mg, 150 µmol, 1.0 eq) with thiol **32** (2.0 eq) in THF (1.00 mL) with PdG3-Xantphos (2 mol%) and Et_3N (2.0 eq); stirring at RT for 3 h. Column chromatography (cyclohexane:EtOAc 1:0 to 7:3) afforded the title compound **39** (181 mg, 104 µmol) in 69% yield as a red foam. $[\alpha]^{20}_D$ = -2.45 (*c* = 0.5 in DMSO); ^{1}H NMR (500 MHz, DMSO) δ = 7.90-7.85 (d, $^3J_{H\text{-}F}$ = 10.0 Hz, 4H, 4Ar-H_{meta}), 7.83-7.79 (m, 4H, 4Ar-H), 7.75-7.70 (m, 4H, 4Ar-H), 7.68-7.58 (m, 8H, 8Ar-H), 7.57-7.53 (m, 2H, 2Ar-H), 7.53-7.46 (m, 16H, 4Ar-H_{meta}, 12Ar-H), 7.42-7.37 (m, 4H, 4Ar-H), 7.34-7.29 (m, 4H, 4Ar-H), 7.27-7.22 (m, 4H, 4Ar-H), 7.20-7.15 (m, 4H, 4Ar-H), 6.10 (d, $^3J_{1,2}$ = 10.0 Hz, 2H, 2H-1), 6.08 (dd, $^3J_{3,4}$ = 9.6 Hz, $^3J_{3,2}$ = 9.2 Hz, 2H, 2H-3), 5.69 (dd, $^3J_{4,5}$ = 9.8 Hz, $^3J_{4,3}$ = 9.6 Hz, 2H, 2H-4), 5.54 (dd, $^3J_{2,1}$ = 10.0 Hz, $^3J_{2,3}$ = 9.2 Hz, 2H, 2H-2), 4.54-4.49 (m, 2H, 2H-5), 3.86-3.75 (m, 4H, 2H-6a, 2H-6b), 0.91 (s, 18H, C(CH_3)$_3$) ppm ; ^{13}C NMR (126 MHz, $CDCl_3$) δ = 165.0, 164.5, 164.4 (6C, 6<u>C</u>OPh), 154.5 (dd, $^1J_{C,F}$ = 261.6 Hz, $^3J_{C,F}$ = 5.0 Hz, 4C, 4Ar-C_{ortho}), 140.0 (2C, 2Ar-C_{para}), 134.9 (8C, 8Ar-C), 134.8 (8C, 8Ar-C), 134.0 (2C, 2Ar-C), 133.8 (2C, 2Ar-C_{ipso}), 133.8, 133.7 (4C, 4Ar-C), 132.2, 132.0 (4C, 4Ar-C), 129.2, 129.1, 128.9, 128.8, 128.7 (24C, 24Ar-C), 128.4, 128.2, 128.1 (6C, 6Ar-C), 127.6 (8C, 8Ar-C), 112.7 (dd, $^2J_{C,F}$ = 23.7 Hz, $^4J_{C,F}$ = 3 Hz, 4C, 4Ar-C_{meta}), 81.3 (2C, 2C-1), 77.5 (2C, 2C-5), 74.0 (2C, 2C-3), 70.1 (2C, 2C-2), 68.4 (2C, 2C-4), 62.3 (2C, 2C-6), 26.2 (6C, 2C(<u>C</u>H_3)$_3$), 18.5 (2C, 2C(<u>C</u>H_3)$_3$) ppm ; ESI HRMS: *m/z*: clcd for $C_{98}H_{86}F_4N_2O_{16}S_2Si_2$ + H^+ = 1743.49662 [M+H^+] found: 1743.49661.

(*E*)-4,4'-*bis*-(1-thiophenyl-2,3,4-tri-*O*-acetyl-6-deoxy-6-thio-β-D-glucopyranosyl) azobenzene (40). Route A: General procedure **A** was applied to 4,4´-di-iodoazobenzene **28** (43 mg, 100 µmol, 1.0 eq) with thiol **34** (2.0 eq) in 1,4-dioxane (0.630 mL) with $Pd(OAc)_2$ (10 mol%) and Xantphos (5 mol%) and Et_3N (2.0 eq); stirring at 100 °C for 1 h. Column chromatography (cyclohexane:EtOAc 4:1 to 3:2) afforded the title compound **40** (73 mg, 72 µmol) in 72% yield as a yellow solid. **Route B**: General procedure **B** was applied to 4,4´-di-iodoazobenzene **28** (65 mg, 150 µmol, 1.0 eq) with thiol **34** (2.0 eq) in THF (1.00 mL) with PdG3-Xantphos (2 mol%) and Et_3N (2.0 eq); stirring at RT for 10 min. Column chromatography (cyclohexane:EtOAc 4:1 to 1:1) afforded the title compound **40** (150 mg, 149 µmol) in quantitative yield as a yellow solid. $[\alpha]^{20}_D$ = +71.6 (*c* = 0.5 in $CHCl_3$); ^{1}H NMR (500 MHz, $CDCl_3$) δ =

7.84-7.80 (m, 4H, 4Ar-H_{ortho}), 7.49-7.46 (m, 4H, 4Ar-H_{SPh}), 7.43-7.39 (m, 4H, 4Ar-H_{meta}), 7.33-7.28 (m, 6H, 6Ar-H_{SPh}), 5.20 (at, $^3J_{3,2}$ = $^3J_{3,4}$ = 9.3 Hz, 2H, 2H-3), 5.03 (at, $^3J_{4,3}$ = 9.3 Hz, $^3J_{4,5}$ = 10.1 Hz, 2H, 2H-4), 5.00 (dd, $^3J_{2,1}$ = 10.1 Hz, $^3J_{2,3}$ = 9.4 Hz, 2H, 2H-2), 4.71 (d, $^3J_{1,2}$ = 10.1 Hz, 2H, 2H-1), 3.73-3.67 (ddd, $^3J_{5\text{-}4}$ = 10.1 Hz, $^3J_{5\text{-}6b}$ = 8.1 Hz, $^3J_{5\text{-}6a}$ = 3.0 Hz, 2H, 2H-5), 3.22 (dd, $^2J_{6a,6b}$ = 14.2 Hz, $^3J_{6a,5}$ = 3.0 Hz, 2H, 2H-6a), 3.12 (dd, $^2J_{6b,6a}$ = 14.2 Hz, $^3J_{6b,5}$ = 8.1 Hz, 2H, 2H-6b), 2.08 (s, 6H, C(O)CH_3), 2.06 (s, 6H, C(O)CH_3), 2.00 (s, 6H, C(O)CH_3) ppm ; ^{13}C NMR (126 MHz, $CDCl_3$) δ = 170.3, 169.8, 169.5 (6C, 6$\underline{C}$(O)CH_3), 150.9 (2C, 2Ar-C_{ipso}), 140.3 (2C, 2Ar-C_{para}), 130.0 (4C, 4Ar-C_{SPh}), 132.0 (2C, 2Ar-C_{SPh}), 129.2 (4C, 4Ar-C_{SPh}), 128.8 (4C, 4Ar-C_{meta}), 128.5 (2C, 2Ar-C_{SPh}), 123.6 (4C, 4Ar-C_{ortho}), 86.3 (2C, 2C-1), 77.1 (2C, 2C-5), 74.0 (2C, 2C-3), 71.6 (2C, 2C-4), 70.2 (2C, 2C-2), 35.3 (2C, 2C-6), 20.9, 20.8 (6C, 6C(O)$\underline{C}H_3$) ppm ; ESI HRMS: *m/z*: clcd for $C_{48}H_{50}N_2O_{14}S_4$ + H^+: 1007.22176 [M+H^+] found: 1007.22047.

(*Z*)-2,9-*bis*-(2,3,4,6-tetra-*O*-acetyl-1-thio-β-D-glucopyranosyl)-11,12-dihydrodibenzo[*c*,*g*][1,2] diazocine (41).

General procedure **B** was applied to 2,9-diiodo-11,12-dihydrodibenzo[1,2]diazocine **30** (35 mg, 75 µmol, 1.0 eq) with thiol **31** (2.0 eq) in THF (1.00 mL) with PdG3-Xantphos (2 mol%) and Et_3N (2.0 eq); stirring at 80 °C for 10 min. Column chromatography (cyclohexane:EtOAc 9:1 to 1:1) afforded the title compound **41** (53 mg, 56 µmol) in 75% yield as a yellow solid. $[\alpha]^{20}_D$ = -39.1 (*c* = 0.5 in $CHCl_3$); ^{1}H NMR (500 MHz, $CDCl_3$) δ = 7.32 (d, ^3J = 8.1 Hz, 1H, H-9, rotamers), 7.27 (d, ^3J = 8.1 Hz, 1H, H-9, rotamers), 7.13 (bs, 2H, 2H-8), 6.80 (d, ^3J = 8.10 Hz, 2H, 2H-11), 5.21 (at, ^3J = 9.3 Hz, 2H, 2H-3), 5.02 (at, ^3J = 9.8 Hz, 2H, 2H-4), 4.92 (at, ^3J = 9.3 Hz, 2H, 2H-2), 4.65 (at, ^3J = 8.5 Hz, 2H, 2H-1), 4.21 (dd, $^2J_{6a,6b}$ = 12.6 Hz, $^3J_{6a,5}$ = 4.8 Hz, 2H, 2H-6a), 4.15 (dd, $^2J_{6b,6a}$ = 12.6 Hz, $^3J_{6b,5}$ = 2.4 Hz, 2H, 2H-6b), 3.70 (ddd, $^3J_{5,4}$ = 10.1 Hz, $^3J_{5,6a}$ = 4.8 Hz, $^3J_{5,6b}$ = 2.4 Hz, 2H, 2H-5), 2.97 (bs, 2H, 2H-13a), 2.76 (bs, 2H, 2H-13b), 2.08 (bs, 6H, C(O)CH_3), 2.06 (s, 6H, C(O)CH_3), 2.02 (s, 6H, C(O)CH_3), 2.00 (s, 6H, C(O)CH_3) ppm ; ^{13}C NMR (126 MHz, $CDCl_3$) δ = 170.5, 170.1, 169.4, 169.2 (8C, 8$\underline{C}$(O)CH_3), 155.2 (2C, 2C-12), 134.5, 134.0 (2C, 2C-8), 131.5, 131.1 (2C, 2C-9), 130.4 (2C, C-7), 128.5 (2C, C-10), 119.6 (2C, 2C-11), 85.4, 85.3 (2C, 2C-1), 75.8 (2C, 2C-5), 73.8 (2C, 2C-3), 69.8 (2C, 2C-2), 68.1 (2C, 2C-4), 62.0 (2C, 2C-6), 31.5, 31.4 (2C, 2C-13), 20.8, 20.7, 20.6, 20.5 (8C, 8C(O)$\underline{C}H_3$) ppm ; ESI HRMS: *m/z*: clcd for $C_{42}H_{42}Cl_6N_4F_4O_{18}S_2$ + H^+: 933.24163 [M+H^+] found: 933.24155.

(*Z*)-2,9-*bis*-(3,4,6-tri-*O*-acetyl-2-deoxy-2-trichloroethoxycarbonylamino-1-thio-β-D-glucopyranosyl)-11,12-dihydrodibenzo[*c*,*g*][1,2]diazocine (42).

General procedure **B** was applied to 2,9-diiodo-11,12-dihydrodibenzo[1,2]diazocine **30** (89.5 mg, 195 µmol, 1.0 eq) with thiol **33** (2.2 eq) in THF (0.980 mL) with PdG3-Xantphos (5 mol%) and Et_3N (2.2 eq); stirring at 80 °C for 30 min. Column chromatography (cyclohexane:EtOAc 9:1 to 1:1) afforded the title compound **42** (139 mg, 116 µmol) in 59% yield as a yellow solid. $[\alpha]^{20}_D$ = -27.8 (*c* = 0.5 in $CHCl_3$); ^{1}H NMR (500MHz, $CDCl_3$) δ = 7.35 (d, ^3J = 8.2 Hz, 1H, H-9, rotamers), 7.28 (d, ^3J = 8.2 Hz, 1H, H-9, rotamers), 7.14 (bs, 2H, 2H-8), 6.81 (d, ^3J = 8.20 Hz, 2H, 2H-11), 5.43 (d, $^3J_{NH,2}$ = 9.1 Hz, 1H, NH), 5.37 (d, $^3J_{NH,2}$ = 9.1 Hz, 1H, NH), 5.28-5.16 (m, 2H, 2H-4), 5.06-4.94 (m, 2H, 2H-3), 4.87-4.64 (m, 6H, 2H-1, 2H-6a, 2H-6b), 4.27-4.09 (m, 4H, 2CH_2CCl_3), 3.79-3.64 (m, 4H, 2H-2, 2H-5), 3.04-2.88 (m, 2H, 2H-13a), 2.82-2.66 (m, 2H, 2H-13b), 2.07 (bs, 6H, C(O)CH_3), 2.03 (s, 6H, C(O)CH_3), 2.01 (bs, 6H, C(O)CH_3) ppm ; ^{13}C NMR (125MHz, $CDCl_3$) δ = 170.7, 170.5, 169.7 (6C, 6C(O)CH_3), 153.9 (2C, 2C-12), 134.3, 133.2 (2C, 2C-8), 131.4, 130.5 (2C, 2C-9), 128.6, 128.5 (4C, 2C-7, 2C-10), 119.7 (2C, 2C-11), 95.4 (2C, 2$CH_2\underline{C}Cl_3$), 86.4, 86.2 (2C, 2C-1), 75.7 (2C, 2C-5), 74.5 (2C, 2$\underline{C}H_2CCl_3$), 73.0 (2C, 2C-4), 68.5, 68.4 (2C, 2C-3), 62.5, 62.3 (2C, 2C-6), 55.0 (2C, 2C-2), 31.7, 31.4 (2C, 2C-13), 20.8, 20.6 (6C, 6C(O)CH_3) ppm ; ESI HRMS: *m/z*: clcd for $C_{42}H_{42}Cl_6N_4F_4O_{18}S_2$ + Na^+: 1217.04284 [M+Na^+] found: 1217.04306.

7.3.2. *Mono*-functionalization of unsymmetrical azobenzenes with different thiols

General procedure C: In a flame dried round bottom flask were loaded the azo derivative, the thiol and PdG3-Xantphos, and vacuum was applied for 15 min. Meanwhile the solvent (dry THF) was degassed by bubbling nitrogen through. Then the flask was filled with a nitrogen atmosphere and the solvent was added, followed by Et_3N. The reaction was stirred at RT for the appropriate time (if heating is required, the flask may be equipped with a nitrogen flushed condenser). Then, the mixture was diluted in EtOAc, washed with 1N HCl and brine, and the aqueous phase was extracted with EtOAc. The combined organic layers were dried over $MgSO_4$, filtered and concentrated *in vacuo*. Column chromatography afforded the pure desired compound.

Table 7.3.1. Results of the *mono*-functionalisation of various azobenzenes (**2**-**5**) with different thiols (**7**, **19**-**22**).

Entry	Azobenzene	R_2SH	Time	Temp.	Product, Yield
1	**43**	**31**	5 min	RT	**50**, 90%
2	**44**	**31**	20 min	RT	**51**, 87%
3	**45**	**31**	30 min	RT	**52**, 93%
4	**45**	**46**	2.5 h	RT	**53**, 86%
5	**45**	**47**	16 h	RT	**54**, 81%
6	**45**	**48**	4 h	70 °C	**55**, 47%
7	**45**	**49**	2 h	RT	**56**, 68%
8[a]	**29**	**31**	15 min	0 °C	**57**, 81%

Conditions: The thiol (1 – 1.2 eq) and azobenzene (1 – 1.2 eq) were stirred in THF (0.24 – 0.3 M) at the appropriate temperature in presence of PdG3-Xantphos (1 – 5 mol%) and Et_3N (1 – 1.4 eq); [a] The reaction was performed at 0 °C, with an excess of azobenzene (2 eq), at a concentration of 0.05 M.

(*E*)-4-(2,3,4,6-tetra-*O*-acetyl-1-thio-β-D-glucopyranosyl) azobenzene (50).

General procedure **C** was applied to 4-iodoazobenzene **43** (92 mg, 300 µmol, 1.0 eq) and thiol **31** (1.0 eq) in THF (1.00 mL) with PdG3-Xantphos (1 mol%) and Et_3N (1.0 eq); stirring at RT for 5 min. Column chromatography (cyclohexane:EtOAc 9:1 to 6:4) afforded the title compound **50** (148 mg, 272 µmol) in 90% yield as a yellow solid. $[\alpha]^{20}_D$ = -24.6 (*c* = 0.5 in $CHCl_3$); ^{1}H NMR (500 MHz, $CDCl_3$) δ = 7.93-7.89 (m, 2H, H-14, H-15), 7.88-7.84 (m, 2H, H-8, H-9), 7.64-7.60 (m, 2H, H-10, H-11), 7.55-7.46 (m, 3H, H-16, H-17, H-18), 5.26 (at, $^3J_{3,2}$ = 9.3 Hz, $J_{3,4}$ = 9.3 Hz, 1H, H-3), 5.08 (at, $^3J_{4,5}$ = 10.1 Hz, $^3J_{4,3}$ = 9.3 Hz, 1H, H-4), 5.05 (dd, $^3J_{1,2}$ = 10.1 Hz, $^3J_{2,3}$ = 9.3 Hz, 1H, H-2), 4.81 (d, $^3J_{1,2}$ = 10.1 Hz, 1H, H-1), 4.25 (dd, $^2J_{6a,6b}$ = 12.4 Hz, $^3J_{6a,5}$ = 5.3 Hz, 1H, H-6a), 4.20 (dd, $^2J_{6b,6a}$ = 12.4 Hz, $^3J_{6b,5}$ = 2.5 Hz, 1H, H-6b), 3.79 (ddd, $^3J_{5,4}$ = 10.1 Hz, $^3J_{5,6a}$ = 5.3 Hz, $^3J_{5,6b}$ = 2.5 Hz, 1H, H-5), 2.10 (s, 6H, C(O)CH_3), 2.03 (s, 3H, C(O)CH_3), 2.00 (s, 3H, C(O)CH_3) ppm ; ^{13}C NMR (126 MHz, $CDCl_3$) δ = 170.7, 170.3, 169.4, 169.3 (4C, 4C(O)CH_3), 152.7 (1C, C-13), 152.2 (1C, C-12), 135.6 (1C, C-7), 132.8 (2C, C-8, C-9), 131.4 (1C, C-18), 129.3 (2C, C-16, C-17), 123.4 (C2, C-10, C-11), 123.1 (2C, C-14, C-15), 85.5 (C-1), 76.1 (C-5), 74.0 (C-3), 70.0 (C-2), 68.3 (C-4), 62.3 (C-6), 20.9, 20.7 (4C, 4C(O)CH_3) ppm ; ESI HRMS: *m/z*: clcd for $C_{26}H_{29}O_9N_2S + H^+$: 545.15883 [M+H$^+$] found: 545.15919.

(*E*)-4-(2,3,4,6-tetra-*O*-acetyl-1-thio-β-D-glucopyranosyl)-4´-bromo azobenzene (51).

General procedure **C** was applied to 4-iodo-4´-bromoazobenzene **44** (116 mg, 300 µmol, 1.0 eq) and thiol **31** (1.0 eq) in THF (1.00 mL) with PdG3-Xantphos (1 mol%) and Et_3N (1.0 eq); stirring at RT for 20 min. Column chromatography (cyclohexane:EtOAc 9:1 to 7:3) afforded the title compound **51** (162 mg,

260 µmol) in 87% yield as a yellow solid. $[\alpha]^{20}_D$ = -19.2 (*c* = 0.5 in $CHCl_3$); ^{1}H NMR (500 MHz, $CDCl_3$) δ = 7.87-7.83 (m, 2H, H-10, H-11), 7.81-7.77 (m, 2H, H-14, H-15), 7.67-7.63 (m, 2H, H-16, H-17), 7.63-7.59 (m, 2H, H-7, H-8), 5.26 (at, $^3J_{3,2}$ = 9.3 Hz, $^3J_{3,4}$ = 9.4 Hz, 1H, H-3), 5.07 (at, $^3J_{4,5}$ = 10.2 Hz, $^3J_{4,3}$ = 9.4 Hz, 1H, H-4), 5.04 (at, $^3J_{2,1}$ = 10.1 Hz, $^3J_{2,3}$ = 9.3 Hz, 1H, H-2), 4.82 (d, $^3J_{1,2}$ = 10.1 Hz, 1H, H-1), 4.25 (dd, $^2J_{6a,6b}$ = 12.4 Hz, $^3J_{6a,5}$ = 5.3 Hz, 1H, H-6a), 4.20 (dd, $^2J_{6b,6a}$ = 12.4 Hz, $^3J_{6b,5}$ = 2.5 Hz, 1H, H-6b), 3.79 (ddd, $^3J_{5,4}$ = 10.2 Hz, $^3J_{5,6a}$ = 5.3 Hz, $^3J_{5,6b}$ = 2.5 Hz, 1H, H-5), 2.10 (s, 6H, C(O)CH_3), 2.03 (s, 3H, C(O)CH_3), 2.00 (s, 3H, C(O)CH_3) ppm ; ^{13}C NMR (126 MHz, $CDCl_3$) δ = 170.7, 170.5, 170.4, 170.3 (4C, 4C(O)CH_3), 152.0 (1C, C-12), 151.4 (1C, C-13), 136.1 (1C, C-7), 132.7 (2C, C-10, C-11), 132.5 (2C, C-16, C-17), 125.9 (1C, C-18), 124.6 (2C, C-14, C-15), 123.5 (2C, C-8, C-9), 85.4 (C-1), 76.1 (C-5), 73.4 (C-3), 70.0 (C-2), 68.3 (C-4), 62.3 (C-6), 20.9, 20.7 (4C, 4C(O)CH_3) ppm ; ESI HRMS: *m/z*: clcd for $C_{26}H_{29}O_9N_2BrS + Na^+$: 645.05128 [M+$Na^+$] found: 645.05042.

(*E*)-4´-(2,3,4,6-tetra-*O*-acetyl-1-thio-β-D-glucopyranosyl)-4´-hydroxy- azobenzene (52).

General procedure **C** was applied to 4-iodo-4´-hydroxyazobenzene **45** (97 mg, 300 µmol, 1.0 eq) and thiol **31** (1.0 eq) in THF (1.00 mL) with PdG3-Xantphos (1 mol%) and Et_3N (1.0 eq); stirring at RT for 30 min. Column chromatography (cyclohexane:EtOAc 9:1 to 7:3) afforded the title compound **52** (155 mg, 277 µmol) in 92% yield as a yellow solid. $[\alpha]^{20}_D$ = -16.7 (*c* = 0.5 in $CHCl_3$); ^{1}H NMR (500 MHz, $CDCl_3$) δ = 7.88-7.83 (m, 2H, H-14, H-15), 7.82-7.78 (m, 2H, H-10, H-11), 7.62-7.57 (m, 2H, H-8, H-9), 6.96-6.91 (m, 2H, H-16, H-17), 6.12 (bs, 1H, OH), 5.27 (at, $^3J_{3,4}$ = 9.5 Hz, $^3J_{3,2}$ = 9.3 Hz, 1H, H-3), 5.08 (at, $^3J_{4,5}$ = 10.1 Hz, $^3J_{4,3}$ = 9.5 Hz, 1H, H-4), 5.04 (dd, $^3J_{2,1}$ = 10.1 Hz, $^3J_{2,3}$ = 9.3 Hz, 1H, H-2), 4.79 (d, $^3J_{1,2}$ = 10.1 Hz, 1H, H-1), 4.26 (dd, $^2J_{6a,6b}$ = 12.3 Hz, $^3J_{6a,5}$ = 5.1 Hz, 1h, H-6a), 4.22 (dd, $^2J_{6b,6a}$ = 12.3 Hz, $^3J_{6b,5}$ = 2.5 Hz, 1h, H-6b), 3.78 (ddd, $^3J_{5,4}$ = 10.1 Hz, $^3J_{5,6a}$ = 5.1 Hz, $^3J_{5,6b}$ = 2.5 Hz, 1H, H-5), 2.11 (bs, 6H, C(O)CH_3), 2.04 (s, 3H, C(O)CH_3), 2.01 (s, 3H, C(O)CH_3) ppm ; ^{13}C NMR (126 MHz, $CDCl_3$) δ = 170.8, 170.3, 169.6, 169.5 (4C, 4C(O)CH_3), 158.9 (1C, C-18), 152.3 (1C, C-12), 147.0 (1C, C-13), 134.2 (1C, C-7), 133.0 (2C, C-8, C-9), 125.2 (2C, C-14, C-15), 123.0 (2C, C-10, C-11), 115.9 (2C, C-16, C-17), 85.4 (C-1), 75.9 (C-5), 73.9 (C-3), 69.9 (C-2), 68.2 (C-4), 62.2 (C-6), 20.8, 20.6 (4C, 4C(O)CH_3) ppm ; ESI HRMS: *m/z*: clcd for $C_{26}H_{29}O_{10}N_2S + H^+$: 561.15374 [M+$H^+$] found: 561.15395.

(*E*)-4-((4-(phenylthio)-4´-hydroxy azobenzene (53). General procedure **C** was applied to 4-iodo-4´-hydroxyazobenzene **45** (78 mg, 241 µmol, 1 eq) and thiophenol **46** (1.2 eq) in THF (0.800 mL) with PdG3-Xantphos (5 mol%) and Et_3N (1.4 eq); stirring at RT for 2.5 h. Automated column chromatography (cyclohexane:EtOAc 1:0 to 4:1 within 15 min) afforded the title compound **53** (64 mg, 207 µmol) in 86% yield, as a brownish solid. ^{1}H NMR (500 MHz, $CDCl_3$) δ = 7.88-7.82 (m, 2H, H-14, H-15), 7.81-7.76 (m, 2H, H-10, H-11), 7.48-7.43 (m, 2H, 2Ar-H_{SPh}), 7.40-7.30 (m, 5H, 3Ar-H_{SPh}, H-8, H-9), 6.97-6.89 (m, 2H, H-16, H-17), 5.35 (bs, 1H, OH) ppm ; ^{13}C NMR (126 MHz, $CDCl_3$) δ = 158.3 (1C, C-18), 151.1 (1C, C-12), 147.2 (1C, C-13), 140.0 (1C, C-7), 134.1 (1C, 1Ar-C_{SPh}), 132.5 (2C, 2Ar-C_{SPh}), 129.8 (2C, C-8, C-9), 129.5 (2C, 2Ar-C_{SPh}), 127.9 (1C, 1Ar-C_{SPh}), 125.0 (2C, C-14, C-15), 123.3 (2C, C-10, C-11), 115.8 (2C, C-16, C-17) ppm ; ESI HRMS: *m/z*: clcd for $C_{18}H_{14}N_2OS + H^+$: 307.08996 [M+H^+] found: 307.08985.

(*E*)-4-((2-hydroxyethyl)thio)-4´-hydroxy azobenzene (54).

General procedure **C** was applied to 4-iodo-4´-hydroxyazobenzene **45** (94 mg, 290 µmol, 1 eq) and 2-mercaptoethanol 47 (1.2 eq) in THF (1.20 mL) with PdG3-Xantphos (5 mol%) and Et_3N (1.2 eq); stirring at RT for 16 h. Automated column chromatography (cyclohexane:EtOAc 9:1 to 45:55 within 15 min) afforded the title compound **54** (65 mg, 235 µmol) in 81% yield, as a brownish solid. ^{1}H NMR (500 MHz, MeOD) δ = 7.82-7.75 (m, 4H, H-14, H-15, H-10, H-11), 7.49-7.43 (m, 2H, H-8, H-9), 6.94-6.88 (m, 2H, H-

16, H-17), 3.75 (t, ^{3}J = 6.8 Hz, 2H, $CH_2\underline{CH_2}OH$), 3.16 (t, ^{3}J = 6.8 Hz, 2H, $\underline{CH_2}CH_2OH$) ppm ; ^{13}C NMR (126 MHz, MeOD) δ = 162.1 (1C, C-18), 152.0 (1C, C-12), 147.6 (1C, C-13), 141.2 (1C, C-7), 129.4 (2C, C-8, C-9), 125.9 (2C, C-14, C-15), 124.0 (2C, C-10, C-11), 116.8 (2C, C-16, C-17), 61.6 (1C, $CH_2\underline{C}H_2OH$), 36.1 (1C, $\underline{C}H_2CH_2OH$), ppm ; ESI HRMS: *m/z*: clcd for $C_{14}H_{13}N_2O_2S$ - H^+: 273.07032 [M-H^+] found: 273.07068.

(*E*)-4-((2-aminoethyl)thio)-4´-hydroxy azobenzene (55).

General procedure **C** was applied to 4-iodo-4´-hydroxyazobenzene **45** (103 mg, 300 µmol, 1.0 eq) and cysteamine **48** (1.0 eq) in THF (1.00 mL) with PdG3-Xantphos (2.5 mol%) and Et_3N (1.0 eq); stirring at 70 °C for 4 h. Column chromatography (DCM/MeOH + 0,1% Et_3N 1:0 to 8:2) afforded the title compound **55** (39 mg, 143 µmol) in 47% yield, as a brownish foam. ^{1}H NMR (500 MHz, DMSO) δ = 7.82-7.75 (m, 4H, H-14, H-15, H-10, H-11), 7.55-7.50 (m, 2H, H-8, H-9), 7.00-6.94 (m, 2H, H-16, H-17), 3.28, 3.18 (m, 2H, $CH_2\underline{CH_2}NH_2$), 2.92 (t, ^{3}J = 7.2 Hz, 2H, $\underline{CH_2}CH_2NH_2$) ppm ; ^{13}C NMR (126 MHz, DMSO) δ = 161.0 (1C, C-18), 149.8 (1C, C-12), 145.0 (1C, C-13), 138.6 (1C, C-7), 127.7 (2C, C-8, C-9), 124.7, 122.7 (4C, C-10, C-11, C-14, C-15), 115.9 (2C, C-16, C-17), 39.2 (1C, $CH_2\underline{C}H_2NH_2$), 31.3 (1C, $\underline{C}H_2CH_2NH_2$), ppm ; ESI HRMS: *m/z*: clcd for $C_{14}H_{15}N_3OS$ + H^+: 274.10086 [M+H^+] found: 274.10064.

(*E*)-4-((R)-2-((tert-butoxycarbonyl)amino)-3-methoxy-3-oxopropyl)thio-4´-hydroxy azobenzene (56).

General procedure **C** was applied to thiol **49** (50.0 µL, 243 µmol, 1.0 eq) and 4-iodo-4´-hydroxyazobenzene **45** (1.2 eq) in THF (1.00 mL) with PdG3-Xantphos (5 mol%) and Et_3N (1.1 eq); stirring at RT for 2 h. Automated column chromatography (cyclohexane:EtOAc 1:0 to 7:3 within 15 min) afforded the title compound **56** (71 mg, 165 µmol) in 68% yield, as an orange foam. $[\alpha]^{20}_D$ = +24.2 (*c* = 0.5 in $CHCl_3$); ^{1}H NMR (500 MHz, $CDCl_3$) δ = 7.84-7.80 (m, 2H, H-14, H-15), 7.80-7.75 (m, 2H, H-10, H-11), 7.49-7.44 (m, 2H, H-8, H-9), 6.95-6.89 (m, 2H, H-16, H-17), 5.41 (d, $^{3}J_{NH,CH}$ = 8.2 Hz, 1H, NH), 4.67-4.58 (m, 1H, CH), 3.60 (s, 3H, OMe), 3.47 (dd, $^{2}J_{Ha,Hb}$ = 14.1 Hz, $^{3}J_{Ha,CH}$ = 5.0 Hz, 1H, Ha), 3.42 (dd, $^{2}J_{Hb,Ha}$ = 14.1 Hz, $^{3}J_{Hb,CH}$ = 5.0 Hz, 1H, Hb), 1.43 (s, 9H, *t*Bu) ppm ; ^{13}C NMR (126 MHz, $CDCl_3$) δ = 171.0 (1C, $\underline{C}(O)OCH_3$), 159.1 (1C, C-18), 155.2 (1C, $HN\underline{C}(O)OC(CH_3)_3$), 151.2 (1C, C-12), 146.8 (1C, C-13), 137.7 (1C, C-7), 130.3 (2C, C-8, C-9), 125.0 (2C, C-14, C-15), 123.1 (2C, C-10, C-11), 115.9 (2C, C-16, C-17), 80.5 (1C, $HNC(O)O\underline{C}(CH_3)_3$), 53.2 (1C, CH), 52.6 (1C, $C(O)O\underline{C}H_3$), 36.6 (1C, CH_2), 28.3 (3C, $HNC(O)OC(\underline{C}H_3)_3$) ppm ; ESI HRMS: *m/z*: clcd for $C_{21}H_{25}N_3O_5S$ + H^+: 432.15877 [M+H^+] found: 432.15829.

(*E*)-2,2',6,6'-tetrafluoro-4-(2,3,4,6-tetra-*O*-acetyl-1-thio-β-D-glucopyranosyl)-4´-iodo azobenzene (57).

General procedure **C** was applied to thiol **31** (55 mg, 150 µmol, 1.0 eq) and 2,2´,6,6´-tetrafluoro-4,4´-di-iodoazobenzene **29** (152 mg, 300 µmol, 2.0 eq) in THF (3.00 mL) with PdG3-Xantphos (1 mol%) and Et_3N (1.0 eq); stirring at 0 °C for 15 min. Column chromatography (cyclohexane:EtOAc 1:0 to 1:1) afforded the title compound **57** (91 mg, 122 µmol) in 81% yield, as an orange solid. $[\alpha]^{20}_D$ = +20.3 (*c* = 0.5 in DMSO); ^{1}H NMR (500 MHz, DMSO) δ = 7.86 (d, $^{3}J_{H-F}$ = 8.6 Hz, 2H, H-16, H-17), 7.42 (d, $^{3}J_{H-F}$ = 10.1 Hz, 2H, H-8, H-9), 5.69 (d, $^{3}J_{1,2}$ = 10.1 Hz, H-1), 5.41 (at, *J* = 9.4 Hz, 1H, H-3), 5.03-4.98 (m, 2H, H-2, H-4), 4.31-4.27 (m, 1H, H-5), 4.17-4.09 (m, 2H, H-6a, H-6b), 2.05 (s, 3H, $C(O)CH_3$), 2.01 (s, 6H, $C(O)CH_3$), 1.97 (s, 3H, $C(O)CH_3$) ppm ; ^{13}C NMR (126 MHz, $CDCl_3$) δ = 170.0, 169.6, 169.4, 169.2 (4C, $4\underline{C}(O)CH_3$), 154.7 (dd, $^{1}J_{C-F}$ = 261.7 Hz, $^{3}J_{C-F}$ = 4.7 Hz, 2C, C-10, C-11), 154.2 (dd, $^{1}J_{C-F}$ = 264.4 Hz, $^{3}J_{C-F}$ = 4.3 Hz, 2C, C-14, C-15), 141.0 (t, $^{3}J_{C-F}$ = 10.9 Hz, 1C, C-7), 130.3 (t, $^{2}J_{C-F}$ = 9.6 Hz, 1C, C-13), 128.8 (t, $^{2}J_{C-F}$ = 9.3 Hz, 1C, C-12), 122.5 (dd, $^{2}J_{C-F}$ = 22.0 Hz, $^{4}J_{C-F}$ = 3.3 Hz, 2C, C-16, C-17), 112.5 (dd, $^{2}J_{C-F}$ = 23.3 Hz, $^{4}J_{C-F}$ = 2.6 Hz, 2C, C-8, C-9), 97.9 (t, $^{3}J_{C,F}$ = 10.1 Hz, 1C, C-18), 81.3 (C-1), 74.6 (C-5), 72.7 (C-3), 69.1, 68.0 (2C, C-2, C-4), 62.1 (C-

6), 20.4, 20.3 (4C, 4C(O)<u>C</u>H$_3$) ppm ; ESI HRMS: *m/z*: clcd for $C_{26}H_{24}O_9N_2F_4IS + H^+$: 743.01778 [M+H$^+$] found: 743.01647.

7.3.3. Hetero-*bis*-functionalization *via* sequential and one-pot procedures

Table 7.3.2. Results of sequential or two-step one-pot synthesis of hetero-*bis*-functionalized azobenzenes.

Substrate	Conditions Step 1	Conditions Step 2	Solvent	Product, Yield
51	**32** (1 eq), Pd^0 (1 mol%), Et$_3$N (1 eq), 60 °C, 15 min	–	1,4-dioxane	**58**, 73%
52	**59** (2 eq), BF$_3$·Et$_2$O (1.3 eq), 3Å MS, 0 °C to RT, 24 h	–	CH_2Cl_2	**60**, 65%
44	**31** (1 eq), Pd^0 (1 mol%), Et$_3$N (1.5 eq), RT, 15 min	**32** (1.5 eq), Pd^0 (1 mol%), Et$_3$N (2.5 eq), 60 °C, 1.5 h	1,4-dioxane	**58**, 73%
44	**31** (1 eq), Pd^0 (1 mol%), Et$_3$N (1.5 eq), RT, 15 min	**49** (1.5 eq), Pd^0 (1 mol%), Et$_3$N (2.5 eq), 60 °C, 1.5 h	1,4-dioxane	**61**, 70%
29	**31** (1 eq), Pd^0 (1 mol%), Et$_3$N (1 eq), -10 °C, 1 h	**32** (1.2 eq), Pd^0 (1 mol%), Et$_3$N (1.2 eq), RT, 30 min	THF	**62**, 51%
45	**31** (1.05 eq), Pd^0 (5 mol%), Et$_3$N (1.1 eq), RT, 2 h	**63** (1.2 eq), K_2CO_3 (3 eq), 80 °C, 2 h	THF (step 1), DMF (step2)	**64**, 57%

Pd^0 = Xantphos-PdG3

(*E*)-4-(2,3,4,6-tetra-*O*-acetyl-1-thio-β-D-glucopyranosyl)-4´-(2´,3´,4´-tri-*O*-benzoyl-6´-*O*-(*tert*-butyldiphenyl)silyl-1-thio-β-D-glucopyranosyl) azobenzene (58).

Sequential synthesis: General procedure **C** was applied to **51** (187 mg, 300 µmol, 1.0 eq) and thiol **32** (1.0 eq) in 1,4-dioxane (3.00 mL) with PdG3-Xantphos (1 mol%) and Et$_3$N (1.0 eq); stirring at 60 °C for 15 min. Column chromatography (cyclohexane:EtOAc 9:1 to 7:3) afforded the title compound **58** (284 mg, 220 µmol) in 73% yield as an orange foam.

One pot synthesis: In a flame dried round bottom flask were loaded the azo derivative **44** (39 mg, 100 µmol, 1.0 eq), the thiol **31** (1.0 eq) and PdG3-Xantphos (1 mol%), and vacuum was applied for 15 min. Meanwhile the solvent (dry 1,4-dioxane) was degassed by bubbling nitrogen through. Then the flask was filled with a nitrogen atmosphere and the solvent (1.00 mL) was added followed by Et$_3$N (1.5 eq). The reaction was stirred at RT for 15 min. Then, thiol **32** (1.5 eq) and further catalyst (1 mol%), which had been kept under vacuum, were added, followed by further Et$_3$N (2.5 eq), and the reaction was stirred at 60 °C for 1.5 h. The mixture was then diluted in EtOAc, washed with HCl 1N and brine, and the aqueous phase was extracted with EtOAc. The combined organic layers were dried over $MgSO_4$, filtered and concentrated *in vacuo*. Column chromatography (cyclohexane:EtOAc 9:1 to 7:3) afforded the title compound **58** (95 mg, 73 µmol) in 73% yield as an orange foam. $[\alpha]^{20}_D$ = +24.1 (*c* = 0.5 in $CHCl_3$); ^{1}H NMR (500 MHz, $CDCl_3$) δ = 7.99-7.95 (m, 2H, 2Ar-H), 7.88-7.83 (m, 4H, 2Ar-H, H-10, H-11), 7.83-7.77 (m, 4H, 2Ar-H, H-14, H-15), 7.73-7.69 (m, 2H, 2Ar-H), 7.68-7.65 (m, 2H, H-16, H-17), 7.63-7.58 (m, 4H, 2Ar-H, H-8, H-9), 7.55-7.51 (m, 2H, 2Ar-H), 7.44-7.24 (m, 11H, 11Ar-H), 7.22-7.17 (m, 2H, 2Ar-H), 5.90 (at, $^3J_{3,4}$ = 9.6 Hz, $^3J_{3,2}$ = 9.4 Hz, 1H, H-3), 5.66 (at, $^3J_{4,5}$ = 10.0 Hz, $^3J_{4,3}$ = 9.6 Hz, 1H, H-4), 5.56 (at, $^3J_{2,1}$ = 10.0 Hz, $^3J_{2,3}$ = 9.4 Hz, 1H, H-2), 5.27 (at, $^3J_{3',2'}$ = $^3J_{3',4'}$ = 9.4 Hz, 1H, H-3'), 5.15 (d, $^3J_{1,2}$ = 10.0 Hz, 1H, H-1), 5.08 (at, $^3J_{4',5'}$ = 10.2 Hz, $^3J_{4',3'}$ = 9.4 Hz, 1H, H-4'), 5.06 (dd, $^3J_{2',1'}$ = 10.1 Hz, $^3J_{2',3'}$ = 9.4 Hz, 1H, H-2'), 4.82 (d, $^3J_{1',2'}$ = 10.1 Hz, 1H, H-1'), 4.26 (dd, $^2J_{6'a,6'b}$ = 12.4 Hz, $^3J_{6'a,5'}$ = 5.3 Hz, 1H, H-6'a), 4.21 (dd, $^2J_{6'b,6'a}$ = 12.4 Hz, $^3J_{6'b,5'}$ = 2.5 Hz, 1H, H-6'b), 4.01-3.96 (m, 1H, H-5), 3.93-3.87 (m, 2H, H-6a, H-6b), 3.79 (ddd, $^3J_{5',4'}$ = 10.2 Hz, $^3J_{5',6'a}$ = 5.3 Hz, $^3J_{6'b,5'}$ = 2.5 Hz, 1H, H-5'), 2.10 (s, 6H, C(O)CH$_3$), 2.03 (s, 3H, C(O)CH$_3$), 2.01 (s, 3H, C(O)CH$_3$), 1.06 (s, 9H, C(CH$_3$)$_3$) ppm ; ^{13}C NMR (126 MHz, $CDCl_3$) δ = 170.7, 170.3, 169.5, 169.4 (4C, 4<u>C</u>(O)CH$_3$), 166.0, 165.2, 165.1 (3C, 3<u>C</u>OPh), 152.1 (C-7), 151.9 (C-18), 136.9 (C-13), 135.9 (C-12), 135.8, 135.7 (4C, 4Ar-C), 133.5, 133.4, 133.3 (3C, 3Ar-C), 133.0, 132.9 (2C, 2Ar-C), 132.7 (2C, C-8, C-9), 132.3

(2C, C-16, C-17), 130.0, 129.9 (6C, 6Ar-C), 129.9, 129.8 (2C, 2Ar-C), 129.3, 129.2, 129.0 (3C, 3Ar-C), 128.6, 128.5, 128.4, 127.9, 127.8 (10C, 10Ar-C), 123.6 (2C, C-14, C-15), 123.4 (2C, C-10, C-11), 85.9 (C-1), 85.5 (C-1'), 79.8 (C-5), 76.1 (C-5'), 74.7 (C-3), 74.0 (C-3'), 70.8 (C-2), 70.0 (C-2'), 68.9 (C-4), 68.3 (C-4'), 62.9 (C-6), 62.3 (C-6'), 26.8 (3C, C($\underline{C}H_3)_3$), 20.9, 20.7 (4C, 4C(O)$\underline{C}H_3$), 19.3 (1C, $\underline{C}(CH_3)_3$) ppm. ESI HRMS: *m/z*: clcd for $C_{69}H_{69}O_{17}N_2S_2Si + H^+$: 1289.38014 [M+H$^+$] found: 1289.38088.

(*E*)-4-(2,3,4,6-tetra-*O*-acetyl-1-thio-β-D-glucopyranosyl)-4'-(2´,3´,4´,6´-tetra-*O*-acetyl-β-D-glucopyranosyloxy)azobenzene (60).

In a flame dried round bottom flask were loaded the azobenzene glycoconjugate **52** (42 mg, 74 µmol) and thioimidate **59** (2.0 eq) and vacuum was applied. After 15 min, activated 3Å molecular sieves (150 mg) was added under N_2 and then dry CH_2Cl_2 (740 µL). The mixture was cooled to 0 °C and $BF_3.OEt_2$ (11.0 µL, 93 µmol, 1.3 eq) was added. The mixture was stirred 15 min at 0 °C and then overnight at RT. Then the mixture was filtered over celite, washed with saturated $NaHCO_3$, dried over $MgSO_4$ and concentrated *in vacuo*. The crude was acetylated with Ac_2O in pyridine, and after removal of the pyridine and Ac_2O, column chromatography (cyclohexane:EtOAc 4:1 to 3:2) afforded the title compound **60** (43 mg, 48 µmol) in 65% yield as an orange solid. $[\alpha]^{20}_D$ = +6.36 (*c* = 0.5 in $CHCl_3$); ^{1}H NMR (500 MHz, $CDCl_3$) δ = 7.92-7.88 (m, 2H, H-14, H-15), 7.85-7.81 (m, 2H, H-10, H-11), 7.63-7.58 (m, 2H, H-8, H-9), 7.14-7.09 (m, 2H, H-16, H-17), 5.36-5.29 (m, 2H, H-2´, H-3´), 5.26 (at, $^3J_{3,4}$ = 9.4 Hz, $^3J_{3,2}$ = 9.3 Hz, 1H, H-3), 5.22-5.17 (m, 2H, H-1´, H-4´), 5.07 (at, $^3J_{4,5}$ = 10.1 Hz, $^3J_{4,3}$ = 9.4 Hz, 1H, H-4), 5.04 (dd, $^3J_{2,1}$ = 10.1 Hz, $^3J_{2,3}$ = 9.3 Hz, 1H, H-2), 4.80 (d, 1H, $^3J_{1,2}$ = 10.1 Hz, 1H, H-1), 4.31 (dd, $^2J_{6'a,6'b}$ = 12.4 Hz, $^3J_{6'a,5'}$ = 5.5 Hz, 1H, H-6´a), 4.25 (dd, $^2J_{6a,6b}$ = 12.3 Hz, $^3J_{6a,5}$ = 5.2 Hz, 1H, H-6a), 4.22-4.17 (m, 2H, H-6b, H-6´b), 3.93 (ddd, $^3J_{5',4'}$ = 10.1 Hz, $^3J_{5',6'a}$ = 5.5 Hz, $^3J_{5',6'b}$ = 2.5 Hz, 1H, H-5´), 3.78 (ddd, $^3J_{5,4}$ = 10.1 Hz, $^3J_{5,6a}$ = 5.2 Hz, $^3J_{5,6b}$ = 2.5 Hz, 1H, H-5), 2.10 (bs, 6H, C(O)CH_3), 2.09 (s, 3H, C(O)CH_3), 2.08 (s, 3H, C(O)CH_3), 2.07 (s, 3H, C(O)CH_3), 2.05 (s, 3H, C(O)CH_3), 2.03 (s, 3H, C(O)CH_3), 2.00 (s, 3H, C(O)CH_3) ppm ; ^{13}C NMR (126 MHz, $CDCl_3$) δ = 170.5, 170.2, 169.4, 169.3, 169.2 (8C, 8$\underline{C}$(O)CH_3), 159.0 (1C, C-18), 152.0 (1C, C-12), 148.5 (1C, C-13), 135.1 (1C, C-7), 132.8 (2C, C-8, C-9), 124.7 (2C, C-14, C-15), 123.1 (2C, C-10, C-11), 117.1 (2C, C-16, C-17), 98.6 (C-1´), 85.3 (C-1), 75.9 (C-5), 73.9 (C-3), 72.6 (C-3´), 72.2 (C-5´), 71.1 (C-2´), 69.9 (C-2), 68.2 (2C, C-4, C-4´), 62.1 (C-6), 61.9 (C-6´), 20.8, 20.7, 20.6 (8C, 8C(O)$\underline{C}H_3$) ppm ; ESI HRMS: *m/z*: clcd for $C_{40}H_{46}O_{19}N_2S_1 + H^+$: 891.24882 [M+H$^+$] found: 891.24779.

(*E*)-4-(2,3,4,6-tetra-*O*-acetyl-1-thio-β-D-glucopyranosyl)-4´-((R)-2-((tert-butoxycarbonyl)amino)-3-methoxy-3-oxopropyl)thio azobenzene (61).

In a flame dried round bottom flask were loaded the azo derivative **3** (39 mg, 100 µmol, 1.0 eq), the thiol **31** (1.0 eq) and PdG3-Xantphos (1 mol%), and vacuum was applied for 15 min. Meanwhile the solvent (dry 1,4-dioxane) was degassed by bubbling nitrogen through. Then the flask was filled with a nitrogen atmosphere and the solvent (1.00 mL) was added followed by Et_3N (1.5 eq). The reaction was stirred at RT for 15 min. Then the rest of the catalyst (1 mol%) and a solution in degassed 1,4-dioxane (1.00 mL) of cysteine derivative **49** (1.5 eq) were added, followed by more Et_3N (2.5 eq), and the reaction was stirred at 60 °C for 1.5 h. The mixture was then diluted in EtOAc, washed with HCl 1N and brine, and the aqueous phase was extracted with EtOAc. The combined organic layers were dried over $MgSO_4$, filtered and concentrated *in vacuo*. Column chromatography (cyclohexane:EtOAc 4:1 to 3:2) afforded the title compound **61** (55 mg, 70 µmol) in 70% yield as an orange foam. $[\alpha]^{20}_D$ = +7.69 (*c* = 0.5 in $CHCl_3$); ^{1}H NMR (500 MHz, $CDCl_3$) δ = 7.87-7.82 (m, 4H, H-10, H-11, H-14, H-15), 7.61 (d, ^3J = 8.4 Hz, 2H, H-8, H-9), 7.49 (d, ^3J = 8.7 Hz, 2H, H-16, H-17), 5.36 (d, $^3J_{NH\text{-}CH}$ = 7.6 Hz, 1H, NH), 5.26 (at, $^3J_{3,4}$ = 9.6 Hz, $^3J_{3,2}$ = 9.2 Hz, 1H, H-3), 5.07 (at, $^3J_{4,5}$ = 10.1 Hz, $^3J_{4,3}$ = 9.6 Hz, 1H, H-4), 5.04 (at, $^3J_{2,1}$ = 10.1 Hz, $^3J_{2,3}$ = 9.2 Hz, 1H, H-2), 4.81 (d, $^3J_{1,2}$ = 10.1 Hz, 1H, H-1), 4.69-4.62 (m, 1H, CH), 4.25 (dd, $^2J_{6a,6b}$ = 12.3 Hz, $^3J_{6a,5}$

= 5.4 Hz, 1H, H-6a), 4.20 (dd, $^{2}J_{6b,6a}$ = 12.3 Hz, $^{3}J_{6b,5}$ = 2.3 Hz, 1H, H-6b), 3.70 (ddd, $^{3}J_{5,4}$ = 10.1 Hz, $^{3}J_{5,6a}$ = 5.4 Hz, $^{3}J_{5,6b}$ = 2.3 Hz, 1H, H-5), 3.63 (s, 3H, $COOCH_3$), 3.55-3.42 (m, 2H, CH_2), 2.11 (s, 3H, $C(O)CH_3$), 2.10 (s, 3H, $C(O)CH_3$), 2.03 (s, 3H, $C(O)CH_3$), 2.00 (s, 3H, $C(O)CH_3$), 1.42 (s, 9H, $C(CH_3)_3$) ppm ; ^{13}C NMR (126 MHz, $CDCl_3$) δ = 170.8 (1C, $\underline{C}OOCH_3$), 170.6, 170.2 169.4, 169.3 (4C, 4$\underline{C}(O)CH_3$), 152.0 (1C, C-12), 150.9 (1C, C-13), 139.6 (1C, C-18), 135.5 (1C, C-7), 132.7 (2C, C-10, C-11), 129.8 (2C, C-14, C-15), 123.5 (2C, C-16, C-17), 123.2 (2C, C-8, C-9), 85.3 (C-1), 80.3 ($\underline{C}(CH_3)_3$), 76.0 (C-5), 73.9 (C-3), 69.9 (C-2), 68.2 (C-4), 62.1 (C-6), 53.3 (1C, $COO\underline{C}H_3$), 52.6 (CH), 36.3 (CH_2), 28.3 ($C(\underline{C}H_3)_3$), 20.8, 20.6 (4C, 4$C(O)\underline{C}H_3$) ppm ; ESI HRMS: *m/z*: clcd for $C_{35}H_{43}N_3O_{13}S_2 + H^+$: 778.23101 [M+H$^+$] found: 778.23040.

(*E*)-2,2',6,6'-tetrafluoro-4-(2,3,4-tri-*O*-benzoyl-6-*O*-(*tert*-butyldiphenyl)silyl-1-thio-β-D-glucopyranosyl)-4'-(2´,3´,4´,6´-tetra-*O*-acetyl-1-thio-β-D-glucopyranosyl) azobenzene (62).

In a flame dried round bottom flask were loaded the azo derivative **29** (101 mg, 200 µmol, 1.0 eq), the thiol **31** (1.0 eq) and PdG3-Xantphos (1 mol%), and vacuum was applied for 15 min. Meanwhile the solvent (THF) was degassed by bubbling nitrogen through. Then the flask was filled with a nitrogen atmosphere and the solvent (4.00 mL) was added followed by Et_3N (1.0 eq). The reaction was stirred at -10 °C for 1 h. Then, thiol **32** (1.2 eq) which had been kept under vacuum with the rest of the catalyst (1 mol%) were added, followed by more Et_3N (1.2 eq), and the reaction was stirred at RT for 30 min. The mixture was then diluted in EtOAc, washed with HCl 1N and brine, and the aqueous phase was extracted with EtOAc. The combined organic layers were dried over $MgSO_4$, filtered and concentrated *in vacuo*. Column chromatography (cyclohexane:EtOAc 9:1 to 1:1) afforded the title compound **62** (140 mg, 103 µmol) in 51% yield as an orange/red foam. $[\alpha]^{20}_D$ = +8.23 (*c* = 0.5 in DMSO); ^{1}H NMR (500 MHz, DMSO) δ = 7.91-7.86 (m, 2H, 2Ar-H), 7.85-7.80 (m, 2H, 2Ar-H), 7.76-7.71 (m, 2H, 2Ar-H), 7.70-7.59 (m, 4H, 4Ar-H), 7.58-7.54 (m, 1H, 1Ar-H), 7.53-7.47 (m, 8H, 6Ar-H, H-16, H-17), 7.45-7.38 (m, 4H, 2Ar-H, H-16, H-17), 7.38-7.31 (m, 2H, 2Ar-H), 7.29-7.24 (m, 2H, 2Ar-H), 7.21-7.15 (m, 2H, 2Ar-H), 6.12 (d, $^{3}J_{1',2'}$ = 10.0 Hz, 1H, H-1´), 6.10 (at, $^{3}J_{3',4'}$ = 9.6 Hz, $^{3}J_{3',2'}$ = 9.2 Hz, 1H, H-3´), 5.71 (at, $^{3}J_{4',5'}$ = 10.2 Hz, $^{3}J_{4',3'}$ = 9.6 Hz, 1H, H-4´), 5.69 (d, $^{3}J_{1,2}$ = 10.1 Hz, 1H, H-1), 5.55 (at, $^{3}J_{2',1'}$ = 10.0 Hz, $^{3}J_{2',3'}$ = 9.2 Hz, 1H, H-2´), 5.41 (at, *J* = 9.4 Hz, 1H, H-3), 5.01 (at, *J* = 9.8 Hz, 2H, H-2, H-4), 4.56-4.49 (m, 1H, H-5´), 4.32-4.26 (m, 1H, H-5), 4.18-4.08 (m, 2H, H-6a, H-6b), 3.88-3.76 (m, 2H, H-6´a, H-6´b), 2.05 (s, 3H, $C(O)CH_3$), 2.02 (bs, 6H, $C(O)CH_3$), 1.97 (s, 3H, $C(O)CH_3$) ppm ; ^{13}C NMR (126 MHz, DMSO) δ = 169.8, 169.4, 169.2, 169.1 (4C, 4$\underline{C}(O)CH_3$), 165.0, 164.5, 164.4 (3C, 3$\underline{C}$(O)Ph), 154.6 (dd, $^{1}J_{C\text{-}F}$ = 262.1 Hz, $^{3}J_{C\text{-}F}$ = 5.2 Hz, 2C, C-14, C-15), 154.5 (dd, $^{1}J_{C\text{-}F}$ = 261.3 Hz, $^{3}J_{C\text{-}F}$ = 5.4 Hz, 2C, C-10, C-11), 140.3 (t, $^{2}J_{C\text{-}F}$ = 11.2 Hz, 1C, C-12), 140.1 (t, $^{2}J_{C\text{-}F}$ = 10.9 Hz, 1C, C-13), 135.0, 134.8 (4C, 4Ar-C), 134.0, 133.8, 133.7 (3C, 3Ar-C), 132.3, 132.0 (2C, 2Ar-C), 129.7 (2C, 2Ar-C), 129.2, 129.1, 129.0, 128.8, 128.7 (12C, 8Ar-C, C-8, C-9, C-16, C-17), 128.5, 128.2, 128.1 (3C, 3Ar-C), 127.6 (4C, 4Ar-C), 112.6 (t, 2C, C-7, C-18), 81.3 (2C, C-1, C-1´), 77.5 (C-5´), 74.5 (C-5), 74.0 (C-3´), 72.6 (C-3), 70.1 (C-2´), 69.0 (C-2 or C-4), 68.4 (C-4´), 67.9 (C-2 or C-4), 62.2 (C-6´), 62.0 (C-6), 26.2 (3C, $C(\underline{C}H_3)_3$), 20.3, 20.2 (4C, 4$C(O)\underline{C}H_3$), 18.5 (1C, $\underline{C}(CH_3)_3$) ppm ; ESI HRMS: *m/z*: clcd for $C_{69}H_{64}F_4N_2O_{17}S_2Si + H^+$: 1361.34246 [M+H$^+$] found: 1361.34282.

(*E*)-4-(2,3,4,6-tetra-*O*-acetyl-1-thio-β-D-glucopyranosyl)-4´-((26-oxo-3,6,9,12-tetraoxa-25-thiaheptacosyl)oxy)azobenzene (64).

General procedure **C** was applied to thiol **31** (20 mg, 55 µmol, 1 eq) and azobenzene **45** (1.05 eq) in THF (0.250 mL) with PdG3-Xantphos (5 mol%) and Et_3N (1.1 eq). After stirring at RT for 2 h, the mixture was concentrated to dryness then the residue dissolved in *N*,*N*-dimethylformamide (0.150 mL) and potassium carbonate (3 eq) was added, followed by tosylate **63** (1.2 eq) dissolved in *N*,*N*-dimethylformamide (0.100 mL). The mixture was heated up to 80 °C then stirred for 2 h. After cooling to RT, the mixture was diluted with ethyl acetate and washed with 2N aq. HCl then with water. The

aqueous phase was extracted with EtOAc, then the combined organic layers were washed with brine, dried over $MgSO_4$, filtered and concentrated *in vacuo*. Column chromatography (cyclohexane:EtOAc 45:55 to 2:3) afforded the title compound **64** (30 mg, 31 µmol) in 57% yield, as an orange oil. $[\alpha]^{20}_D$ = -5.03 (*c* = 0.5 in $CHCl_3$); ^{1}H NMR (500 MHz, $CDCl_3$) δ = 7.93-7.88 (m, 2H, H-14, H-15), 7.84-7.79 (m, 2H, H-8, H-9), 7.62-7.57 (m, 2H, H-10, H-11), 7.06-7.00 (m, 2H, H-16, H-17), 5.26 (at, $^3J_{3,2}$ = $^3J_{3,4}$ = 9.4 Hz, 1H, H-3), 5.07 (at, $^3J_{4,5}$ = 10.2 Hz, $^3J_{4,3}$ = 9.4 Hz, 1H, H-4), 5.04 (dd, $^3J_{2,1}$ = 10.1 Hz, $^3J_{2,3}$ = 9.4 Hz, 1H, H-2), 4.80 (d, $^3J_{1,2}$ = 10.1 Hz, 1H, H-1), 4.29-4.16 (m, 4H, H-6_a, H-6_b, PhOC$\underline{H}_2$CH_2O), 3.92-3.88 (m, 2H, PhOCH_2C$\underline{H}_2$O), 3.78 (ddd, $^3J_{5,4}$ = 10.1 Hz, $^3J_{5,6a}$ = 5.3 Hz, $^3J_{5,6a}$ = 2.4 Hz, 1H, H-5), 3.76-3.73 (m, 2H, PEG-CH_2), 3.71-3.63 (m, 8H, PEG-CH_2), 3.60-3.56 (m, 2H, PEG-CH_2), 3.47-3.40 (m, 2H, OC$\underline{H}_2$CH_2CH_2), 2.88-2.83 (m, 2H, C$\underline{H}_2$SC(O)CH_3), 2.32 (s, 3H, SC(O)CH_3), 2.11 (s, 3H, OC(O)CH_3), 2.10 (s, 3H, OC(O)CH_3), 2.03 (s, 3H, OC(O)CH_3), 2.00 (s, 3H, OC(O)CH_3), 1.59-1.53 (m, 4H, Aliph-CH_2), 1.36-1.24 (m, 14H, Aliph-CH_2) ppm ; ^{13}C NMR (126 MHz, $CDCl_3$) δ = 196.1 (1C, S$\underline{C}$(O)CH_3), 170.6, 170.2, 169.4, 169.3 (4C, 4O$\underline{C}$(O)CH_3), 161.6 (1C, C-18), 152.3 (1C, C-12), 147.0 (1C, C-13), 134.6 (1C, C-7), 132.8 (2C, C-8, C-9), 124.9 (2C, C-14, C-15), 123.0 (2C, C-10, C-11), 114.9 (2C, C-16, C-17), 85.5 (C-1), 75.9 (C-5), 73.9 (C-3), 71.6 (1C, O$\underline{C}$H$_2$CH$_2$CH$_2$), 70.9 (1C, PEG-CH_2), 70.7, 70.6 (4C, 4PEG-CH_2), 70.1 (1C, PEG-CH_2), 69.9 (C-2), 69.6 (1C, PhOCH$_2\underline{C}$H$_2$O), 68.2 (C-4), 67.8 (PhO$\underline{C}$H$_2$CH$_2$O), 62.2 (C-6), 30.7 (SC(O)$\underline{C}$H$_3$), 29.6, 29.5, 29.4, 29.2, 29.1, 28.8, 26.1 (11C, 11Aliph-CH_2), 20.8, 20.6 (4C, 4OC(O)CH_3) ; ESI HRMS: *m/z*: clcd for $C_{47}H_{68}N_2O_{15}S_2$ + H^+: 965.41339 [M+H^+] found: 965.41156.

7.3.4. Oxidation of glycosidic sulfur atoms

(*E*)-4-(2,3,4,6-tetra-*O*-acetyl-1-thio-β-D-glucopyranosyl)-4´-methoxy azobenzene (65).

To the azo derivative **45** (200 mg, 617 µmol, 1 eq) in DMF (6.2 mL), was added *t*BuOK (76 mg, 680 µmol, 1.1 eq) at RT. The mixture was stirred 5 min, and then methyl iodide (58 µL, 926 µmol, 1.5 eq) was added. After 2 h, the reaction was diluted with EtOAc and washed twice with HCl 1N. Then the organics were dried over $MgSO_4$ and concentrated in *vacuo*. The obtained residue was dried under vacuum for 2 h, then were added PdG3/Xantphos (1 mol%) and the thiol **31** (1 eq) under N_2 atmosphere. Then THF (5.7 mL) was added followed by Et_3N (94 µL, 678 µmol, 1.2 eq). The mixture was stirred at RT for 10 min. Then it was diluted with EtOAc, washed with HCl 1N, the organics were dried over $MgSO_4$ and concentrated in *vacuo*. Column chromatography (cyclohexane:EtOAc 8:2 to 7:3) afforded the title compound **65** (253 mg, 440 µmol) in 71% yield over two steps. ^{1}H NMR (500 MHz, $CDCl_3$) δ = 7.94-7.89 (m, 2H, H-14, H-15), 7.84-7.80 (m, 2H, H10, H-11), 7.62-7.58 (m, 2H, H-8, H-9), 7.04-6.99 (m, 2H, H-16, H-17), 5.26 (at, $^3J_{3,4}$ = 9.6 Hz, $^3J_{3,2}$ = 9.3 Hz, 1H, H-3), 5.07 (at, $^3J_{4,5}$ = 10.1 Hz, $^3J_{4,3}$ = 9.6 Hz, 1H, H-4), 5.04 (dd, $^3J_{2,1}$ = 10.1 hz, $^3J_{2,3}$ = 9.3 Hz, 1H, H-2), 4.80 (d, $^3J_{1,2}$ = 10.1 Hz, 1H, H-1), 4.25 (dd, $^2J_{6a,6b}$ = 12.3 Hz, $^3J_{6a,5}$ = 5.3 Hz, 1H, H-6a), 4.20 (dd, $^2J_{6b,6a}$ = 12.3 Hz, $^3J_{6b,5}$ = 2.5 Hz, 1H, H-6b), 3.90 (s, 3H, OCH_3), 3.77 (ddd, $^3J_{5,4}$ = 10.1 Hz, $^3J_{5,6a}$ = 5.3 Hz, $^3J_{5,6b}$ = 2.5 Hz, 1H, H-5), 2.10 (bs, 6H, C(O)CH_3), 2.03 (s, 3H, C(O)CH_3), 2.00 (s, 3H, C(O)CH_3) ppm ; ^{13}C NMR (126 MHz, $CDCl_3$) δ = 170.6, 170.2, 169.4. 169.3 (4C, 4$\underline{C}$(O)CH_3), 162.3 (1C, C-18), 152.3 (1C, C-12), 147.0 (1C, C-13), 134.05 (1C, C-7), 134.5 (2C, C-8, C-9), 124.9 (2C, C-14, C-15), 123.0 (2C, C-10, C-11), 114.3 (2C, C-16, C-17), 85.5 (C-1), 75.9 (C-5), 73.9 (C-3), 69.9 (C-2), 68.2 (C-4), 62.1 (C-6), 55.6 (OCH_3), 20.8, 20.7, 20.6 (4C, 4C(O)$\underline{C}$H$_3$) ESI HRMS: *m/z*: clcd for $C_{27}H_{30}N_2O_{10}S$ + H^+: 575.16939 [M+H^+] found: 575.16942.

(*R*,*S*)-(*E*)-4-(2,3,4,6-tetra-*O*-acetyl-β-D-glucopyranosyl-1-sulfinyl) azobenzene (66a).

To **50** (102 mg, 187 µmol, 1.0 eq) in CH_2Cl_2 (1.87 mL) was added 70% *meta*-chloroperbenzoic acid (69 mg, 1.5 eq) at RT. The mixture was stirred for 2h. Then Et_3N (50 µL) was added, and the crude mixture was directly purified by column chromatography (cyclohexane:Et_2O 1:1 to 0:1) to afford sulfoxide

derivative **66a** (45 mg, 81 µmol) in 43% yield as an orange solid, and sulfone derivative **66b** (57 mg, 99 µmol) in 53% yield as a pale orange solid. Note that sulfoxide **66a** was obtained as a 2.2:1 mixture of diastereomers which were not separated. ^{1}H NMR (500 MHz, $CDCl_3$) δ = 8.09-8.03 (m, 2.9H, H-10, H-11), 7.98-7.92 (m, 2.9H, H-14, H-15), 7.88-7.83 (m, 2H, H-7, H-9), 7.83-7.78 (m, 0.9 H, H-7, H-9), 7.59-7.49 (m, 4.35H, H-16, H-17, H-18), 5.38 (at, $^{3}J_{2,1}$ = 9.8 Hz, $^{3}J_{2,3}$ = 9.1 Hz, 0.45H, H-2), 5.33-5.24 (m, 2.45H, H-2, H-3), 5.01 (dd, $^{3}J_{4,5}$ = 10.0 Hz, $^{3}J_{4,3}$ = 9.5 Hz, 0.45H, H-4), 4.97 (dd, $^{3}J_{4,5}$ = 10.1 Hz, $^{3}J_{4,3}$ = 9.3 Hz, 1H, H-4), 4.47 (d, $^{3}J_{1,2}$ = 9.5 Hz, 1H, H-1), 4.33 (d, $^{3}J_{1,2}$ = 9.8 Hz, 0.45H, H-1), 4.29-4.09 (m, 2.45H, H-6a, H-6b), 4.03 (dd, $^{2}J_{6a,6b}$ 12.4 Hz, $^{3}J_{6b,5}$ = 2.2 Hz, 0.45Hz, H-6b), 3.73 (ddd, $^{3}J_{5,4}$ = 10.1 Hz, $^{3}J_{5,6b}$ = 4.5 Hz, $^{3}J_{5,6a}$ = 2.4 Hz, 1H, H-5), 3.62 (ddd, $^{3}J_{5,4}$ = 10.0 Hz, $^{3}J_{5,6a}$ = 5.8 Hz, $^{3}J_{5,6b}$ = 2.2 Hz, 0.45H, H-5), 2.11 (s, 1.35H, $C(O)CH_3$), 2.02 (s, 1.35H, $C(O)CH_3$), 2.01 (s, 3H, $C(O)CH_3$), 2.00 (s, 4.35H, $C(O)CH_3$), 1.97 (s, 3H, $C(O)CH_3$), 1.96 (s, 3H, $C(O)CH_3$), 1.91 (s, 1.35H, $C(O)CH_3$) ppm ; ^{13}C NMR (126 MHz, $CDCl_3$) δ = 170.4, 170.1, 169.4, 169.2, 169.1, 169.0 (5.8C, 4$\underline{C}(O)CH_3$, 1.8$\underline{C}(O)CH_3$), 154.6 (1.45C, C-12), 152.4 (1.45C, C-13), 141.1, 140.8 (1.45C, C-7), 131.9, 131.8 (1.45C, C-18), 129.2 (2.9C, C-16, C-17), 126.8, 126.6 (2.9C, C-8, C-9), 123.2, 123.1 (5.8C, C-10, C-11, C-14, C-15), 92.5, 90.0 (1.45C, C-1), 76.7, 76.4 (1.45C, C-5), 73.8, 73.5 (1.45C, C-3), 67.7, 67.6, 67.5, 67.4 (2.9 C, C-2, C-4), 61.7, 61.3 (1.45C, C-6), 20.7, 20.6, 20.5 (5.8C, 4C(O)CH_3, 1.8C(O)CH_3) ppm ; ESI HRMS: *m/z*: clcd for $C_{26}H_{28}N_2O_{10}S + H^+$: 561.15374 [M+H$^+$] found: 561.15394.

(*E*)-4-(2,3,4,6-tetra-*O*-acetyl-β-D-glucopyranosyl-1-sulfonyl) azobenzene (66b).

$[\alpha]^{20}_D$ = -46.5 (*c* = 0.5 in $CHCl_3$); ^{1}H NMR (500 MHz, $CDCl_3$) δ = 8.10-8.03 (m, 4H, H-8, H-9, H-10, H-11), 8.00-7.94 (m, 2H, H-14, H-15), 7.59-7.52 (m, 3H, H-16, H-17, H-18), 5.31-5.23 (m, 2H, h-2, H-3), 4.94-4.88 (m, 1H, H-4), 4.58-4.51 (m, 1H, H-1), 4.18-4.13 (m, 2H, H-6a, H-6b), 3.77-3.71 (m, 1H, H-5), 2.15 (s, 3H, $C(O)CH_3$), 2.00 (bs, 6H, $C(O)CH_3$), 1.96 (s, 3H, $C(O)CH_3$) ppm ; ^{13}C NMR (126 MHz, $CDCl_3$) δ = 170.3, 170.0, 169.4, 169.2 (4C, 4$\underline{C}(O)CH_3$), 156.0 (1C, C-12), 152.4 (1C, C-13), 135.6 (1C, C-7), 132.3 (1C, C-18), 131.8 (2C, C-8, C-9), 129.3 (2C, C-16, C-17), 123.4 (2C, C-14, C-15), 122.9 (2C, C-10, C-11), 88.9 (C-1), 76.3 (C-5), 73.3 (C-3), 67.2 (C-4), 66.9 (C-2), 61.1 (C-6), 20.7, 20.6, 20.5 (4C, 4C(O)CH_3) ppm ; ESI HRMS: *m/z*: clcd for $C_{26}H_{28}O_{11}N_2S + H^+$: 577.14866 [M+H$^+$] found: 577.14774.

(*E*)-4-(2,3,4,6-tetra-*O*-acetyl-β-D-glucopyranosyl-1-sulfinyl)-4´-methoxy azobenzene (67a)

To **65** (40 mg, 70 µmol, 1 eq) in CH_2Cl_2 (0.7 mL) was added 70% *meta*-chloroperbenzoic acid (26 mg, 104 µmol, 1.5 eq), and the mixture was stirred for 1 h at RT. Then it was directly purified by column chromatography (cyclohexane:Et_2O 1:1 to 0:1) to afford the title compound **67a** (20 mg, 34 µmol) in 48% yield along with an α/β mixture of **67b** (21 mg, 35 µmol, 49%). Note that pure **β-67b** was sinthesized independently. ^{1}H NMR (500 MHz, $CDCl_3$) δ = 8.03-7.99 (m, 3.2H, H-10, H-11), 7.97-7.92 (m, 3.2H, H-14, H-15), 7.84-7.81 (m, 2H, H-8, H-9), 7.80-7.76 (m, 1.2H, H-8, H-9), 7.06-7.01 (m, 3.2H, H-16, H-17), 5.37 (m, 0.6H, H-2), 5.34-5.24 (m, 2.6H, 1.6H-2, 1H-3), 5.04-4.94 (m, 1.6 H, H-4), 4.46 (d, $^{3}J_{1,2}$ = 9.4 Hz, 1H, H-1), 4.31 (d, $^{3}J_{1,2}$ = 9.8 Hz, 0.6H, H-1), 4.19-4.09 (m, 2.6H, 1.6H-6a, 1H-6b), 4.30 (dd, $^{2}J_{6b,6a}$ = 12.4, $^{3}J_{6b,5}$ = 2.2 Hz, 0.6H, H-6b), 3.91 (s, 4.8H, OCH_3), 3.71 (ddd, $^{3}J_{5,4}$ = 10.1 Hz, $^{3}J_{5,6b}$ = 4.5 Hz, $^{3}J_{5,6a}$ = 2.4 Hz, 1H, H-5), 3.62 (ddd, $^{3}J_{5,4}$ = 10.1 Hz, $^{3}J_{5,6a}$ = 5.9 Hz, $^{3}J_{5,6b}$ = 2.2 Hz, 0.6H, H-5), 2.10 (s, 1.8H, $C(O)CH_3$), 2.01 (s, 1.8H, $C(O)CH_3$), 2.00 (s, 7.8H, $C(O)CH_3$), 1.96 (bs, 6H, $C(O)CH_3$), 1.91 (s, 1.8H, $C(O)CH_3$) ppm ; ^{13}C NMR (126 MHz, $CDCl_3$) δ = 170.4, 170.1, 169.4, 169.2, 169.1, 169.0 (6.4C, $\underline{C}(O)CH_3$), 168.8 (1.6C, C-18), 154.8 (1.6C, C-12), 146.9 (1.6C, C-13), 140.3 (1C, C-7), 140.0 (0.6C, C-7), 126.7, 126.6 (3.2C, C-8, C-9), 125.2 (3.2C, C-14, C-15), 122.4 (3.2C, C-10, C-11), 114.4 (3.2C, C-16, C-17), 92.4, 90.1 (1.6C, C-1), 76.6, 76.4 (1.6C, C-5), 73.8, 73.5 (1.6C, C-3), 67.7 (0.6C, C-4), 67.6 (1C, C-2), 67.5 (0.6C, C-2), 67.4 (1C, C-4), 61.7, 61.3 (1.6C, C-6), 55.7 (1.6C, OCH_3), 20.6, 20.5 (6.4C, C(O)$\underline{C}H_3$) ppm ; ESI HRMS: *m/z*: clcd for $C_{27}H_{30}O_{11}N_2S + H^+$: 591.16431 [M+H$^+$] found: 591.16451.

(*E*)-4-(2,3,4,6-tetra-*O*-acetyl-β-D-glucopyranosyl-1-sulfonyl)-4´-methoxy azobenzene (67b)

To **65** (100 mg, 174 µmol, 1eq) in CH_2Cl_2 (1.7 mL) was added 70% *meta*-chloroperbenzoic acid (83 mg, 339 µmol, 1.95 eq), at -40 °C. After 3 h, Amberlyst A21 was added, and after 5 min the solution was directly purified by column chromatography (cyclohexane:EtOAc 7:3) to afford the title compound **67b** (33 mg, 54 µmol) in 31% yield. ^{1}H NMR (500 MHz, $CDCl_3$) δ = 8.06-7.95 (m, 6H, H-8, H-9, H-10, H-11, H-14, H-15), 7.07-7.02 (m, 2H, H-16, H-17), 5.31-5.23 (m, 2H, H-2, H-3), 4.94-4.87 (m, 1H, H-4), 4.55-4.51 (m, 1H, H-1), 4.17-4.12 (d, $^3J_{6a,5}$ = $^3J_{6b,5}$ = 3.6 Hz, 2H, H-6a, H-6b), 3.92 (s, 3H, OCH_3), 3.73 (dt, $^3J_{5,4}$ = 10.0 Hz, $^3J_{5,6a}$ = $^3J_{5,6b}$ = 3.6 Hz, 1H, H-5), 2.15 (s, 3H, C(O)CH_3), 2.00 (bs, 6H, C(O)CH_3), 1.95 (s, 3H, $\underline{C}$(O)CH_3) ppm ; ^{13}C NMR (126 MHz, $CDCl_3$) δ = 170.3, 170.0, 169.4, 169.1 (4C, 4$\underline{C}$(O)CH_3), 163.2 (1C, C-18), 156.3 (1C, C12), 146.9 (1C, C-13), 134.4 (1C, C-7), 131.7 (2C, C-8, C-9), 125.6 (2C, C-14, C-15), 122.6 (2C, C-10, C-11), 114.4 (2C, C-16, C17), 88.9 (C-1), 76.3 (C-5), 73.3 (C-3), 67.3 (C-4), 67.0 (C-2), 61.2 (C-6), 55.7 (OCH_3), 20.7, 20.6, 20.5 (4C, 4C(O)$\underline{C}H_3$) ppm ; ESI HRMS: *m/z*: clcd for $C_{27}H_{30}O_{12}N_2S$ + H^+:607.15922 [M+H^+] found: 607.15942.

(*E*)-4-(2,3,4,6-tetra-*O*-acetyl-β-D-glucopyranosyl-1-sulfonyl)-4´-bromo azobenzene (68).

To **51** (93 mg, 150 µmol, 1.0 eq) in CH_2Cl_2 (1.5 mL) was added 70% *meta*-chloroperbenzoic acid (74 mg, 300 µmol, 2.0 eq) at RT. The mixture was stirred for 1.5 h. Then the mixture was diluted with EtOAc, washed with NaOH 1M (3x). The water phase was extracted with EtOAc and the combined organic phases were washed with brine, then dried over $MgSO_4$ and concentrated *in vacuo*. Column chromatography (cyclohexane:EtOAc 9:1 to 3:2) afforded the title compound **68** (86 mg, 131 µmol) in 87% yield as an orange/red solid. $[\alpha]^{20}_D$ = -50.6 (*c* = 0.5 in $CHCl_3$); ^{1}H NMR (500 MHz, $CDCl_3$) δ = 8.09-8.03 (m, 4H, H-8, H-9, H-10, H-11), 7.87-7.83 (m, 2H, H-14, H-15), 7.72-7.68 (m, 2H, H-16, H-17), 5.29-5.23 (m, 2H, H-2, H-3), 4.93-4.87 (m, 1H, H-4), 4.57-4.52 (m, 1H, H-1), 4.16-4.14 (m, 2H, H-6a, H-6b), 3.77-3.72 (m, 1H, H-5), 2.15 (s, 3H, $\underline{C}$(O)CH_3), 2.00 (s, 3H, C(O)CH_3), 1.99 (s, 3H, C(O)CH_3), 1.96 (s, 3H, C(O)CH_3) ppm ; ^{13}C NMR (126 MHz, $CDCl_3$) δ = 170.3, 170.0, 169.4, 169.2 (4C, 4$\underline{C}$(O)CH_3), 155.7 (1C, C-12), 151.1 (1C, C-13), 135.9 (1C, C-7), 132.6 (2C, C-16, C-17), 131.9 (2C, C-8, C-9), 127.1 (1C, C-18), 124.8 (2C, C-14, C-15), 123.0 (C-10, C-11), 88.9 (C-1), 76.3 (C-5), 73.3 (C-3), 67.2 (C-4), 66.9 (C-2), 61.1 (C-6), 20.7, 20.6, 20.5 (4C, 4C(O)$\underline{C}H_3$) ppm ; ESI HRMS: *m/z*: clcd for $C_{26}H_{27}BrN_2O_{11}S$ + Na^+: 677.04111 [M+Na^+] found: 677.04077.

(*E*)-2,2',6,6'-tetrafluoro-4-(2,3,4,6-tetra-*O*-acetyl-β-D-glucopyranosyl-1-sulfonyl)-4´-iodo azobenzene (69).

To **57** (72 mg, 97 µmol, 1.0 eq) in CH_2Cl_2 (1 mL) was added 70% *meta*-chloroperbenzoic acid (53 mg, 214 µmol, 2.2 eq) at RT. The mixture was stirred for 2 h. Then the mixture was diluted with EtOAc, washed with NaOH 1M (3x). The water phase was extracted with EtOAc and the combined organic phases were washed with brine, then dried over $MgSO_4$ and concentrated *in vacuo*. Column chromatography (cyclohexane:EtOAc 4:1 to 6:4) afforded the title compound **69** (51 mg, 66 µmol) in 68% yield as an orange/red solid. $[\alpha]^{20}_D$ = -1.18 (*c* = 0.5 in DMSO); ^{1}H NMR (500 MHz, $CDCl_3$) δ = 7.93 (d, $^3J_{H,F}$ = 9.0 Hz, 2H, H-16, H-17), 7.72 (d, $^3J_{H,F}$ = 7.7 Hz, 2H, H-8, H-9), 5.41 (d, $^3J_{1,2}$ = 9.7 Hz, 1H, H-1), 5.36 (t, $^3J_{3,2}$ = $^3J_{3,4}$ = 9.3 Hz, 1H, H-3), 5.26 (at, $^3J_{2,1}$ = 9.7 Hz, $^3J_{2,3}$ = 9.3 Hz, 1H, H-2), 4.94 (at, $^3J_{4,5}$ = 9.9 Hz, $^3J_{4,3}$ = 9.3 Hz, 1H, H-4), 4.14-4.05 (m, 3H, H-5, H-6a, H-6b), 2.07 (s, 3H, C(O)CH_3), 1.98 (s, 3H, C(O)CH_3), 1.95 (s, 3H, C(O)CH_3), 1.90 (s, 3H, C(O)CH_3) ppm ; ^{13}C NMR (126 MHz, $CDCl_3$) δ = 169.7, 169.4, 169.0, 168.8 (4C, 4$\underline{C}$(O)CH_3), 154.3 (dd, $^1J_{C,F}$ = 267.0 Hz, $^3J_{C,F}$ = 4.0 Hz, 2C, C-14, C-15), 153.5 (dd, $^1J_{C,F}$ = 262.8

Hz, $^{3}J_{C,F}$ = 3.1 Hz, 2C, C-10, C-11), 137.2 (t, $^{3}J_{C,F}$ = 8.7 Hz, 1C, C-7), 134.5 (t, $^{2}J_{C,F}$ = 10.4 Hz, 1C, C-12), 129.8 (t, $^{2}J_{C,F}$ = 9.5 Hz, 1C, C-13), 122.6 (dd, $^{2}J_{C,F}$ = 22.0 Hz, $^{4}J_{C,F}$ = 3.3 Hz, 2C, C-16, C-17), 115.0 (d, $^{2}J_{C,F}$ = 23.4 Hz, 2C, C-8, C-9), 100.2 (t, $^{3}J_{C,F}$ = 10.1 Hz, 1C, C-18), 87.1 (C-1), 74.9 (C-5), 72.3 (C-3), 67.0 (C-4), 66.1 (C-2), 61.0 (C-6), 20.3, 20.2, 20.1, 20.0 (4C, 4C(O)<u>C</u>H$_3$) ; ESI HRMS: *m/z*: clcd for $C_{26}H_{23}F_4IN_2O_{11}S$ + H^+: 775.00761 [M+H^+] found: 775.00746.

(*E*)-4-(2,3,4,6-tetra-*O*-acetyl-β-D-glucopyranosyl-1-sulfonyl)-4´-(2´,3´,4´,6´-tetra-*O*-acetyl-1-thio-β-D-glucopyranosyl) azobenzene (70).

General procedure **C** was applied to **68** (66 mg, 100 µmol, 1 eq) and thiol **31** (1 eq) in 1,4-dioxane (330 µL) with PdG3-Xantphos (1 mol%) and Et_3N (1 eq); stirring at 70 °C for 6 h. Column chromatography (CH_2Cl_2:Et_2O 9:1 to 7:3) afforded a fraction of 55 mg containing impurities along with the target compound. The residue was dissolved in a minimal amount of CH_2Cl_2, diluted with Et_2O, and precipitated by addition of cyclohexane and filtered to afford the pure title compound **70** (43 mg, 46 µmol) in 46% yield as a red solid. $[\alpha]^{20}_D$ = -33.7 (*c* = 0.5 in $CHCl_3$); ^{1}H NMR (500 MHz, $CDCl_3$) δ = 8.09-8.03 (m, 4H, H-8, H-9, H-10, H-11), 7.94-7.89 (m, 2H, H-14, H-15), 7.66-7.62 (m, 2H, H-16, H-17), 5.30-5.23 (m, 3H, H-2, H-3, H-3´), 5.12-5.04 (m, 2H, H-2´, H-4´), 4.94-4.88 (m, 1H, H-4), 4.86 (d, $^{3}J_{1´,2´}$ = 10.1 Hz, 1H, H-1´), 4.58-4.52 (m, 1H, H-1), 4.27 (dd, $^{2}J_{6´a,6´b}$ = 12.3 Hz, $^{3}J_{6´a,5}$ = 5.3 Hz, 1H, H-6´a), 4.22 (dd, $^{2}J_{6´b,6´a}$ = 12.3 Hz, $^{3}J_{6´b,5´}$ = 2.5 Hz, 1H, H-6´b), 4.16 (d, $^{3}J_{6a,5}$ = $^{3}J_{6b,5}$ = 3.5 Hz, 2H, H-6a, H-6b), 3.82 (ddd, $^{3}J_{5´,4´}$ = 10.1 Hz, $^{3}J_{5´,6´a}$ = 5.3 Hz, $^{3}J_{5´,6´b}$ = 2.5 Hz, 1H, H-5´), 3.75 (ddd, $^{3}J_{5,4}$ = 10.1 Hz, $^{3}J_{5,6a}$ = $^{3}J_{5,6b}$ = 3.5 Hz, 1H, H-5), 2.15 (s, 3H, C(O)CH$_3$), 2.12 (s, 3H, C(O)CH$_3$), 2.11 (s, 3H, C(O)CH$_3$), 2.04 (s, 3H, C(O)CH$_3$), 2.01 (s, 3H, C(O)CH$_3$), 2.11 (bs, 6H, C(O)CH$_3$), 1.96 (s, 3H, C(O)CH$_3$) ppm ; ^{13}C NMR (126 MHz, $CDCl_3$) δ = 170.5, 170.2, 170.1, 170.0, 169.4, 169.3, 169.2 (8C, 8<u>C</u>(O)CH$_3$), 155.8 (1C, C-12), 151.6 (1C, C-13), 137.6 (1C, C-18), 135.8 (1C, C-7), 132.2 (2C, C-16, C-17), 131.9 (2C, C-8, C-9), 123.7 (2C, C-14, C-15), 123.0 (2C, C-10, C-11), 88.9 (C-1), 85.0 (C-1´), 76.3 (C-5), 76.0 (C-5´), 73.8 (C-3´), 73.3 (C-3), 69.8 (C-2´), 68.1 (C-4´), 67.2 (C-4), 66.9 (C-2), 62.1 (C-6´), 61.1 (C-6), 20.8, 20.7, 20.6, 20.5 (8C, 8C(O)<u>C</u>H$_3$) ppm ; ESI HRMS: *m/z*: clcd for $C_{40}H_{47}O_{20}N_2S_2$ + H^+: 939.21581 [M+H^+] found: 939.21541.

(*E*)-2,2',6,6'-tetrafluoro-4-(2,3,4,6-tetra-*O*-acetyl-β-D-glucopyranosyl-1-sulfonyl)-4´-(2´,3´,4´,6´-tetra-*O*-acetyl-1-thio-β-D-glucopyranosyl) azobenzene (71).

General procedure **C** was applied to **69** (51 mg, 66 µmol, 1.0 eq) and thiol **31** (1.0 eq) in 1,4-dioxane (0.660 mL) with PdG3-Xantphos (1 mol%) and Et_3N (1.0 eq); stirring at RT for 1 h. Column chromatography (CH_2Cl_2:Et_2O 95:5 to 9:1) afforded the title compound **71** (39 mg, 39 µmol) in 59% yield as a red solid. $[\alpha]^{20}_D$ = +0.444 (*c* = 0.5 in DMSO); ^{1}H NMR (500 MHz, $CDCl_3$) δ = 7.71 (d, $^{3}J_{H,F}$ = 7.7 Hz, 2H, H-8, H-9), 7.48 (d, $^{3}J_{H,F}$ = 10.4 Hz, 2H, H-16, H-17), 5.74 (d, $^{3}J_{1´,2´}$ = 10.0 Hz, 1H, H-1´), 5.44-5.38 (m, 2H, H-1, H-3´), 5.35 (t, $^{3}J_{3,2}$ = $^{3}J_{3,4}$ = 9.4 Hz, 1H, H-3), 5.25 (at, $^{3}J_{2,1}$ = 9.6 Hz, $^{3}J_{2,3}$ = 9.4 Hz, 1H, H-2), 5.06-4.99 (m, 2H, H-2´, H-4´), 4.93 (at, $^{3}J_{4,5}$ = 9.8 Hz, $^{3}J_{4,3}$ = 9.4 Hz, 1H, H-4), 4.33-4.28 (m, 1H, H-5´), 4.15-4.06 (m, 5H, H-5, H-6a, H-6b, H-6´a, H-6´b), 2.06 (s, 3H, C(O)CH$_3$), 2.06 (s, 3H, C(O)CH$_3$), 2.02 (s, 3H, C(O)CH$_3$), 2.02 (s, 3H, C(O)CH$_3$), 1.98 (s, 3H, C(O)CH$_3$), 1.98 (s, 3H, C(O)CH$_3$), 1.95 (s, 3H, C(O)CH$_3$), 1.90 (s, 3H, C(O)CH$_3$) ppm ; ^{13}C NMR (126 MHz, $CDCl_3$) δ = 169.8, 169.7, 169.4, 169.3, 169.1, 169.0, 168.8 (8C, 8<u>C</u>(O)CH$_3$), 154.9 (dd, $^{1}J_{C,F}$ = 263.5 Hz, $^{3}J_{C,F}$ = 4.5 Hz, 2C, C-14, C-15), 153.5 (dd, $^{1}J_{C,F}$ = 262.5 Hz, $^{3}J_{C,F}$ = 2.9 Hz, 2C, C-10, C-11), 142.9 (t, $^{3}J_{C,F}$ = 11.4 Hz, 1C, C-18), 136.8 (t, $^{3}J_{C,F}$ = 8.6 Hz, 1C, C-7), 134.7 (t, $^{2}J_{C,F}$ = 10.5 Hz, 1C, C-12), 128.3 (t, $^{2}J_{C,F}$ = 9.3 Hz, 1C, C-13), 114.9 (d, $^{2}J_{C,F}$ = 26.2 Hz, 2C, C-8, C-9), 112.2 (d, $^{2}J_{C,F}$ = 23.2 Hz, 2C, C-16, C-17), 87.1 (C-1), 81.0 (C-1´), 74.9 (C-5´), 74.5 (C-5), 72.6 (C-3´), 72.3 (C-3), 68.9 (C-2´), 67.9 (C-4´), 67.0 (C-4), 66.1 (C-2), 62.0 (C-6´), 61.1 (C-6), 20.3, 20.2, 20.1, 20.0 (8C, 8C(O)<u>C</u>H$_3$) ppm ; ESI HRMS: *m/z*: clcd for $C_{40}H_{42}O_{20}N_2F_4S_2$ + Na^+: 1033.16007 [M+Na^+] found: 1033.15872.

(*E*)-4,4´-*bis*-(2,3,4,6-tetra-*O*-acetyl-β-D-glucopyranosyl-1-sulfonyl) azobenzene (72).

To **35** (30 mg, 33 µmol, 1.0 eq) in CH_2Cl_2 (330 µL) was added 70% meta-chloroperbenzoic acid (36 mg, 146 µmol, 4.4 eq) at RT and the mixture was stirred for 3 h. Then it was diluted with EtOAc, washed with NaOH 1M (3x) and brine. The water phase was extracted with EtOAc and the combined organic phases were washed with brine, then dried over $MgSO_4$ and concentrated *in vacuo*. Column chromatography (CH_2Cl_2:EtOAc 9:1 to 7:3) afforded the title compound **72** (25 mg, 26 µmol) in 79% yield as a pale red solid. $[\alpha]^{20}_D$ = -36.9 (*c* = 0.5 in DMSO); ^{1}H NMR (500 MHz, $CDCl_3$) δ = 8.12 (s, 8H, 4Ar-H_{ortho}, 4Ar-H_{meta}), 5.30-5.23 (m, 4H, H-2, H-3), 4.94-4.88 (m, 2H, H-4), 4.59-4.55 (m, 2H, H-1), 4.22-4.14 (m, 2H, H-6a, H-6b), 3.79-3.74 (m, 2H, H-5), 2.16 (s, 6H, C(O)CH_3) , 2.01 (s, 6H, C(O)CH_3), 2.00 (s, 6H, C(O)CH_3), 1.98 (s, 6H, C(O)CH_3) ppm ; ^{13}C NMR (126 MHz, $CDCl_3$) δ = 170.2, 170.0, 169.4, 169.2 (4C, 4$\underline{C}$(O)CH_3), 155.4 (2C, 2Ar-C_{ipso}), 136.9 (2C, 2Ar-C_{para}), 132.1 (4C, 4Ar-C_{meta}), 123.3 (4C, 4Ar-C_{ortho}), 89.0 (C-1), 76.4 (C-5), 73.3 (C-3), 67.2 (C-4), 66.9 (C-2), 61.1 (C-6), 20.7, 20.6, 20.5 (4C, 4C(O)$\underline{C}H_3$) ppm ; ESI HRMS: *m/z*: clcd for $C_{40}H_{46}N_2O_{22}S_2 + H^+$: 971.20564 [M+$H^+$] found: 971.20535.

(*E*)-2,2',6,6'-tetrafluoro-4,4´-*bis*-(2,3,4,6-tetra-*O*-acetyl-β-D-glucopyranosyl-1-sulfonyl) azobenzene (73).

To **36** (77 mg, 79 µmol, 1.0 eq) in CH_2Cl_2 (780 µL) was added 70% meta-chloroperbenzoic acid (85 mg, 346 µmol, 4.4 eq) at RT and the mixture was stirred for 3 h. Then Then it was diluted with EtOAc, washed with NaOH 1M (3x). The water phase was extracted with EtOAc and the combined organic phases were washed with brine, then dried over $MgSO_4$ and concentrated *in vacuo*. Column chromatography (CH_2Cl_2:EtOAc 9:1 to 4:1) afforded the title compound **73** (64 mg, 61 µmol) in 78% yield as a pale red solid. $[\alpha]^{20}_D$ = -1.67 (*c* = 0.5 in DMSO); ^{1}H NMR (500 MHz, $CDCl_3$) δ = 7.76 (d, $^2J_{H,F}$ = 7.9 Hz, 4H, 4Ar-H_{meta}), 5.42 (d, $^3J_{1,2}$ = 9.7 Hz, 2H, H-1), 5.36 (t, $^3J_{3,2}$ = $^3J_{3,4}$ = 9.3 Hz, 2H, H-3), 5.28 (at, $^3J_{2,1}$ = 9.7 Hz, $^3J_{2,3}$ = 9.3 Hz, 2H, H-2), 4.96 (at, $^3J_{4,5}$ = 9.9 Hz, $^3J_{4,3}$ = 9.3 Hz, 2H, H-4), 4.15-4.05 (m, 6H, H-5, H-6a, H-6b), 2.07 (s, 6H, C(O)CH_3), 1.98 (s, 6H, C(O)CH_3), 1.95 (s, 6H, C(O)CH_3), 1.90 (s, 6H, C(O)CH_3) ppm ; ^{13}C NMR (126 MHz, $CDCl_3$) δ = 169.8, 169.6, 169.2, 169.0 (8C, 8$\underline{C}$(O)CH_3), 153.9 (dd, $^1J_{C,F}$ = 263.9 Hz, $^3J_{C,F}$ = 2.7 Hz, 4C, 4Ar-C_{ortho}), 138.4 (t, $^3J_{C,F}$ = 8.7 Hz, 2C, 2Ar-C_{para}), 134.2 (t, $^2J_{C,F}$ = 10.2 Hz, 2C, 2Ar-C_{ipso}), 115.3 (dd, $^2J_{C,F}$ = 22.4 Hz, $^4J_{C,F}$ = 3.4 Hz, 4C, 4Ar-C_{meta}), 87.3 (C-1), 75.1 (C-5), 72.5 (C-3), 67.1 (C-4), 66.2 (C-2), 61.1 (C-6), 20.4, 20.2, 20.1 (8C, 8C(O)$\underline{C}H_3$) ppm ; ESI HRMS: *m/z*: clcd for $C_{40}H_{42}F_4N_2O_{22}S_2 + Na^+$: 1065.14990 [M+$Na^+$] found: 1065.14969.

7.3.5. Photochromic properties of selected AB glycoconjugates

7.3.5.1. Compound 50

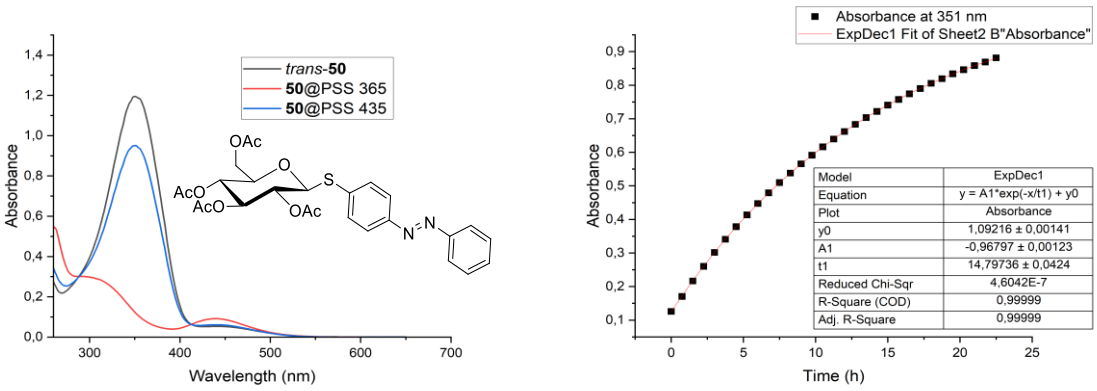

Figure 7.3.2. Left: UV-vis spectra of molecule **50** at 25 °C in DMSO (50 µM) in the *trans* state (black line), and after 2 min irradiation at 365 nm (red line) and 435 nm (blue line); Right: Exponential growth of the absorbance at 351 nm of a *cis*/*trans* mixture of **50** after irradiation at 365 nm in DMSO (50 µM) at 40 °C; The rate constant is given by: $k = 1/t_1$.

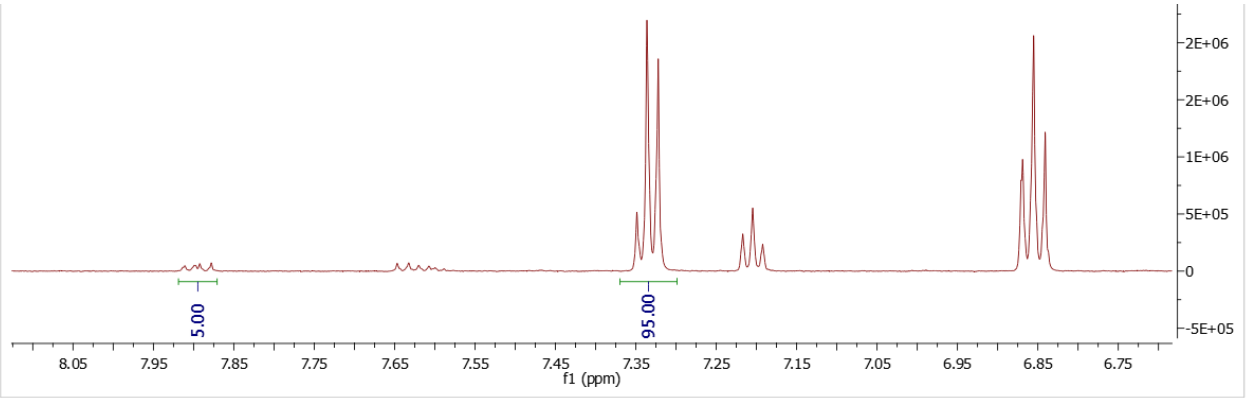

Figure 7.3.3. Expansion in the aromatic region of the ^{1}H NMR spectrum (DMSO-d_6, 300 K) of an equilibrium mixture of *trans* and *cis*-**50** (1 mM) after irradiation at 365 nm (2 min).

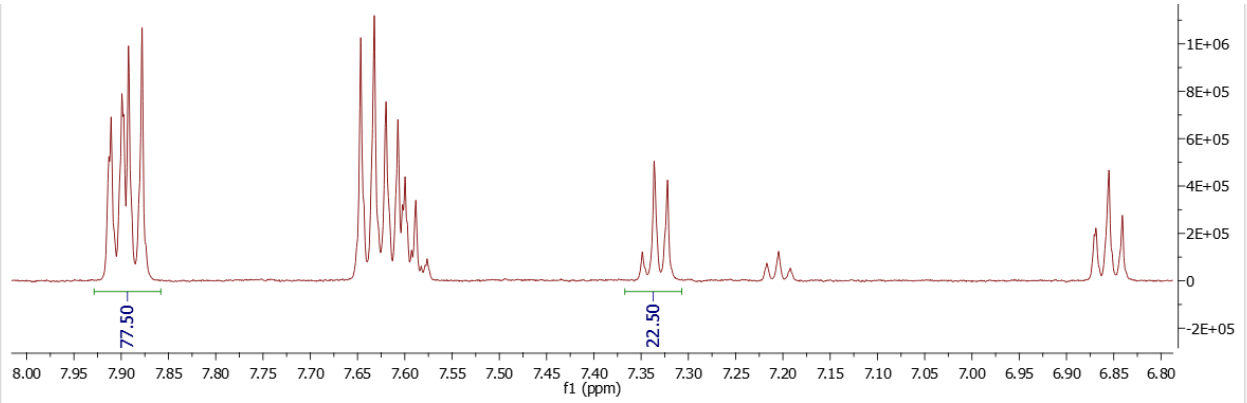

Figure 7.3.4. Expansion in the aromatic region of the ^{1}H NMR spectrum (DMSO-d_6, 300 K) of an equilibrium mixture of *trans* and *cis*-**50** (1 mM) after irradiation at 435 nm (2 min).

7.3.5.2. Compound 66a

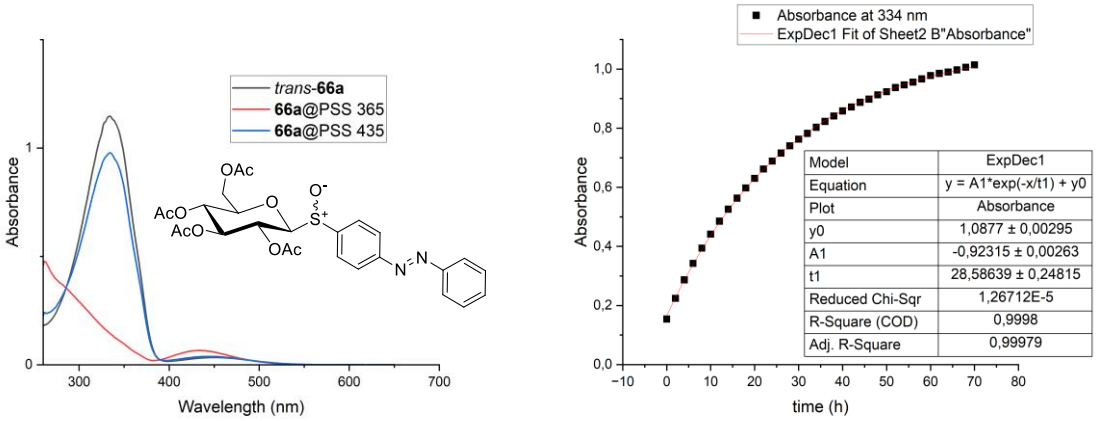

Figure 7.3.5. Left: UV-vis spectra of molecule **66a** at 25 °C in DMSO (50 µM) in the *trans* state (black line), and after 2 min irradiation at 365 nm (red line) and 435 nm (blue line); Right: Exponential growth of the absorbance at 334 nm of a *cis*/*trans* mixture of **66a** after irradiation at 365 nm in DMSO (50 µM) at 40 °C; The rate constant is given by: $k = 1/t_1$.

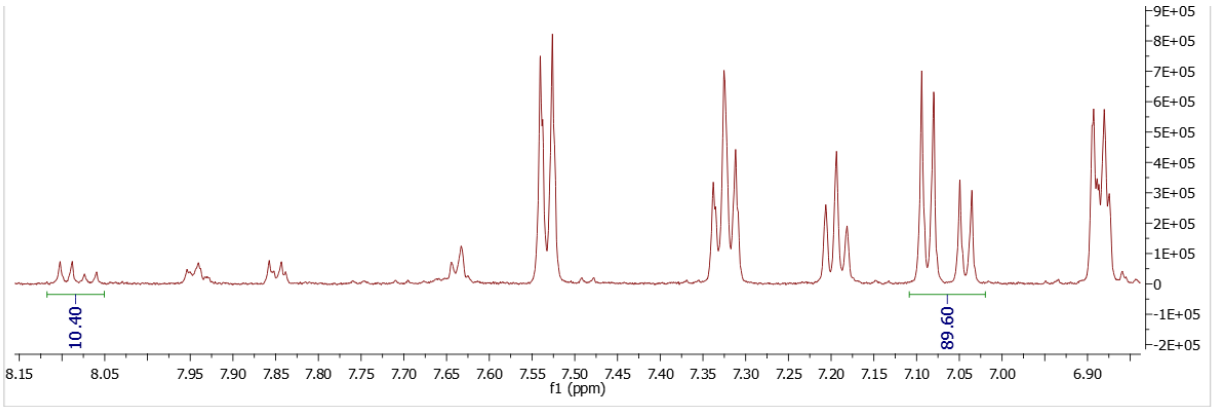

Figure 7.3.6. Expansion in the aromatic region of the ^{1}H NMR spectrum (DMSO-d_6, 300 K) of an equilibrium mixture of *trans* and *cis*-**66a** (1 mM) after irradiation at 365 nm (2 min).

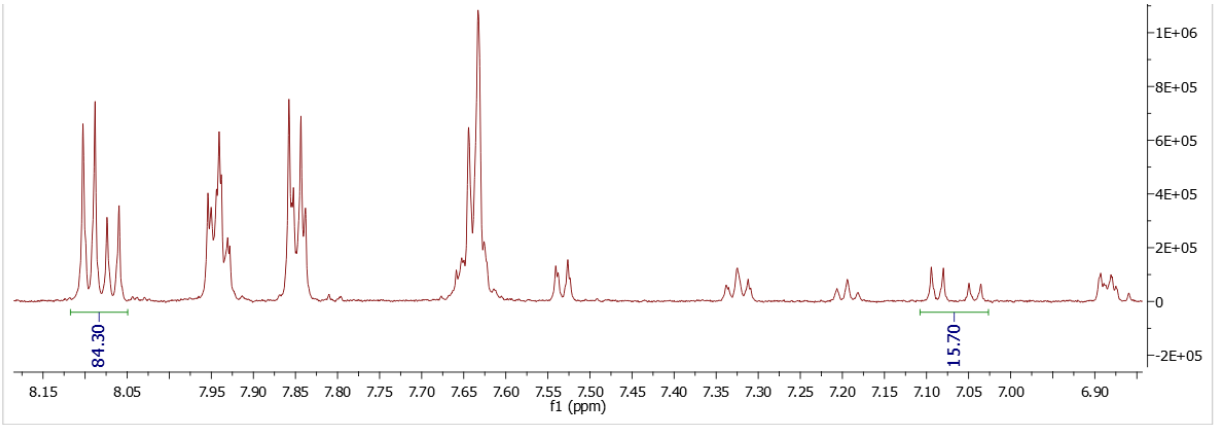

Figure 7.3.7. Expansion in the aromatic region of the ^{1}H NMR spectrum (DMSO-d_6, 300 K) of an equilibrium mixture of *trans* and *cis*-**66a** (1 mM) after irradiation at 435 nm (2 min).

7.3.5.3. Compound 66b

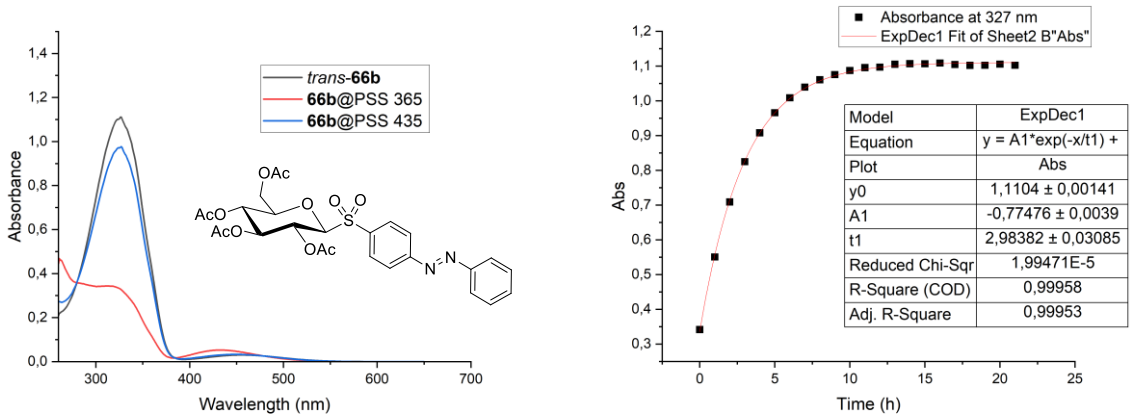

Figure 7.3.8. Left: UV-vis spectra of molecule **66b** at 25 °C in DMSO (50 µM) in the *trans* state (black line), and after 2 min irradiation at 365 nm (red line) and 435 nm (blue line); Right: Exponential growth of the absorbance at 327 nm of a *cis*/*trans* mixture of **66b** after irradiation at 365 nm in DMSO (50 µM) at 40 °C; The rate constant is given by: $k = 1/t_1$.

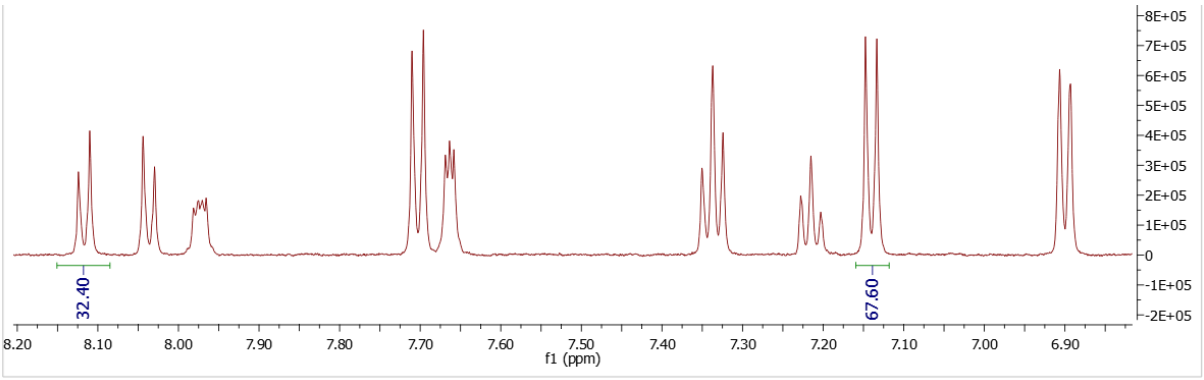

Figure 7.3.9. Expansion in the aromatic region of the ^{1}H NMR spectrum (DMSO-d_6, 300 K) of an equilibrium mixture of *trans* and *cis*-**66b** (1 mM) after irradiation at 365 nm (2 min).

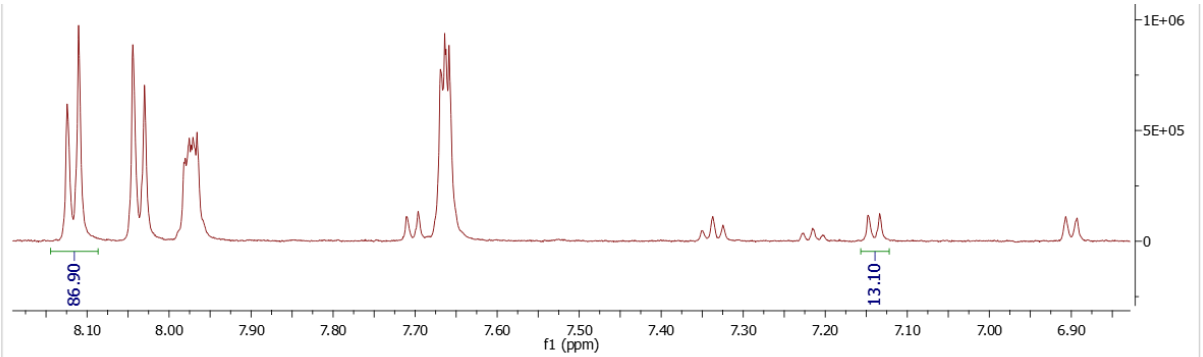

Figure 7.3.10. Expansion in the aromatic region of the ^{1}H NMR spectrum (DMSO-d_6, 300 K) of an equilibrium mixture of *trans* and *cis*-**66b** (1 mM) after irradiation at 435 nm (2 min).

7.3.5.4. Compound 65

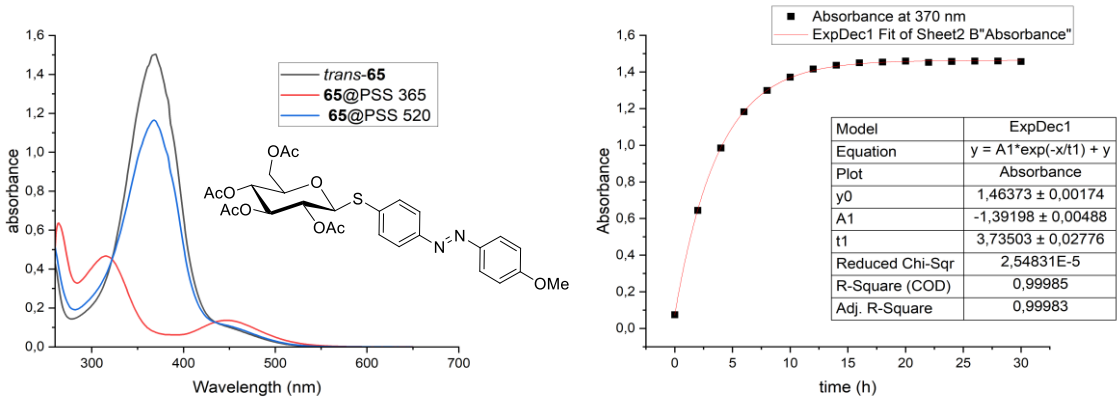

Figure 7.3.11. Left: UV-vis spectra of molecule **65** at 25 °C in DMSO (50 µM) in the *trans* state (black line), and after 2 min irradiation at 365 nm (red line) and 435 nm (blue line); Right: Exponential growth of the absorbance at 370 nm of a *cis*/*trans* mixture of **65** after irradiation at 365 nm in DMSO (50 µM) at 40 °C; The rate constant is given by: $k = 1/t_1$.

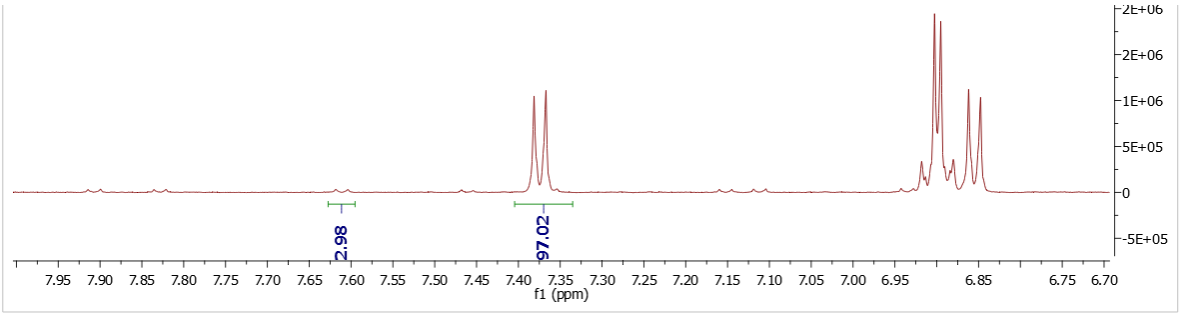

Figure 7.3.12. Expansion in the aromatic region of the ^{1}H NMR spectrum (DMSO-d_6, 300 K) of an equilibrium mixture of *trans* and *cis*-**65** (1 mM) after irradiation at 365 nm (2 min).

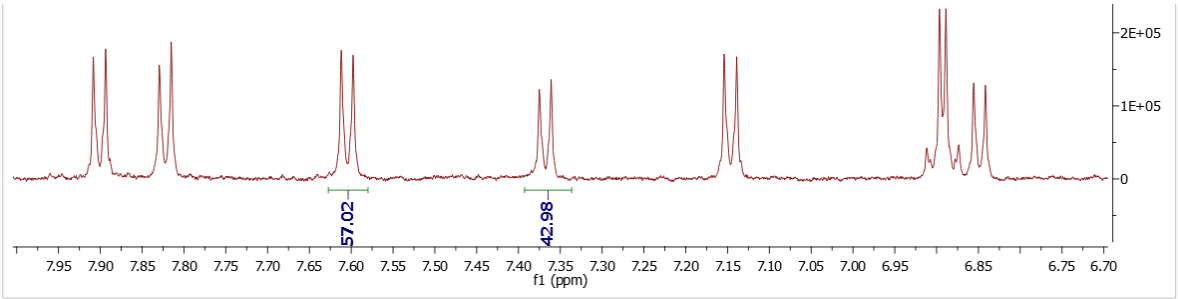

Figure 7.3.13. Expansion in the aromatic region of the ^{1}H NMR spectrum (DMSO-d_6, 300 K) of an equilibrium mixture of *trans* and *cis*-**65** (1 mM) after irradiation at 435 nm (2 min).

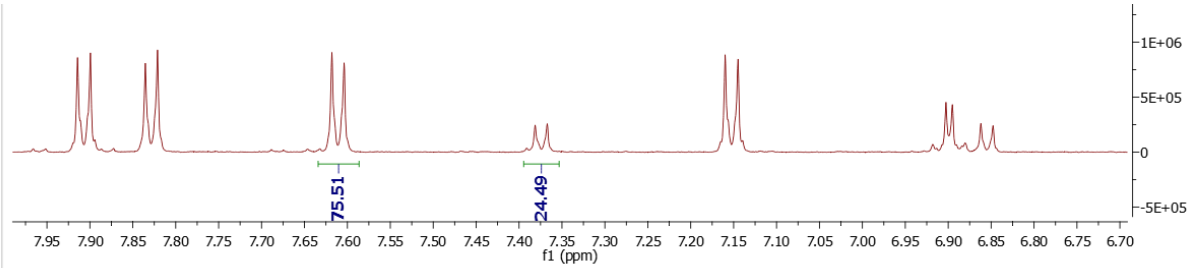

Figure 7.3.14. Expansion in the aromatic region of the ^{1}H NMR spectrum (DMSO-d_6, 300 K) of an equilibrium mixture of *trans* and *cis*-**65** (1 mM) after irradiation at 520 nm (2 min).

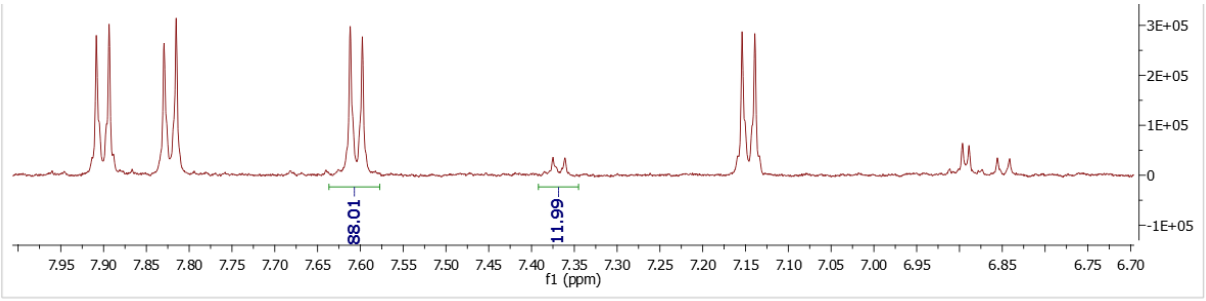

Figure 7.3.15. Expansion in the aromatic region of the ^{1}H NMR spectrum (DMSO-d_6, 300 K) of an equilibrium mixture of *trans* and *cis*-**65** (1 mM) after irradiation at 435 nm for 2 min, and then 590 nm for 5 min.

7.3.5.5. Compound 67a

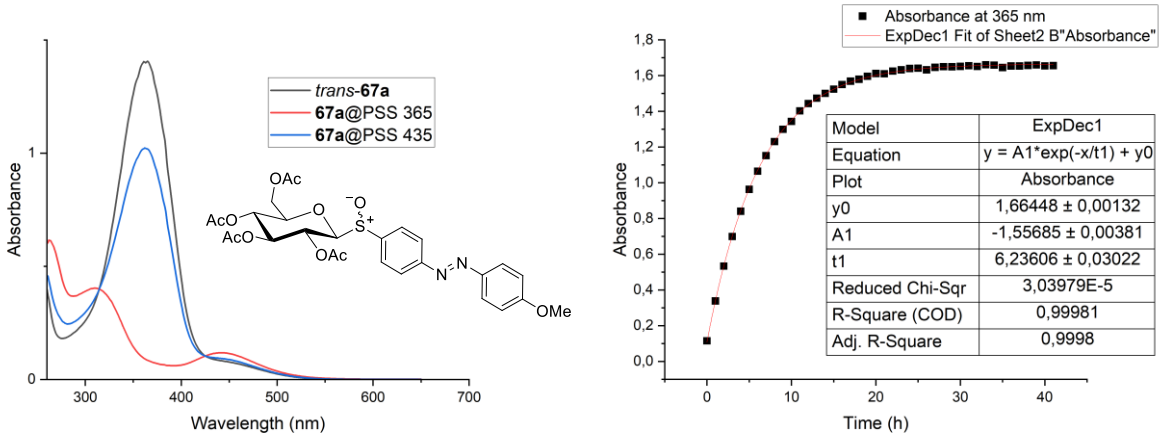

Figure 7.3.16. Left: UV-vis spectra of molecule **67a** at 25 °C in DMSO (50 µM) in the *trans* state (black line), and after 2 min irradiation at 365 nm (red line) and 435 nm (blue line); Right: Exponential growth of the absorbance at 365 nm of a *cis*/*trans* mixture of **67a** after irradiation at 365 nm in DMSO (50 µM) at 40 °C; The rate constant is given by: $k = 1/t_1$.

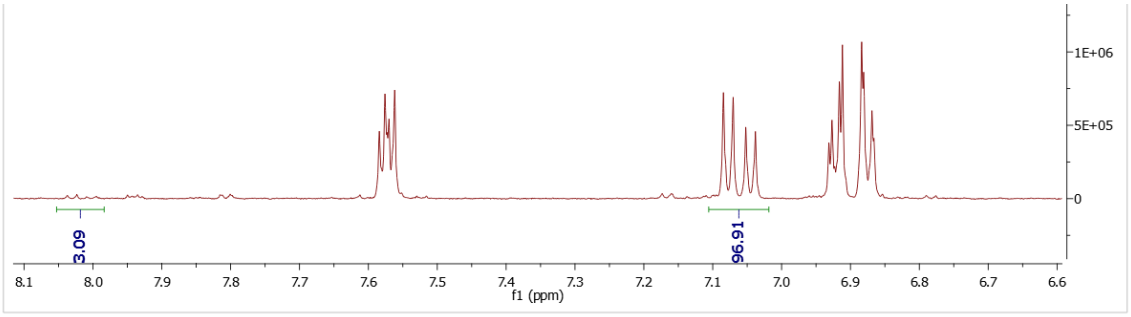

Figure 7.3.17. Expansion in the aromatic region of the ^{1}H NMR spectrum (DMSO-d_6, 300 K) of an equilibrium mixture of *trans* and *cis*-**67a** (1 mM) after irradiation at 365 nm (2 min).

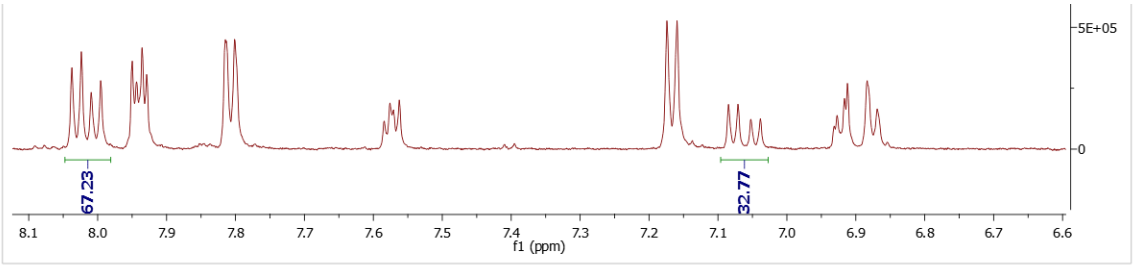

Figure 7.3.18. Expansion in the aromatic region of the ^{1}H NMR spectrum (DMSO-d_6, 300 K) of an equilibrium mixture of *trans* and *cis*-**67a** (1 mM) after irradiation at 435 nm (2 min).

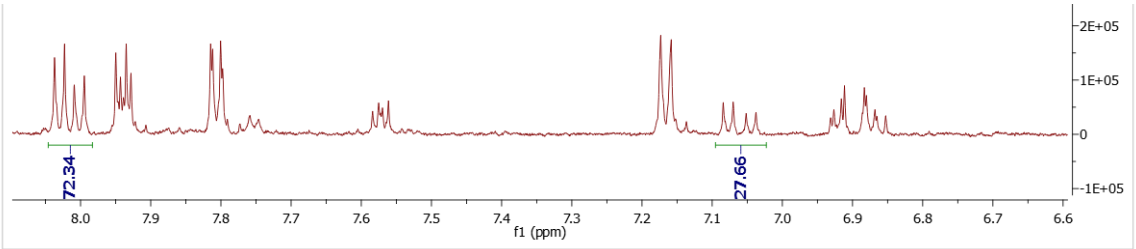

Figure 7.3.19. Expansion in the aromatic region of the ^{1}H NMR spectrum (DMSO-d_6, 300 K) of an equilibrium mixture of *trans* and *cis*-**67a** (1 mM) after irradiation at 520 nm (2 min).

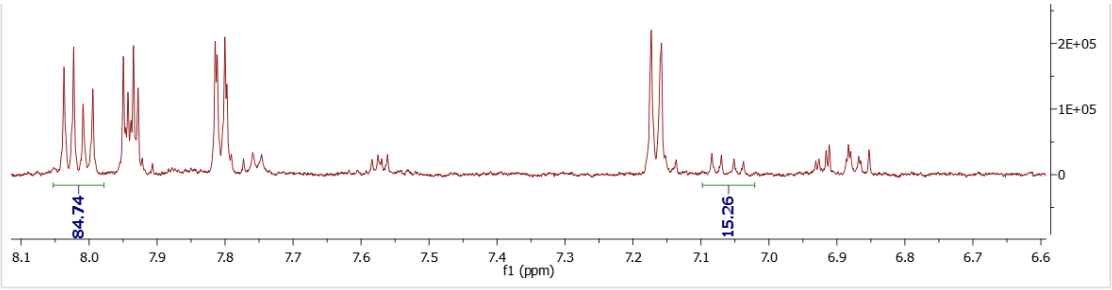

Figure 7.3.20. Expansion in the aromatic region of the ^{1}H NMR spectrum (DMSO-d_6, 300 K) of an equilibrium mixture of *trans* and *cis*-**67a** (1 mM) after irradiation at 520 nm for 2 min and 590 nm for 5 min.

7.3.5.6. Compound 67b

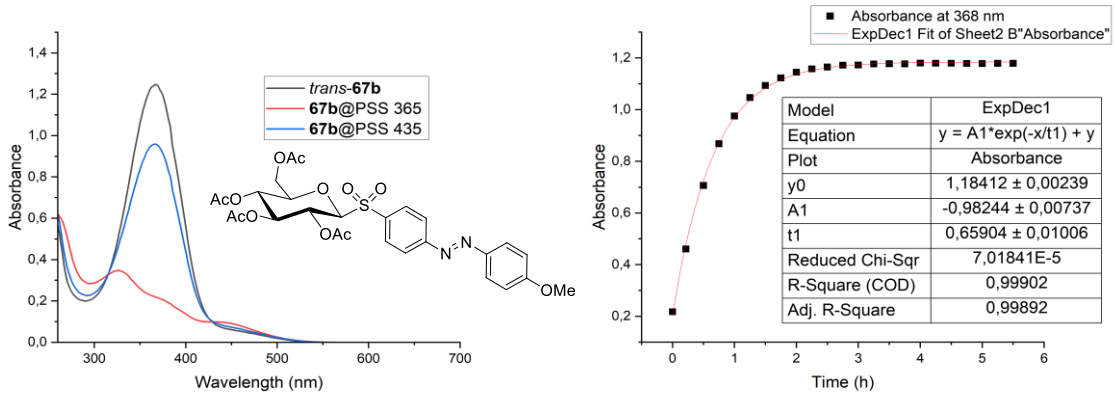

Figure 7.3.21. Left: UV-vis spectra of molecule **67b** at 25 °C in DMSO (50 µM) in the *trans* state (black line), and after 2 min irradiation at 365 nm (red line) and 435 nm (blue line); Right: Exponential growth of the absorbance at 368 nm of a *cis*/*trans* mixture of **67b** after irradiation at 365 nm in DMSO (50 µM) at 40 °C; The rate constant is given by: $k = 1/t_1$.

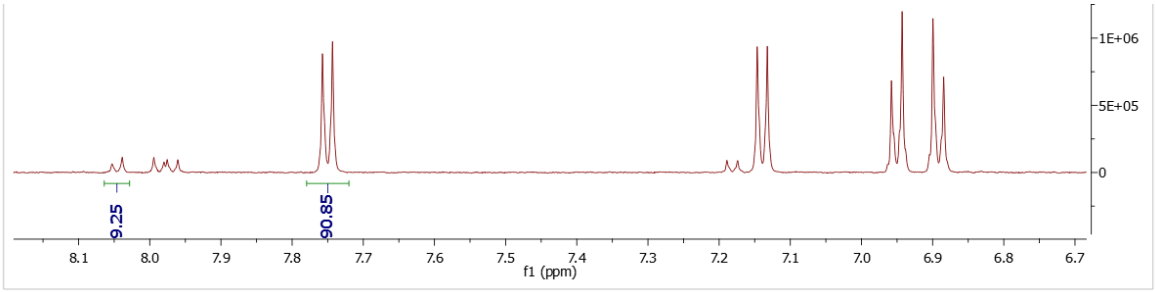

Figure 7.3.22. Expansion in the aromatic region of the ^{1}H NMR spectrum (DMSO-d_6, 300 K) of an equilibrium mixture of *trans* and *cis*-**67b** (1 mM) after irradiation at 365 nm for 2 min.

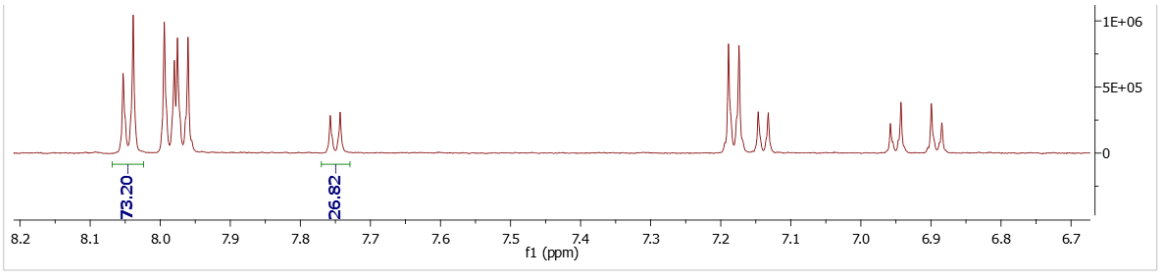

Figure 7.3.23. Expansion in the aromatic region of the ^{1}H NMR spectrum (DMSO-d_6, 300 K) of an equilibrium mixture of *trans* and *cis*-**67b** (1 mM) after irradiation at 435 nm for 2 min.

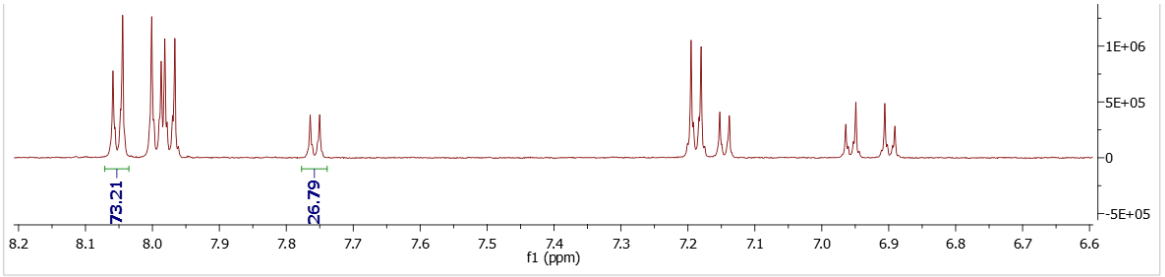

Figure 7.3.24. Expansion in the aromatic region of the ^{1}H NMR spectrum (DMSO-d_6, 300 K) of an equilibrium mixture of *trans* and *cis*-**67b** (1 mM) after irradiation at 520 nm for 2 min.

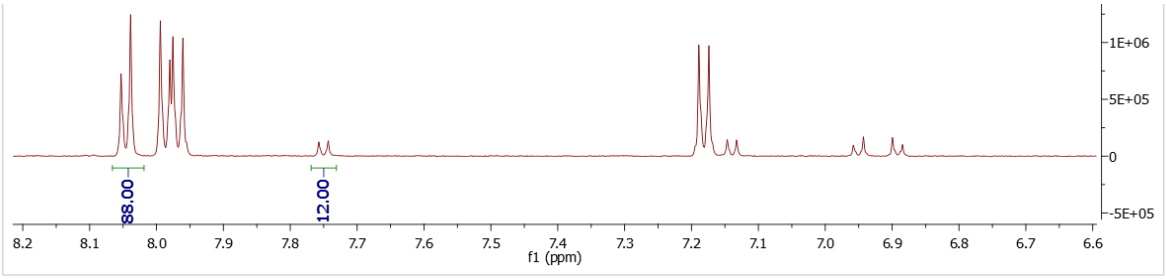

Figure 7.3.25. Expansion in the aromatic region of the ^{1}H NMR spectrum (DMSO-d_6, 300 K) of an equilibrium mixture of *trans* and *cis*-**67b** (1 mM) after irradiation at 435 nm for 2 min and then 590 for 10 min.

7.3.5.7. Compound 35

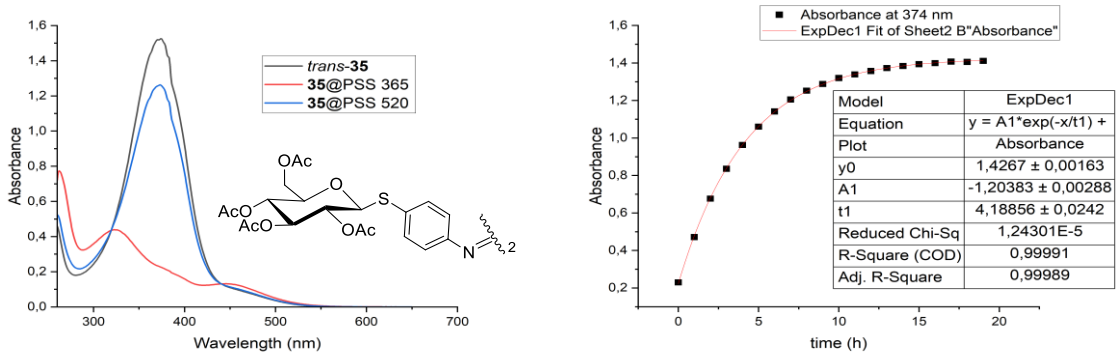

Figure 7.3.26. Left: UV-vis spectra of molecule **35** at 25 °C in DMSO (50 µM) in the *trans* state (black line), and after 2 min irradiation at 365 nm (red line) and 435 nm (blue line); Right: Exponential growth of the absorbance at 374 nm of a *cis*/*trans* mixture of **35** after irradiation at 365 nm in DMSO (50 µM) at 40 °C; The rate constant is given by: $k = 1/t_1$.

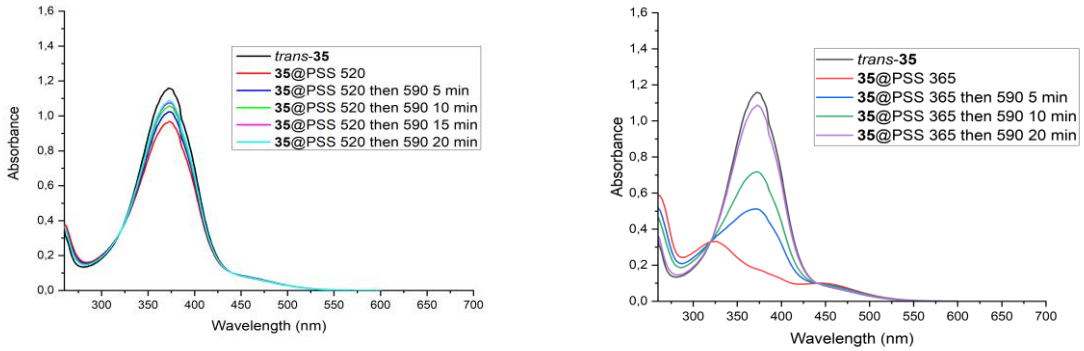

Figure 7.3.27. UV-vis analysis of the time required to reach the PSS 590 nm at 25 °C in DMSO (50 µM) starting from the *cis*/*trans* mixture of **35** at PSS 520 nm (left), and starting from the *cis*/*trans* mixture of **35** at PSS 365 nm (right).

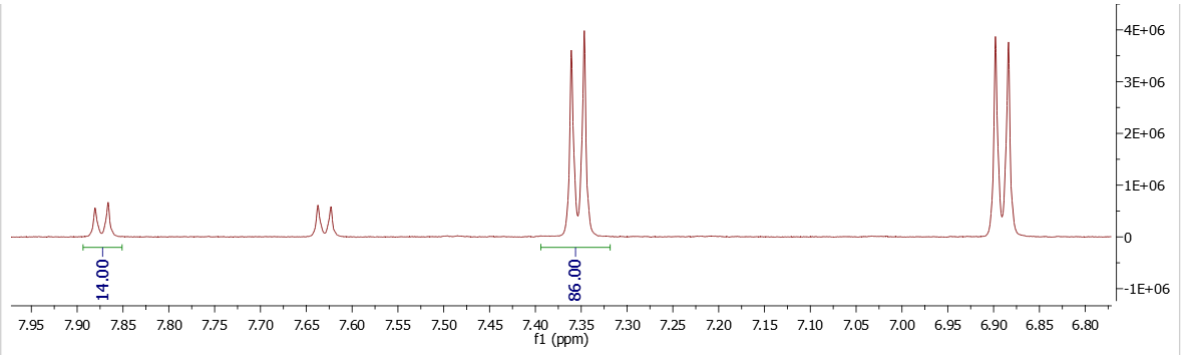

Figure 7.3.28. Expansion in the aromatic region of the ^{1}H NMR spectrum (DMSO-d_6, 300 K) of an equilibrium mixture of *trans* and *cis*-**35** (1 mM) after irradiation at 365 nm (2 min).

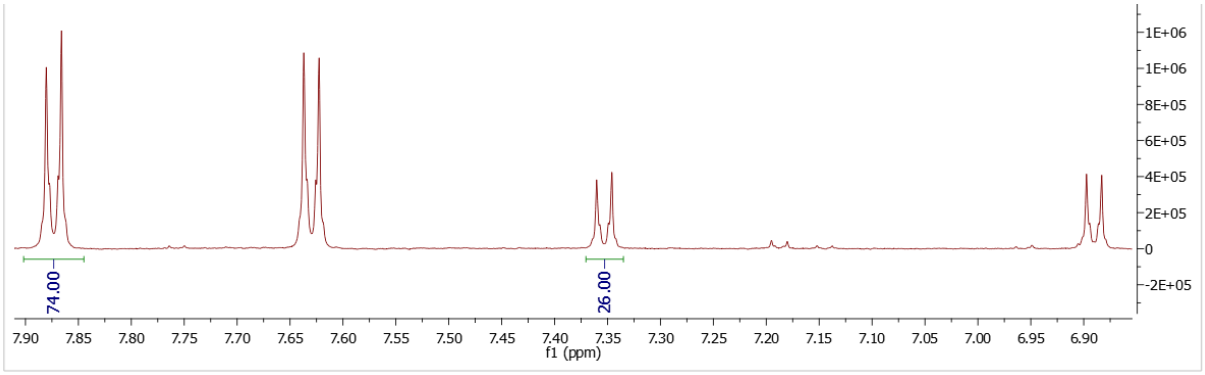

Figure 7.3.29. Expansion in the aromatic region of the ^{1}H NMR spectrum (DMSO-d_6, 300 K) of an equilibrium mixture of *trans* and *cis*-**35** (1 mM) after irradiation at 435 nm (2 min).

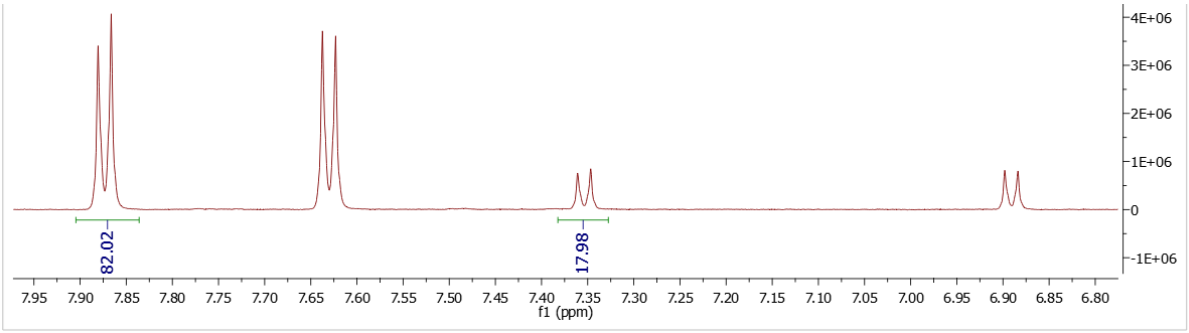

Figure 7.3.30. Expansion in the aromatic region of the ^{1}H NMR spectrum (DMSO-d_6, 300 K) of an equilibrium mixture of *trans* and *cis*-**35** (1 mM) after irradiation at 520 nm (2 min).

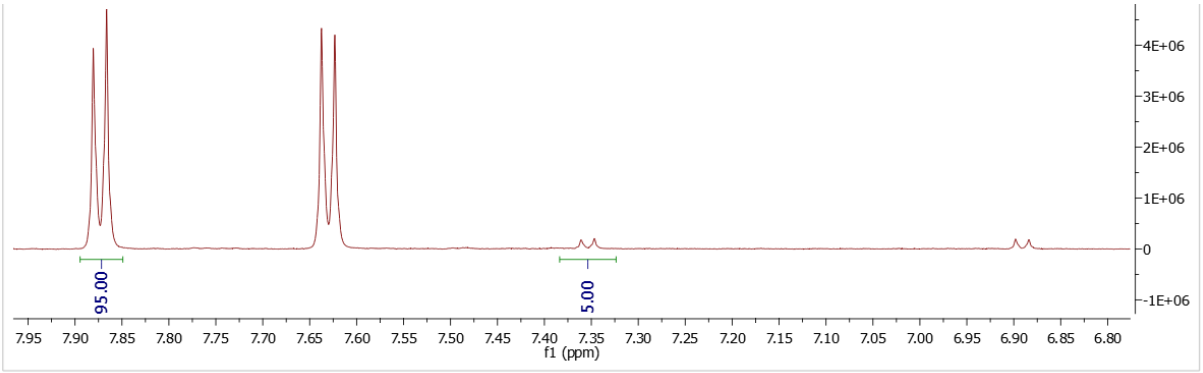

Figure 7.3.31. Expansion in the aromatic region of the ^{1}H NMR spectrum (DMSO-d_6, 300 K) of an equilibrium mixture of *trans* and *cis*-**11** (1 mM) after irradiation at 590 nm (15 min after PSS 520 nm).

7.3.5.8. Compound 70

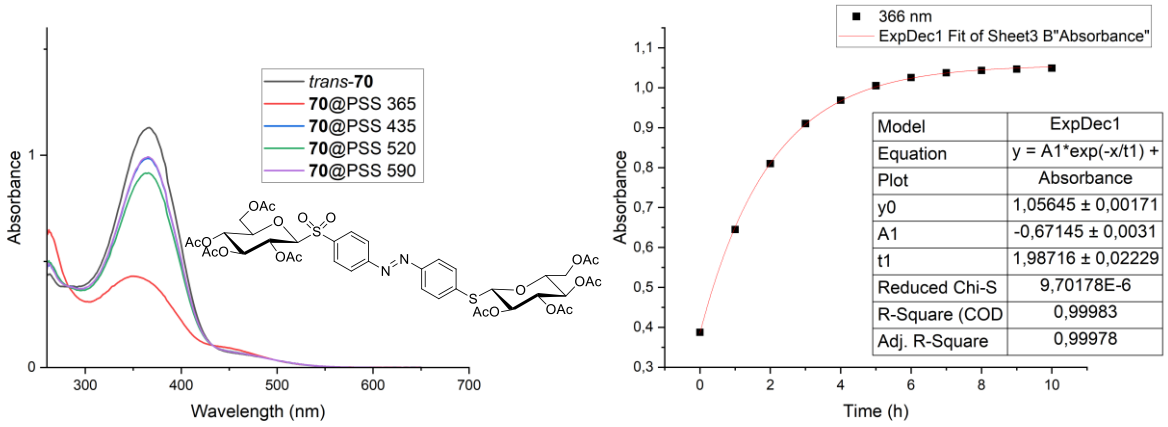

Figure 7.3.32. Left: UV-vis spectra of molecule **70** at 25 °C in DMSO (50 µM) in the *trans* state (black line), and after 2 min irradiation at 365 nm (red line), 435 nm (blue line) and 520 nm (green line), and 5 min irradiation at 590 nm after the PSS 520 (violet line); Right: Exponential growth of the absorbance at 366 nm of a *cis*/*trans* mixture of **70** after irradiation at 365 nm in DMSO (50 µM) at 40 °C; The rate constant is given by: $k = 1/t_1$.

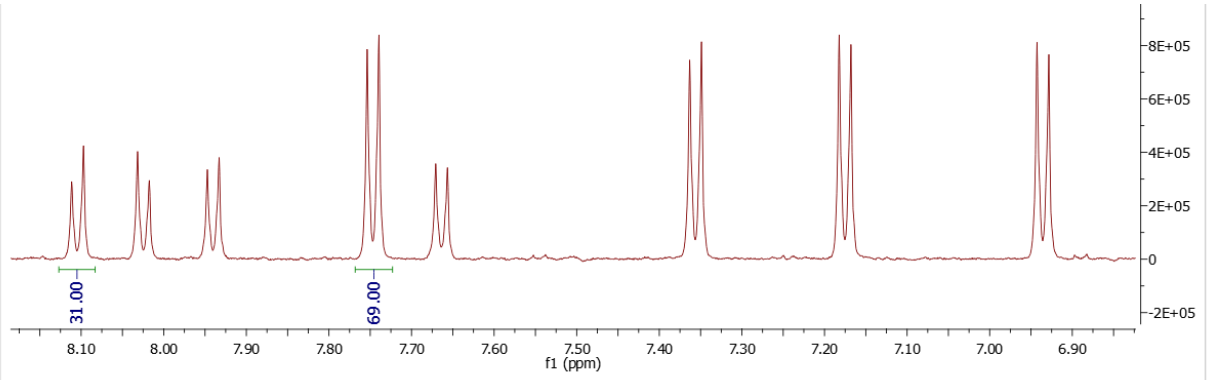

Figure 7.3.33. Expansion in the aromatic region of the ^{1}H NMR spectrum (DMSO-d_6, 300 K) of an equilibrium mixture of *trans* and *cis*-**70** (1 mM) after irradiation at 365 nm (2 min).

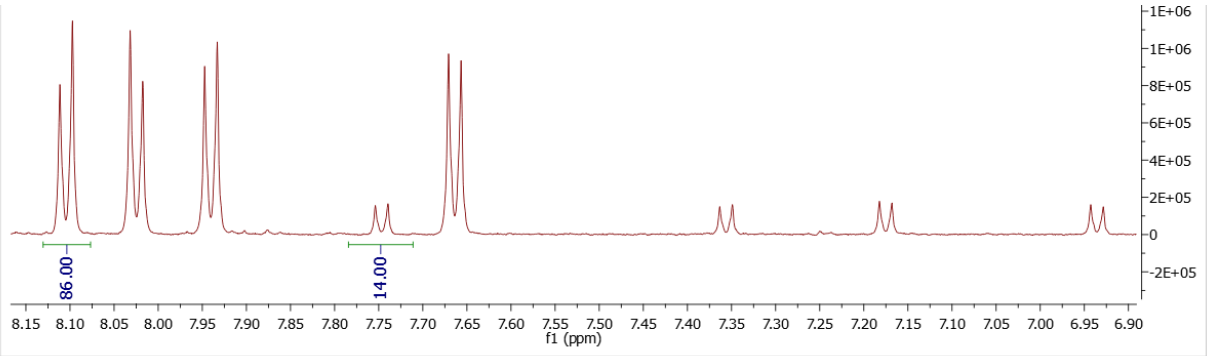

Figure 7.3.34. Expansion in the aromatic region of the ^{1}H NMR spectrum (DMSO-d_6, 300 K) of an equilibrium mixture of *trans* and *cis*-**70** (1 mM) after irradiation at 435 nm (2 min).

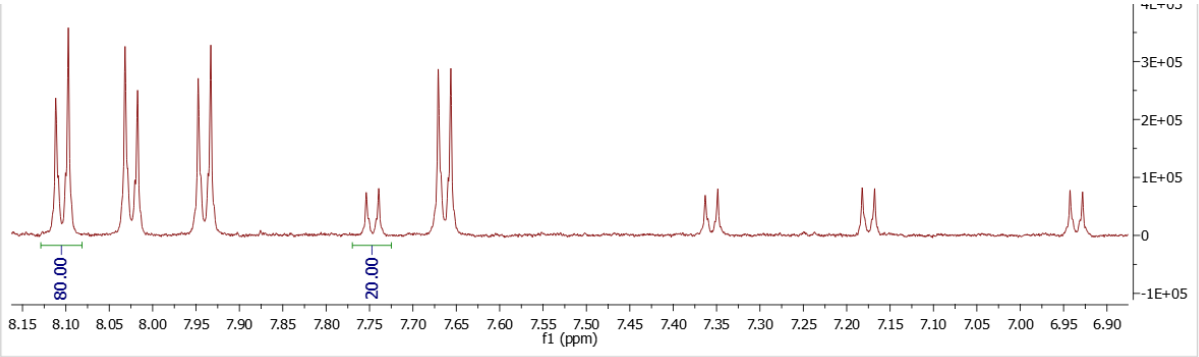

Figure 7.3.35. Expansion in the aromatic region of the ^{1}H NMR spectrum (DMSO-d_6, 300 K) of an equilibrium mixture of *trans* and *cis*-**70** (1 mM) after irradiation at 520 nm (2 min).

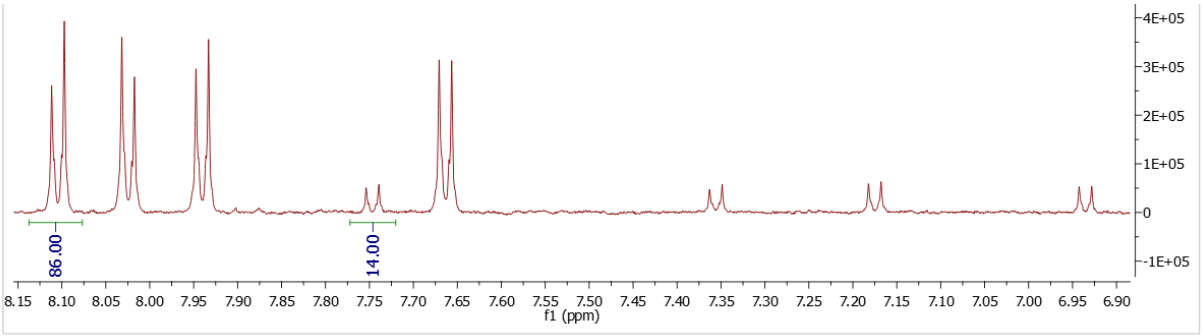

Figure 7.3.36. Expansion in the aromatic region of the ^{1}H NMR spectrum (DMSO-d_6, 300 K) of an equilibrium mixture of *trans* and *cis*-**70** (1 mM) after irradiation at 590 nm (5 min after PSS 520 nm).

7.3.5.9. Compound 36

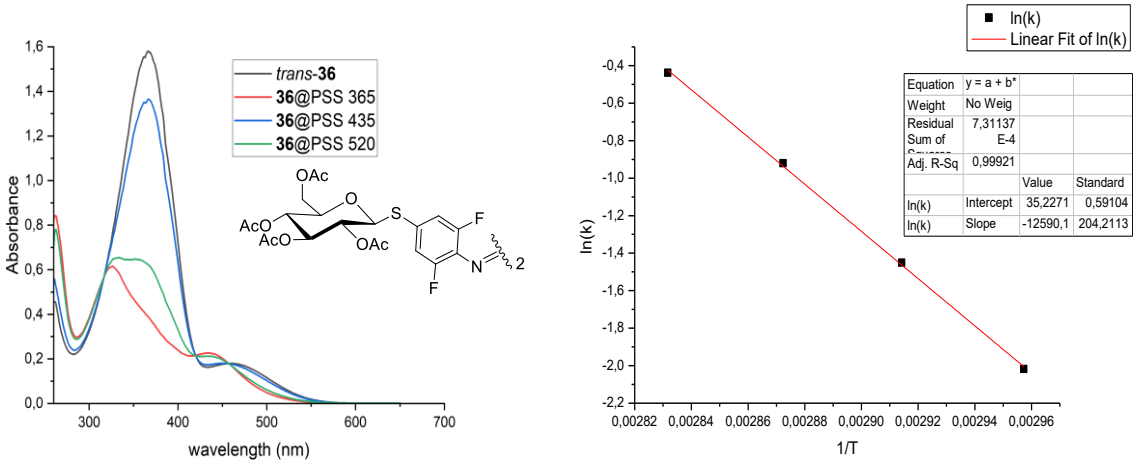

Figure 7.3.37. Left: UV-vis spectra of molecule **36** at 25 °C in DMSO (50 µM) in the *trans* state (black line), and after 2 min irradiation at 365 nm (red line), 435 nm (blue line) and 520 nm (green line); Right: Linearized Arrhenius plot ln(k) = f(1/T) for compound **36**; the ordinate at the origin gives the natural logarithm of the pre-exponential factor ln*A* and the slope gives $\frac{Ea}{R}$.

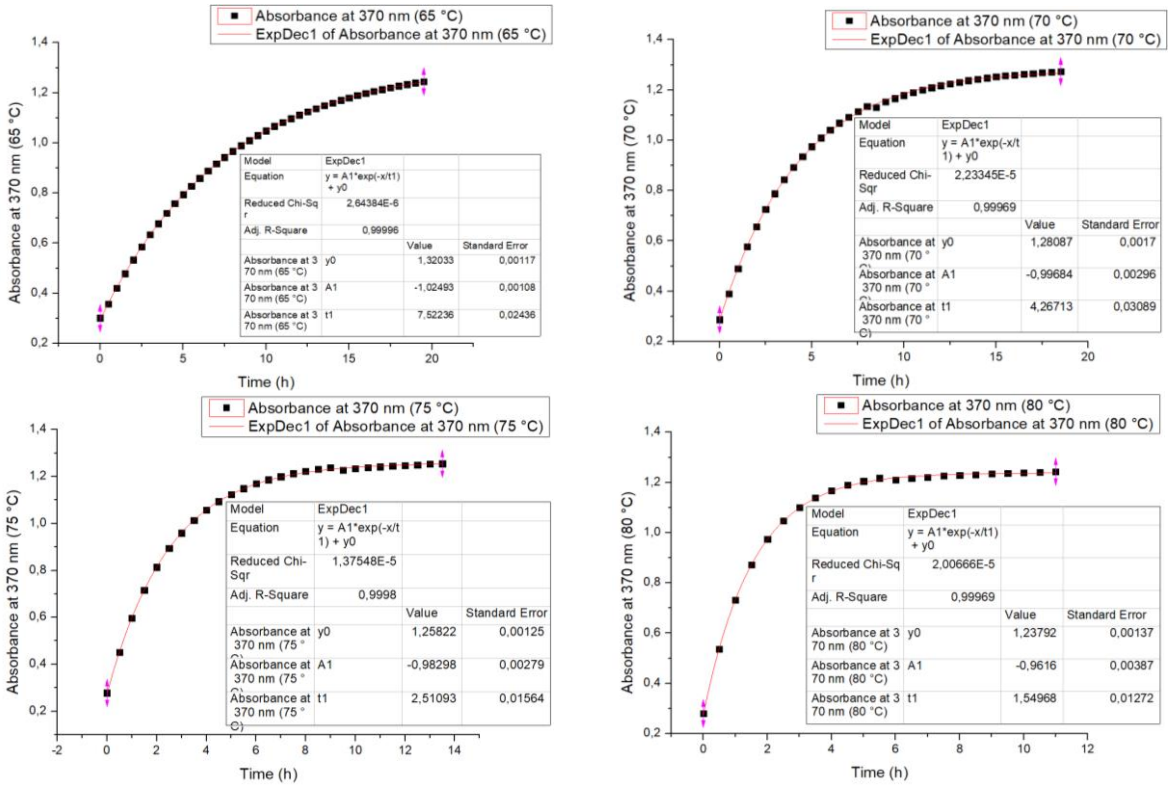

Figure 7.3.38. Exponential growth of the absorbance at 370 nm of a *cis*/*trans* mixture of **36** after irradiation at 365 nm in DMSO (50 µM) at 65, 70, 75 and 80 °C; The rate constant at each temperature is given by: $k_T = 1/t_1$.

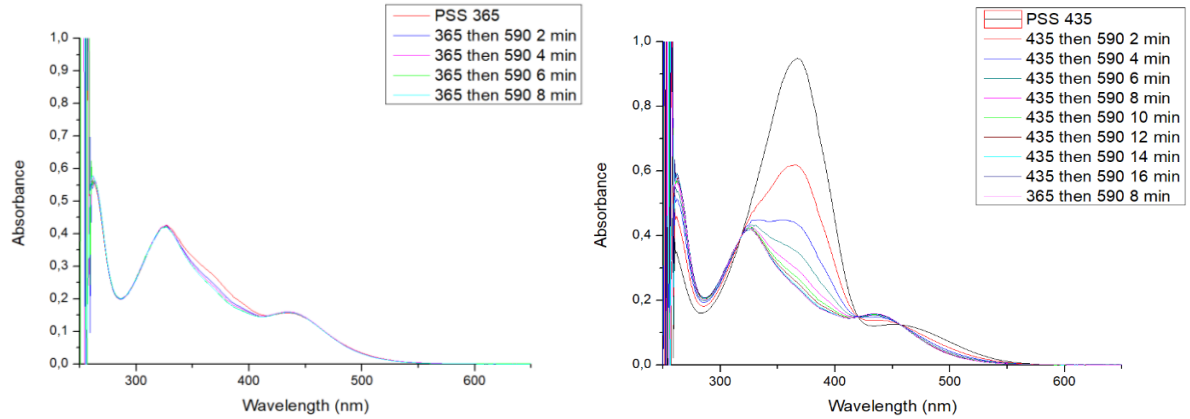

Figure 7.3.39. UV-vis analysis of the time required to reach the PSS 590 nm at 25 °C in DMSO (50 µM) starting from the *cis*/*trans* mixture of **36** at PSS 365 nm (left), and starting from the *cis*/*trans* mixture of **36** at PSS 435 nm (right).

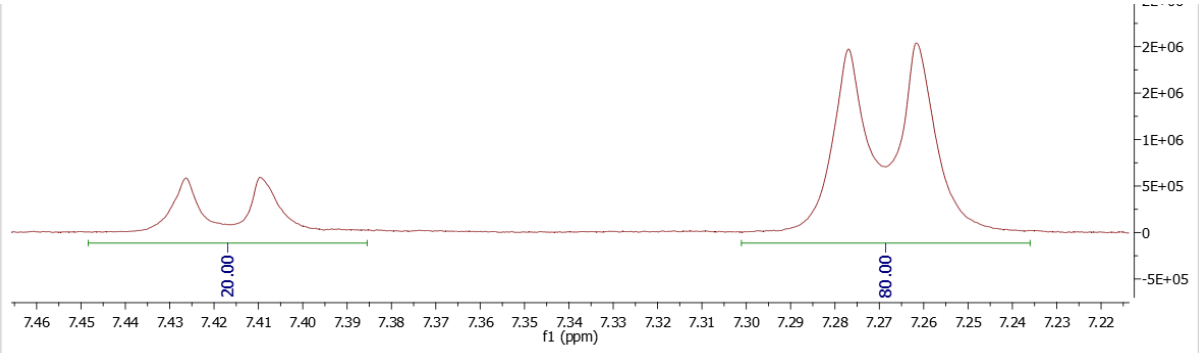

Figure 7.3.40. Expansion in the aromatic region of the ^{1}H NMR spectrum (DMSO-d_6, 300 K) of an equilibrium mixture of *trans* and *cis*-**36** (1 mM) after irradiation at 365 nm (2 min).

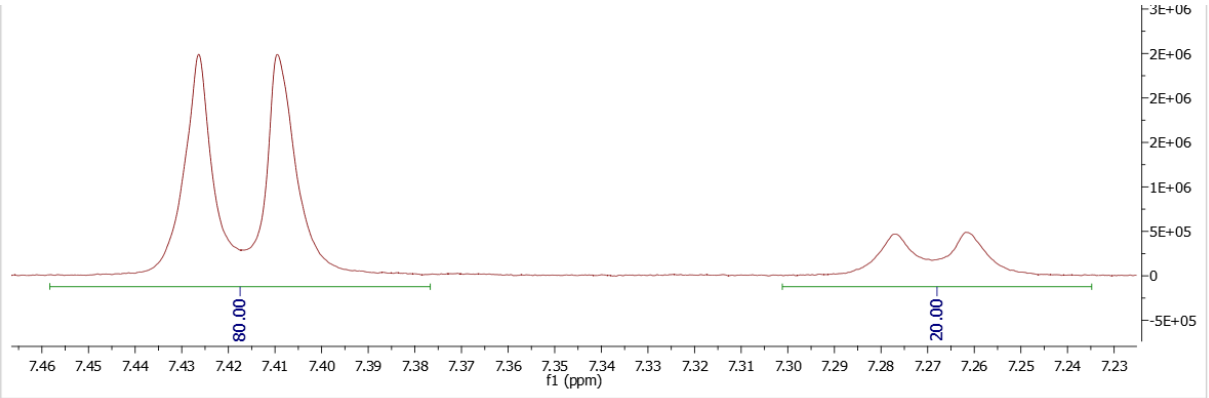

Figure 7.3.41. Expansion in the aromatic region of the ^{1}H NMR spectrum (DMSO-d_6, 300 K) of an equilibrium mixture of *trans* and *cis*-**36** (1 mM) after irradiation at 435 nm (2 min).

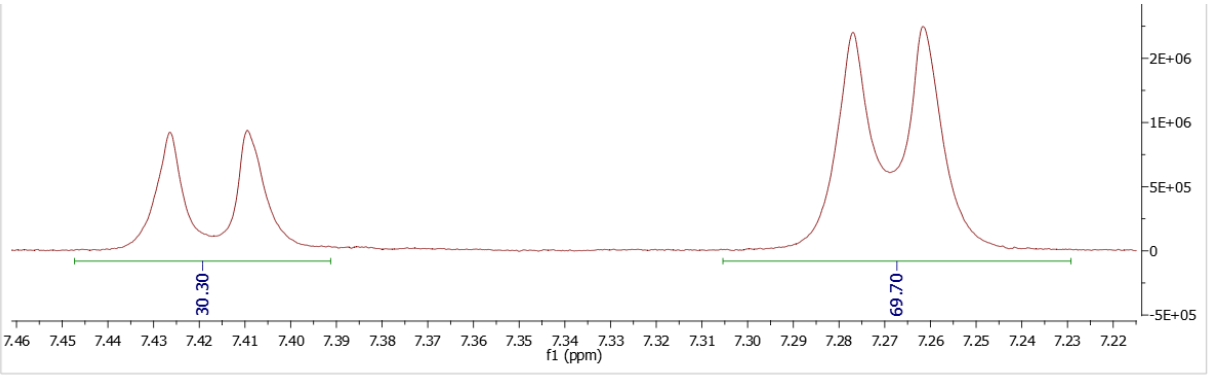

Figure 7.3.42. Expansion in the aromatic region of the ^{1}H NMR spectrum (DMSO-d_6, 300 K) of an equilibrium mixture of *trans* and *cis*-**36** (1 mM) after irradiation at 520 nm (2 min).

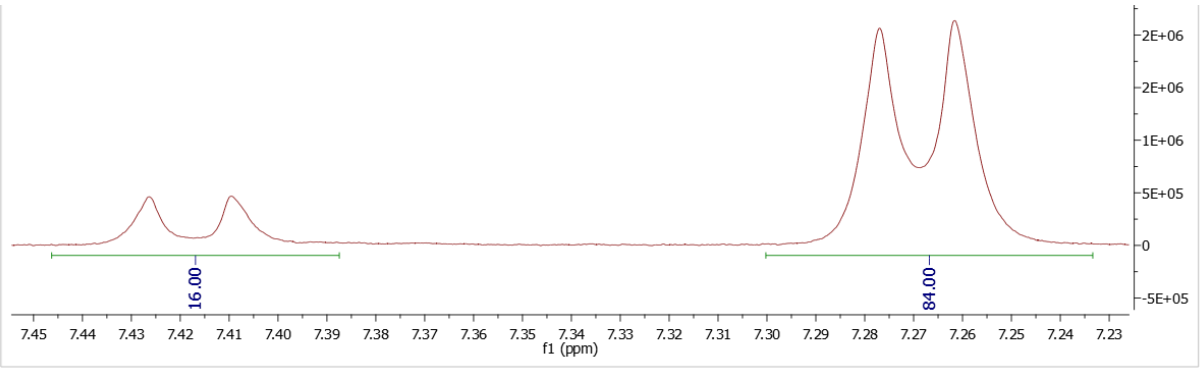

Figure 7.3.43. Expansion in the aromatic region of the ^{1}H NMR spectrum (DMSO-d_6, 300 K) of an equilibrium mixture of *trans* and *cis*-**36** (1 mM) after irradiation at 590 nm (10 min irradiation after PSS 365).

7.3.5.10. Compound 71

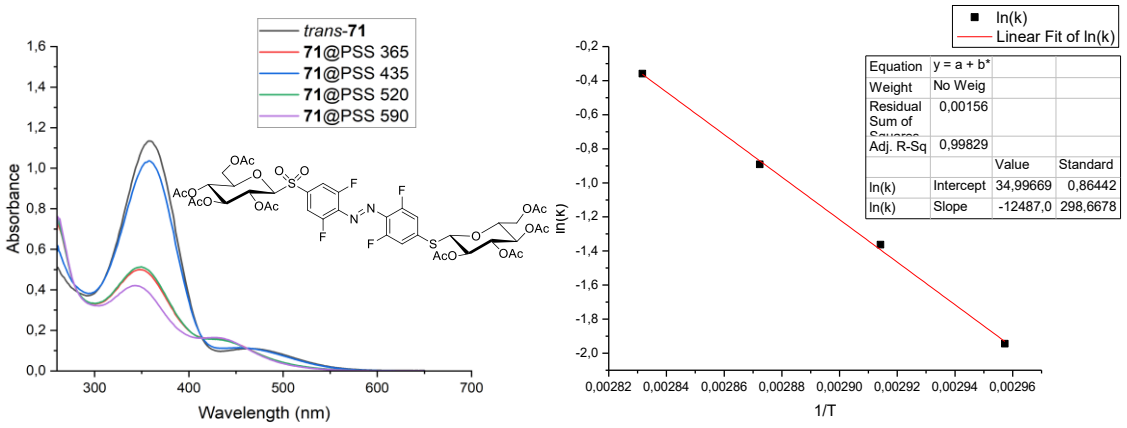

Figure 7.3.44. Left: UV-vis spectra of molecule **71** at 25 °C in DMSO (50 µM) in the *trans* state (black line), and after 2 min irradiation at 365 nm (red line), 435 nm (blue line), 520 nm (green line), and 10 min irradiation at 590 nm (violet line); Right: Linearized Arrhenius plot ln (k) = f(1/T) for compound **71**; the ordinate at the origin gives the natural logarithm of the pre-exponential factor ln*A* and the slope gives $\frac{Ea}{R}$.

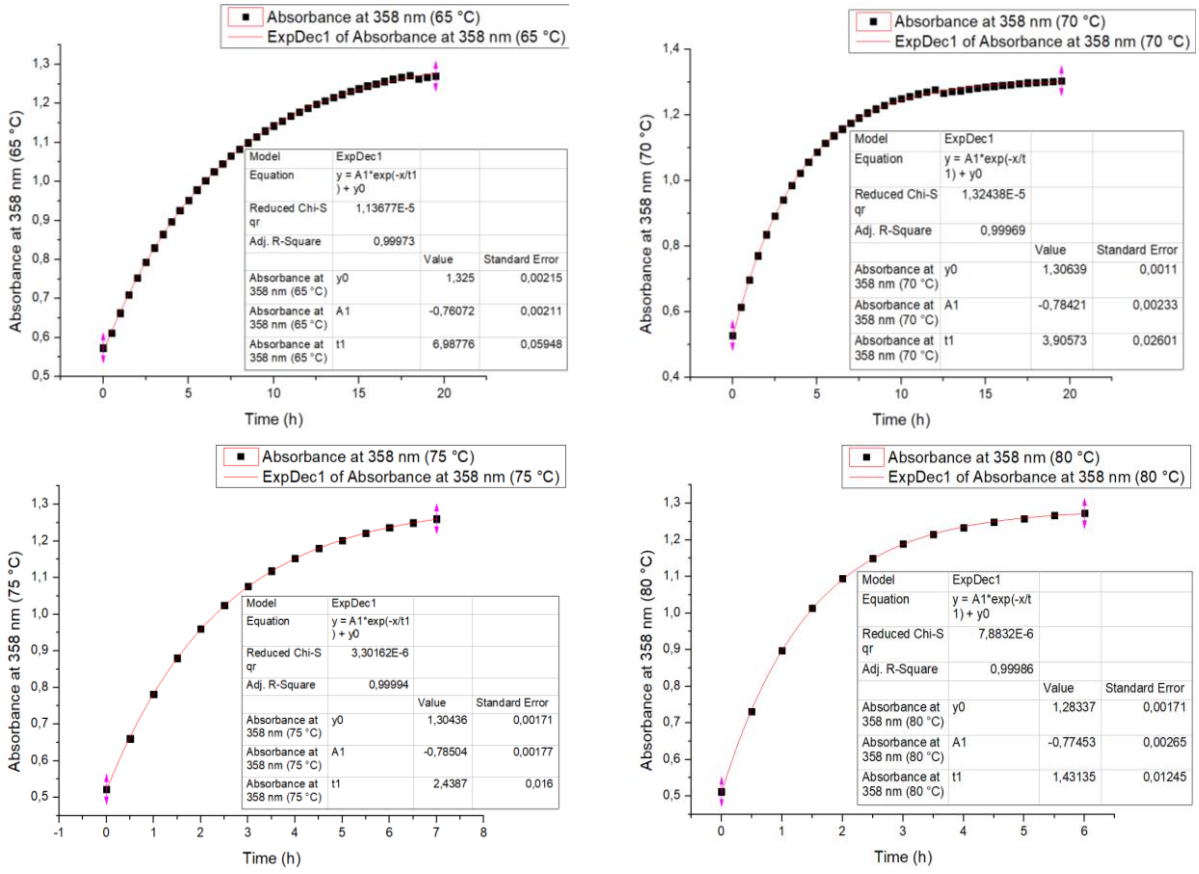

Figure 7.3.45. Exponential growth of the absorbance at 358 nm of a *cis*/*trans* mixture of **71** after irradiation at 365 nm in DMSO (50 µM) at 65, 70, 75 and 80 °C; The rate constant at each temperature is given by: $k_T = 1/t_1$.

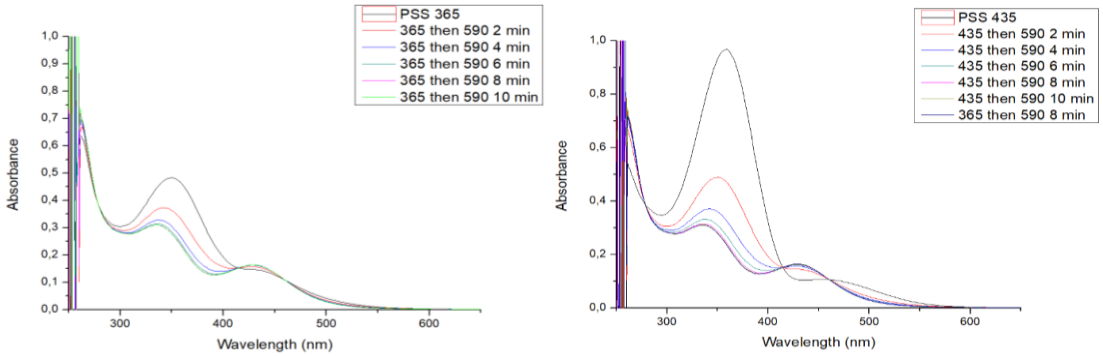

Figure 7.3.46. UV-vis analysis of the time required to reach the PSS 590 nm at 25 °C in DMSO (50 µM) starting from the *cis*/*trans* mixture of **70** at PSS 365 nm (left), and starting from the *cis*/*trans* mixture of **70** at PSS 435 nm (right).

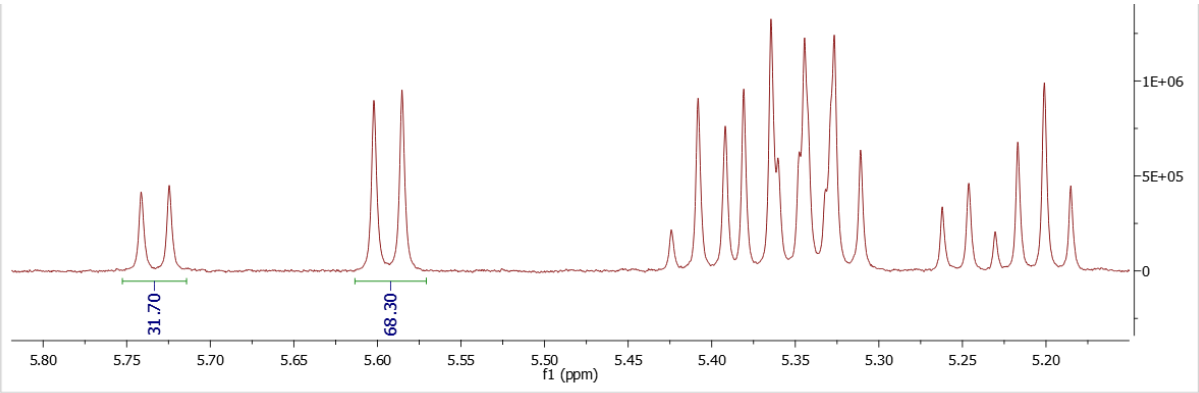

Figure 7.3.47. Expansion in the carbohydrate region of the ^{1}H NMR spectrum (DMSO-d_6, 300 K) of an equilibrium mixture of *trans* and *cis*-**71** (1 mM) after irradiation at 365 nm (2 min).

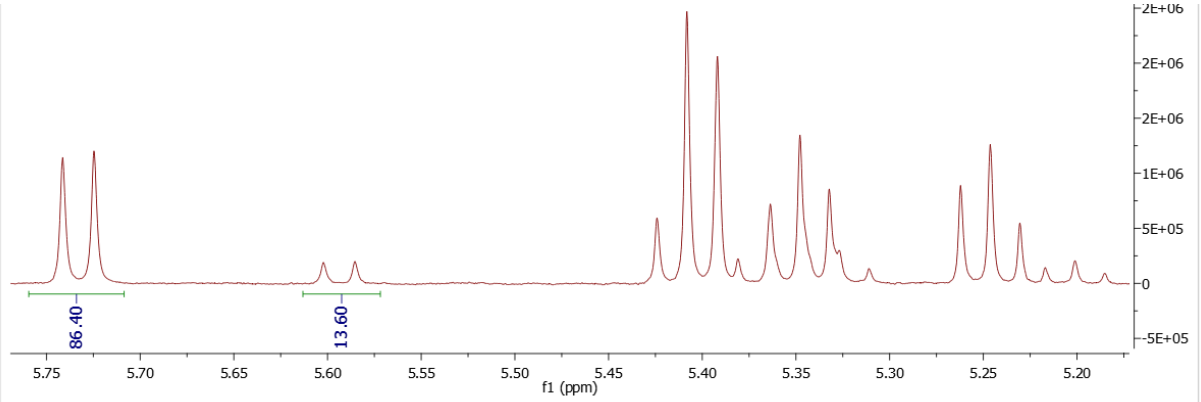

Figure 7.3.48. Expansion in the carbohydrate region of the ^{1}H NMR spectrum (DMSO-d_6, 300 K) of an equilibrium mixture of *trans* and *cis*-**71** (1 mM) after irradiation at 435 nm (2 min).

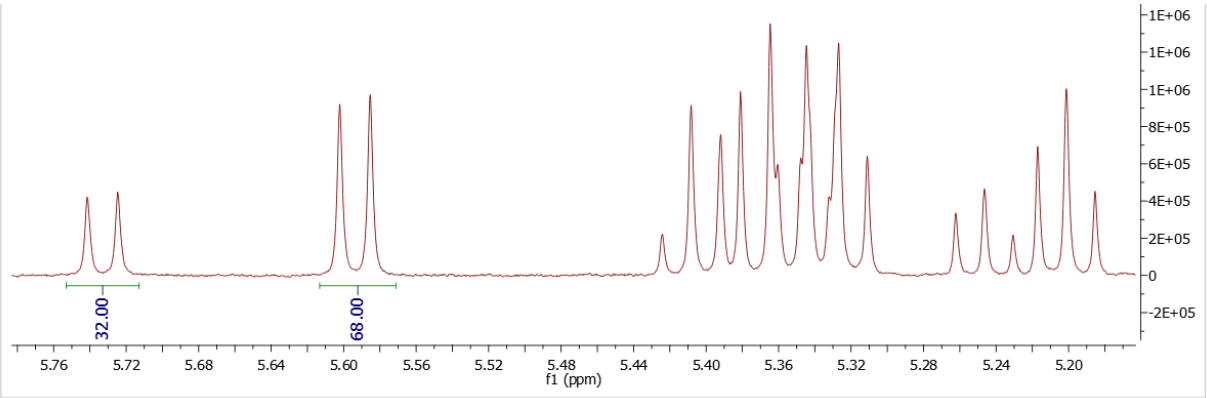

Figure 7.3.49. Expansion in the carbohydrate region of the ^{1}H NMR spectrum (DMSO-d_6, 300 K) of an equilibrium mixture of *trans* and *cis*-**71** (1 mM) after irradiation at 520 nm (2 min).

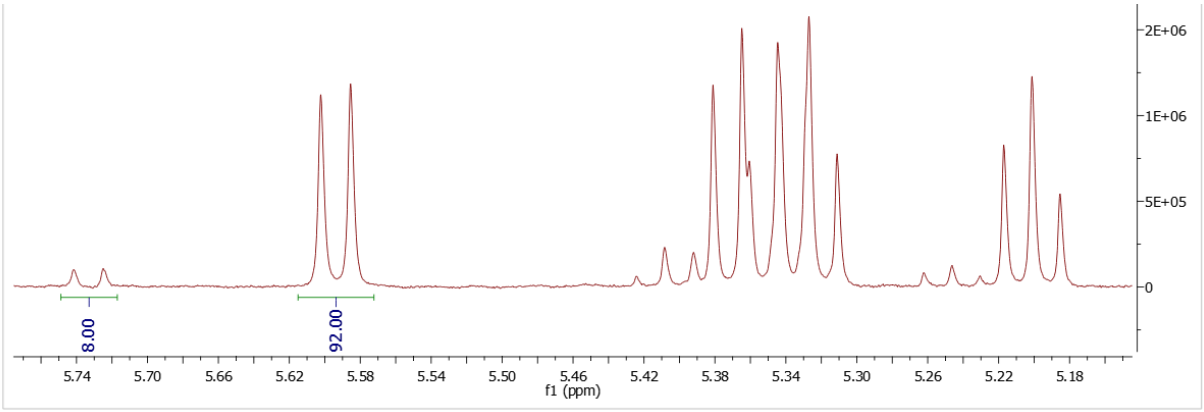

Figure 7.3.50. Expansion in the aromatic region of the ^{1}H NMR spectrum (DMSO-d_6, 300 K) of an equilibrium mixture of *trans* and *cis*-**71** (1 mM) after irradiation at 590 nm (14 min after PSS 365).

7.3.5.11. Compound 73

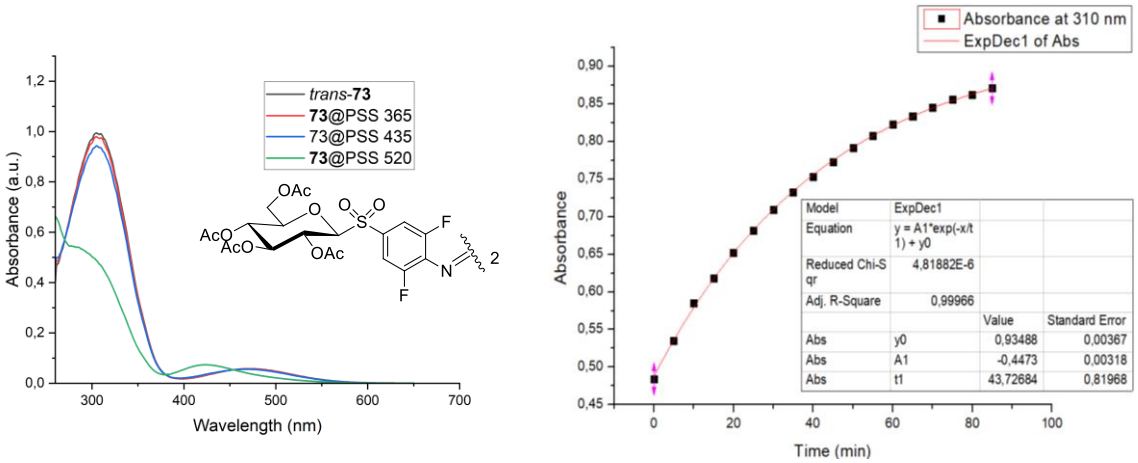

Figure 7.3.51. Left: UV-vis spectra of molecule **73** at 25 °C in DMSO (50 µM) in the *trans* state (black line), and after 2 min irradiation at 365 nm (red line), and 435 nm (blue line), and 520 nm (green line); Right: Exponential growth of the absorbance at 310 nm of a *cis*/*trans* mixture of **73** after irradiation at 365 nm in DMSO (50µM) at 40 °C; The rate constant is given by: $k = 1/t_1$.

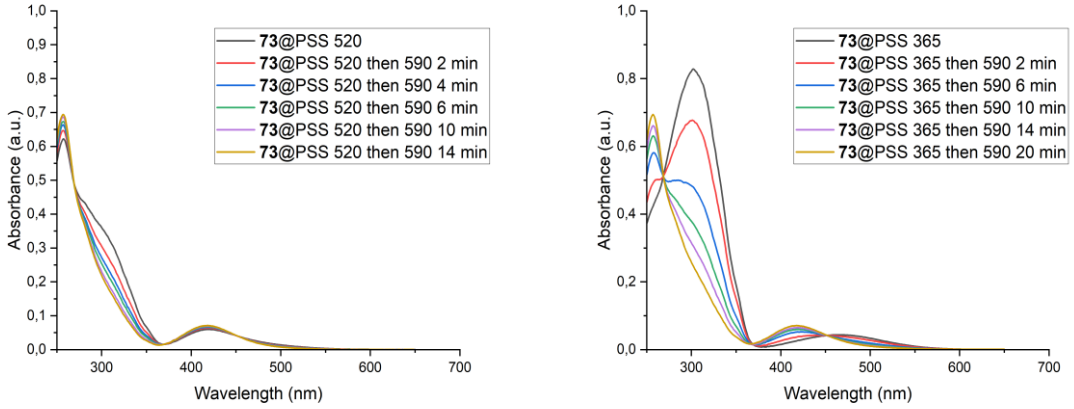

Figure 7.3.52. UV-vis analysis of the time required to reach the PSS 590 nm starting from the *cis*/*trans* mixture of **73** in MeCN (50 µM) at PSS 520 nm (left), and starting from the *cis*/*trans* mixture of **73** in MeCN (50 µM) at PSS 365 nm (right).

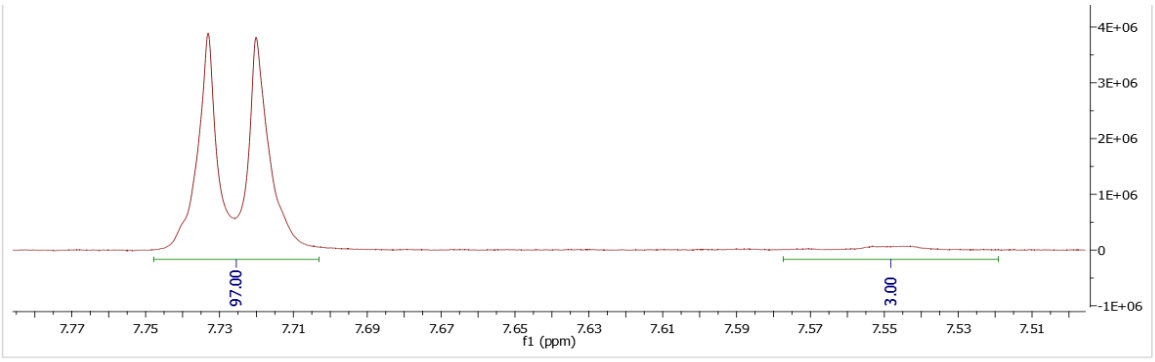

Figure 7.3.53. Expansion in the aromatic region of the ^{1}H NMR spectrum (MeCN-d_3, 300 K) of an equilibrium mixture of *trans* and *cis*-**73** (1mM) after irradiation at 365 nm (2 min).

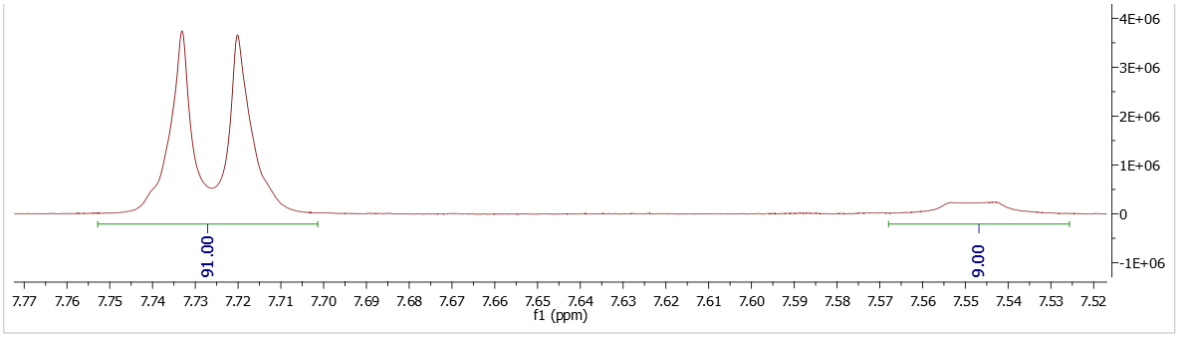

Figure 7.3.54. Expansion in the aromatic region of the ^{1}H NMR spectrum (MeCN-d_3, 300 K) of an equilibrium mixture of *trans* and *cis*-**73** (1mM) after irradiation at 435 nm (2 min).

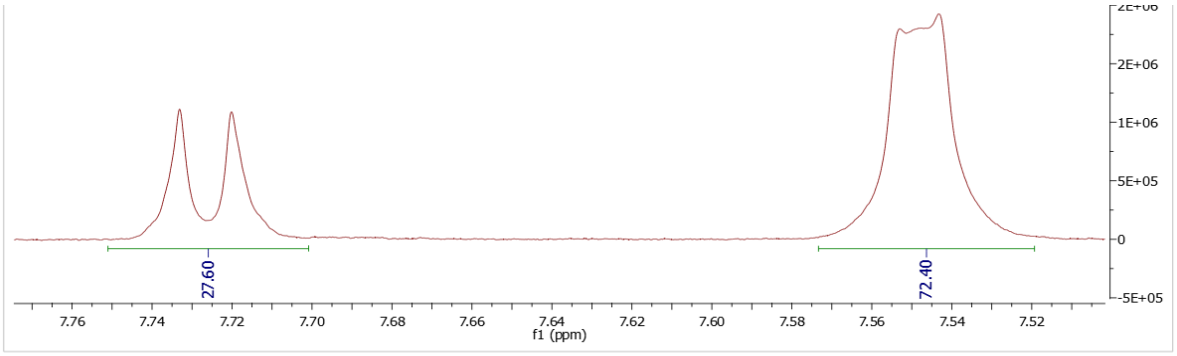

Figure 7.3.55. Expansion in the aromatic region of the ^{1}H NMR spectrum (MeCN-d_3, 300 K) of an equilibrium mixture of *trans* and *cis*-**73** (1mM) after irradiation at 520 nm (2 min).

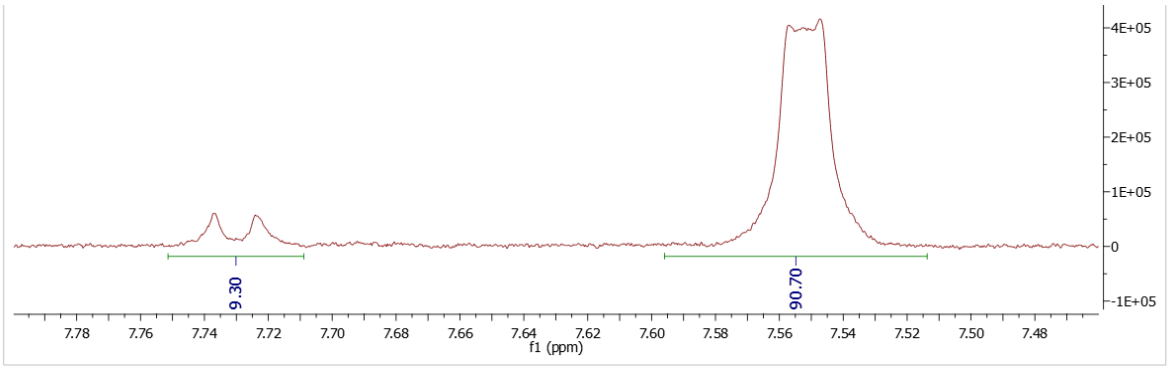

Figure 7.3.56. Expansion in the aromatic region of the ^{1}H NMR spectrum (MeCN-d_3, 300 K) of an equilibrium mixture of *trans* and *cis*-**73** (1mM) after irradiation at 590 nm (20 min irradiation after PSS 520).

Compound 41

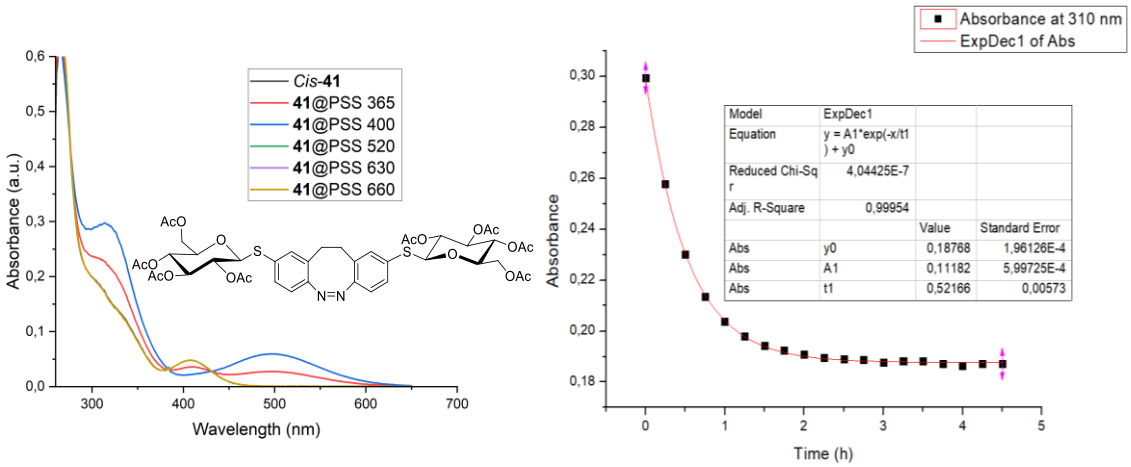

Figure 7.3.57. Left: UV-vis spectra of molecule **41** at 25 °C in DMSO (50 µM) in the *cis* state (black line), and after 2 min irradiation at 365 nm (red line), 400 nm (blue line), and 30 s irradiation at 520 nm (green line), 630 nm (violet line) and 660 nm (ochre line); Right: Exponential decay of the absorbance at 310 nm of a *cis*/*trans* mixture of **41** after irradiation at 400 nm in DMSO (50µM) at 40 °C; The rate constant is given by: $k = 1/t_1$.

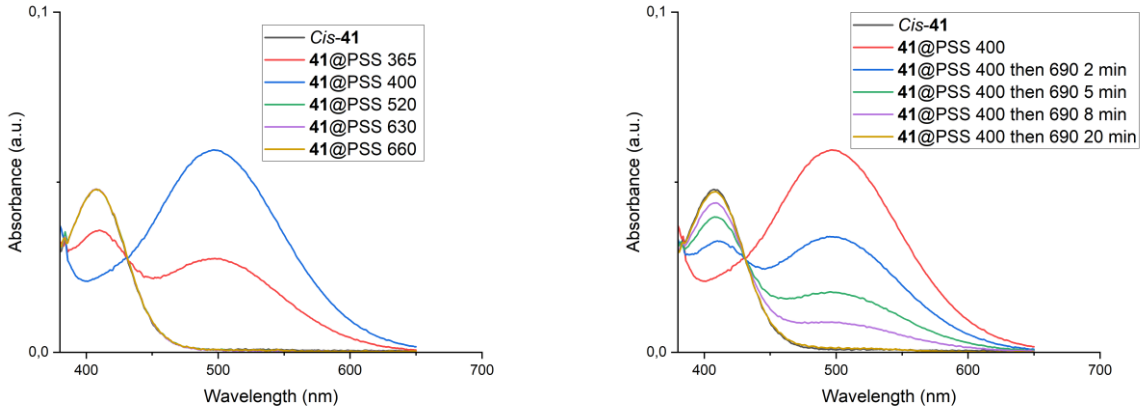

Figure 7.3.58. Left: Zoom in the n→π* region of the UV-vis spectra of **41** at different PSS; Right: UV-vis analysis in the n→π* region of the time required to reach the PSS 690 nm starting from the *cis*/*trans* mixture of **41** in DMSO (50 µM, 25 °C) at PSS 400 nm.

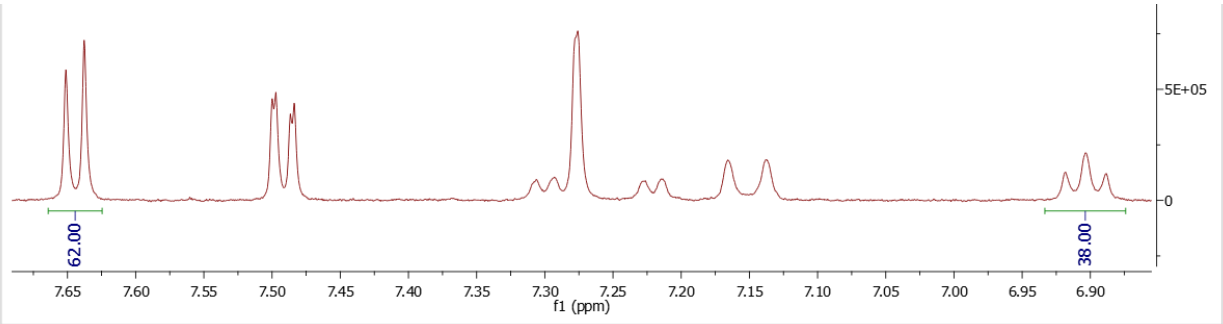

Figure 7.3.59. Expansion in the aromatic region of the ^{1}H NMR spectrum (DMSO-d_6, 300 K) of an equilibrium mixture of *trans* and *cis*-**41** (1 mM) after irradiation at 365 nm (2 min).

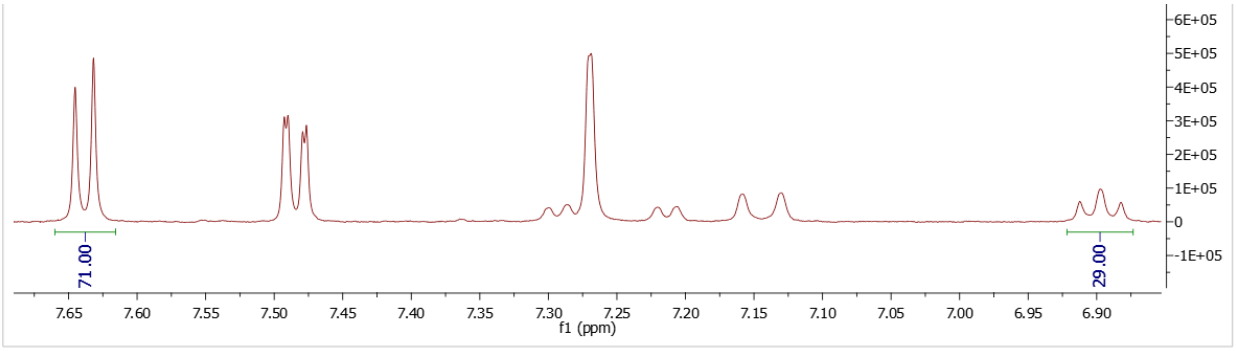

Figure 7.3.60. Expansion in the aromatic region of the ^{1}H NMR spectrum (DMSO-d_6, 300 K) of an equilibrium mixture of *trans* and *cis*-**41** (1 mM) after irradiation at 400 nm (2 min).

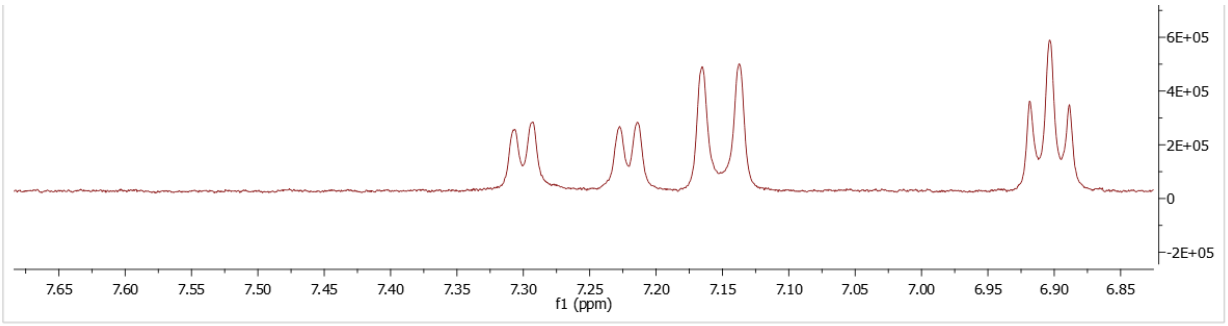

Figure 7.3.61. Expansion in the aromatic region of the ^{1}H NMR spectrum (DMSO-d_6, 300 K) of an equilibrium mixture of *trans* and *cis*-**41** (1 mM) after irradiation at 520 nm (2 min).

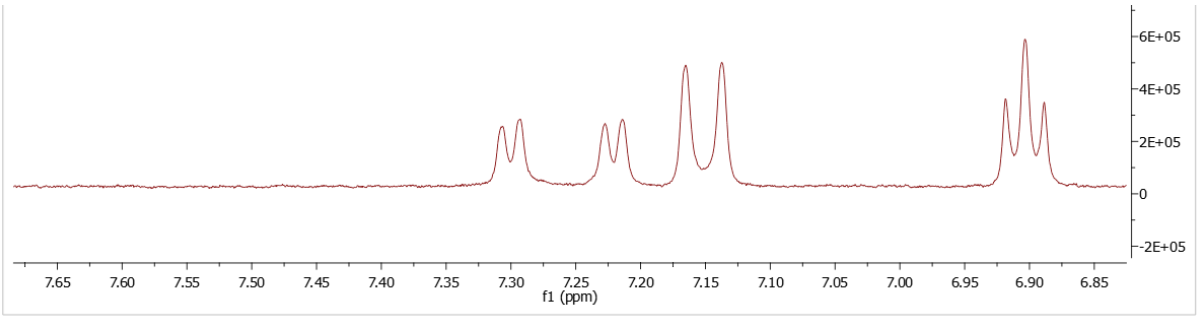

Figure 7.3.62. Expansion in the aromatic region of the ^{1}H NMR spectrum (DMSO-d_6, 300 K) of an equilibrium mixture of *trans* and *cis*-**41** (1 mM) after irradiation at 590 nm (2 min irradiation after PSS 365).

7.3.6. Orthogonal switching experiments

7.3.6.1. Orthogonal switching with a mixture of 35 and 73

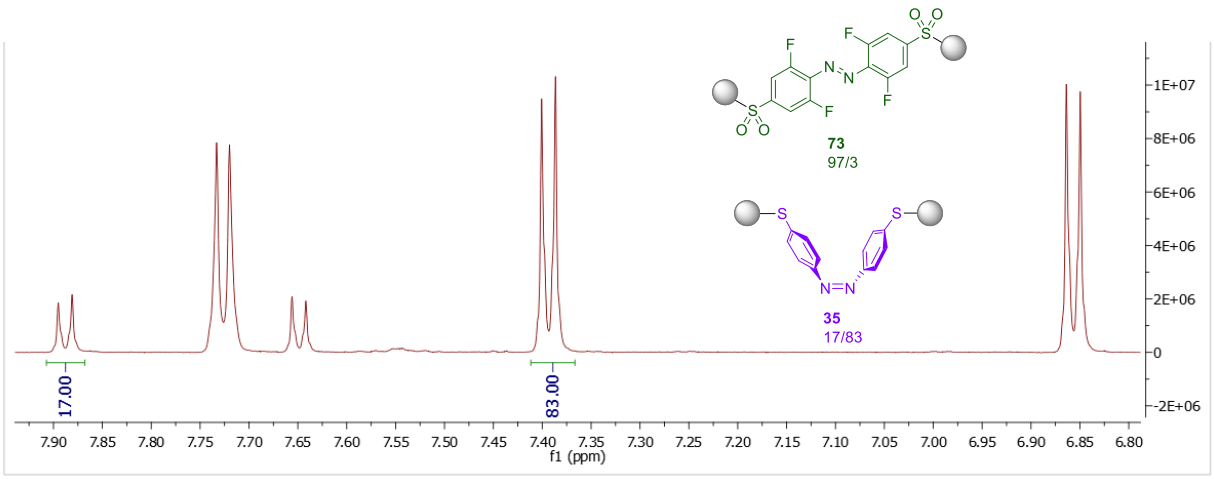

Figure 7.3.63. Expansion in the aromatic region of the ^{1}H NMR spectrum of an equilibrium mixture of **35** and **73** in d_3-MeCN (500 µM) after irradiation at 365 nm (2 min), with integration of the proportion of *trans* and *cis*-**35**.

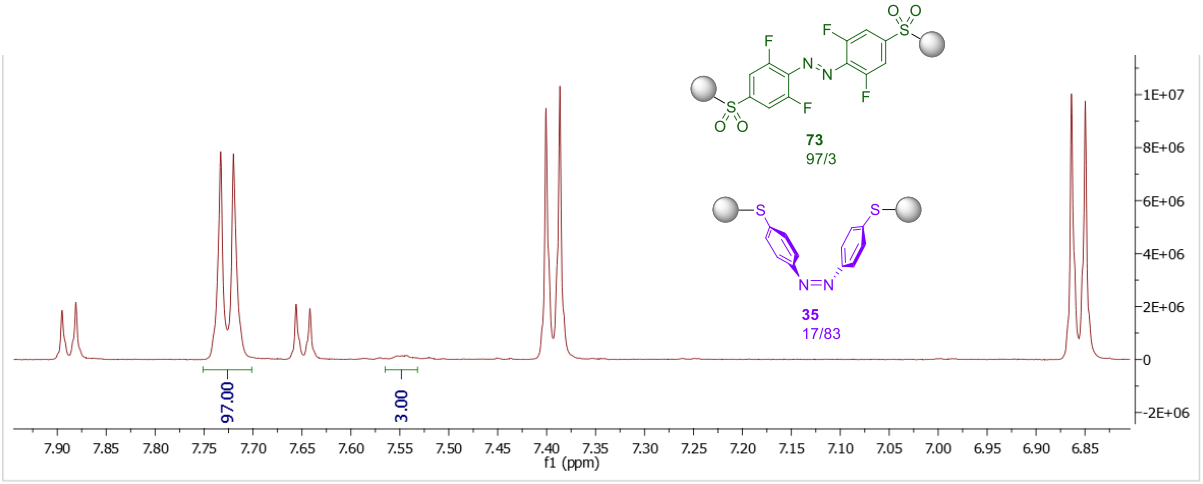

Figure 7.3.64. Expansion in the aromatic region of the ^{1}H NMR spectrum of an equilibrium mixture of **35** and **73** in d_3-MeCN (500 µM) after irradiation at 365 nm (2 min), with integration of the proportion of *trans* and *cis*-**73**.

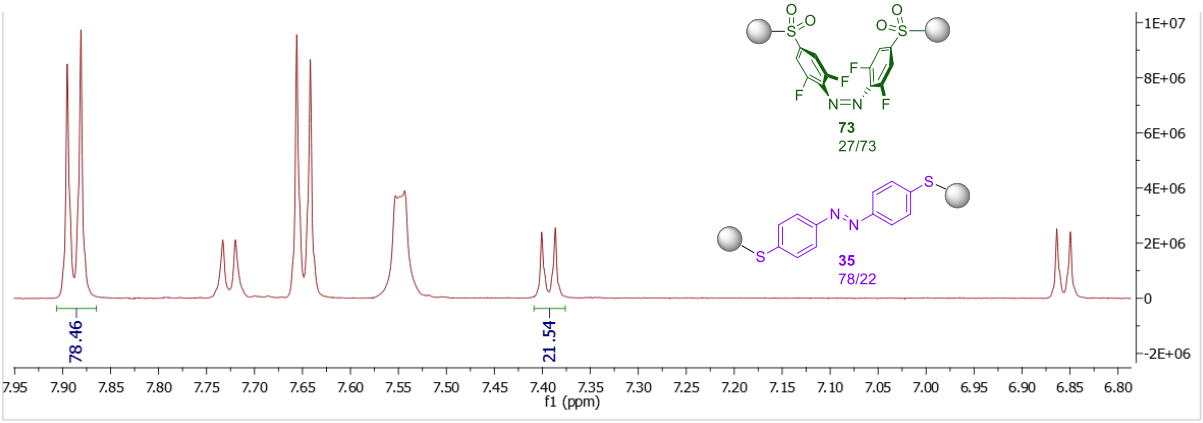

Figure 7.3.65. Expansion in the aromatic region of the ^{1}H NMR spectrum of an equilibrium mixture of **35** and **73** in d_3-MeCN (500 µM) after irradiation at 520 nm (2 min), with integration of the proportion of *trans* and *cis*-**35**.

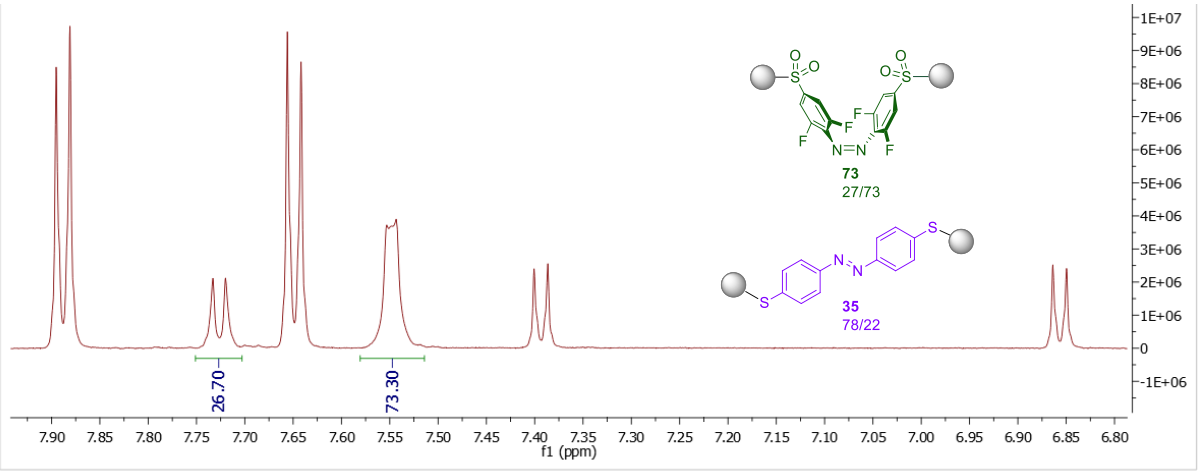

Figure 7.3.66. Expansion in the aromatic region of the ^{1}H NMR spectrum of an equilibrium mixture of **35** and **73** in d_3-MeCN (500 µM) after irradiation at 520 nm (2 min), with integration of the proportion of *trans* and *cis*-**73**.

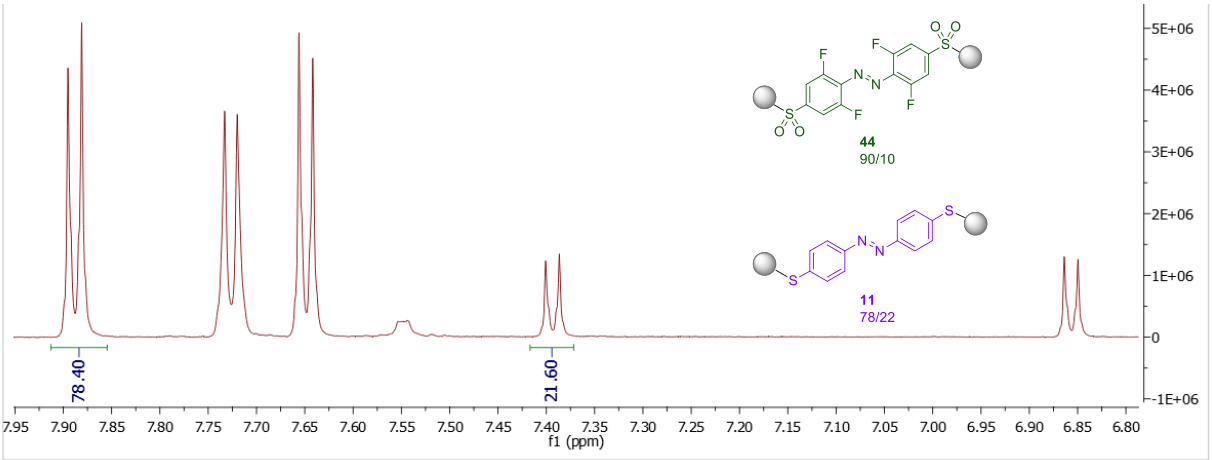

Figure 7.3.67. Expansion in the aromatic region of the ^{1}H NMR spectrum of an equilibrium mixture of **35** and **73** in d_3-MeCN (500 µM) after irradiation at 435 nm (2 min), with integration of the proportion of *trans* and *cis*-**35**.

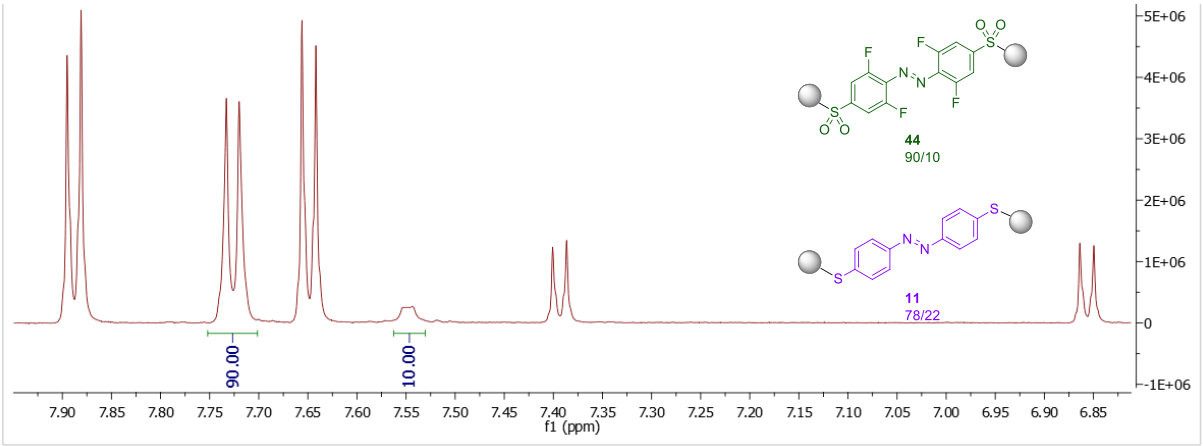

Figure 7.3.68. Expansion in the aromatic region of the ^{1}H NMR spectrum of an equilibrium mixture of **35** and **73** in d_3-MeCN (500 µM) after irradiation at 435 nm (2 min), with integration of the proportion of *trans* and *cis*-**73**.

7.3.6.2. Orthogonal switching with a mixture of 41 and 73

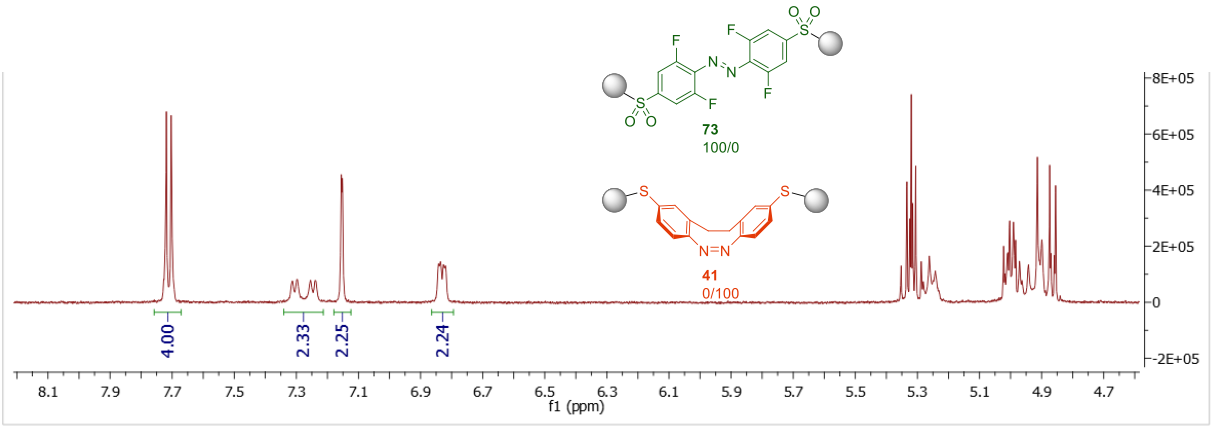

Figure 7.3.69. Expansion in the aromatic region of the ^{1}H NMR spectrum of a mixture of **17** and **44** in d_3-MeCN (500 µM) in the ground state.

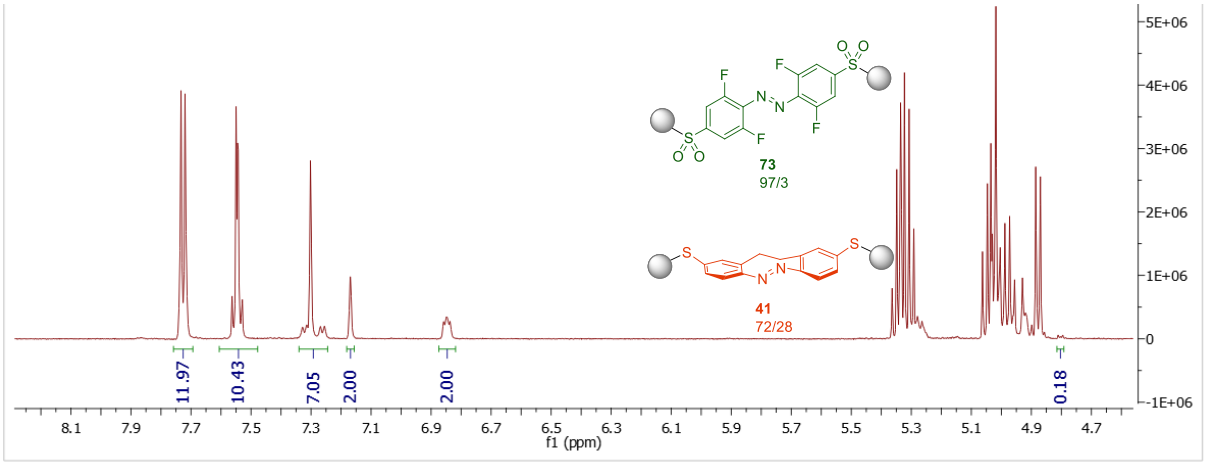

Figure 7.3.70. Expansion in the aromatic region of the ^{1}H NMR spectrum of an equilibrium mixture of **41** and **73** in d_3-MeCN (500 µM) after irradiation at 400 nm (2 min), with integration of the proportion of each isomer. For *trans*-**41**: (7.05-2)/7.05 = 0.72 = 72%; for *cis*-**73**: (0.18x2)/(11.97+0.36) = 0.029 = 2.9%.

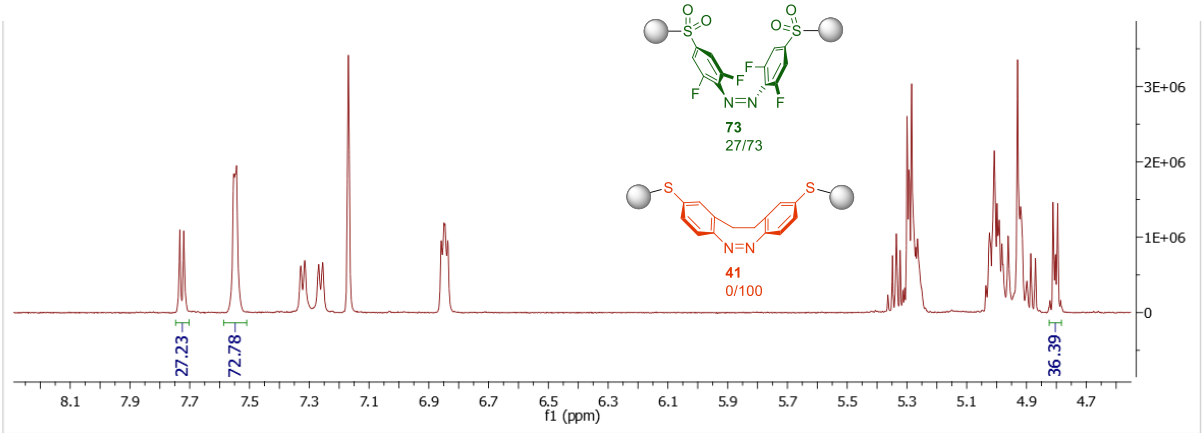

Figure 7.3.71. Expansion in the aromatic region of the ^{1}H NMR spectrum of an equilibrium mixture of **41** and **73** in d_3-MeCN (500 µM) after irradiation at 520 nm (2 min), with integration of the proportion *trans* and *cis* **73**. Note that *cis*-**41** was quantitatively recovered.

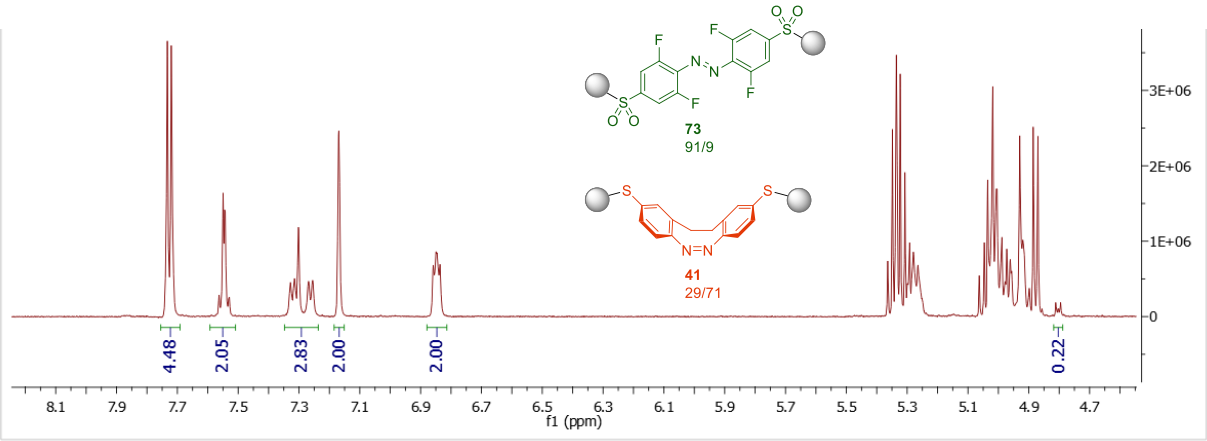

Figure 7.3.72. Expansion in the aromatic region of the ^{1}H NMR spectrum of an equilibrium mixture of **41** and **73** in d_3-MeCN (500 µM) after irradiation at 435 nm (2 min), with integration of the proportion of each isomer. For *trans*-**41**: (2.83-2)/2.83 = 0.29 = 29%; for *cis*-**73**: (0.22x2)/(4.48+0.44) = 0.089 = 8.9%.

7.4. Synthesis of AB-glycophanes

7.4.1. Macrocyclization *via* thiourea bridging

General procedure: The di-isothiocyanate **1** (20 mg, 22.9 µmol, 1 eq)[268e] was dissolved in DMSO (1 mM) and the solution was irradiated at 365 nm for 10 min. Then was added a DMSO solution (100 mM, 1.05 eq) of the diamine dropwise at RT. The mixture was stirred for 2 h and then diluted with EtOAc, washed with water (2x) and brine (2x), and then the organics were dried over $MgSO_4$ and concentrated in *vacuo*. Column chromatography (cyclohexane:EtOAc) afforded the pure macrocycle.

Macrocycle (74)

Macrocycle **74** (17.8 mg, 18.8 µmol), was isolated in 82% yield as a yellow solid. $[\alpha]^{20}_D$ = +405 (*c* = 0.1 in $CHCl_3$); ^{1}H NMR (500 MHz, DMSO) δ = 7.75 (d, ^3J = 8.9 Hz, 4H, 4Ar-H_{ortho}), 7.47 (bs, 2H, 2NH), 7.26 (bs, 2H, 2NH), 7.15 (d, ^3J = 8.9 Hz, 4H, 4Ar-H_{meta}), 5.51 (bs, 2H, H-1), 5.44 (at, $^3J_{3,2}$ = 9.4 Hz, $^3J_{3,4}$ = 9.6 Hz, 2H, H-3), 5.14 (dd, $J_{2,3}$ = 9.4 Hz, $J_{2,1}$ = 8.2 Hz, 2H, H-2), 4.88 (at, $^3J_{4,3}$ = 9.6 Hz, $^3J_{4,5}$ = 9.5 Hz, 2H, H-4), 4.23-4.07 (m, 2H, H-5), 3.97-3.81 (m, 2H, H-6a), 3.29-3.13 (m, 6H, H-6b, 2N-CH_2), 2.09 (s, 6H, CH_3CO), 2.05 (s, 6H, CH_3CO), 1.99 (s, 6H, CH_3CO), 1.83-1.66 (m, 2H, NCH_2-C$\underline{H}_2$) ppm; ^{13}C NMR (126 MHz, DMSO) δ = 169.5, 169.16 (6C, 6$CH_3\underline{C}O$), 157.5 (2C, 2Ar-C_{para}), 147.8 (2C, 2Ar-C_{ipso}), 123.7 (4C, 4Ar-C_{ortho}), 118.4 (4C, 4Ar-C_{meta}), 97.0 (C-1), 72.2 (C-3), 71.0 (C-5), 70.7 (C-2), 70.6 (C-4), 44.2 (C-6), 28.0 (N$\underline{C}H_2$), 22.1 (NCH_2-$\underline{C}H_2$), 20.2 (6C, 6$\underline{C}H_3CO$) ppm; ESI HRMS: *m/z*: calcd for $C_{41}H_{50}O_{16}N_6S_2$ + Na^+: 969.26141 [M + H^+] found: 969.26169.

Macrocycle (75)

Macrocycle **75** (15.6 mg, 16.3 µmol) was isolated in 71% yield as a yellow solid. $[\alpha]^{20}_D$ = +365 (*c* = 0.1 in $CHCl_3$); ^{1}H NMR (500 MHz, DMSO) δ = 7.75 (d, ^3J = 8.9 Hz, 4H, 4Ar-H_{ortho}), 7.54 (bs, 2H, 2NH), 7.31 (bs, 2H, 2NH), 7.17 (bs, 4H, 4Ar-H_{meta}), 5.47 (bs, 2H, H-1), 5.42 (at, $^3J_{3,2}$ = 9.3 Hz, $^3J_{3,4}$ = 9.6 Hz, 2H, H-3), 5.13 (dd, $^3J_{2,3}$ = 9.3 Hz, $^3J_{2,1}$ = 8.1 Hz, 2H, H-2), 4.87 (at, $^3J_{4,3}$ = 9.6 Hz, $^3J_{4,5}$ = 9.5 Hz, 2H, H-4), 4.25 (bs, 2H, H-5), 3.86 (bs, 2H, H-6a), 3.40-3.12 (m, 6H, H-6b, 2N-CH_2), 2.07 (s, 6H, CH_3CO), 2.04 (s, 6H, CH_3CO), 1.98 (s, 6H, CH_3CO), 1.52 (bs, 4H, NCH_2-C$\underline{H}_2$-C$\underline{H}_2$-CH_2N) ppm; ^{13}C NMR (126 MHz, DMSO) δ = 169.8, 169.7, 169.4 (6C, 6$CH_3\underline{C}O$), 158.0 (2C, 2Ar-C_{para}), 147.9 (2C, 2Ar-C_{ipso}), 123.8 (4C, 4Ar-C_{ortho}), 118.5 (4C, 4Ar-C_{meta}), 97.2 (C-1), 72.3 (C-3), 70.9 (C-5), 70.8 (4C, C-2, C-4), 44.5 (C-6), 26.3 (N$\underline{C}H_2$), 20.6, 20.5, 20.4 (6C, 6$\underline{C}H_3CO$) ppm; ESI HRMS: *m/z*: calcd for $C_{42}H_{52}O_{16}N_6S_2$ + H^+: 961.29453 [M + H^+] found: 961.29440.

Macrocycle (76)

Macrocycle **76** (11.3 mg, 12.1 µmol) was isolated in 53% yield as a yellow solid. $[\alpha]^{20}_D$ = +1178 (*c* = 0.1 in $CHCl_3$); ^{1}H NMR (500 MHz, DMSO) δ = 7.75 (d, ^3J = 8.9 Hz, 4H, 4Ar-H_{ortho}), 7.33 (bs, 2H, 2NH), 7.16 (d, ^3J = 8.9 Hz, 4H, 4Ar-H_{meta}), 7.09 (bs, 2H, 2NH), 5.46 (d, $^3J_{1,2}$ = 8.1 Hz, 2H, H-1), 5.42 (at, $^3J_{3,2}$ = 9.4 Hz, $^3J_{3,4}$ = 9.4 Hz), 5.12 (dd, $^3J_{2,3}$ = 9.4 Hz, $^3J_{2,1}$ = 8.1 Hz, 2H, H-2), 4.85 (at, $^3J_{4,3}$ = 9.4 Hz, $^3J_{4,5}$ = 9.6 Hz, 2H, H-4), 4.14-4.05 (m, 2H, H-5), 3.69-3.58 (m, 2H, H-6a), 3.45-3.27 (m, 4H, H-6b + N-CH_2), 3.26-3.13 (m, 2H, N-CH_2), 2.09 (s, 6H, CH_3CO), 2.03 (s, 6H, CH_3CO), 1.99 (s, 6H, CH_3CO) ppm; ^{13}C NMR (126 MHz, DMSO) δ = 169.5, 169.2 (6C, 6$CH_3\underline{C}O$), 157.1 (2C, 2Ar-C_{para}), 148.0 (2C, 2Ar-C_{ipso}), 123.6 (4C, 4Ar-C_{ortho}), 119.5 (4C, 4Ar-C_{meta}), 97.2 (C-1), 72.3 (C-3), 71.0 (C-4), 70.7, 70.8 (C-2, C-5), 44.2 (C-6), 42.6 (N$\underline{C}H_2$), 20.4, 20.3 (6C, 6$\underline{C}H_3CO$) ppm; ESI HRMS: *m/z*: calcd for $C_{40}H_{49}O_{16}N_6S_2$ + H^+: 933.26410 [M + H^+] found: 961.26172.

Macrocycle (77)

Macrocycle **77** (12.5 mg, 12.7 µmol) was isolated after 5 days of reaction in 56% yield as a yellow solid. $[\alpha]^{20}_{D}$ = +527 (*c* = 0.1 in $CHCl_3$); ^{1}H NMR (500 MHz, DMSO) δ = 9.66 (bs, 2H, 2Ar-NH), 7.70 (bs, 2H, 2NH), 7.60-7.48 (m, 8H, 4Ar-H_{ortho} + C_6H_4), 7.13 (d, ^3J = 9.0 Hz, 4H, 4Ar-H_{meta}), 5.54-5.43 (m, 4H, H-1, H-3), 5.16 (dd, $^3J_{2,3}$ = 9.5 Hz, $^3J_{2,1}$ = 8.2 Hz, 2H, H-2), 4.93 (at, $^3J_{4,5}$ = 9.5 Hz, 2H, H-4), 4.60-4.48 (m, 2H, H-5), 3.98-3.86 (m, 2H, H-6a), 3.37-3.29 (m, 2H, H-6b), 2.08 (s, 6H, CH_3CO), 2.07 (s, 6H, CH_3CO), 2.00 (s, 6H, CH_3CO) ppm; ^{13}C NMR (126 MHz, DMSO) δ = 169.6, 169.5, 169.2 (6C, 6$CH_3\underline{C}O$), 157.9 (2C, 2Ar-C_{para}), 147.4 (2C, 2Ar-C_{ipso}), 135.4 (2C, 2Ar-C_{para} C_6H_4), 123.8 (4C, 4Ar-C_{ortho}), 121.3 (4C, C_6H_4), 117.7 (2C, 2Ar-C_{meta}), 97.3 (C-1), 72.3 (C-3), 71.2 (C-4), 70.5 (C-2), 69.7 (C-5), 43.8 (C-6) ppm; ESI HRMS: *m/z*: calcd for $C_{44}H_{48}O_{16}N_6S_2$ + H^+: 981.26410 [M + H^+] found: 981.26280.

7.4.2. Macrocyclization *via* palladium-catalyzed thioarylation

Compounds **17**, **81**, **82**, **83**, **89** and **90** were synthesized according to known procedures.[230e,354,358] To avoid overloading the document, and because their characterization was incomplete, compounds **84**-**88** and **96**-**100** are not described.

DMAB-Dithioacetate (87´)

To thiol **90** (240 mg, 630 µmol, 2eq) and Et_3N (87 µL, 624 µmol, 1.98 eq) in CH_2Cl_2 (3.15 mL) was added the azobenzene **83** (116 mg, 315 µmol, 1 eq) at RT. The mixture was stirred 15 min, then it was directly purified by column chromatography (cyclohexane:EtOAc 3:2 to 1:1), to afford the desired compound **87´** (278 mg, 287 µmol) in 91% yield as an orange solid. ^{1}H NMR (500 MHz, $CDCl_3$) δ = 7.88 (d, ^3J = 8.4 Hz, 4H, 4Ar-H_{ortho}), 7.48 (d, ^3J = 8.4 Hz, 4H, 4Ar-H_{meta}), 5.12 (at, $^3J_{3,4}$ = 9.5 Hz, $^3J_{3,2}$ = 9.1 Hz, 2H, H-3), 5.07 (at, $^3J_{2,1}$ = 9.9 Hz, $^3J_{2,3}$ = 9.1 Hz, 2H, H-2), 4.98 (at, $^3J_{4,3}$ = 9.5 Hz, $^3J_{4,5}$ = 9.6 Hz, 2H, H-4), 4.31 (d, $^3J_{1,2}$ = 9.9 Hz, 2H, H-1), 4.02 (d, ^2J = 12.9 Hz, 2H, CH_2a), 3.88 (d, ^2J = 12.9 Hz, 2H, CH_2b), 3.56 (ddd, $^3J_{5,4}$ = 9.6 Hz, $^3J_{5,6b}$ = 7.1 Hz, $^3J_{5,6a}$ = 3.0 Hz, 2H, H-5), 3.27 (dd, $^2J_{6a,6b}$ = 14.3 Hz, $^3J_{6a,5}$ = 3.0 Hz, 2H, H-6a), 3.06 (dd, $^2J_{6b,6a}$ = 14.3 Hz, $^3J_{6b,5}$ = 7.1 Hz, 2H, H-6b), 2.37 (s, 6H, SC(O)CH_3), 2.07 (s, 6H, OC(O)CH_3), 2.02 (s, 6H, OC(O)CH_3), 1.98 8s, 6H, OC(O)CH_3) ppm; ^{13}C NMR (126 MHz, $CDCl_3$) δ = 194.6 (2C, S$\underline{C}$(O)CH_3), 170.1, 169.8, 169.5 (6C, 6O$\underline{C}$(O)CH_3), 151.8 (2C, Ar-C_{ipso}), 140.2 (2C, Ar-C_{para}), 129.9 (4C, Ar-C_{meta}), 123.1 (4C, Ar-C_{ortho}), 81.7 (C-1), 77.0 (C-5), 73.6 (C-3), 70.5 (C-4), 69.8 (C-2), 33.3 ($\underline{C}H_2$), 30.5 (SC(O)CH_3), 30.4 (C-6), 20.6 (6C, 6OC(O)CH_3) ppm; ESI HRMS: *m/z*: calcd for $C_{42}H_{50}O_{16}N_2S_4$ + NH_4^+ : 984.23814 [M + NH_4^+] found: 984.23468.

DMAB-Dithiol (88´)

To **87´** (225 mg, 233 µmol) in *N*,*N*-dimethylacetamide (2.3 mL) were added Et_3N (32 µL, 233 µmol, 1 eq) and dithiotreitol (215 mg, 1.4 mmol, 6 eq) at RT. The mixture was stirred overnight, then it was diluted with EtOAc, washed twice with HCl 1N, and once with sat. aq. $NaHCO_3$ solution. Then the organics were dried over $MgSO_4$ and concentrated in *vacuo*. Column chromatography (CH_2Cl_2:acetone 98:2 to 96:4) afforded the dithiol **88´** (135 mg, 154 µmol) in 66% yield as an orange solid. ^{1}H NMR (500 MHz, $CDCl_3$) δ = 7.89 (d, ^3J = 8.7 Hz, 4H, 4Ar-H_{ortho}), 7.51 (d, ^3J = 8.7 Hz, 4H, 4Ar-H_{meta}), 5.14 (at, $^3J_{3,4}$ = 9.6 Hz, $^3J_{3,2}$ = 9.0 Hz, 2H, H-3), 5.07 (at, $^3J_{2,1}$ = 10.0 Hz, $^3J_{2,3}$ = 9.0 Hz, 2H, H-2), 5.01 (at, $^3J_{4,5}$ = $^3J_{4,3}$ = 9.6 Hz, 2H, H-4), 4.37 (d, $^3J_{1,2}$ = 10.0 Hz, 2H, H-1), 4.06 (d, ^2J = 13.2 Hz, 2H, CH_2a), 3.90 (d, ^2J = 13.2 Hz, 2H, CH_2b), 3.50 (ddd, $^3J_{5,4}$ = 9.6 Hz, $^3J_{5,6a}$ = 6.5 Hz, $^3J_{5,6b}$ = 3.9 Hz, 2H, H-5), 2.68-2.62 (m, 4H, H-6a, H-6b), 2.03

(s, 6H, CH_3CO), 2.02 (s, 6H, CH_3CO), 1.99 (s, 6H, CH_3CO), 1.73 (dd, $^3J_{SH,6a}$ = 8.0 Hz, $^3J_{SH,6a}$ = 9.1 Hz, 2H, SH) ppm; ^{13}C NMR (126 MHz, $CDCl_3$) δ = 170.1, 169.6, 169.5 (6C, 6O<u>C</u>(O)CH_3), 151.9 (2C, 2Ar-C_{ipso}), 140.3 (2C, 2Ar-C_{para}), 129.9 (4C, 4Ar-C_{meta}), 123.2 (4C, 4Ar-C_{ortho}), 81.9 (C-1), 78.5 (C-5), 73.7 (C-3), 71.0 (C-4), 69.9 (C-2), 33.6 (<u>C</u>H_2), 26.3 (C-6), 20.7, 20.6 (6C, 6OC(O)<u>C</u>H_3) ppm; ESI HRMS: *m/z*: calcd for $C_{38}H_{46}O_{14}N_2S_4 + NH_4^+$: 900.21701 [M + NH_4^+] found: 900.21338.

Macrocycle (91)

The dithiol **88´** (10 mg, 11.3 µmol), the 4,4´-diiodoazobenzene **28** (4.9 mg, 11.3 µmol, 1 eq) and the catalyst PdG3-Xantphos (1 mg, 1.13 µmol, 10 mol%) were charged in a flask and put under vacuum. Meanwhile the solvent (THF) was degassed by bubbling N_2 through. Then, the solvent (4.52 mL, 2.5 mM) was added to the reaction flask under N_2, and then Et_3N (3.2 µL, 22.6 µmol, 2 eq) was added at RT. After 1 h, the reaction was diluted with EtOAc, washed with HCl 1N and brine, and then the organics were dried over $MgSO_4$ and concentrated in *vacuo*. Column chromatography (CH_2Cl_2:acetone 98:2 to 95:5) afforded macrocycle **91** (8.4 mg, 7.92 µmol) in 70% yield as an orange solid. ^{1}H NMR (500 MHz, $CDCl_3$) δ = 8.03 (d, ^3J = 8.8 Hz, 4H, 4Ar-H_{ortho} DSAB), 7.43 (d, ^3J = 8.8 Hz, 4H, 4Ar-H_{meta} DSAB), 7.33 (d, ^3J = 8.3 Hz, 4H, 4Ar-H_{ortho} DMAB), 7.10 (d, ^3J = 8.3 Hz, 4H, 4Ar-H_{meta} DMAB), 5.10-4.98 (m, 6H, H-2, H-3, H-4), 4.02 (d, ^2J = 12.9 Hz, 2H, CH_2a), 3.98 (d, $^3J_{1,2}$ = 9.3 Hz, 2H, H-1), 3.68 (d, ^2J = 12.9 Hz, 2H, CH_2b), 3.63-3.56 (m, 2H, H-5), 3.48-3.41 (m, 2H, H-6a), 3.00 (dd, $^2J_{6b,6a}$ = 15.5 Hz, $^3J_{6b,5}$ = 9.3 Hz, 2H, H-6b), 2.14 (s, 6H, CH_3CO), 1.99 (s, 6H, CH_3CO), 1.96 (s, 6H, CH_3CO) ppm; ^{13}C NMR (126 MHz, $CDCl_3$) δ = 170.1, 169.7, 169.4 (6C, 6O<u>C</u>(O)CH_3), 151.2 (2C, 2Ar-C_{ipso} DMAB), 150.3 (2C, 2Ar-C_{ipso} DSAB), 139.7 (2C, 2Ar-C_{para} DSAB), 139.4 (2C, 2Ar-C_{para} DMAB), 129.9 (4C, 4Ar-C_{meta} DMAB), 126.6 (4C, 4Ar-C_{meta} DSAB), 124.1 (4C, 4Ar-C_{ortho} DSAB), 123.0 (4C, 4Ar-C_{ortho} DMAB), 80.8 (C-1), 74.1 (C-5), 73.7, 72.2, 69.7 (C-2, C-3, C-4), 33.0 (<u>C</u>H_2 DMAB), 32.7 (C-6), 20.8, 20.6 (6C, 6OC(O)<u>C</u>H_3) ppm; ESI HRMS: *m/z*: calcd for $C_{50}H_{53}O_{14}N_4S_4 + H^+$: 1061.24356 [M + H^+] found: 1061.24306.

Macrocycle (92)

The dithiol **88´** (10 mg, 11.3 µmol), the 4,4´-diiodo-2,2´,6,6´-tetrafluoroazobenzene **29** (5.7 mg, 11.3 µmol, 1 eq) and the catalyst PdG3-Xantphos (1 mg, 1.13 µmol, 10 mol%) were charged in a flask and put under vacuum. Meanwhile the solvent (THF) was degassed by bubbling N_2 through. Then, the solvent (2.26 mL, 5 mM) was added to the reaction flask under N_2, and then Et_3N (3.2 µL, 22.6 µmol, 2 eq) was added at RT. After 2 h, the reaction was diluted with EtOAc, washed with HCl 1N and brine, and then the organics were dried over $MgSO_4$ and concentrated in *vacuo*. Column chromatography (CH_2Cl_2:acetone 98:2 to 95:5) afforded macrocycle **92** (7 mg, 6.18 µmol) in 55% yield as a red solid. ^{1}H NMR (500 MHz, DMSO-*d*$_6$) δ = 7.45 (d, ^3J = 8.4 Hz, 4H, 4Ar-H_{ortho} DSAB), 7.39 (d, $^3J_{H,F}$ = 10.7 Hz, 4H, 4Ar-H_{meta} TFAB), 7.21 (d, ^3J = 8.4 Hz, 4H, 4Ar-H_{meta} DSAB), 5.33 (at, $^3J_{3,2}$ = 9.4 Hz, $^3J_{3,4}$ = 9.2 Hz, 2H, H-3), 4.95 (at, $^3J_{4,5}$ = 9.6 Hz, $^3J_{4,3}$ = 9.2 Hz, 2H, H-4), 4.91 (at, $^3J_{2,1}$ = 10.0 Hz, $^3J_{2,3}$ = 9.4 Hz, 2H, H-2), 4.60 (d, $^3J_{1,2}$ = 10.0 Hz, 2H, H-1), 4.04-3.96 (m, 2H, H-5), 3.92 (d, ^2J = 13.0 Hz, 2H, CH_2a), 3.76 (d, ^2J = 13.0 Hz, 2H, CH_2b), 3.74-3.68 (m, 2H, H-6a), 3.13 (dd, $^2J_{6b,6a}$ = 15.5 Hz, $^3J_{6b,5}$ = 9.2 Hz, 2H, H-6b), 2.07 (s, 6H, CH_3CO), 1.95 (s, 6H, CH_3CO), 1.93 (s, 6H, CH_3CO) ppm; ^{13}C NMR (126 MHz, DMSO-*d*$_6$) δ = 169.6, 169.5, 169.2 (6C, 6O<u>C</u>(O)CH_3), 155.3 (dd, $^1J_{C,F}$ = 262.6 Hz, $^3J_{C,F}$ = 4.7 Hz, 4C, 4Ar-C_{ortho} TFAB), 150.3 (2C, 2Ar-C_{ipso} DMAB), 144.2 (t, $^3J_{C,F}$ = 10.7 Hz, 2C, 2Ar-C_{para} TFAB), 140.8 (2C, 2Ar-C_{para} DMAB), 130.0 (4C, 4Ar-C_{meta} DMAB), 127.7 (t, $^2J_{C,F}$ = 8.8 Hz, 2C, 2Ar-C_{ipso} TFAB), 122.4 (4C, 4Ar-C_{ortho} DMAB), 110.6 (d, $^2J_{C,F}$ = 23.7 Hz, 4C, 4Ar-C_{meta} TFAB), 79.3 (C-1), 73.5 (C-5), 72.9 (C-3), 71.3 (C-4), 69.7 (C-2), 31.8 (C-6), 31.7 (<u>C</u>H_2 DMAB), 20.7, 20.4, 20.3 (6C, 6OC(O)<u>C</u>H_3) ppm; ESI HRMS: *m/z*: calcd for $C_{50}H_{49}O_{14}N_4F_4S_4 + H^+$: 1133.20587 [M + H^+] found: 1133.20602.

Macrocycle (78)

To macrocycle **91** (17.1 mg, 16.1 µmol) in CH_2Cl_2:MeOH (4:1, 1.6 mL) was added MeONa (1M in MeOH, 5 µL), at RT. The reaction was stirred for 3 h, then Amberlyte IR 120 H^+ was added, and the mixture was stirred another 10 min. Then it was filtered and concentrated in *vacuo*. Column chromatography (CH_2Cl_2:MeOH 9:1 then MeOH:H_2O 9:1) afforded the macrocycle **78** (12 mg, 14.8 µmol) in 92% yield as an orange solid. $[\alpha]^{20}_D$ = +234 (*c* = 0.2 in DMSO); ^{1}H NMR (500 MHz, DMSO-*d*$_6$) δ = 7.99 (d, ^3J = 8.9 Hz, 4H, 4Ar-H_{ortho} DSAB), 7.54 (d, ^3J = 8.9 Hz, 4H, 4Ar-H_{meta} DSAB), 7.14 (d, ^3J = 8.2 Hz, 4H, 4Ar-H_{ortho} DMAB), 7.07 (d, ^3J = 8.2 Hz, 4H, 4Ar-H_{meta} DMAB), 5.45 (d, $^3J_{OH,H-4}$ = 5.9 Hz, 2H, OH-4), 5.24 (d, $^3J_{OH,H-3}$ = 4.8 Hz, 2H, OH-3), 5.15 (d, $^3J_{OH,H-2}$ = 5.9 Hz, 2H, OH-2), 3.96-3.88 (m, 4H, H-6a, CH_2a), 3.73 (d, ^2J = 12.8 Hz, 2H, CH_2b), 3.63 (d, $^3J_{1,2}$ = 9.6 Hz, 2H, H-1), 3.31-3.24 (m, 2H, H-5), 3.15-3.06 (m, 4H, H-2, H-4), 3.05-2.95 (m, 4H, H-3, H-6b) ppm; ^{13}C NMR (126 MHz, DMSO-*d*$_6$) δ = 150.0 (2C, 2Ar-C_{ipso} DMAB), 149.1 (2C, 2Ar-C_{ipso} DSAB), 141.6 (2C, 2Ar-C_{para} DMAB), 141.1 (2C, 2Ar-C_{para} DSAB), 130.0 (4C, 4Ar-C_{meta} DMAB), 126.1 (4C, 4Ar-C_{meta} DSAB), 123.5 (4C, 4Ar-C_{ortho} DSAB), 122.2 (4C, 4Ar-C_{ortho} DMAB), 81.9 (C-1), 78.2 (C-3), 74.9 (C-5), 74.1 (C-4), 72.6 (C-2), 32.2 (C-6), 31.3 ($\underline{C}H_2$ DMAB) ppm; ESI HRMS: *m/z*: calcd for $C_{38}H_{41}O_8N_4S_4$ + H^+ : 809.18017 [M + H^+] found: 809.17941.

Macrocycle (79)

To macrocycle **92** (20 mg, 17.7 µmol) in CH_2Cl_2:MeOH (1:1, 2 mL) was added MeONa (5.4 M in MeOH, 3 drops) at RT. The reaction was stirred for 2 h, then Amberlyte IR 120 H^+ was added, and the mixture was stirred another 10 min. Then it was filtered and concentrated in *vacuo*. During the concentration, the product precipitated. The remaining solvent was pipetted in another flask, and the solid was rinsed with EtOAc, affording the desired compound **79** (15.4 mg, 17.5 µmol) in 99% yield as an orange solid. $[\alpha]^{20}_D$ = +920 (*c* = 0.44 in DMSO); ^{1}H NMR (500 MHz, DMSO-*d*$_6$) δ = 7.39-7.33 (m, 8H, 4Ar-H_{meta}TFAB, 4Ar-H_{ortho} DMAB), 7.2 (d, ^3J = 8.4 Hz, 4H, 4Ar-H_{meta} DMAB), 5.35 (d, $^3J_{OH,H-4}$ = 5.8 Hz, 2H,OH-4), 5.18 (d, $^3J_{OH,H-3}$ = 4.3 Hz, 2H, OH-3), 5.16 (d, $^3J_{OH,H-2}$ = 5.2 Hz, 2H, OH-2), 3.93 (d, ^2J = 12.8 Hz, 2H, CH_2a), 3.86-3.79 (m, 4H, H-1, H-6a), 3.76 (d, ^2J = 12.8 Hz, 2H, CH_2b), 3.30-3.24 (m, 2H, H-5), 3.17-3.05 (m, 8H, H-2, H-3, H-4, H-6b) ppm; ^{13}C NMR (126 MHz, DMSO-*d*$_6$) δ = 155.5 (dd, $^1J_{C,F}$ = 261.6 Hz, $^3J_{C,F}$ = 4.9 Hz, 4C, 4Ar-C_{ortho} TFAB), 150.1 (2C, 2Ar-C_{ipso} DMAB), 145.0 (t, $^3J_{C,F}$ = 11.0 Hz, 2C, 2Ar-C_{para} TFAB), 141.7 (2C, 2Ar-C_{para} DMAB), 130.0 (4C, 4Ar-C_{meta} DMAB), 127.4 (t, $^2J_{C,F}$ = 8.9 Hz, 2C, 2Ar-C_{ipso} TFAB), 122.1 (4C, 4Ar-C_{ortho} DMAB), 110.0 (d, $^2J_{C,F}$ = 23.3 Hz, 4C, 4Ar-C_{meta} TFAB), 82.4 (C-1), 77.8 (C-3), 75.9 (C-5), 73.6 (C-4), 72.6 (C-2), 32.6 (C-6), 31.4 ($\underline{C}H_2$ DMAB) ppm; ESI HRMS: *m/z*: calcd for $C_{38}H_{37}O_8N_4F_4S_4$ + H^+ : 881.14249 [M + H^+] found: 881.14213.

CAB-dithioacetate (93)

General procedure **B** (part 7.3.1) was applied to 2,9-diiodo-11,12-dihydrodibenzo[1,2]diazocine **30** (31 mg, 67 µmol, 1.0 eq) with thiol **90** (2.0 eq) in THF (1.3 mL) with PdG3-Xantphos (2 mol%) and Et_3N (2.0 eq); stirring at 80 °C for 10 min. Column chromatography (cyclohexane:EtOAc 3:2) afforded the compound **93** (48.4 mg, 50.2 µmol) in 75% yield as a yellow solid. ^{1}H NMR (500 MHz, $CDCl_3$) δ = 7.33-7.24 (m, 2H, 2H-9), 7.16 (bs, 2H, 2H-8), 6.83 (d, ^3J = 8.3 Hz, 2H, 2H-11), 5.19-5.14 (m, 2H, H-3), 4.94-4.85 (m, 4H, H-2, H-4), 4.60 (bs, 2H, H-1), 3.62 (bs, 2H, H-5), 3.30-3.18 (m, 2H, H-6a), 3.12-2.94 (m, 4H, H-6b, CH_2a CAB), 2.88-2.76 (bs, 2H, CH_2b CAB), 2.35 (s, 6H, SC(O)CH_3), 2.07 (s, 6H, OC(O)CH_3), 2.05 (s, 6H, OC(O)CH_3), 1.98 (s, 6H, OC(O)CH_3) ppm; ^{13}C NMR (126 MHz, $CDCl_3$) δ = 194.5 (2C, S$\underline{C}$(O)CH_3), 170.3, 169.4 (6C, O$\underline{C}$(O)CH_3), 155.4 (2C, 2C-12), 134.7, 134.3 (2C, 2C-8), 131.7, 131.6 (2C, 2C-9), 130.4 (2C, 2C-

7), 128.7 (2C, 2C-10), 119.7 (2C, 2C-11), 85.3, 85.2 (C-1), 77.1 (C-5), 73.9 (C-3), 70.4, 70.3, 70.0, (4C, C-4, C-2), 31.7 (2C, CH_2 CAB), 30.6 (2C, SC(O)$\underline{C}H_3$), 30.4 (2C, C-6), 20.8, 20.7 (6C, 6 OC(O)$\underline{C}H_3$) ppm; ESI HRMS: *m/z*: calcd for $C_{42}H_{48}O_{16}N_2S_4 + NH_4^+$: 982.22249 [M + NH_4^+] found: 982.21967.

CAB-dithiol (94)

To **93** (40 mg, 47 µmol) and dithiotreitol (32 mg, 207 µmol, 5 eq) in *N*,*N*-dimethylacetamide (0.82 mL) was added Et_3N at RT. The mixture was stirred overnight, then it was diluted with EtOAc, washed with HCl 1N (3x), and the organics were dried over $MgSO_4$ and concentrated. Column chromatography (CH_2Cl_2:acetone 95:5) afforded the dithiol **94** (15.3 mg, 17.4 µmol) in 37% yield as a yellow solid. Due to the very small quantity obtained only an NMR was measured to identify the product. ^{1}H NMR (500 MHz, $CDCl_3$) δ = 7.31-7.26 (m, 2H, 2H-9), 7.20 (bs, 2H, 2H-8), 6.81 (d, ^3J = 8.5 Hz, 2H, 2H-11), 5.19 (at, ^3J = 9.3 Hz, 2H, H-3), 4.97-4.88 (m, 4H, H-2, H-4), 4.71 (d, $^3J_{1,2}$ = 10.2 Hz, 2H, H-1), 3.55 (bs, 2H, H-5), 3.00-2.89 (m, 2H, CH_2a CAB), 2.82-2.71 (m, 2H, CH_2b CAB), 2.67-2.56 (m, 4H, H-6a, H-6b), 2.05 (bs, 6H, OC(O)CH_3), 2.03 (s, 6H, OC(O)CH_3), 1.98 (s, 6H, OC(O)CH_3), 1.70-1.62 (m, 2H, SH) ppm; ^{13}C NMR (126 MHz, $CDCl_3$) δ = 170.3, 169.7, 169.4 (6C, O$\underline{C}$(O)CH_3), 155.2 (2C, 2C-12), 133.8, 133.6 (2C, 2C-8), 131.0 (2C, 2C-9), 130.8 (2C, 2C-7), 128.8 (2C, 2C-10), 119.9, 119.8 (2C, 2C-11), 85.2 (C-1), 78.9, 78.8 (C-5), 73.8 (C-3), 70.9, 70.2 (4C, C-2, C-4), 31.6 (2C, CH_2 CAB), 26.3 (C-6), 20.9, 20.8, 20.7 (6C, 6 OC(O)$\underline{C}H_3$) ppm.

Macrocycle (95)

Dithiol **94** (15 mg, 17 µmol) was charged in a flask and put under vacuum. In a separate flask the 4,4´-diiodoazobenzene **28** (7.4 mg, 17 µmol, 1eq) and the catalyst PdG3-Xantphos (1.6 mg, 1.7 µmol, 10 mol%) were charged and put under vacuum. Meanwhile the solvent (THF) was degassed by bubbling N_2 through. Then, the solvent (6.8 mL, 2.5 mM) was added to **94** under N_2, and the solution was irradiated at 405 nm for 10 min. Then, the catalyst and the azo derivative **28** were added under N_2, and finally Et_3N (4.7 µL, 34 µmol, 2 eq) was added at RT. After 20 min, the mixture was diluted with EtOAc, washed with HCl 1 N, and the organics were dried over $MgSO_4$ and concentrated in *vacuo*. Column chromatography (CH_2Cl_2:acetone 98:2 to 9:1) afforded the macrocycle **95** (4.6 mg, 4.3 µmol) in 26% yield as a yellow residue. Once again, only the NMR characterization was done. ^{1}H NMR (500 MHz, $CDCl_3$) δ =7.92-7.86 (m, 4H, 4Ar-H_{ortho} DSAB), 7.69 (d, 2H, ^3J = 8.2 Hz, 2Ar-H_{meta} DSAB), 7.66 (d, 2H, ^3J = 8.2 Hz, 2Ar-H_{meta} DSAB), 6.58 (s, 1H, H-8), 6.49 (s, 1H, H-8´), 6.36 (d, ^3J = 8.2 Hz, 1H, H-10), 6.30 (bs, 2H, H-9, H-9´), 6.14 (bs, 1H , H-10´), 5.20-5.12 (m, 2H, H-3, H-3´), 5.10-5.00 (m, 2H, H-4, H-4´), 4.81 (at, $^3J_{2,1}$ = 9.9 Hz, $^3J_{2,3}$ = 9.3 Hz, 1H, H-2), 4.62 (at, $^3J_{2´,1´}$ = 9.9 Hz, $^3J_{2´,3´}$ = 9.3 Hz, 1H, H-2´), 4.55 (d, $^3J_{1,2}$ = 9.9 Hz, 1H, H-1), 4.41 (d, $^3J_{1´,2´}$ = 9.9 Hz, 1H, H-1´), 3.80-3.68 (m, 2H, H-5, H-5´), 3.29-3.18 (m, 2H, H-6a, H-6a´), 3.10-2.99 (m, 2H, H-6b, H-6b´), 2.78-2.65 (m, 2H, CH_2a CAB), 2.43-2.27 (m, 2H, CH_2b CAB), 2.08 (s, 3H, OC(O)CH_3), 2.06 (s, 3H, OC(O)CH_3), 2.04 (s, 3H, OC(O)CH_3), 2.02 (s, 3H, OC(O)CH_3), 1.99 (s, 3H, OC(O)CH_3), 1.96 (s, 3H, OC(O)CH_3) ppm; ^{13}C NMR (126 MHz, $CDCl_3$) δ = 170.2, 169.6, 169.5, 169.3, 168.9 (6C, O$\underline{C}$(O)CH_3), 155.5, 155.2 (2C, C-12, C-12´), 150.9, 150.5 (2C, 2Ar-C_{ipso} DSAB), 140.6, 140.5 (2C, 2Ar-C_{para} DSAB), 136.6 (2C, C-8), 134.7 (C-8´), 133.8 (C-9), 132.2 (4C,2Ar-C_{meta} DSAB, C-10, C-9´), 129.5 (3C, 2Ar-C_{meta} DSAB, C-10´), 127.8, 127.7 (3C, C-11, C-11´, C-7´), 123.4, 123.3 (4C, 4Ar-C_{ortho} DSAB), 119.1, 118.8 (2C, C-11, C-11´), 85.9, 85.3 (C-1, C-1´), 80.4, 79.1 (C-5, C-5´), 74.1, 73.9 (C-3, C-3´), 70.5 (C-4, C-4´), 70.1 (C-2), 69.7 (C-2´), 35.9, 33.8 (C-6, C-6´), 31.3, 30.8 (CH_2a, CH_2b CAB), 20.8, 20.7, 20.6 (6C, OC(O)$\underline{C}H_3$) ppm.

DMAB-*bis*-conjugate (101)

To the diol **85** (48 mg, 39 µmol) in CH_2Cl_2:MeOH (1:1, 1 mL) was added MeONa (5.4 M in MeOH, 1 drop) at RT. The mixture was stirred for 2 h, then Amberlyte IR 120 H^+ was added, and after further stirring for 10 min, the mixture was filtered and concentrated. The crude was dissolved in MeOH and the product was precipitated with Et_2O, to afford the compound **101** in 73% yield as an orange solid. ^{1}H NMR (500 MHz, DMSO-d_6) δ = 7.84 (d, ^3J = 8.4 Hz, 4H, 4Ar-H_{ortho}), 7.56 (d, ^3J = 8.4 Hz, 4H, 4Ar-H_{meta}), 5.12 (bs, 2H, OH), 5.02 (bs, 2H, OH), 4.94 (bs, 2H, OH), 4.68 (m, 2H, OH-6), 4.07-4.00 (m, 4H, CH_2a, H-1), 3.87 (d, ^2J = 13.1 Hz, 2H, CH_2b), 3.78-3.72 (m, 2H, H-6a), 3.50-3.43 (m, 2H, H-6b), 3.11-3.01 (m, 8H, H-2, H-3, H-4, H-5) ppm; ^{13}C NMR (126 MHz, DMSO-d_6) δ = 150.8 (2C, 2Ar-C_{ipso}), 142.4 (2C, 2Ar-C_{para}), 130.2 (4C, 4Ar-C_{meta}), 122.6 (4C, 4Ar-C_{ortho}), 82.8 (C-1), 81.2 (C-5), 78.3 (C-3), 73.2 (C-2), 70.3 (C-4), 61.4 (C-6), 31.9 ($\underline{C}H_2$) ppm; ESI HRMS: *m/z*: calcd for $C_{26}H_{34}O_{10}N_2S_2$ + Na^+: 621.15624 [M + Na^+] found: 621.15381.

DSAB-*bis*-conjugate (103)

General procedure **B** (part 7.3.1) was applied to 4,4´-diiodoazobenzene **28** (15 mg, 34.6 µmol) with thiol **102** (2.0 eq) in THF (1 mL) with PdG3-Xantphos (2 mol%) and Et_3N (2.0 eq); stirring at RT for 10 min. Then, crude residue was dissolved in CH_2Cl_2:MeOH (1:1, 2 mL) and K_2CO_3 (7 mg, 1.5 eq) was added at RT. After 2 h, Amberlyte IR 120 H^+ was added, and after further stirring for 10 min, the mixture was filtered and concentrated. Column chromatography (CH_2Cl_2:MeOH 1:0 to 8:2) afforded the compound **103** (20.7 mg, 34.6 µmol) in a quantitative yield as an orange solid. ^{1}H NMR (500 MHz, DMSO-d_6) δ = 7.81 (d, ^3J = 8.6 Hz, 4H, 4Ar-H_{ortho}), 7.50 (d, ^3J = 8.6 Hz, 4H, 4Ar-H_{meta}), 5.28 (d, $^3J_{OH,H-4}$ = 5.7 Hz, 2H,OH-4), 4.89 (d, $^3J_{OH,H-3}$ = 4.9 Hz, 2H,OH-3), 4.80 (d, $^3J_{OH,H-2}$ = 6.4 Hz, 2H,OH-2), 4.54 (d, $^3J_{1,2}$ = 3.7 Hz, 1H, H-1), 3.59-3.52 (m, 4H, H-5, H-6a), 3.40-3.35 (m, 2H, H-3), 3.27-3.21 (m, 8H, OMe, H-2), 3.12-3.04 (m, 4H, H-6b, H-4) ppm; ^{13}C NMR (126 MHz, DMSO-d_6) δ = 149.4 (2C, 2Ar-C_{ipso}), 142.1 (2C, 2Ar-C_{para}), 127.1 (4C, 4Ar-C_{meta}), 123.1 (4C, 4Ar-C_{ortho}), 99.8 (C-1), 73.4 (C-4), 73.1 (C-5), 71.9 (C-2), 70.5 (C-3), 54.3 (OMe), 34.1 (C-6) ppm; ESI HRMS: *m/z*: calcd for $C_{26}H_{34}O_{10}N_2S_2$ + Na^+: 621.15471 [M + Na^+] found: 621.15356.

TFAB-*bis*-conjugate (104)

General procedure **B** (part 7.3.1) was applied to 4,4´-diiodoazobenzene **28** (15 mg, 34.6 µmol) with thiol **102** (2.0 eq) in THF (1 mL) with PdG3-Xantphos (2 mol%) and Et_3N (2.0 eq); stirring at RT for 10 min. Then, crude residue was dissolved in CH_2Cl_2:MeOH (1:1, 2 mL) and K_2CO_3 (7 mg, 1.5 eq) was added at RT. After 2 h, Amberlyte IR 120 H^+ was added, and after further stirring for 10 min, the mixture was filtered and concentrated. The crude was then dissolved in water, and washed with EtOAc. Then it was concentrated until 2-3 mL of water remained, and allowed to crystallize overnight in the fridge. The solid was filtered and dried by co-evaporation with toluene to afford the compound **104** (20 mg, 29.8 µmol) in 75% yield. ^{1}H NMR (500 MHz, DMSO-d_6) δ = 7.30 (d, $^3J_{H,F}$ = 10.6 Hz, 4H, 4Ar-H_{meta}), 5.34 (d, $^3J_{OH,H-4}$ = 5.8 Hz, 2H, OH-4), 4.92 (d, $^3J_{OH,H-3}$ = 5.1 Hz, 2H, OH-3), 4.83 (d, $^3J_{OH,H-2}$ = 6.4 Hz, 2H, OH-2), 4.54 (d, $^3J_{1,2}$ = 3.6 Hz, 2H, H-1), 3.62-3.51 (m, 4H, H-5, H-6a), 3.37-3.33 (m, 2H, H-3), 3.24 (s, 6H, OMe) 3.19-3.13 (m, 2H, H-6b), 3.11-3.06 (m, 2H, H-4) ppm; ^{13}C NMR (126 MHz, DMSO-d_6) δ = 155.9, 154.2 (4C, 4Ar-C_{ortho}), 145.6 (2C, 2Ar-C_{para}), 127.5 (2C, 2Ar-C_{ipso}), 110.2, 110.0 (4C, 4Ar-C_{meta}), 99.9 (C-1), 73.2 (C-4), 73.1 (C-3), 71.2 (C-2), 70.5 (C-5), 54.4 (OMe), 33.7 (C-6) ppm; ESI HRMS: *m/z*: calcd for $C_{26}H_{34}O_{10}N_2F_4S_2$ + Na^+: 693.11702 [M + Na^+] found: 693.11689.

7.5. Photochromic properties of the synthesized AB-glycophanes

7.5.1. Properties of AB glycophanes 74-77

Extinction coefficients (ε) were calculated using the Beer-Lambert law (see equation below), plotting the absorbance at the respective λ_{max} against the concentration (5 different concentrations in a range of 2.10^{-5} to 6.10^{-5} mol.L^{-1}). A linear fit gave the value of ε as the slope of the linear plot.

$$A = \varepsilon \cdot c \cdot l$$

A = absorbance

ε = extinction coefficient = slope of the plot

c = molar concentration in mol.L^{-1}

l = optical path length in cm

Macrocycle 74:

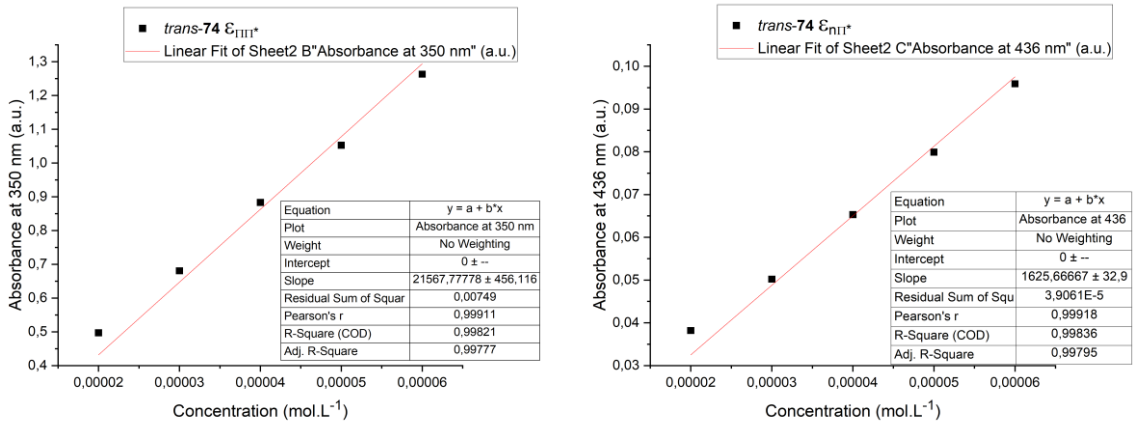

Figure 7.5.1. Plot of the absorbance at the λ_{max} and $\lambda_{n\rightarrow\pi^*}$ against the concentration for *trans*-**74**; the slope of the linear fit gives the value of the molar extinction coefficient ε. Measured at 298 K in DMSO in concentrations from 2.10^{-5} to 6.10^{-5} mol.L^{-1} (left) *trans*-**74**, absorbance at 350 nm; (right) *trans*-**74**, absorbance at 436 nm.

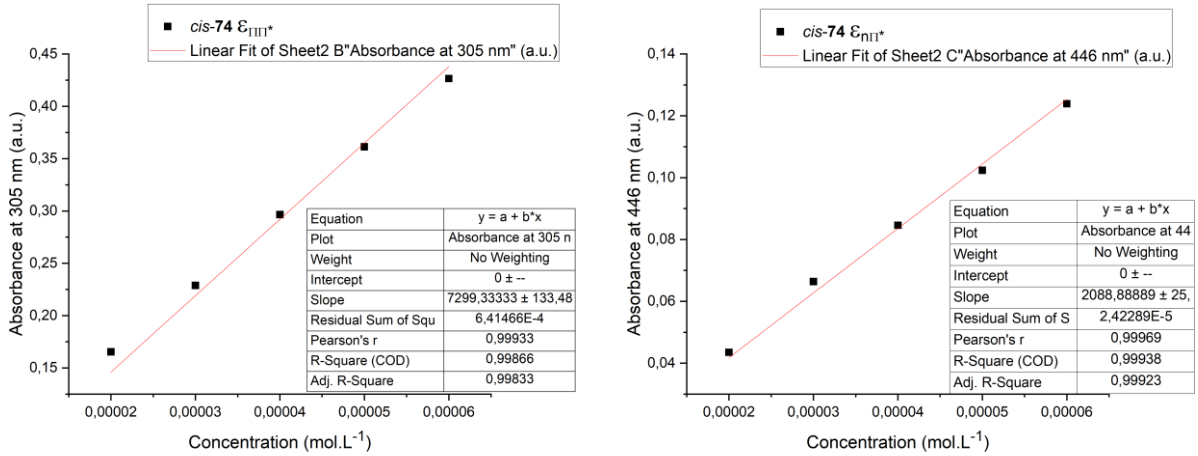

Figure 7.5.2. Plot of the absorbance at the λ_{max} and $\lambda_{n\rightarrow\pi^*}$ against the concentration for **74** at the PSS 365; the slope of the linear fit gives the value of the molar extinction coefficient ε. Measured at 298 K in DMSO in concentrations from 2.10^{-5} to 6.10^{-5} mol.L^{-1} (left) *cis*-**74**, absorbance at 305 nm; (right) *cis*-**74**, absorbance at 446 nm.

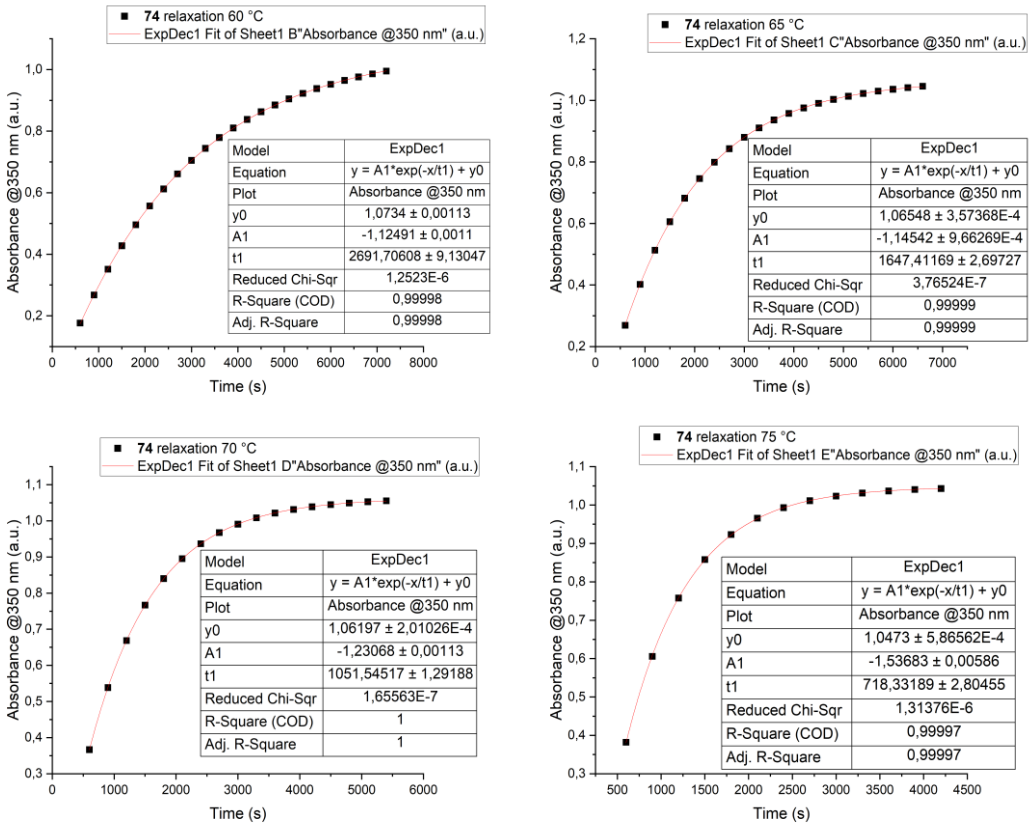

Figure 7.5.3. Exponential growth of the absorbance at 350 nm of a *cis*/*trans* mixture of **74** after irradiation at 365 nm in DMSO (50µM) at 60, 65, 70 and 75 °C. The rate constant at each temperature is given by: $k_T = 1/t_1$.

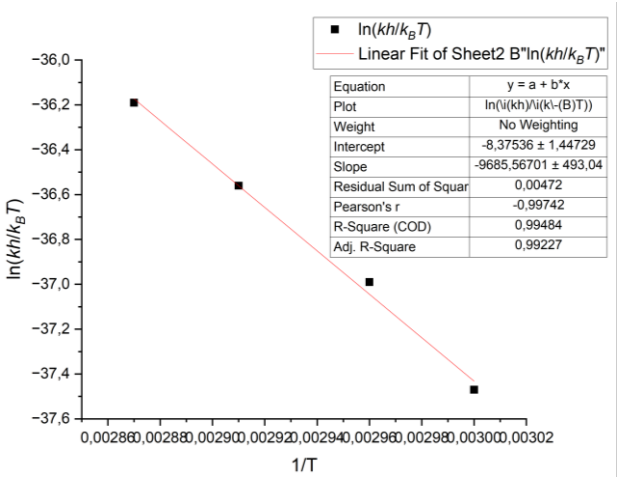

Figure 7.5.4. Eyring plot for macrocycle **74**. The slope of the linear fit gives the value $\frac{\Delta H^{\neq}}{R}$ and the ordinate at the origin $\frac{\Delta S^{\neq}}{R}$.

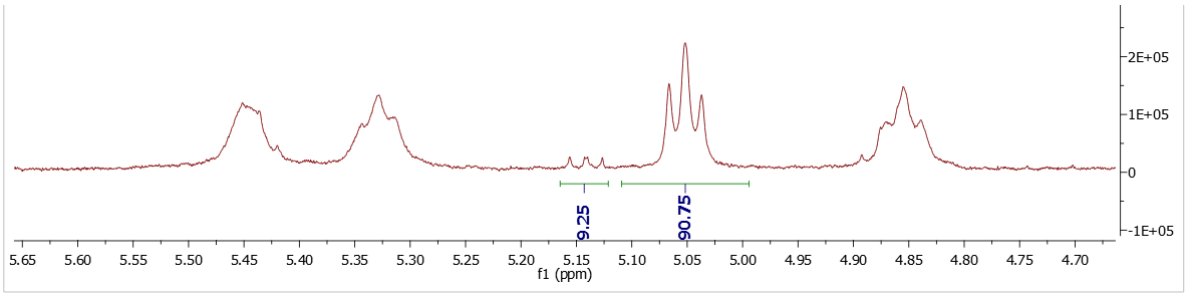

Figure 7.5.5. Expansion in the carbohydrate region of the ^{1}H NMR spectrum (DMSO-d_6, 300 K) of an equilibrium mixture of *trans* and *cis*-**74** (1 mM) after irradiation at 365 nm (2 min).

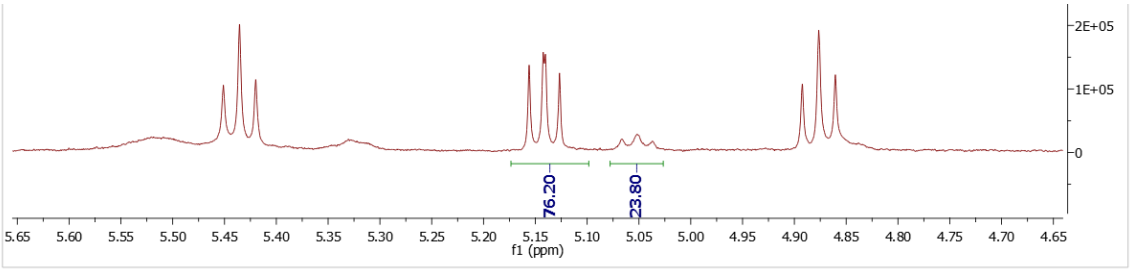

Figure 7.5.6. Expansion in the carbohydrate region of the ^{1}H NMR spectrum (DMSO-d_6, 300 K) of an equilibrium mixture of *trans* and *cis*-**74** (1 mM) after irradiation at 520 nm (2 min).

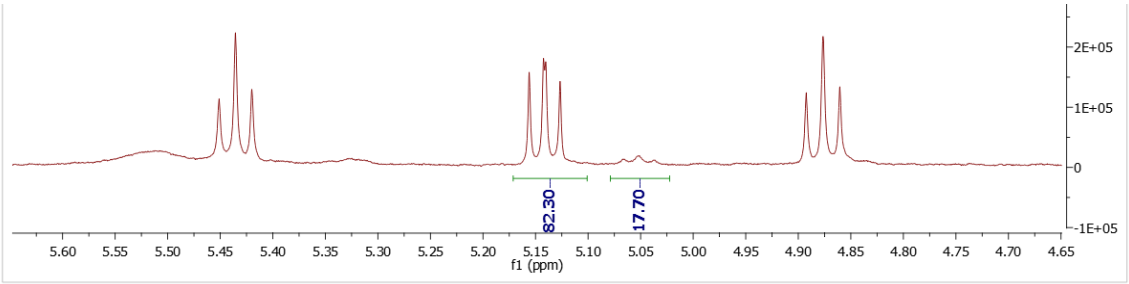

Figure 7.5.7. Expansion in the carbohydrate region of the ^{1}H NMR spectrum (DMSO-d_6, 300 K) of a mixture of *trans* and *cis*-**74** (1 mM) after irradiation at 520 nm (2 min) followed by 625 nm (10 min).

Macrocycle 75:

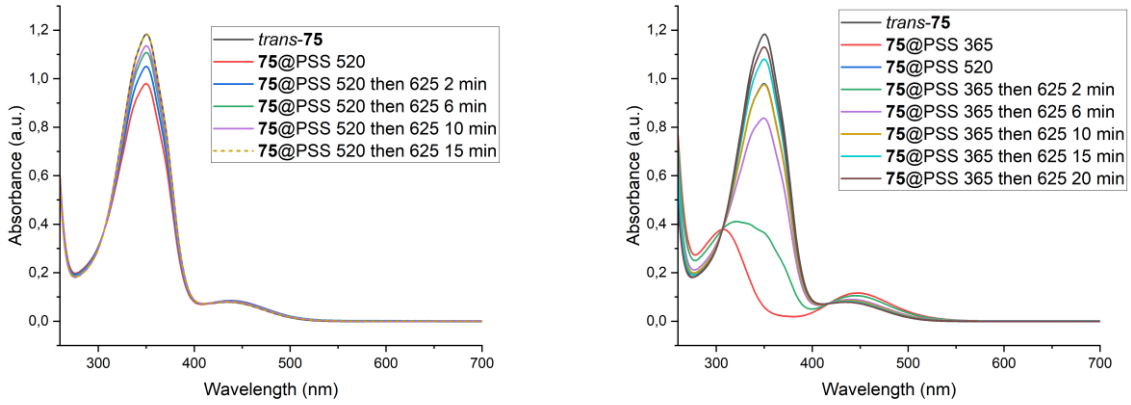

Figure 7.5.8. Evolution of the UV-vis spectra of macrocycle **75** in DMSO (50 µM) at 298 K upon irradiation with red-light, starting from the PSS 520 (left) or the PSS 365 (right).

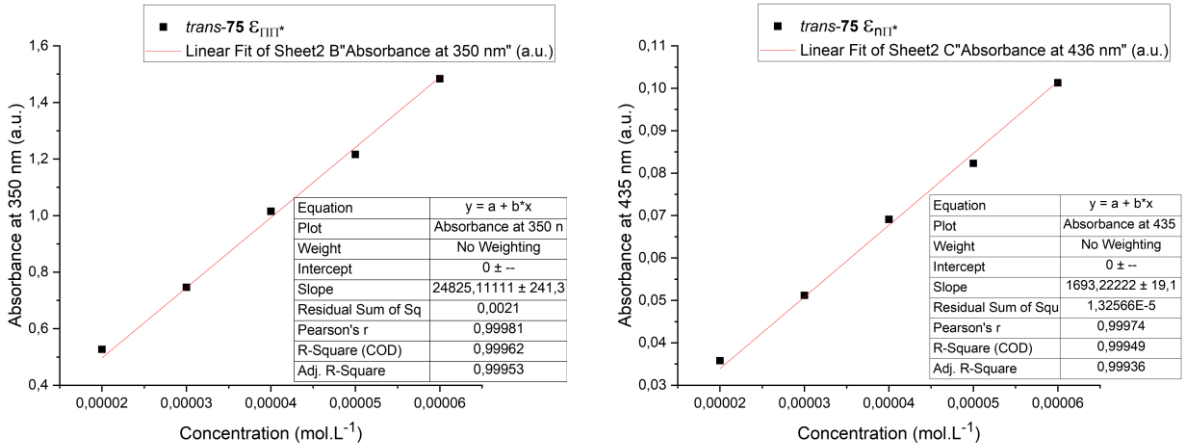

Figure 7.5.9. Plot of the absorbance at the λ_{max} and $\lambda_{n\rightarrow\pi^*}$ against the concentration for *trans*-**75**; the slope of the linear fit gives the value of the molar extinction coefficient ε. Measured at 298 K in DMSO in concentrations from 2.10^{-5} to 6.10^{-5} mol.L^{-1} (left) *trans*-**75**, absorbance at 350 nm; (right) *trans*-**75**, absorbance at 436 nm.

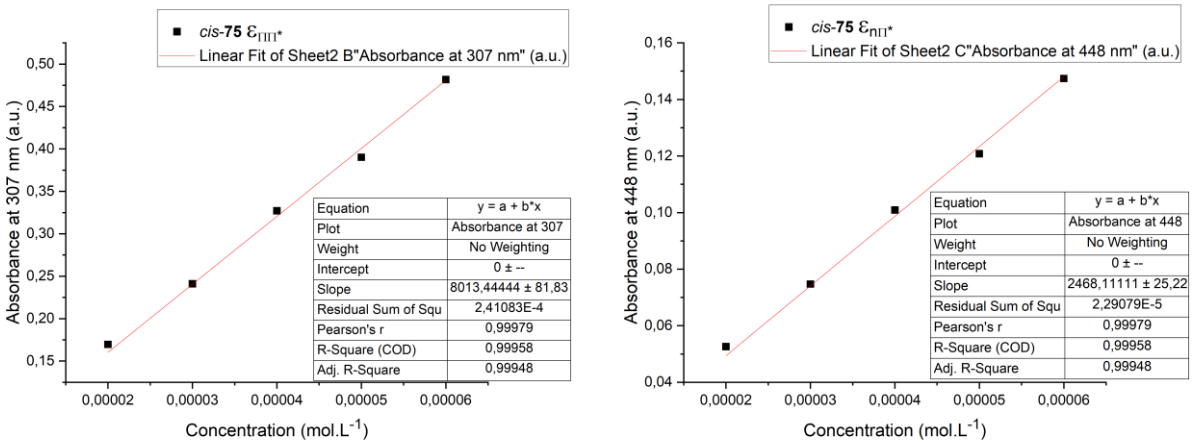

Figure 7.5.10. Plot of the absorbance at the λ_{max} and $\lambda_{n\rightarrow\pi^*}$ against the concentration for **75** at the PSS 365; the slope of the linear fit gives the value of the molar extinction coefficient ε. Measured at 298 K in DMSO in concentrations from 2.10^{-5} to 6.10^{-5} mol.L^{-1} (left) *cis*-**75**, absorbance at 307 nm; (right) *cis*-**75**, absorbance at 448 nm.

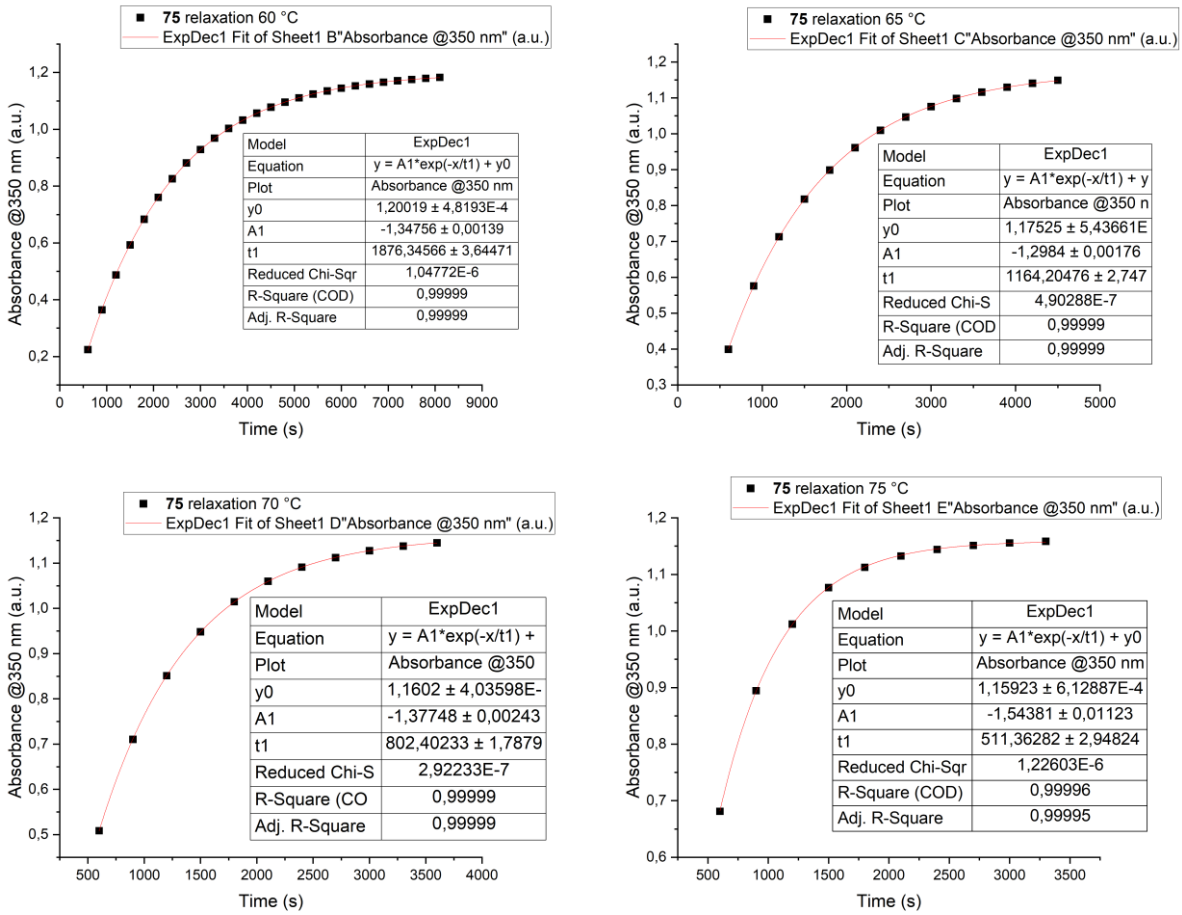

Figure 7.5.11. Exponential growth of the absorbance at 350 nm of a *cis*/*trans* mixture of **75** after irradiation at 365 nm in DMSO (50µM) at 60, 65, 70 and 75 °C. The rate constant at each temperature is given by: $k_T = 1/t_1$.

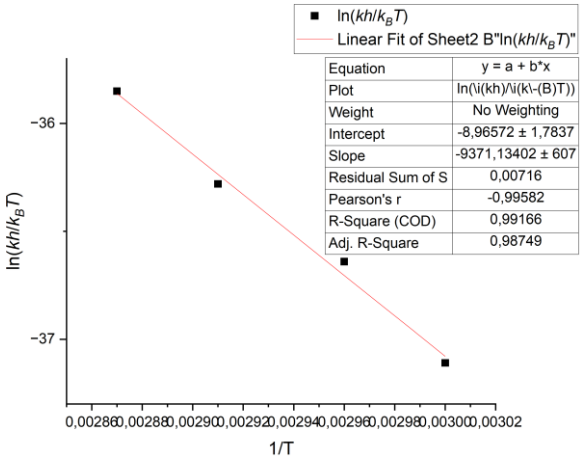

Figure 7.5.12. Eyring plot for macrocycle **74**. The slope of the linear fit gives the value $\frac{\Delta H^{\neq}}{\mathrm{R}}$ and the ordinate at the origin $\frac{\Delta S^{\neq}}{\mathrm{R}}$.

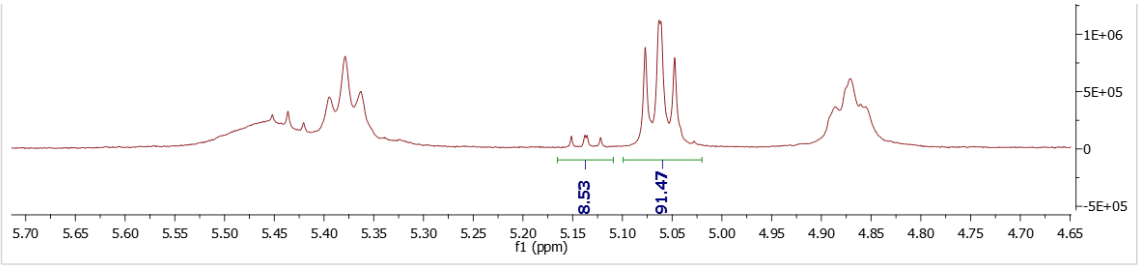

Figure 7.5.13. Expansion in the carbohydrate region of the ^{1}H NMR spectrum (DMSO-d_6, 300 K) of an equilibrium mixture of *trans* and *cis*-**75** (1 mM) after irradiation at 365 nm (2 min).

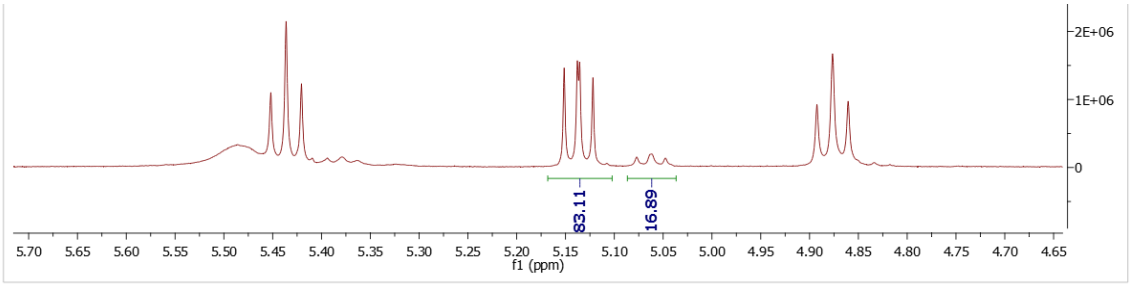

Figure 7.5.14. Expansion in the carbohydrate region of the ^{1}H NMR spectrum (DMSO-d_6, 300 K) of an equilibrium mixture of *trans* and *cis*-**75** (1 mM) after irradiation at 520 nm (2 min).

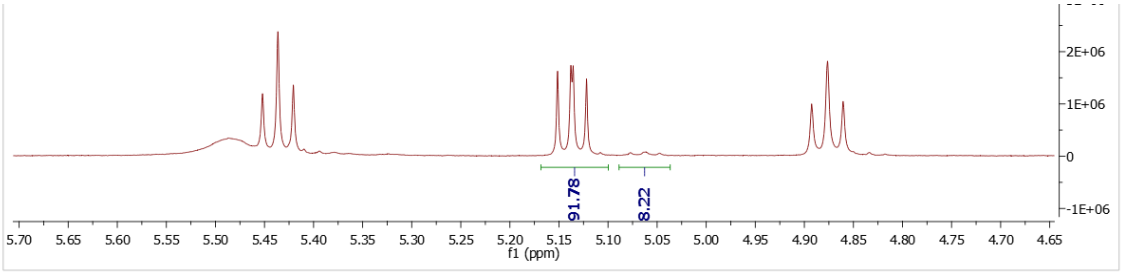

Figure 7.5.15. Expansion in the carbohydrate region of the ^{1}H NMR spectrum (DMSO-d_6, 300 K) of a mixture of *trans* and *cis*-**75** (1 mM) after irradiation at 520 nm (2 min) followed by 625 nm (10 min).

Macrocycle 76

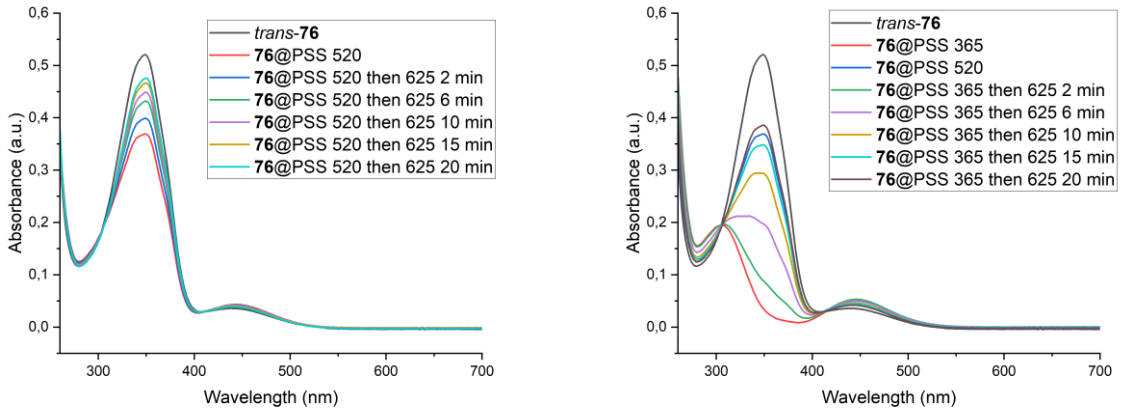

Figure 7.5.16. Evolution of the UV-vis spectra of macrocycle **76** in DMSO (50 µM) at 298 K upon irradiation with red-light, starting from the PSS 520 (left) or the PSS 365 (right).

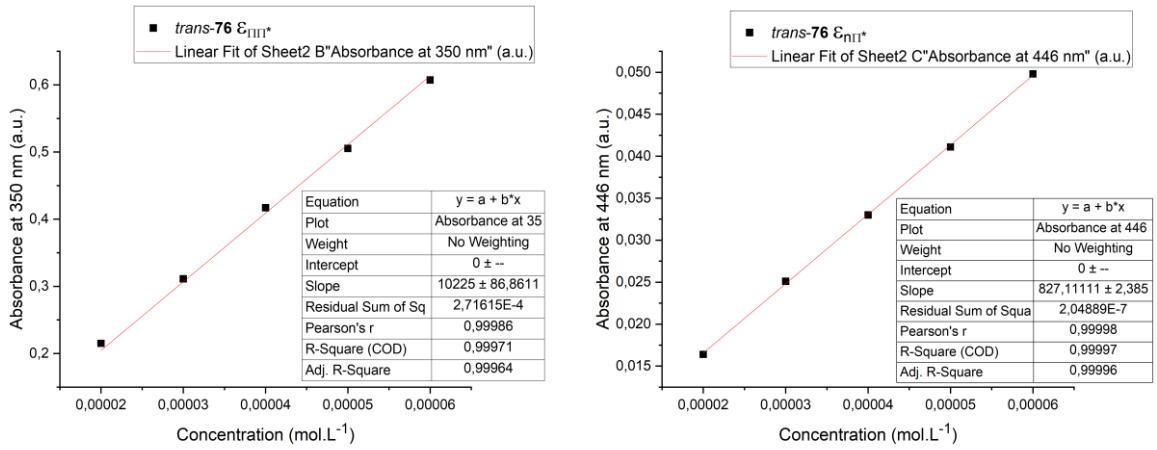

Figure 7.5.17. Plot of the absorbance at the λ_{max} and $\lambda_{n\rightarrow\pi^*}$ against the concentration for *trans*-**76**; the slope of the linear fit gives the value of the molar extinction coefficient ε. Measured at 298 K in DMSO in concentrations from 2.10^{-5} to 6.10^{-5} mol.L^{-1} (left) *trans*-**76**, absorbance at 350 nm; (right) *trans*-**76**, absorbance at 446 nm.

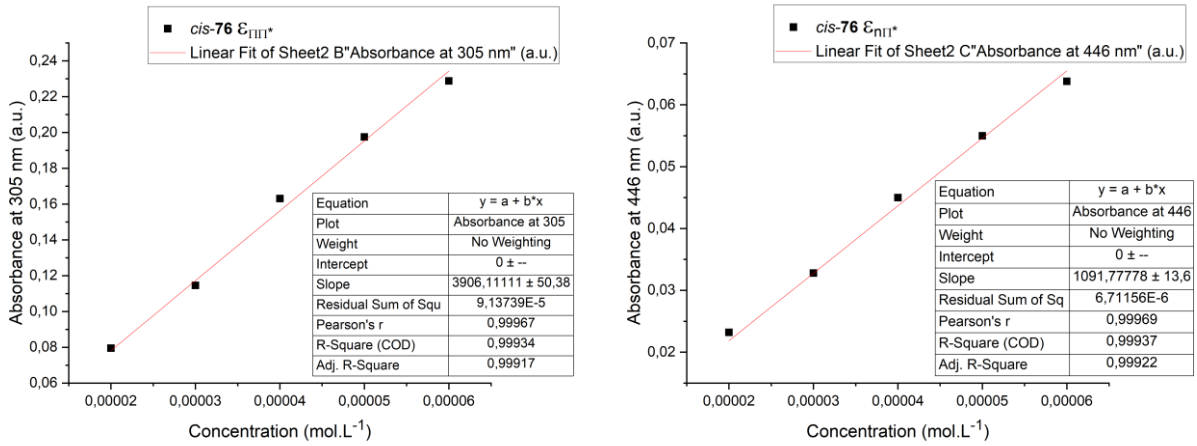

Figure 7.5.18. Plot of the absorbance at the λ_{max} and $\lambda_{n\rightarrow\pi^*}$ against the concentration for **76** at the PSS 365; the slope of the linear fit gives the value of the molar extinction coefficient ε. Measured at 298 K in DMSO in concentrations from 2.10^{-5} to 6.10^{-5} mol.L^{-1}; (left) *cis*-**76**, absorbance at 305 nm; (right) *cis*-**76**, absorbance at 446 nm.

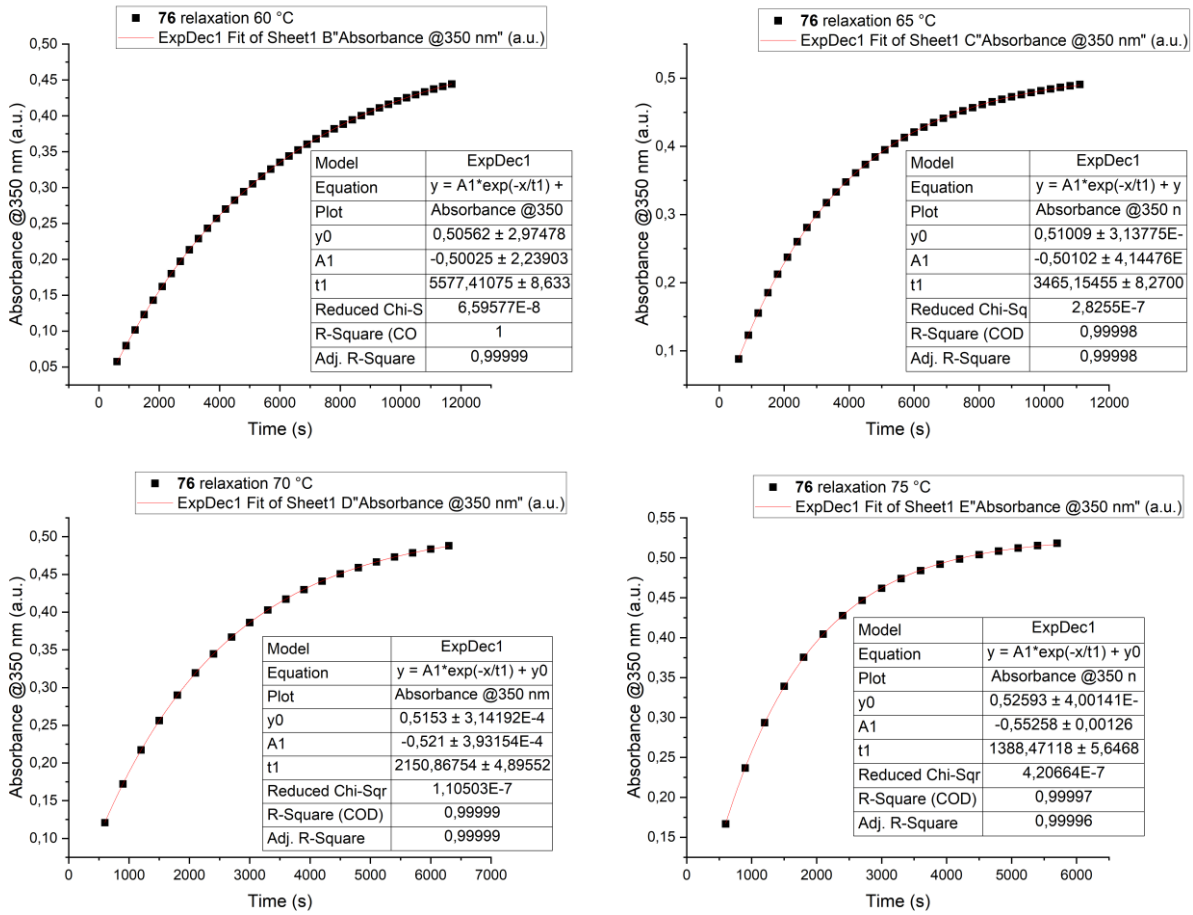

Figure 7.5.19. Exponential growth of the absorbance at 350 nm of a *cis*/*trans* mixture of **76** after irradiation at 365 nm in DMSO (50µM) at 60, 65, 70 and 75 °C. The rate constant at each temperature is given by: $k_T = 1/t_1$.

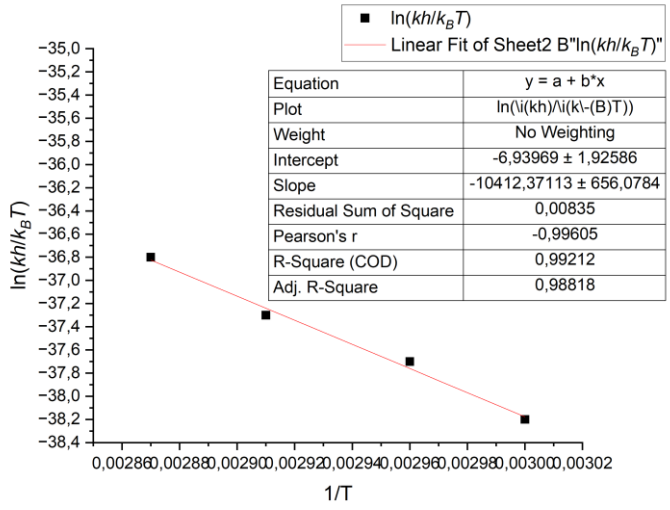

Figure 7.5.20. Eyring plot for macrocycle **76**. The slope of the linear fit gives the value $\frac{\Delta H^{\neq}}{\mathrm{R}}$ and the ordinate at the origin $\frac{\Delta S^{\neq}}{\mathrm{R}}$.

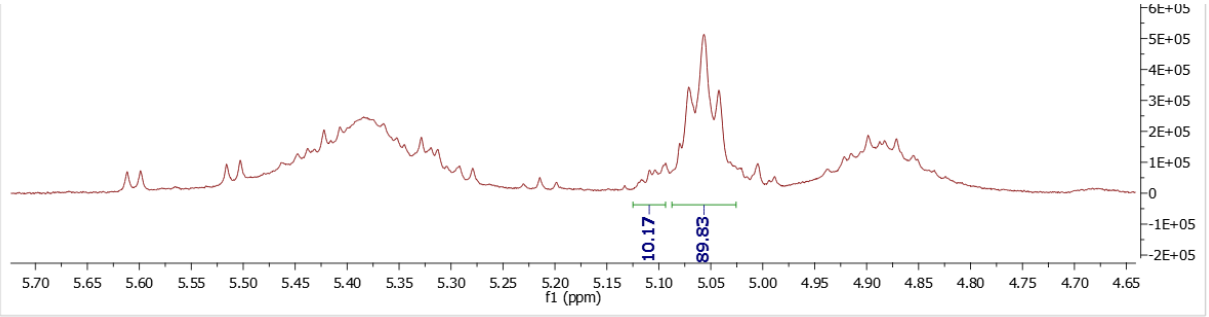

Figure 7.5.21. Expansion in the carbohydrate region of the ^{1}H NMR spectrum (DMSO-d_6, 300 K) of an equilibrium mixture of *trans* and *cis*-**76** (1 mM) after irradiation at 365 nm (2 min).

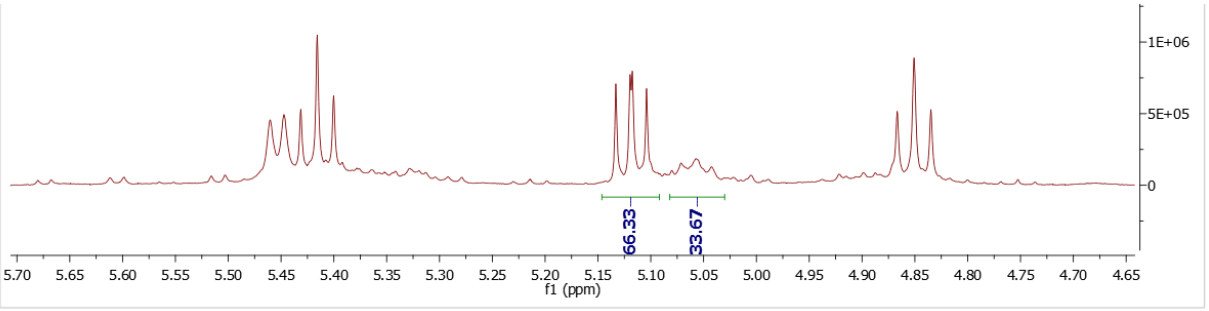

Figure 7.5.22. Expansion in the carbohydrate region of the ^{1}H NMR spectrum (DMSO-d_6, 300 K) of an equilibrium mixture of *trans* and *cis*-**76** (1 mM) after irradiation at 520 nm (2 min).

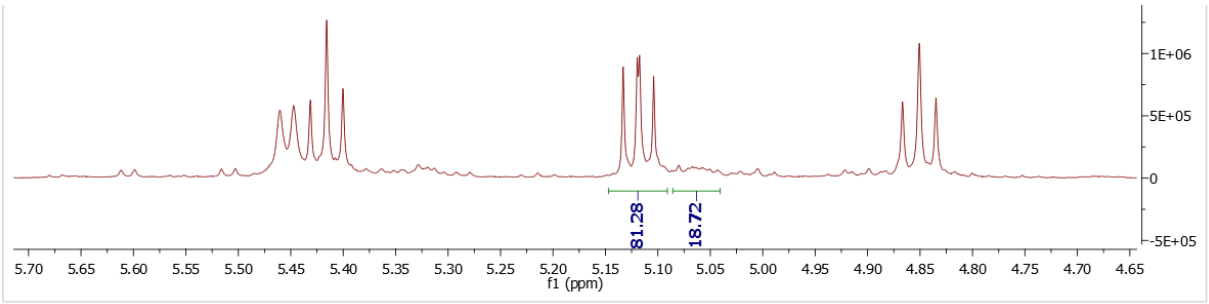

Figure 7.5.23. Expansion in the carbohydrate region of the ^{1}H NMR spectrum (DMSO-d_6, 300 K) of a mixture of *trans* and *cis*-**76** (1 mM) after irradiation at 520 nm (2 min) followed by 625 nm (10 min).

Note: In the case of macrocycle **76**, some signals that were not present in the first spectrum taken after chromatography (Figure 7.5.24), started appearing after several switching forth and back. It seems that these new signals also change upon irradiation. At this point it is not known whether this could be a contamination during the preparation of the solutions, or perhaps hints of the very minor presence of the isomer of opposite helical chirality. For example, the intensity of the doublet at 5.61 ppm changes from one PSS to the other, and the doublet at 5.67 ppm is not present in the PSS 365 whereas it appears in the PSS 520 and fades away again after red-light irradiation. Similarly, the triplet at 5.21 ppm seems to disappear when converting the macrocycle further to the ground state. Of course this raises doubts about the accuracy of the integration, but the obtained values fit well with the evolution of the UV-Vis spectra and the observed trends with the macrocycles **74**, **75** and **77** and **105**.

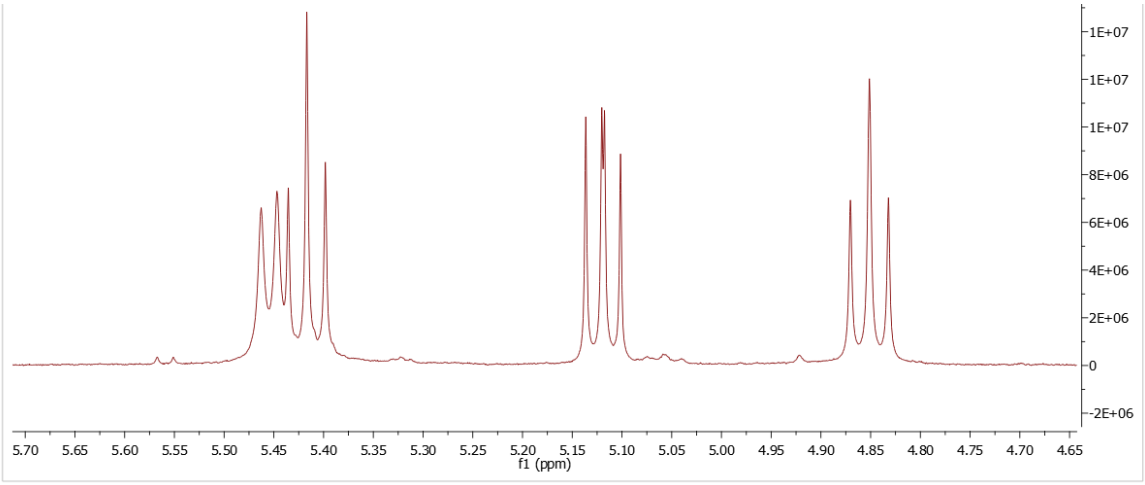

Figure 7.5.24. Expansion in the carbohydrate region of the ^{1}H NMR spectrum (DMSO-d_6, 300 K) of *trans*-**76** directly after purification by column chromatography. The signal at 5.56 ppm is nearly completely absent in the spectra from the PSS, while other signals appeared upon irradiation.

Macrocycle 77

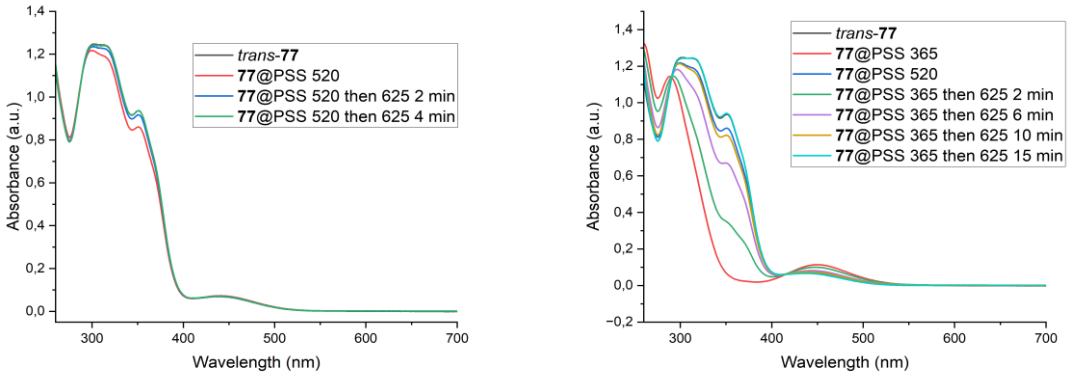

Figure 7.5.25. Evolution of the UV-vis spectra of macrocycle **77** in DMSO (50 µM) at 298 K upon irradiation with red-light, starting from the PSS 520 (left) or the PSS 365 (right).

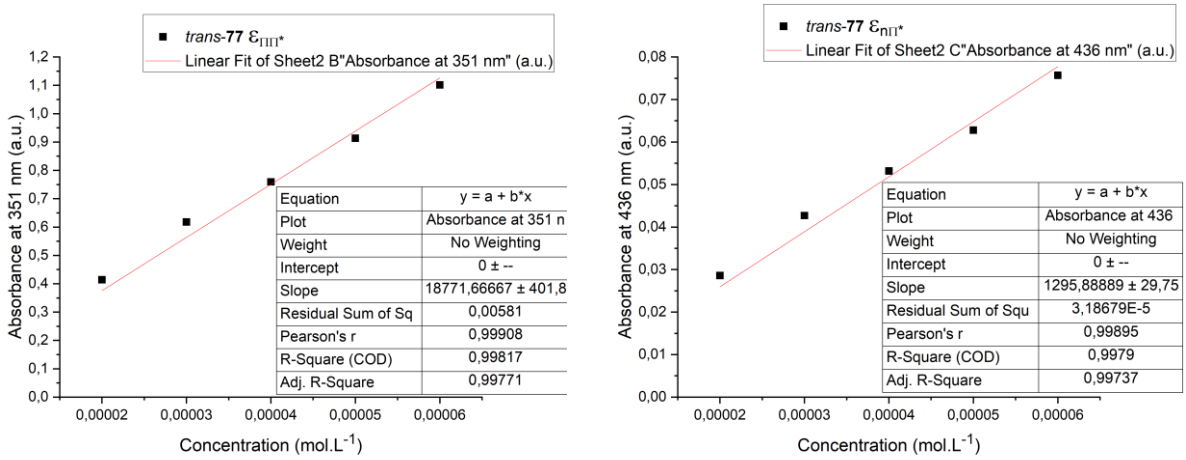

Figure 7.5.26. Plot of the absorbance at the λ_{max} and $\lambda_{n\rightarrow\pi^*}$ against the concentration for *trans*-**77**; the slope of the linear fit gives the value of the molar extinction coefficient ε. Measured at 298 K in DMSO in concentrations from 2.10^{-5} to 6.10^{-5} mol.L^{-1}; (left) *trans*-**77**, absorbance at 351 nm; (right) *trans*-**77**, absorbance at 436 nm.

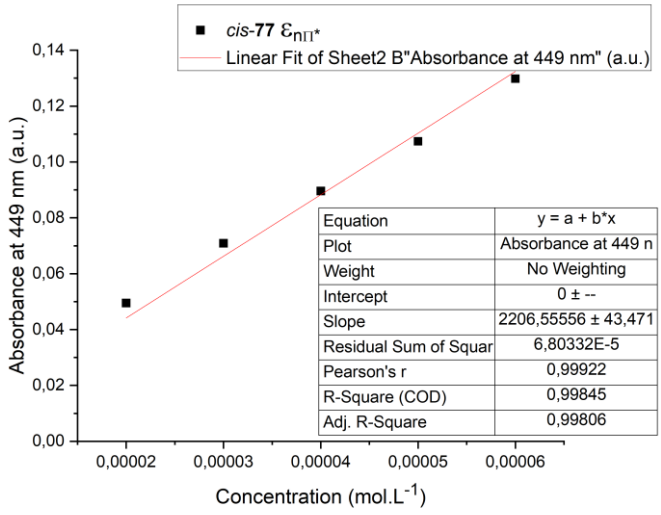

Figure 7.5.27. Plot of the absorbance at the $\lambda_{n\rightarrow\pi^*}$ (449 nm) against the concentration for **76** at the PSS 365; the slope of the linear fit gives the value of the molar extinction coefficient ε. Measured at 298 K in DMSO in concentrations from 2.10^{-5} to 6.10^{-5} mol.L^{-1}.

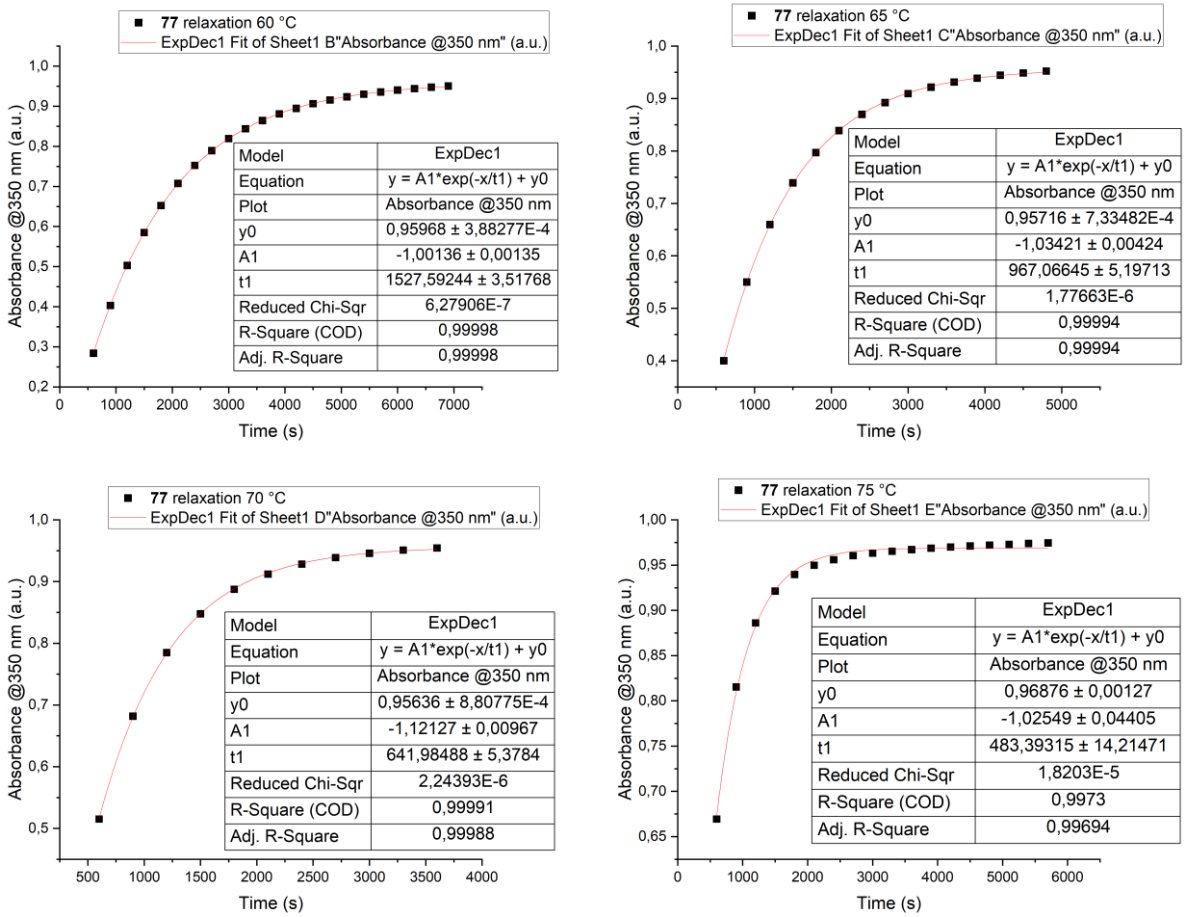

Figure 7.5.28. Exponential growth of the absorbance at 350 nm of a *cis*/*trans* mixture of **77** after irradiation at 365 nm in DMSO (50µM) at 60, 65, 70 and 75 °C. The rate constant at each temperature is given by: $k_T = 1/t_1$.

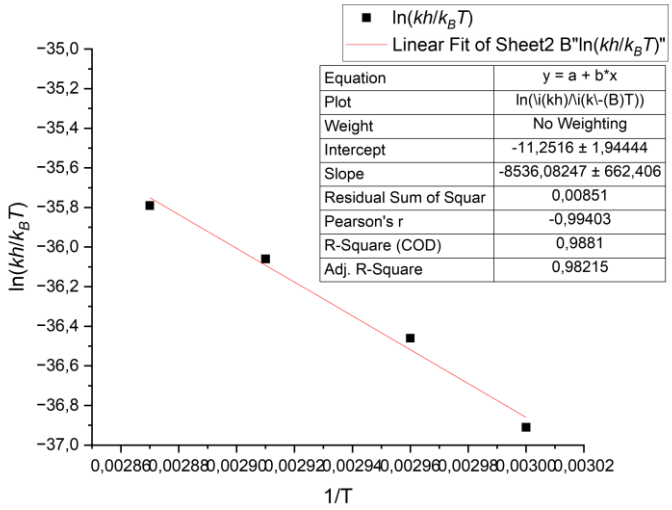

Figure 7.5.29. Eyring plot for macrocycle **77**. The slope of the linear fit gives the value $\frac{\Delta H^{\neq}}{\mathrm{R}}$ and the ordinate at the origin $\frac{\Delta S^{\neq}}{\mathrm{R}}$.

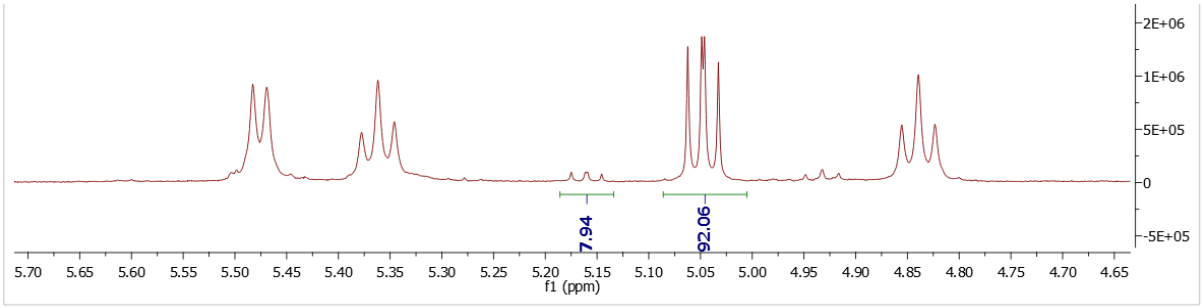

Figure 7.5.30. Expansion in the carbohydrate region of the ^{1}H NMR spectrum (DMSO-d_6, 300 K) of an equilibrium mixture of *trans* and *cis*-**77** (1 mM) after irradiation at 365 nm (2 min).

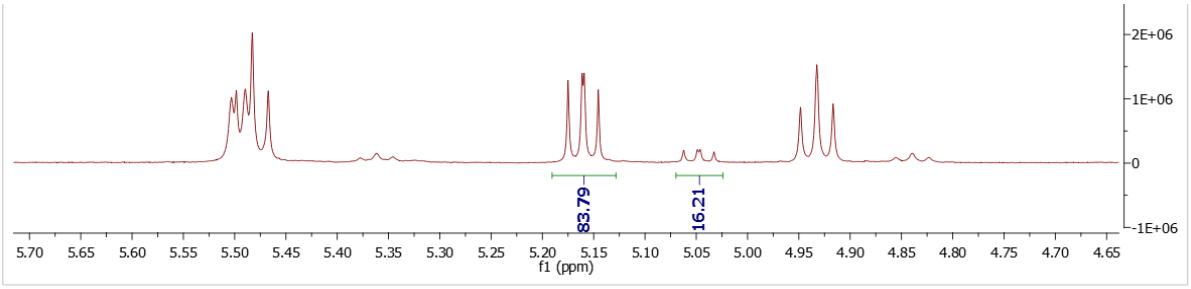

Figure 7.5.31. Expansion in the carbohydrate region of the ^{1}H NMR spectrum (DMSO-d_6, 300 K) of an equilibrium mixture of *trans* and *cis*-**77** (1 mM) after irradiation at 520 nm (2 min).

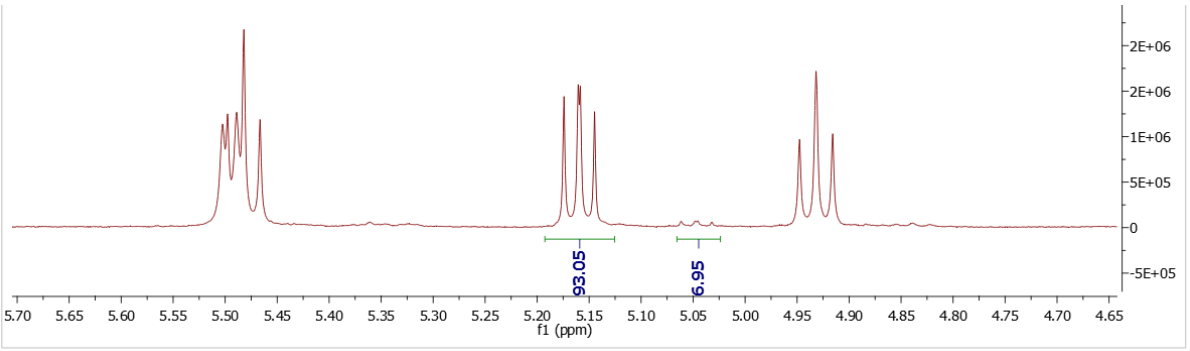

Figure 7.5.32. Expansion in the carbohydrate region of the ^{1}H NMR spectrum (DMSO-d_6, 300 K) of a mixture of *trans* and *cis*-**77** (1 mM) after irradiation at 520 nm (2 min) followed by 625 nm (10 min).

Compensation relationship

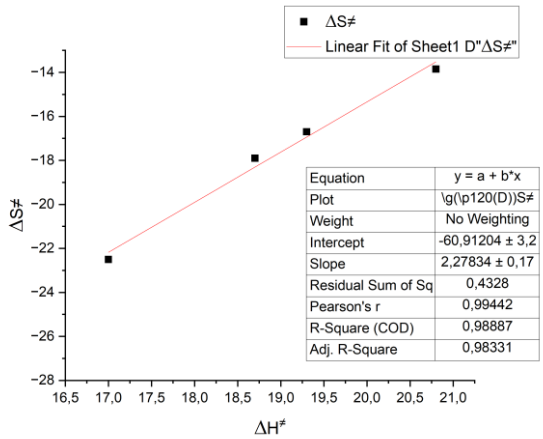

Figure 7.5.33. Enthalpy-entropy compensation plot for compounds **74**-**77**.

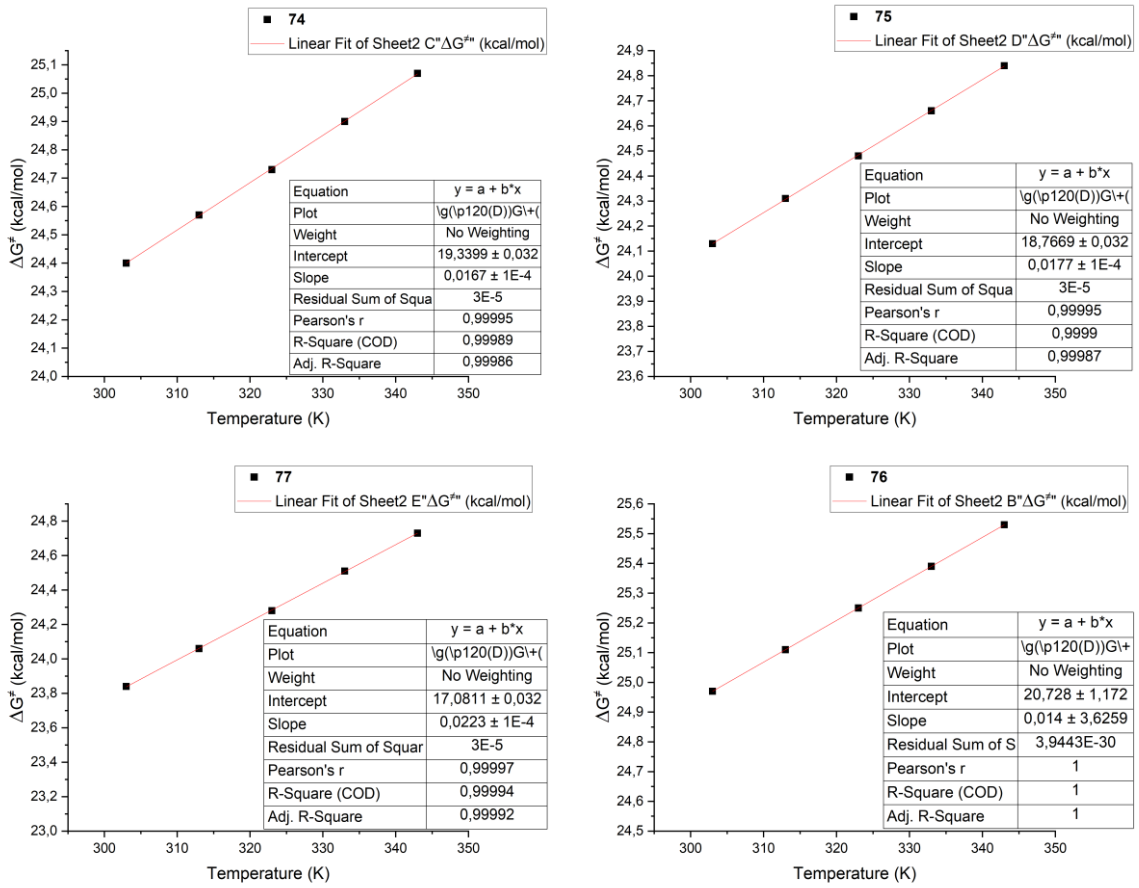

Figure 7.5.34. van't Hoff plot for compounds **74**-**77**. The linear fits give linear function equations, and the resolution of f(x) = g(x) gives the intersection between each functions, of which the abscissa corresponds to the isokinetic temperature.

7.5.2. Properties of glycoazobenzenophanes 78, 79 and 95

7.5.2.1. Thermal relaxation of linear conjugates 101, 103 and 104

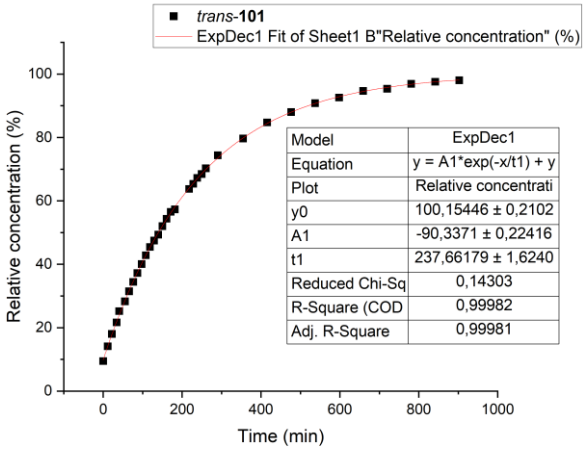

Figure 7.5.35. NMR monitoring (600 MHz, 323 K) of the exponential growth of the concentration of *trans*-**101** starting from a *cis*/*trans* mixture of **101** after irradiation at 365 nm in DMSO-d_6 (1 mM); The rate constant is given by: $k = 1/t_1$.

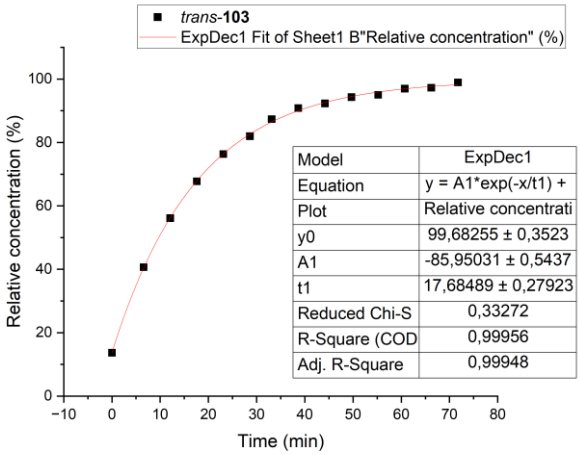

Figure 7.5.36. NMR monitoring (600 MHz, 323 K) of the exponential growth of the concentration of *trans*-**103** starting from a *cis*/*trans* mixture of **103** after irradiation at 385 nm in DMSO-d_6 (1 mM); The rate constant is given by: $k = 1/t_1$.

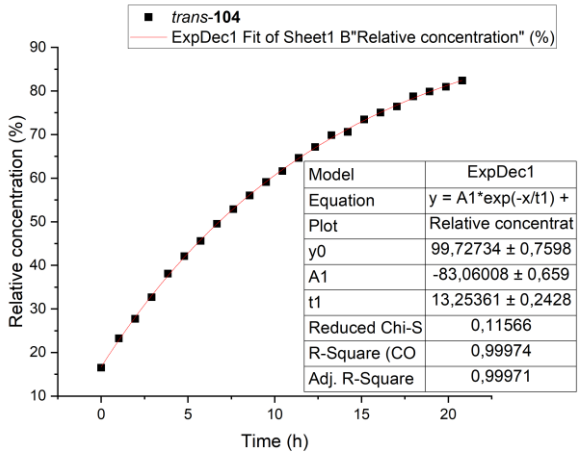

Figure 7.5.37. NMR monitoring (600 MHz, 323 K) of the exponential growth of the concentration of *trans*-**104** starting from a *cis*/*trans* mixture of **104** after irradiation at 385 nm in DMSO-d_6 (1 mM); The rate constant is given by: $k = 1/t_1$.

7.5.2.2. Determination of the PSS composition of linear conjugates 101, 103 and 104

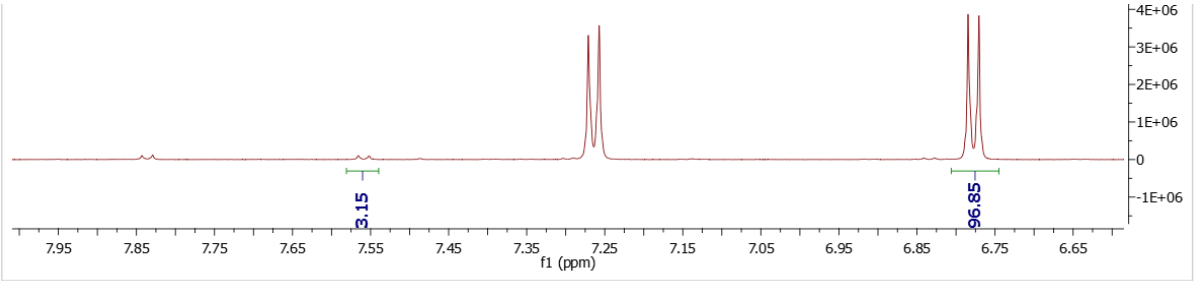

Figure 7.5.38. Expansion in the aromatic region of the ^{1}H NMR spectrum (DMSO-d_6, 300 K) of an equilibrium mixture of *trans* and *cis*-**101** (1 mM) after irradiation at 365 nm (2 min).

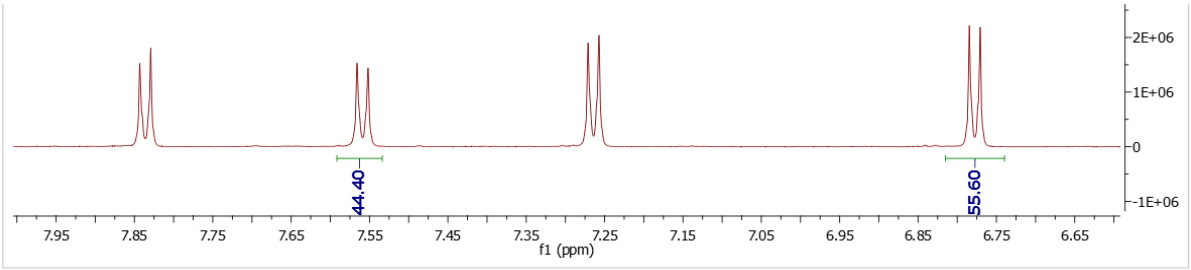

Figure 7.5.39. Expansion in the aromatic region of the ^{1}H NMR spectrum (DMSO-d_6, 300 K) of an equilibrium mixture of *trans* and *cis*-**101** (1 mM) after irradiation at 385 nm (2 min).

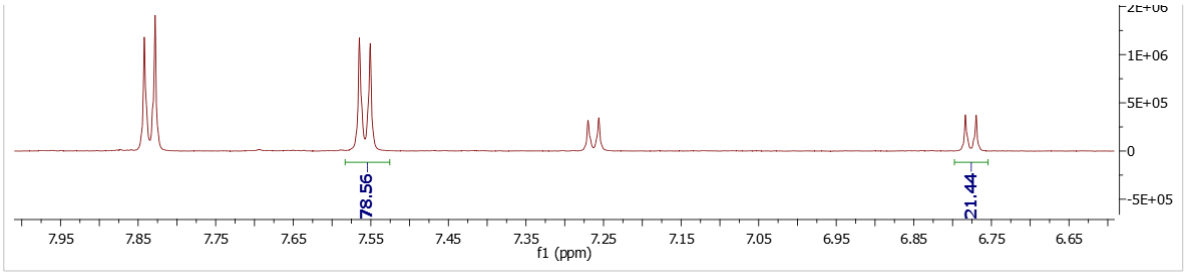

Figure 7.5.40. Expansion in the aromatic region of the ^{1}H NMR spectrum (DMSO-d_6, 300 K) of an equilibrium mixture of *trans* and *cis*-**101** (1 mM) after irradiation at 405 nm (2 min).

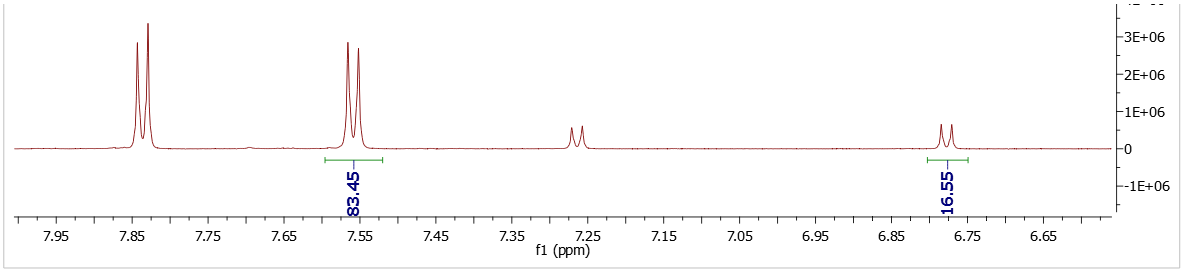

Figure 7.5.41. Expansion in the aromatic region of the ^{1}H NMR spectrum (DMSO-d_6, 300 K) of an equilibrium mixture of *trans* and *cis*-**101** (1 mM) after irradiation at 435 nm (2 min).

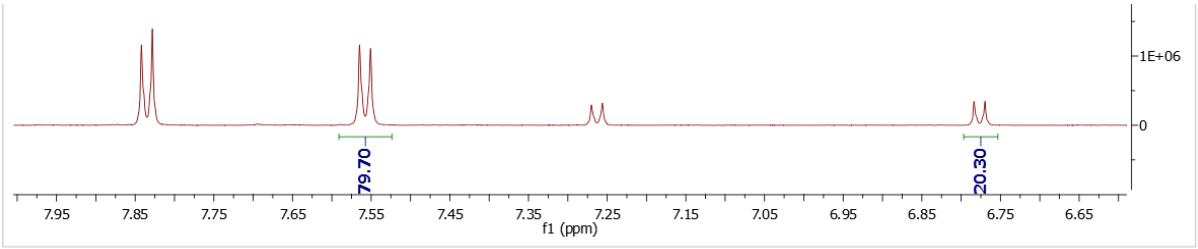

Figure 7.5.42. Expansion in the aromatic region of the ^{1}H NMR spectrum (DMSO-d_6, 300 K) of an equilibrium mixture of *trans* and *cis*-**101** (1 mM) after irradiation at 435 nm (2 min).

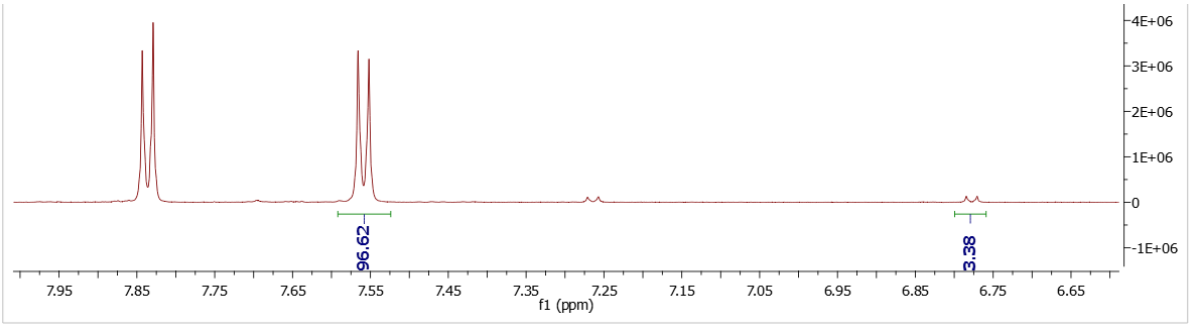

Figure 7.5.43. Expansion in the aromatic region of the ^{1}H NMR spectrum (DMSO-d_6, 300 K) of an equilibrium mixture of *trans* and *cis*-**101** (1 mM) after irradiation at 470 nm (2 min) followed by 625 nm (15 min).

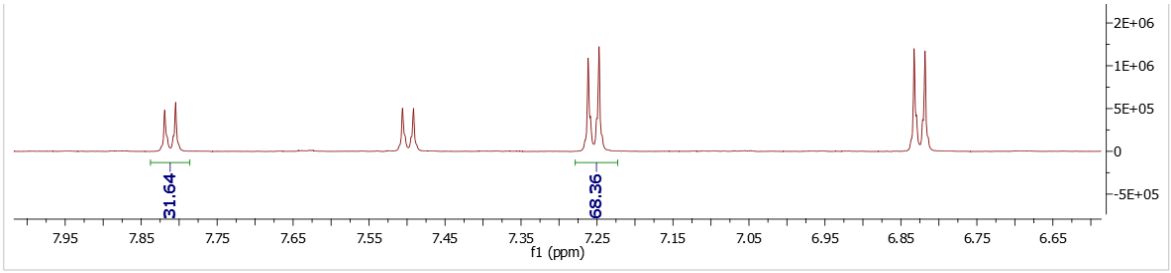

Figure 7.5.44. Expansion in the aromatic region of the ^{1}H NMR spectrum (DMSO-d_6, 300 K) of an equilibrium mixture of *trans* and *cis*-**103** (1 mM) after irradiation at 365 nm (2 min).

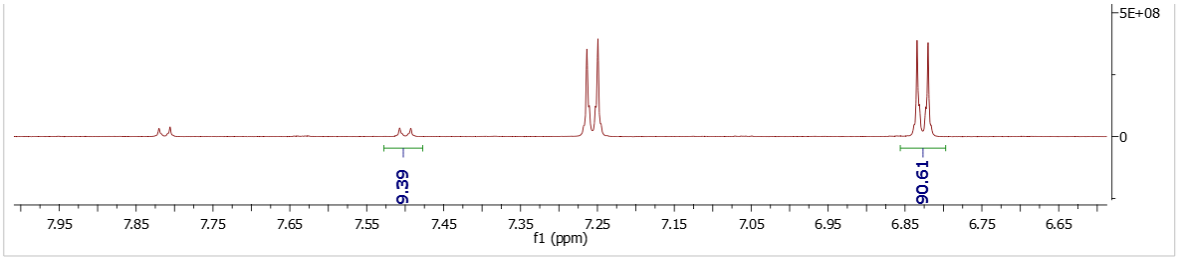

Figure 7.5.45. Expansion in the aromatic region of the ^{1}H NMR spectrum (DMSO-d_6, 300 K) of an equilibrium mixture of *trans* and *cis*-**103** (1 mM) after irradiation at 385 nm (2 min).

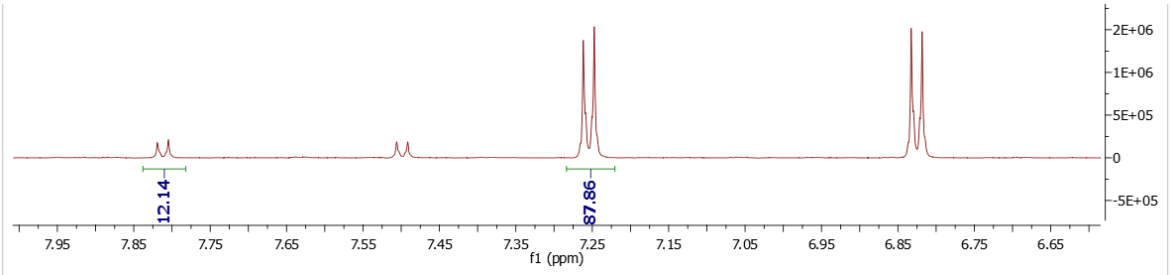

Figure 7.5.46. Expansion in the aromatic region of the ^{1}H NMR spectrum (DMSO-d_6, 300 K) of an equilibrium mixture of *trans* and *cis*-**103** (1 mM) after irradiation at 405 nm (2 min).

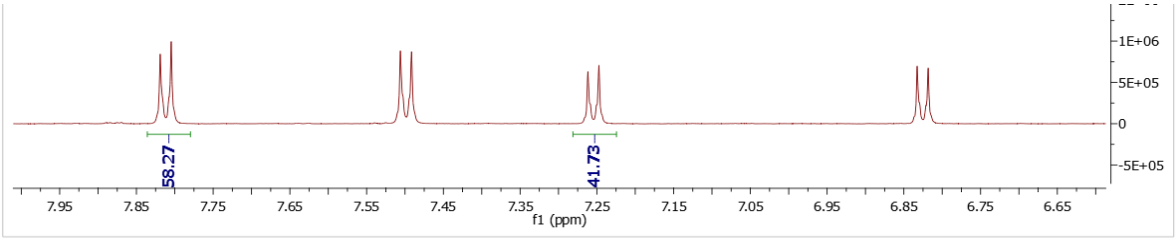

Figure 7.5.47. Expansion in the aromatic region of the ^{1}H NMR spectrum (DMSO-d_6, 300 K) of an equilibrium mixture of *trans* and *cis*-**103** (1 mM) after irradiation at 470 nm (2 min).

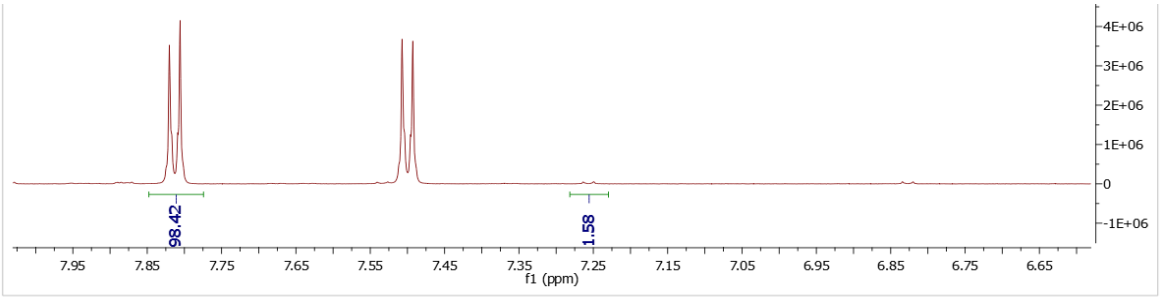

Figure 7.5.48. Expansion in the aromatic region of the ^{1}H NMR spectrum (DMSO-d_6, 300 K) of an equilibrium mixture of *trans* and *cis*-**103** (1 mM) after irradiation at 470 nm (2 min) followed by 625 nm (10 min).

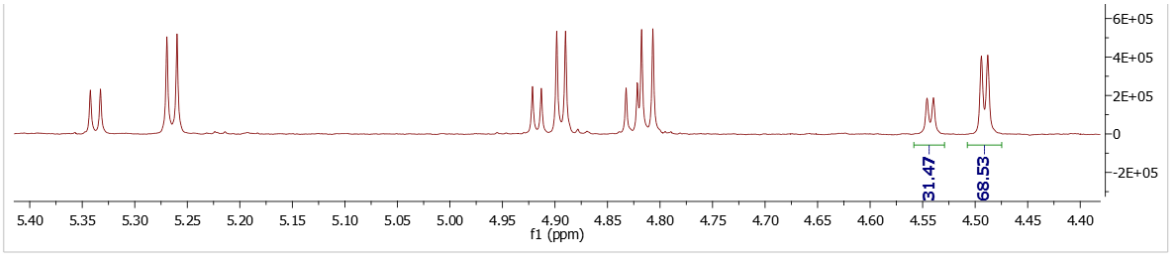

Figure 7.5.49. Expansion in the carbohydrate region of the ^{1}H NMR spectrum (DMSO-d_6, 300 K) of an equilibrium mixture of *trans* and *cis*-**104** (1 mM) after irradiation at 365 nm (2 min).

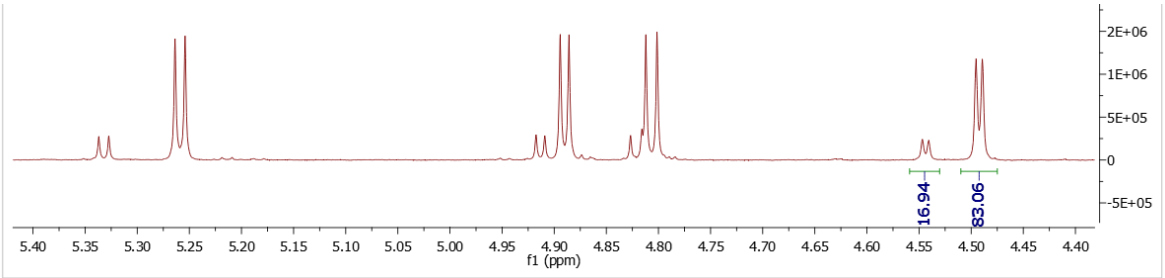

Figure 7.5.50. Expansion in the carbohydrate region of the ^{1}H NMR spectrum (DMSO-d_6, 300 K) of an equilibrium mixture of *trans* and *cis*-**104** (1 mM) after irradiation at 385 nm (2 min).

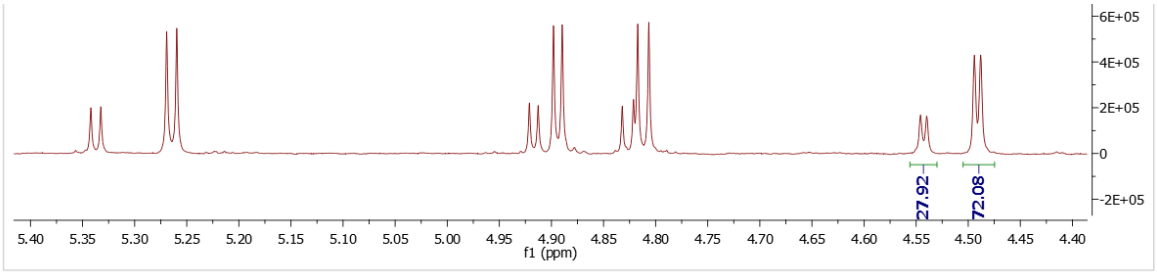

Figure 7.5.51. Expansion in the carbohydrate region of the ^{1}H NMR spectrum (DMSO-d_6, 300 K) of an equilibrium mixture of *trans* and *cis*-**104** (1 mM) after irradiation at 405 nm (2 min).

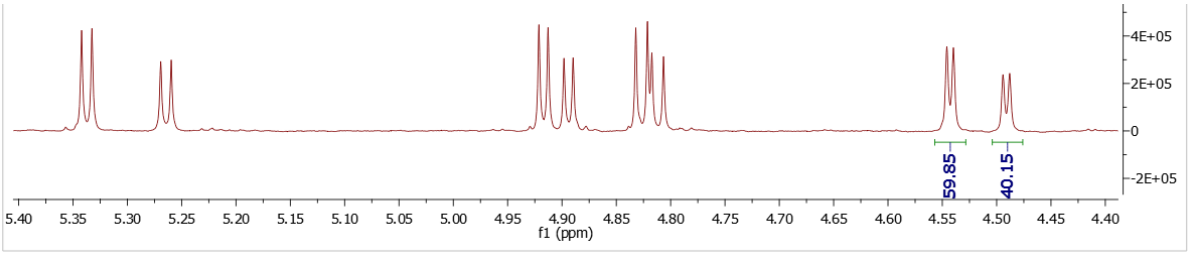

Figure 7.5.52. Expansion in the carbohydrate region of the ^{1}H NMR spectrum (DMSO-d_6, 300 K) of an equilibrium mixture of *trans* and *cis*-**104** (1 mM) after irradiation at 470 nm (2 min).

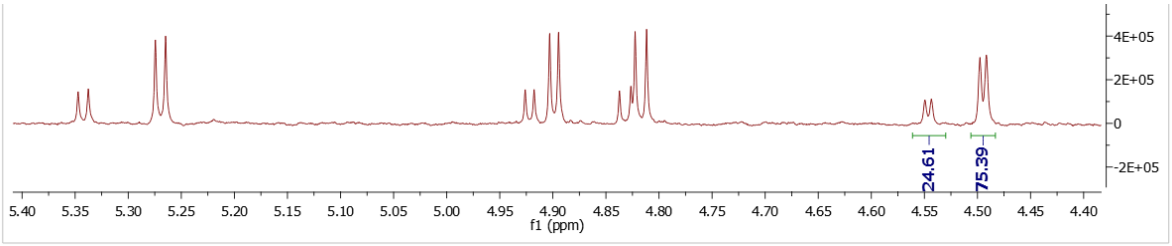

Figure 7.5.53. Expansion in the carbohydrate region of the ^{1}H NMR spectrum (DMSO-d_6, 300 K) of an equilibrium mixture of *trans* and *cis*-**104** (1 mM) after irradiation at 625 nm (12 min).

7.5.2.3. Thermal relaxation of glycoazobenzenophanes 78 and 79

The fitting of the thermal relaxation data was performed by Prof. V. Pimienta, Paul Sabatier University, Toulouse. A homemade program SA was used to fit the kinetic data. The corresponding differential equations were integrated numerically using a semi-implicit Runge-Kutta method. The unknown parameters were fitted automatically using an iterative algorithm of the Powell type, designed to minimize the residual quadratic error E = Σj Σi [cij - eij]2/(n ·N) where cij and eij are the computed and experimental values of concentrations respectively, n is the number of data point in a given run, and N is the number of runs.

The thermal relaxation of macrocycles **78** and **79** is described by the following differential equations:

$$\frac{dA(t)}{dt} = -k_1A(t) - k_2A(t) \quad (1)$$

$$\frac{dB(t)}{dt} = k_1A(t) - k_3B(t) \quad (2)$$

$$\frac{dC(t)}{dt} = k_2A(t) - k_4C(t) \quad (3)$$

$$\frac{dD(t)}{dt} = k_3B(t) + k_4C(t) \quad (4)$$

With $A(t) = [Z,Z]_t$, $B(t) = [Z,E]_t$, $C(t) = [E,Z]_t$ and $D(t) = [E,E]_t$.

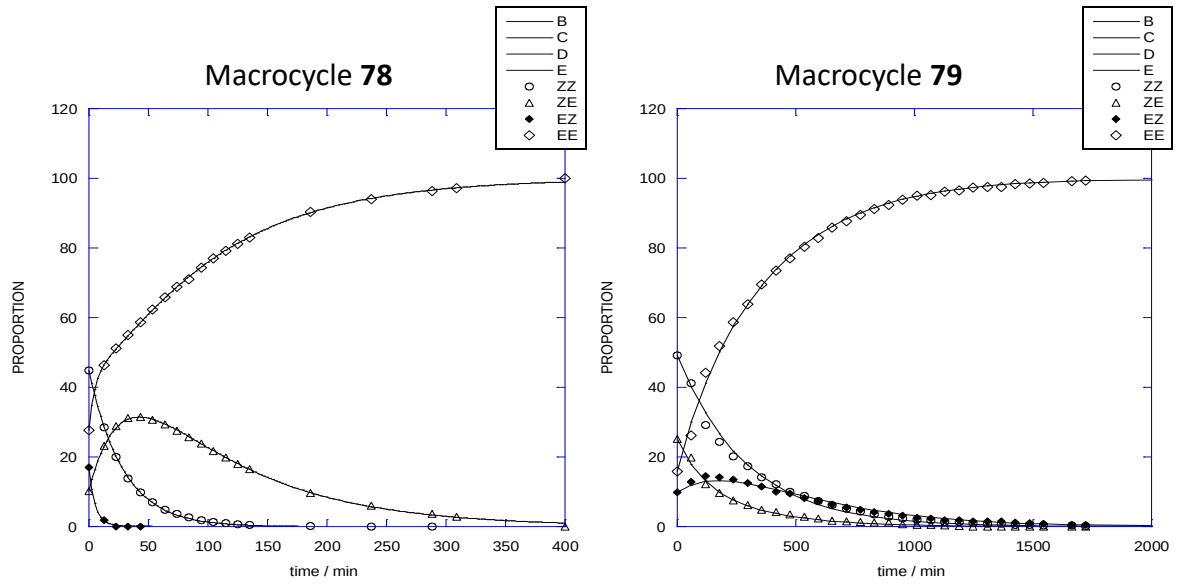

Figure 7.5.54. Fits of the kinetic traces of thermal reversal of PSS mixtures of macrocycles **78** (left) and **79** (right) after irradiation at 365 nm. The obtained values for the thermal relaxation constants are given in Tables 5.6 and 5.9.

7.5.2.4. Determination of the PSS composition for macrocycle 78

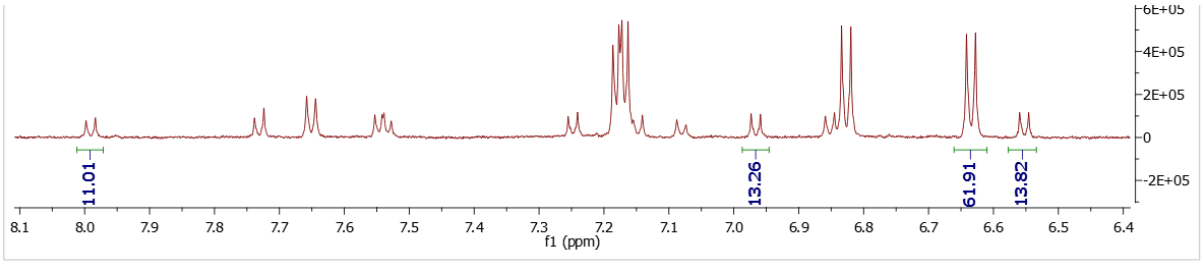

Figure 7.5.55. Expansion in the aromatic region of the ^{1}H NMR spectrum (DMSO-d_6, 300 K) of an equilibrium mixture of (*E*,*E*), (*Z*,*E*), (*E*,*Z*) and (*Z*,*Z*)-**78** (1 mM) after irradiation at 365 nm (6 min).

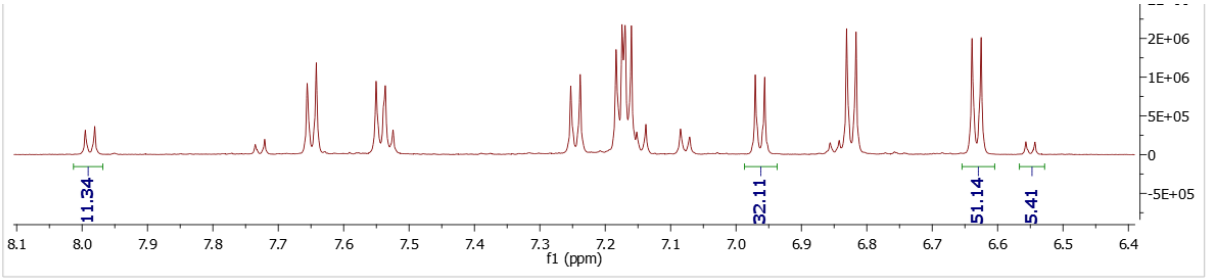

Figure 7.5.56. Expansion in the aromatic region of the ^{1}H NMR spectrum (DMSO-d_6, 300 K) of an equilibrium mixture of (*E*,*E*), (*Z*,*E*), (*E*,*Z*) and (*Z*,*Z*)-**78** (1 mM) after irradiation at 385 nm (2 min).

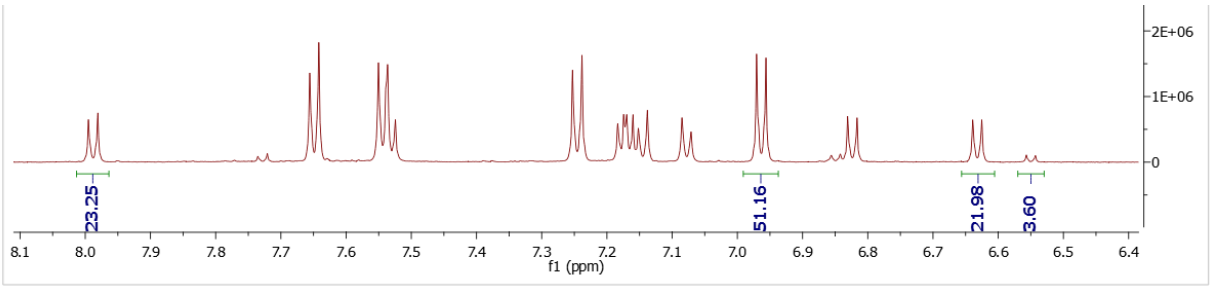

Figure 7.5.57. Expansion in the aromatic region of the ^{1}H NMR spectrum (DMSO-d_6, 300 K) of an equilibrium mixture of (*E*,*E*), (*Z*,*E*), (*E*,*Z*) and (*Z*,*Z*)-**78** (1 mM) after irradiation at 405 nm (2 min).

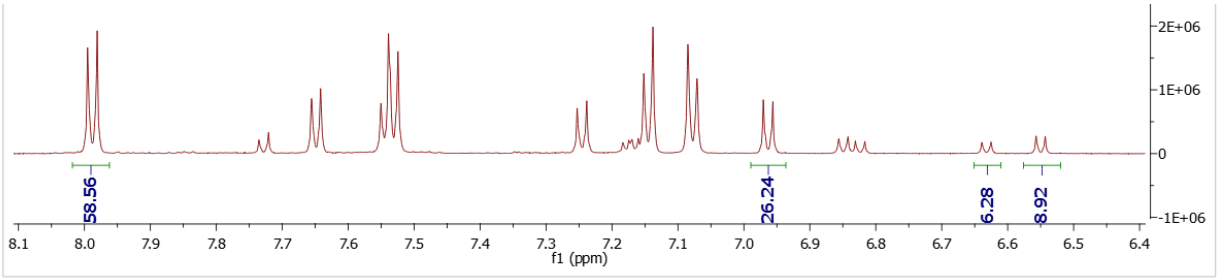

Figure 7.5.58. Expansion in the aromatic region of the ^{1}H NMR spectrum (DMSO-d_6, 300 K) of an equilibrium mixture of (*E*,*E*), (*Z*,*E*), (*E*,*Z*) and (*Z*,*Z*)-**78** (1 mM) after irradiation at 470 nm (2 min).

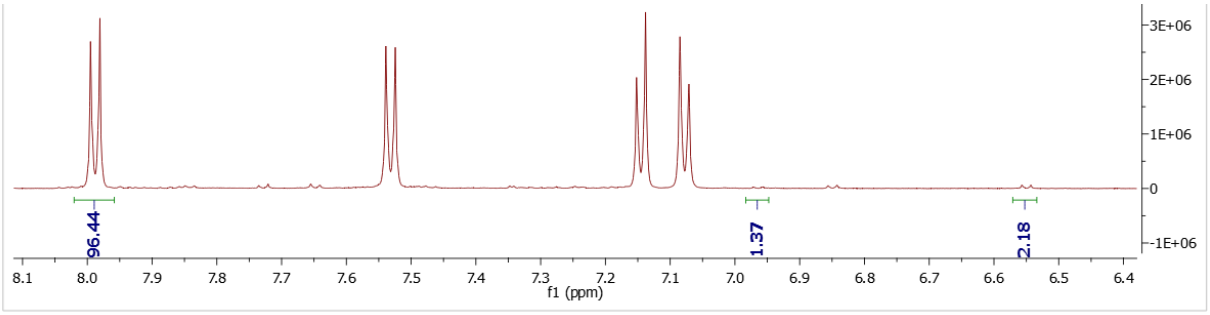

Figure 7.5.59. Expansion in the aromatic region of the ^{1}H NMR spectrum (DMSO-d_6, 300 K) of an equilibrium mixture of (*E*,*E*), (*Z*,*E*), (*E*,*Z*) and (*Z*,*Z*)-**78** (1 mM) after irradiation at 625 nm (15 min).

7.5.2.5. Selective multistate switching of macrocycle 78

Cycle 1:

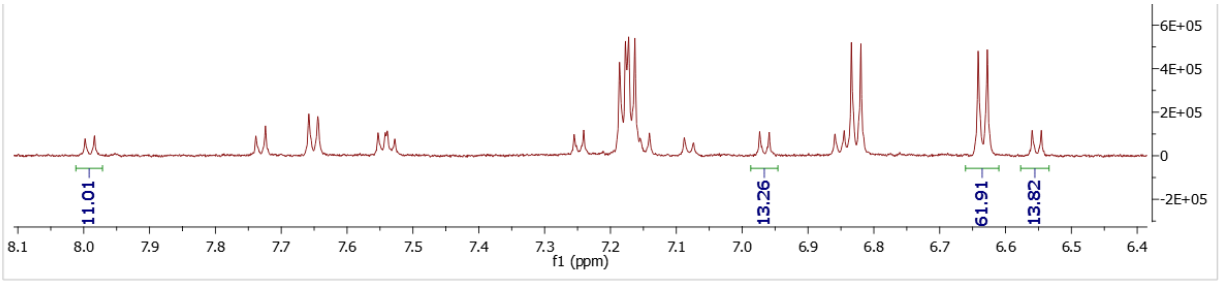

Figure 7.5.60. Expansion in the aromatic region of the ^{1}H NMR spectrum (DMSO-d_6, 300 K) of an equilibrium mixture of (*E*,*E*), (*Z*,*E*), (*E*,*Z*) and (*Z*,*Z*)-**78** (1 mM) after irradiation at 365 nm (6 min).

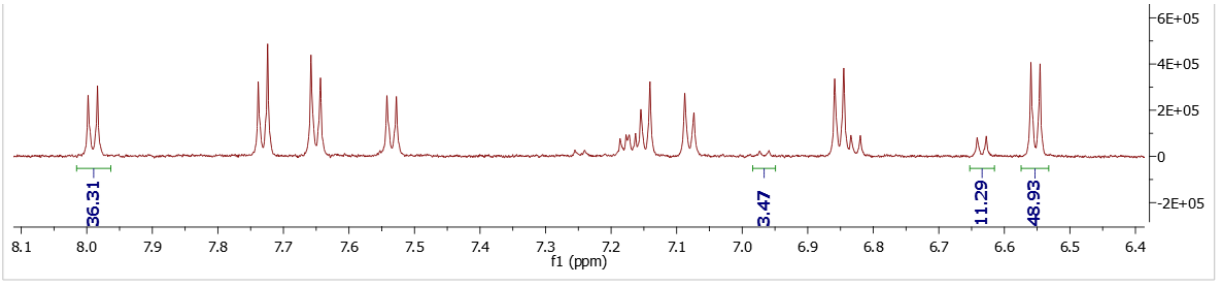

Figure 7.5.61. Expansion in the aromatic region of the ^{1}H NMR spectrum (DMSO-d_6, 300 K) of a mixture of (*E*,*E*), (*Z*,*E*), (*E*,*Z*) and (*Z*,*Z*)-**78** (1 mM) after irradiation at 365 nm (6 min) followed by 625 nm (1 min).

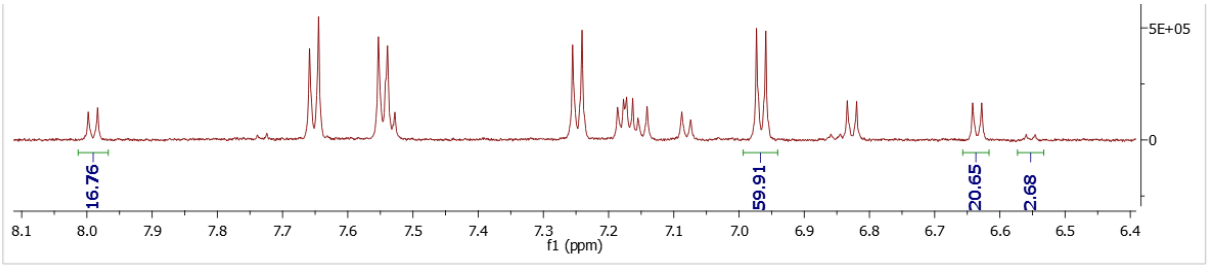

Figure 7.5.62. Expansion in the aromatic region of the ^{1}H NMR spectrum (DMSO-d_6, 300 K) of an equilibrium mixture of (*E*,*E*), (*Z*,*E*), (*E*,*Z*) and (*Z*,*Z*)-**78** (1 mM) after irradiation at 365 nm (6 min) followed by 625 nm (1 min) and 405 nm (2 min).

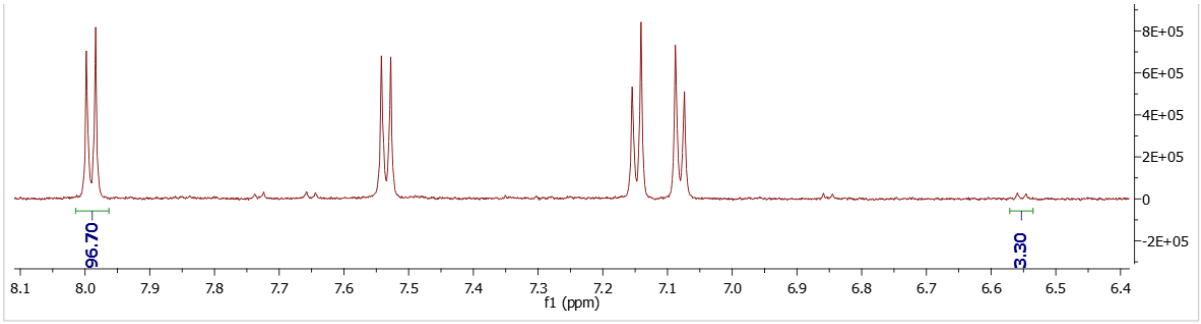

Figure 7.5.63. Expansion in the aromatic region of the ^{1}H NMR spectrum (DMSO-d_6, 300 K) of an equilibrium mixture of (*E*,*E*), (*Z*,*E*), (*E*,*Z*) and (*Z*,*Z*)-**78** (1 mM) after irradiation at 365 nm (6 min) followed by 625 nm (1 min), 405 nm (2 min) and 625 nm (20 min).

Cycle 2:

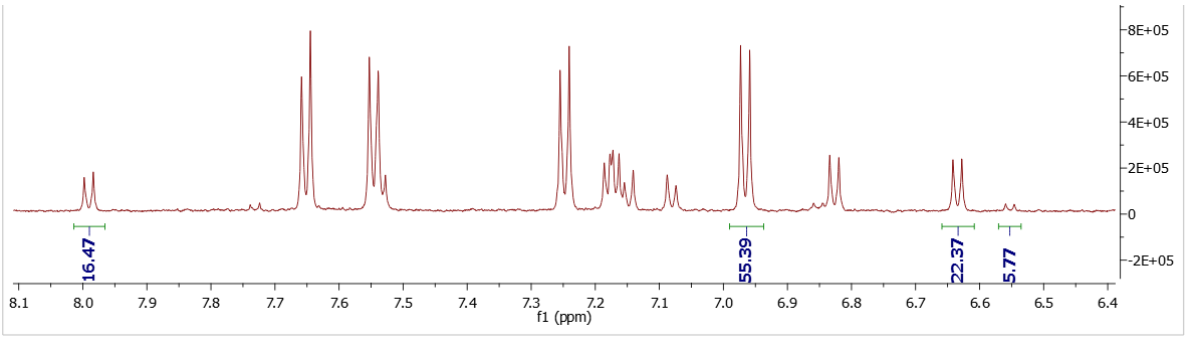

Figure 7.5.64. Expansion in the aromatic region of the ^{1}H NMR spectrum (DMSO-d_6, 300 K) of an equilibrium mixture of (*E*,*E*), (*Z*,*E*), (*E*,*Z*) and (*Z*,*Z*)-**78** (1 mM) after irradiation at 405 nm (2 min).

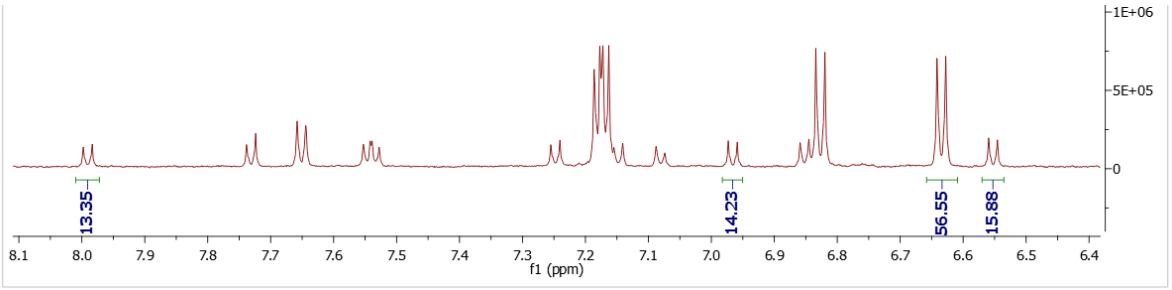

Figure 7.5.65. Expansion in the aromatic region of the ^{1}H NMR spectrum (DMSO-d_6, 300 K) of an equilibrium mixture of (*E*,*E*), (*Z*,*E*), (*E*,*Z*) and (*Z*,*Z*)-**78** (1 mM) after irradiation at 405 nm (2 min) followed by 365 nm (4 min).

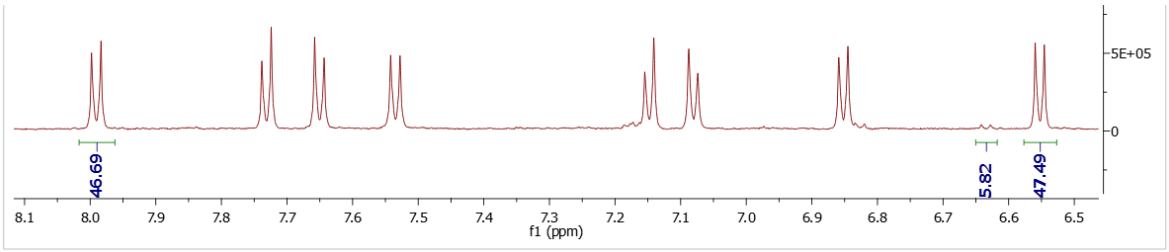

Figure 7.5.66. Expansion in the aromatic region of the ^{1}H NMR spectrum (DMSO-d_6, 300 K) of a mixture of (*E*,*E*), (*Z*,*E*), (*E*,*Z*) and (*Z*,*Z*)-**78** (1 mM) after irradiation at 405 nm (2 min) followed by 365 nm (4 min) and 625 nm (2 min).

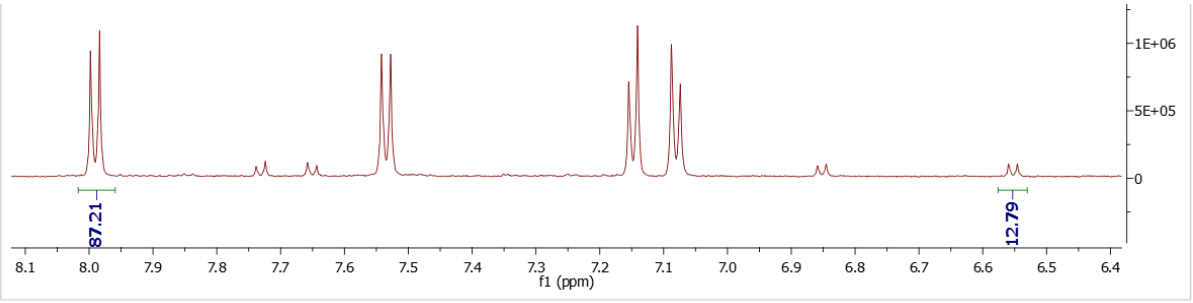

Figure 7.5.67. Expansion in the aromatic region of the ^{1}H NMR spectrum (DMSO-d_6, 300 K) of a mixture of (*E*,*E*), (*Z*,*E*), (*E*,*Z*) and (*Z*,*Z*)-**78** (1 mM) after irradiation at 405 nm (2 min) followed by 365 nm (4 min) and 625 nm (22 min).

7.5.2.6. Determination of the PSS composition for macrocycle 79

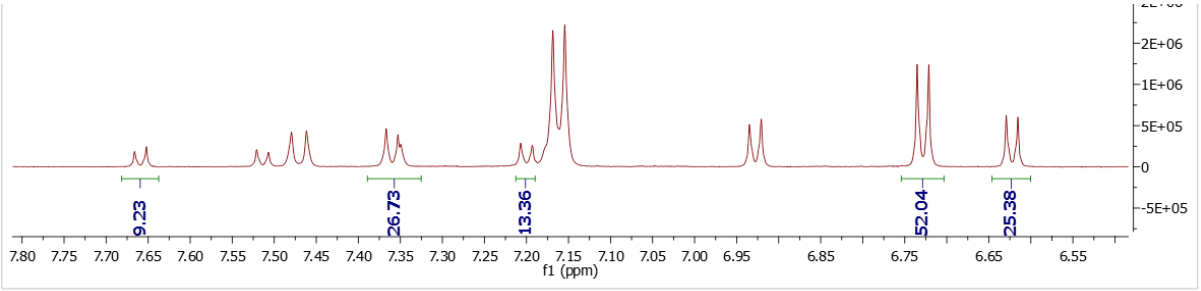

Figure 7.5.68. Expansion in the aromatic region of the ^{1}H NMR spectrum (DMSO-d_6, 300 K) of an equilibrium mixture of (*E*,*E*), (*Z*,*E*), (*E*,*Z*) and (*Z*,*Z*)-**79** (1 mM) after irradiation at 365 nm (2 min); the signal at 7.36 ppm was integrated to ascertain the accurate integration of the signal at 7.20 ppm.

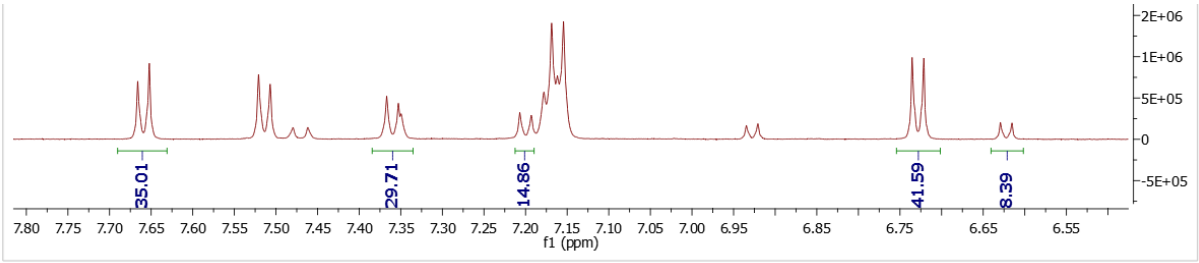

Figure 7.5.69. Expansion in the aromatic region of the ^{1}H NMR spectrum (DMSO-d_6, 300 K) of an equilibrium mixture of (*E*,*E*), (*Z*,*E*), (*E*,*Z*) and (*Z*,*Z*)-**79** (1 mM) after irradiation at 385 nm (2 min); the signal at 7.36 ppm was integrated to ascertain the accurate integration of the signal at 7.20 ppm.

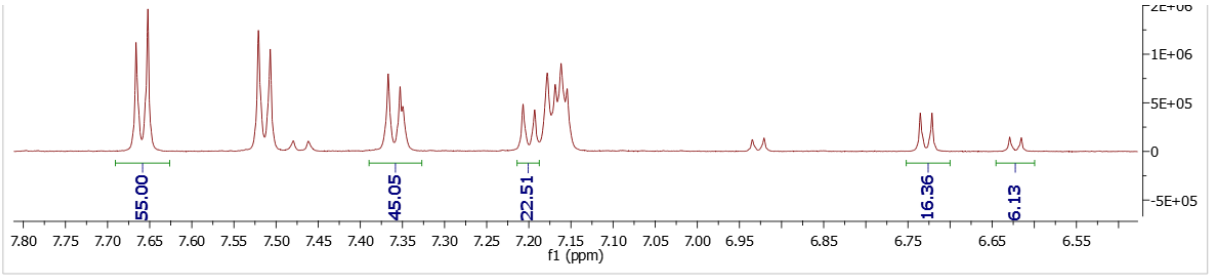

Figure 7.5.70. Expansion in the aromatic region of the ^{1}H NMR spectrum (DMSO-d_6, 300 K) of an equilibrium mixture of (*E*,*E*), (*Z*,*E*), (*E*,*Z*) and (*Z*,*Z*)-**79** (1 mM) after irradiation at 405 nm (2 min); the signal at 7.36 ppm was integrated to ascertain the accurate integration of the signal at 7.20 ppm.

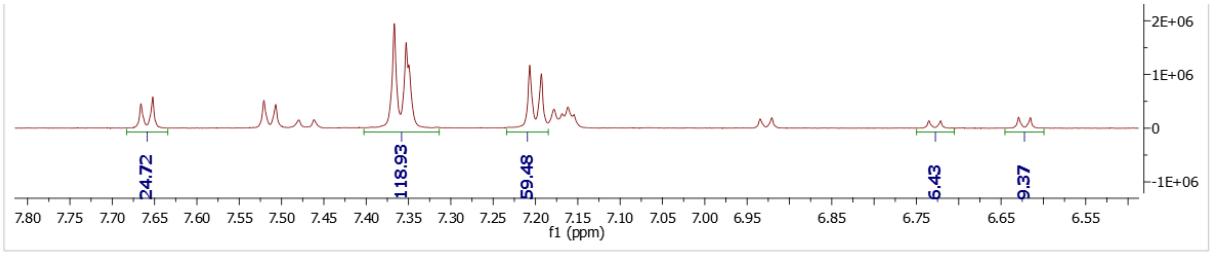

Figure 7.5.71. Expansion in the aromatic region of the ^{1}H NMR spectrum (DMSO-d_6, 300 K) of an equilibrium mixture of (*E*,*E*), (*Z*,*E*), (*E*,*Z*) and (*Z*,*Z*)-**79** (1 mM) after irradiation at 470 nm (2 min); the signal at 7.36 ppm was integrated to ascertain the accurate integration of the signal at 7.20 ppm.

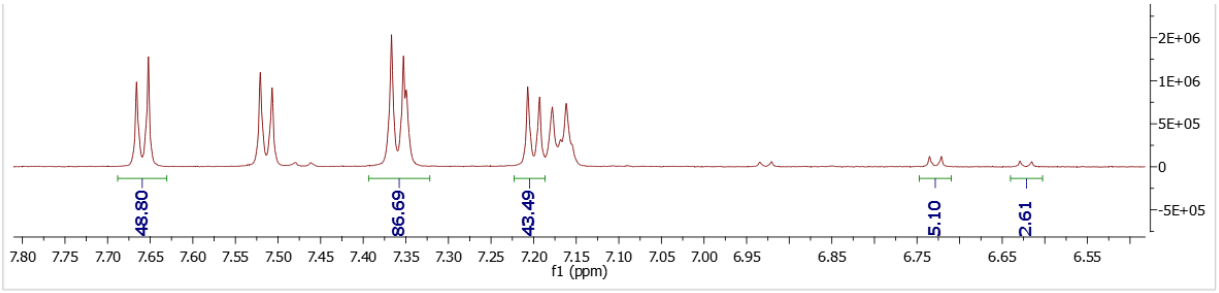

Figure 7.5.72. Expansion in the aromatic region of the ^{1}H NMR spectrum (DMSO-d_6, 300 K) of a mixture of (*E*,*E*), (*Z*,*E*), (*E*,*Z*) and (*Z*,*Z*)-**79** (1 mM) after irradiation at 470 nm (2 min) followed by irradiation at 625 nm (5 min); the signal at 7.36 ppm was integrated to ascertain the accurate integration of the signal at 7.20 ppm.

7.5.2.7. Determination of the PSS composition for macrocycle 95

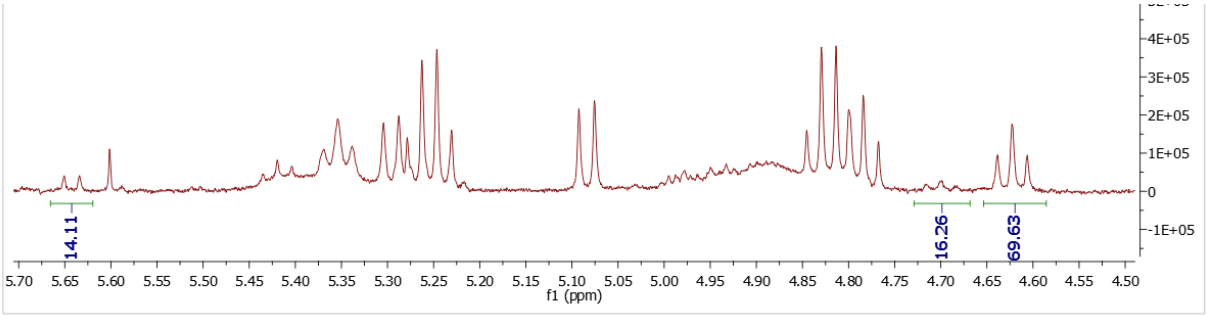

Figure 7.5.73. Expansion in the aromatic region of the ^{1}H NMR spectrum (DMSO-d_6, 300 K) of an equilibrium mixture of (*E*,*E*), (*Z*,*E*), (*E*,*Z*) and (*Z*,*Z*)-**95** (1 mM) after irradiation at 385 nm (2 min).

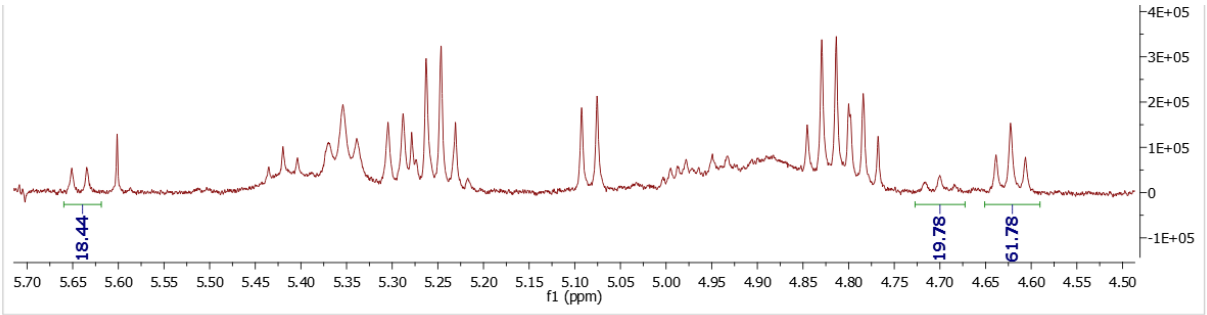

Figure 7.5.74. Expansion in the aromatic region of the ^{1}H NMR spectrum (DMSO-d_6, 300 K) of an equilibrium mixture of (*E*,*E*), (*Z*,*E*), (*E*,*Z*) and (*Z*,*Z*)-**95** (1 mM) after irradiation at 405 nm (2 min).

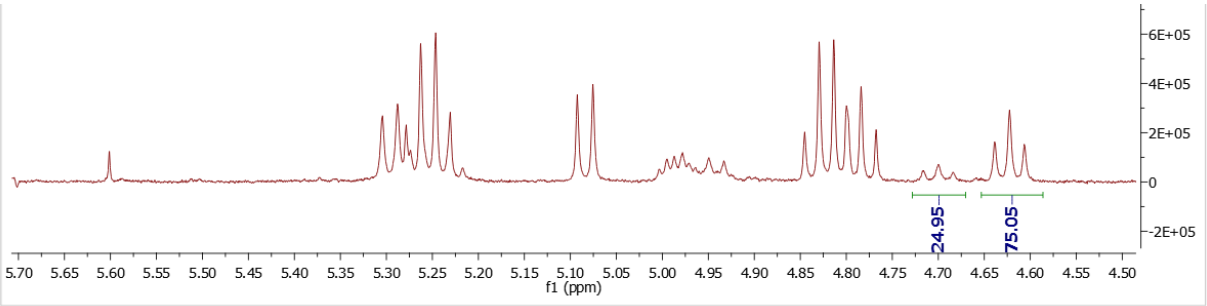

Figure 7.5.75. Expansion in the aromatic region of the ^{1}H NMR spectrum (DMSO-d_6, 300 K) of a mixture of (*E*,*E*), (*Z*,*E*), (*E*,*Z*) and (*Z*,*Z*)-**95** (1 mM) after irradiation at 405 nm (2 min) followed by 660 nm (30 s).

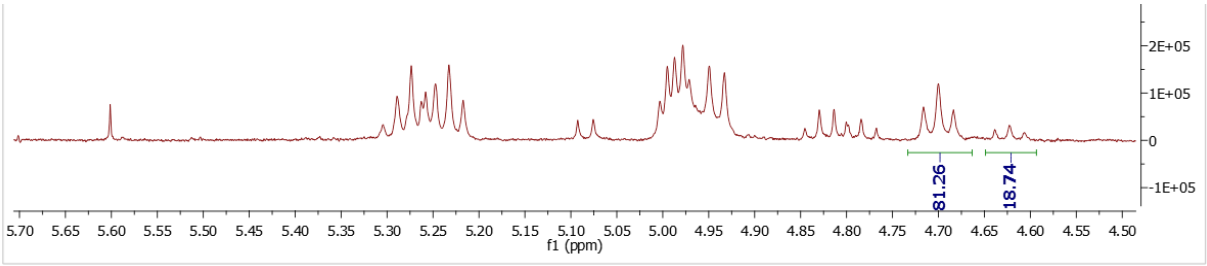

Figure 7.5.76. Expansion in the aromatic region of the ^{1}H NMR spectrum (DMSO-d_6, 300 K) of an equilibrium mixture of (*E*,*E*), (*Z*,*E*), (*E*,*Z*) and (*Z*,*Z*)-**95** (1 mM) after irradiation at 520 nm (2 min).

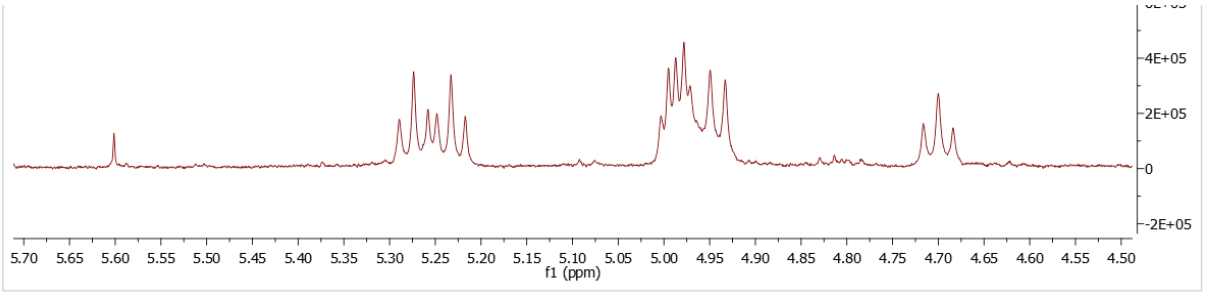

Figure 7.5.77. Expansion in the aromatic region of the ^{1}H NMR spectrum (DMSO-d_6, 300 K) of a mixture of (*E*,*E*), (*Z*,*E*), (*E*,*Z*) and (*Z*,*Z*)-**95** (1 mM) after irradiation at 520 nm (2 min) followed by 625 nm (5 min). The integrals are not shown because of a too small signal-over-noise ratio for the integration of (*Z*,*Z*)-**95**.

7.6. NMR spectra of the synthesized compounds

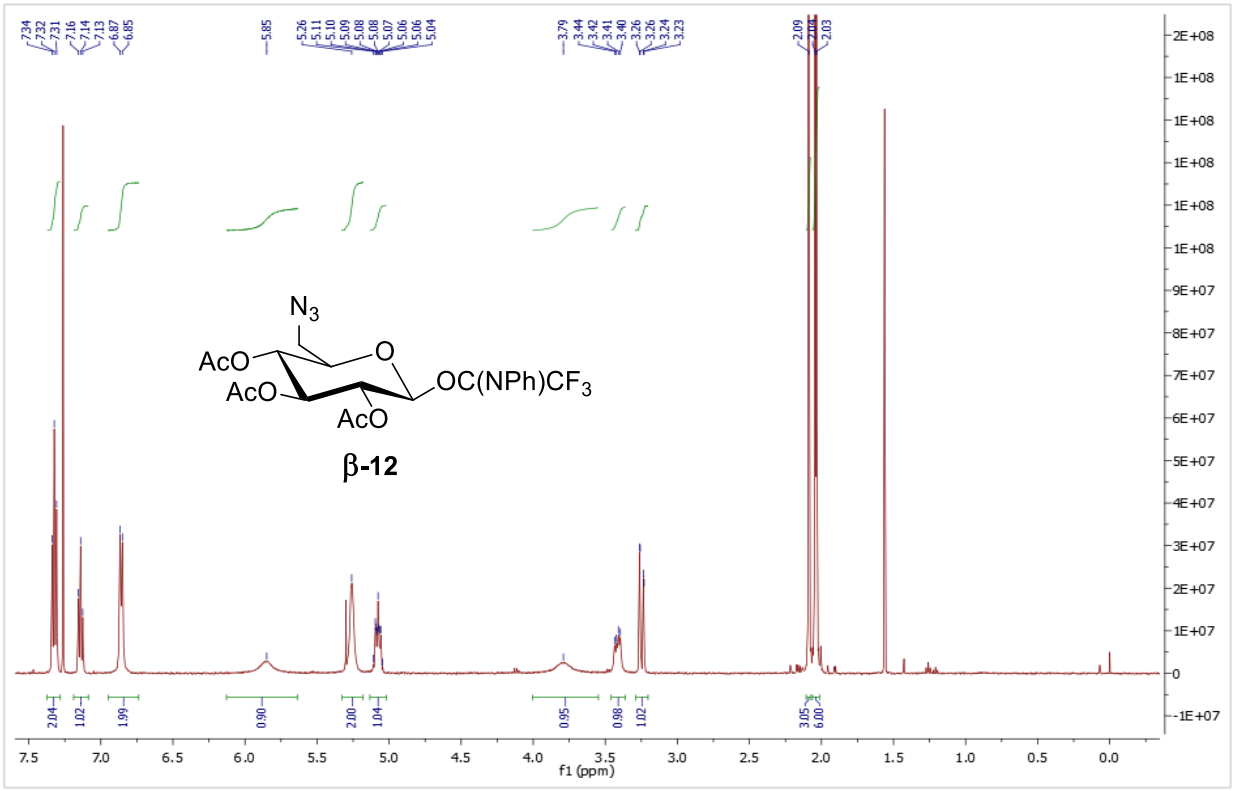

Figure 7.6.1. ^{1}H NMR spectrum of **β-12** (500 MHz, $CDCl_3$, 300 K).

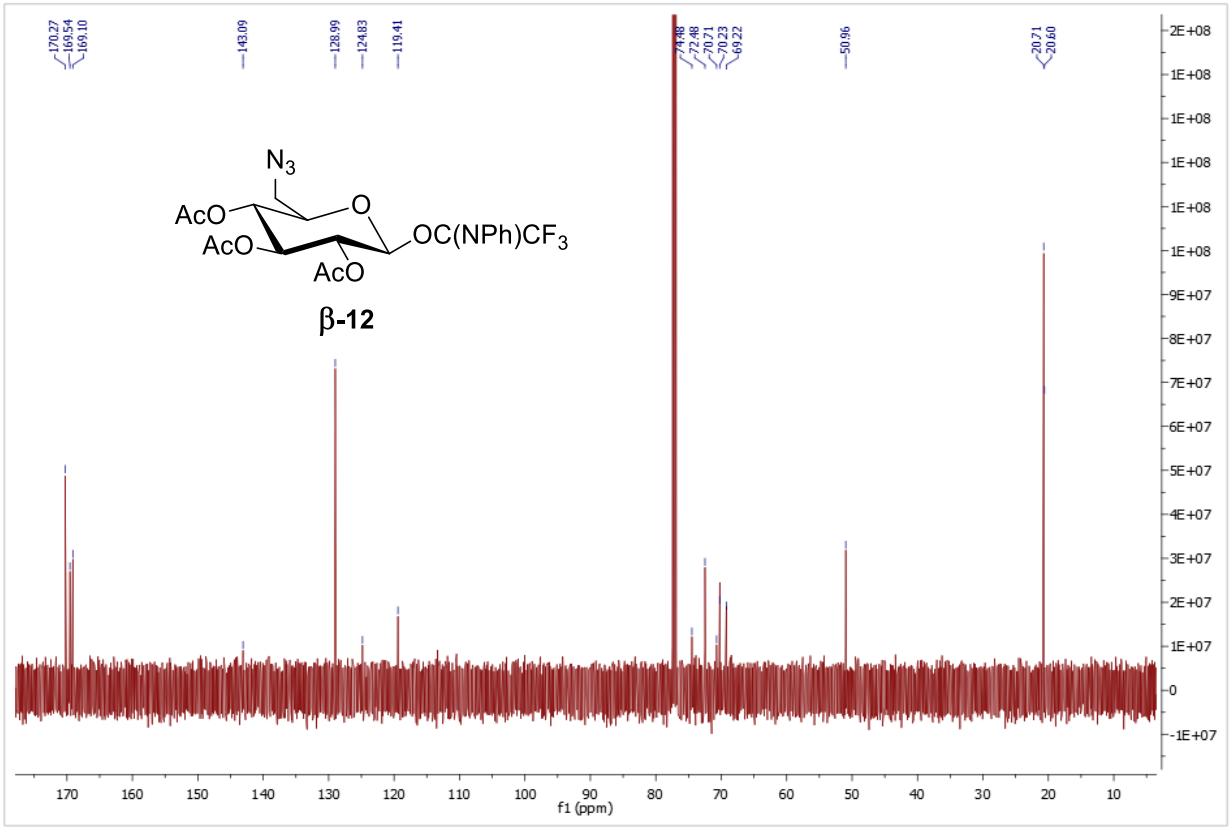

Figure 7.6.2. ^{13}C NMR spectrum of **β-12** (126 MHz, $CDCl_3$, 300 K).

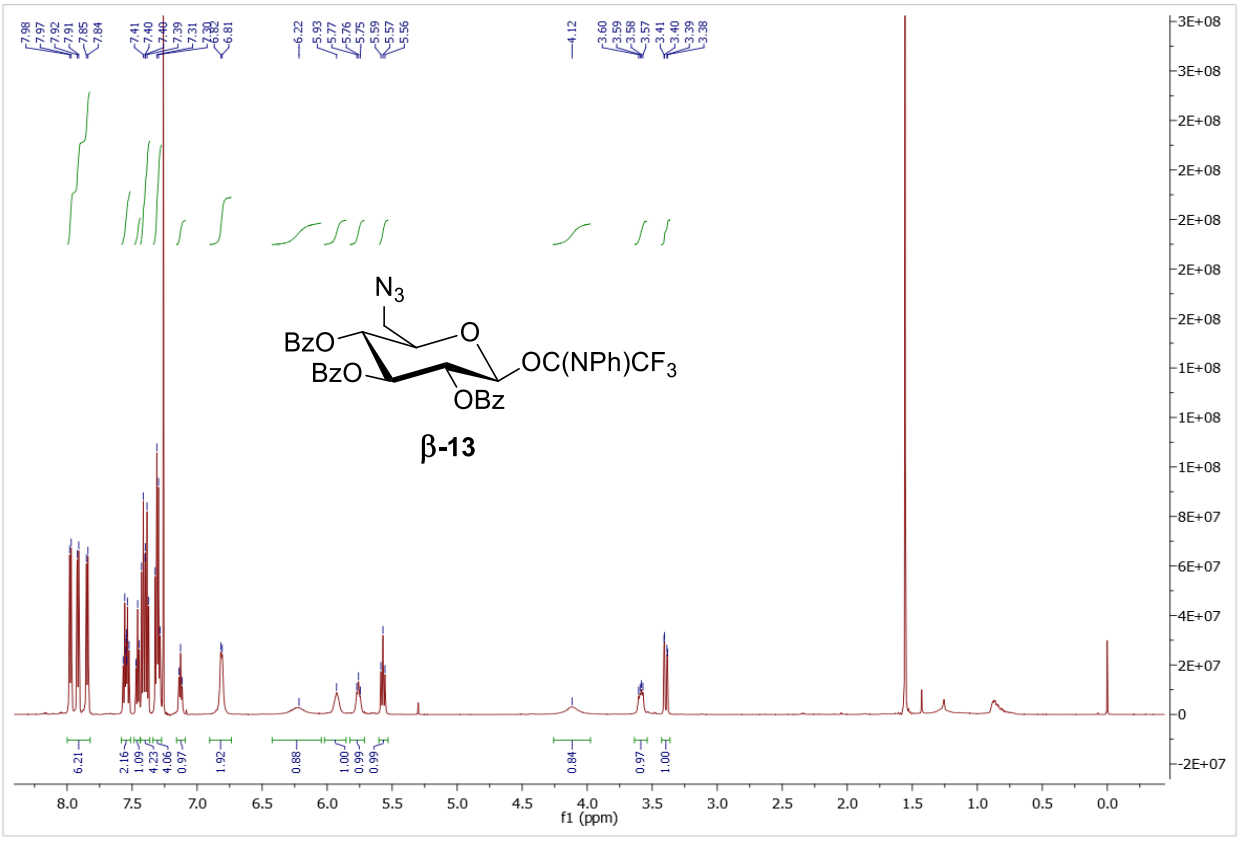

Figure 7.6.3. ^{1}H NMR spectrum of **β-13** (500 MHz, $CDCl_3$, 300 K).

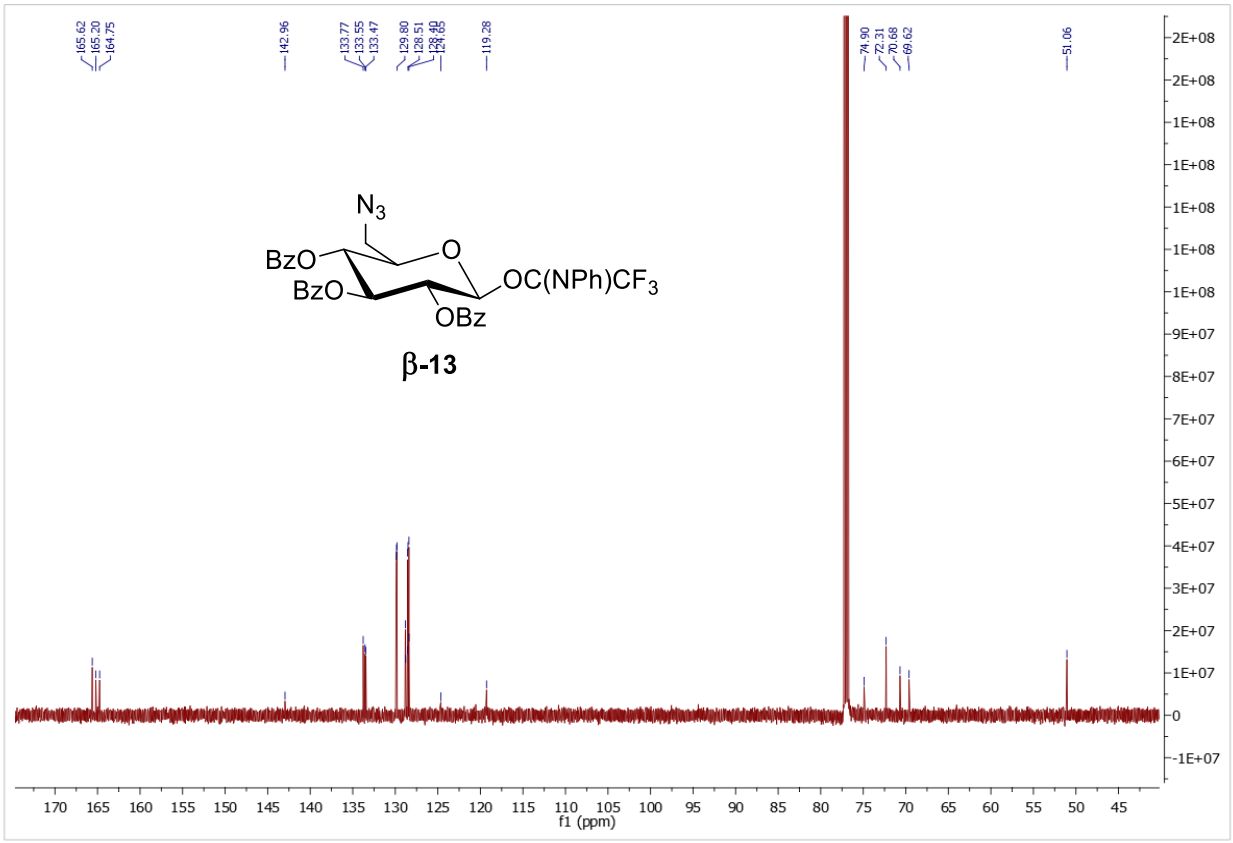

Figure 7.6.4. ^{13}C NMR spectrum of **β-13** (126 MHz, $CDCl_3$, 300 K).

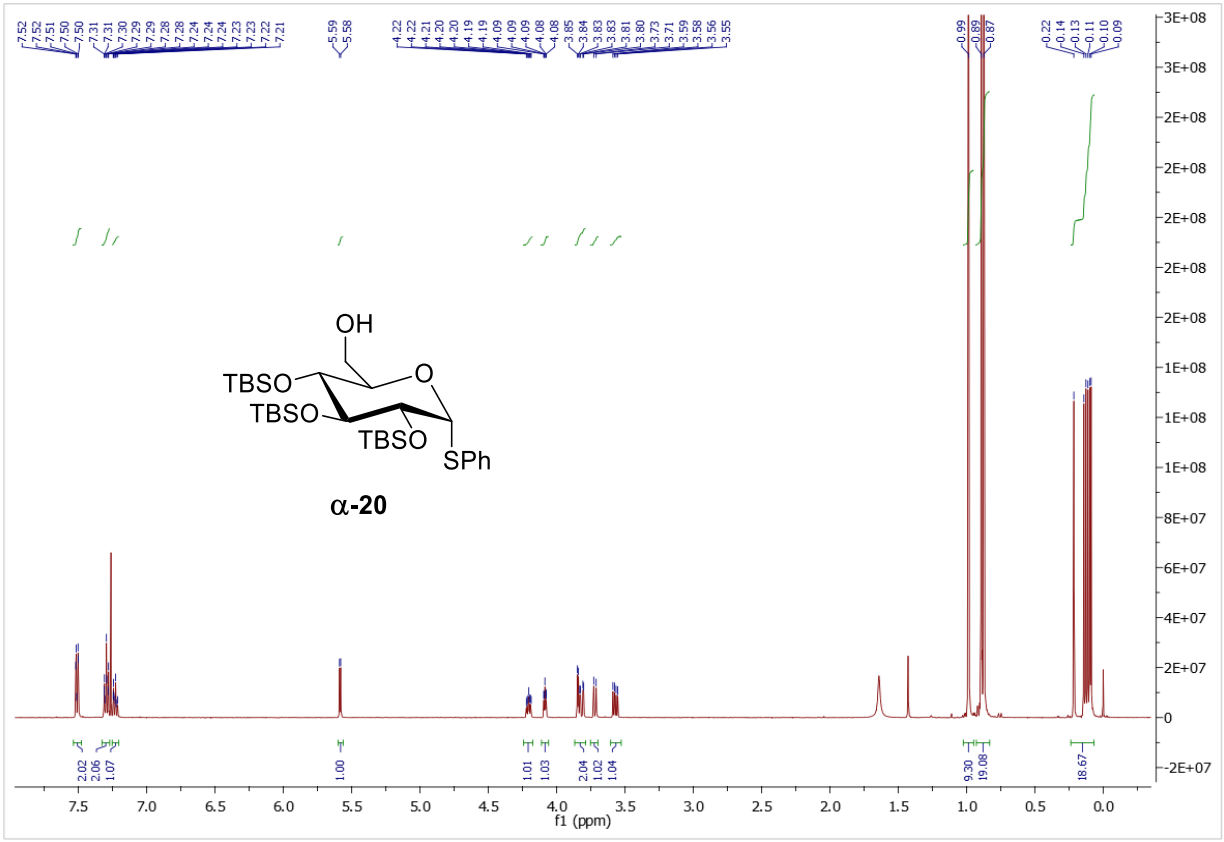

Figure 7.6.5. ^{1}H NMR spectrum of **α-20** (500 MHz, $CDCl_3$, 300 K).

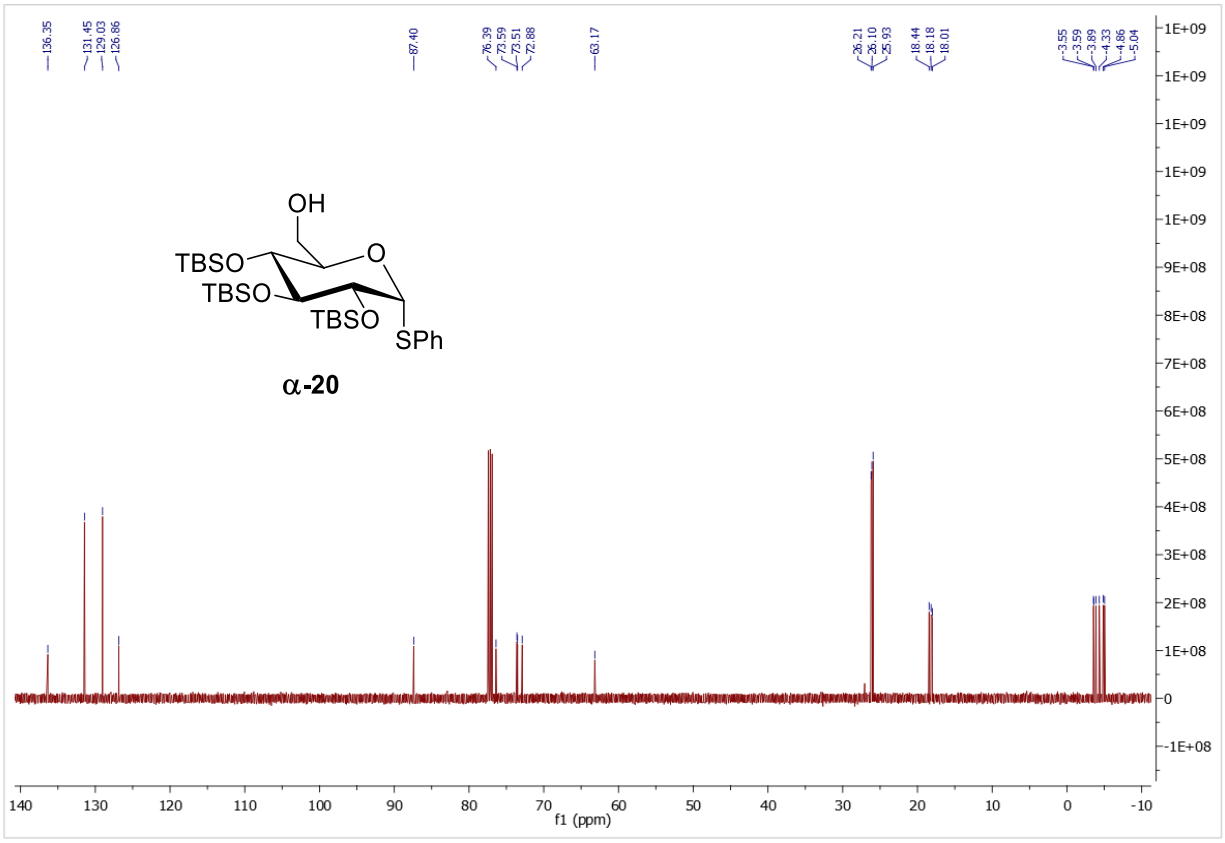

Figure 7.6.6. ^{13}C NMR spectrum of **α-20** (126 MHz, $CDCl_3$, 300 K).

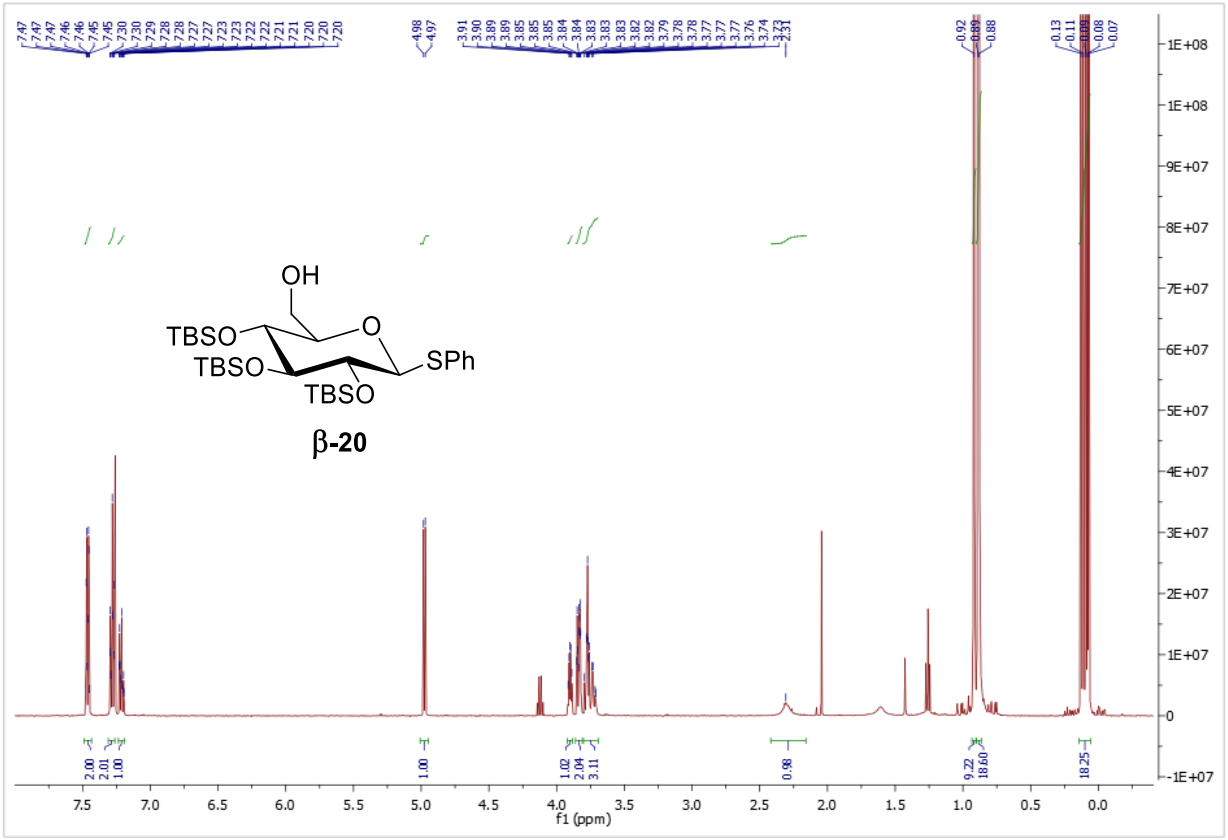

Figure 7.6.7. ^{1}H NMR spectrum of **β-20** (500 MHz, $CDCl_3$, 300 K).

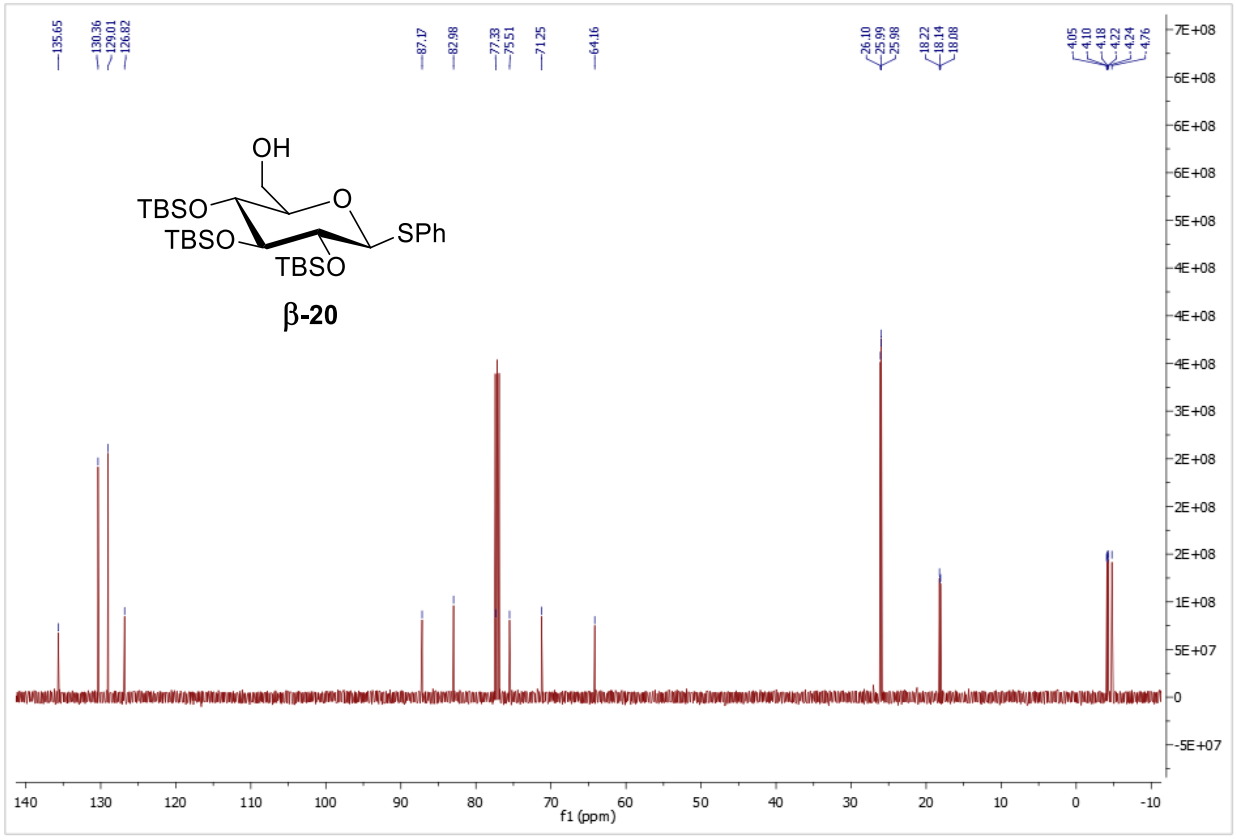

Figure 7.6.8. ^{13}C NMR spectrum of **β-20** (126 MHz, $CDCl_3$, 300 K).

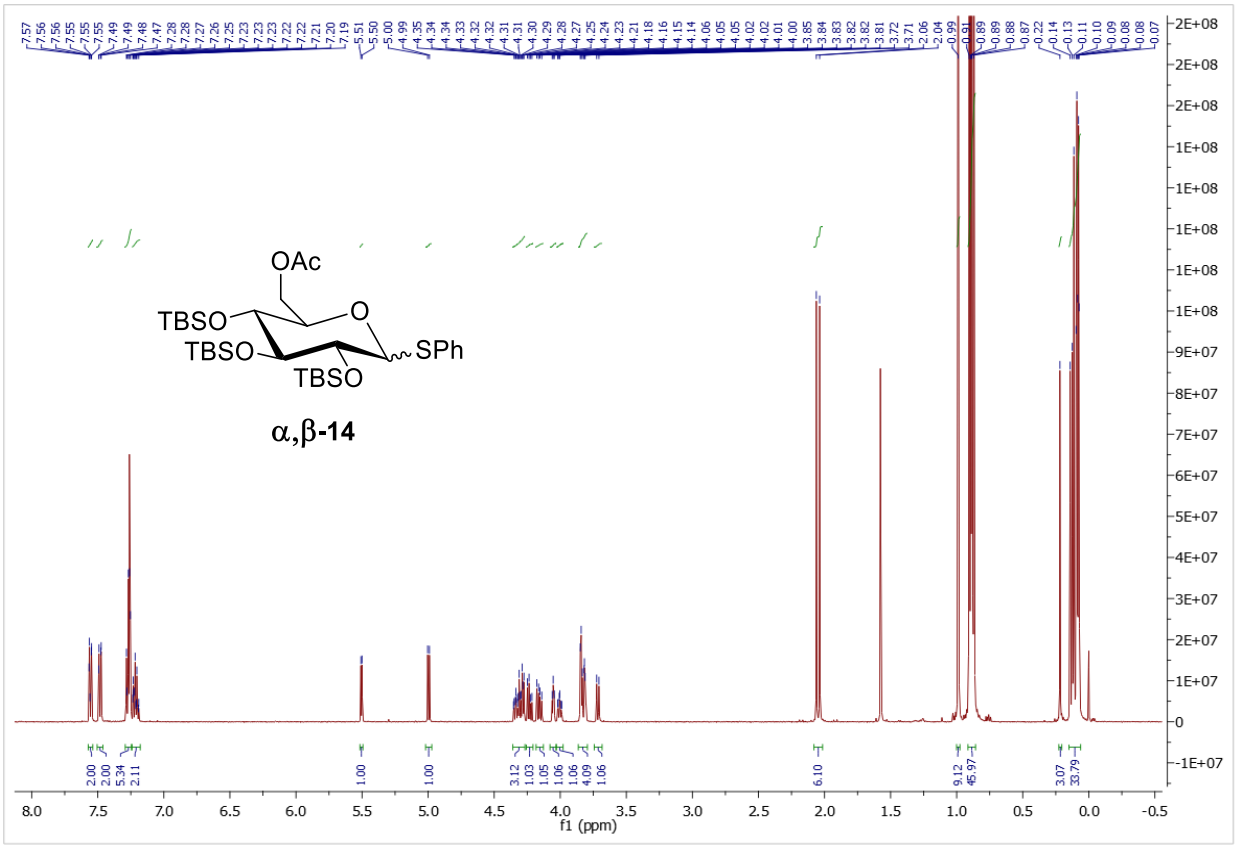

Figure 7.6.9. ^{1}H NMR spectrum of **α,β-14** (500 MHz, $CDCl_3$, 300 K).

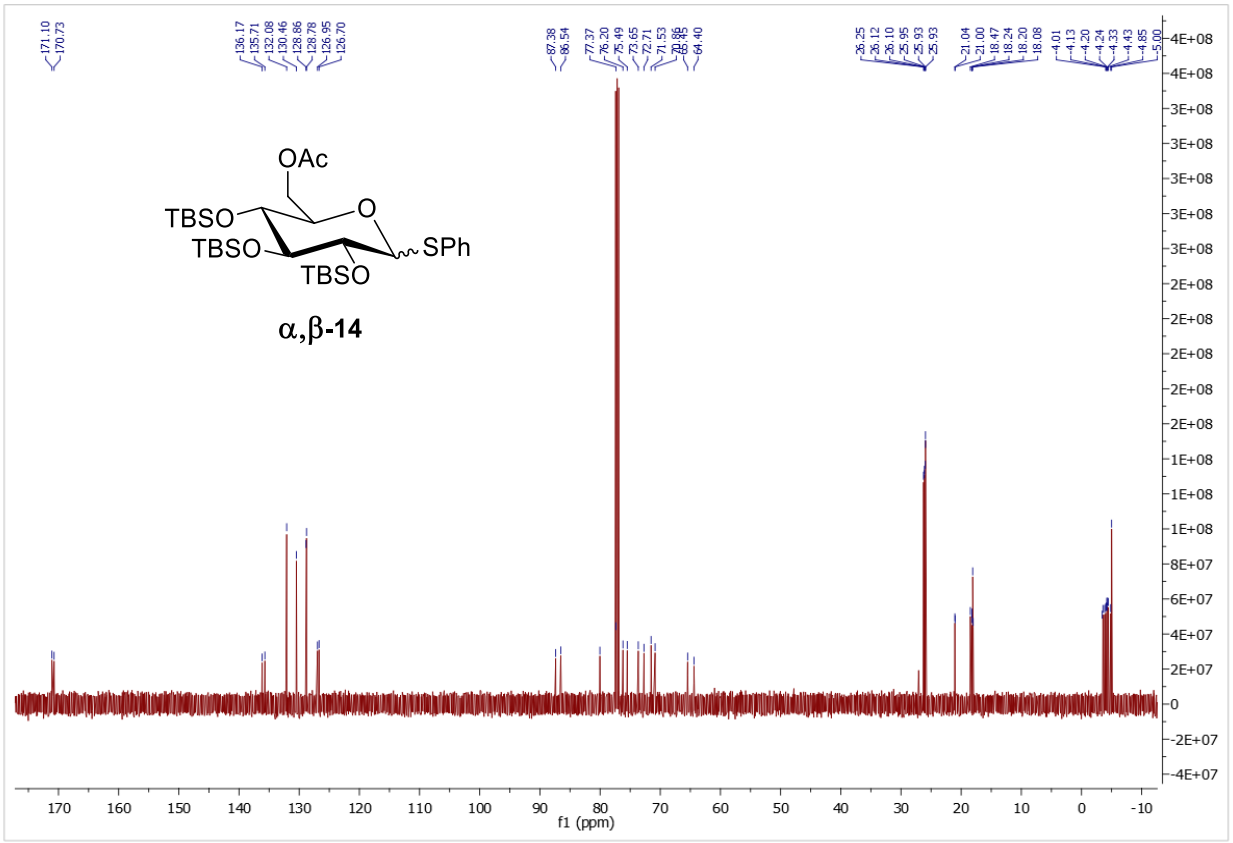

Figure 7.6.10. ^{13}C NMR spectrum of **α,β-14** (126 MHz, $CDCl_3$, 300 K).

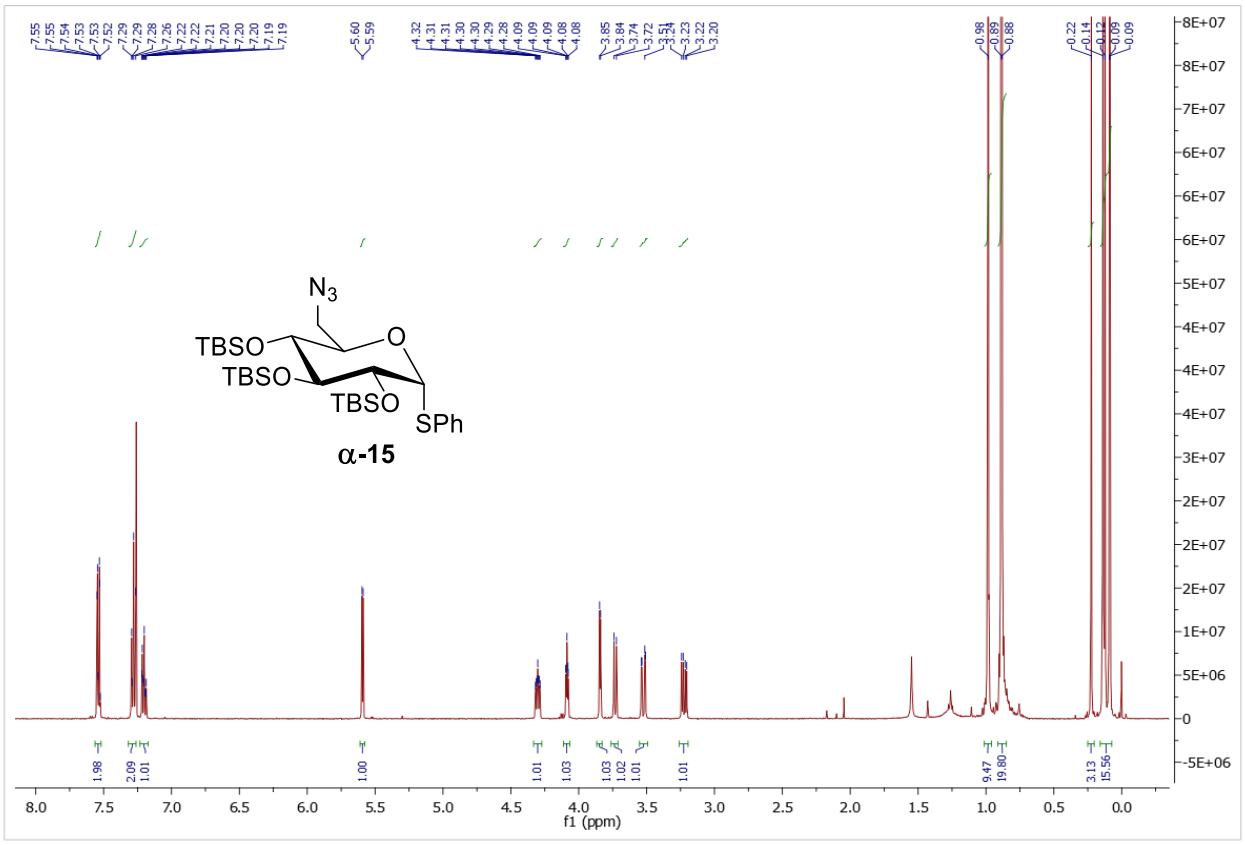

Figure 7.6.11. ^{1}H NMR spectrum of **α-15** (500 MHz, $CDCl_3$, 300 K).

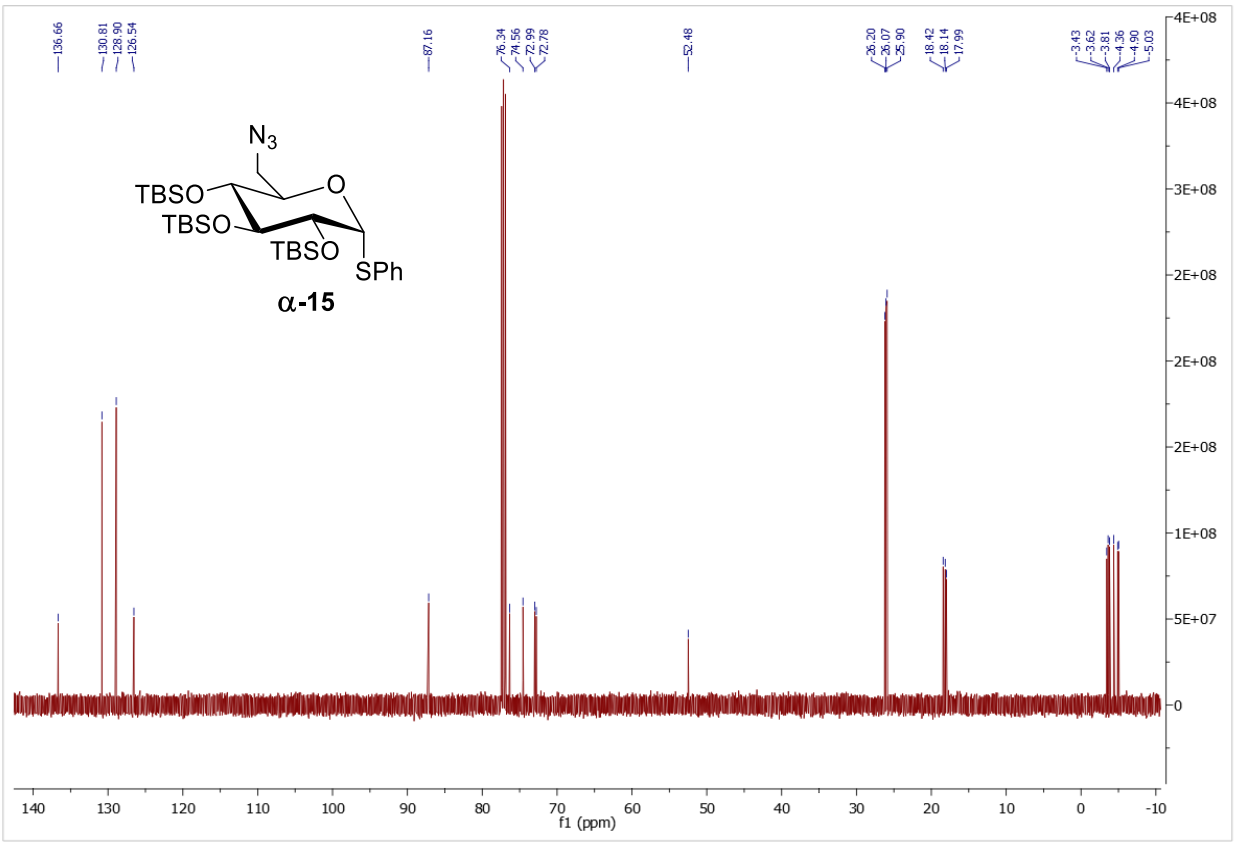

Figure 7.6.12. ^{13}C NMR spectrum of **α-15** (126 MHz, $CDCl_3$, 300 K).

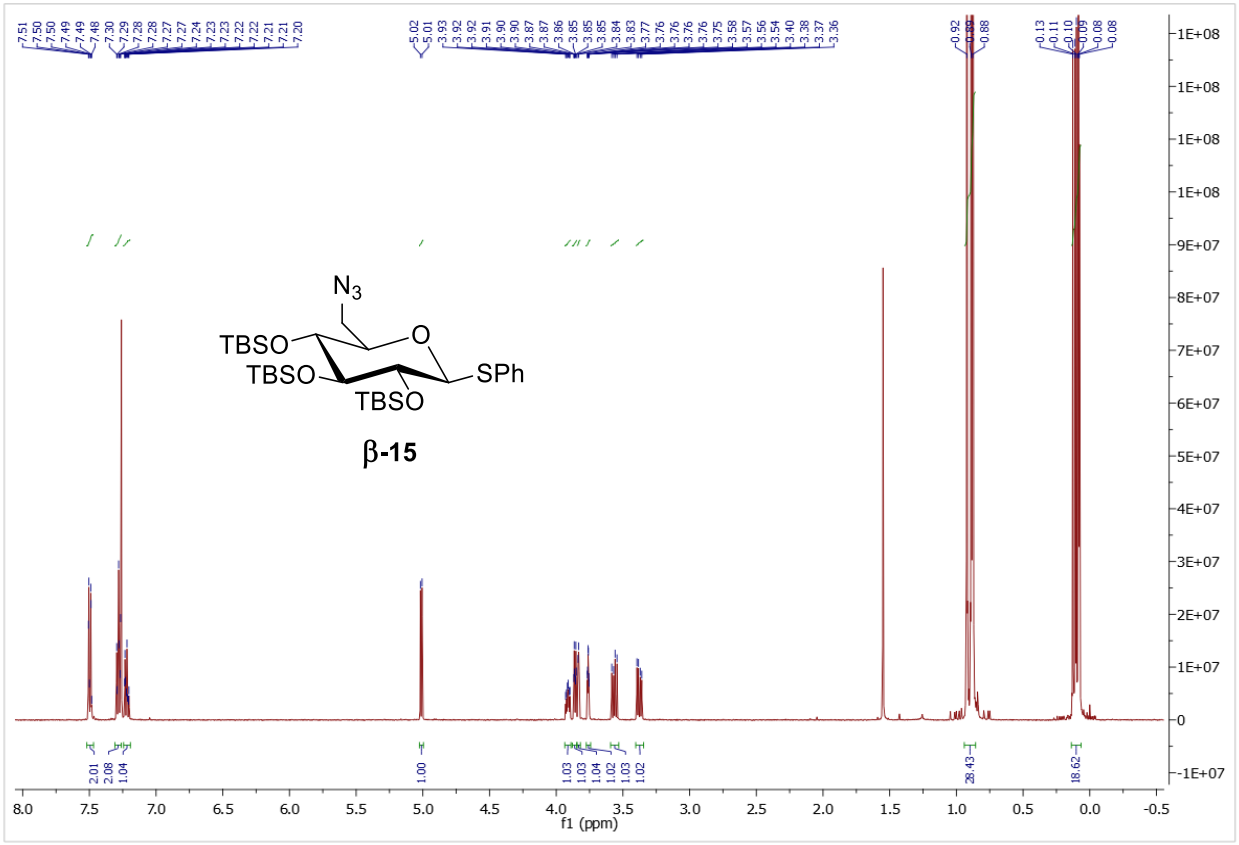

Figure 7.6.13. ^{1}H NMR spectrum of **β-15** (500 MHz, $CDCl_3$, 300 K).

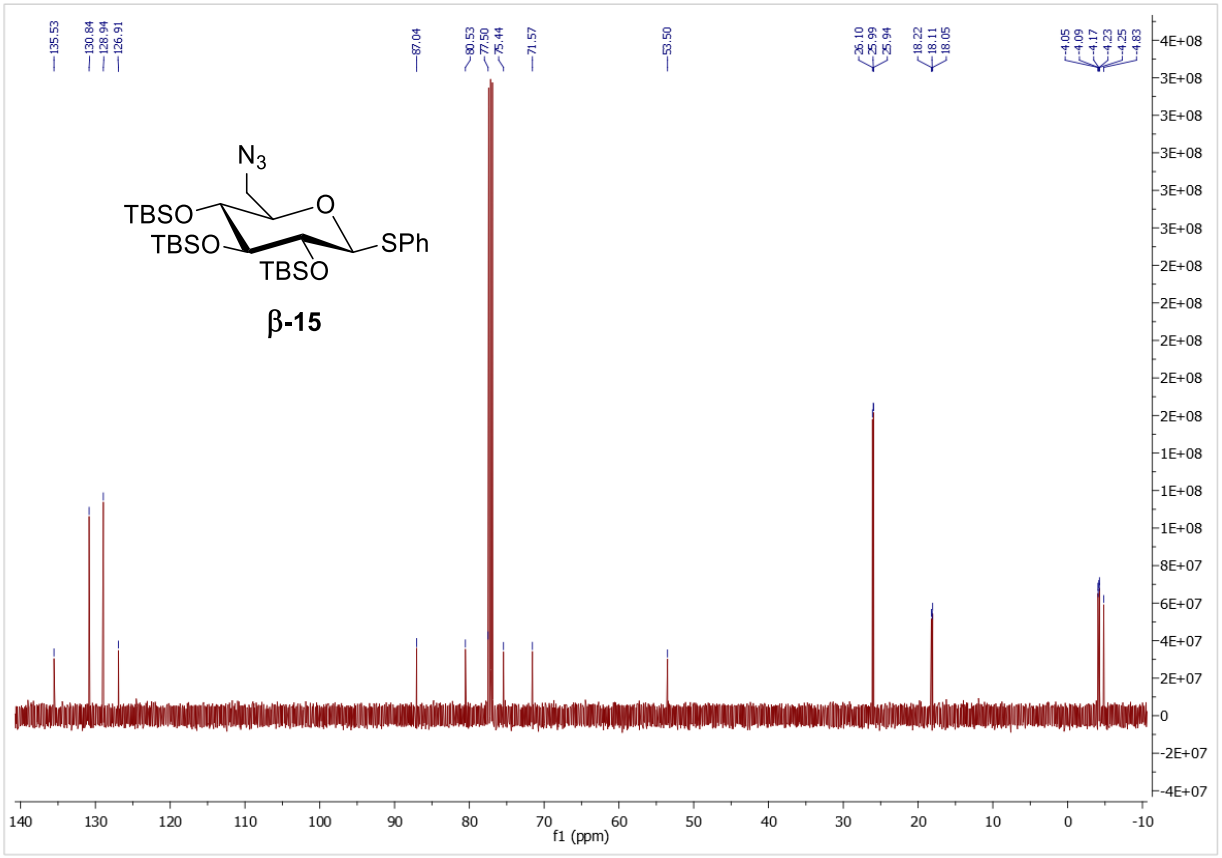

Figure 7.6.14. ^{13}C NMR spectrum of **β-15** (126 MHz, $CDCl_3$, 300 K).

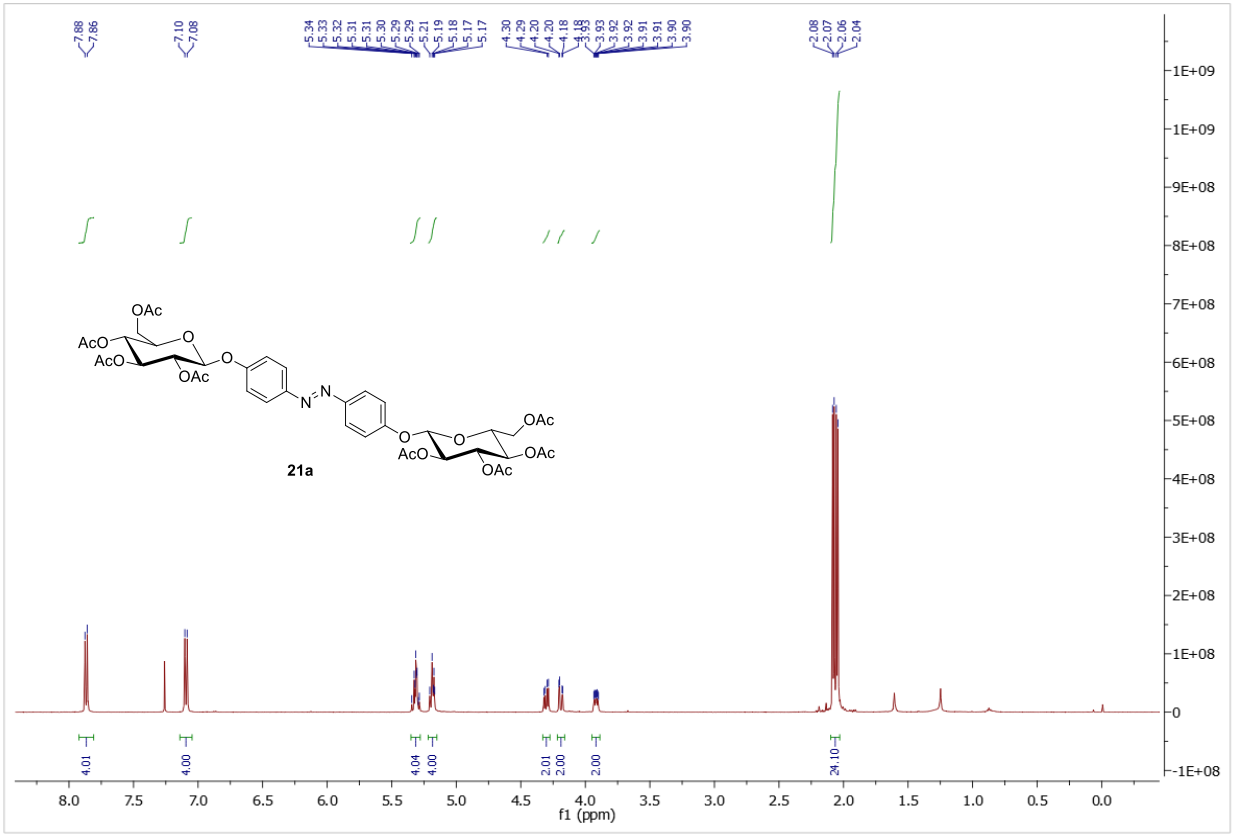

Figure 7.6.15. ^{1}H NMR spectrum of **21a** (500 MHz, $CDCl_3$, 300 K).

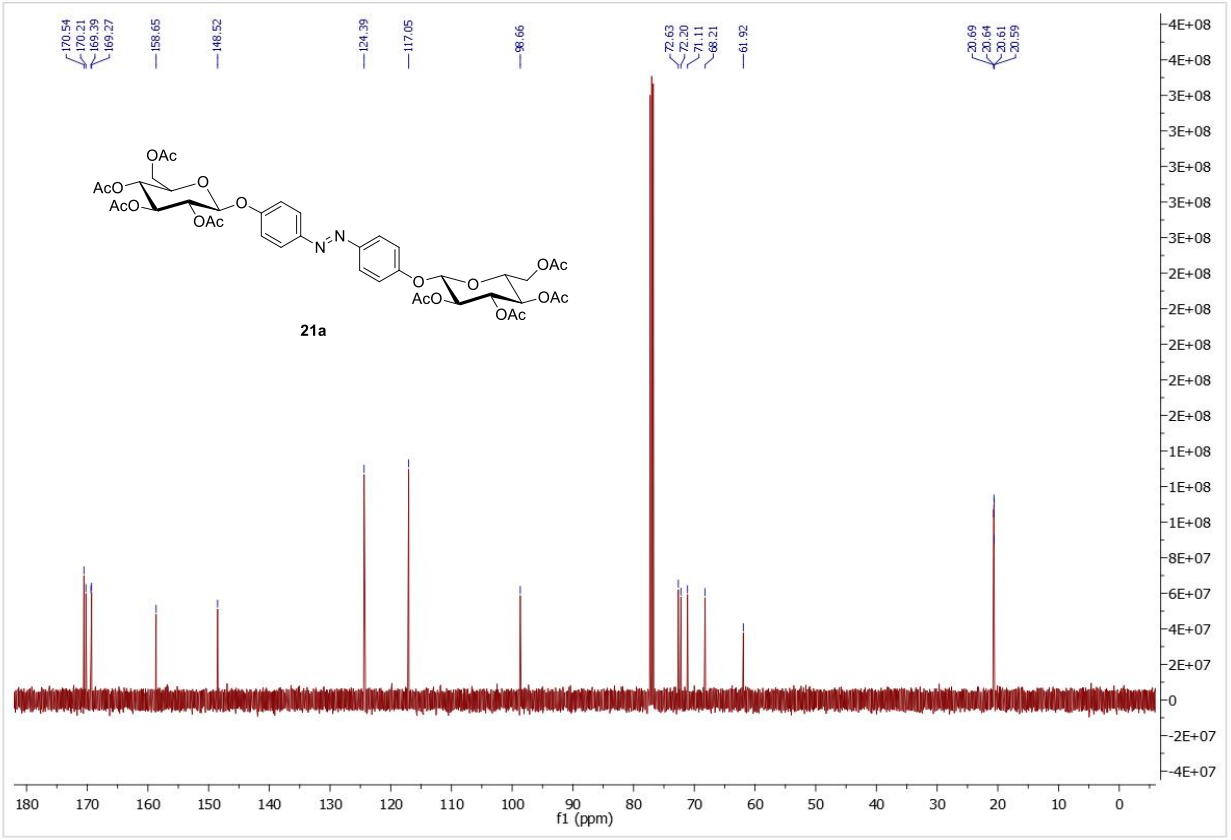

Figure 7.6.16. ^{13}C NMR spectrum of **21a** (126 MHz, $CDCl_3$, 300 K).

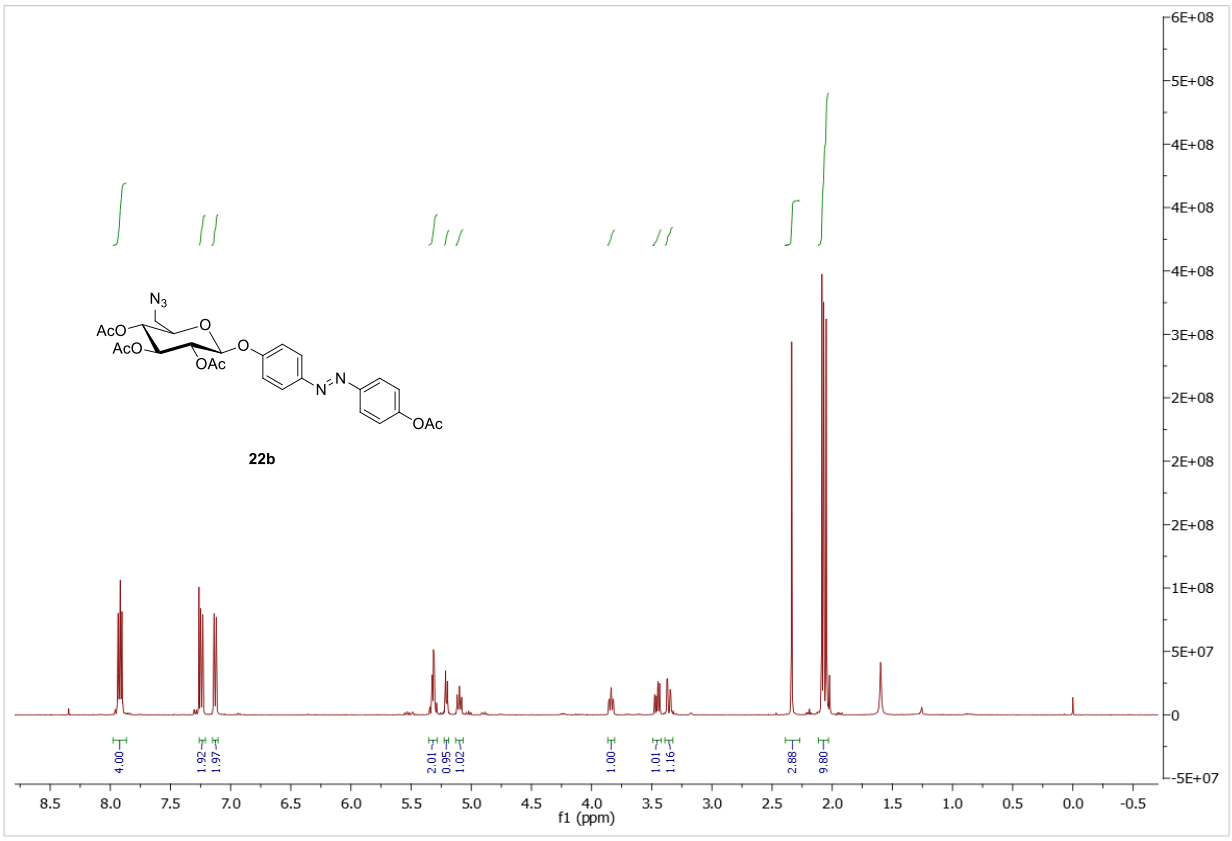

Figure 7.6.17. ^{1}H NMR spectrum of **22b** (500 MHz, $CDCl_3$, 300 K).

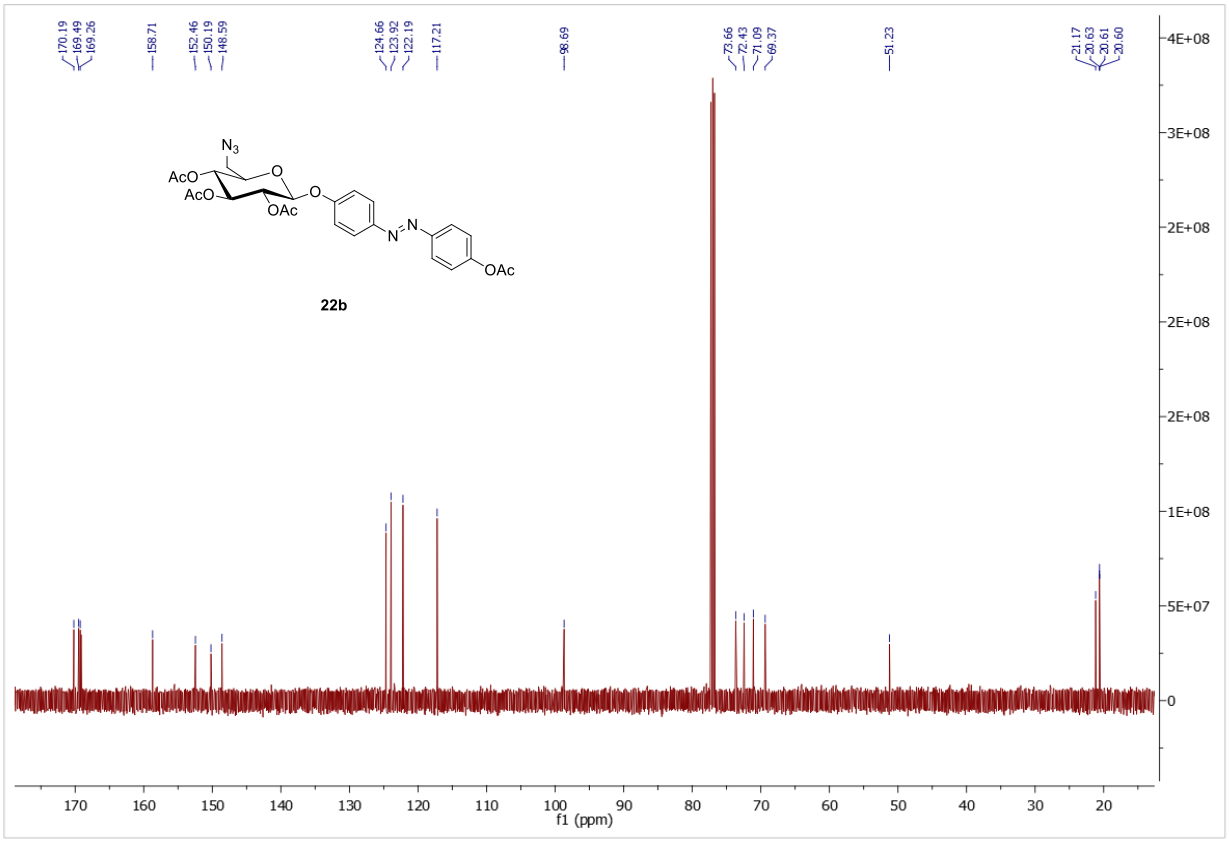

Figure 7.6.18. ^{13}C NMR spectrum of **22b** (126 MHz, $CDCl_3$, 300 K).

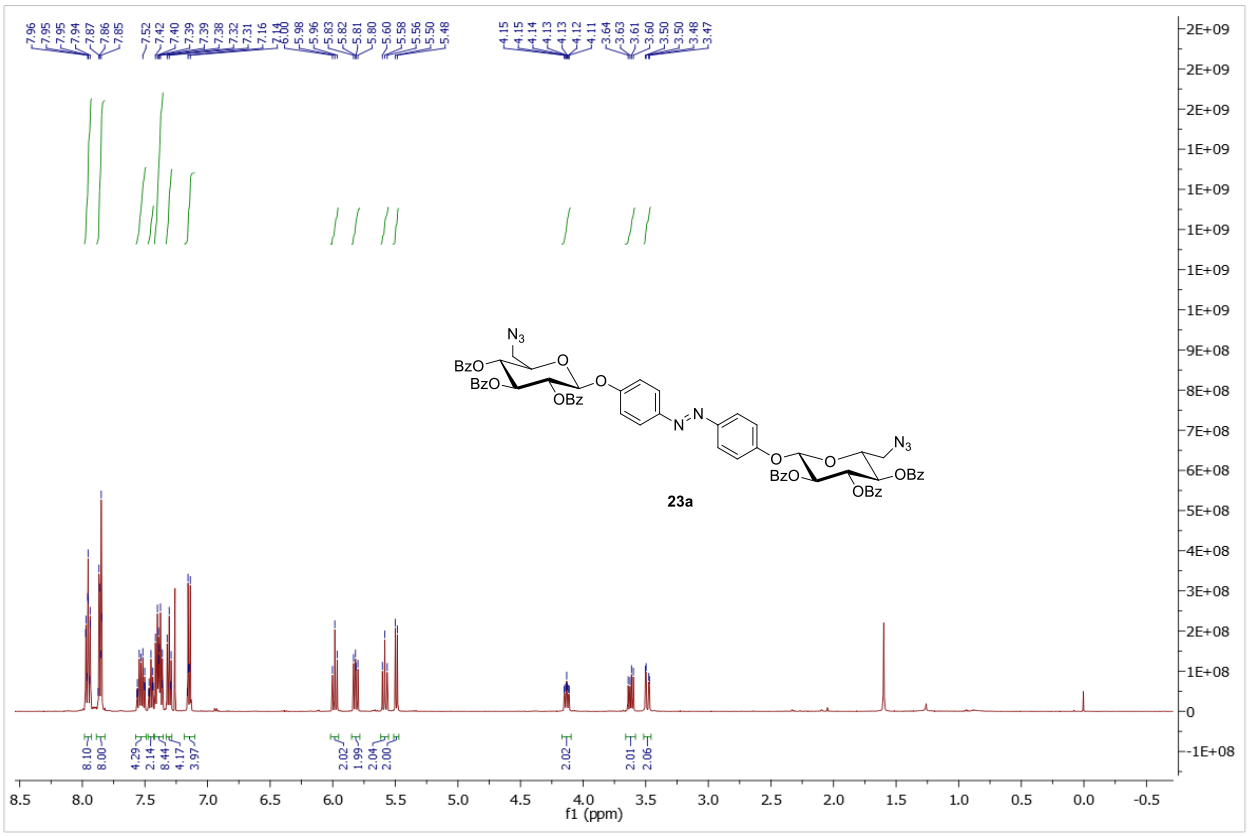

Figure 7.6.19. ^{1}H NMR spectrum of **23a** (500 MHz, $CDCl_3$, 300 K).

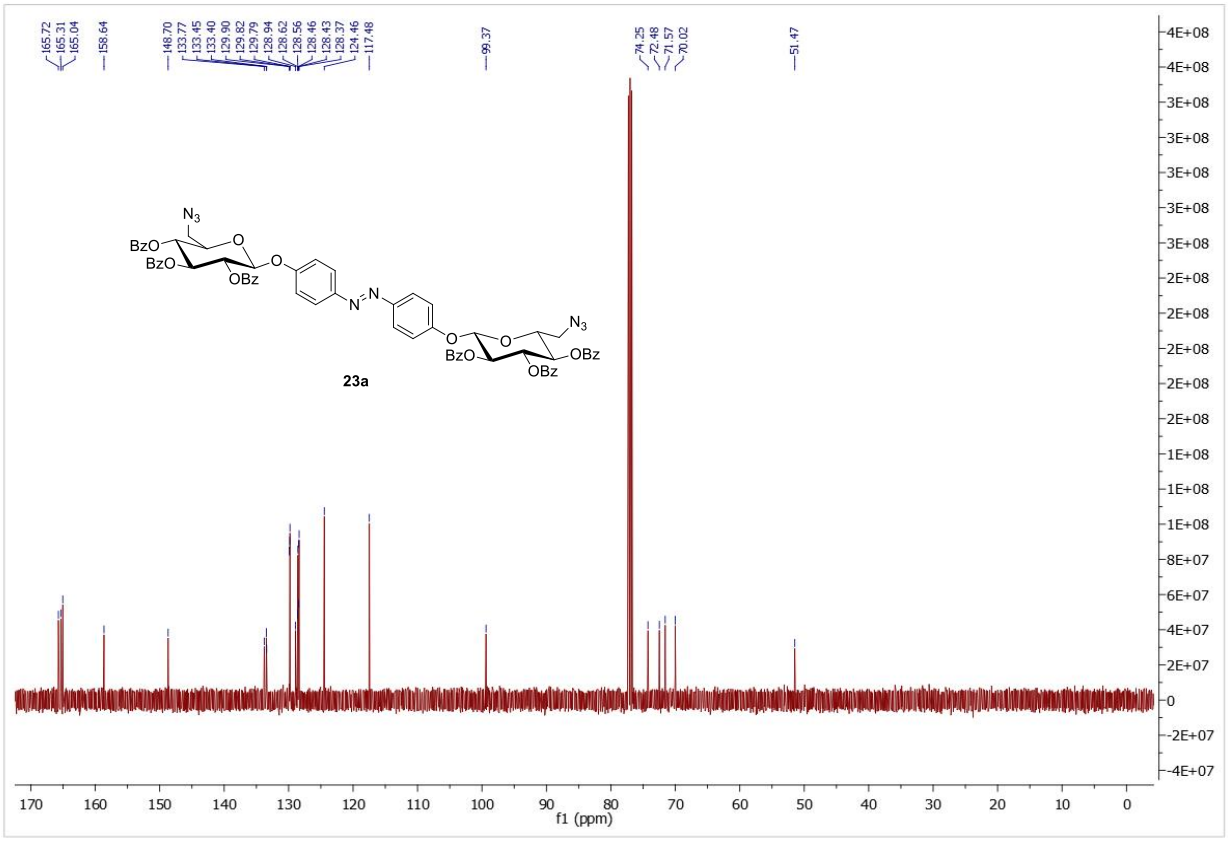

Figure 7.6.20. ^{13}C NMR spectrum of **23a** (126 MHz, $CDCl_3$, 300 K).

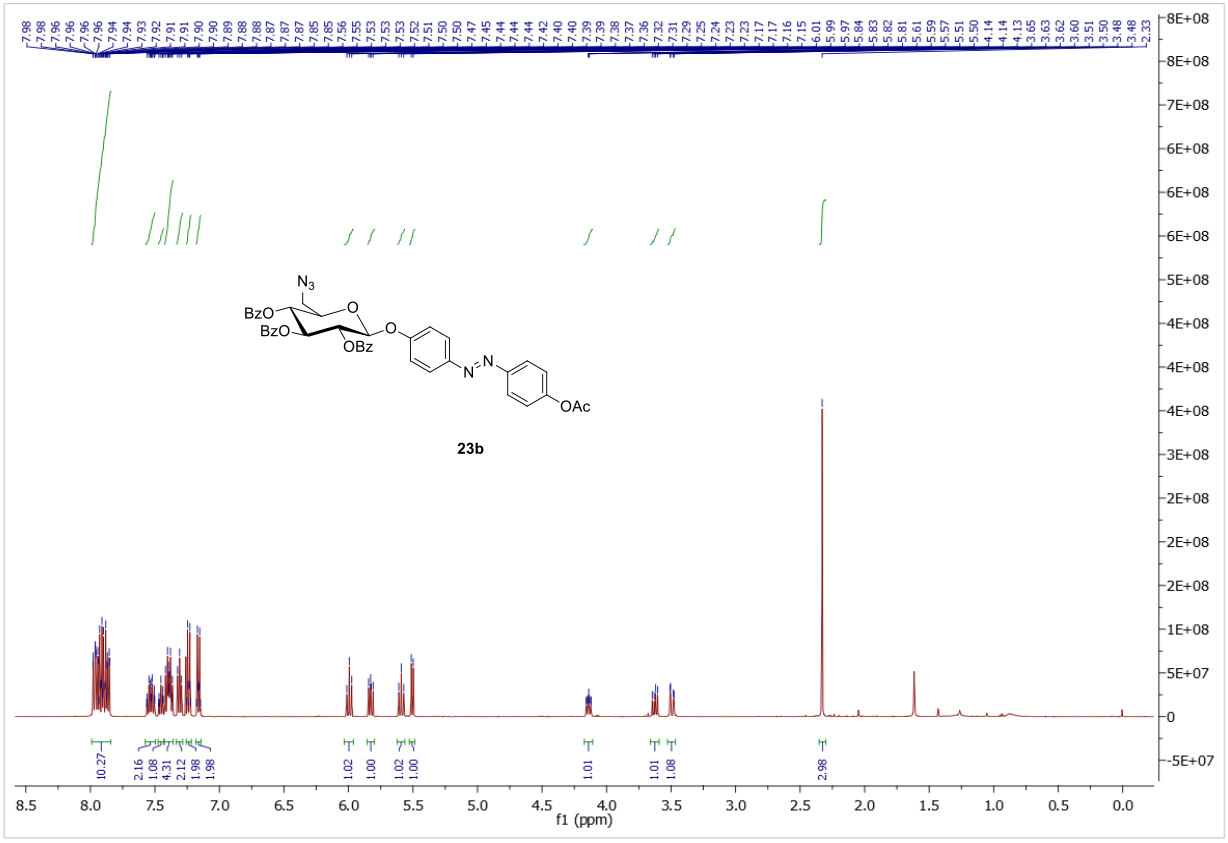

Figure 7.6.21: ^{1}H NMR spectrum of **23b** (500 MHz, $CDCl_3$, 300 K).

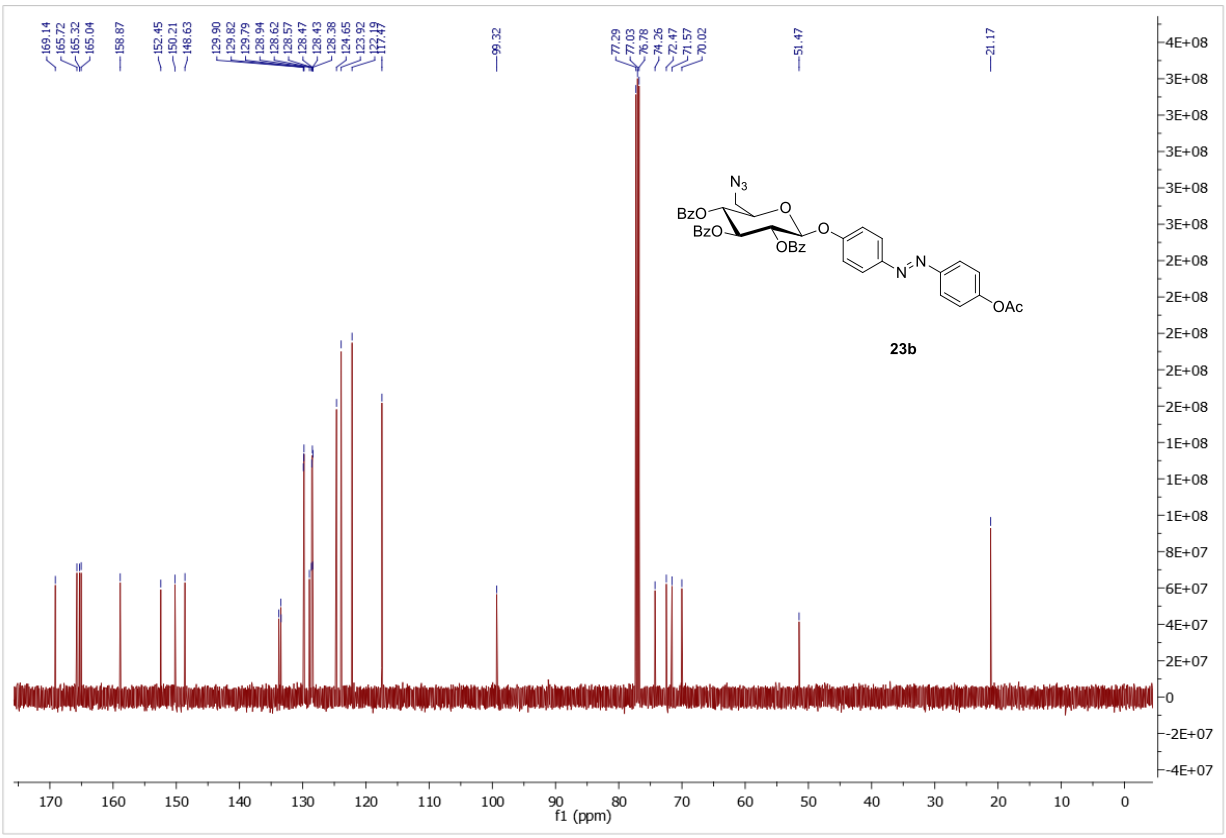

Figure 7.6.22. ^{13}C NMR spectrum of **23b** (126 MHz, $CDCl_3$, 300 K).

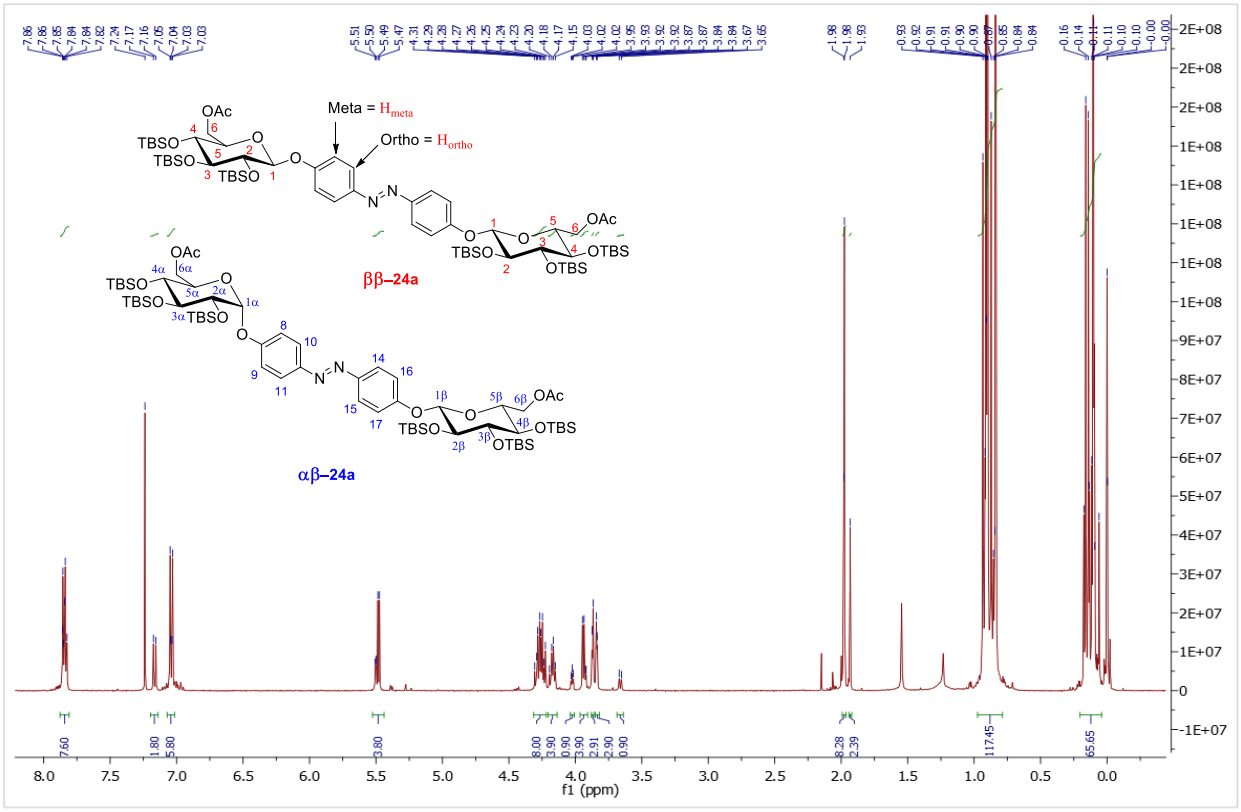

Figure 7.6.23. ^{1}H NMR spectrum of a mixture (**αβ**:**ββ**; 47:53) of **24a**, (500 MHz, $CDCl_3$, 300 K).

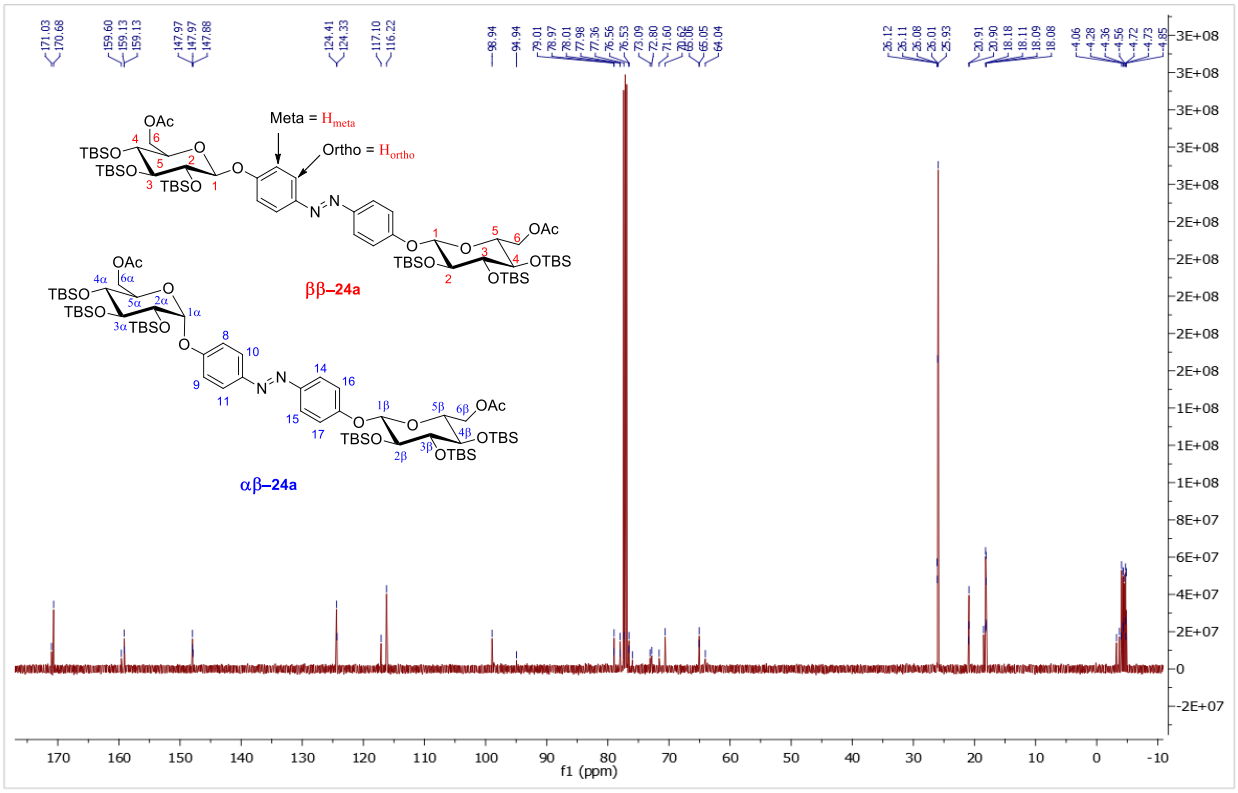

Figure 7.6.24: ^{13}C NMR spectrum of a mixture (**αβ**:**ββ**; 47:53) of **24a**, (126 MHz, $CDCl_3$, 300 K).

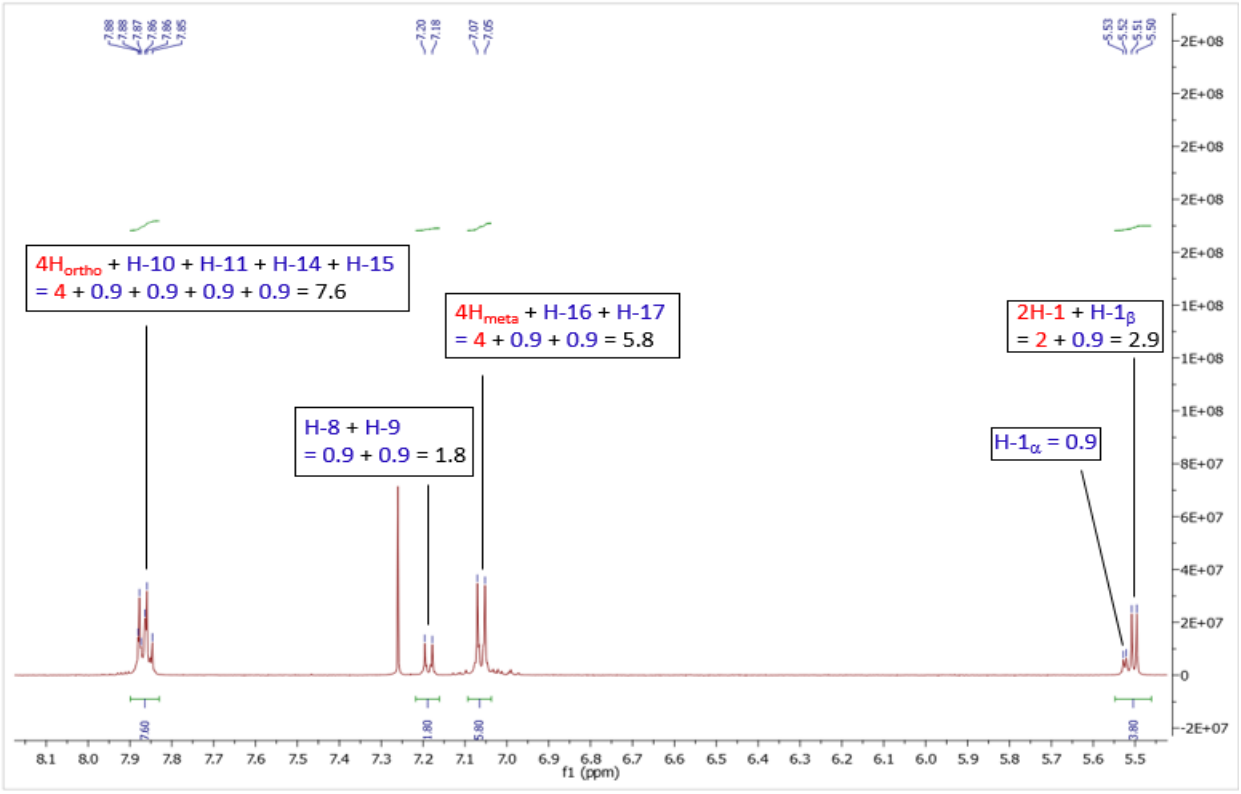

Figure 7.6.25: Expansion of the ^{1}H NMR spectrum of a mixture (**αβ**:**ββ**; 47:53) of **24a** in the aromatic region, (500 MHz, $CDCl_3$, 300 K).

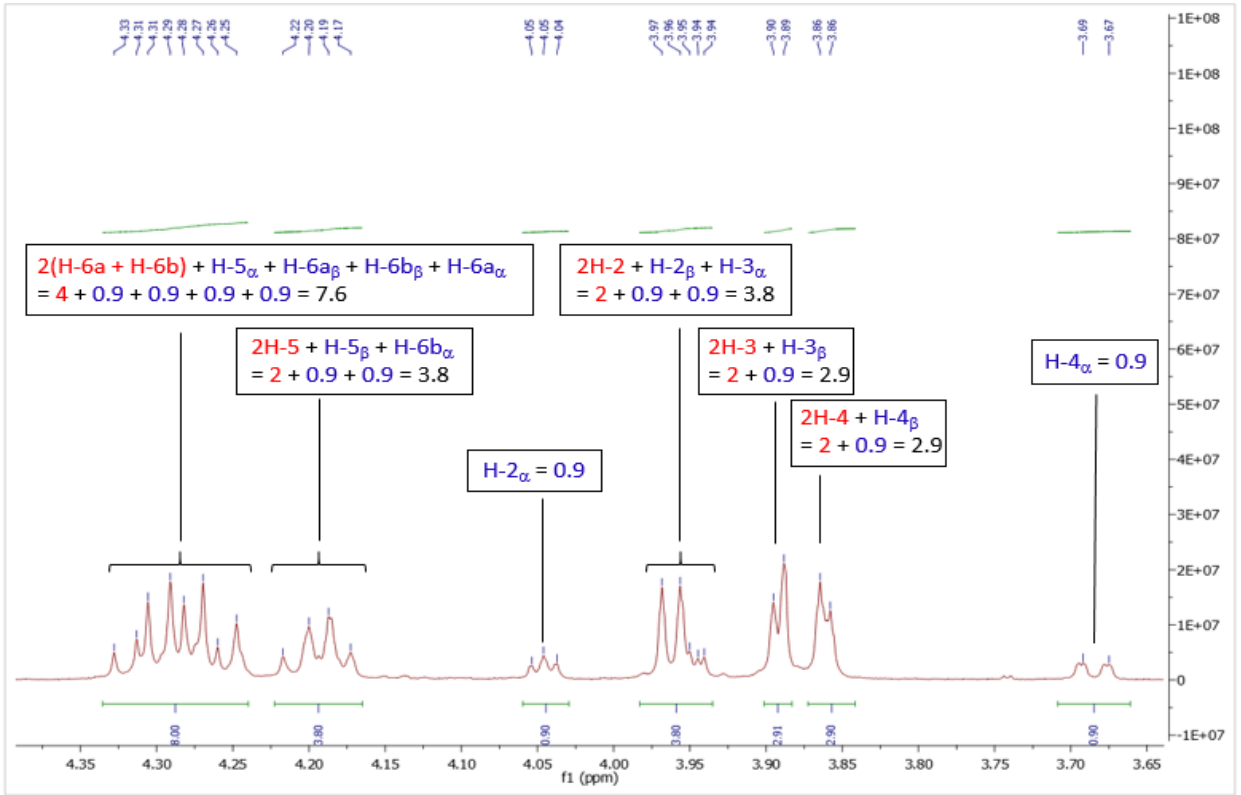

Figure 7.6.26. Expansion of the ^{1}H NMR spectrum of a mixture (**αβ**:**ββ**; 47:53) of **24a** in the carbohydrate region, (500 MHz, $CDCl_3$, 300 K).

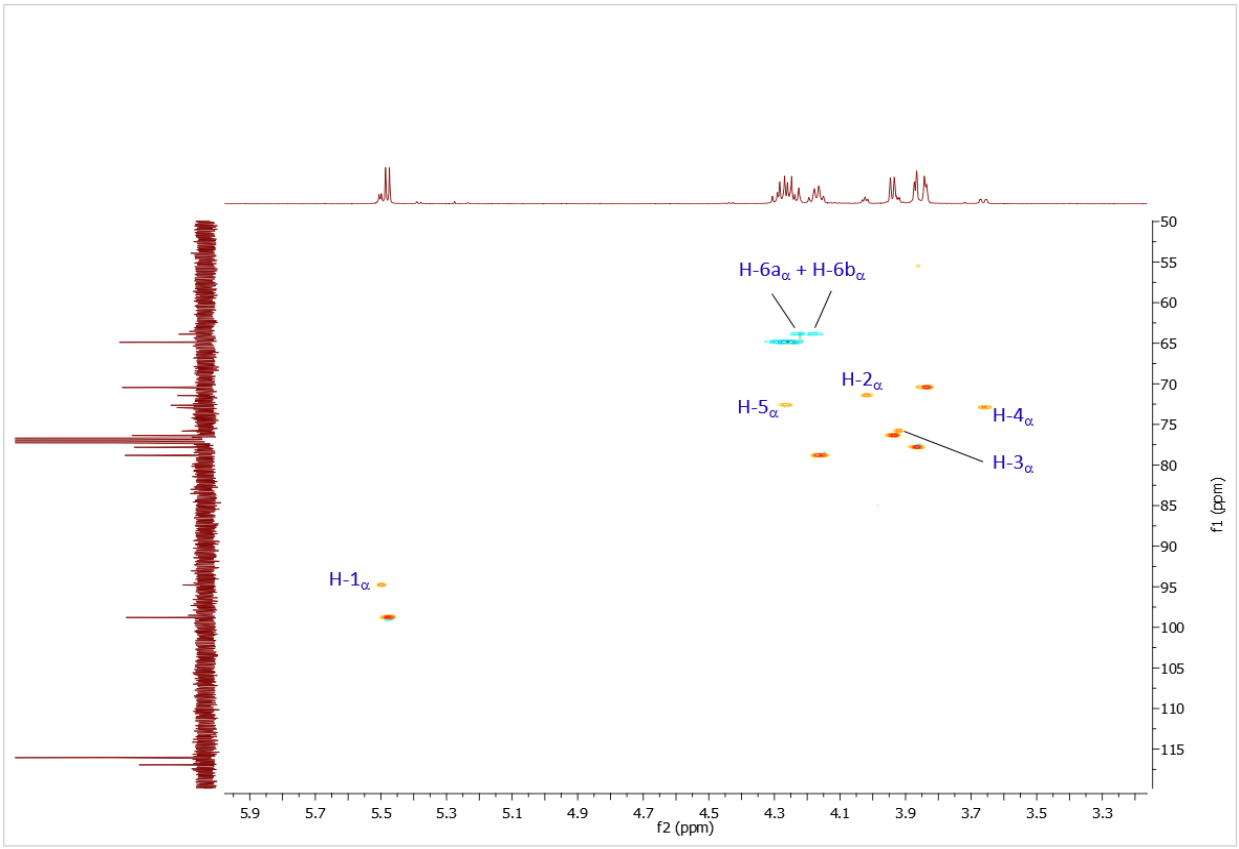

Figure 7.6.27. Expansion of the ^{1}H-^{13}C HSQC spectrum of a mixture (**αβ**:**ββ**; 47:53) of **24a** in the carbohydrate region, (500 MHz, $CDCl_3$, 300 K).

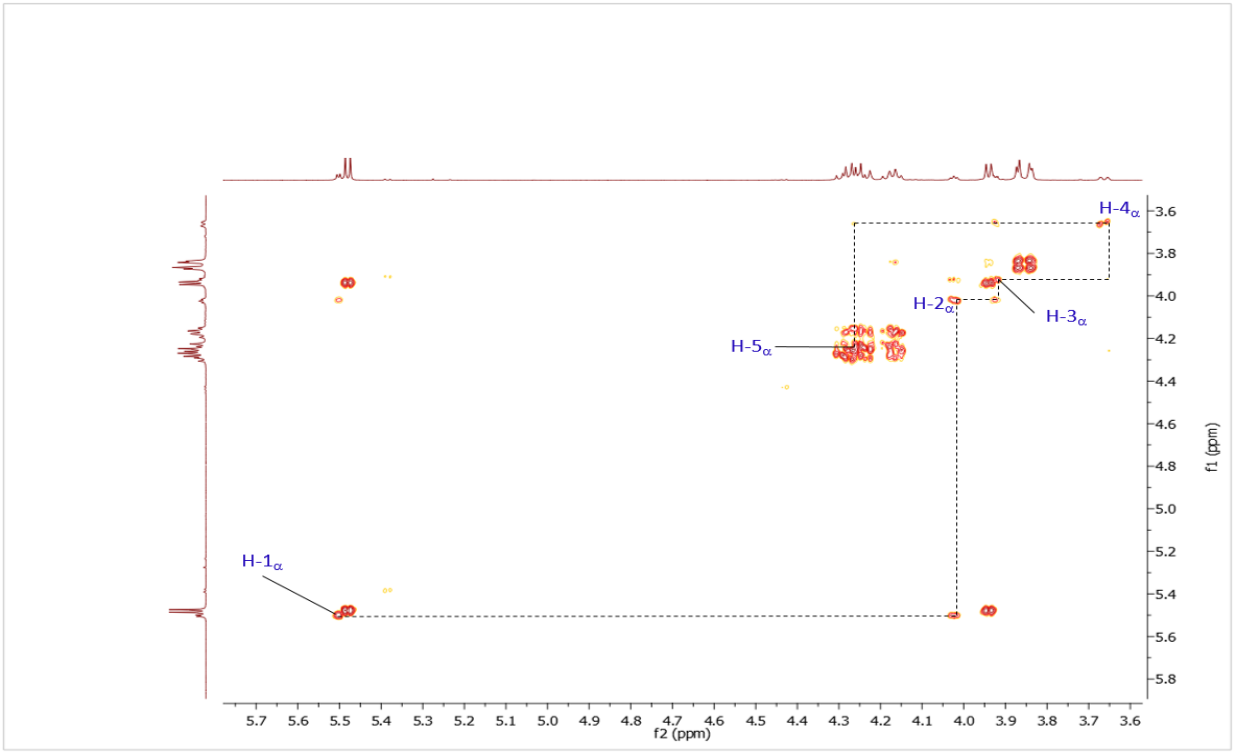

Figure 7.6.28. Expansion of the ^{1}H-^{1}H COSY spectrum of a mixture (**αβ**:**ββ**; 47:53) of **24a** in the carbohydrate region, (500 MHz, $CDCl_3$, 300 K).

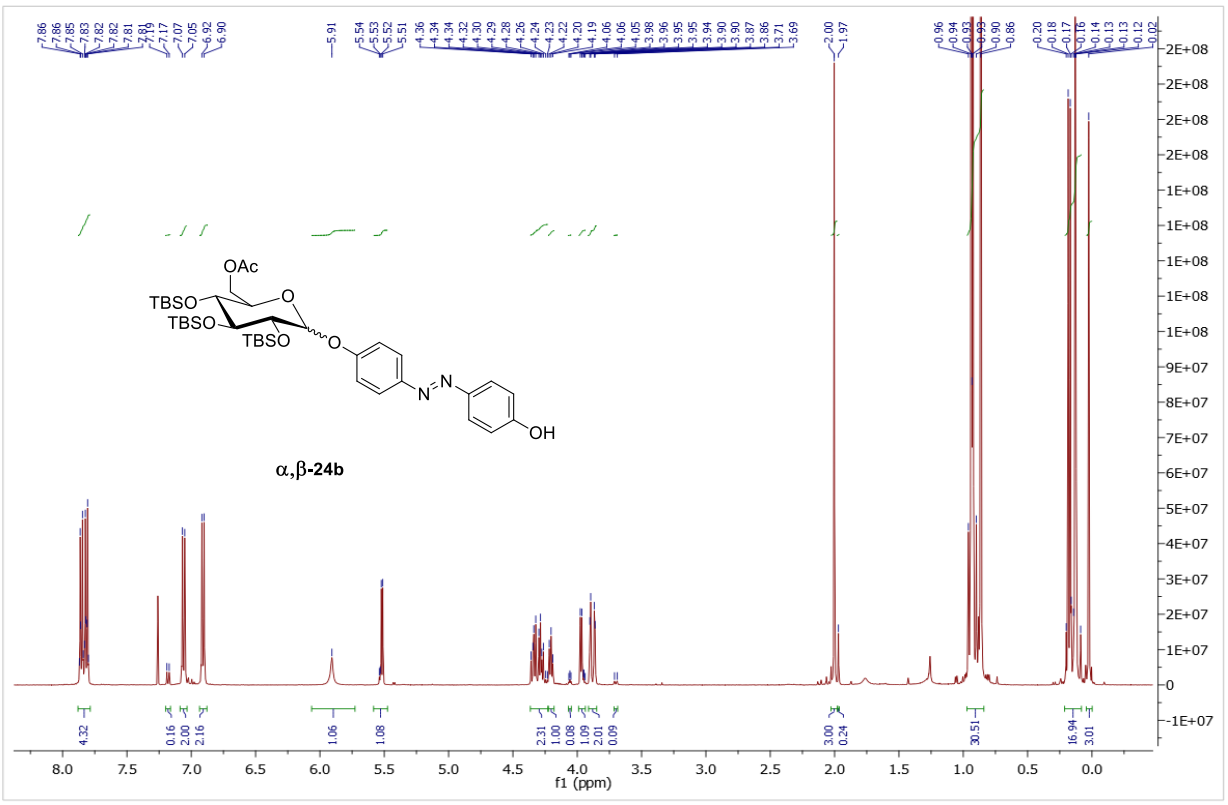

Figure 7.6.29. ^{1}H NMR spectrum of a mixture (**α**:**β**; 7:93) of **24b**, (500 MHz, $CDCl_3$, 300 K).

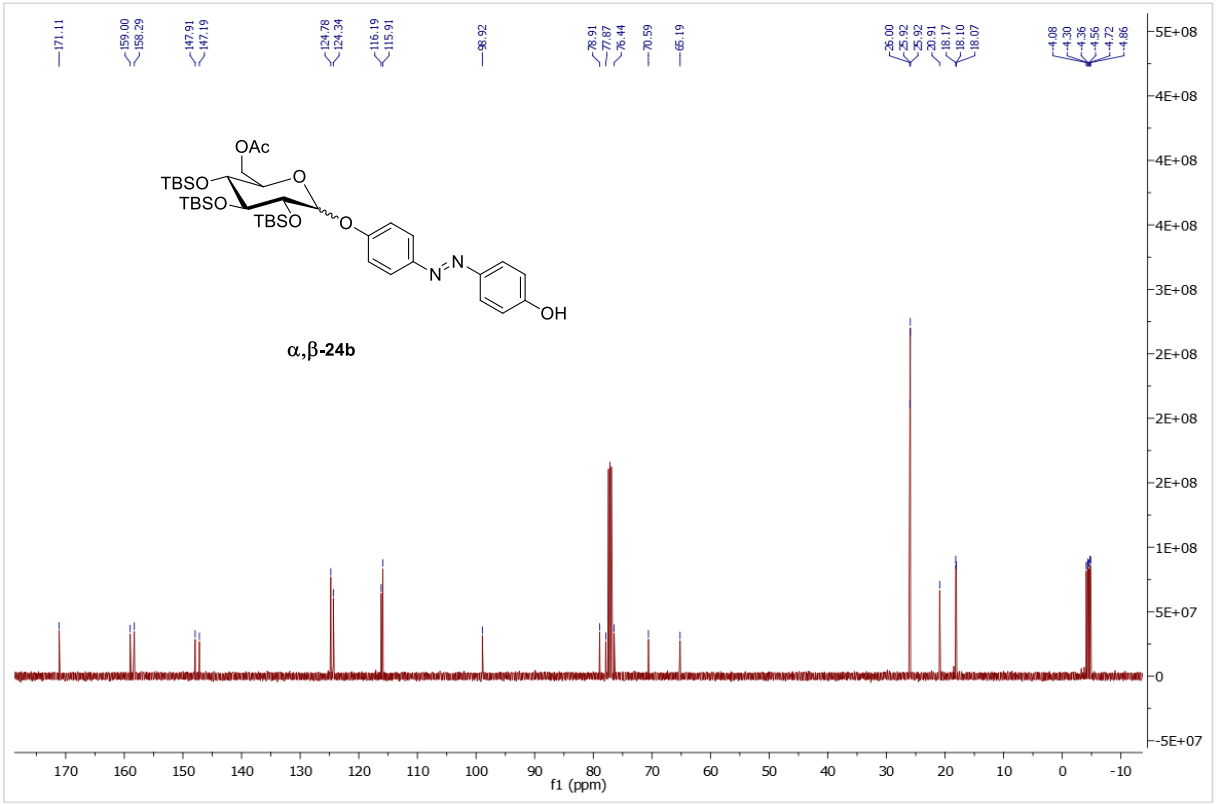

Figure 7.6.30. ^{13}C NMR spectrum of a mixture (**α**:**β**; 7:93) of **24b**, (126 MHz, $CDCl_3$, 300 K).

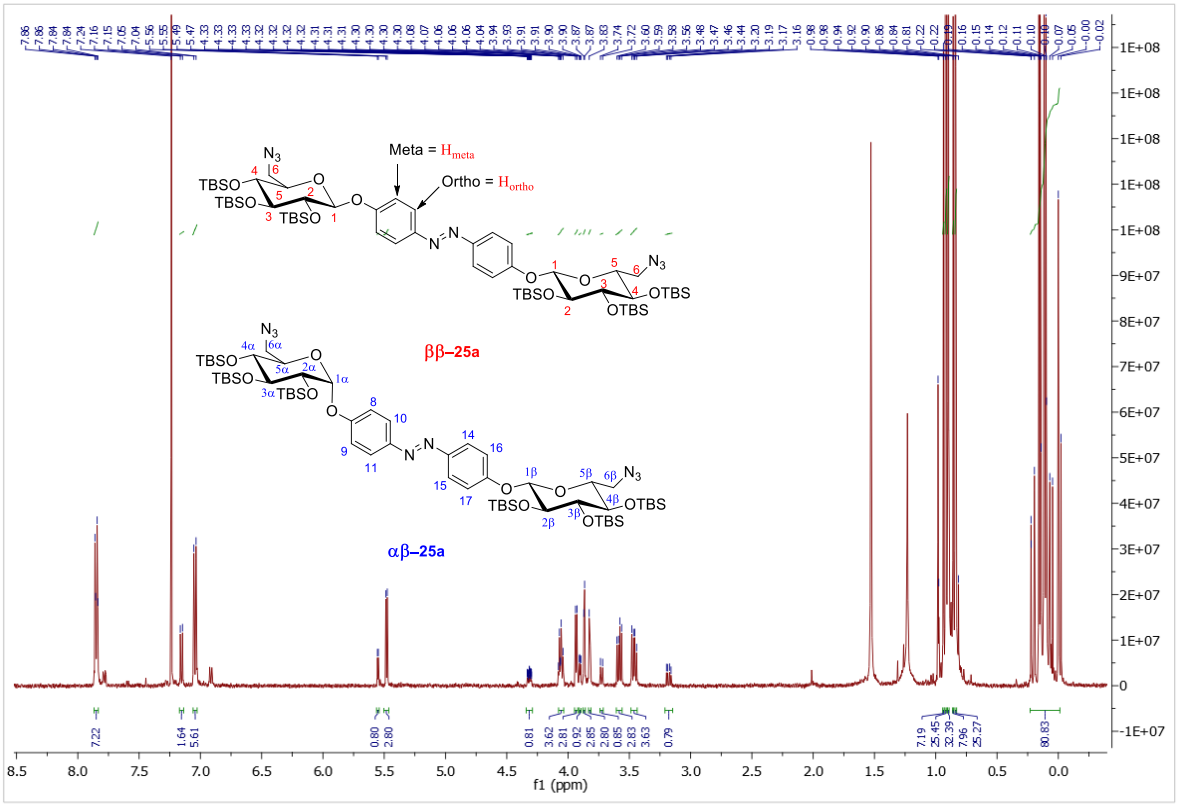

Figure 7.6.31. ^{1}H NMR spectrum of a mixture (**αβ:ββ**; 44:56) of **25a**, (500 MHz, $CDCl_3$, 300 K).

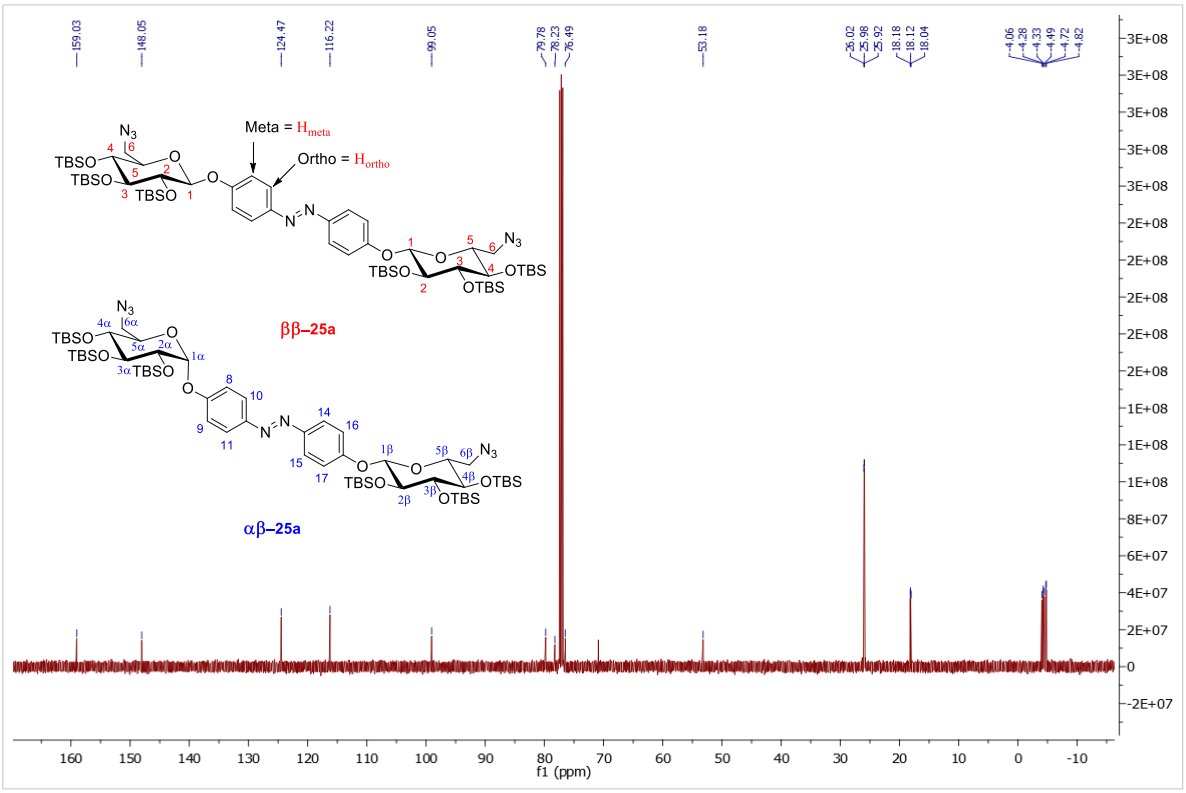

Figure 7.6.32. ^{13}C NMR spectrum of a mixture (**αβ:ββ**; 44:56) of **25a**, (126 MHz, $CDCl_3$, 300 K).

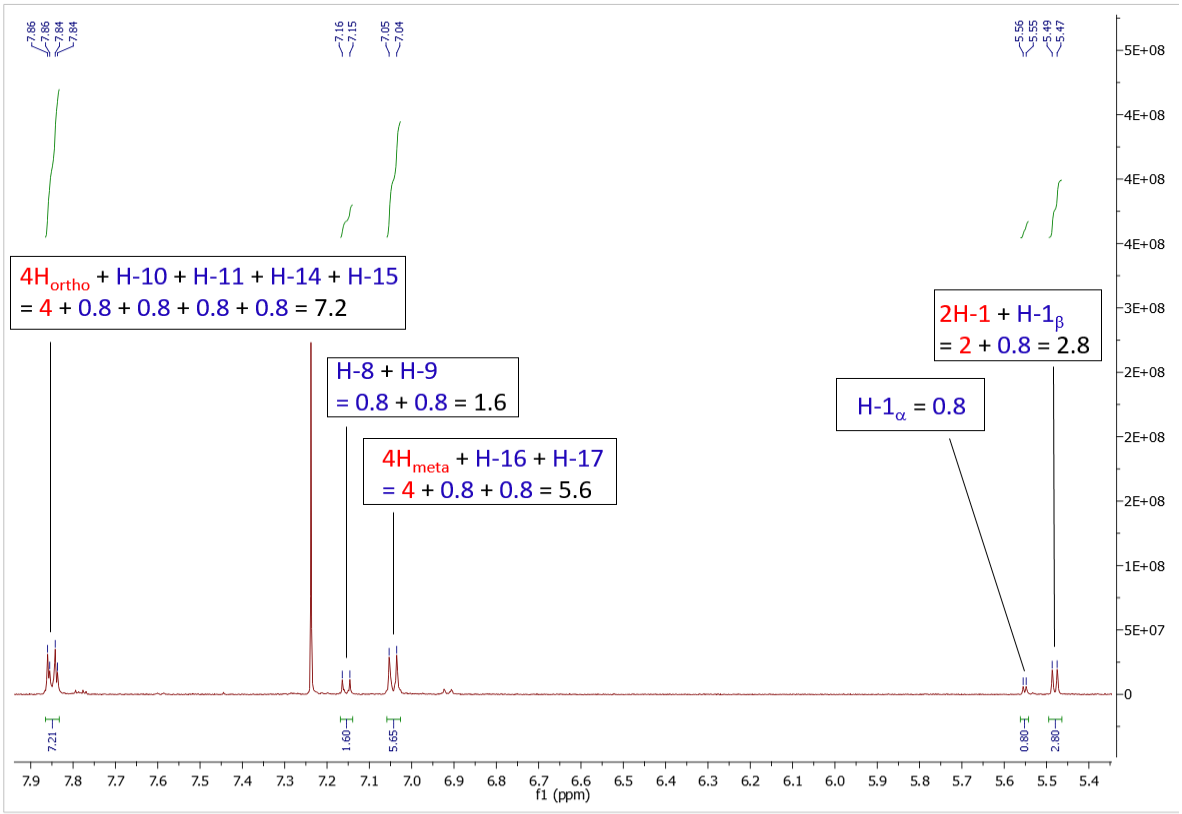

Figure 7.6.33. Expansion of the ^{1}H NMR spectrum of a mixture (**αβ:ββ**; 44:56) of **25a** in the aromatic region, (500 MHz, $CDCl_3$, 300 K).

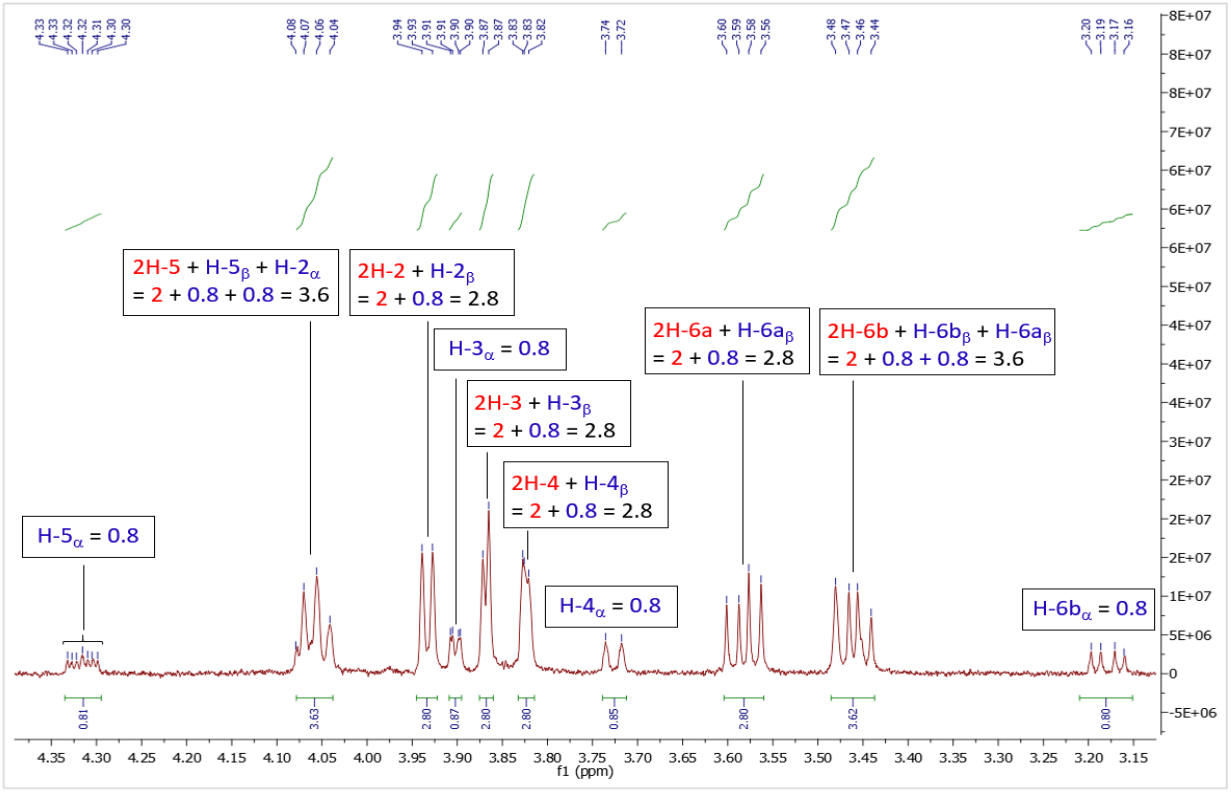

Figure 7.6.34. Expansion of the ^{1}H NMR spectrum of a mixture (**αβ:ββ**; 44:56) of **25a** in the carbohydrate region, (500 MHz, $CDCl_3$, 300 K).

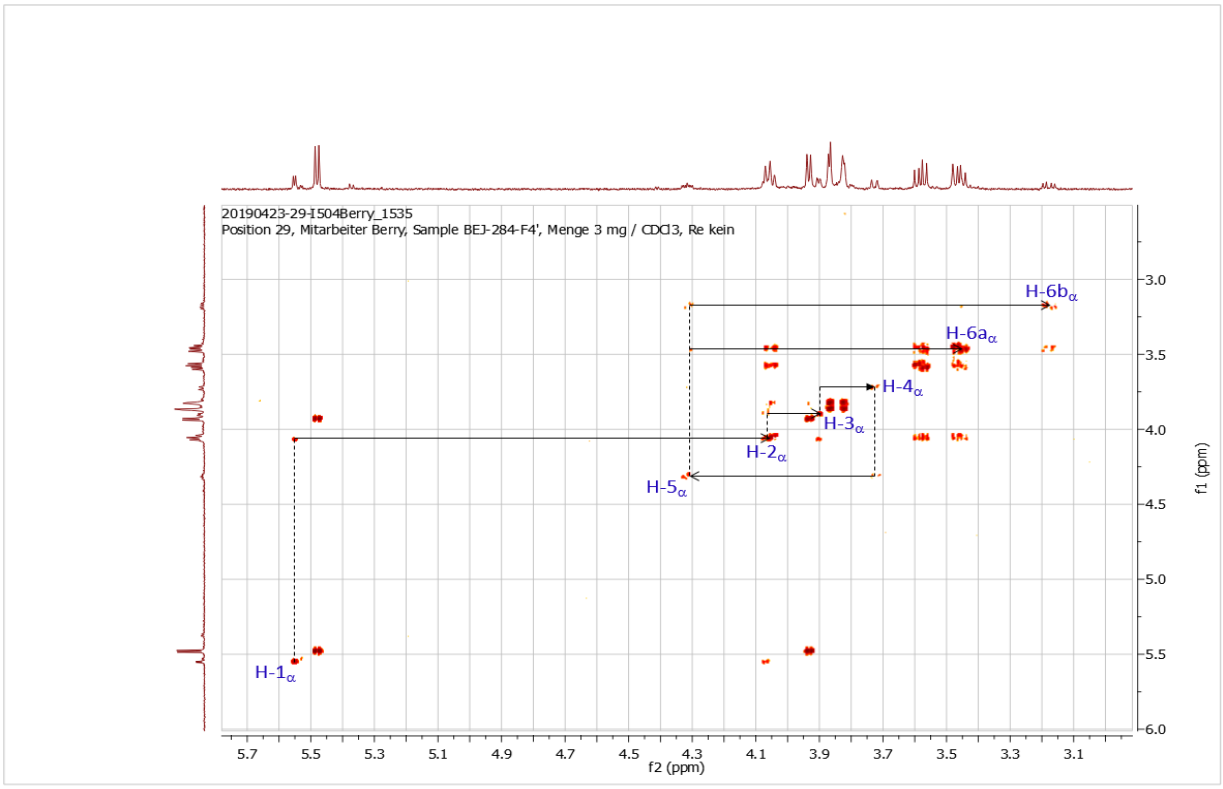

Figure 7.6.35. Expansion of the ^{1}H-^{1}H COSY spectrum of a mixture (**αβ:ββ**; 44:56) of **25a** in the carbohydrate region, (500 MHz, $CDCl_3$, 300 K).

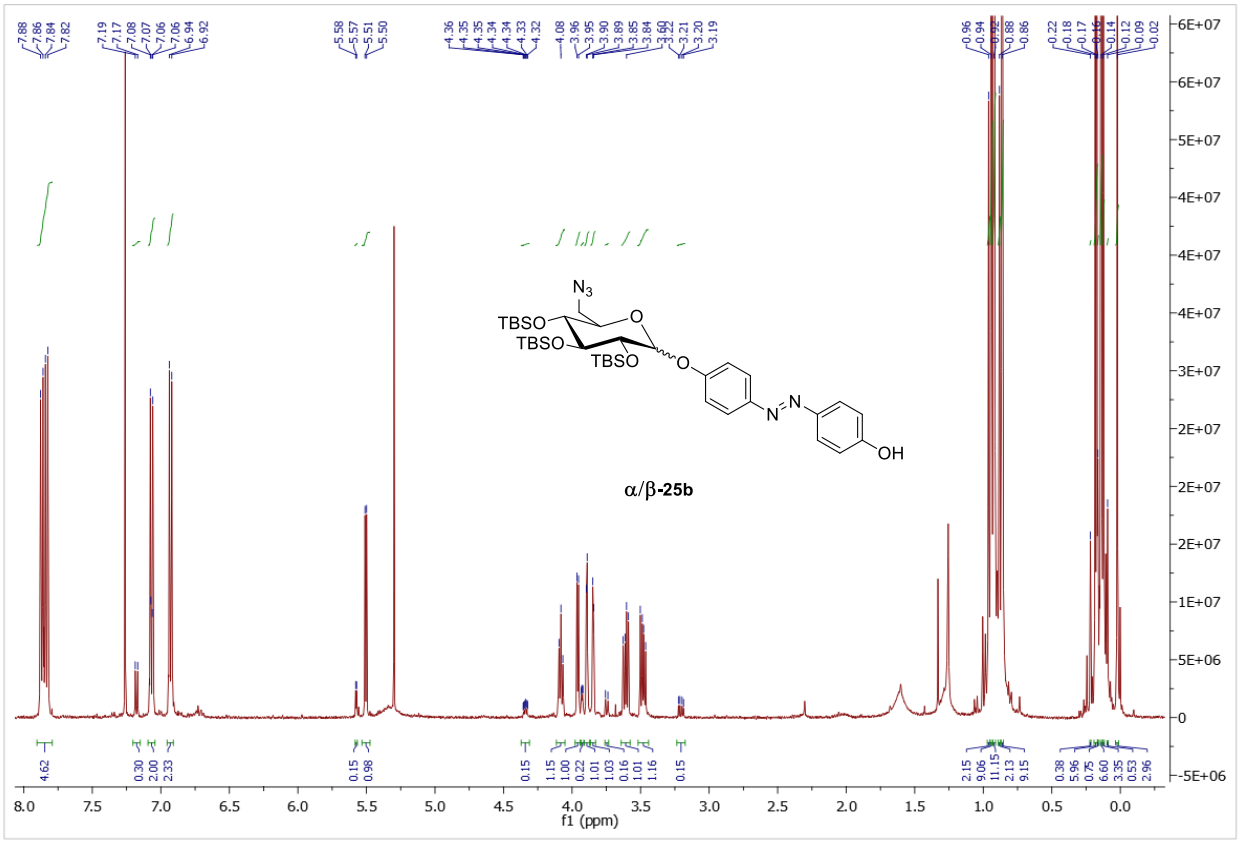

Figure 7.6.36. ^{1}H NMR spectrum of a mixture (**α**:**β**; 13:87) of **25b**, (500 MHz, $CDCl_3$, 300 K).

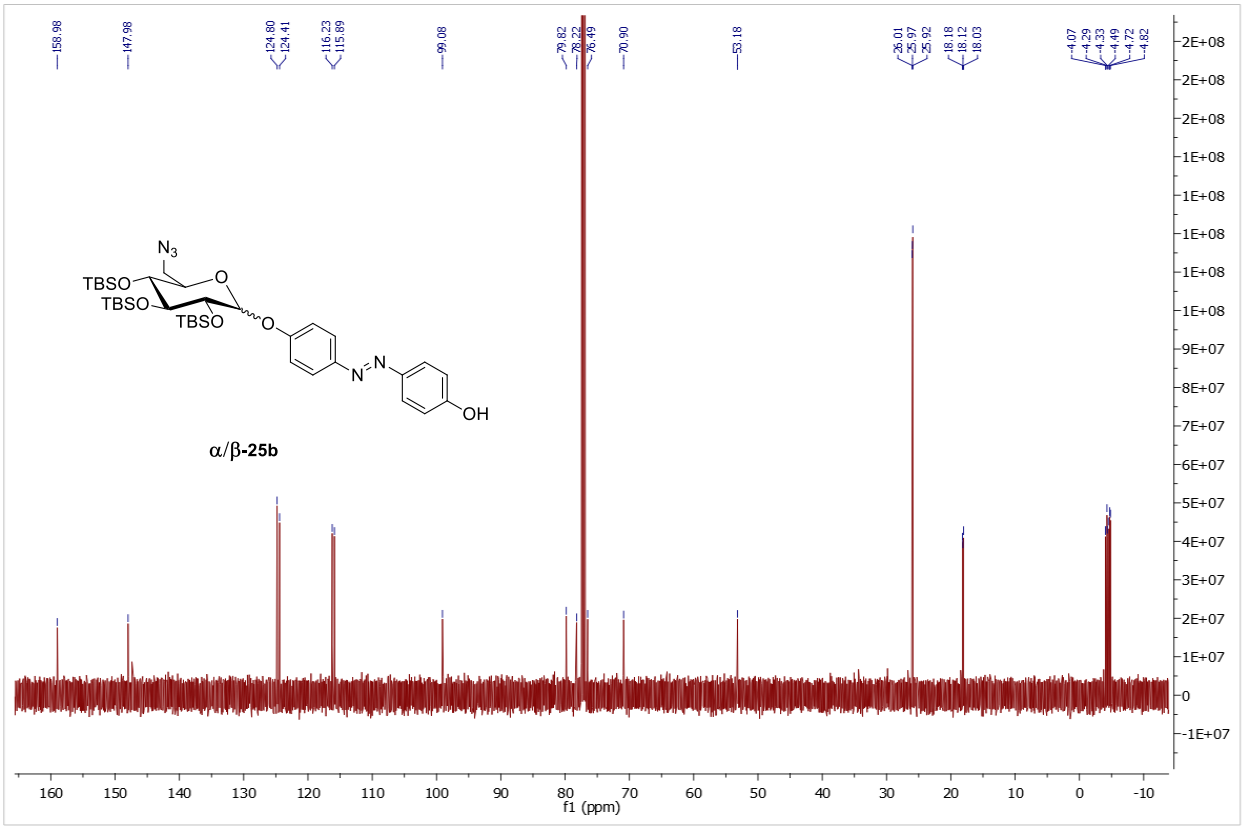

Figure 7.6.37: ^{13}C NMR spectrum of a mixture (**α:β**; 13:87) of **25b**, (126 MHz, $CDCl_3$, 300 K).

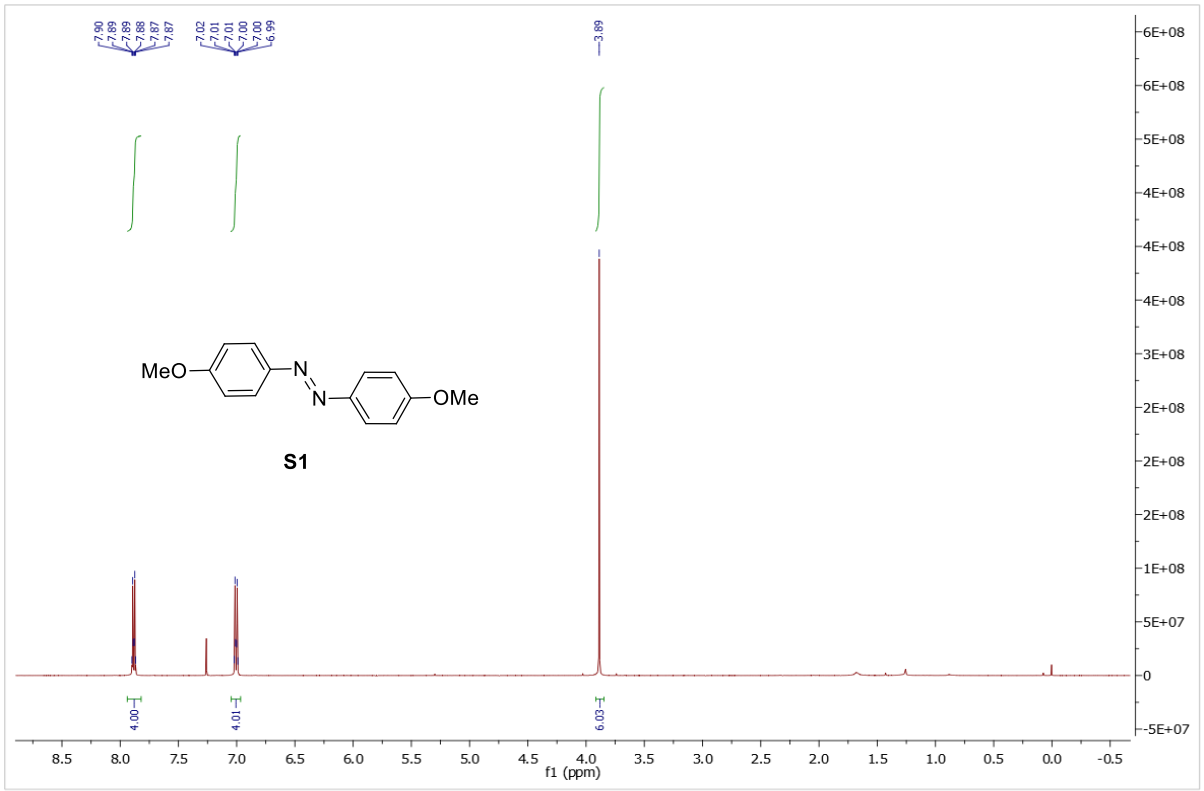

Figure 7.6.38: ^{1}H NMR spectrum of *p,p´*-dimethoxyazobenzene **S1** (500 MHz, $CDCl_3$, 300 K).

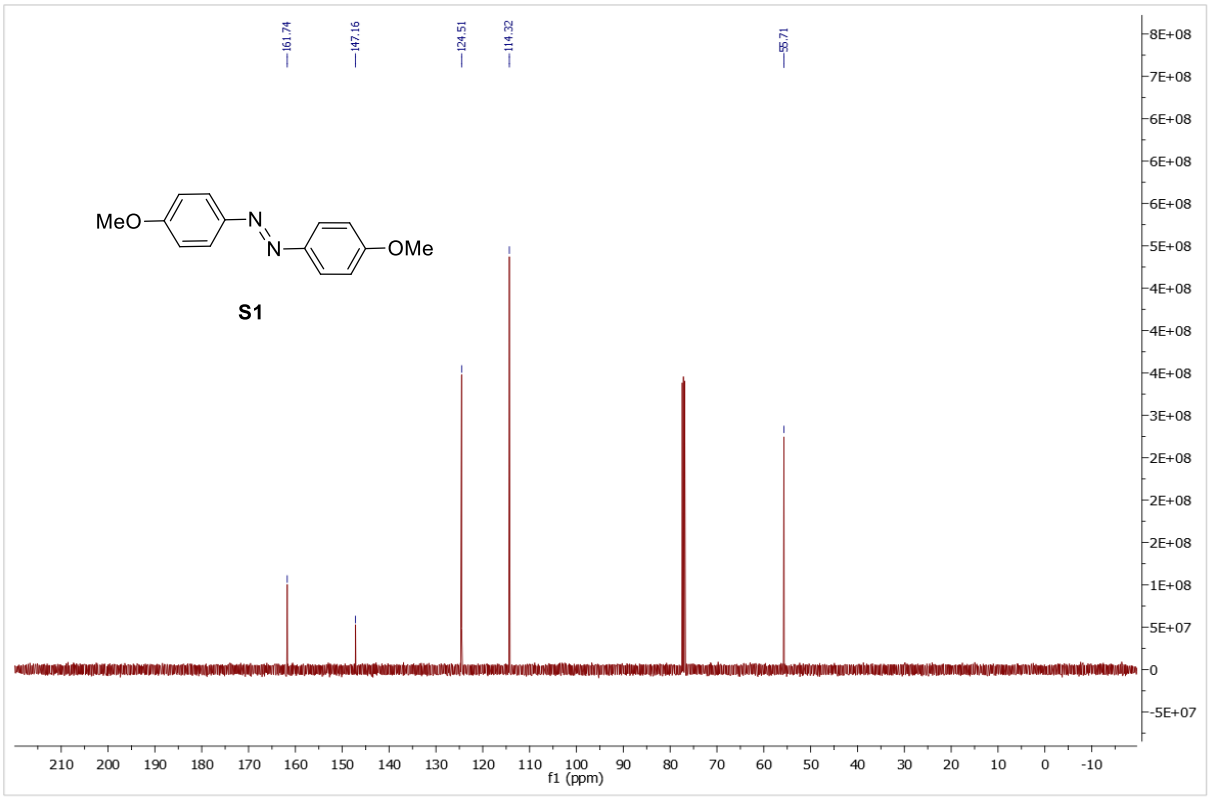

Figure 7.6.39: ^{13}C NMR spectrum of *p,p´*-dimethoxyazobenzene **S1** (126 MHz, $CDCl_3$, 300 K).

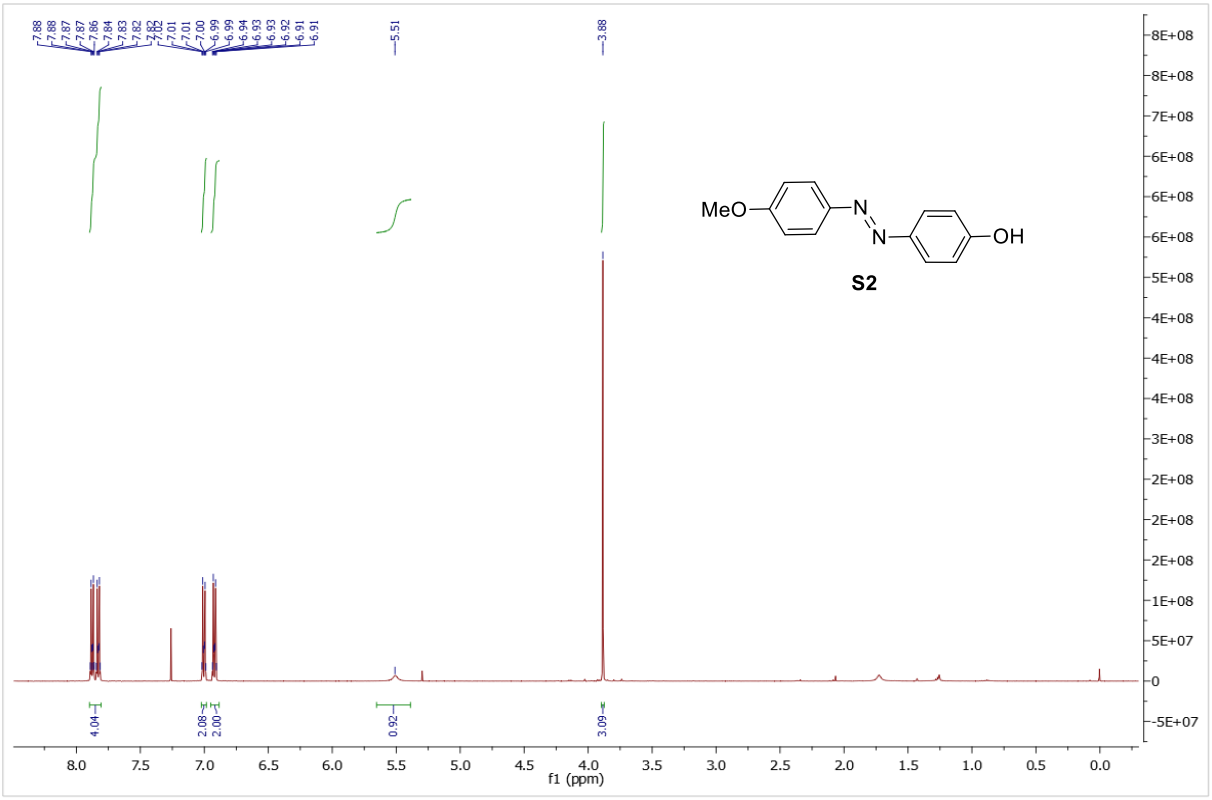

Figure 7.6.40. ^{1}H NMR spectrum of *p*-methoxy-*p´*-hydroxyazobenzene **S2** (500 MHz, $CDCl_3$, 300 K).

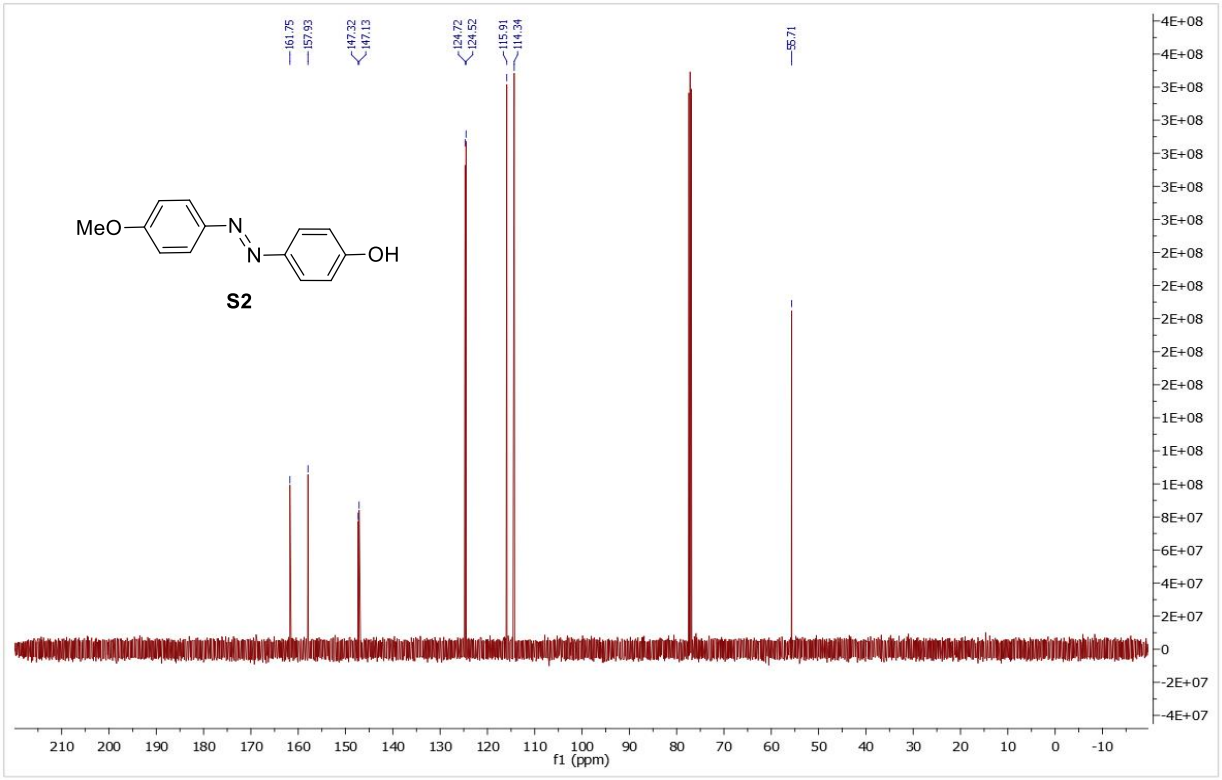

Figure 7.6.41. ^{13}C NMR spectrum of *p*-methoxy-*p´*-hydroxyazobenzene **S2** (126 MHz, $CDCl_3$, 300 K).

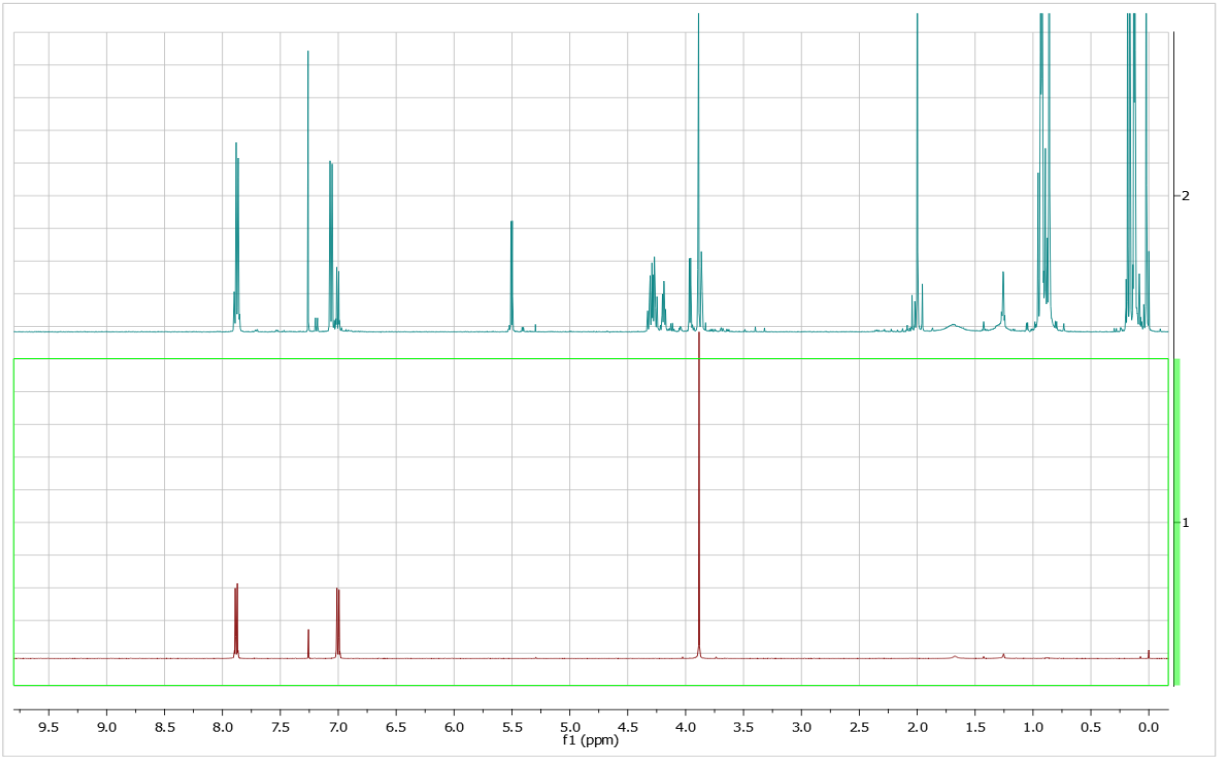

Figure 7.6.42. Superimposition of the ^{1}H spectrum of a mixture of **αβ/ββ-24a** and *p,p´*-dimethoxyazobenzene (top, green) with the spectrum of pure *p,p´*-dimethoxyazobenzene (bottom, red).

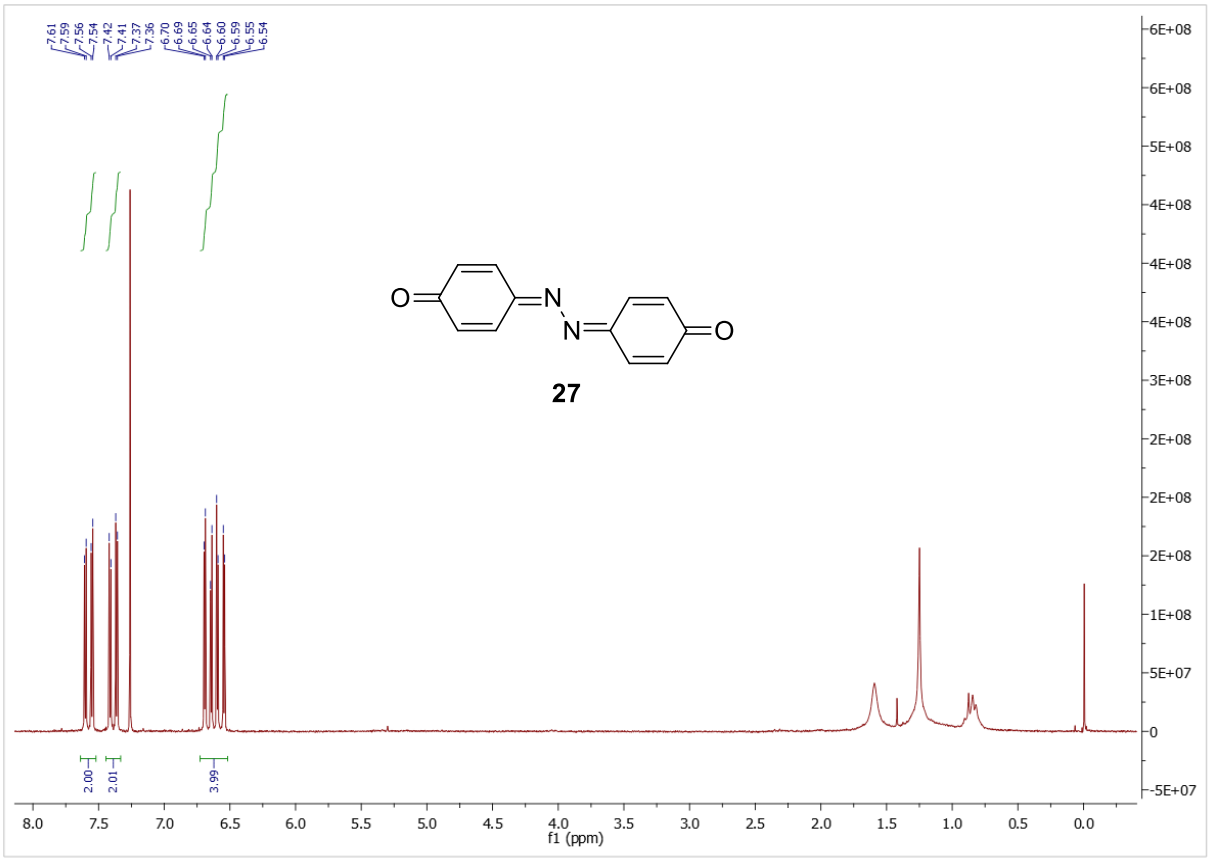

Figure 7.6.43. ^{1}H NMR spectrum of **27**, (500 MHz, $CDCl_3$, 300 K).

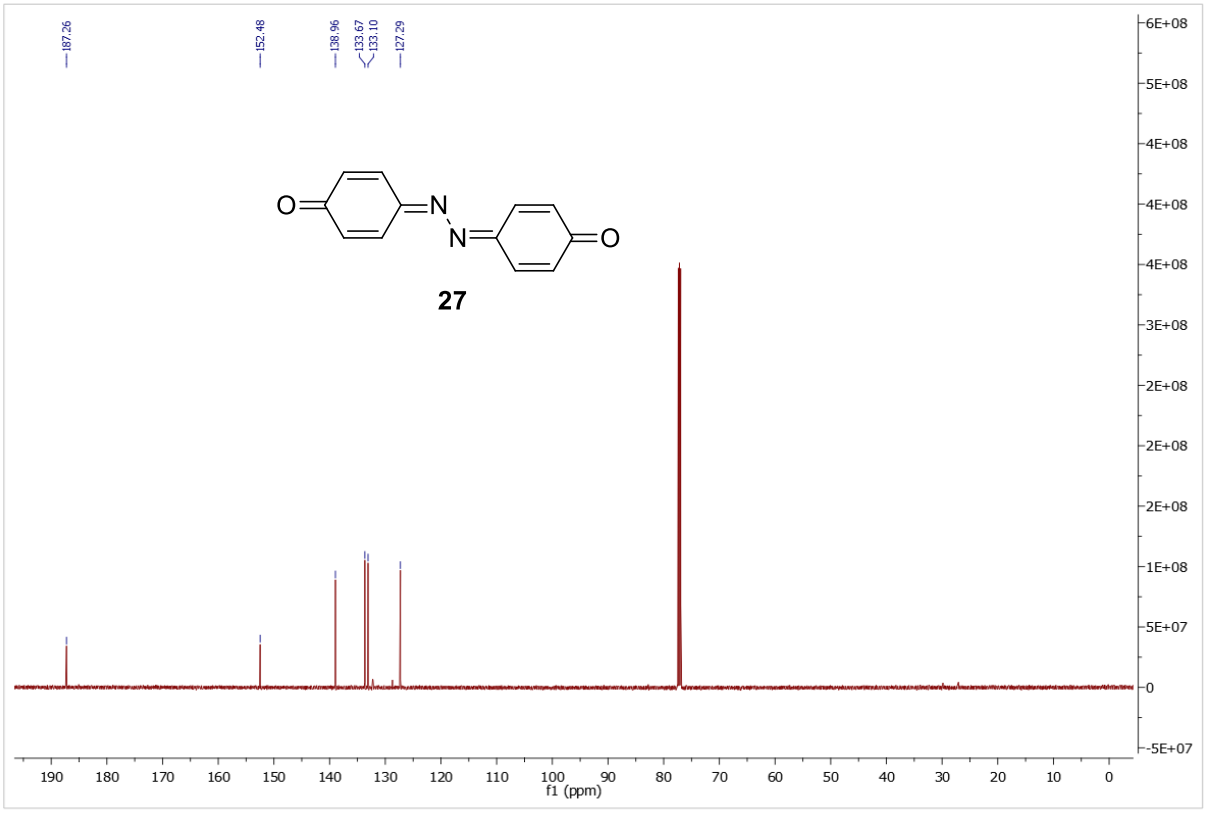

Figure 7.6.44. ^{13}C NMR spectrum of **27**, (126 MHz, $CDCl_3$, 300 K).

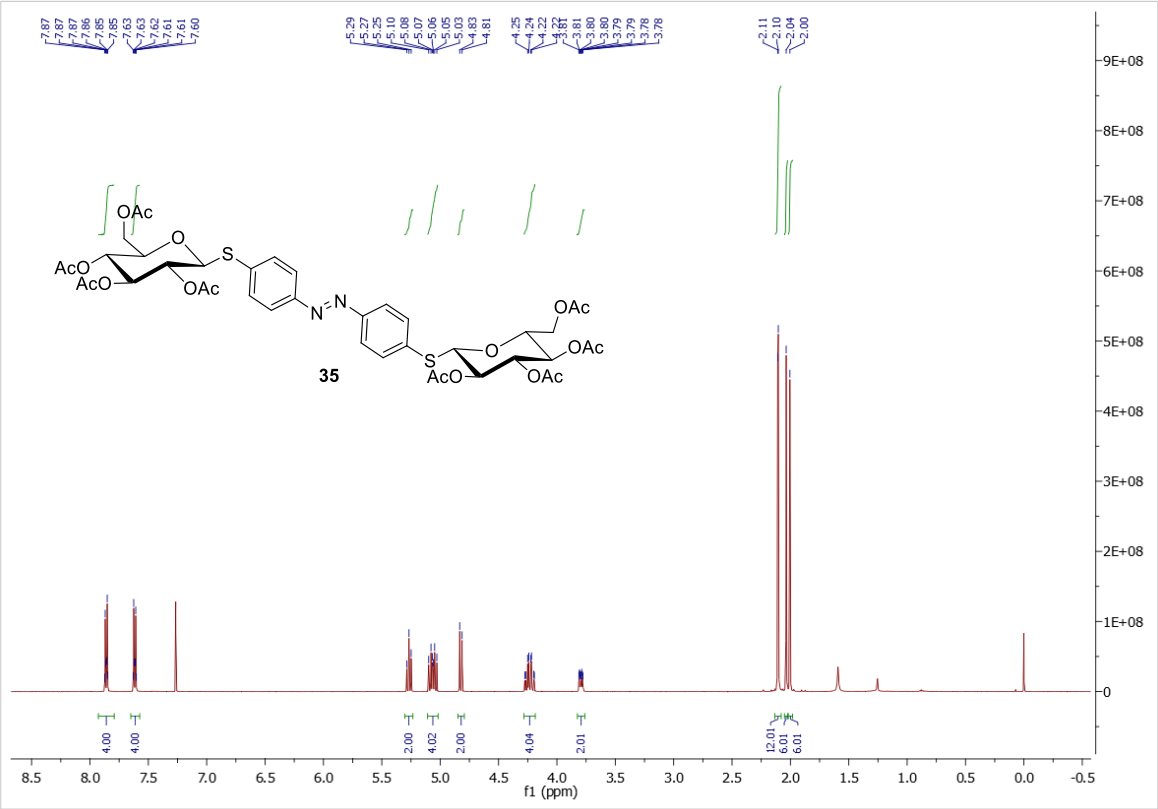

Figure 7.6.45. ^{1}H NMR spectrum of **35** (500 MHz, $CDCl_3$, 300 K).

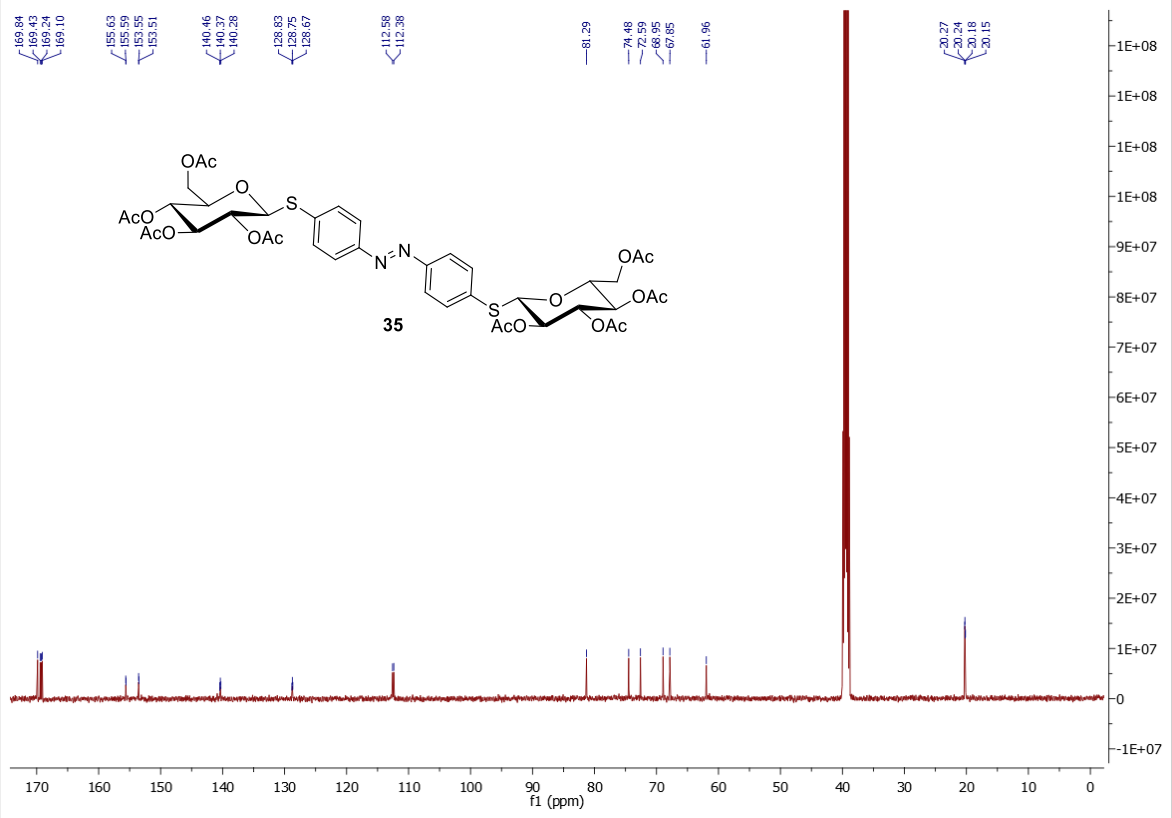

Figure 7.6.46. ^{13}C NMR spectrum of **35** (126 MHz, $CDCl_3$, 300 K).

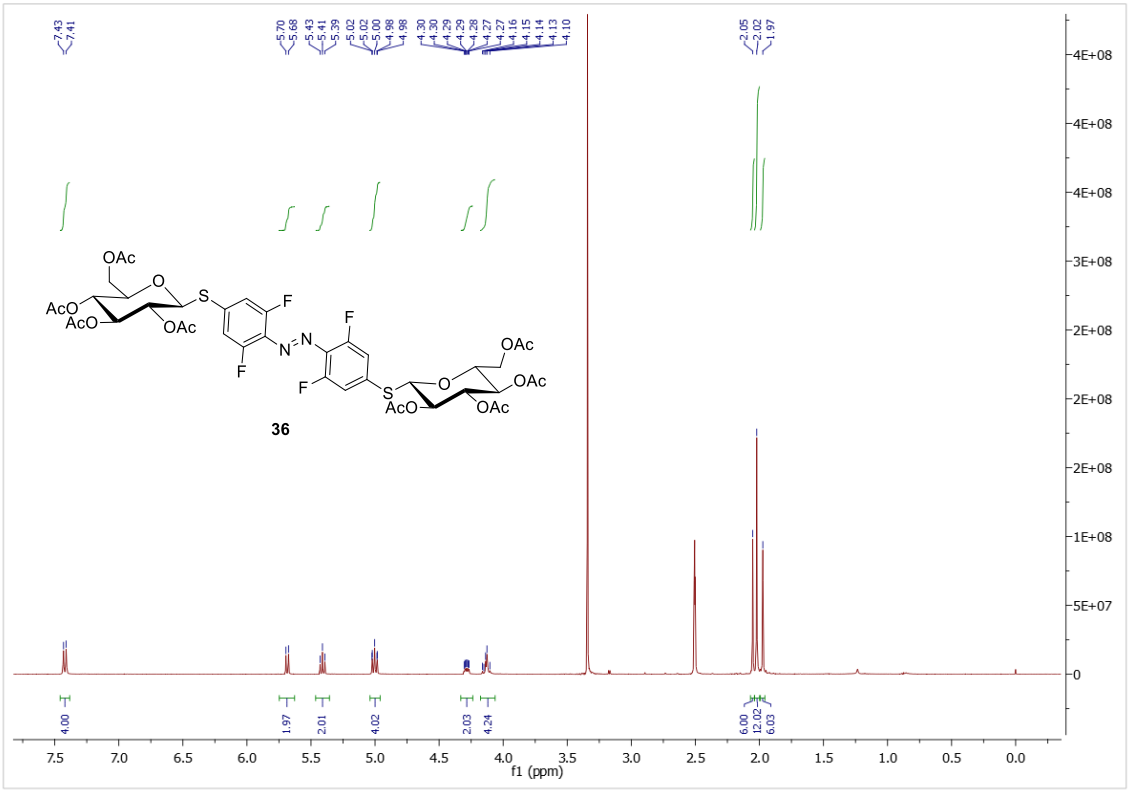

Figure 7.6.47. ^{1}H NMR spectrum of **36** (500 MHz, DMSO-d_6, 300 K).

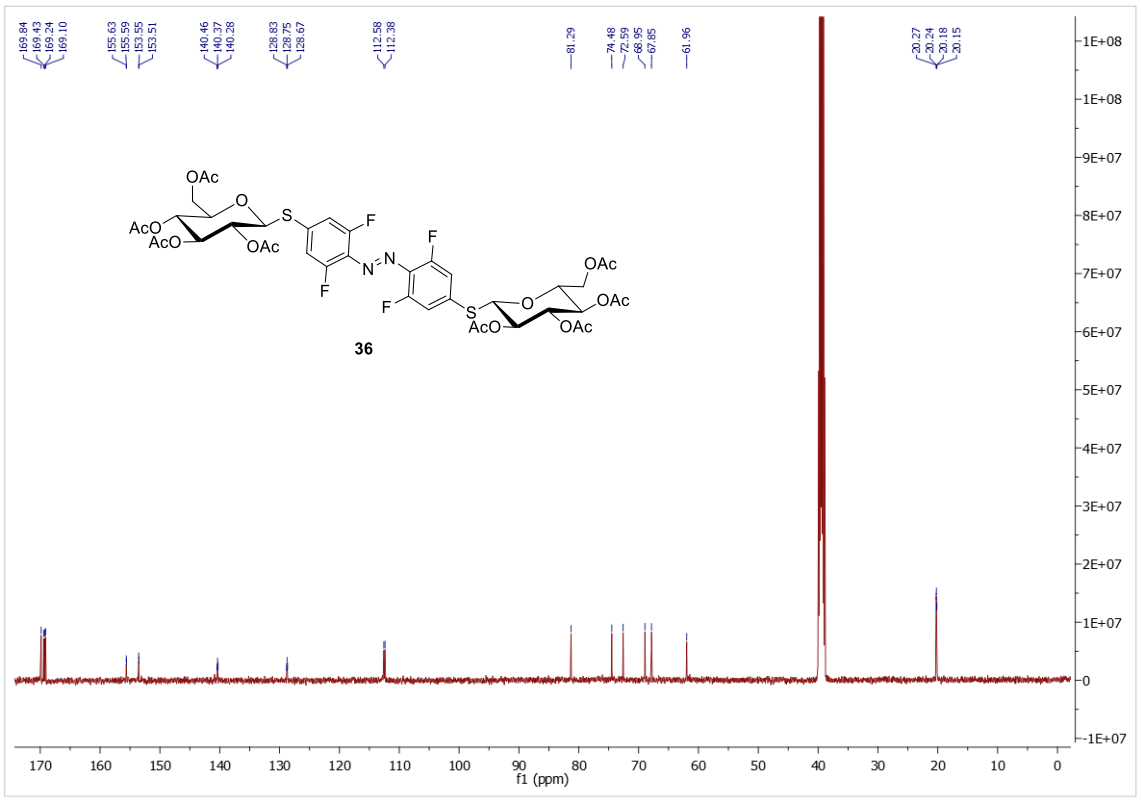

Figure 7.6.48. ^{13}C NMR spectrum of **36** (126 MHz, DMSO-d_6, 300 K).

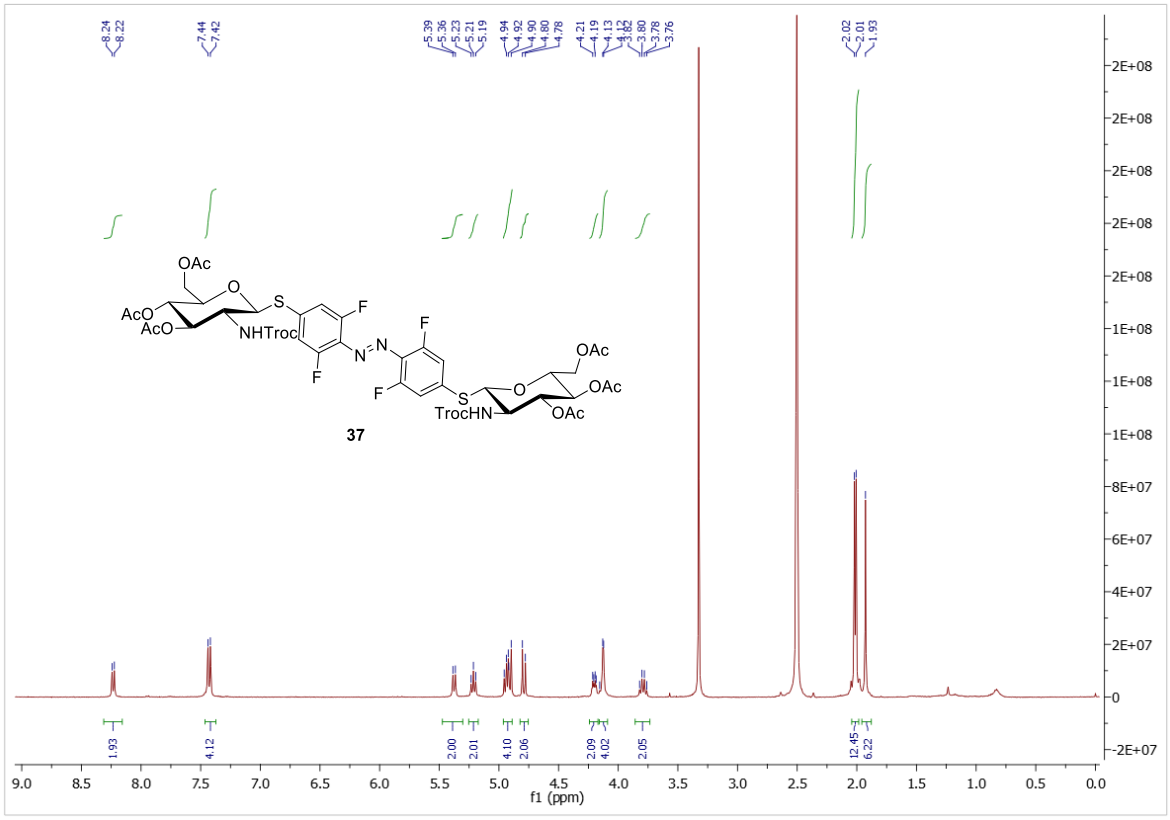

Figure 7.6.49. ^{1}H NMR spectrum of **37** (500 MHz, DMSO-d_6, 300 K).

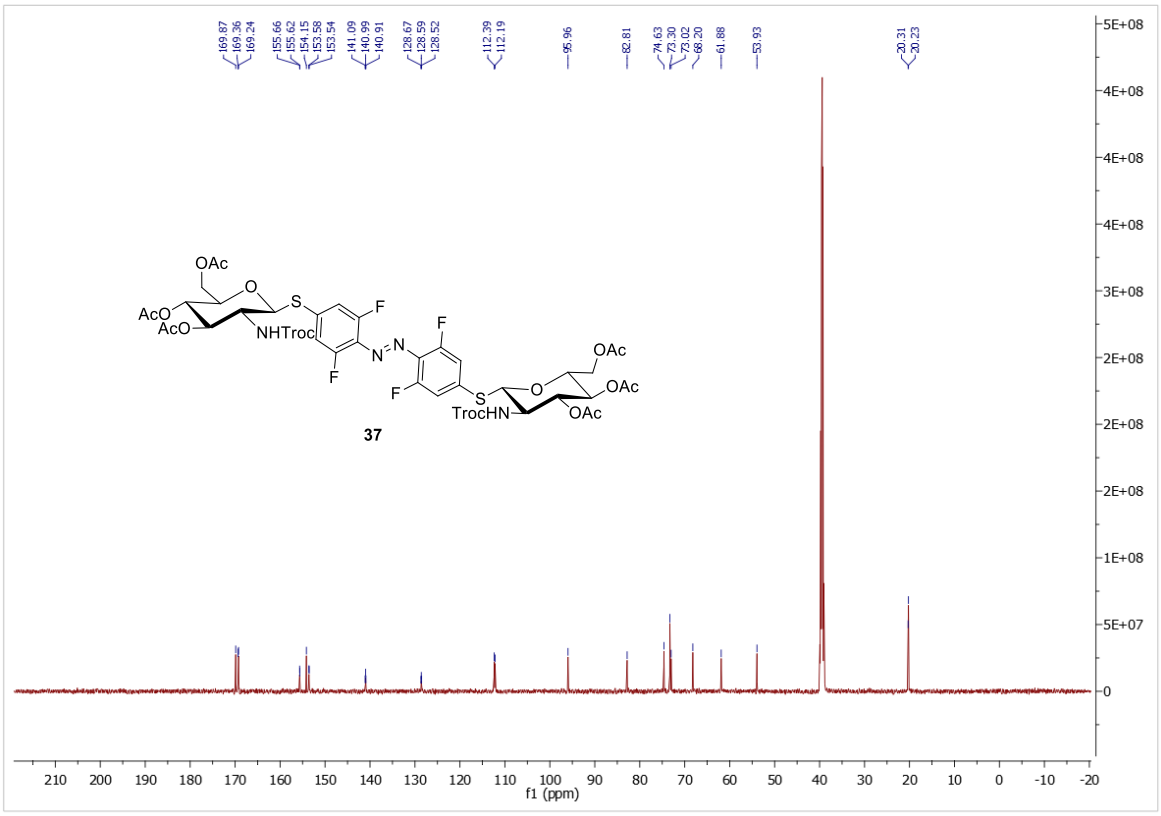

Figure 7.6.50. ^{13}C NMR spectrum of **37** (126 MHz, DMSO-d_6, 300 K).

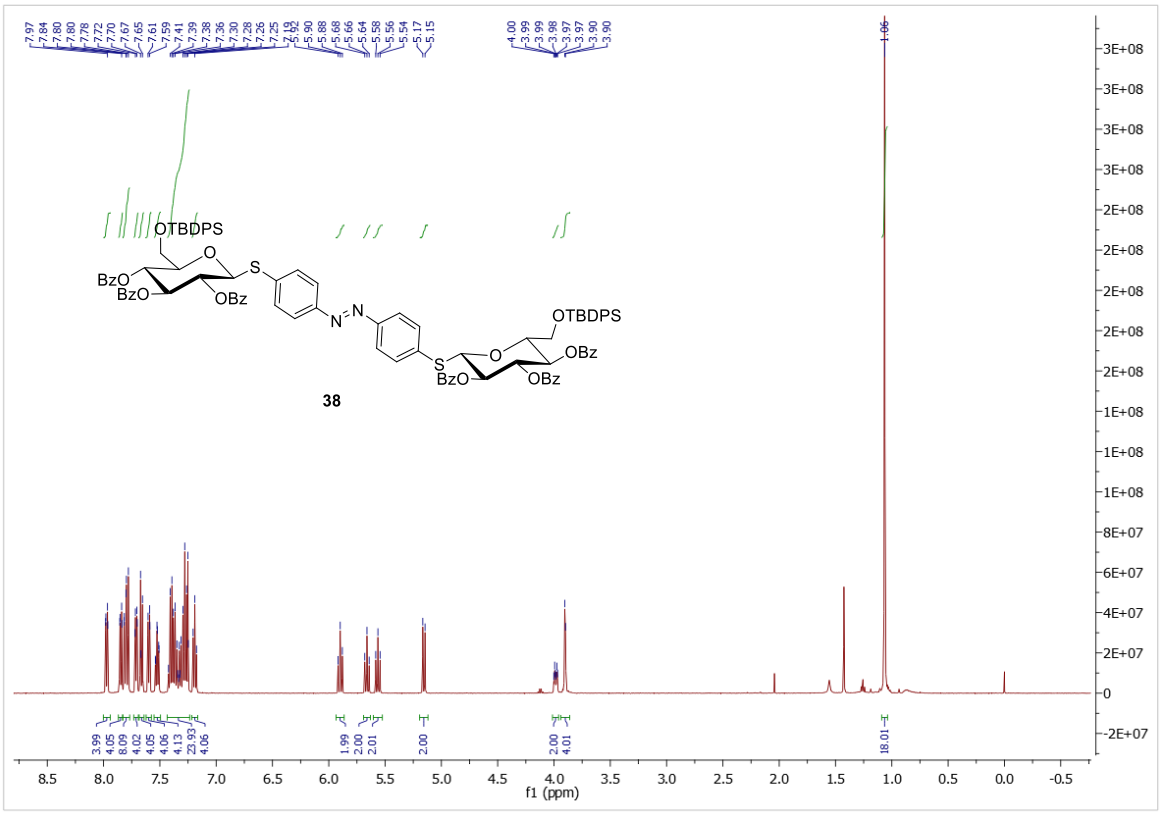

Figure 7.6.51. ^{1}H NMR spectrum of **38** (500 MHz, $CDCl_3$, 300 K).

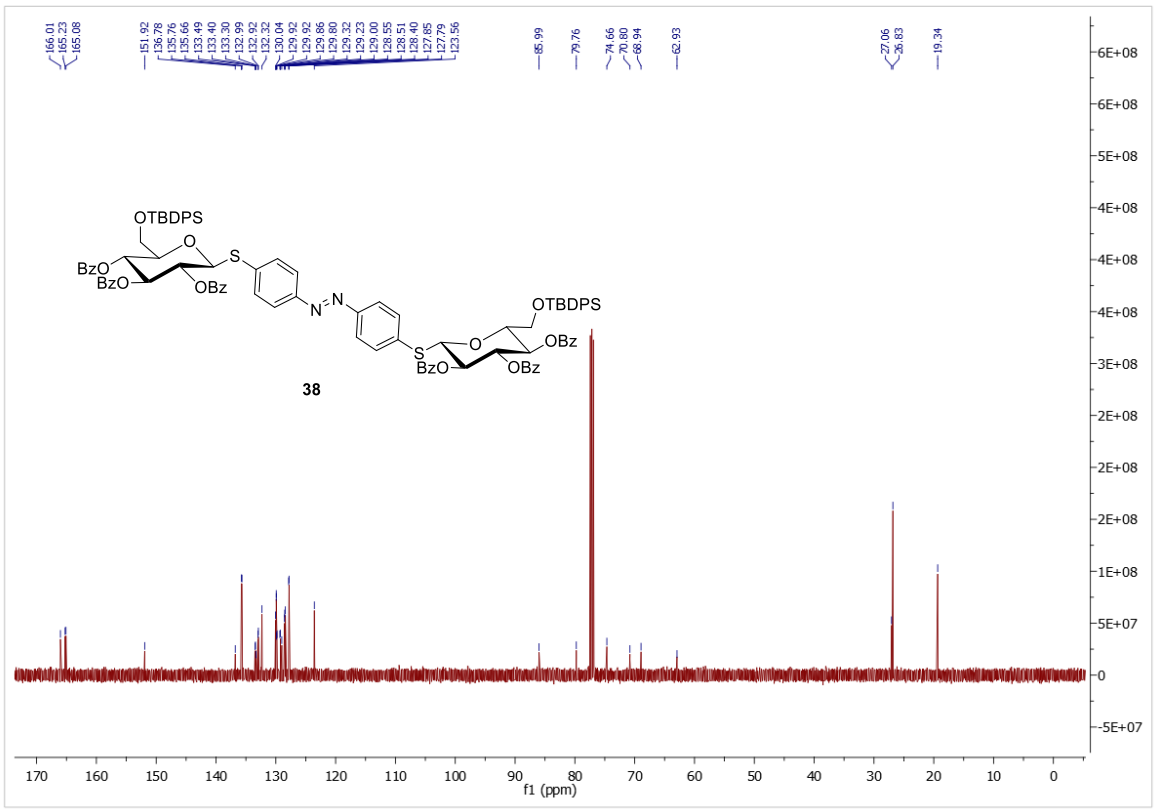

Figure 7.6.52. ^{13}C NMR spectrum of **38** (126 MHz, $CDCl_3$, 300 K).

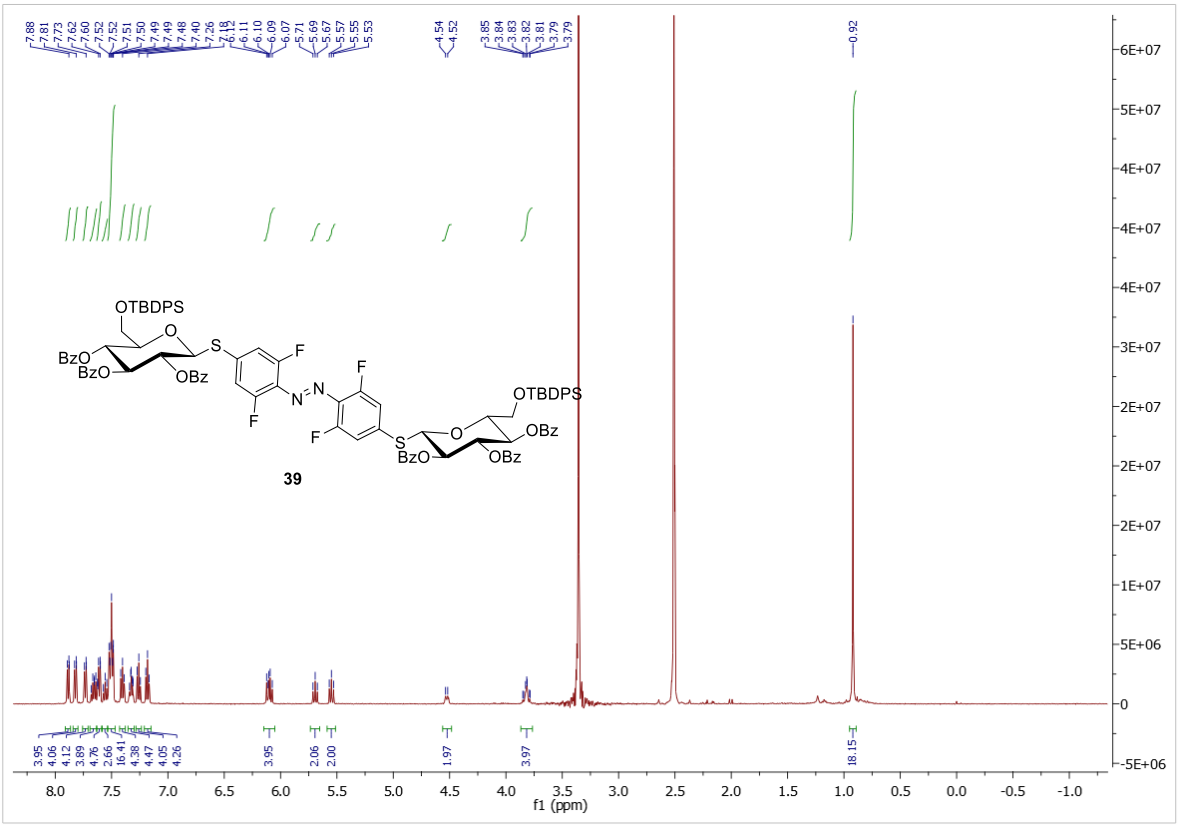

Figure 7.6.53. ^{1}H NMR spectrum of **39** (500 MHz, DMSO-d_6, 300 K).

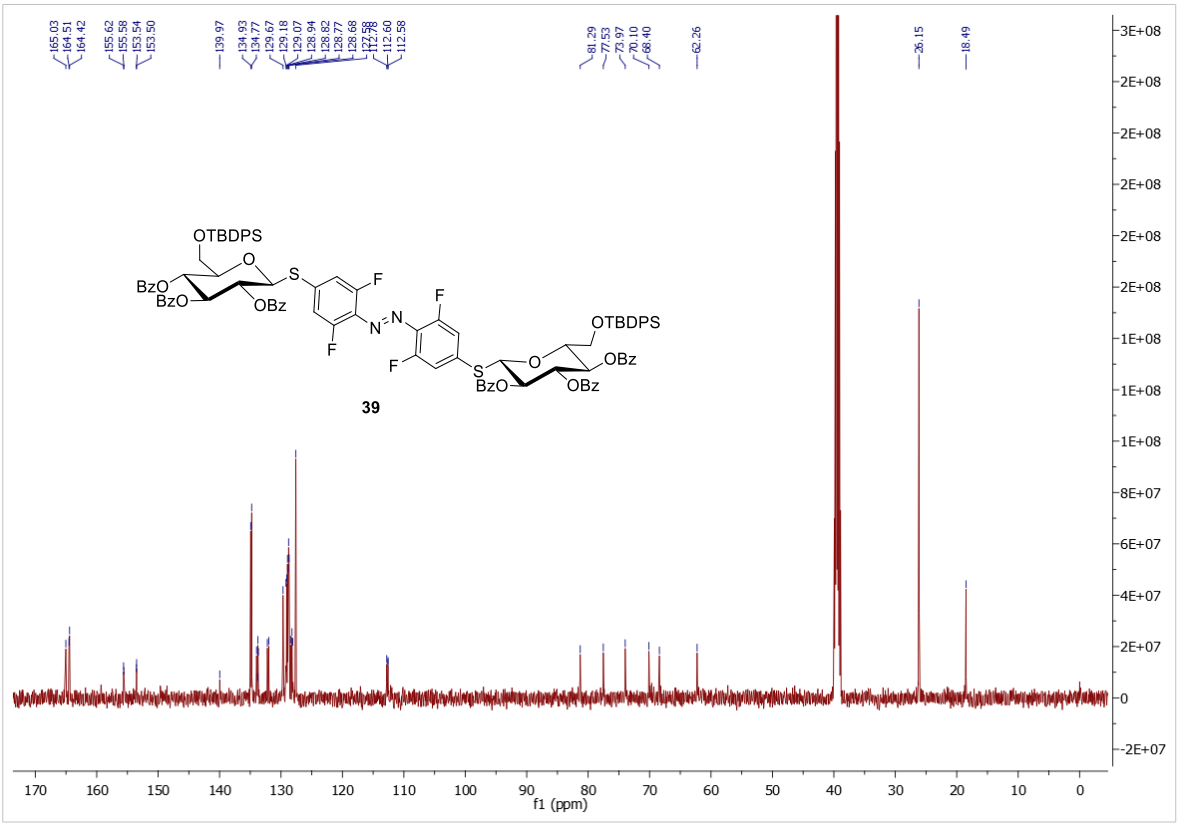

Figure 7.6.54. ^{13}C NMR spectrum of **39** (126 MHz, DMSO-d_6, 300 K).

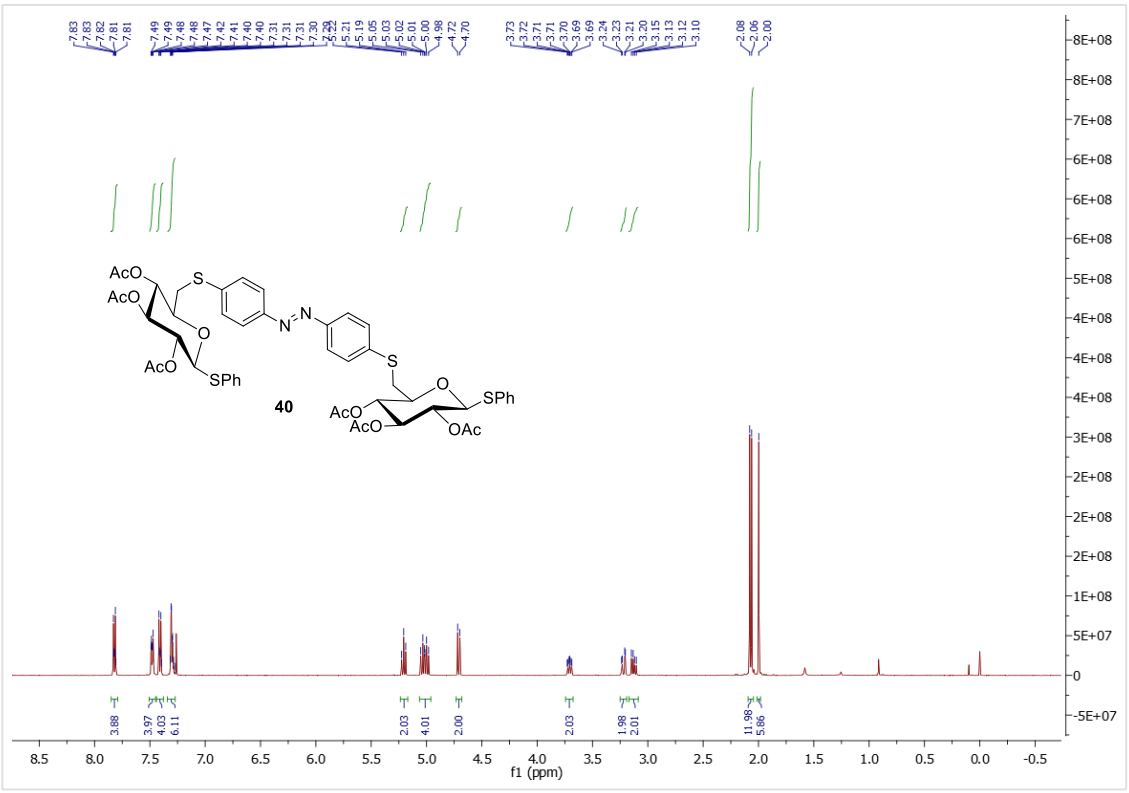

Figure 7.6.55. ^{1}H NMR spectrum of **40** (500 MHz, $CDCl_3$, 300 K).

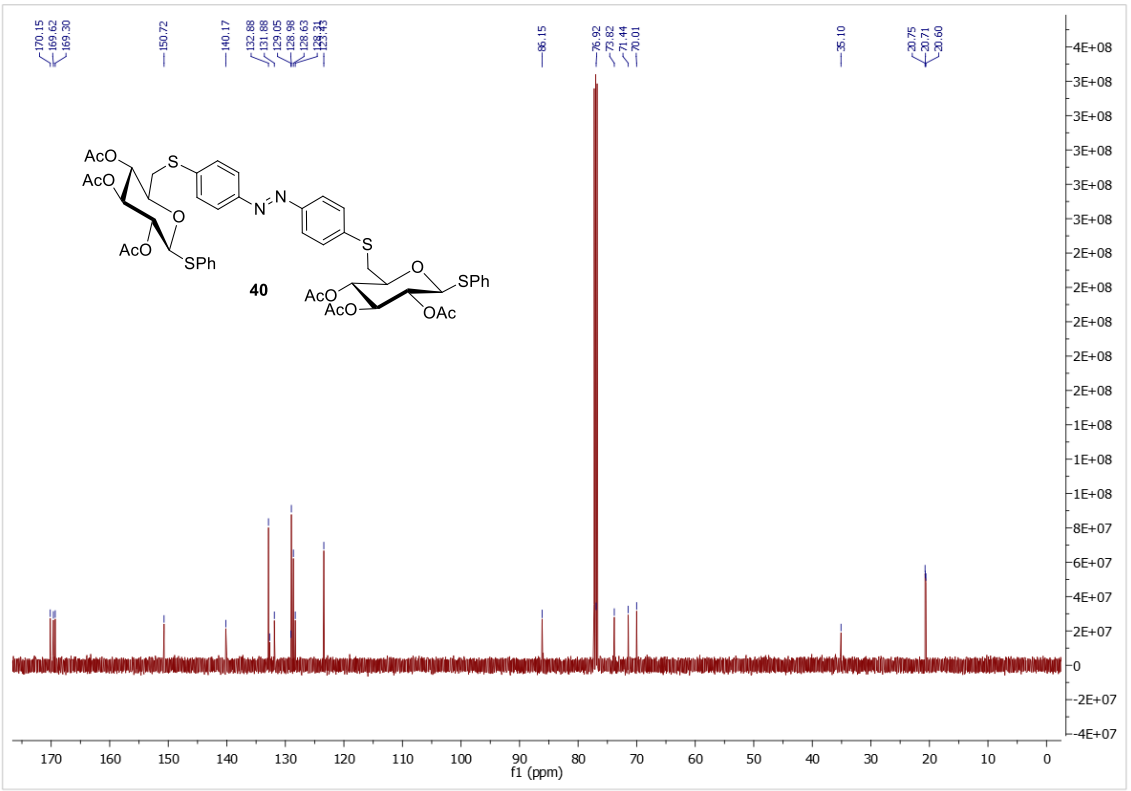

Figure 7.6.56. ^{13}C NMR spectrum of **40** (126 MHz, $CDCl_3$, 300 K).

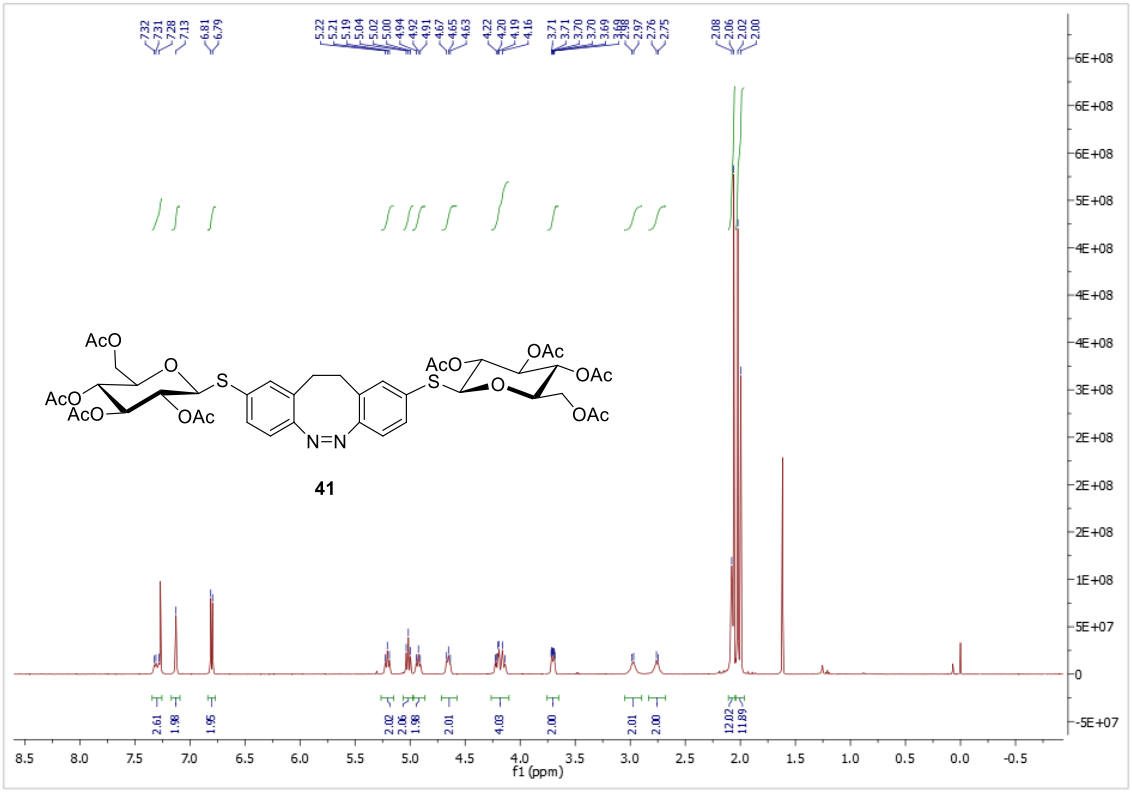

Figure 7.6.57. ^{1}H NMR spectrum of **41** (500 MHz, $CDCl_3$, 300 K).

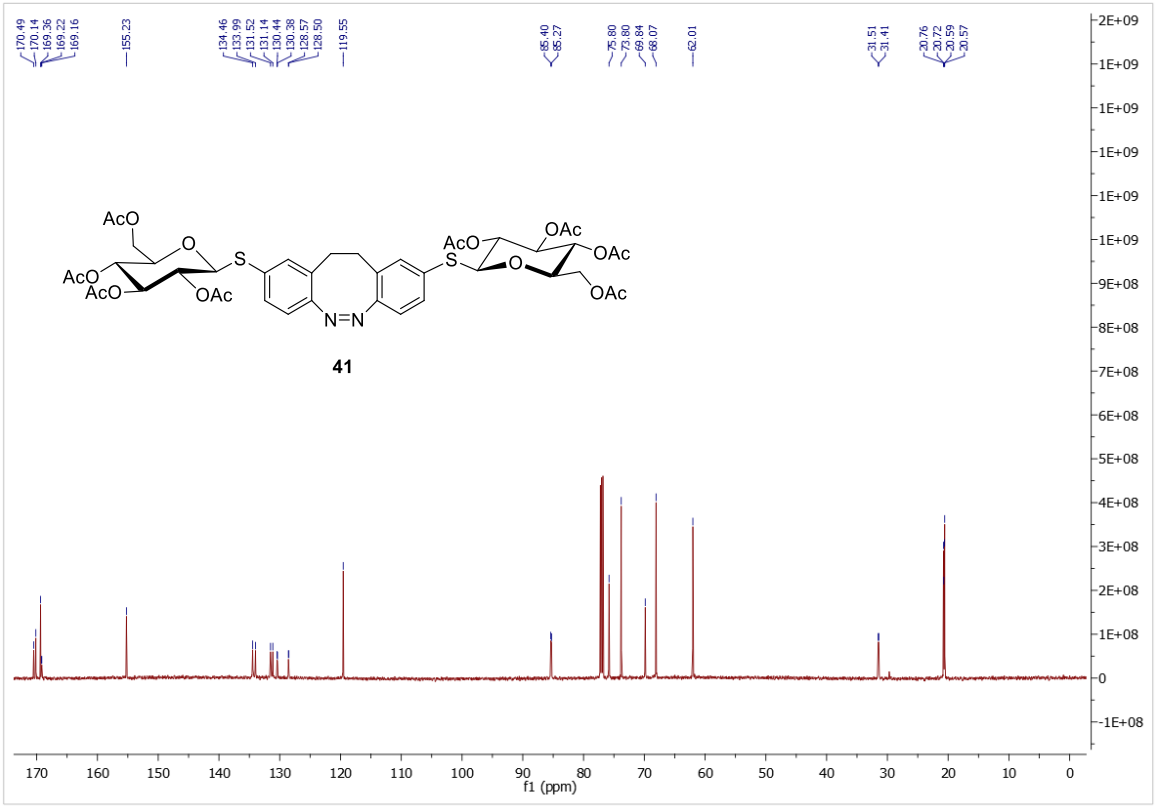

Figure 7.6.58. ^{13}C NMR spectrum of **41** (126 MHz, $CDCl_3$, 300 K).

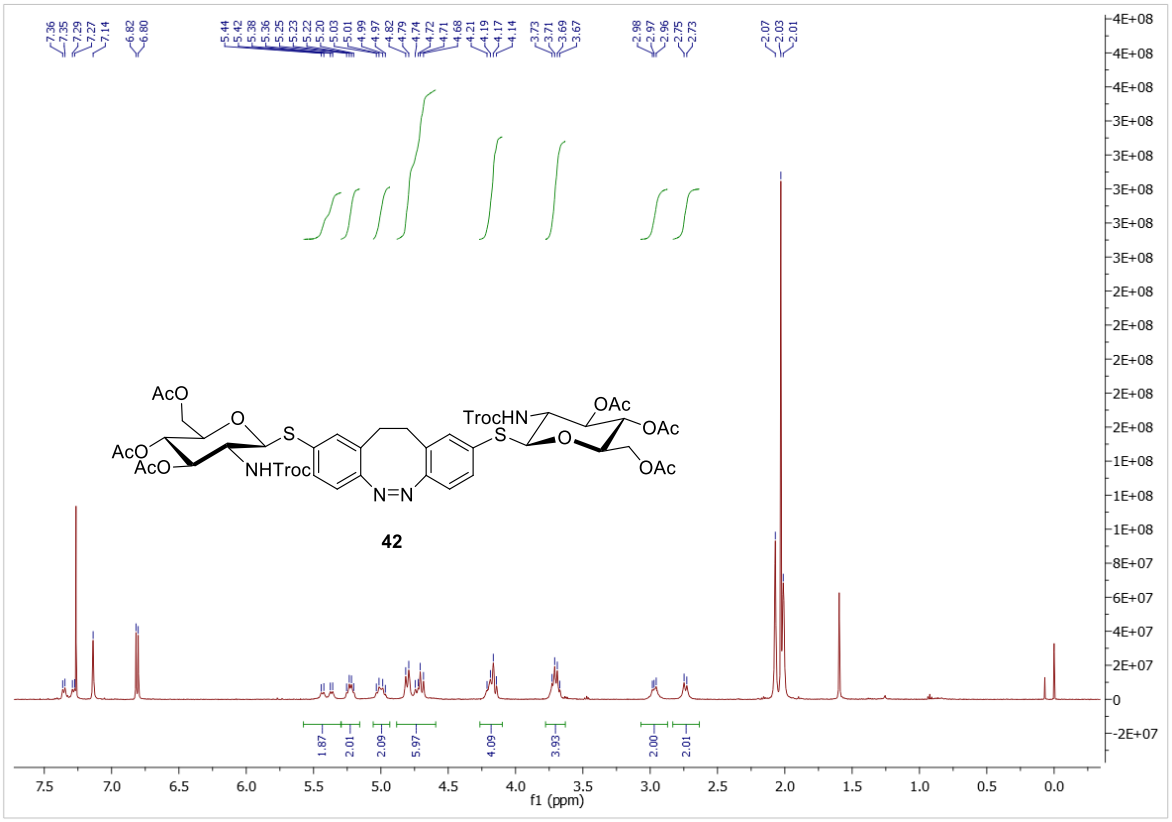

Figure 7.6.59. ^{1}H NMR spectrum of **42** (500 MHz, $CDCl_3$, 300 K).

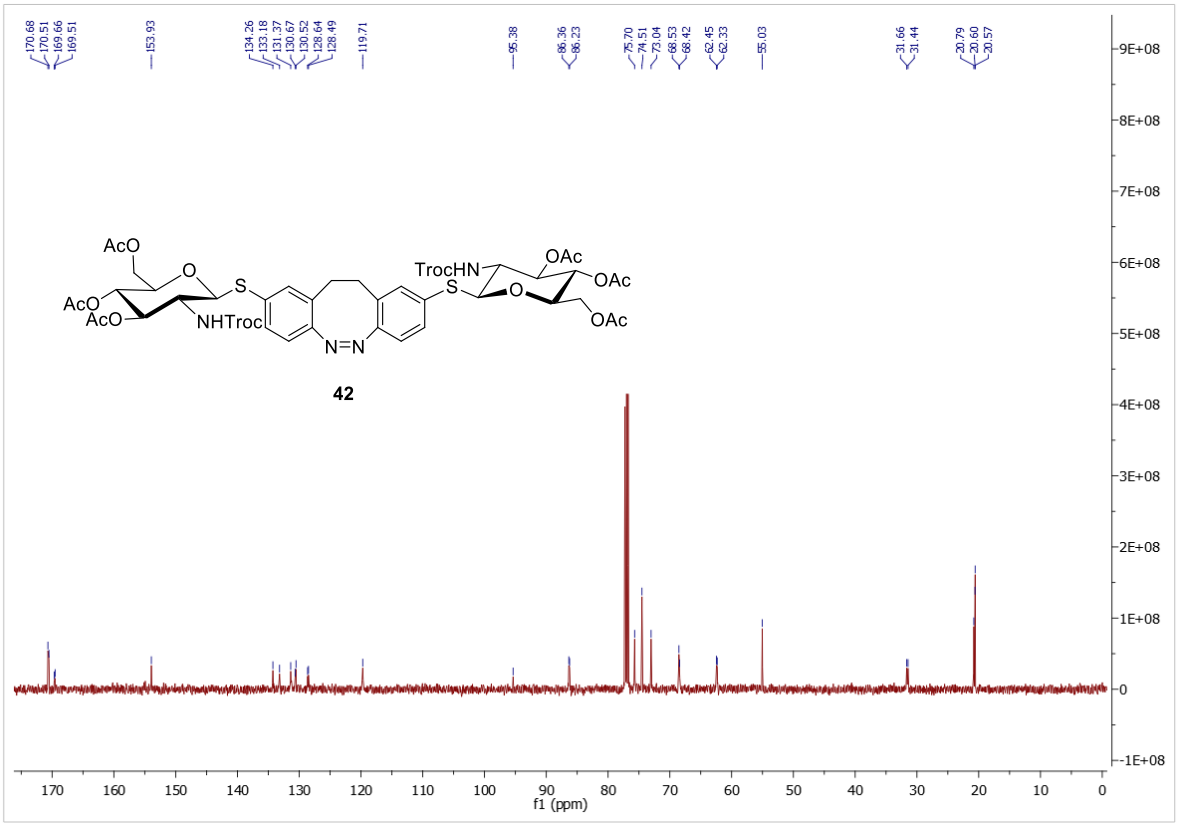

Figure 7.6.60. ^{13}C NMR spectrum of **42** (126 MHz, $CDCl_3$, 300 K).

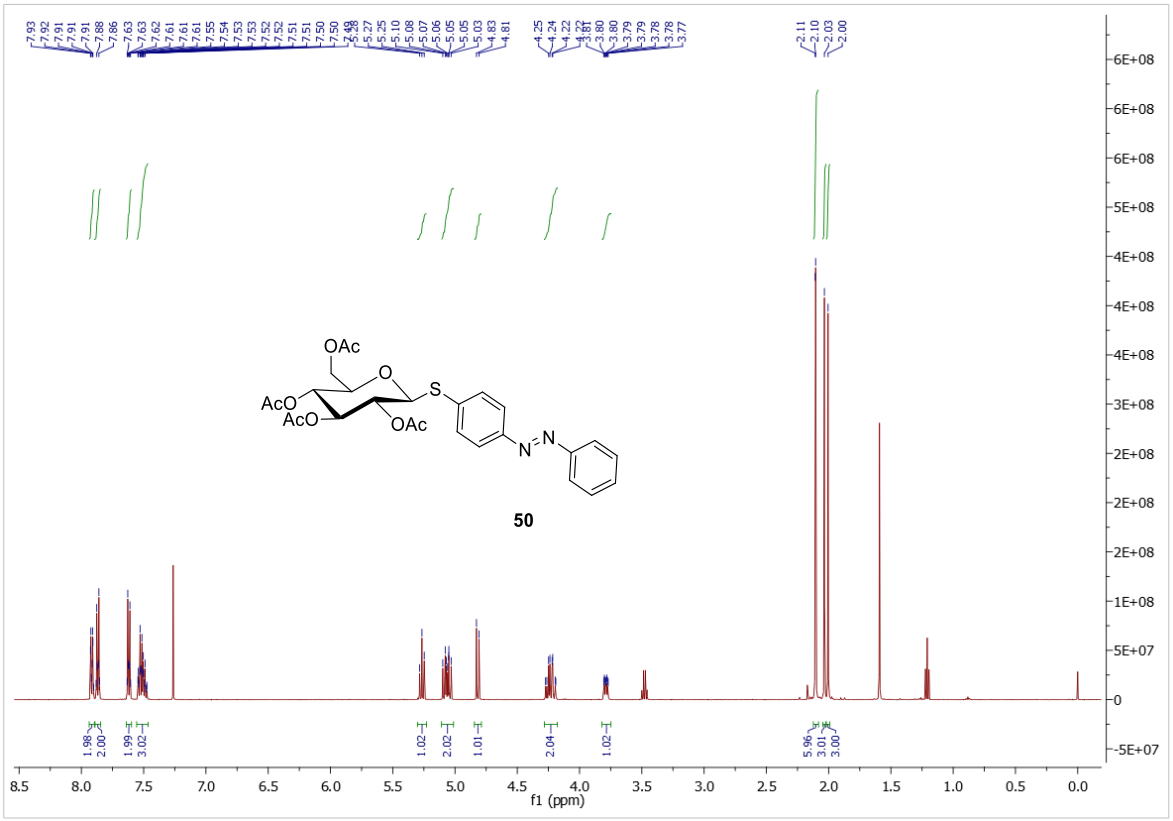

Figure 7.6.61. ^{1}H NMR spectrum of **50** (500 MHz, $CDCl_3$, 300 K).

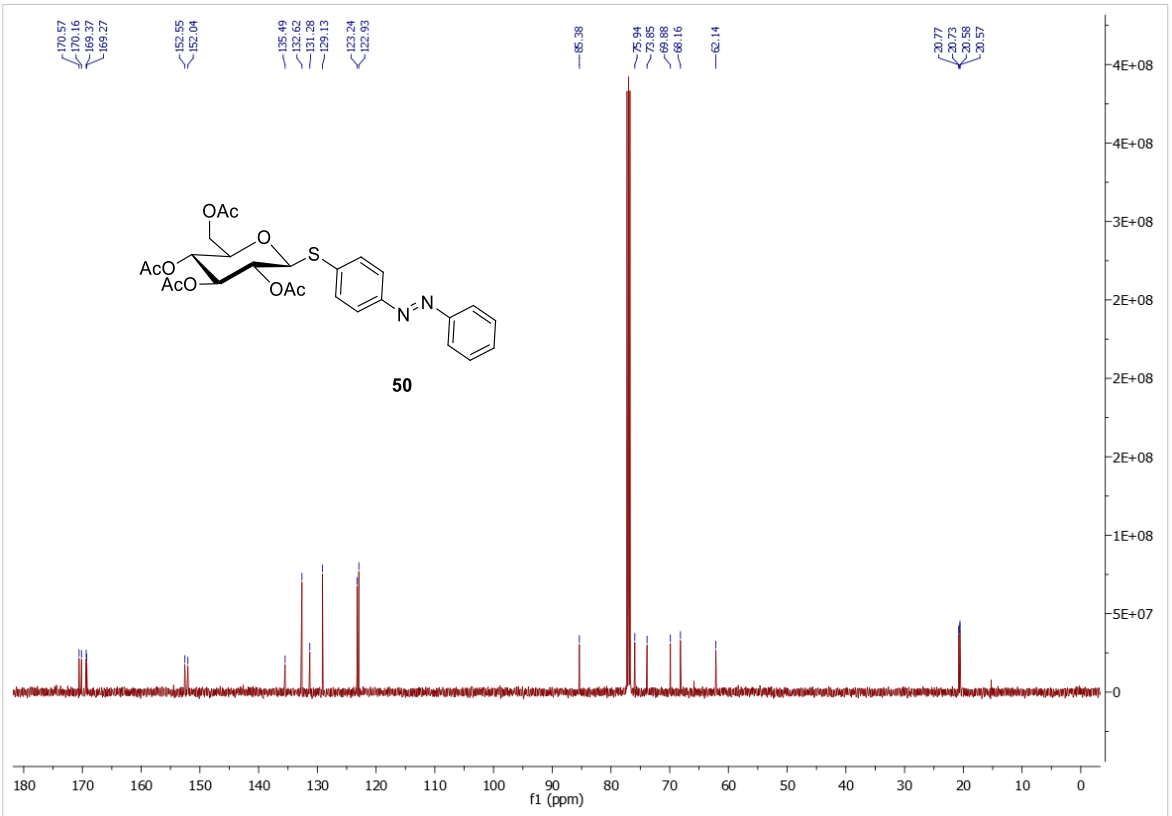

Figure 7.6.62. ^{13}C NMR spectrum of **50** (126 MHz, $CDCl_3$, 300 K).

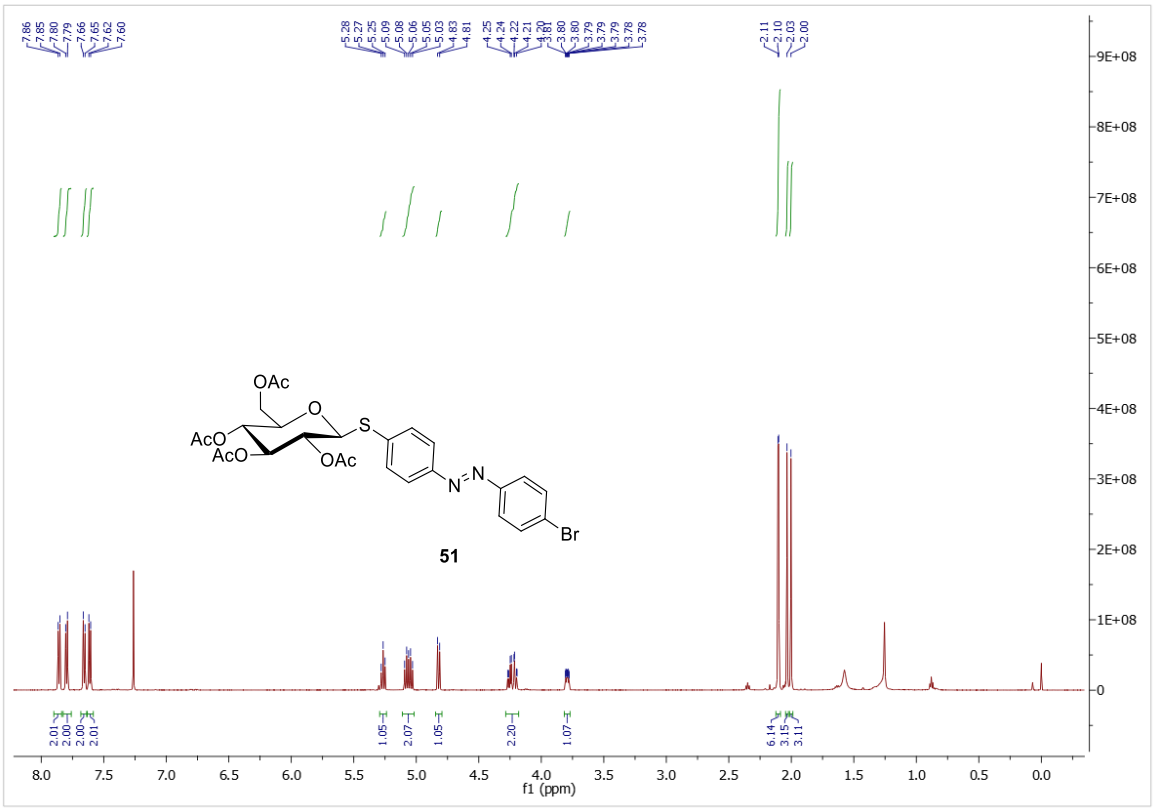

Figure 7.6.63. ^{1}H NMR spectrum of **51** (500 MHz, $CDCl_3$, 300 K).

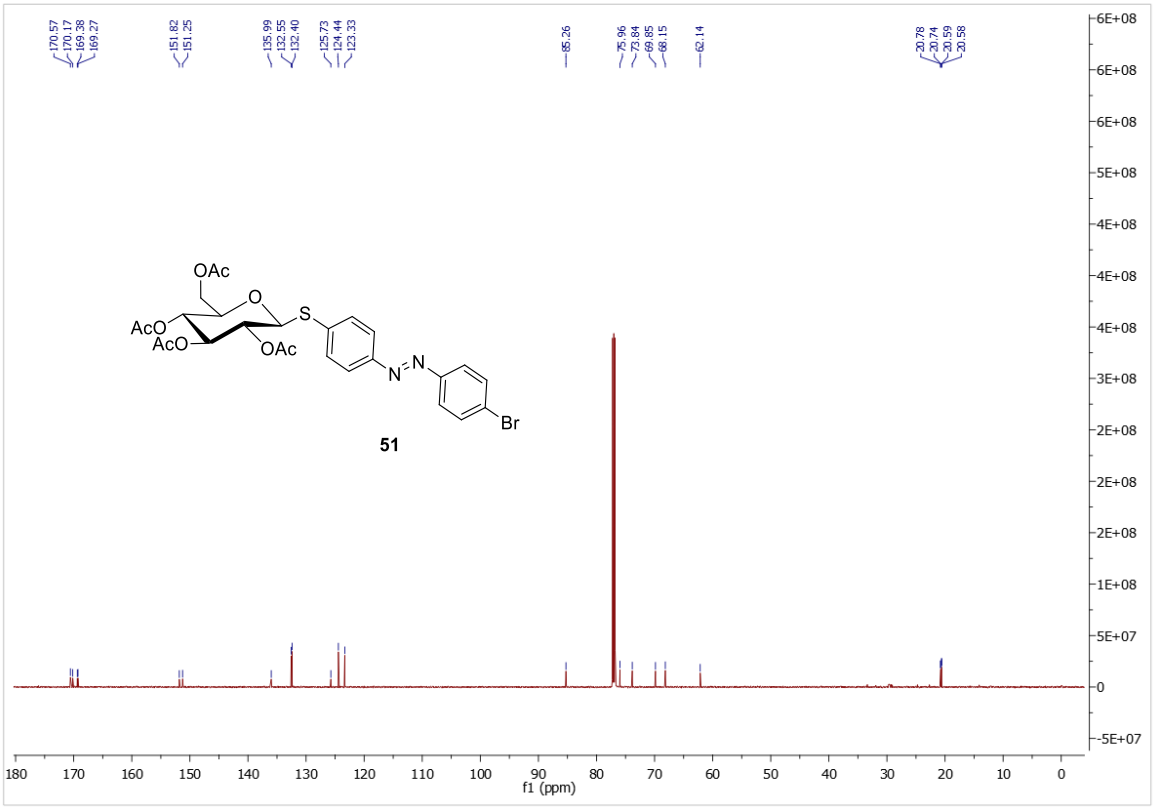

Figure 7.6.64. ^{13}C NMR spectrum of **51** (126 MHz, $CDCl_3$, 300 K).

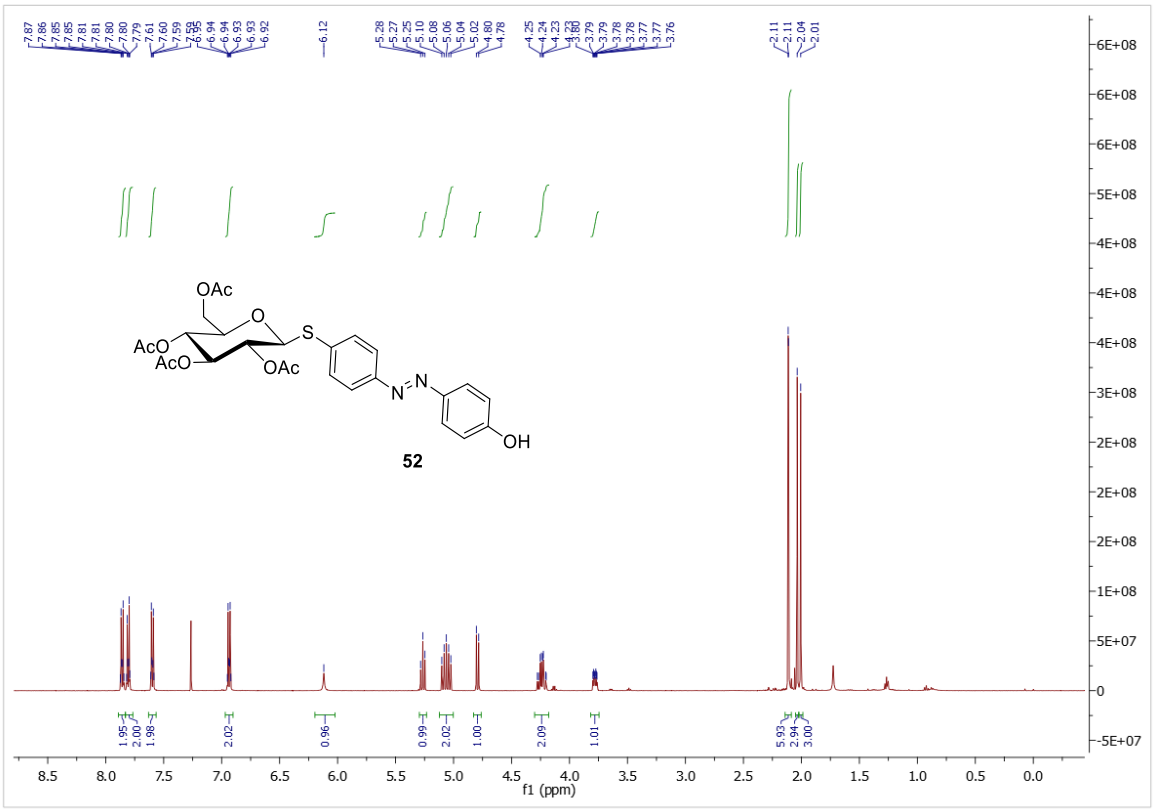

Figure 7.6.65. ^{1}H NMR spectrum of **52** (500 MHz, $CDCl_3$, 300 K).

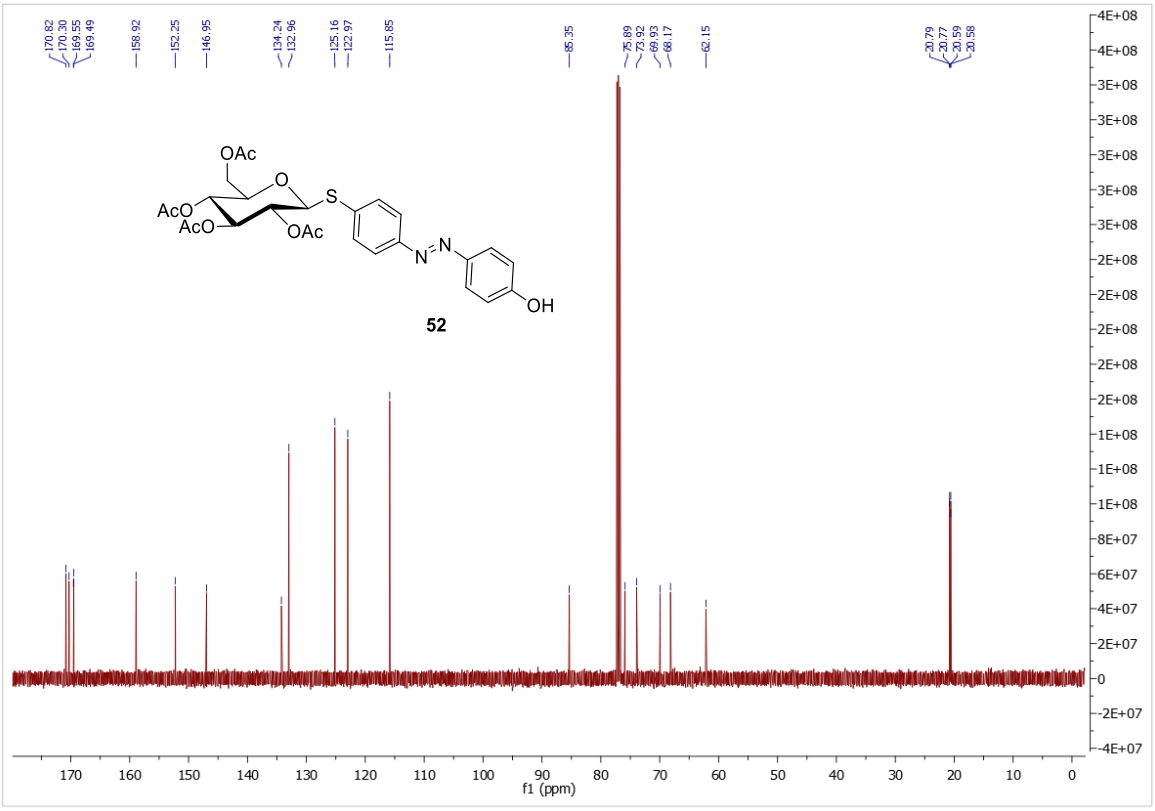

Figure 7.6.66. ^{13}C NMR spectrum of **52** (126 MHz, $CDCl_3$, 300 K).

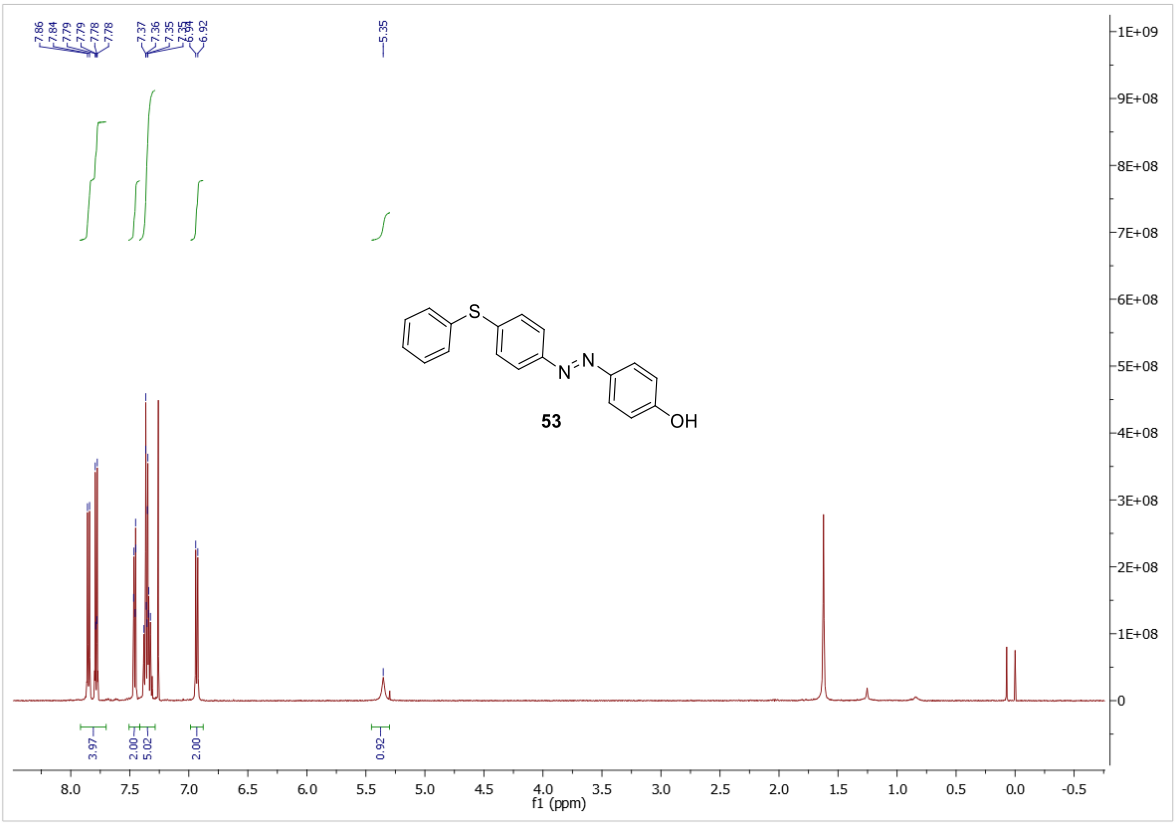

Figure 7.6.67. ^{1}H NMR spectrum of **53** (500 MHz, $CDCl_3$, 300 K).

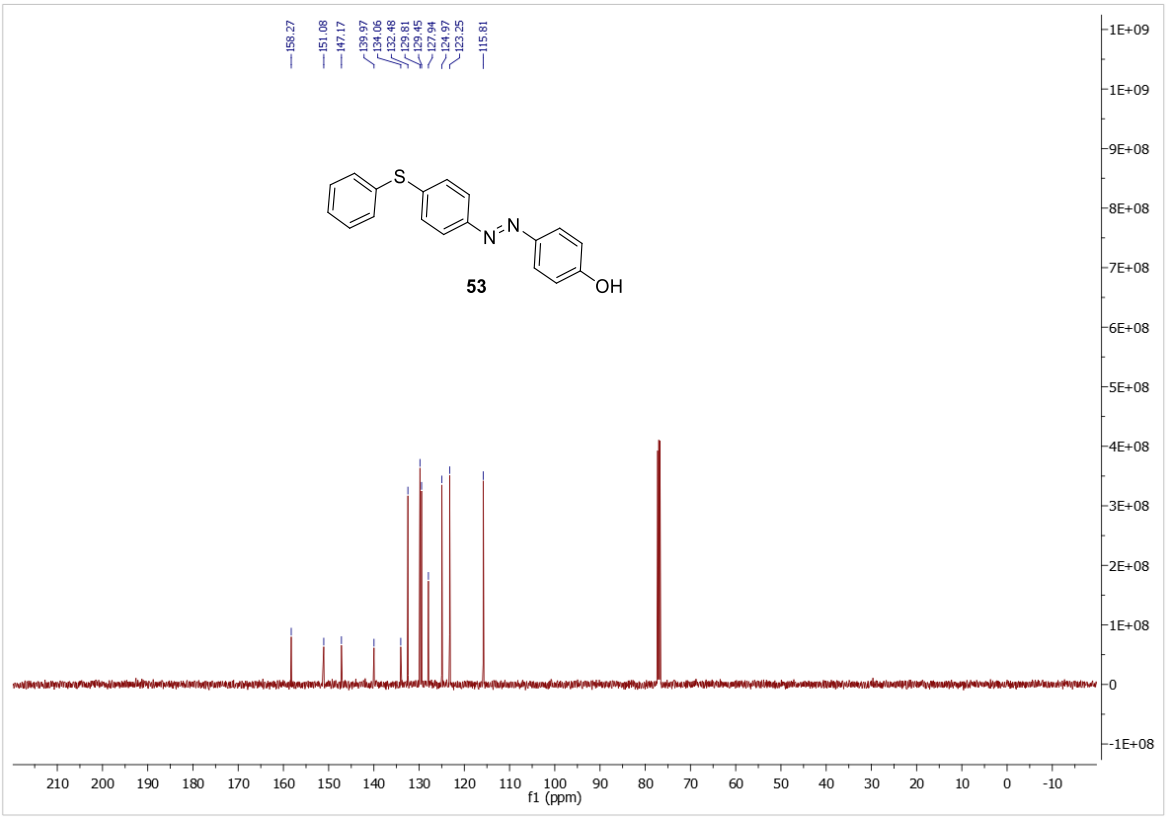

Figure 7.6.68. ^{13}C NMR spectrum of **53** (126 MHz, $CDCl_3$, 300 K).

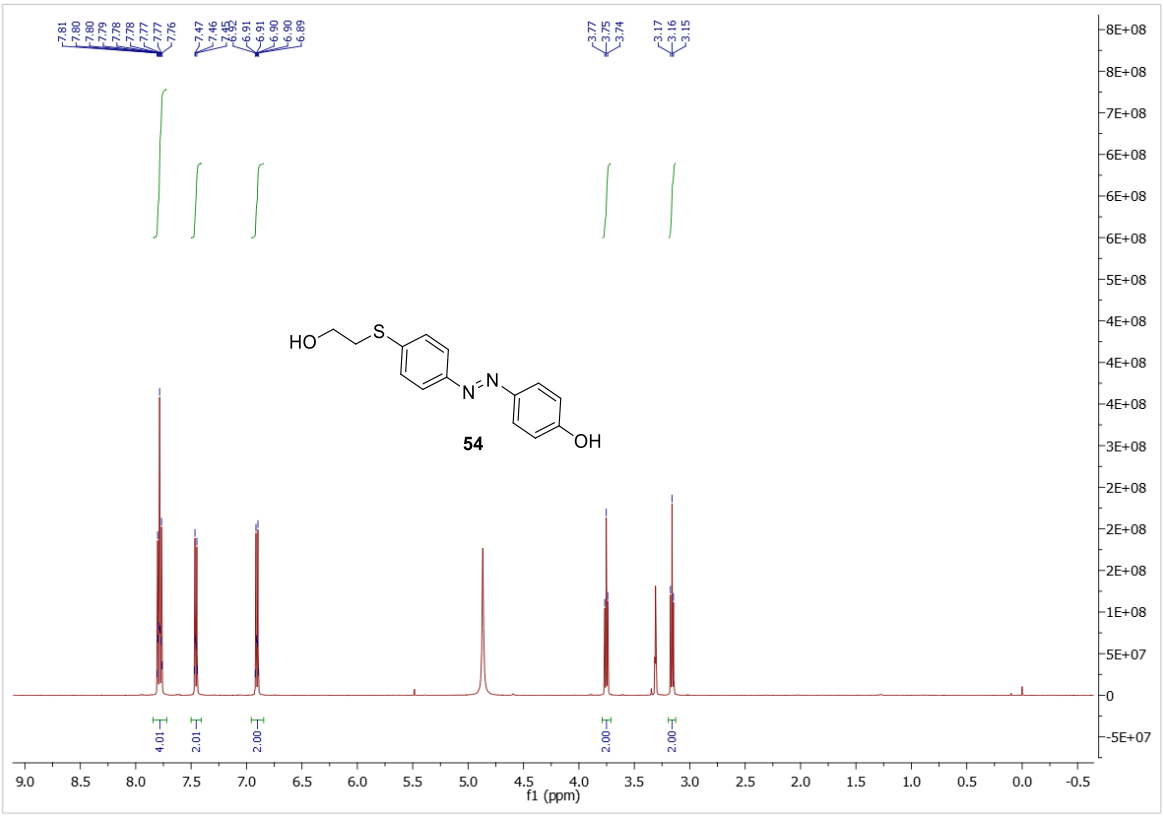

Figure 7.6.69. ^{1}H NMR spectrum of **54** (500 MHz, MeOD, 300 K).

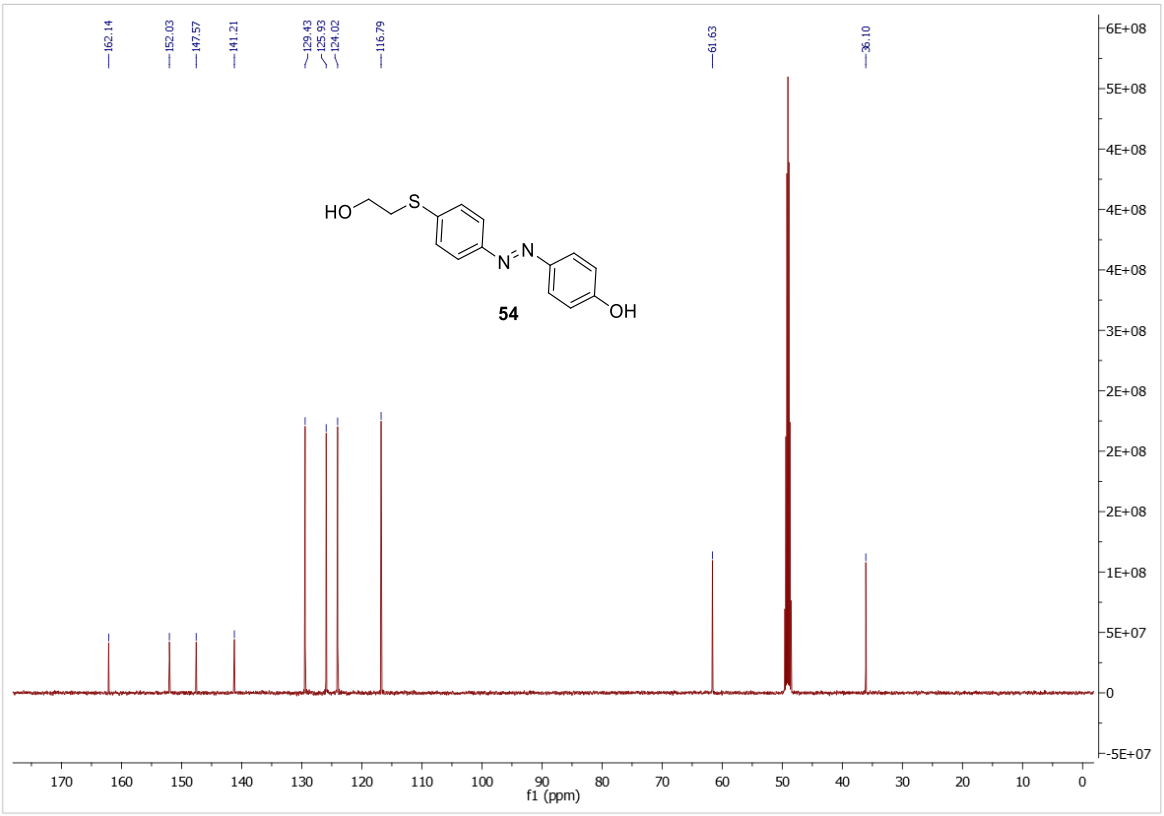

Figure 7.6.70. ^{13}C NMR spectrum of **54** (126 MHz, MeOD, 300 K).

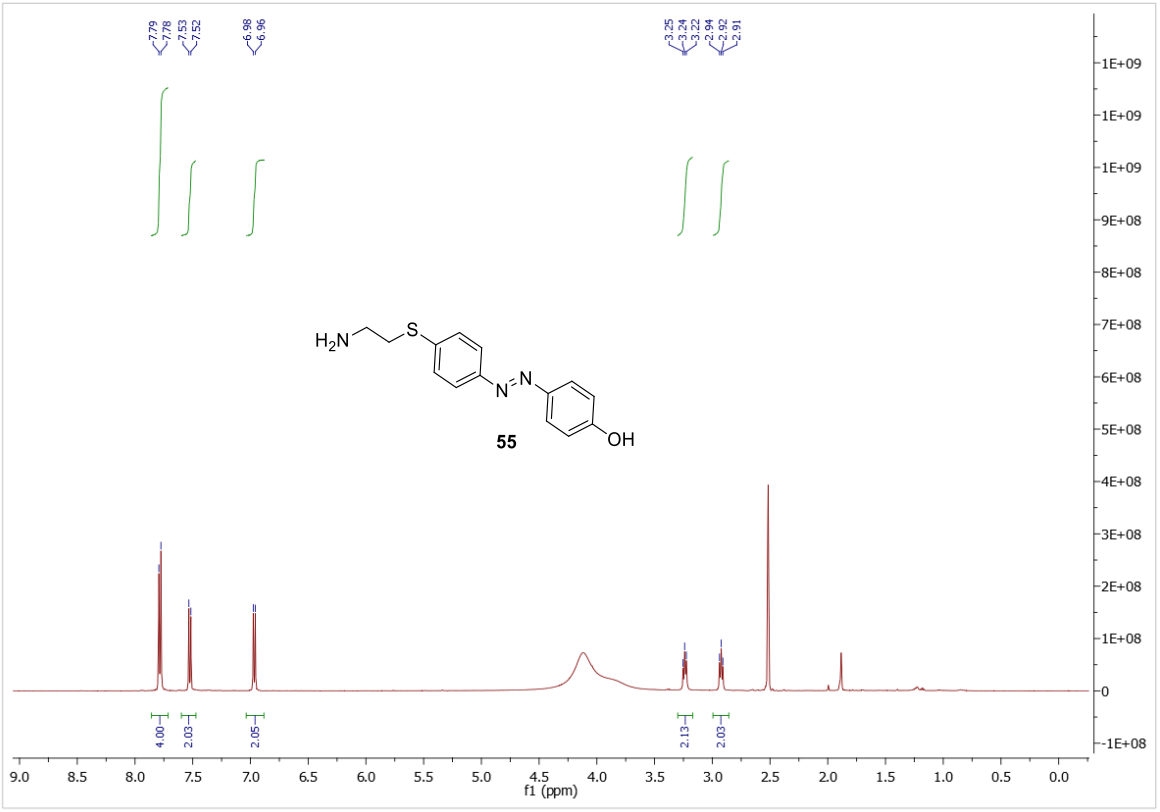

Figure 7.6.71. ^{1}H NMR spectrum of **55** (500 MHz, DMSO-d_6, 300 K).

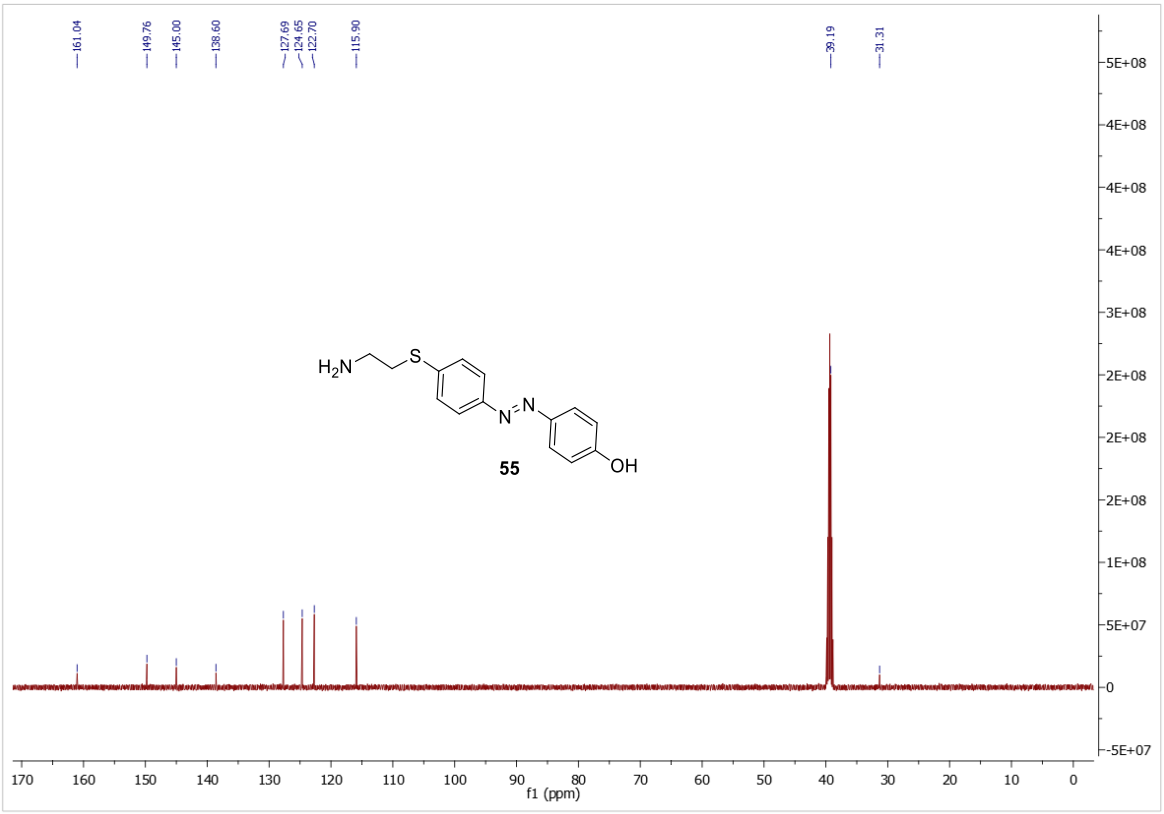

Figure 7.6.72. ^{13}C NMR spectrum of **55** (126 MHz, DMSO-d_6, 300 K).

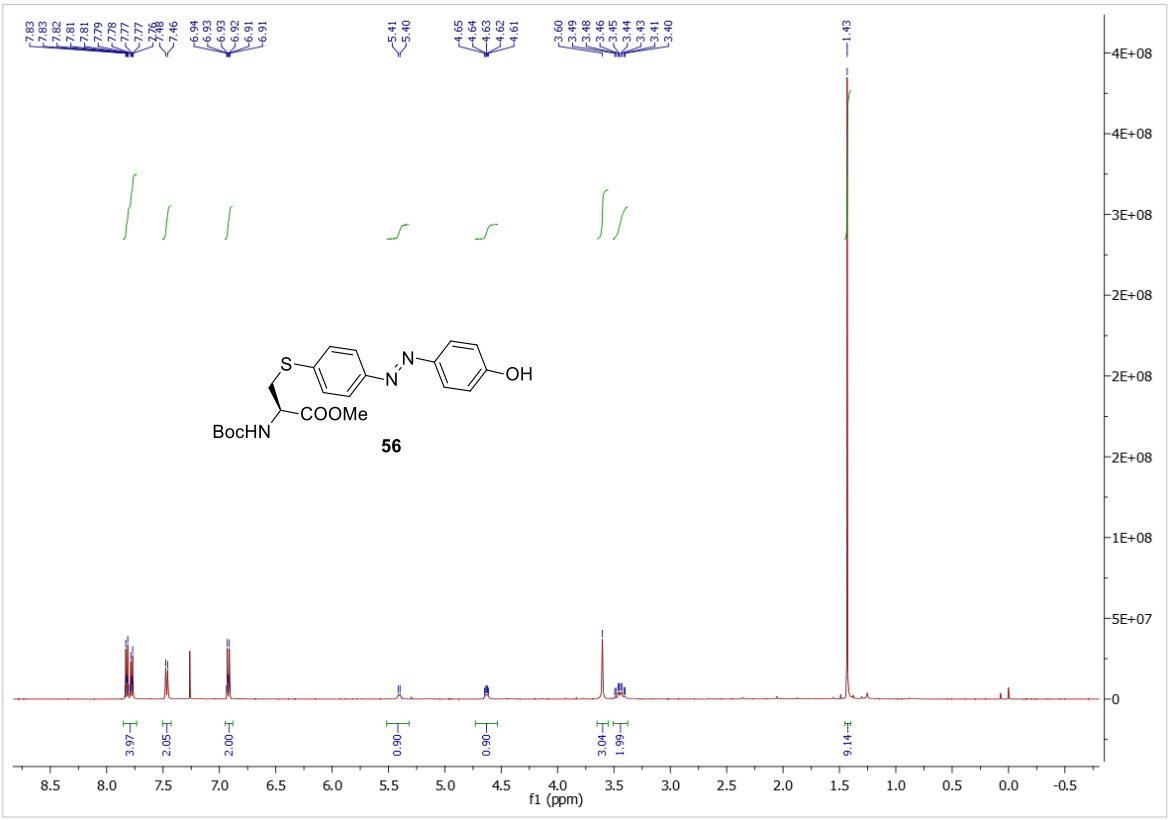

Figure 7.6.73. ^{1}H NMR spectrum of **56** (500 MHz, $CDCl_3$, 300 K).

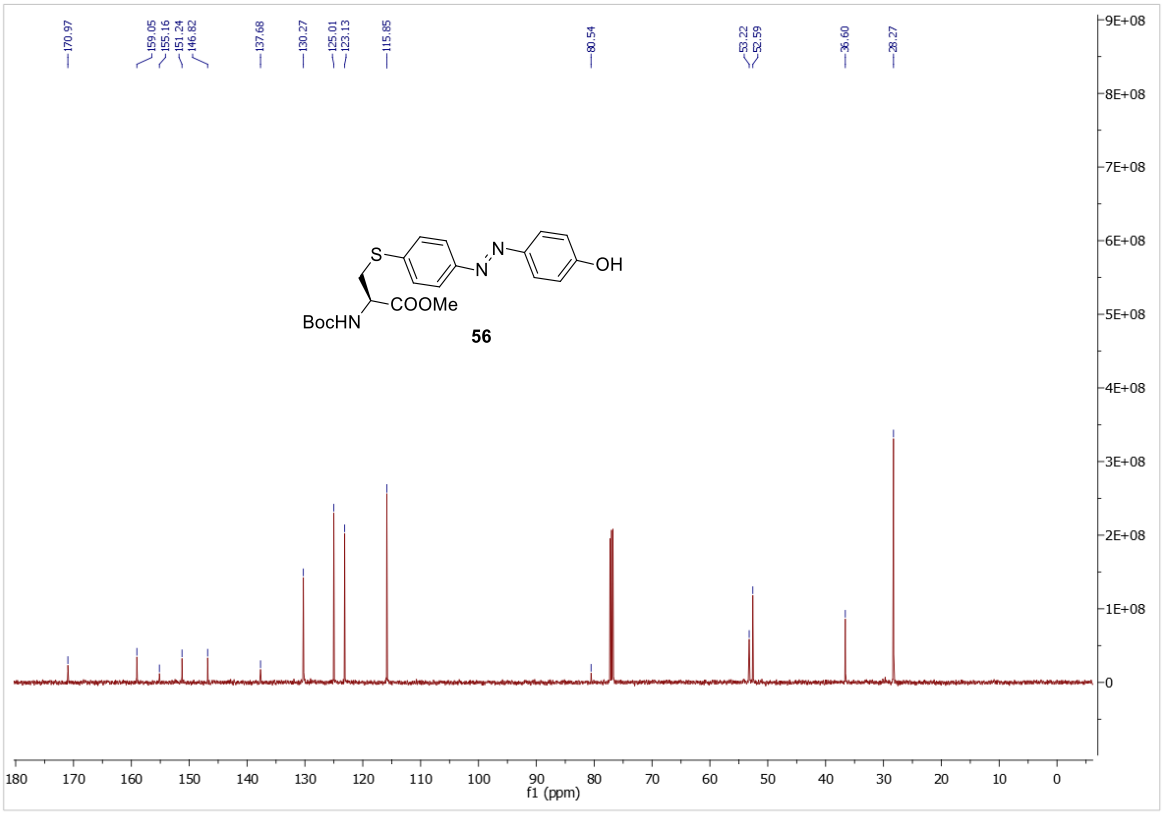

Figure 7.6.74. ^{13}C NMR spectrum of **56** (126 MHz, $CDCl_3$, 300 K).

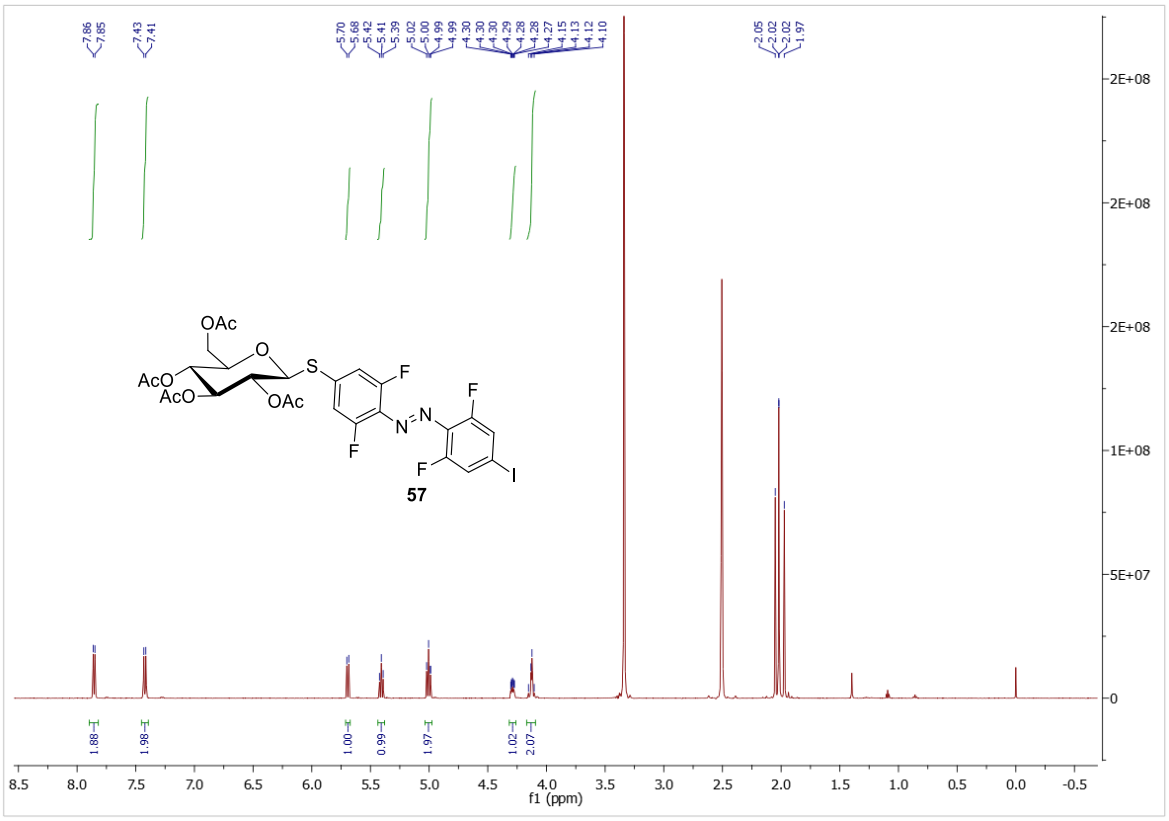

Figure 7.6.75. ^{1}H NMR spectrum of **57** (500 MHz, DMSO-d_6, 300 K).

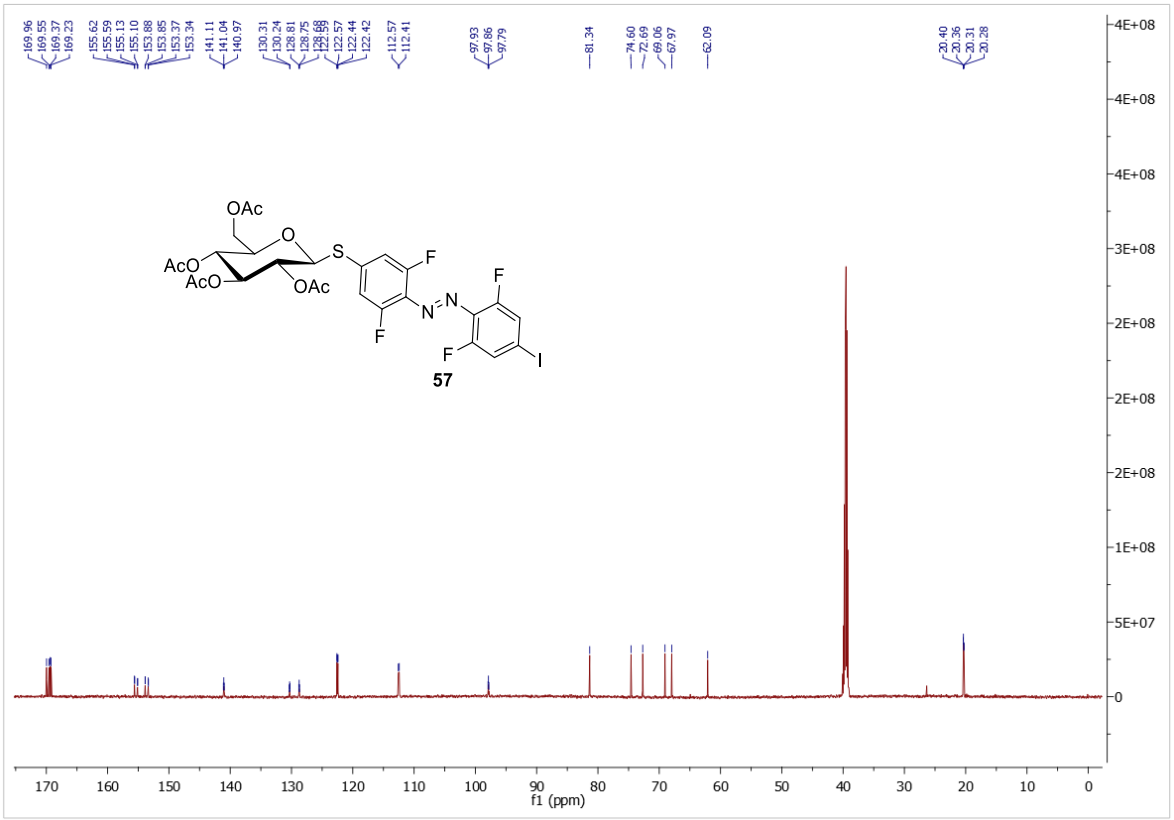

Figure 7.6.76. ^{13}C NMR spectrum of **57** (126 MHz, DMSO-d_6, 300 K).

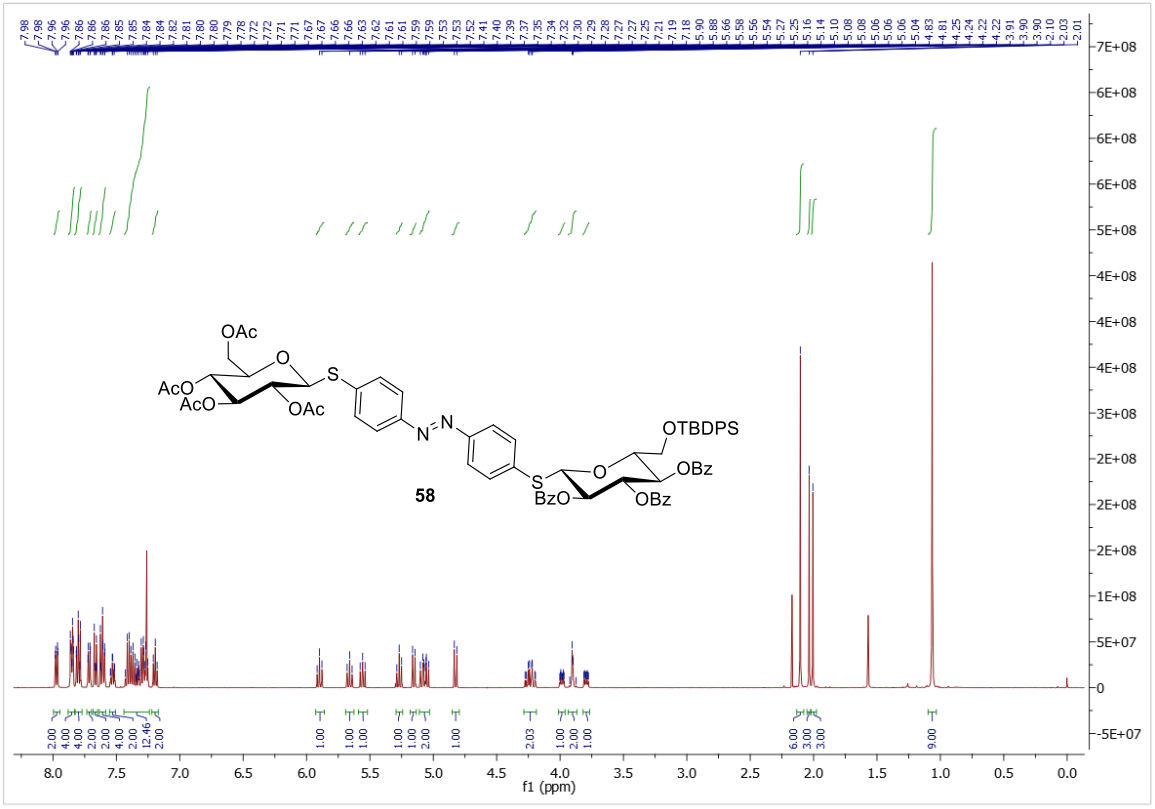

Figure 7.6.77. ^{1}H NMR spectrum of **58** (500 MHz, $CDCl_3$, 300 K).

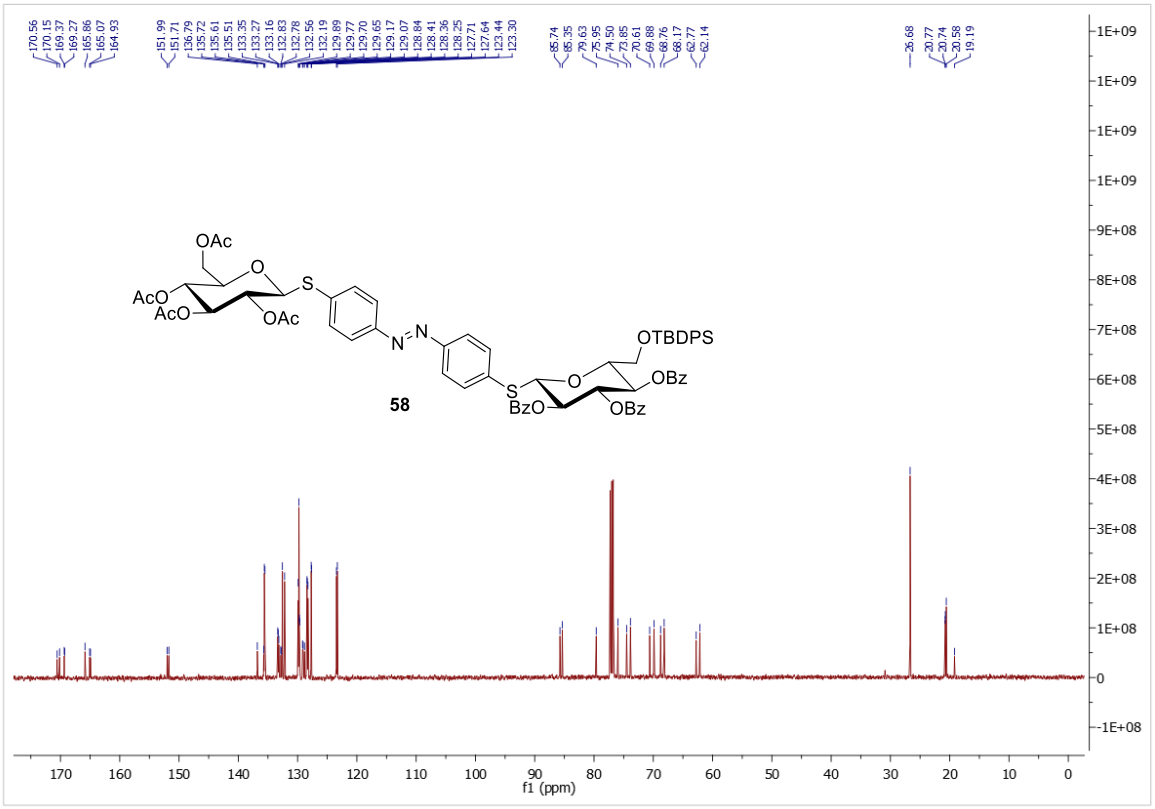

Figure 7.6.78. ^{13}C NMR spectrum of **58** (126 MHz, $CDCl_3$, 300 K).

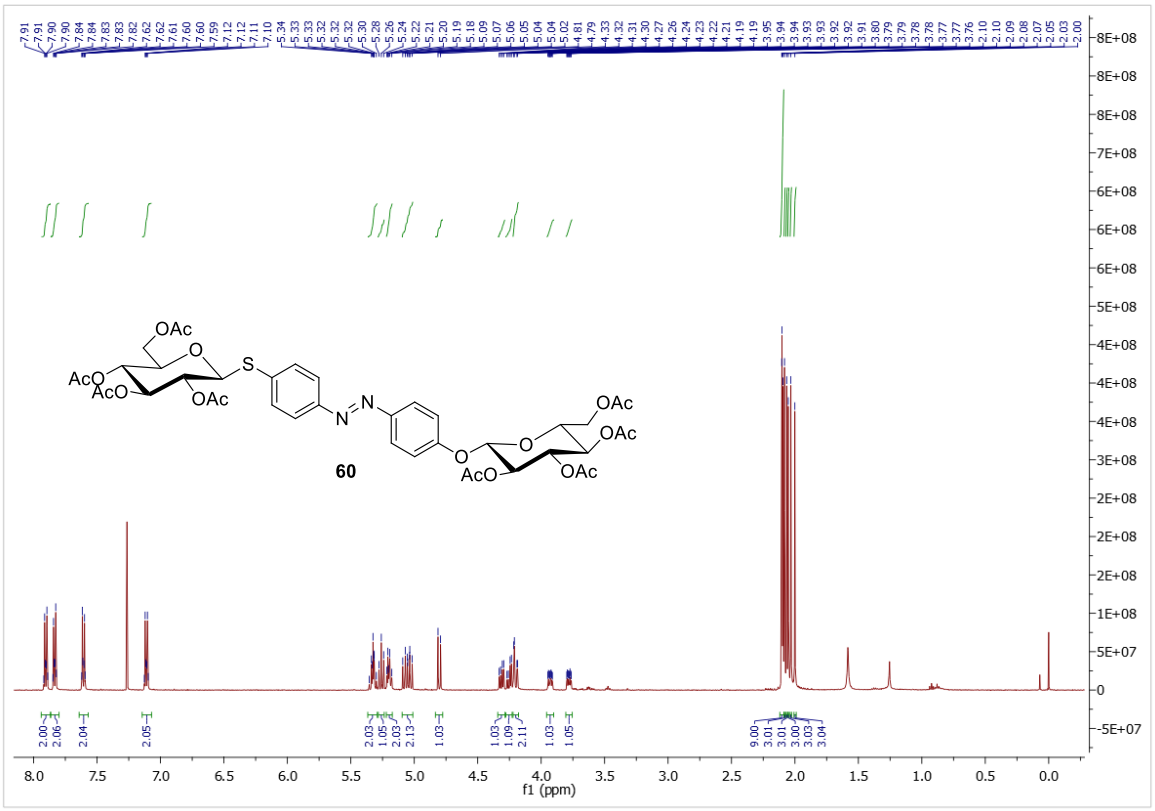

Figure 7.6.79. ^{1}H NMR spectrum of **60** (500 MHz, $CDCl_3$, 300 K).

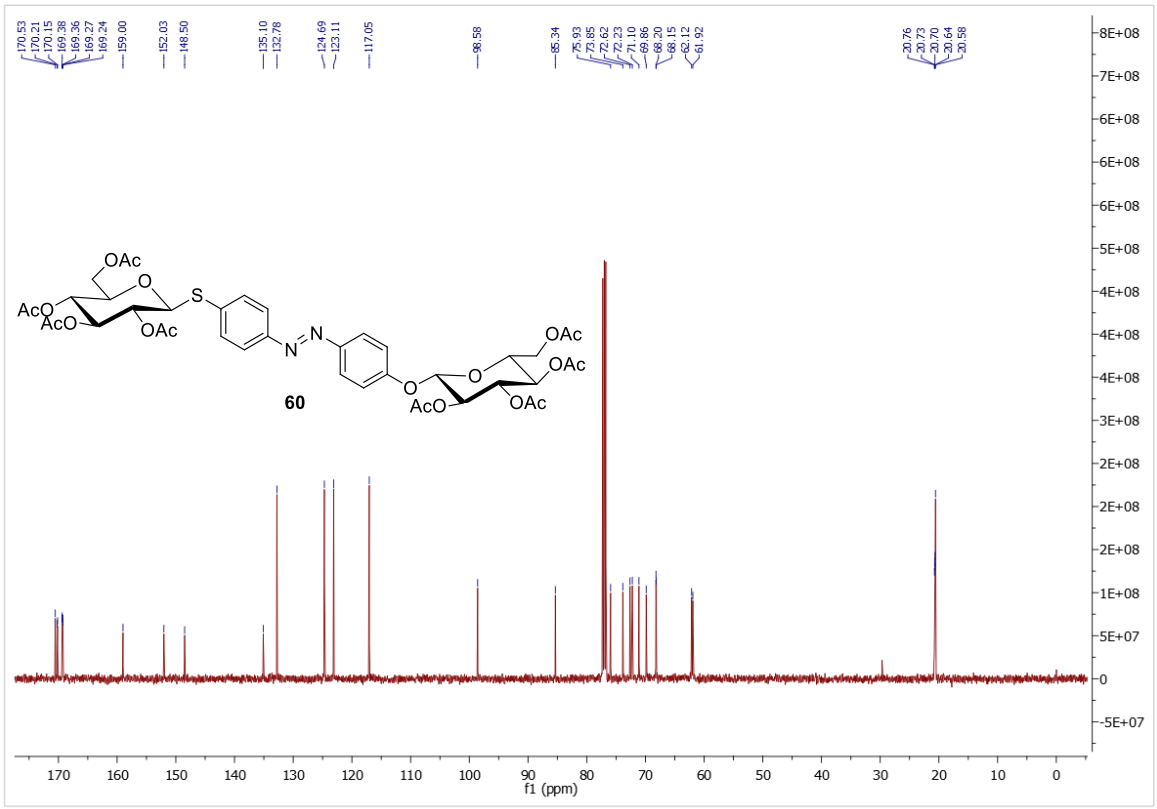

Figure 7.6.80. ^{13}C NMR spectrum of **60** (126 MHz, $CDCl_3$, 300 K).

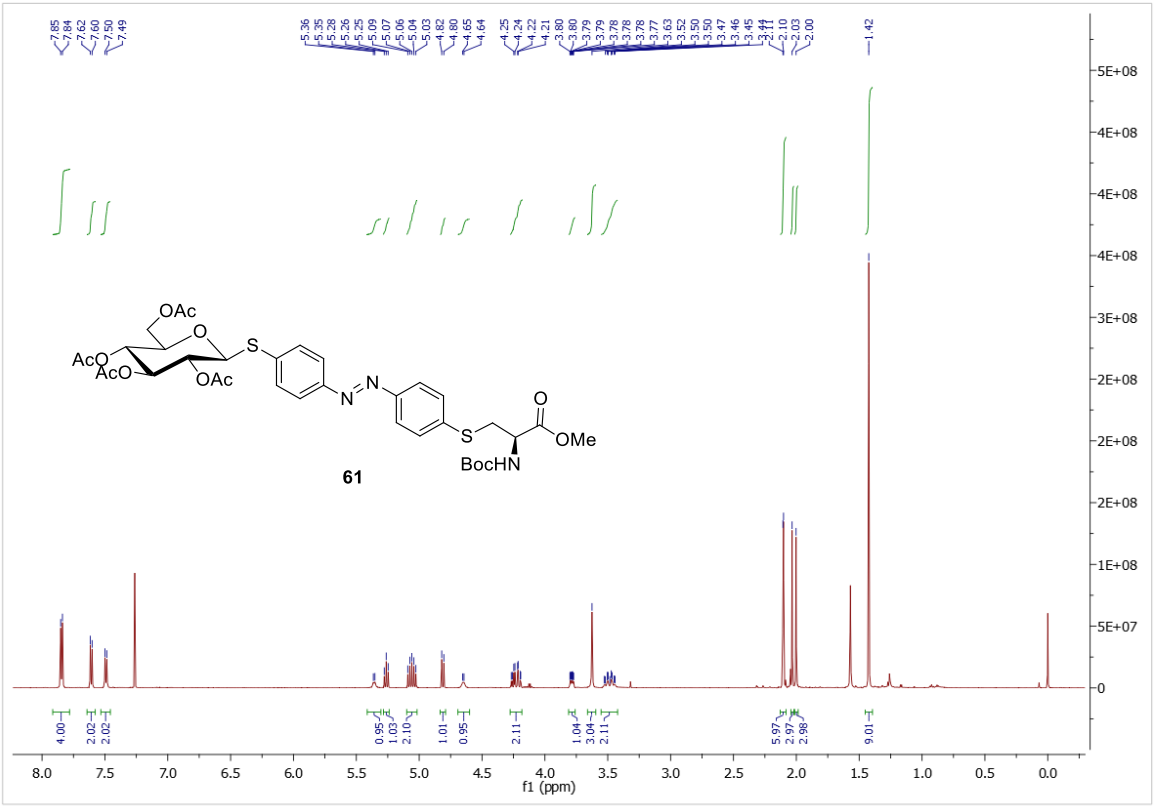

Figure 7.6.81. ^{1}H NMR spectrum of **61** (500 MHz, $CDCl_3$, 300 K).

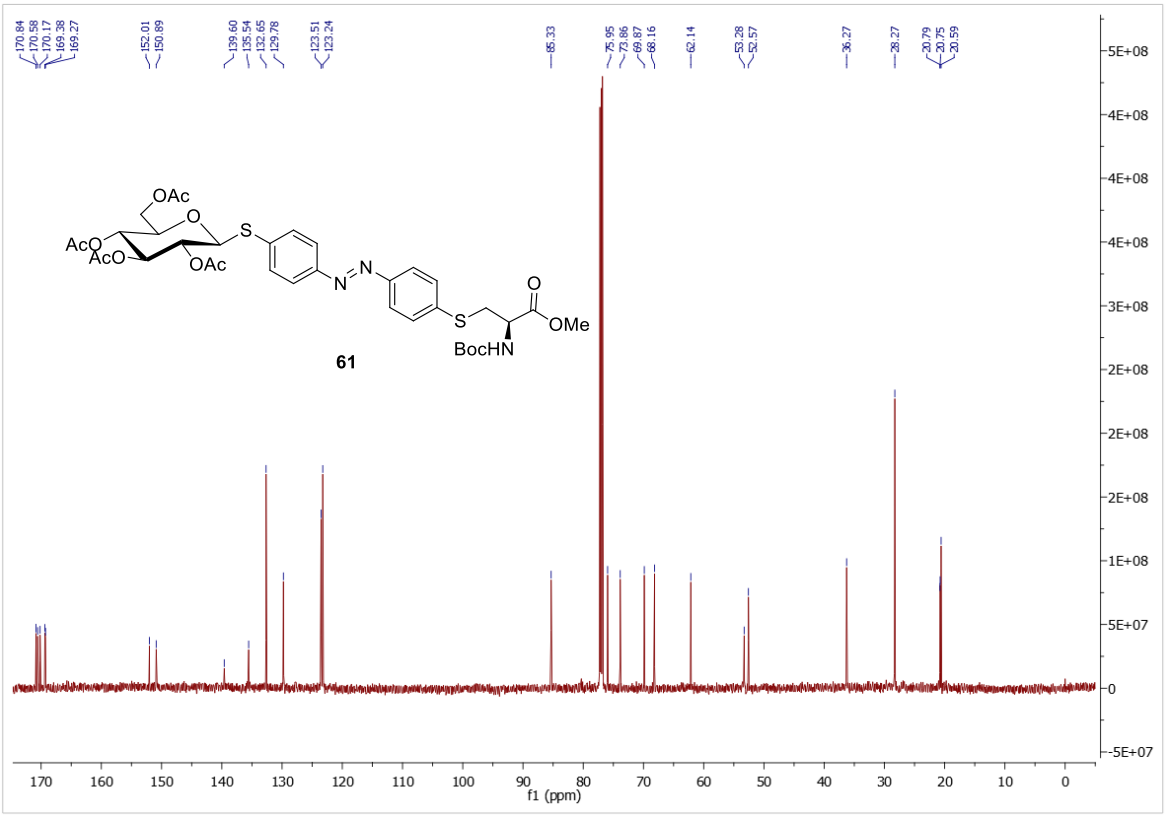

Figure 7.6.82. ^{13}C NMR spectrum of **61** (126 MHz, $CDCl_3$, 300 K).

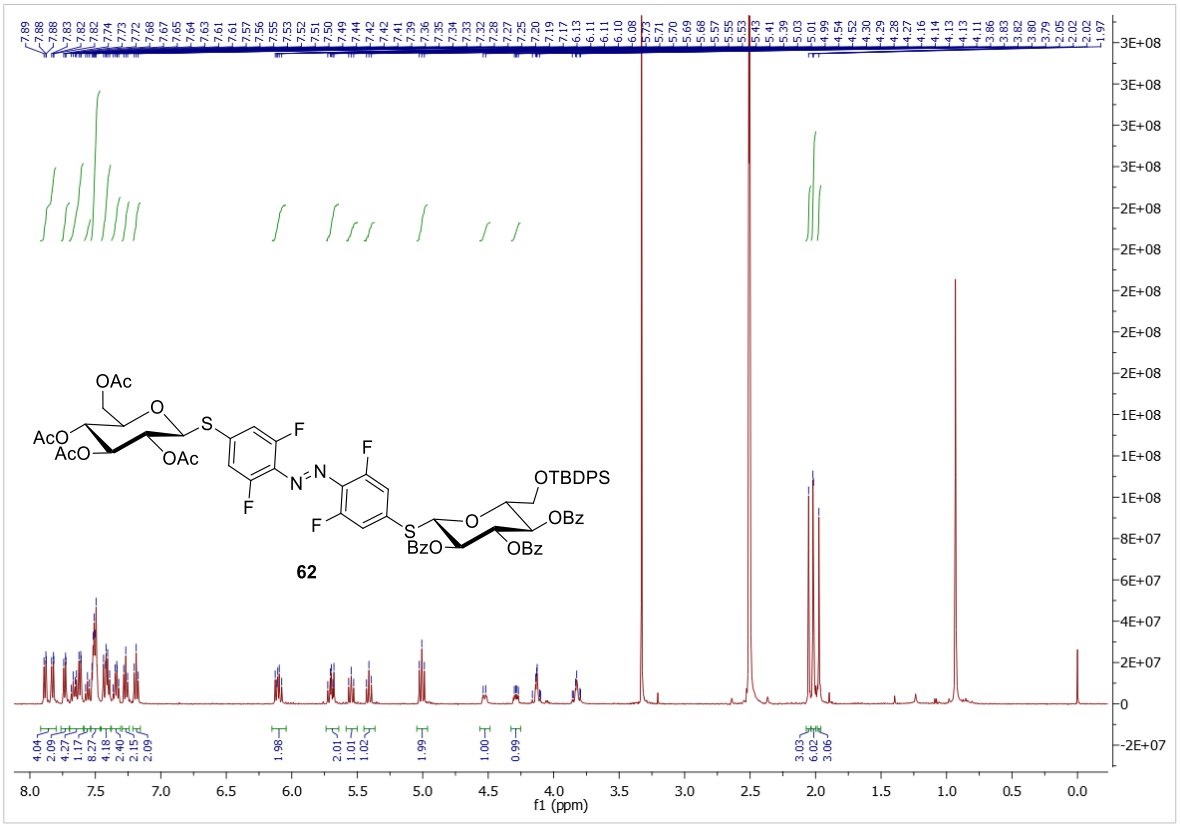

Figure 7.6.83. ^{1}H NMR spectrum of **62** (500 MHz, DMSO-d_6, 300 K).

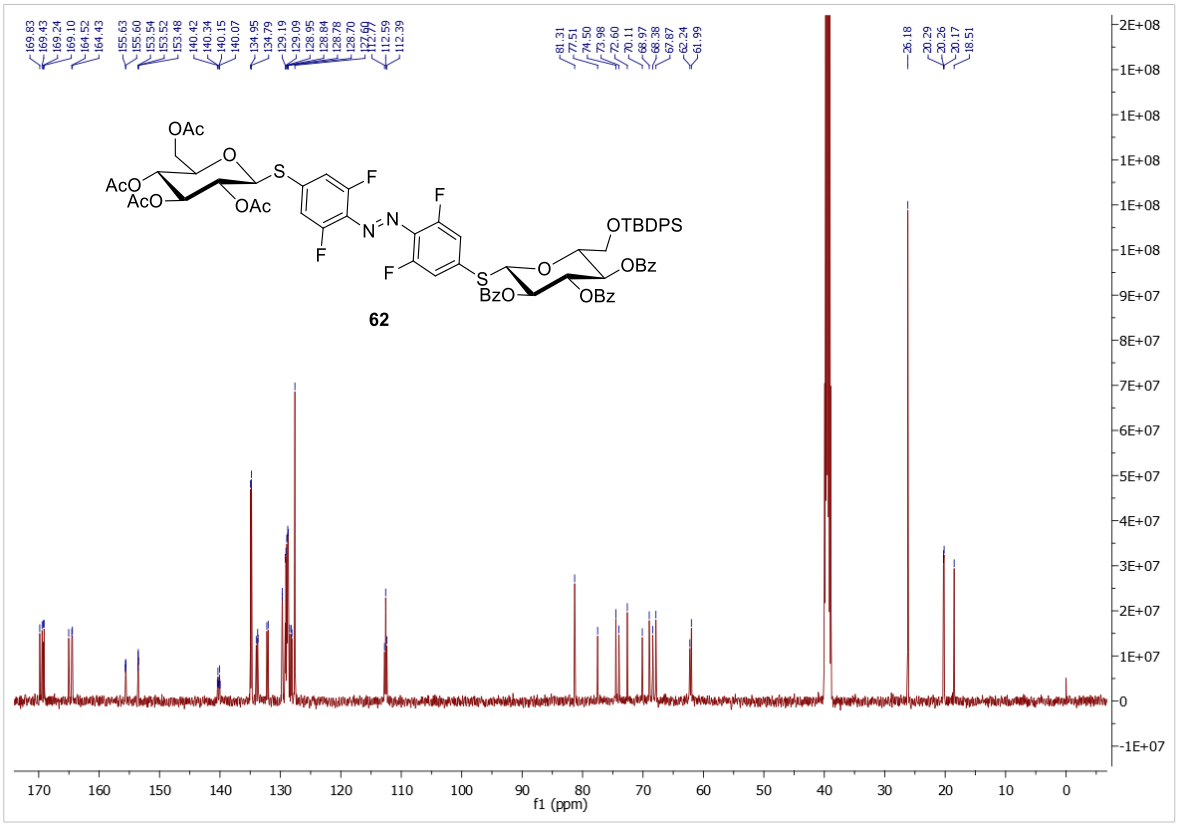

Figure 7.6.84. ^{13}C NMR spectrum of **62** (126 MHz, DMSO-d_6, 300 K).

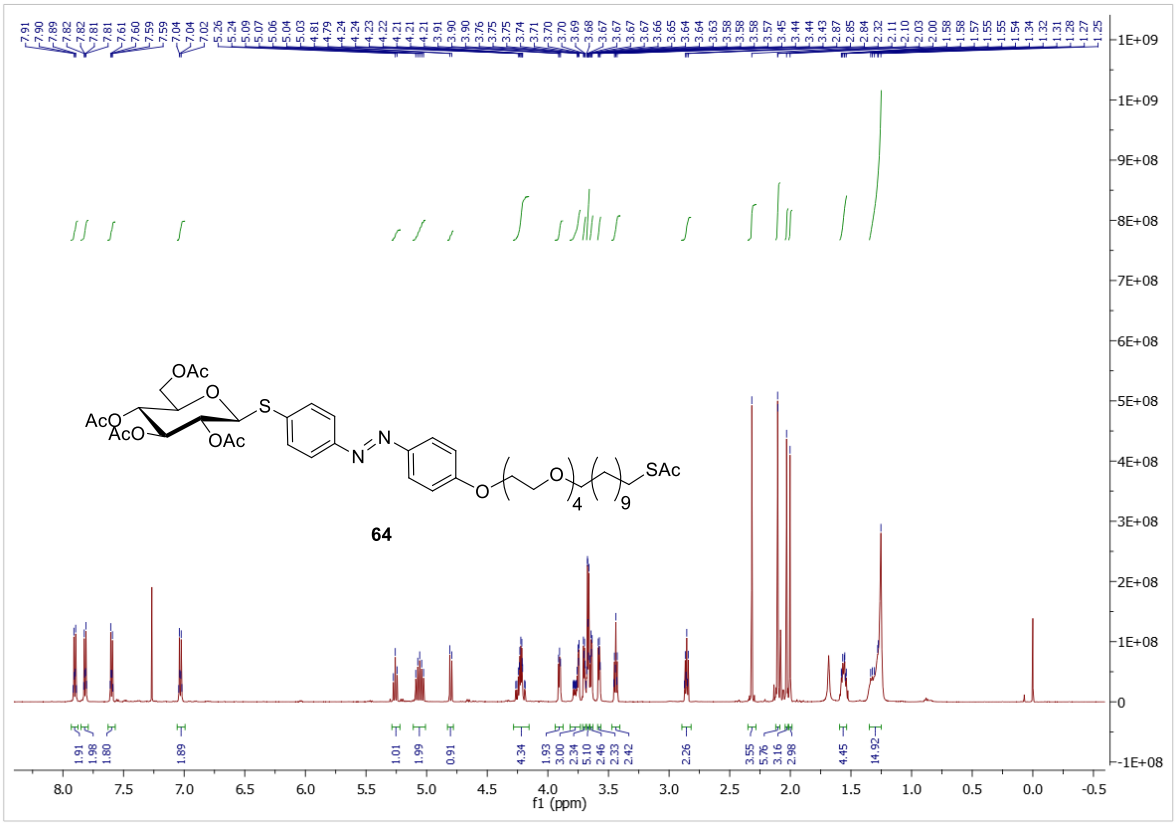

Figure 7.6.85. ^{1}H NMR spectrum of **64** (500 MHz, $CDCl_3$, 300 K).

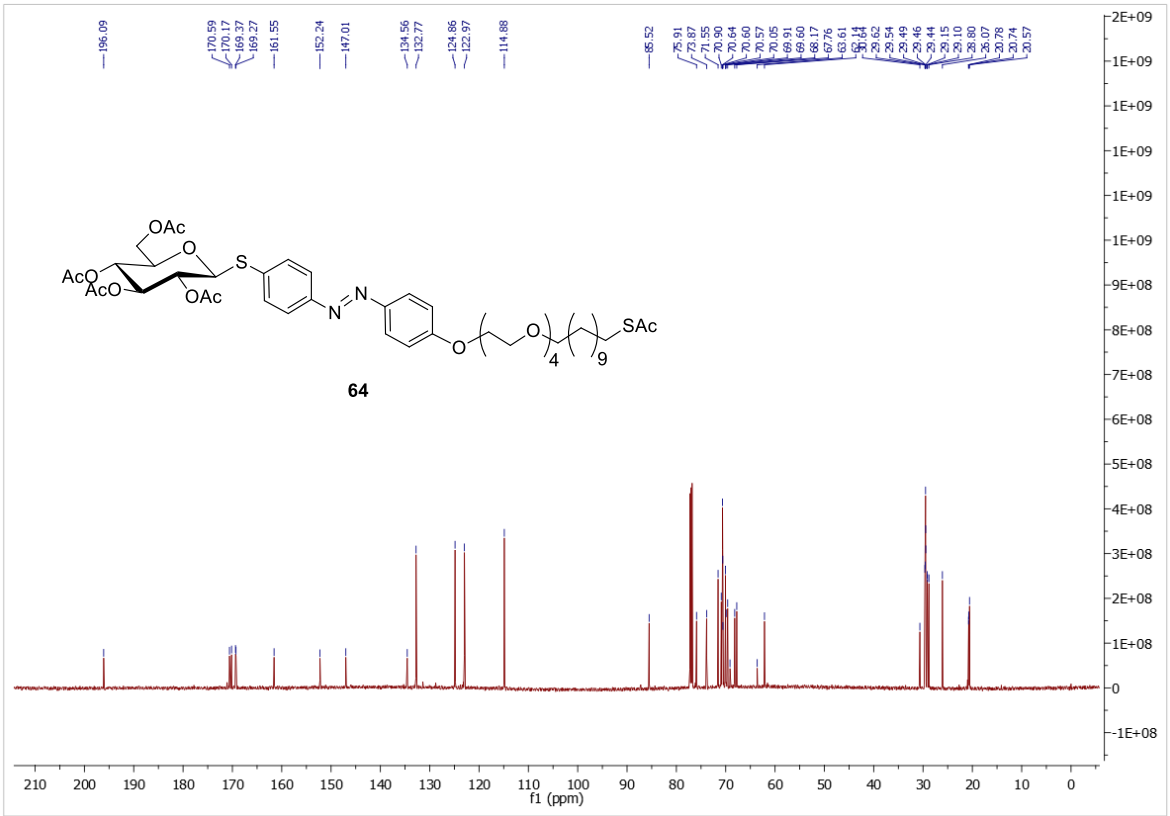

Figure 7.6.86. ^{13}C NMR spectrum of **64** (126 MHz, $CDCl_3$, 300 K).

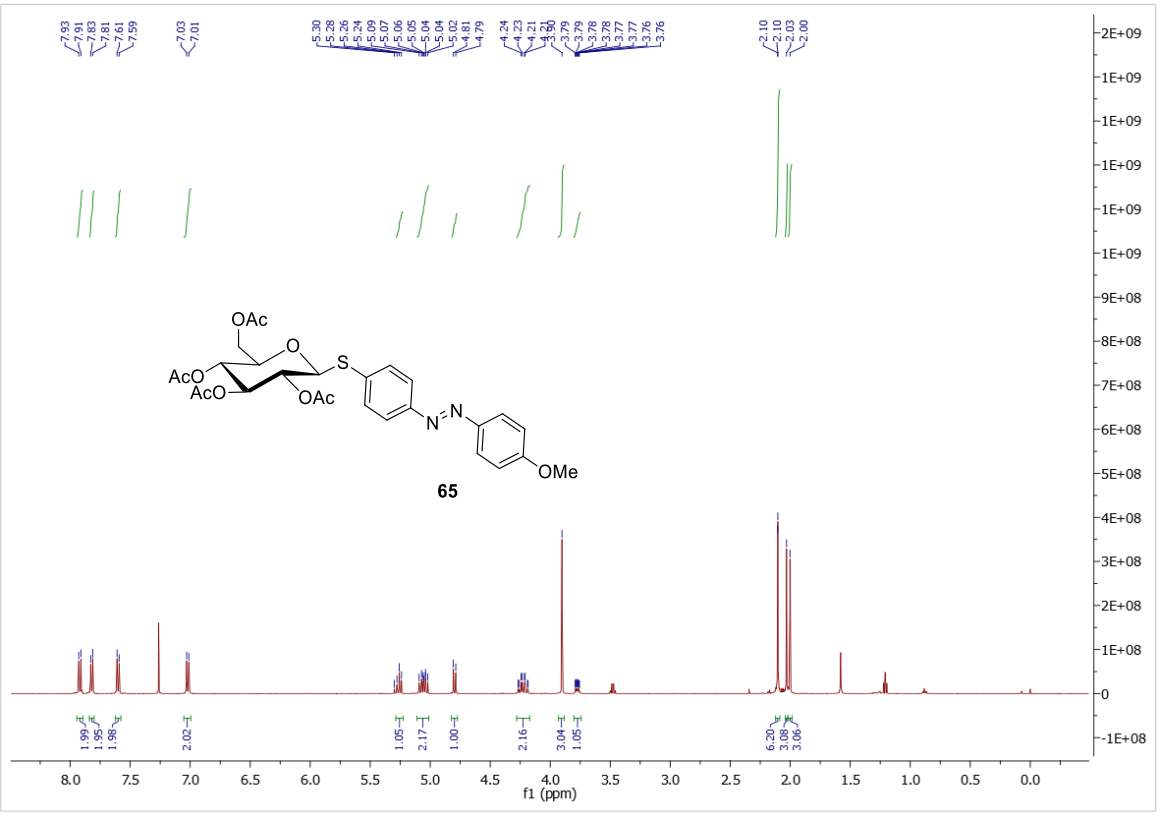

Figure 7.6.87. ^{1}H NMR spectrum of **65** (500 MHz, $CDCl_3$, 300 K).

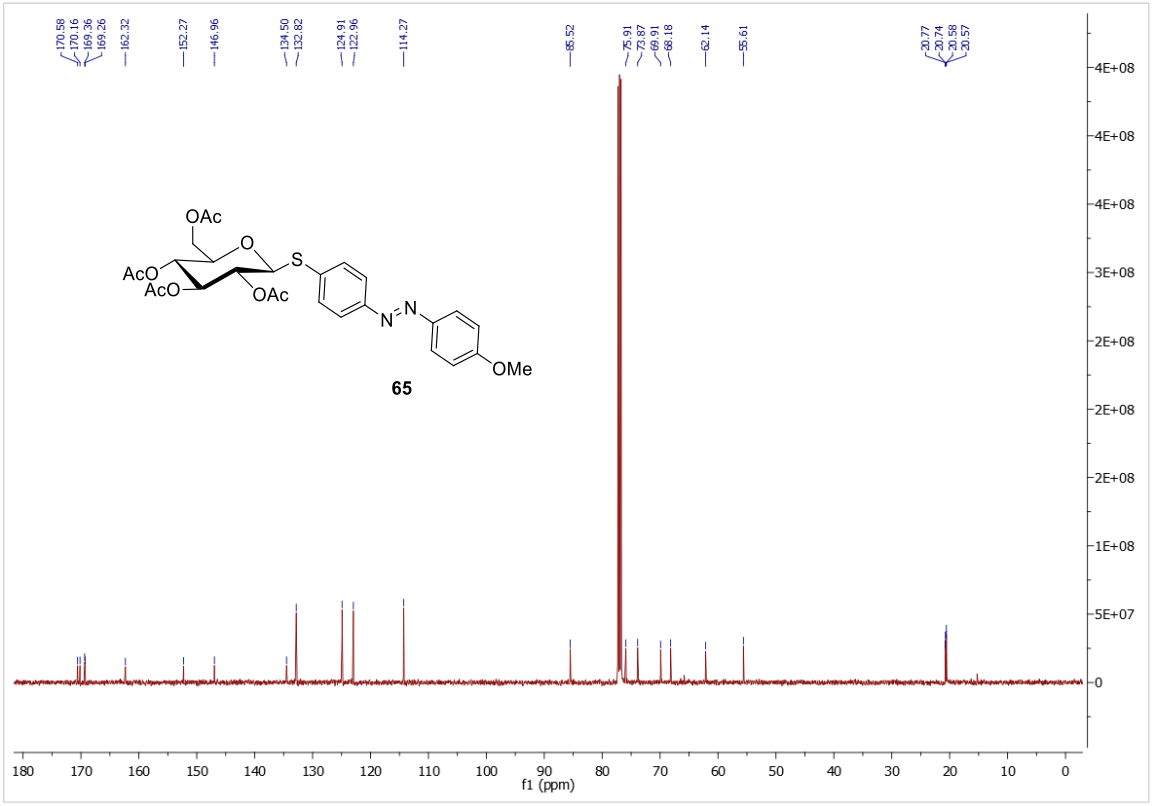

Figure 7.6.88. ^{13}C NMR spectrum of **65** (126 MHz, $CDCl_3$, 300 K).

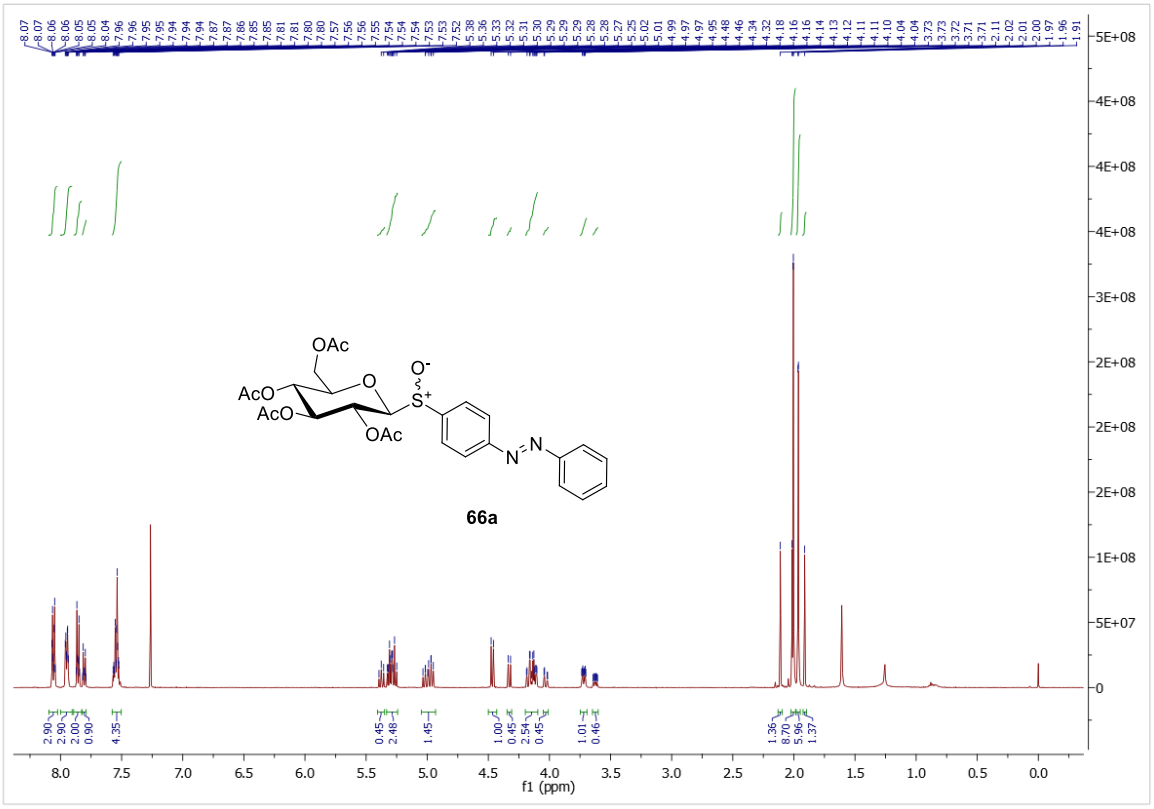

Figure 7.6.89. ^{1}H NMR spectrum of **66a** (500 MHz, $CDCl_3$, 300 K).

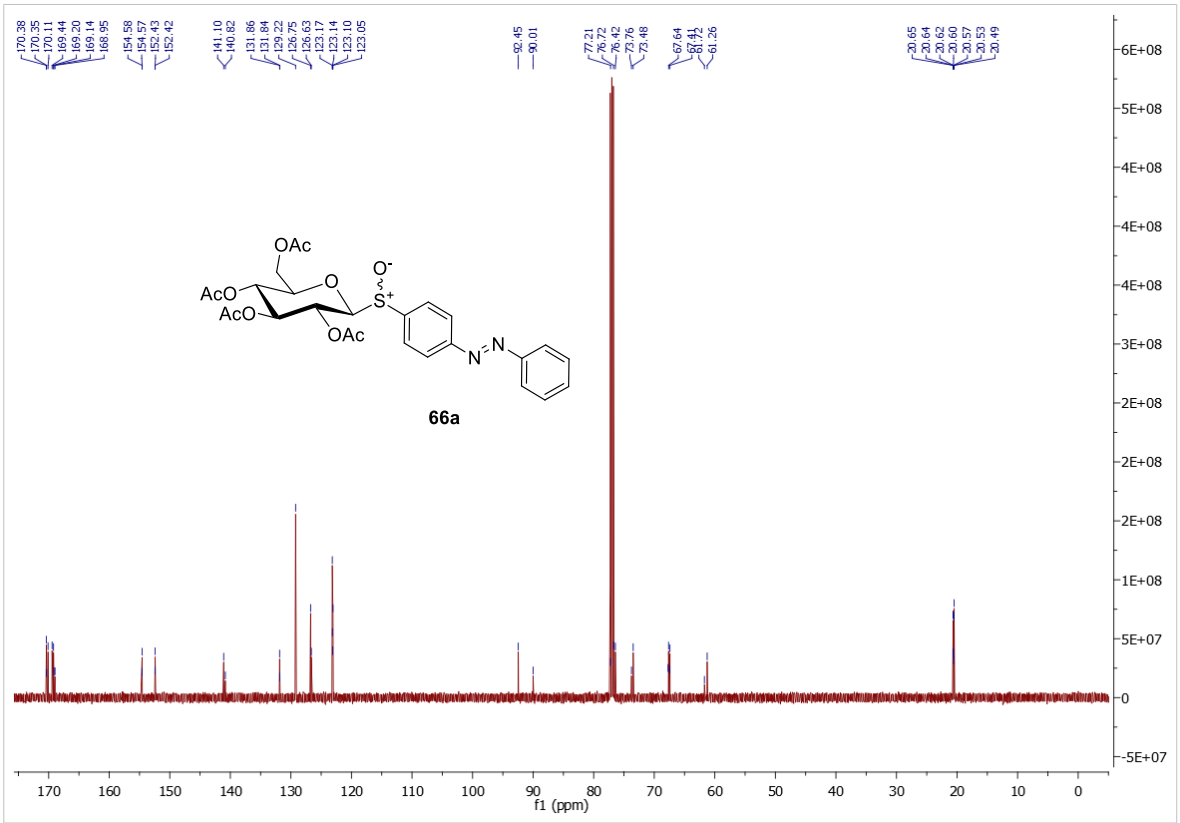

Figure 7.6.90. ^{13}C NMR spectrum of **66a** (126 MHz, $CDCl_3$, 300 K).

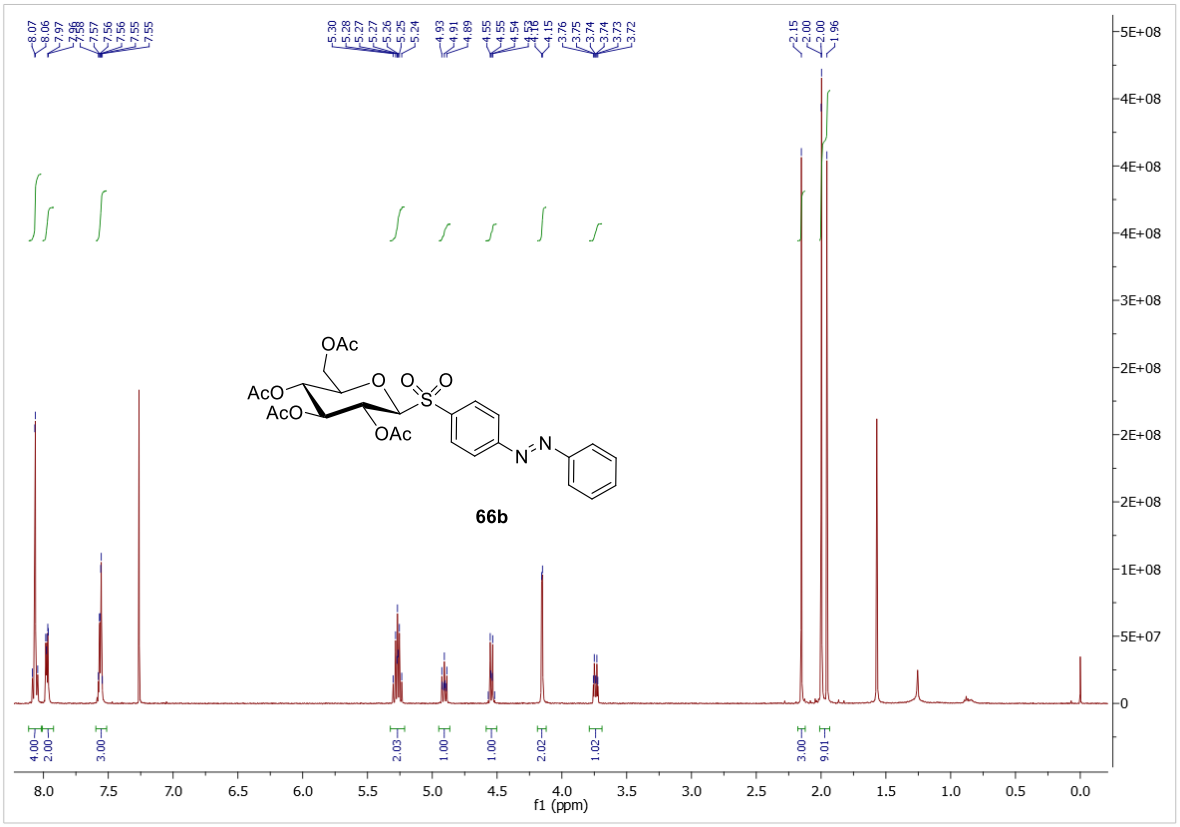

Figure 7.6.91. ^{1}H NMR spectrum of **66b** (500 MHz, $CDCl_3$, 300 K).

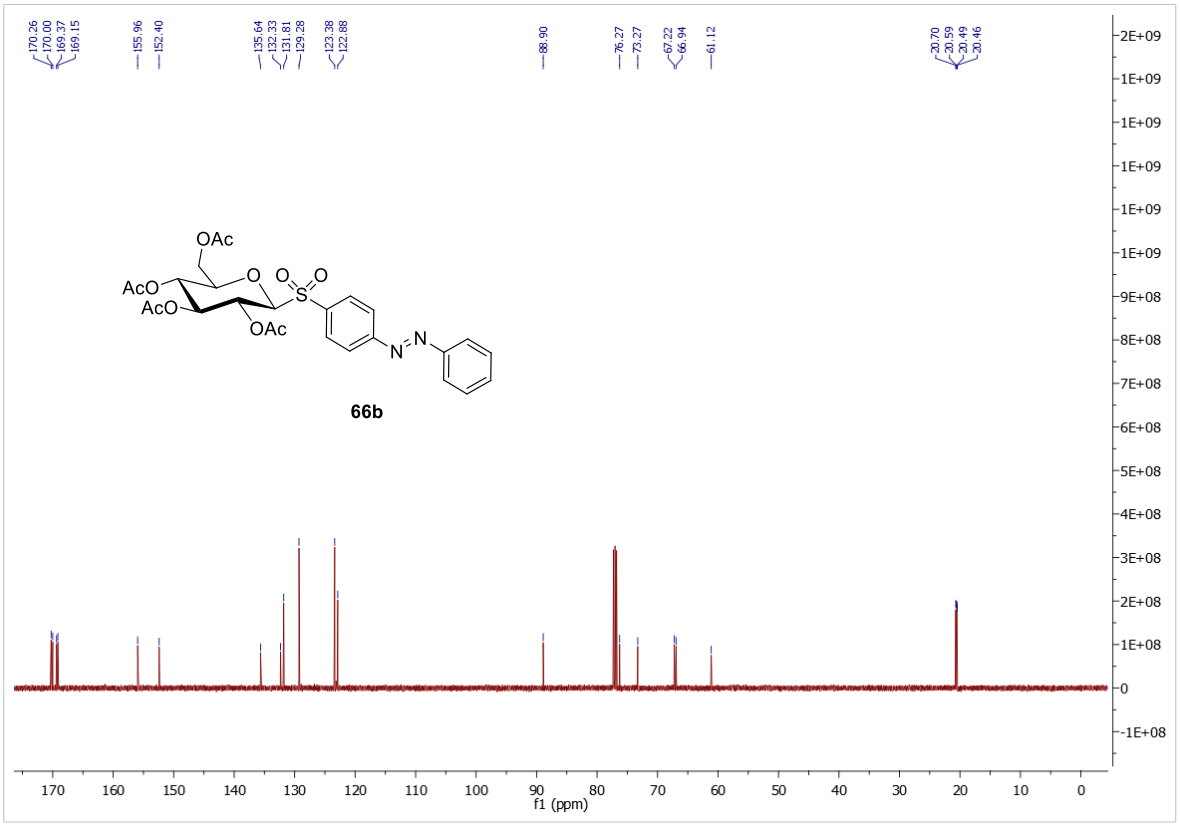

Figure 7.6.92. ^{13}C NMR spectrum of **66b** (126 MHz, $CDCl_3$, 300 K).

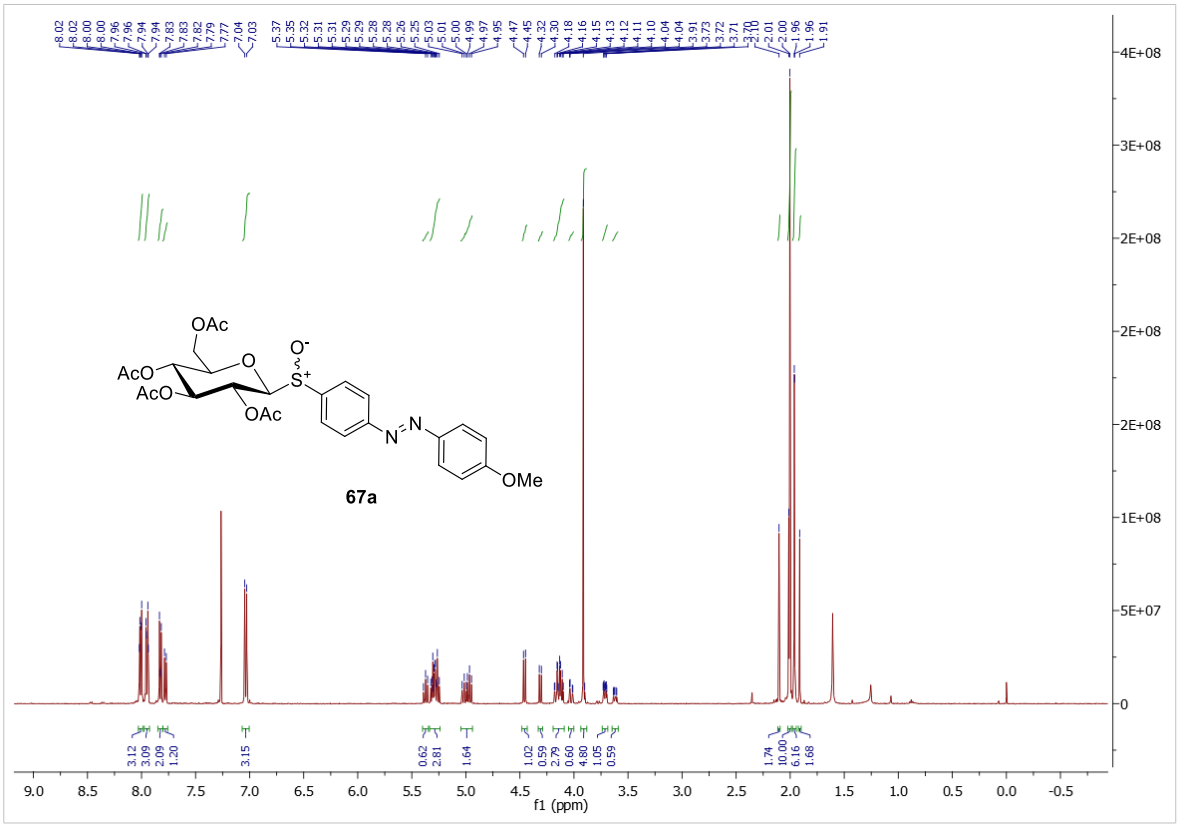

Figure 7.6.93. ^{1}H NMR spectrum of **67a** (500 MHz, $CDCl_3$, 300 K).

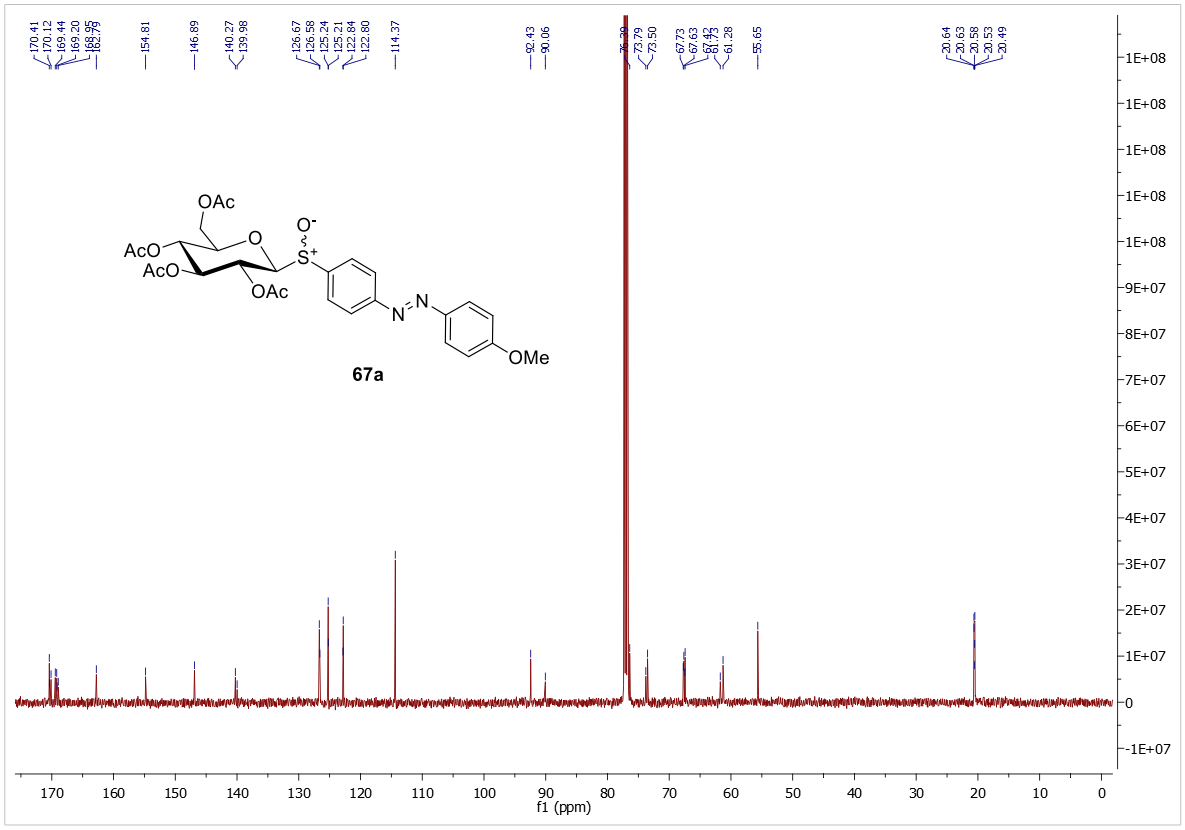

Figure 7.6.94. ^{13}C NMR spectrum of **67a** (126 MHz, $CDCl_3$, 300 K).

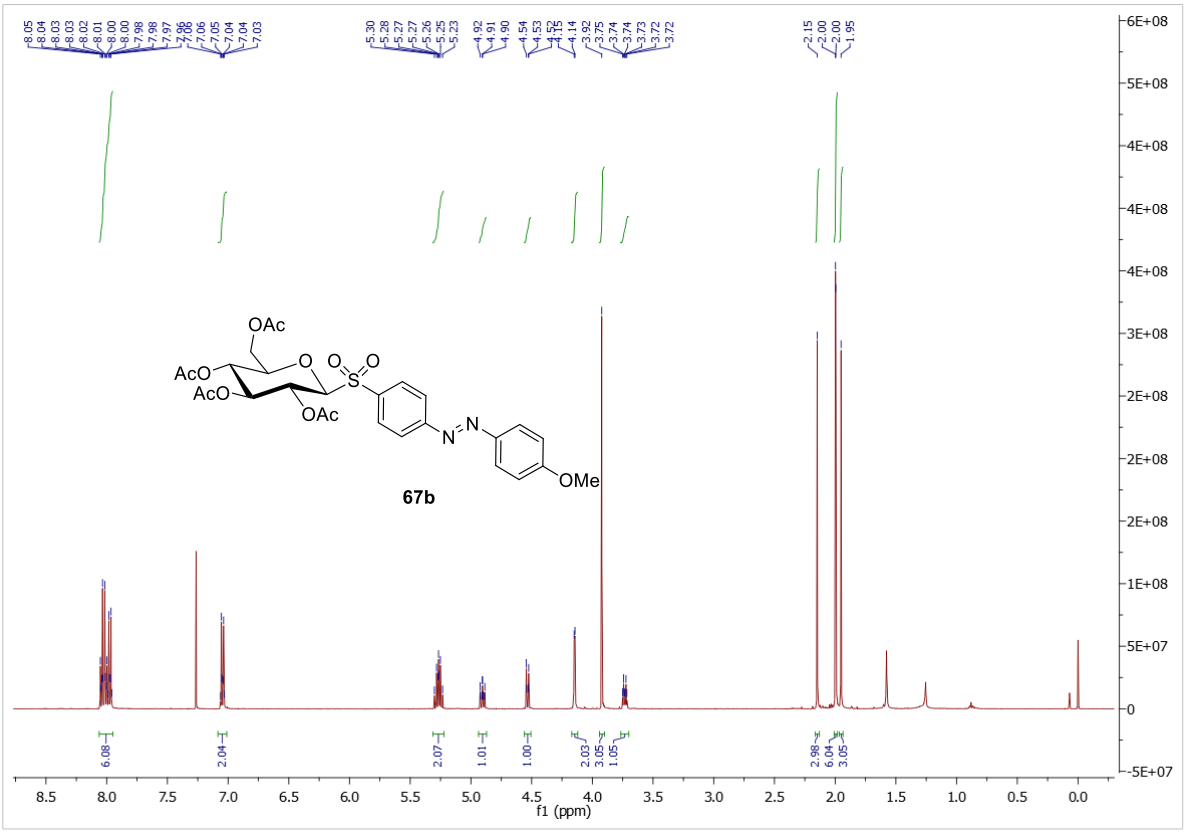

Figure 7.6.95. ^{1}H NMR spectrum of **67b** (500 MHz, $CDCl_3$, 300 K).

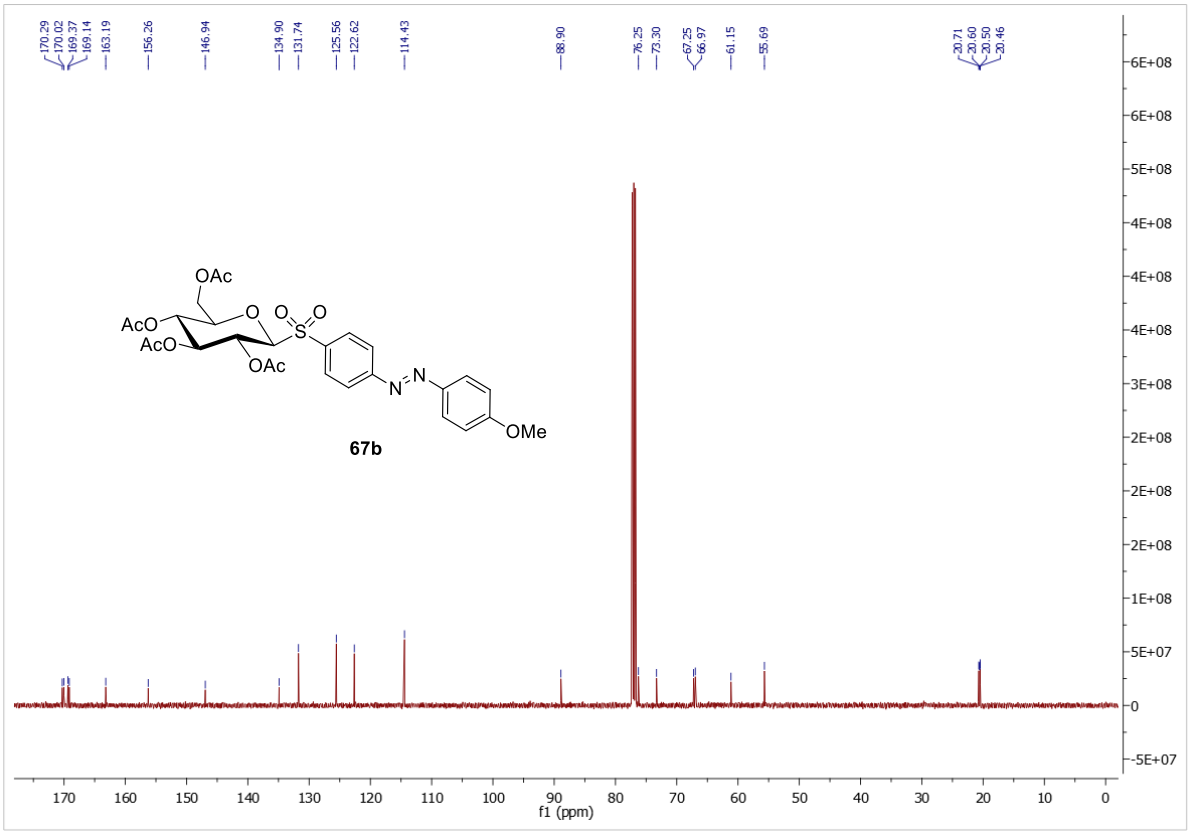

Figure 7.6.96. ^{13}C NMR spectrum of **67b** (126 MHz, $CDCl_3$, 300 K).

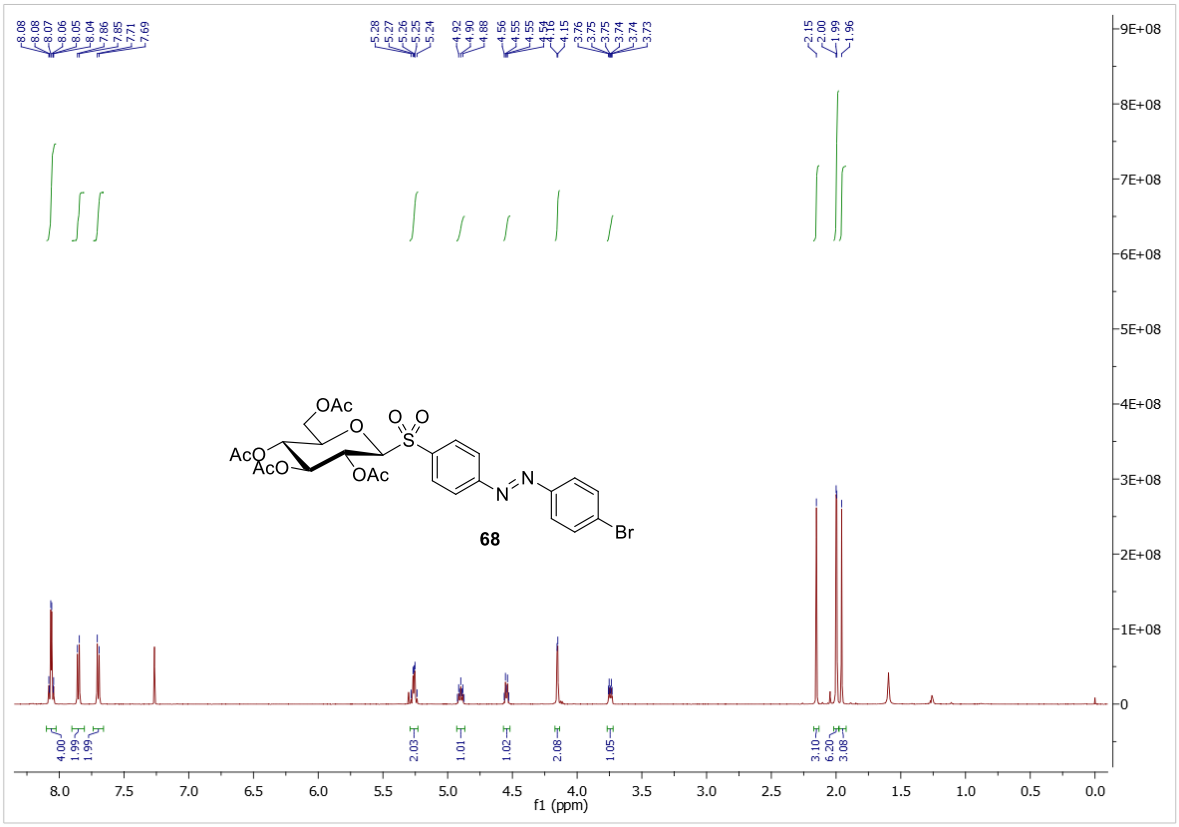

Figure 7.6.97. ^{1}H NMR spectrum of **68** (500 MHz, $CDCl_3$, 300 K).

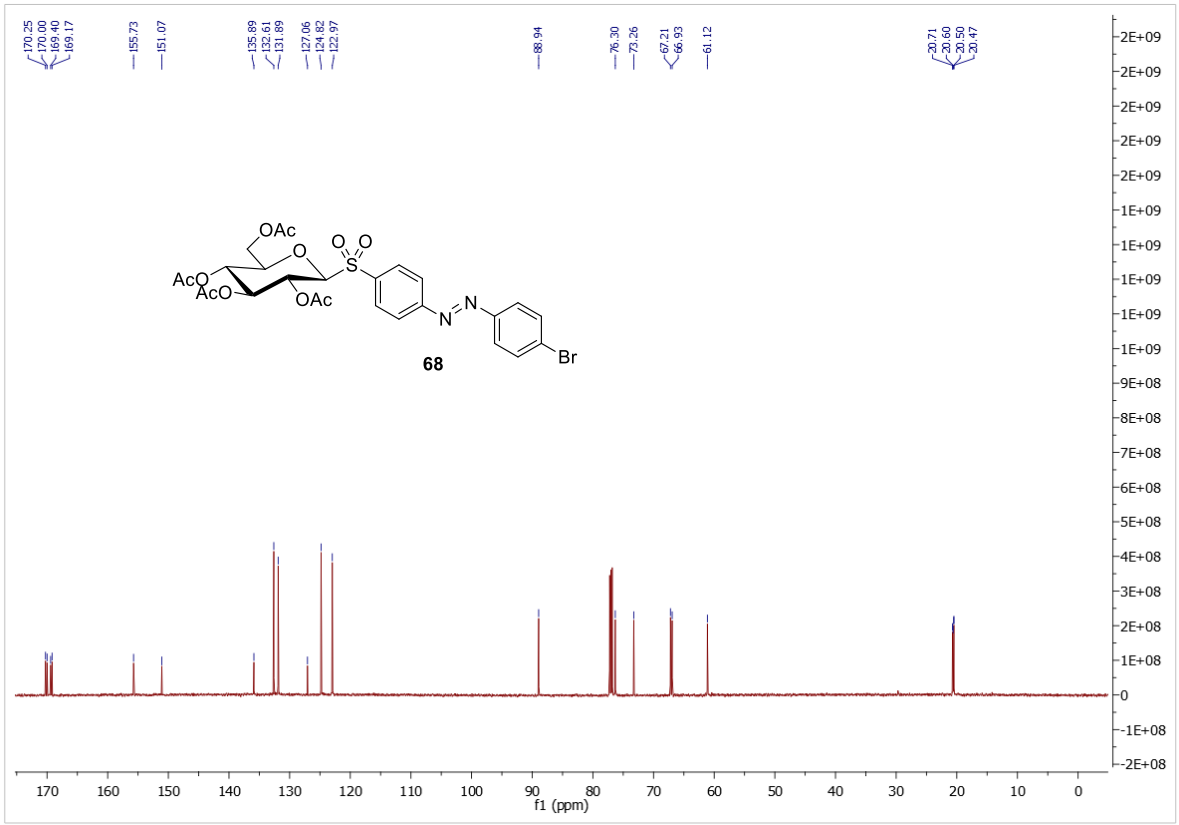

Figure 7.6.98. ^{13}C NMR spectrum of **68** (126 MHz, $CDCl_3$, 300 K).

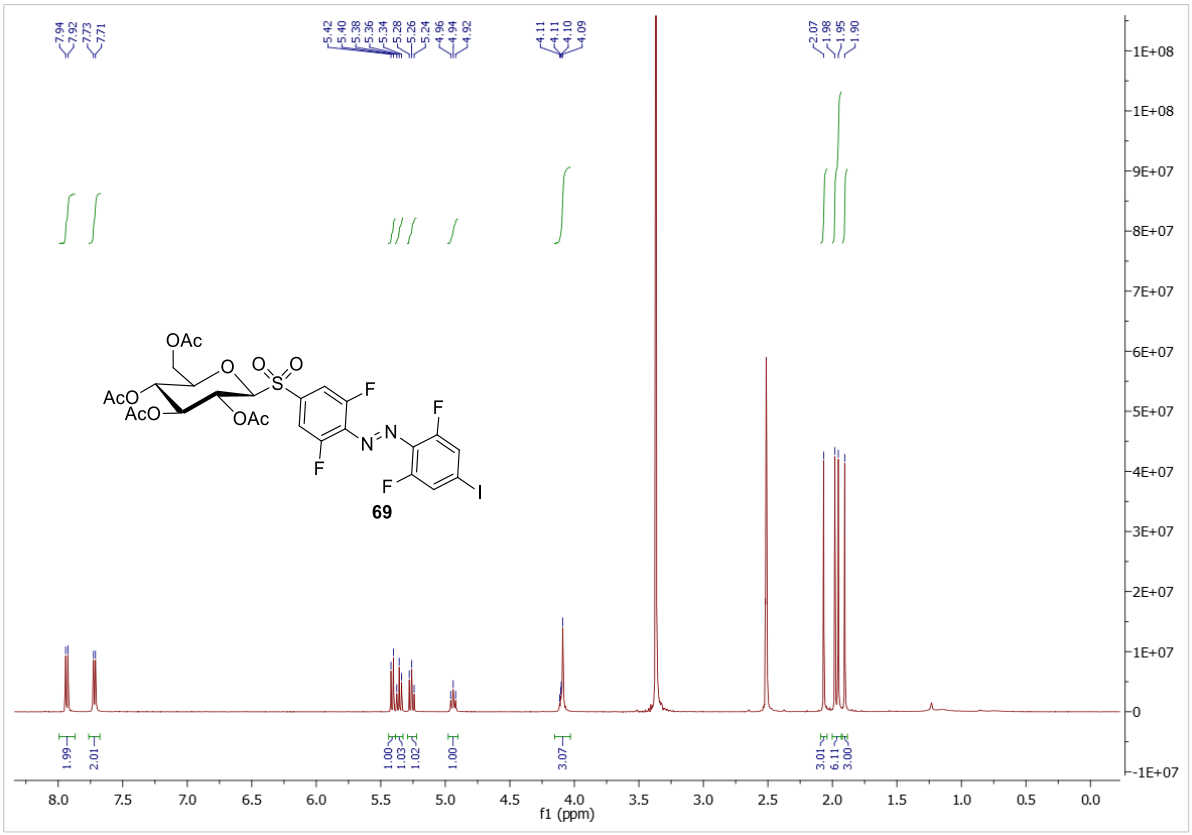

Figure 7.6.99. ^{1}H NMR spectrum of **69** (500 MHz, DMSO-d_6, 300 K).

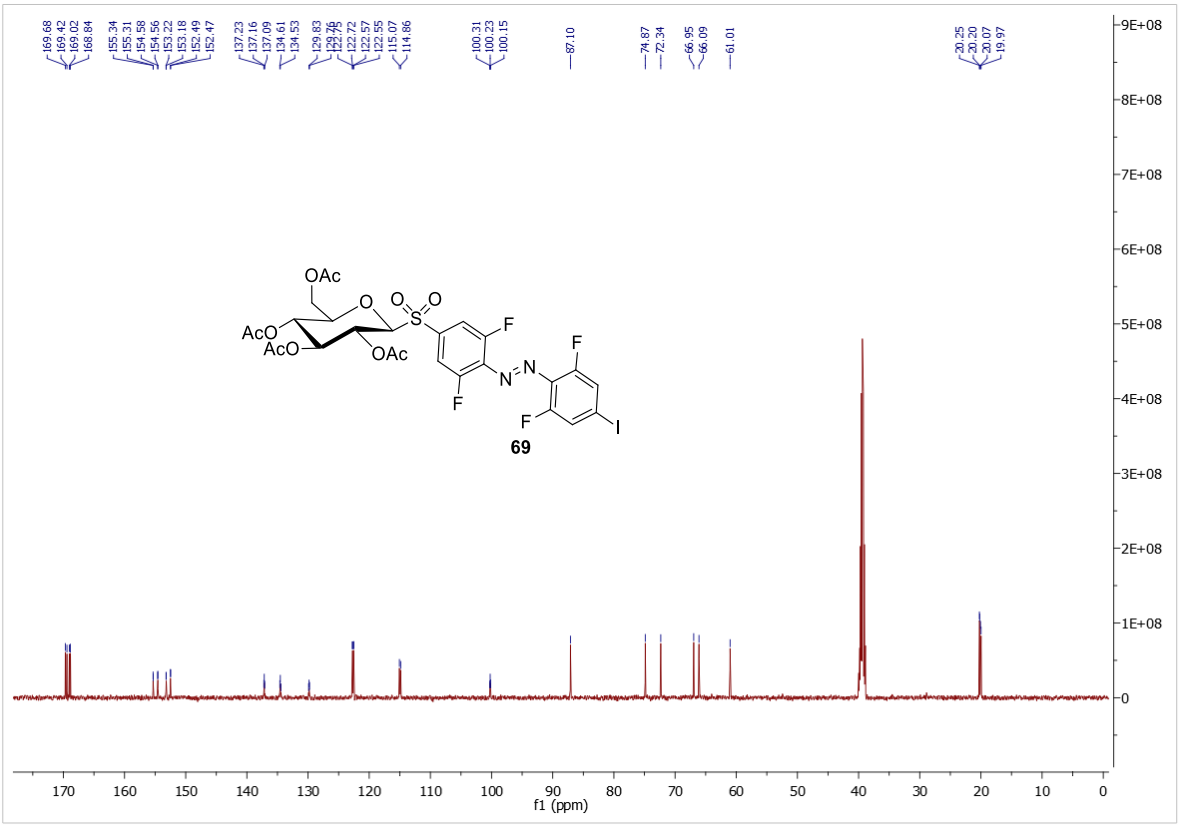

Figure 7.6.100. ^{13}C NMR spectrum of **69** (126 MHz, DMSO-d_6, 300 K).

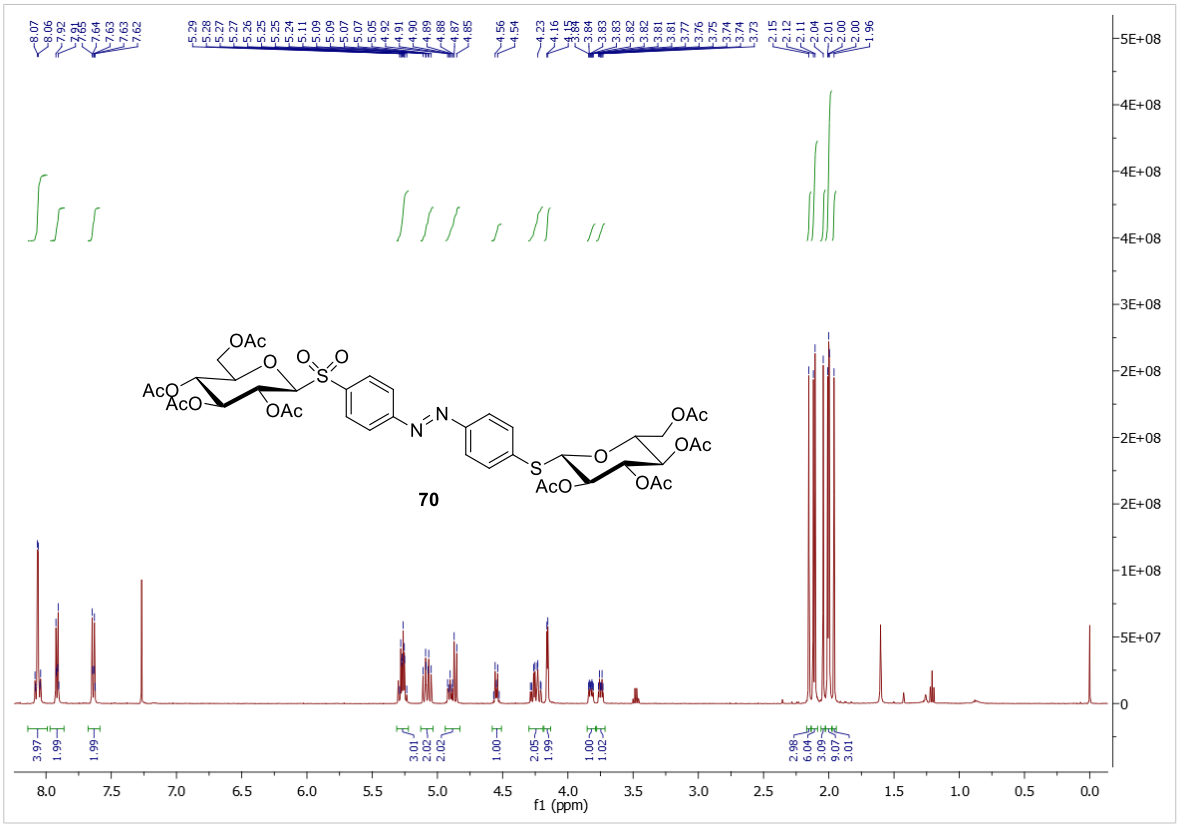

Figure 7.6.101. ^{1}H NMR spectrum of **70** (500 MHz, $CDCl_3$, 300 K).

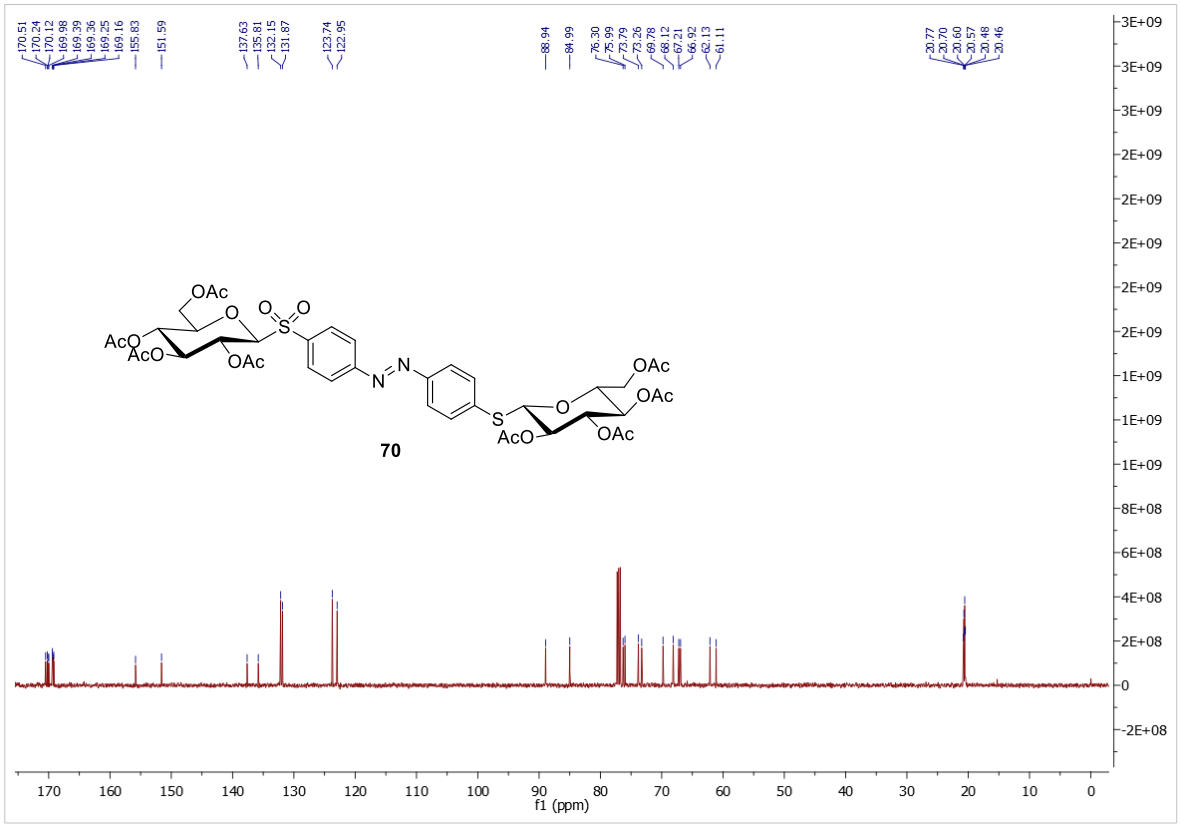

Figure 7.6.102. ^{13}C NMR spectrum of **70** (126 MHz, $CDCl_3$, 300 K).

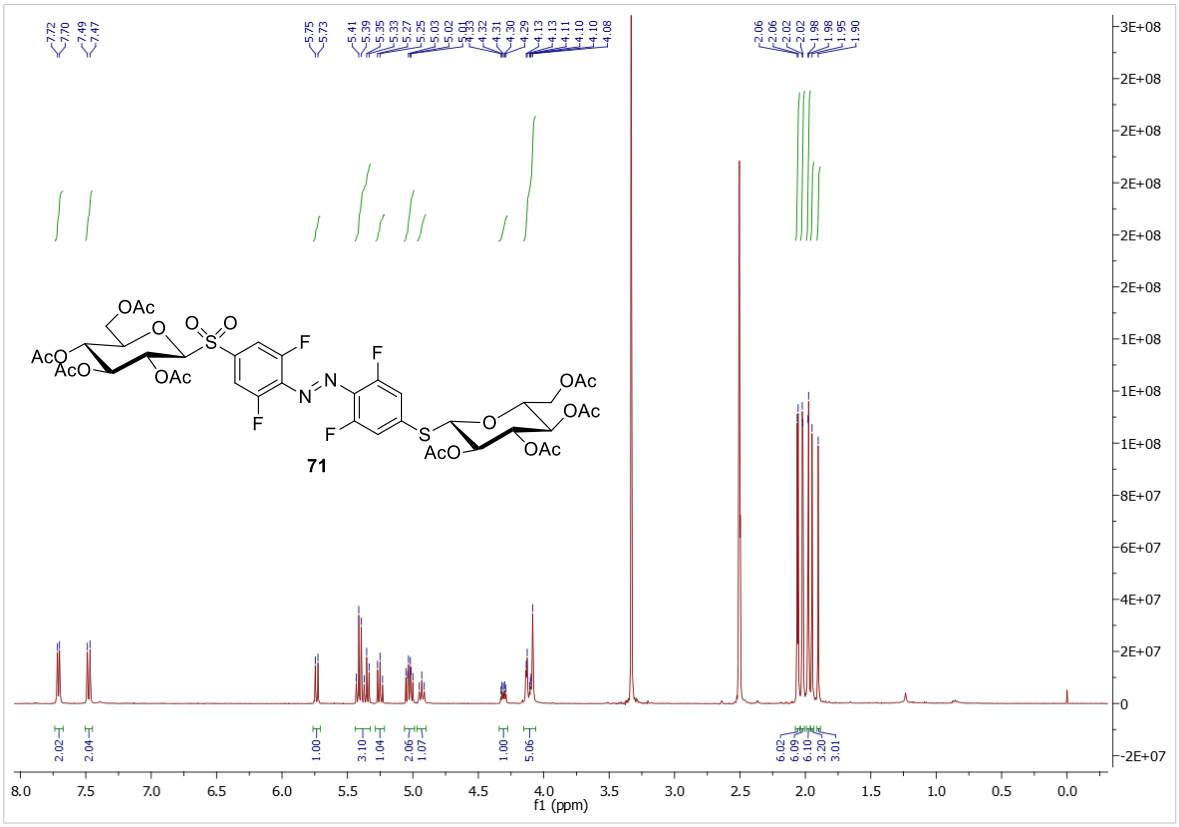

Figure 7.6.103. ^{1}H NMR spectrum of **71** (500 MHz, DMSO-d_6, 300 K).

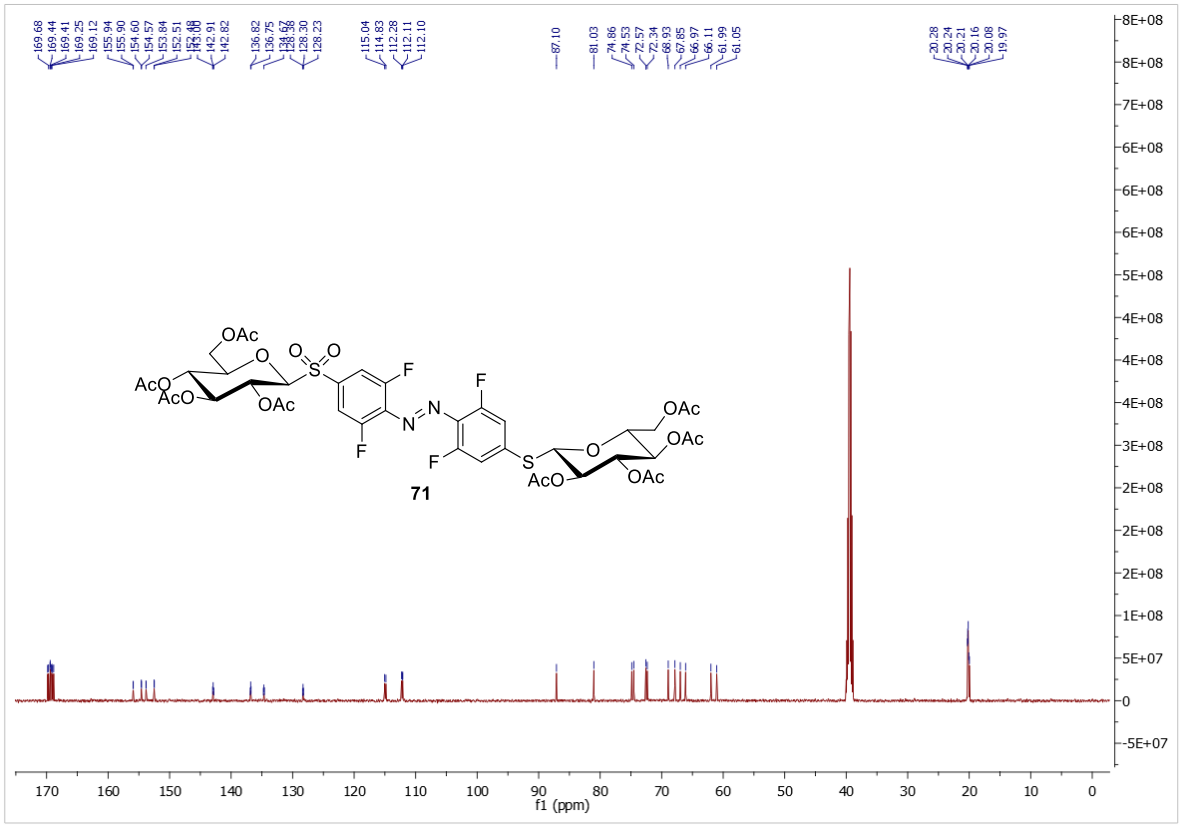

Figure 7.6.104. ^{13}C NMR spectrum of **71** (126 MHz, DMSO-d_6, 300 K).

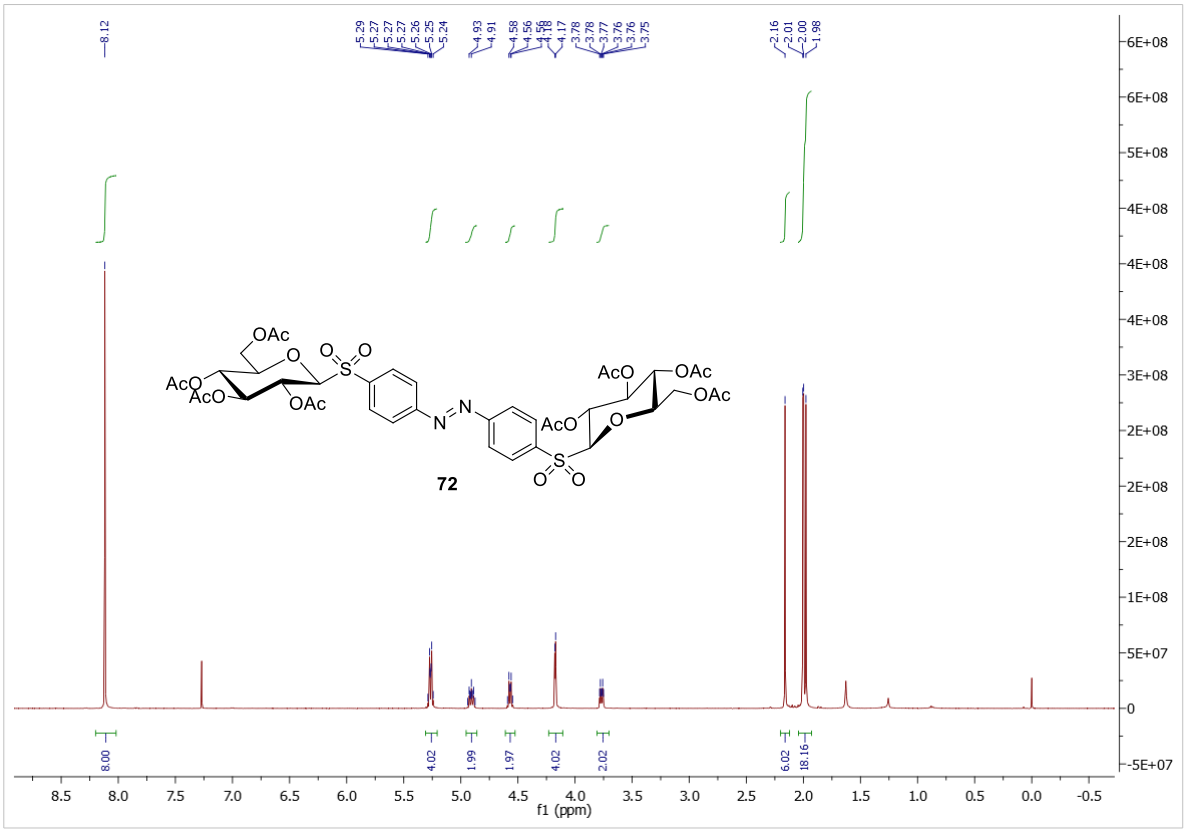

Figure 7.6.105. ^{1}H NMR spectrum of **72** (500 MHz, $CDCl_3$, 300 K).

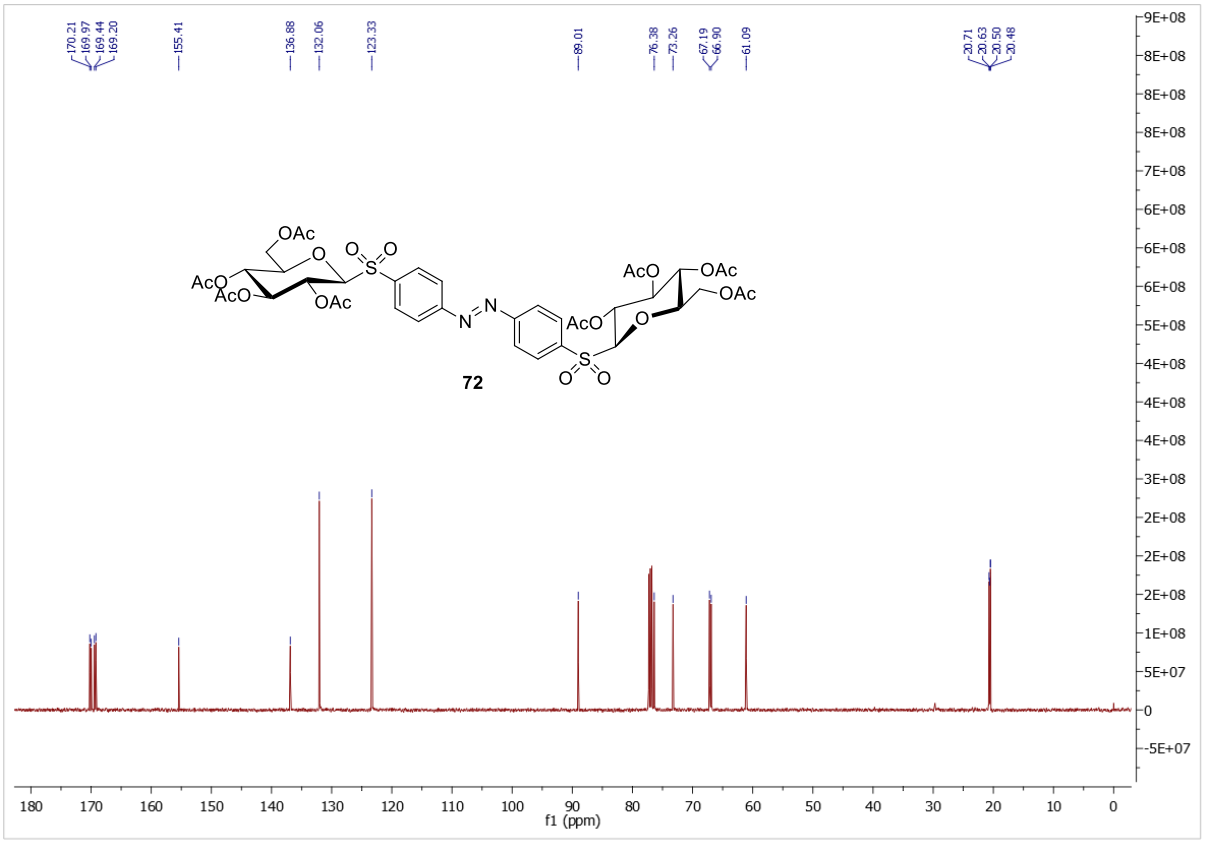

Figure 7.6.106. ^{13}C NMR spectrum of **72** (126 MHz, $CDCl_3$, 300 K).

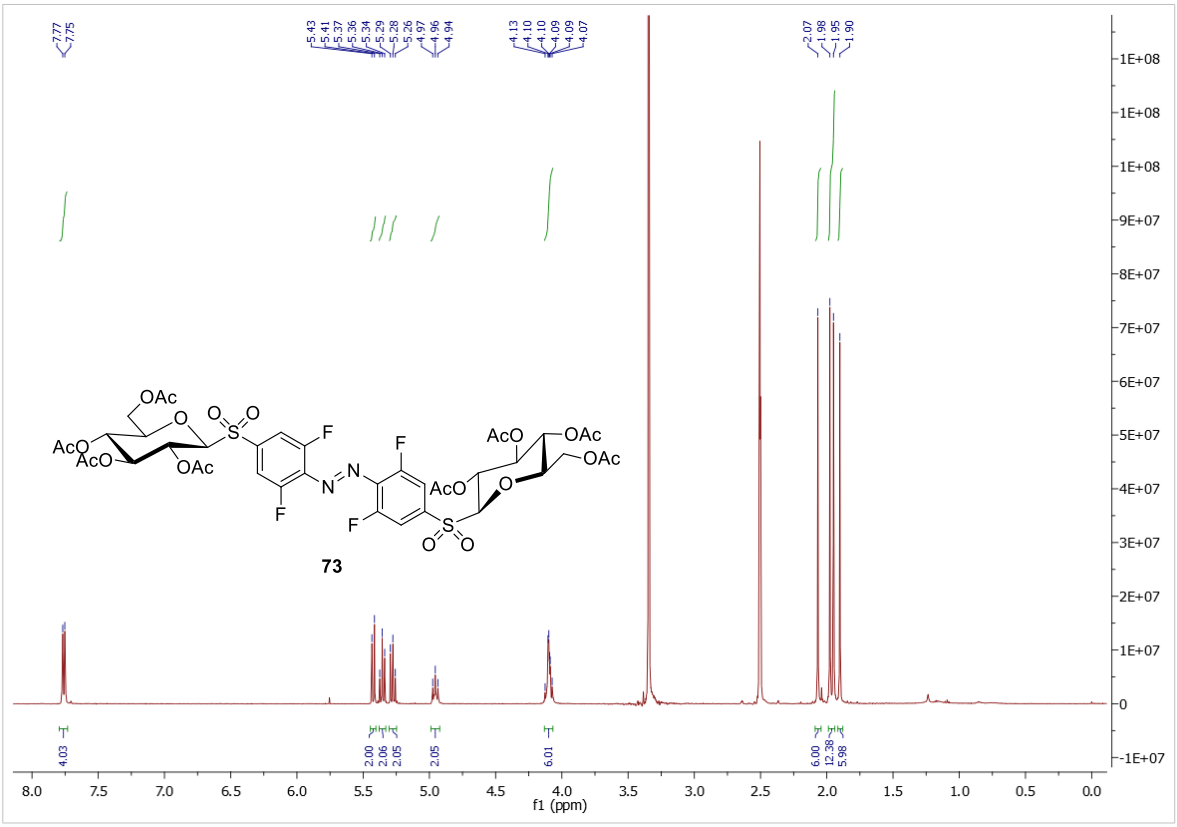

Figure 7.6.107. ^{1}H NMR spectrum of **73** (500 MHz, DMSO-d_6, 300 K).

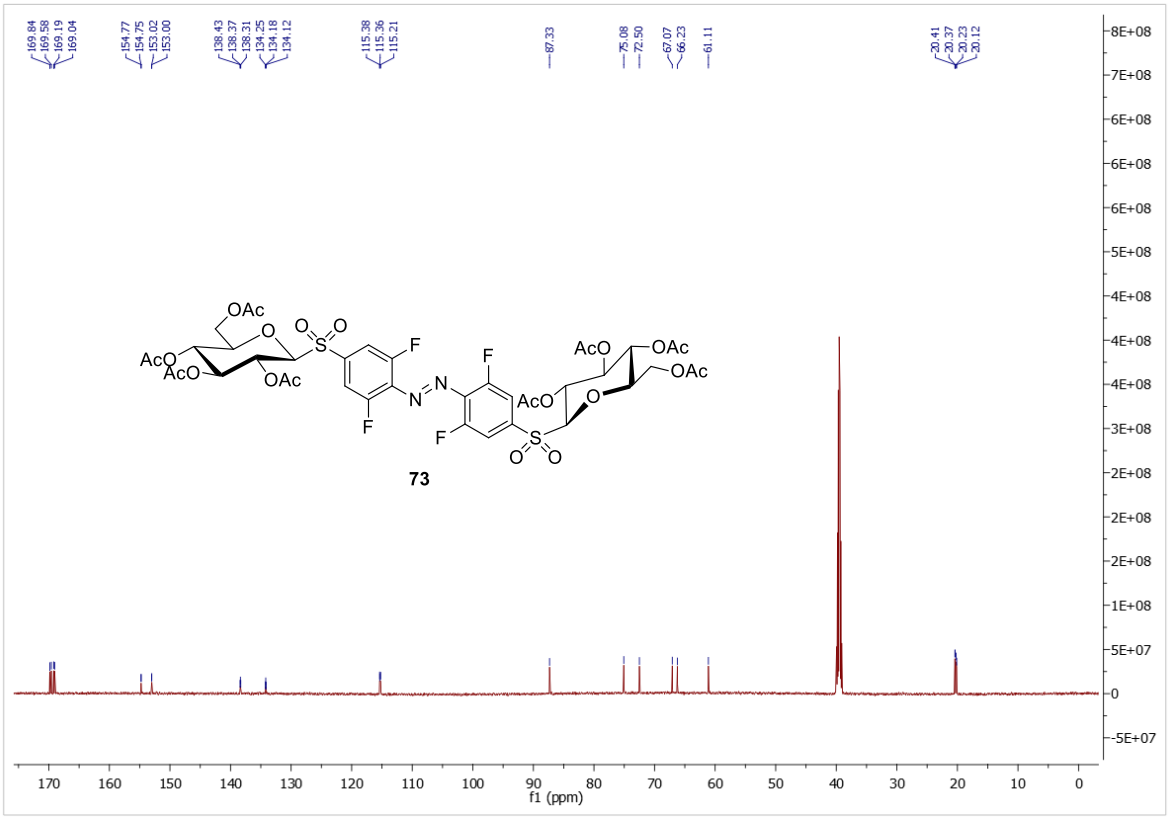

Figure 7.6.108. ^{13}C NMR spectrum of **73** (126 MHz, DMSO-d_6, 300 K).

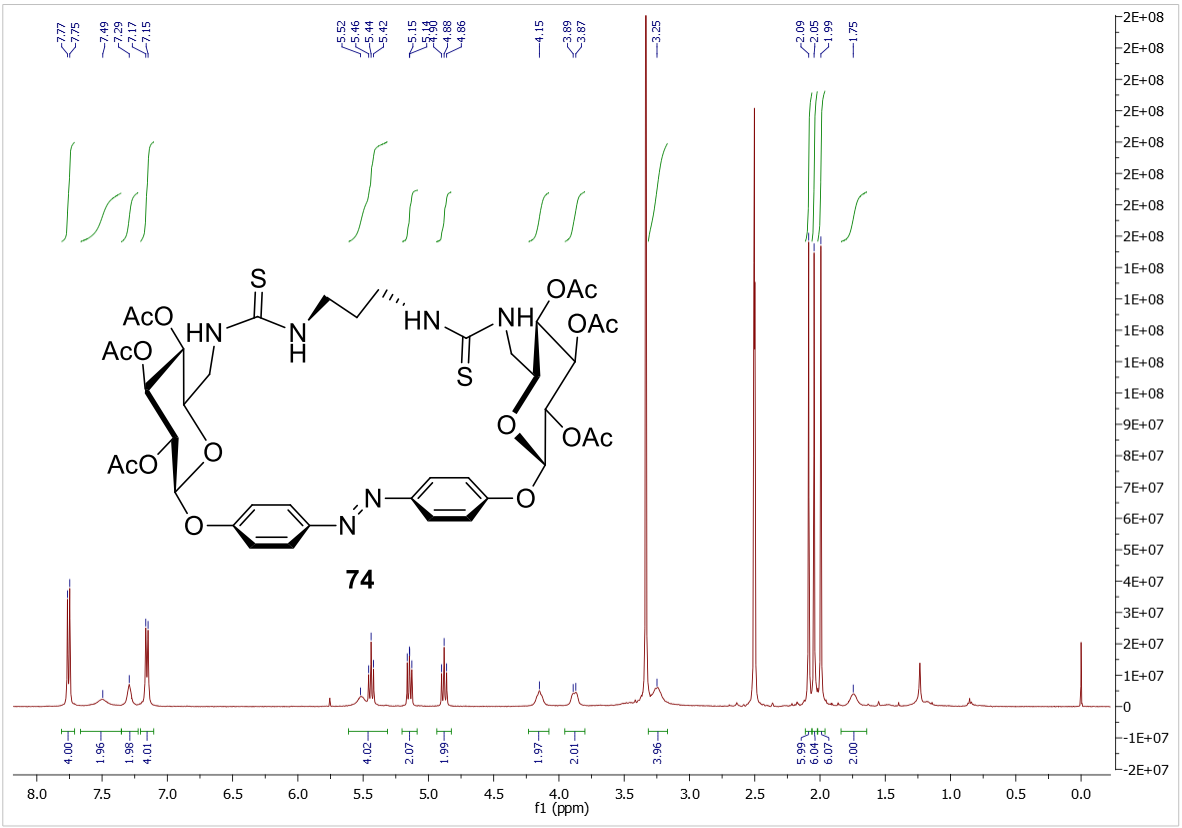

Figure 7.6.109. ^{1}H NMR spectrum of **74** (500 MHz, DMSO-d_6, 300 K).

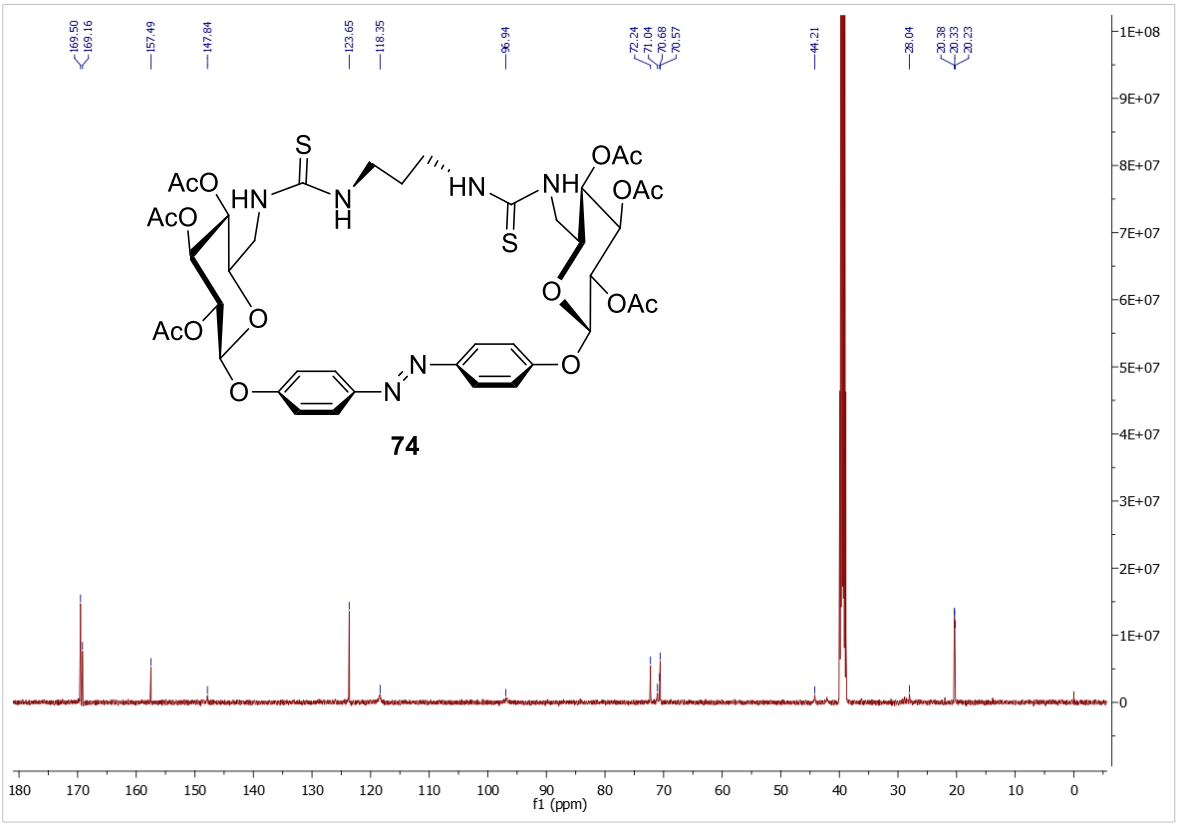

Figure 7.6.110. ^{13}C NMR spectrum of **74** (126 MHz, DMSO-d_6, 300 K).

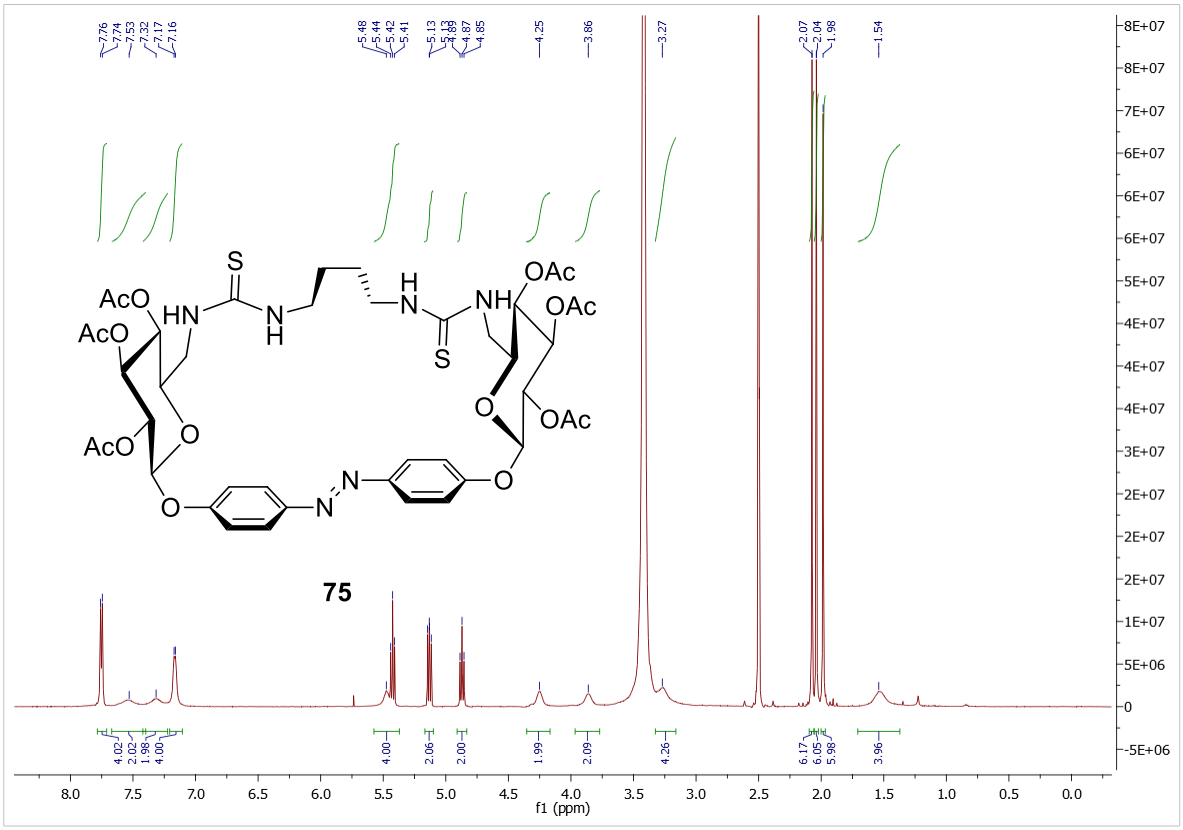

Figure 7.6.111. ^{1}H NMR spectrum of **75** (500 MHz, DMSO-d_6, 300 K).

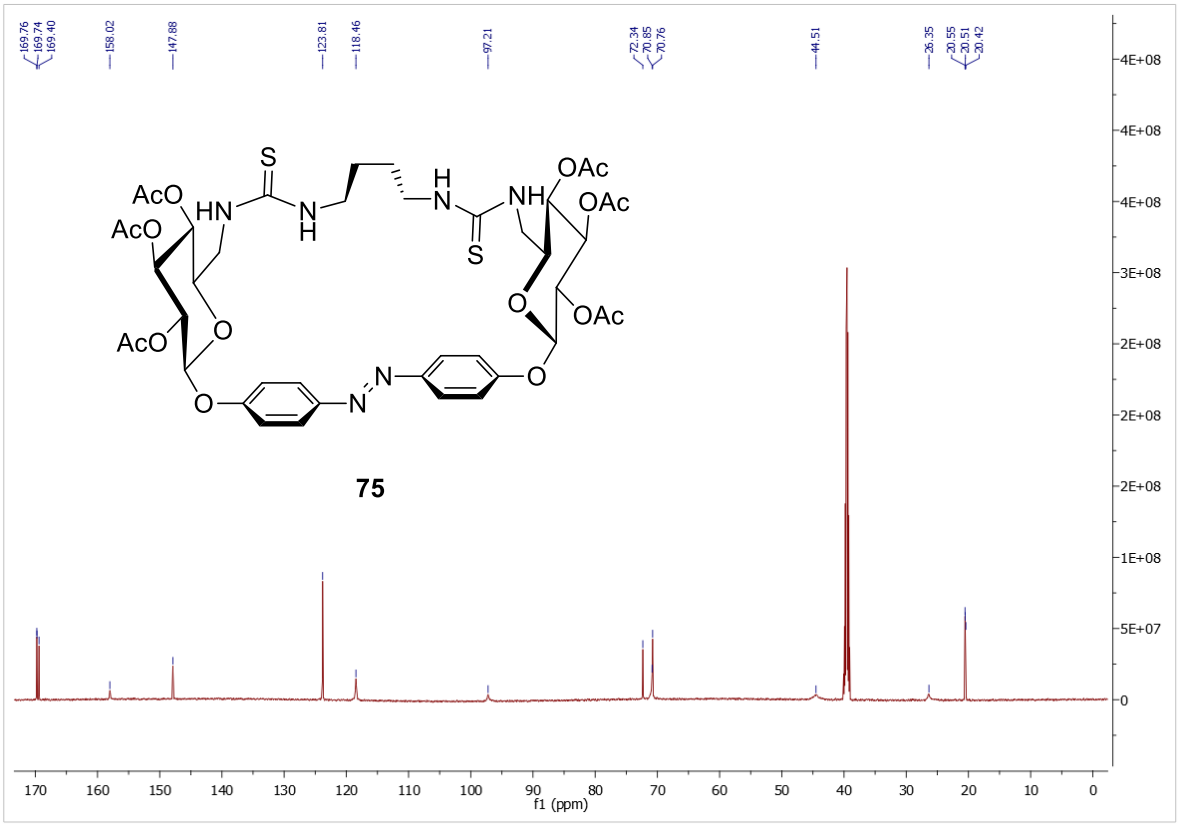

Figure 7.6.112. ^{13}C NMR spectrum of **75** (126 MHz, DMSO-d_6, 300 K).

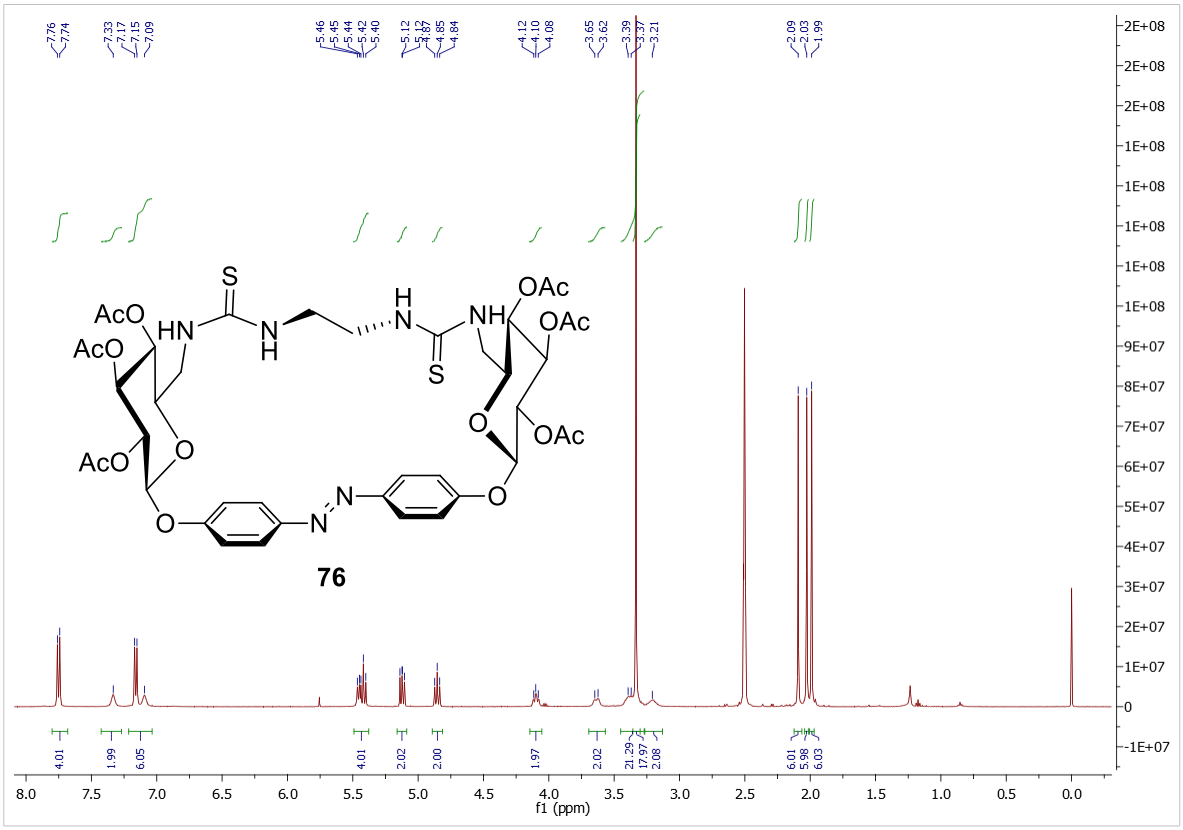

Figure 7.6.113. ^{1}H NMR spectrum of **76** (500 MHz, DMSO-d_6, 300 K).

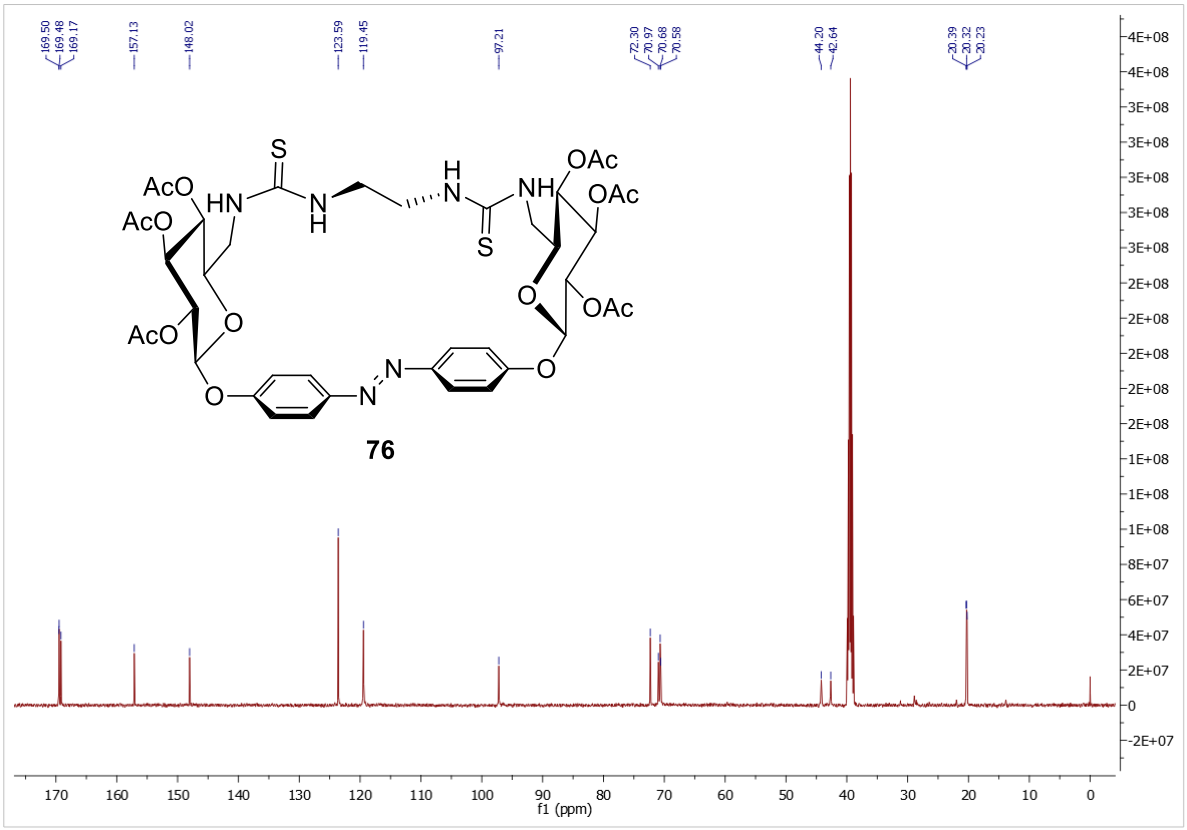

Figure 7.6.114. ^{13}C NMR spectrum of **76** (126 MHz, DMSO-d_6, 300 K).

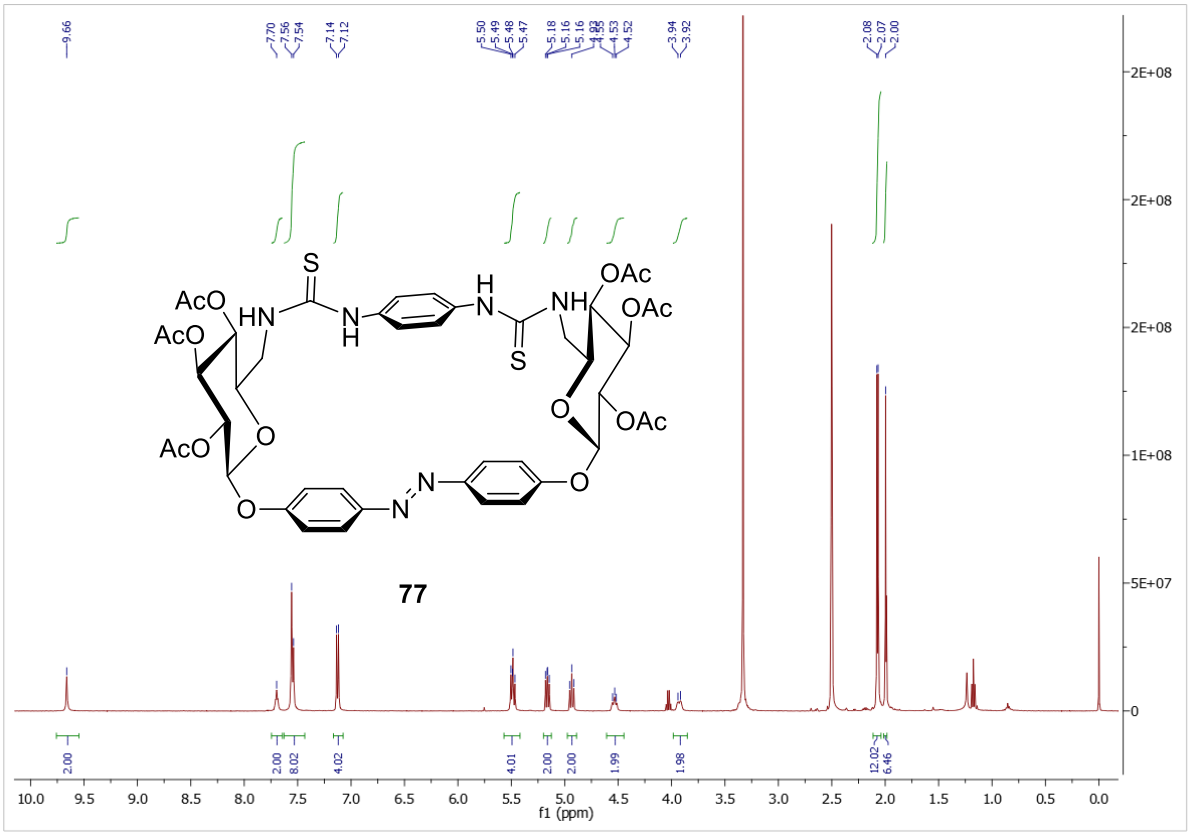

Figure 7.6.115. ^{1}H NMR spectrum of **77** (500 MHz, DMSO-d_6, 300 K).

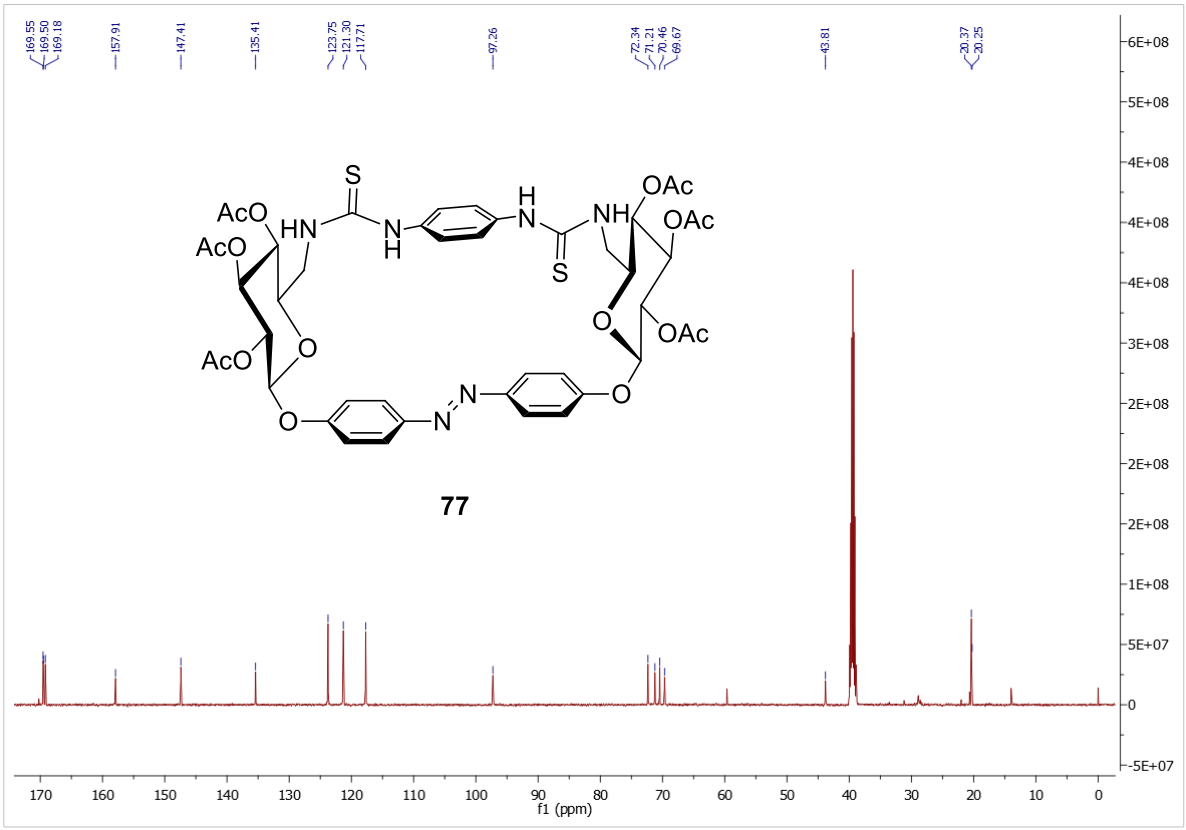

Figure 7.6.116. ^{13}C NMR spectrum of **77** (126 MHz, DMSO-d_6, 300 K).

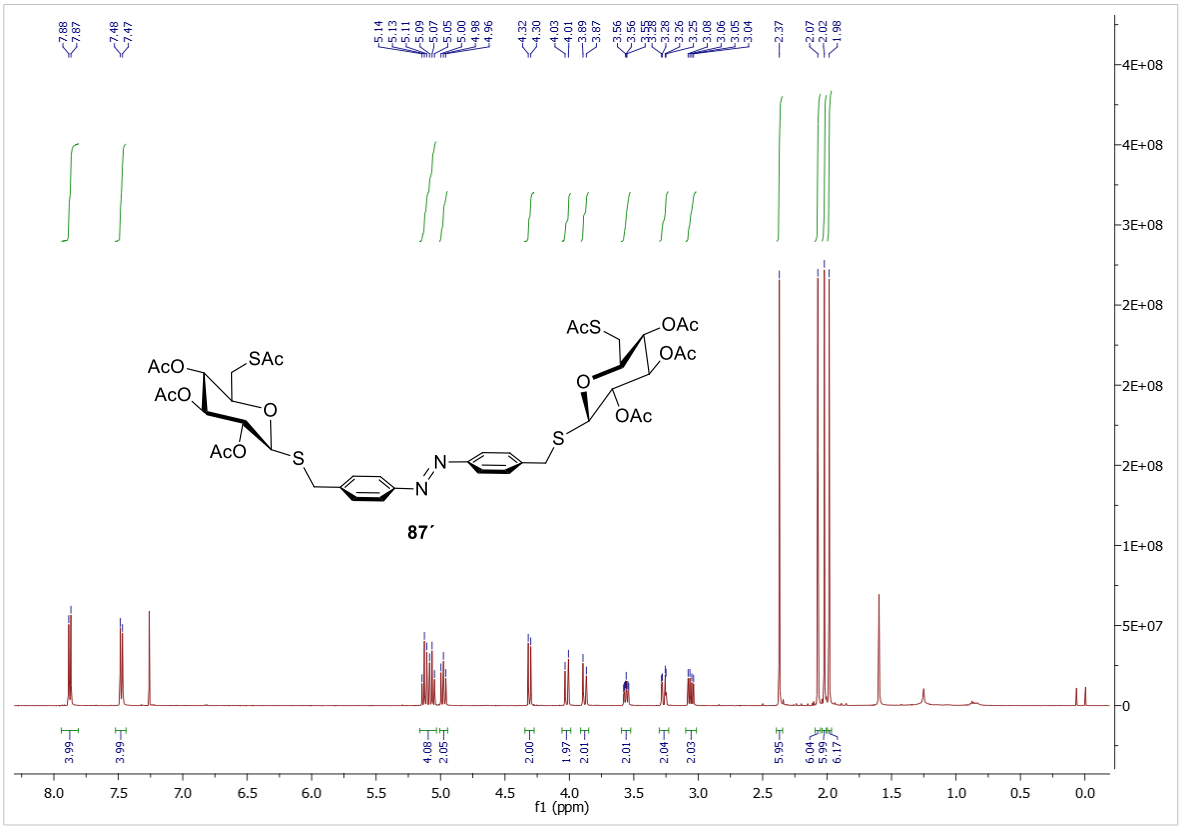

Figure 7.6.117. ^{1}H NMR spectrum of **87´** (500 MHz, $CDCl_3$, 300 K).

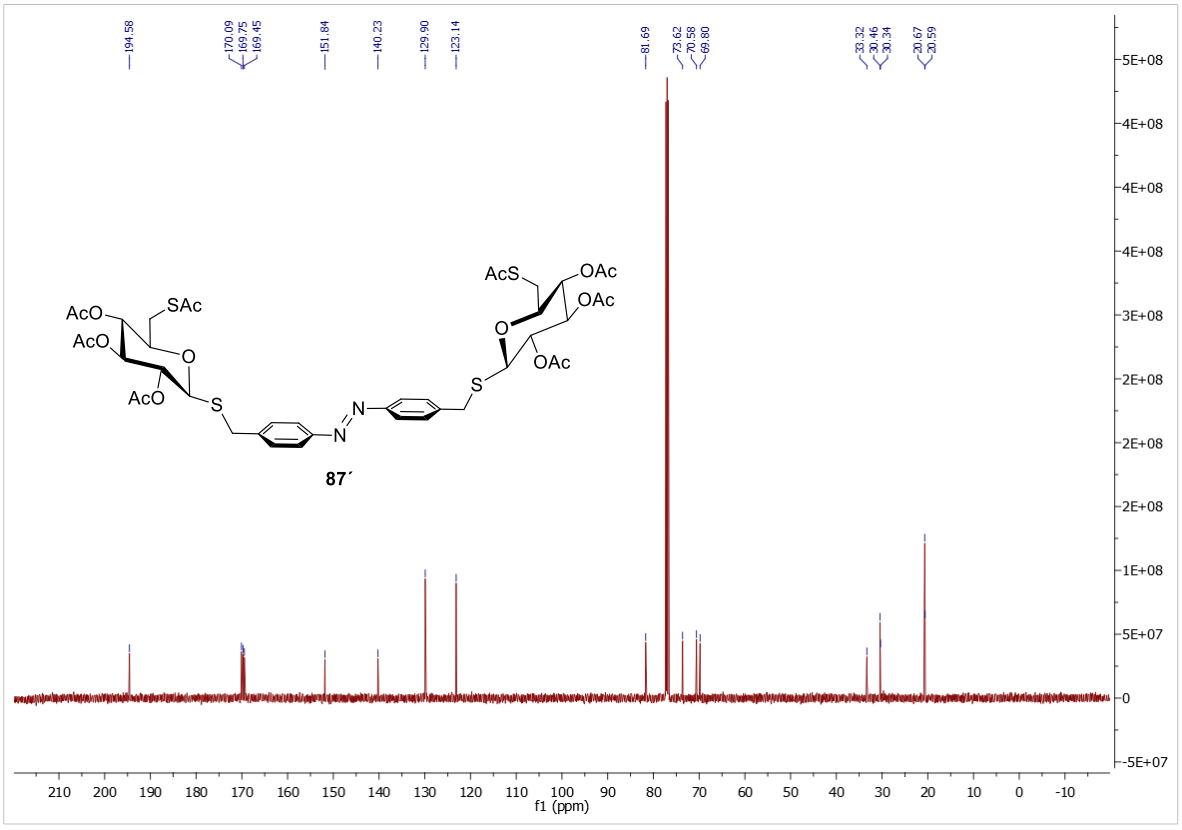

Figure 7.6.118. ^{13}C NMR spectrum of **87´** (126 MHz, $CDCl_3$, 300 K).

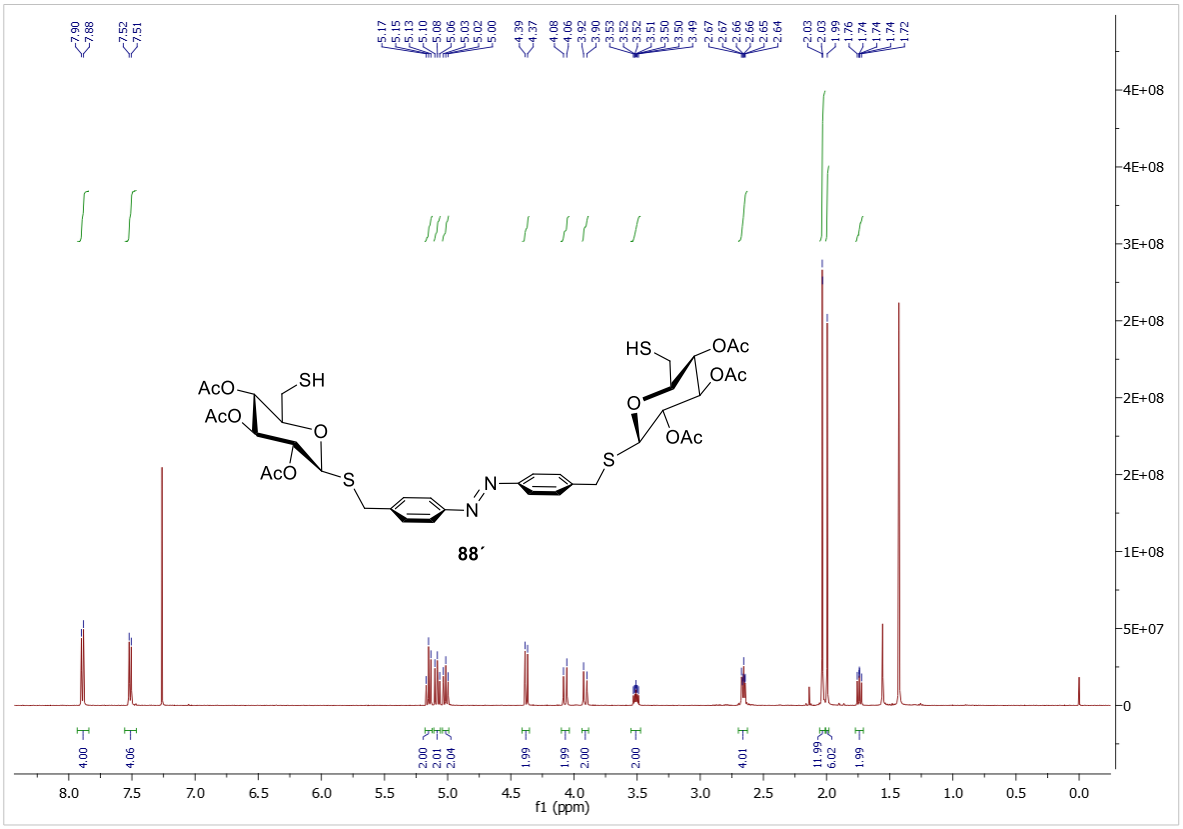

Figure 7.6.119. ^{1}H NMR spectrum of **88´** (500 MHz, $CDCl_3$, 300 K).

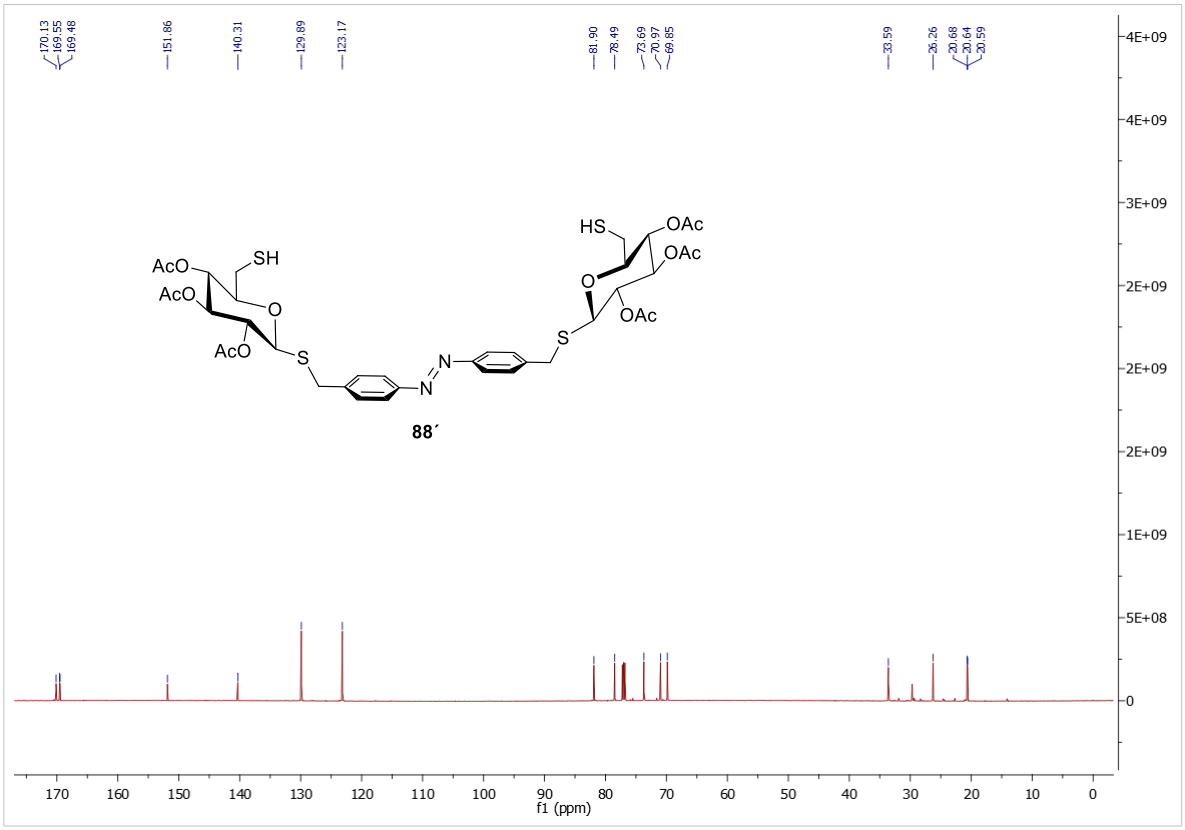

Figure 7.6.120. ^{13}C NMR spectrum of **88´** (126 MHz, $CDCl_3$, 300 K).

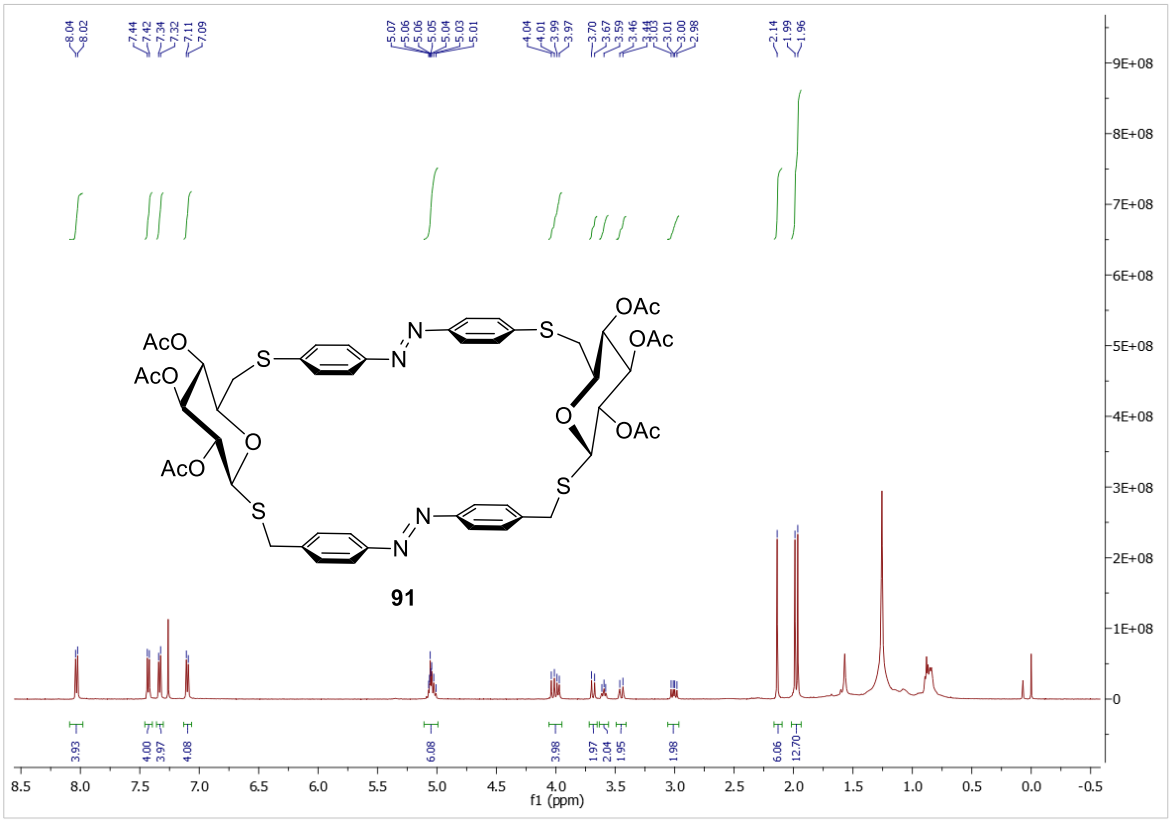

Figure 7.6.121. ^{1}H NMR spectrum of **91** (500 MHz, $CDCl_3$, 300 K).

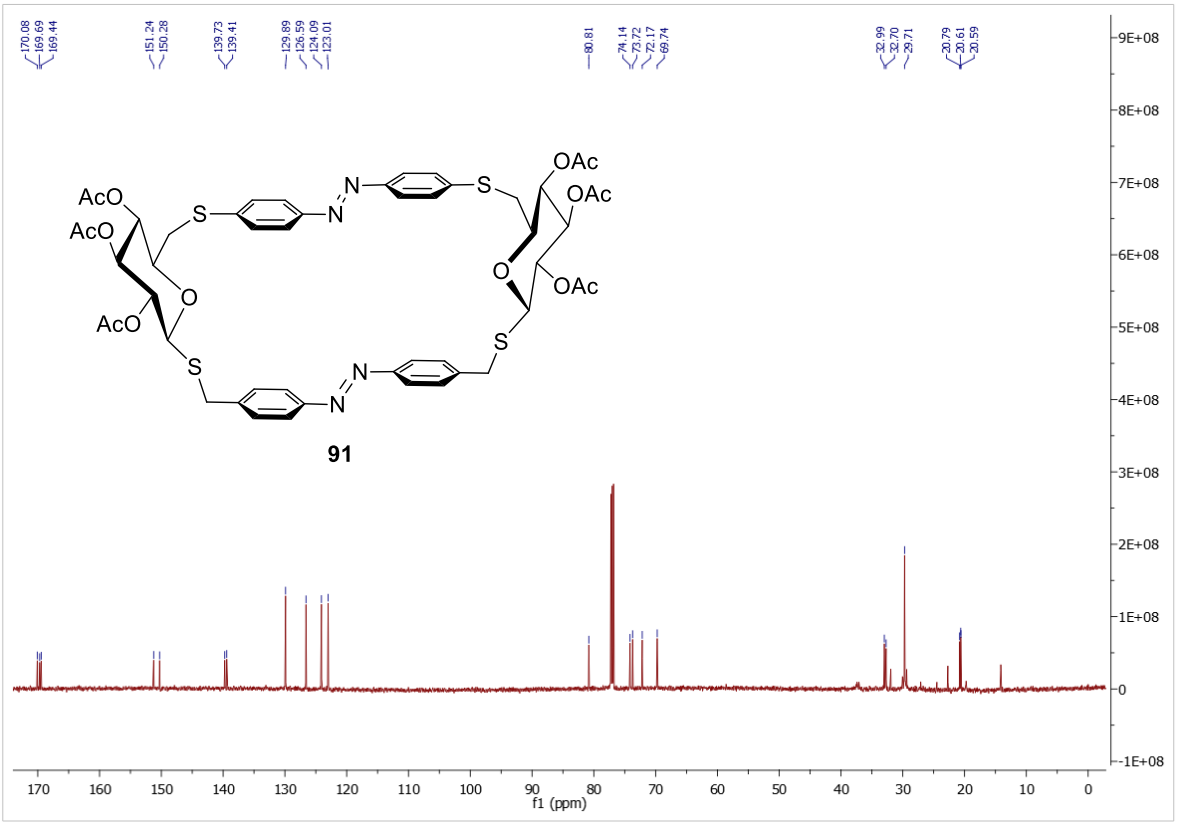

Figure 7.6.122. ^{13}C NMR spectrum of **91** (126 MHz, $CDCl_3$, 300 K).

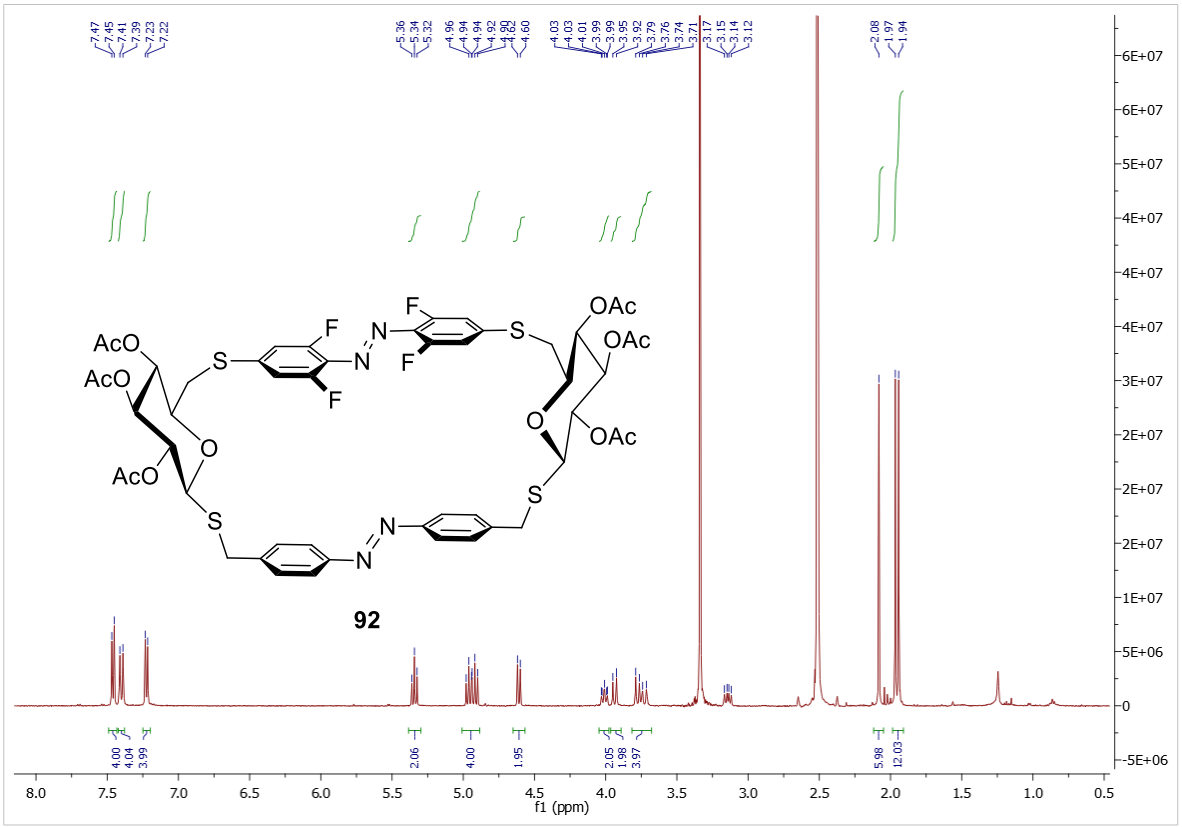

Figure 7.6.123. ^{1}H NMR spectrum of **92** (500 MHz, DMSO-d_6, 300 K).

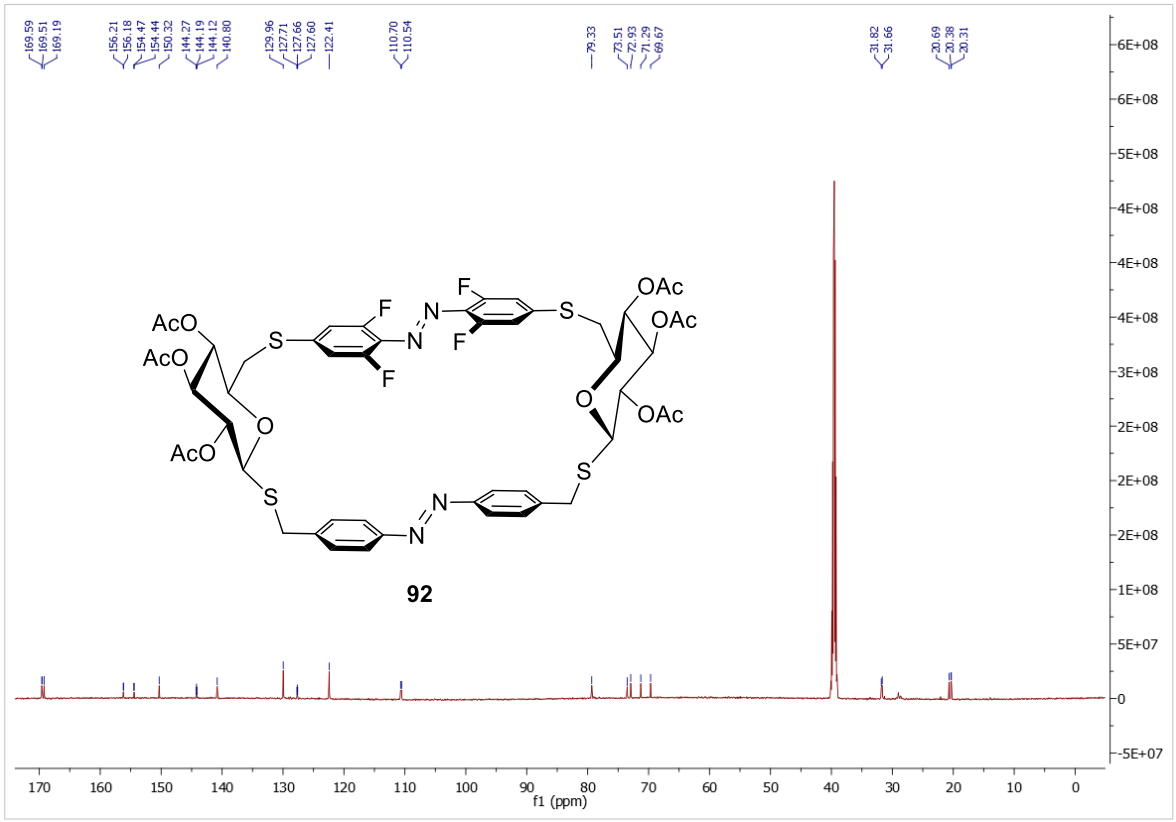

Figure 7.6.124. ^{13}C NMR spectrum of **92** (126 MHz, DMSO-d_6, 300 K).

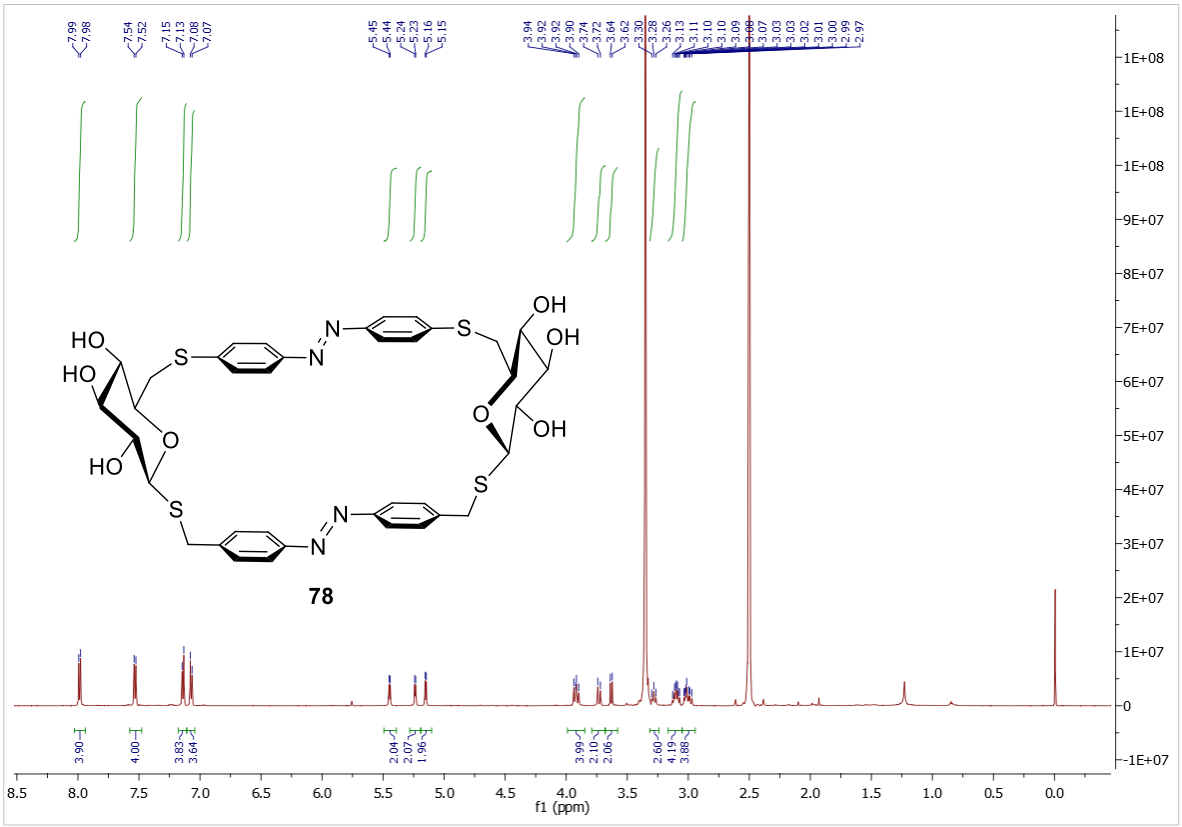

Figure 7.6.125. ^{1}H NMR spectrum of **78** (500 MHz, DMSO-d_6, 300 K).

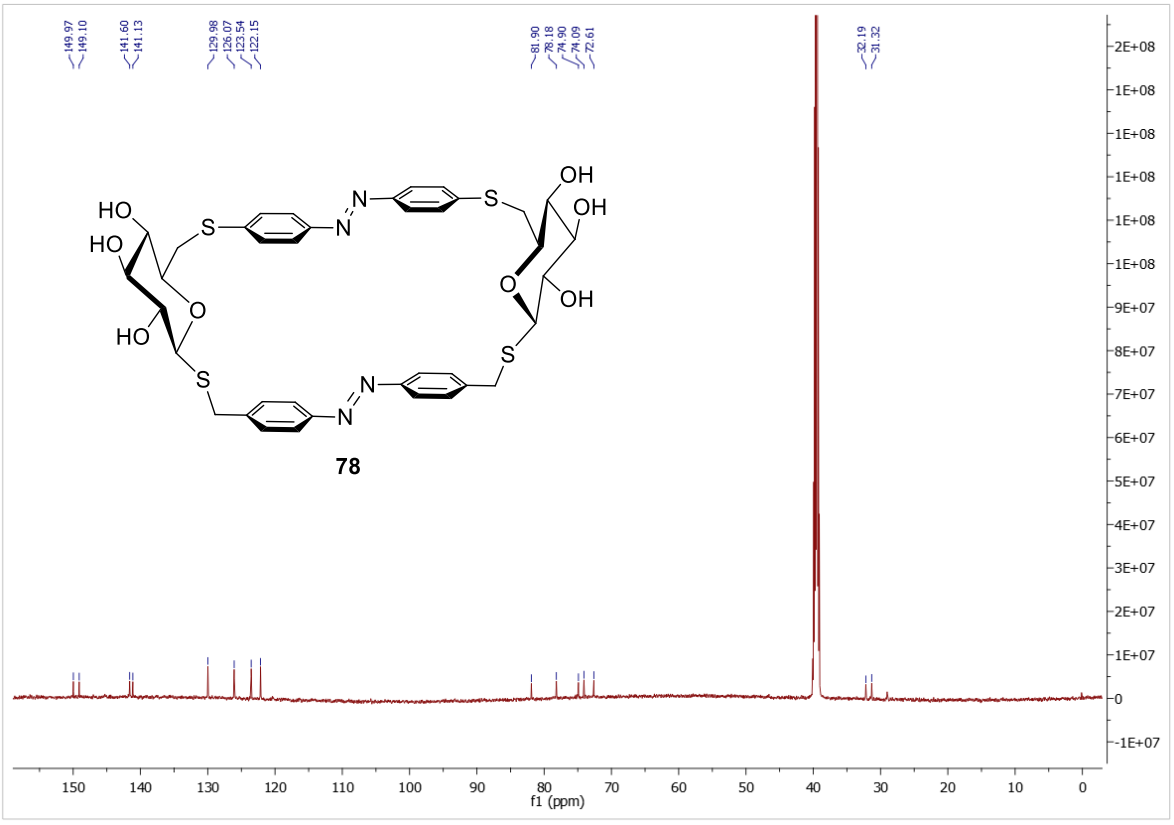

Figure 7.6.126. ^{13}C NMR spectrum of **78** (126 MHz, DMSO-d_6, 300 K).

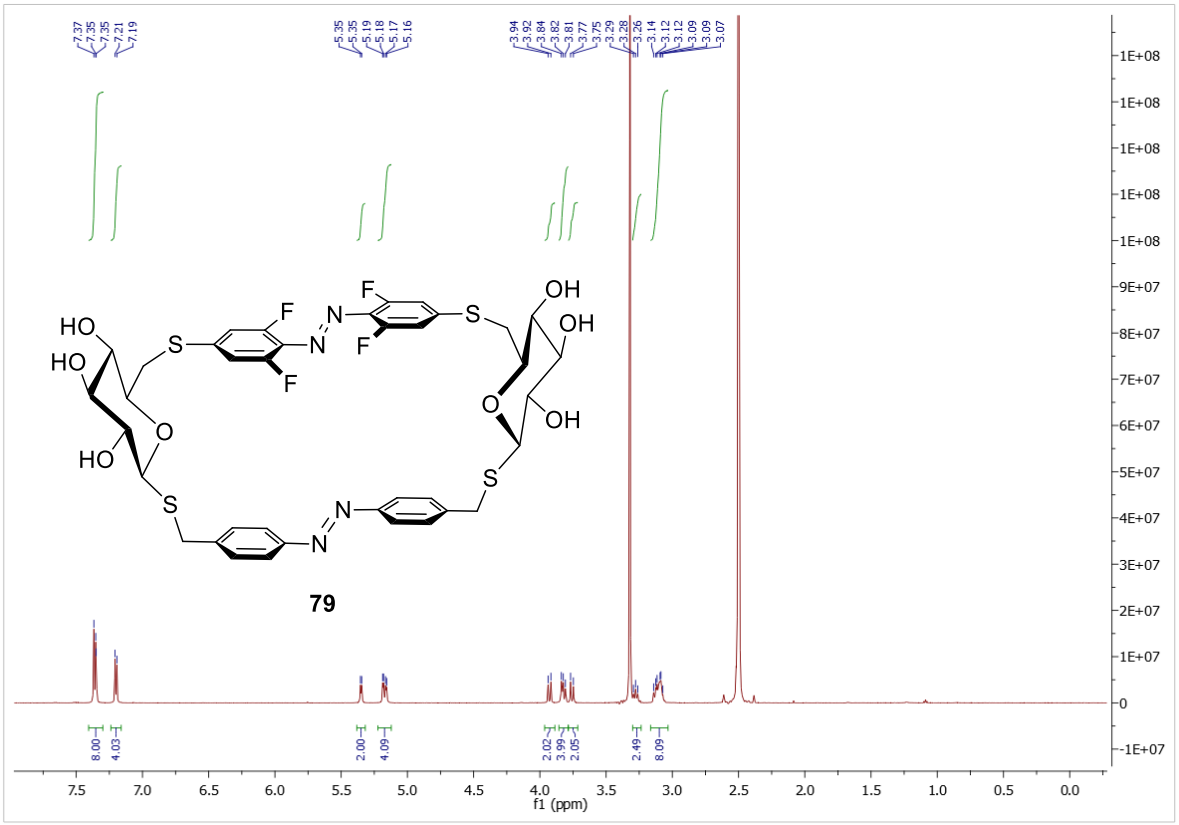

Figure 7.6.127. ^{1}H NMR spectrum of **79** (500 MHz, DMSO-d_6, 300 K).

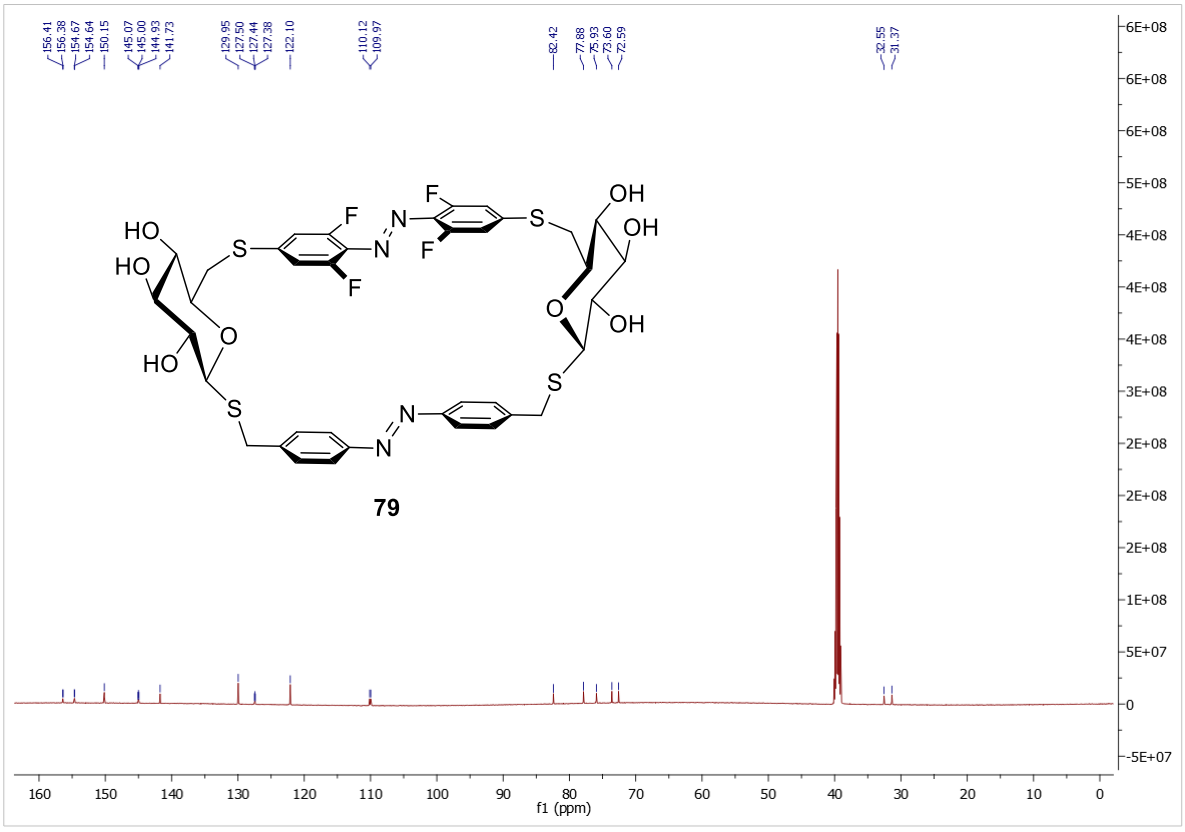

Figure 7.6.128. ^{13}C NMR spectrum of **79** (126 MHz, DMSO-d_6, 300 K).

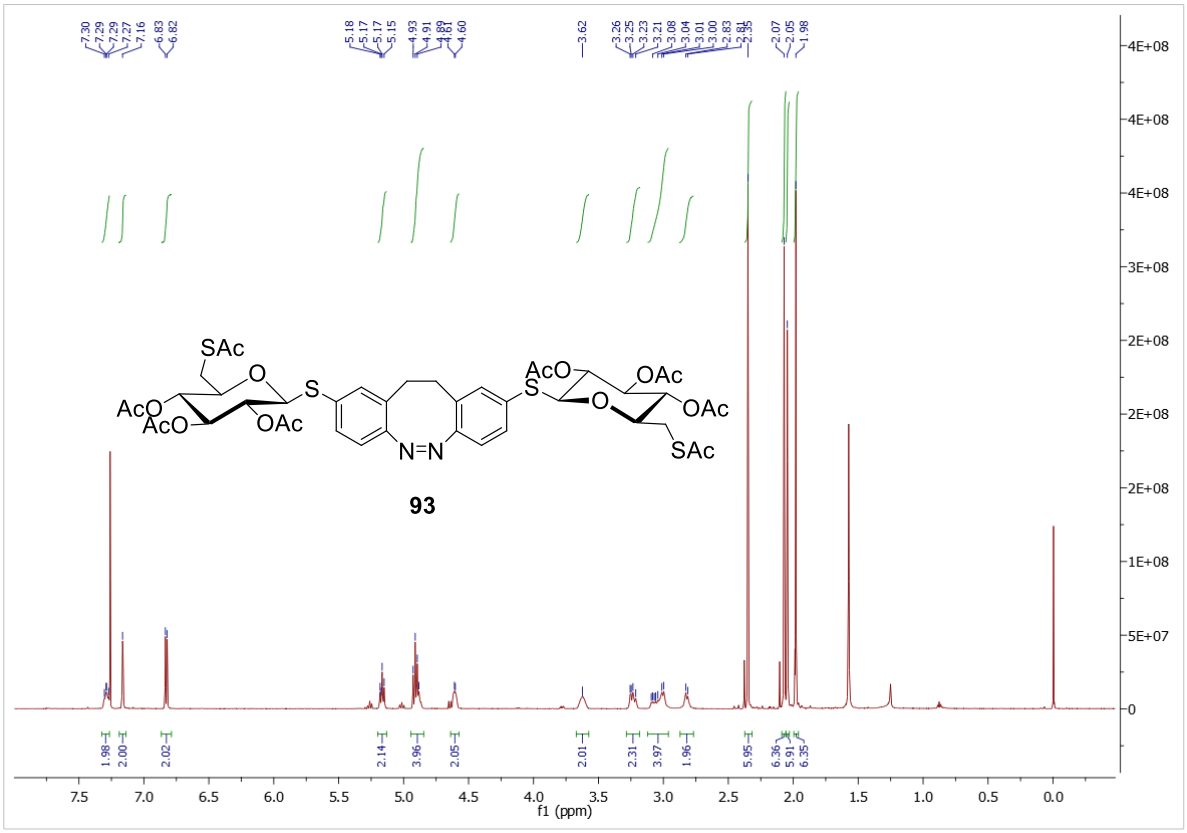

Figure 7.6.129. ^{1}H NMR spectrum of **93** (500 MHz, $CDCl_3$, 300 K).

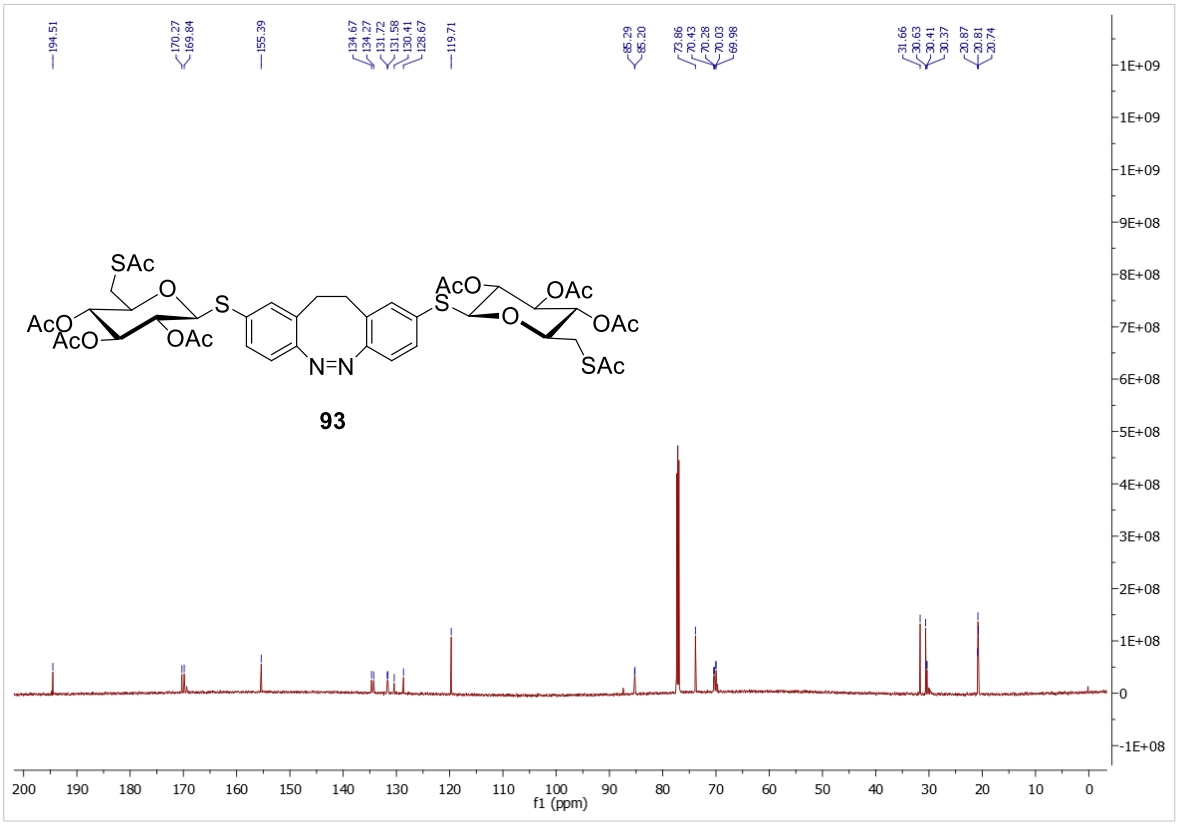

Figure 7.6.130. ^{13}C NMR spectrum of **93** (126 MHz, $CDCl_3$, 300 K).

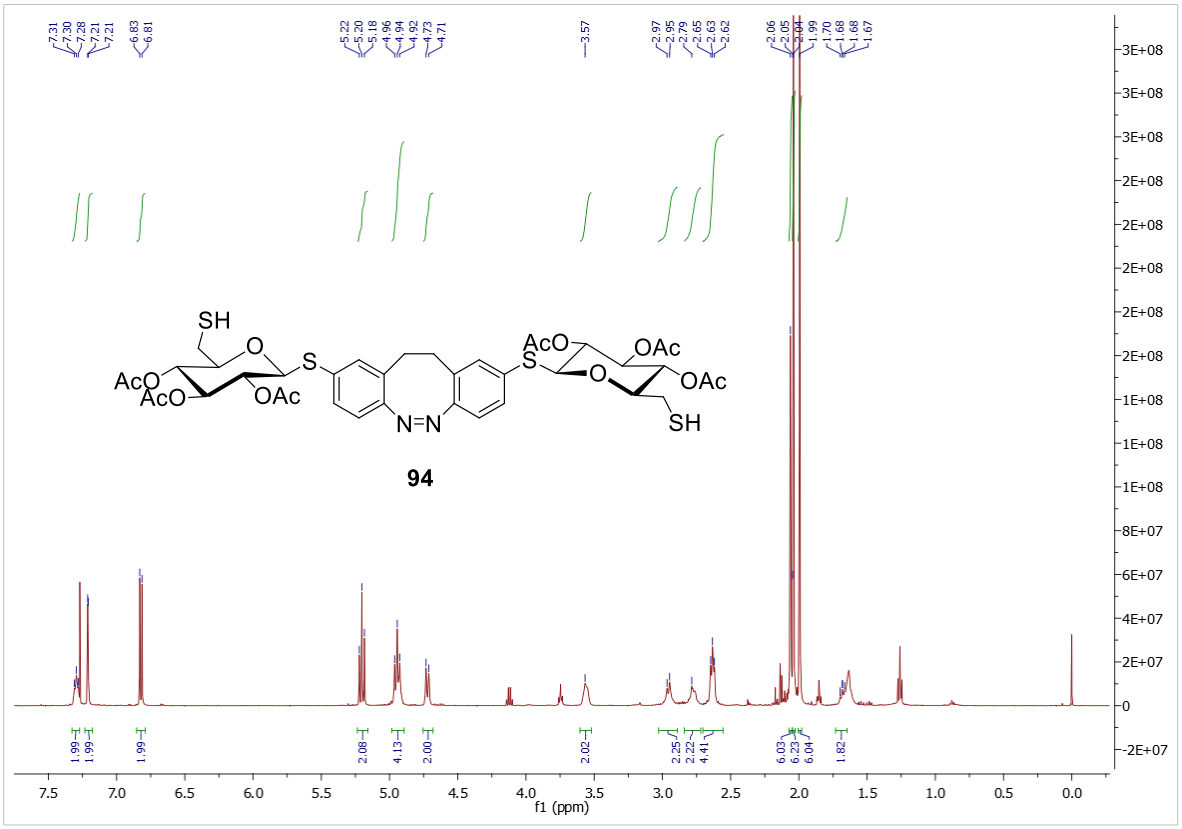

Figure 7.6.131. ^{1}H NMR spectrum of **94** (500 MHz, $CDCl_3$, 300 K).

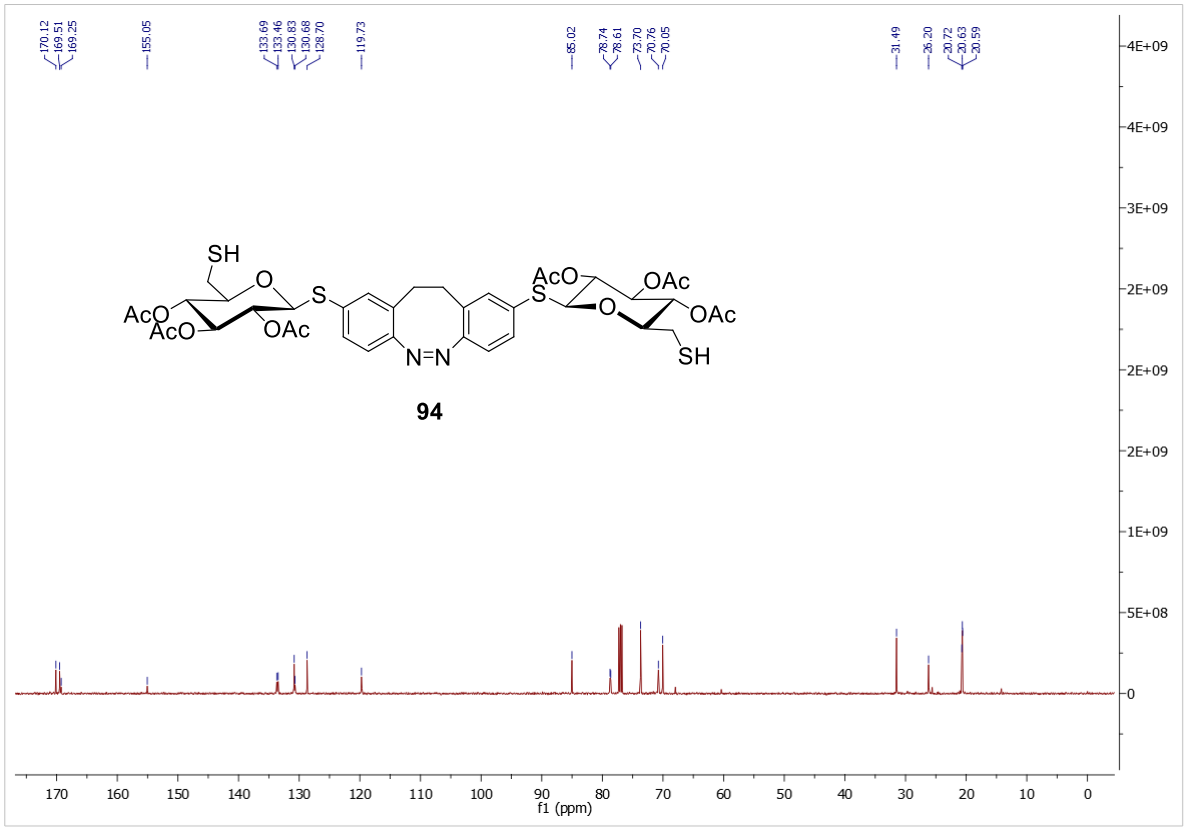

Figure 7.6.132. ^{13}C NMR spectrum of **94** (126 MHz, $CDCl_3$, 300 K).

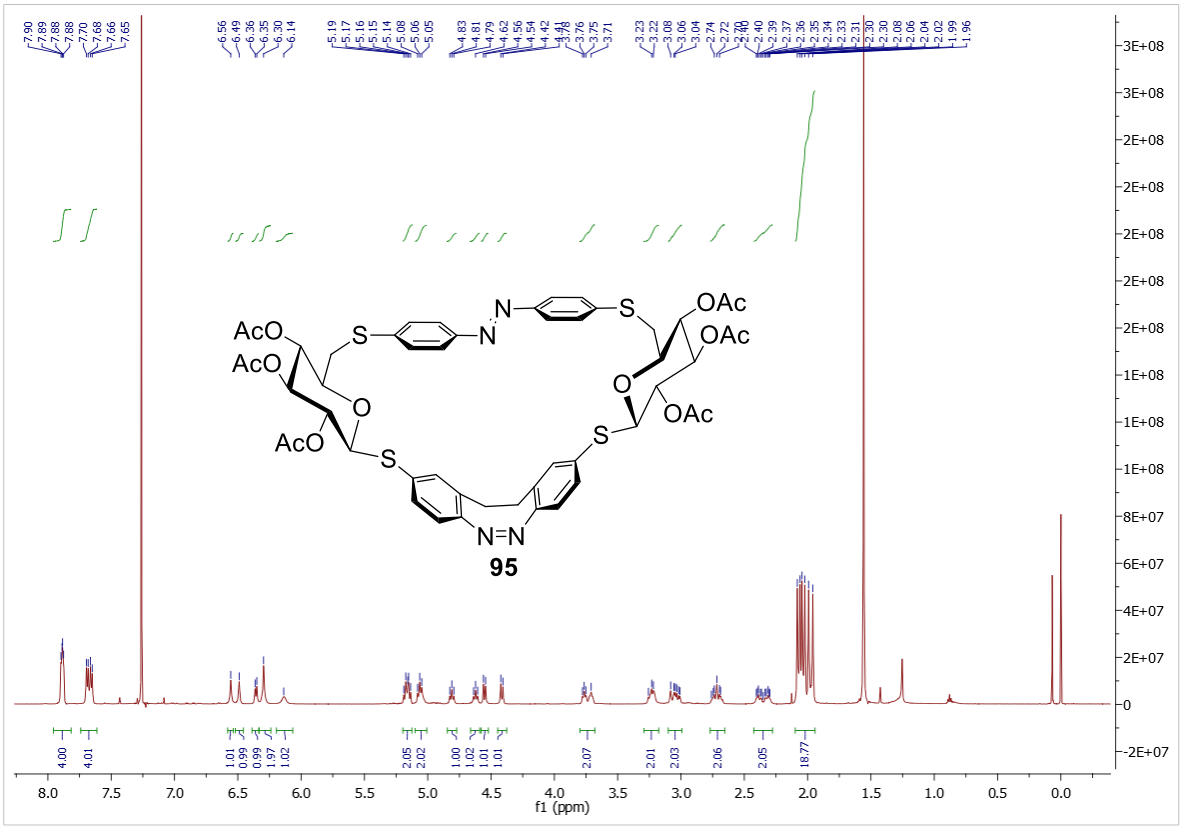

Figure 7.6.133. ^{1}H NMR spectrum of **95** (500 MHz, $CDCl_3$, 300 K).

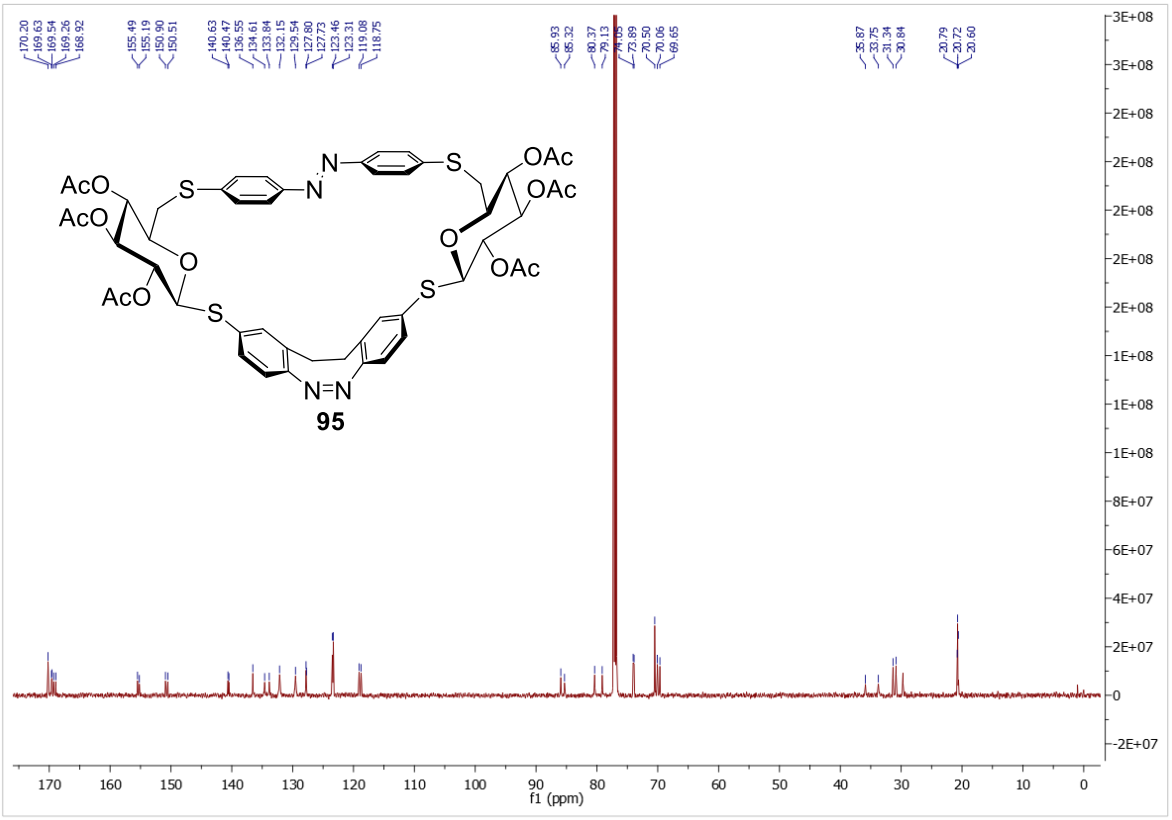

Figure 7.6.134. ^{13}C NMR spectrum of **95** (126 MHz, $CDCl_3$, 300 K).

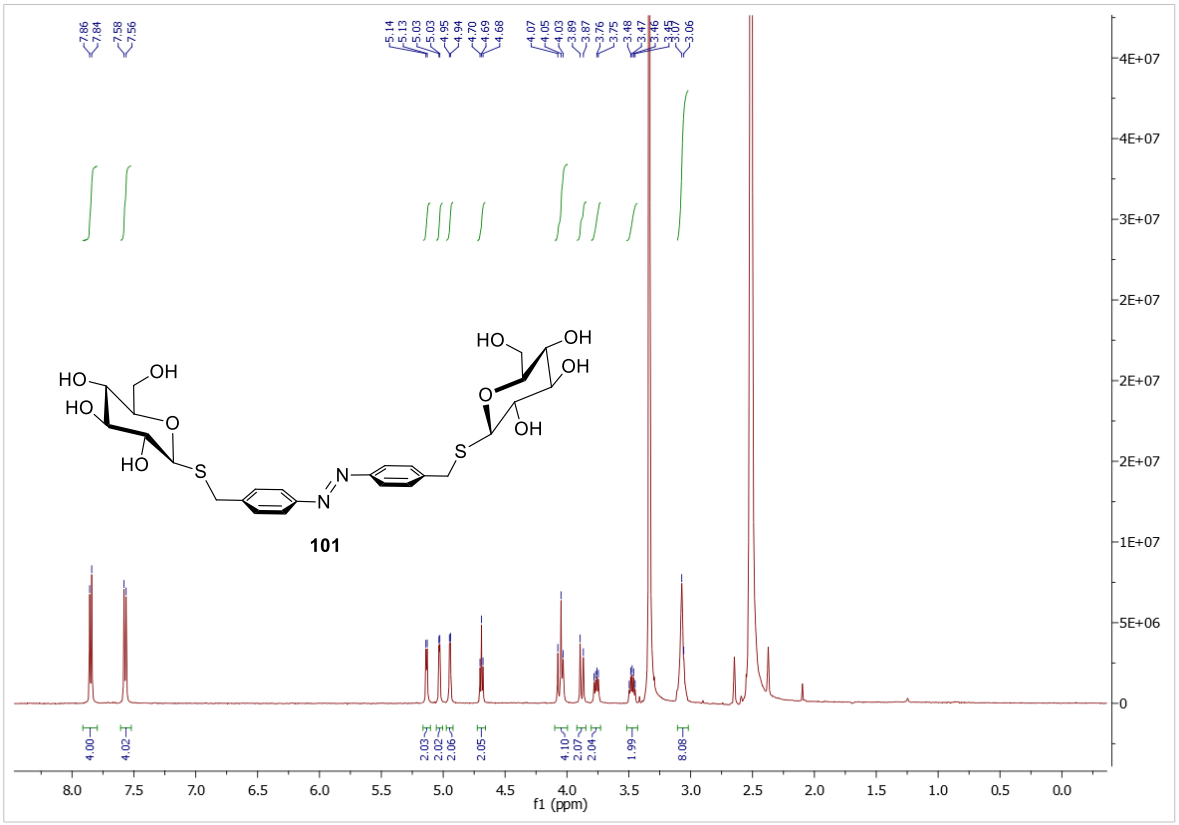

Figure 7.6.135. ^{1}H NMR spectrum of **101** (500 MHz, DMSO-d_6, 300 K).

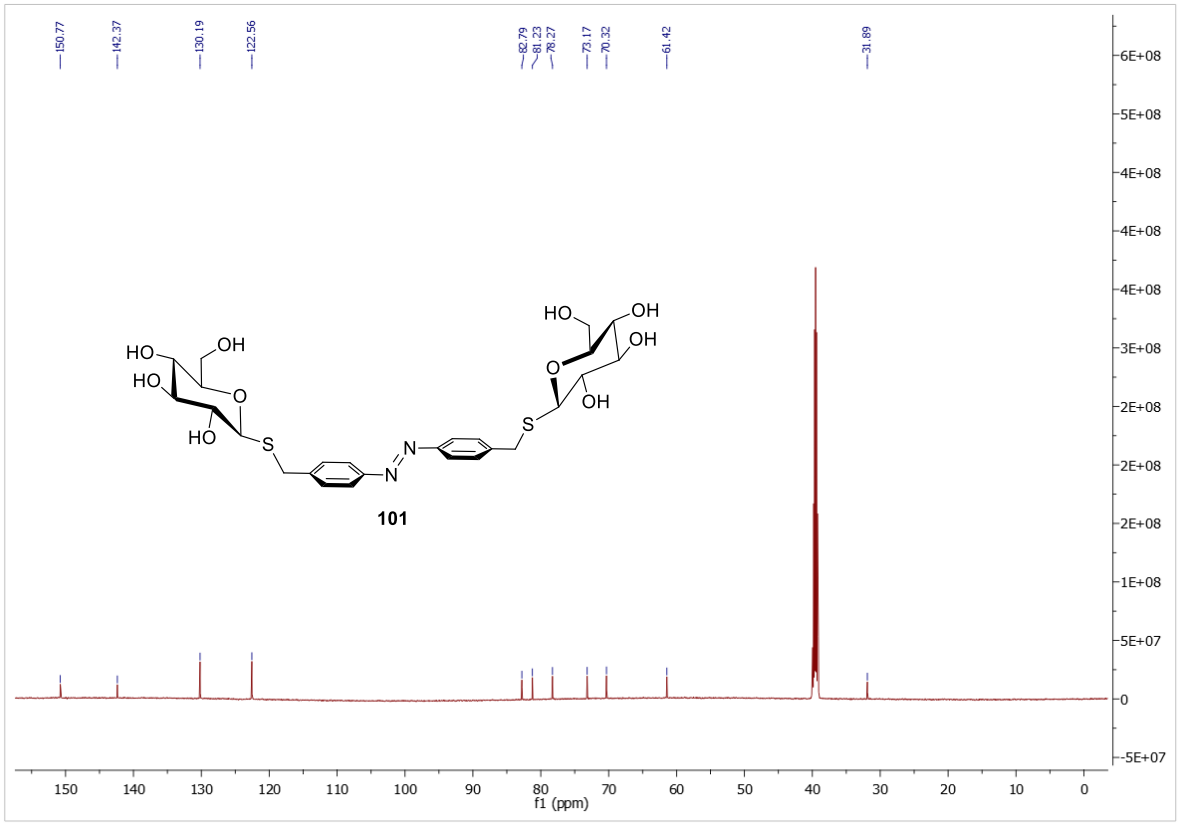

Figure 7.6.136. ^{13}C NMR spectrum of **101** (126 MHz, DMSO-d_6, 300 K).

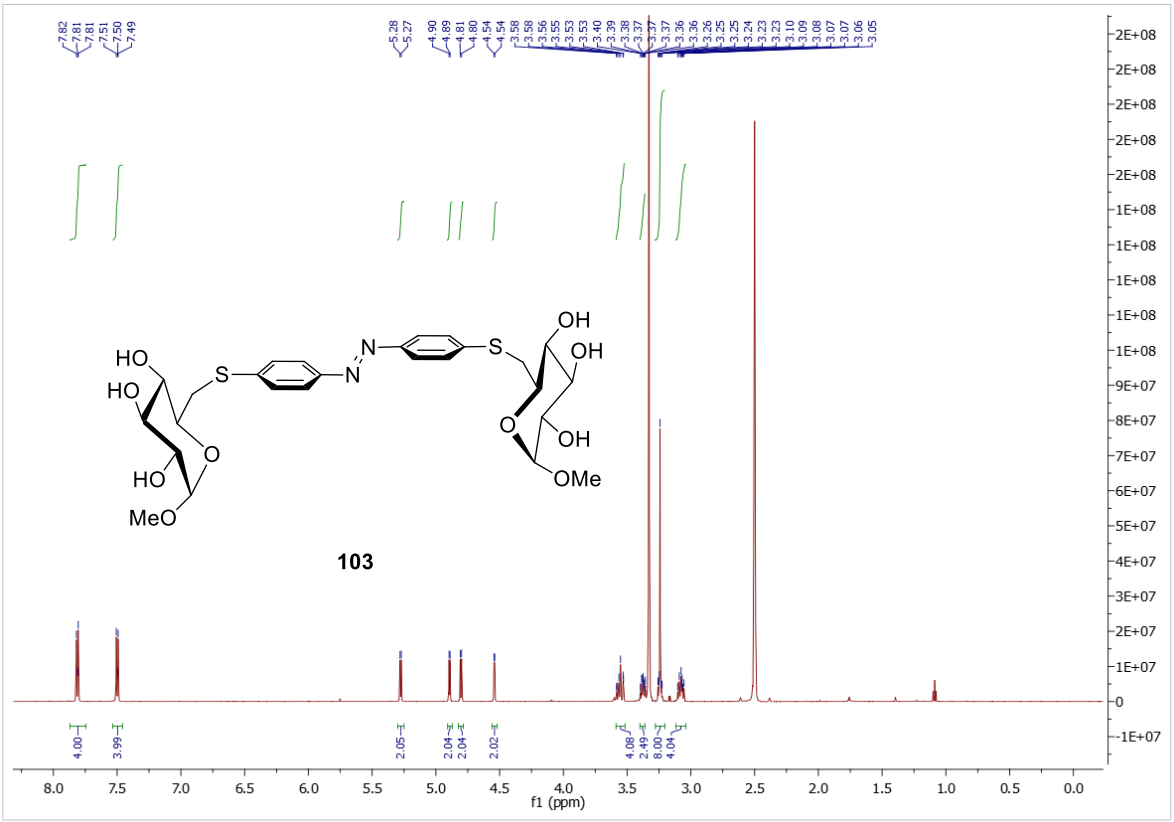

Figure 7.6.137. ^{1}H NMR spectrum of **103** (500 MHz, DMSO-d_6, 300 K).

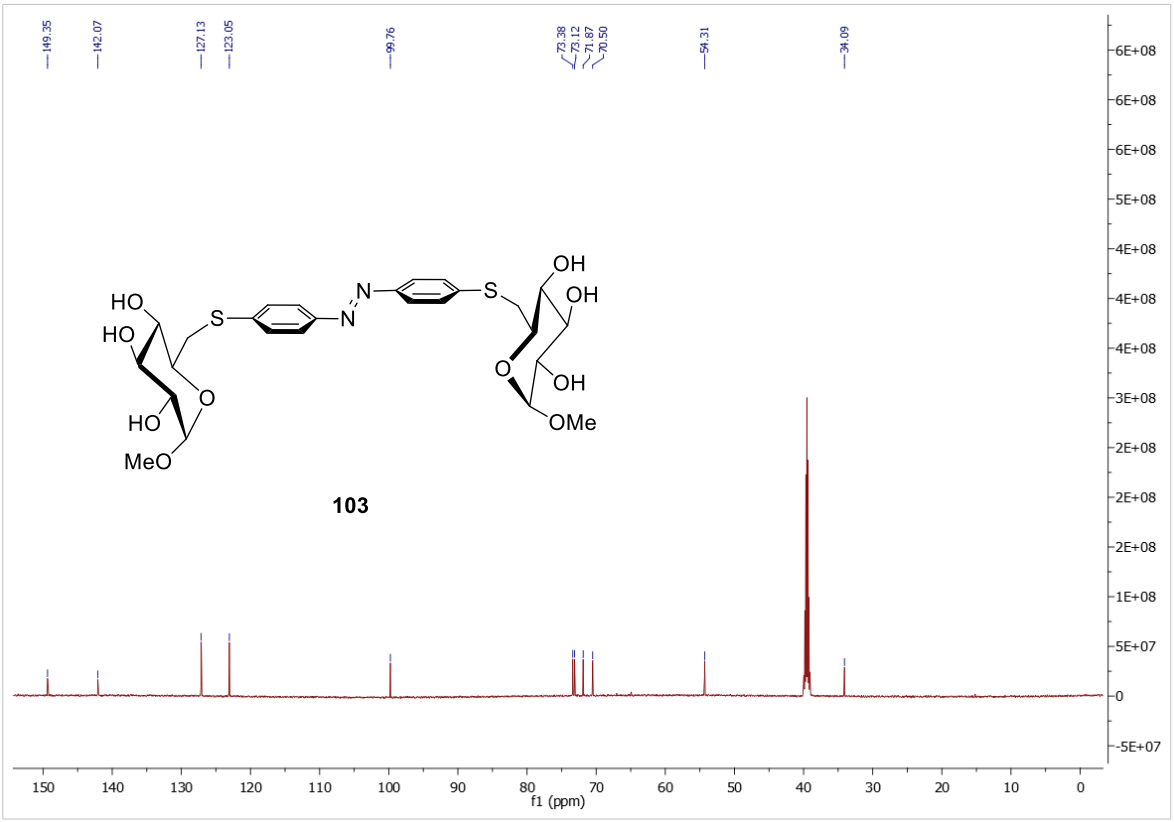

Figure 7.6.138. ^{13}C NMR spectrum of **103** (126 MHz, DMSO-d_6, 300 K).

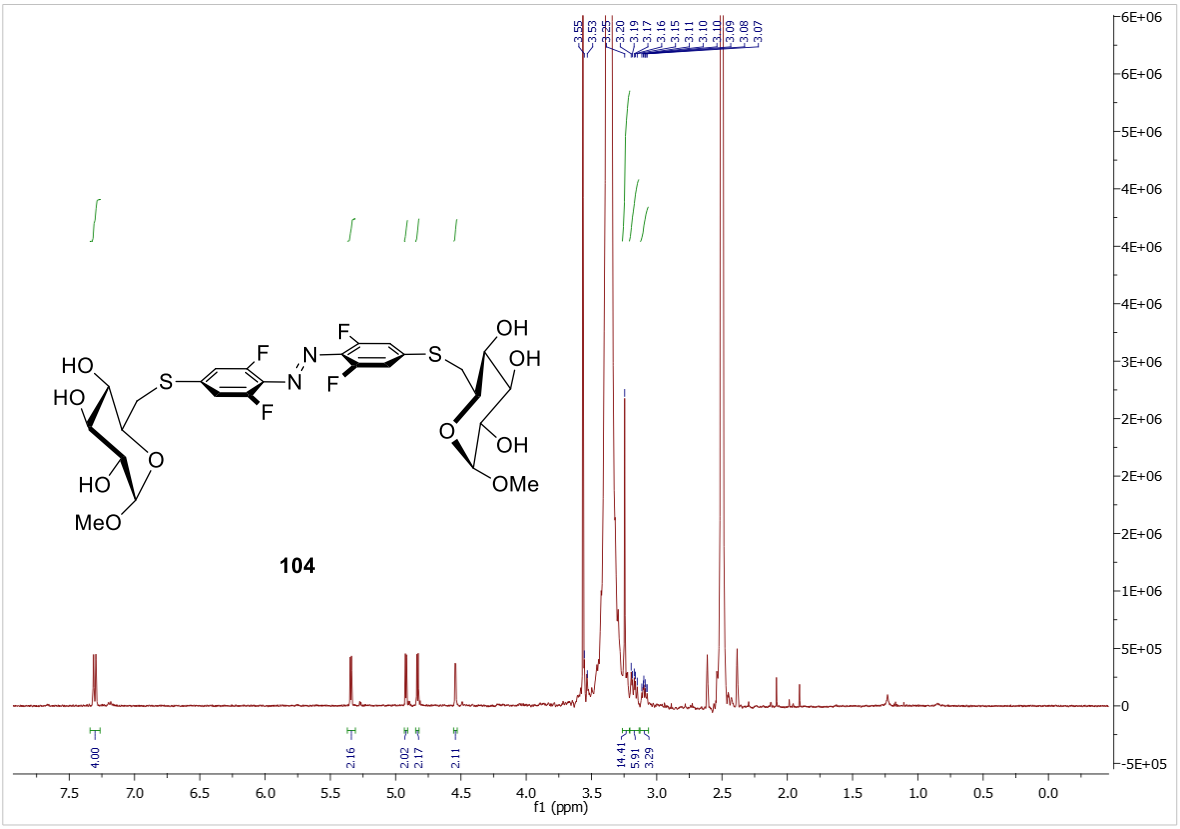

Figure 7.6.139. ^{1}H NMR spectrum of **104** (500 MHz, DMSO-d_6, 300 K).

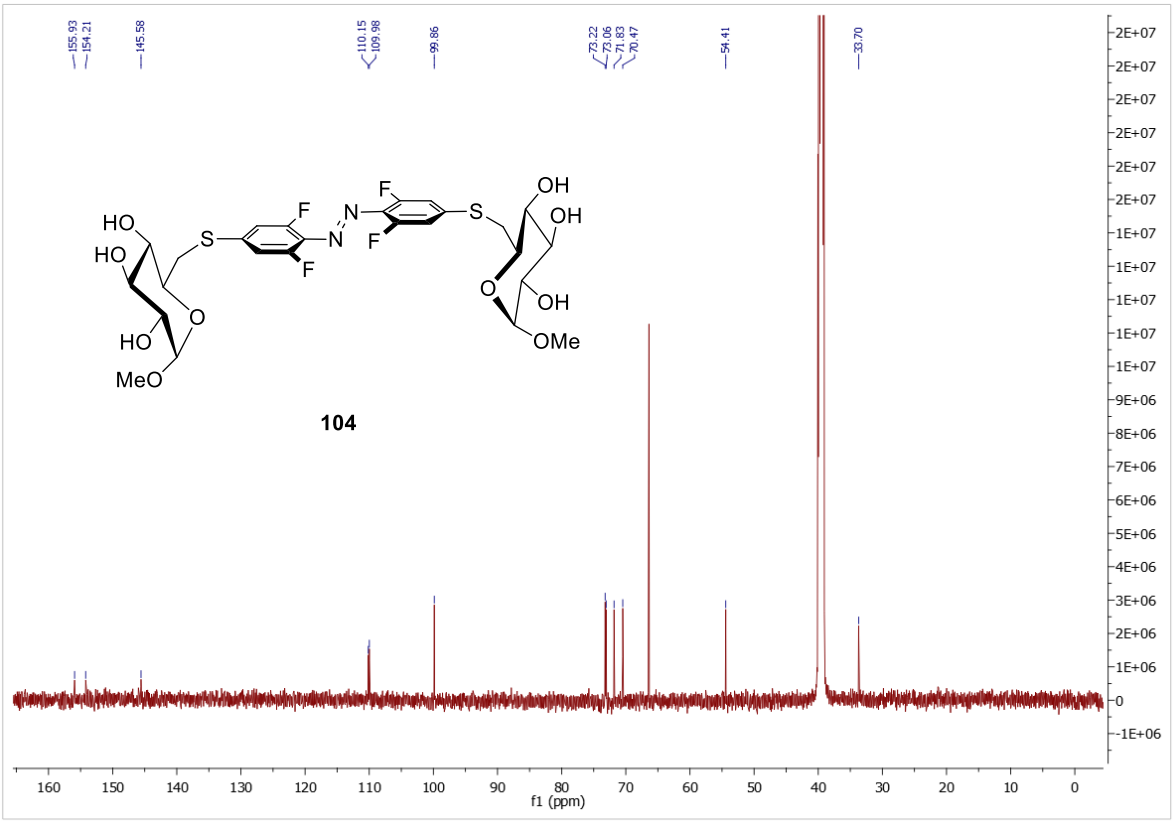

Figure 7.6.140. ^{13}C NMR spectrum of **104** (126 MHz, DMSO-d_6, 300 K).

8. References

1. A. R. Battersby, *Nat. Prod. Rep.*, **2000**, 17, 507–526.
2. (a) R. B. Woodward, *Pure Appl. Chem.*, **1973**, 33, 145-178; (b) A. Eschenmoser and C. E. Winter, *Science*, **1977**, 196, 1410–1420.
3. David J. Newman and Gordon M. Cragg, Chapter 1: Bioactive Macrocycles from Nature, in *Macrocycles in Drug Discovery*, J. Levin Ed., pp. 1–36, **2014.**
4. E. M. Driggers, S. P. Hale, J. Lee and N. K. Terrett, *Nature*, **2008**, 7, 608–624.
5. G. G. Zhanel, M. Dueck, D. J. Hoban, L. M. Vercaigne, J. M. Embil, A. S. Gin and J. A. Karlowsky, *Drugs*, **2001**, 61, 444–489.
6. F. Giordanetto and J. Kihlberg, *J. Med. Chem.* **2014**, 57, 278–295.
7. G. G. Zhanel, M. Walters, A. Noreddin, L. M. Vercaigne, A. Wierzbowski, J. M. Embil, A. S. Gin, S. Douthwaite and D. J. Hoban, *Drugs*, **2002**, 62, 1771–1795.
8. S. H. Joo, *Biomol. Ther.*, **2012**, 20, 19–26.
9. M. Rybak, B. Lomaestro, J. C. Rotschafer, R. Moellering, W. Craig, M. Billeter, J. R. Dalovisio and D. P. Levine, *Am. J. Health Syst. Pharm.* **2009**, 66, 82–98.
10. A. Okano, N. A. Isley, and D. L. Boger, *Proc. Natl. Acad. Sci.*, **2017**, 114, 5052–5061.
11. H. G. Kang, D. Zhang, N. Degauque, C. Mariat, S. Alexopoulos and X. X. Zheng, *Am. J. Transplant.*, **2007**, 1907–1916.
12. H. J. Kang and H. J. Park, *Biochemistry*, **2009**, 48, 31, 7392–7398.
13. J. M. Lehn, *Supramolecular Chemistry, Concepts and Perspectives*, Wiley-VCH, Weinheim, **1995**.
14. K. Ariga and T. Kunitake, *Supramolecular Chemistry, Fondamentals and Applications*, Springer, Heidelberg, **2006**.
15. (a) C. J. Pedersen, *Science*, **1988**, 241, 536–540; (b) C. J. Pedersen *J. Am. Chem. Soc. 1967, 89, 7017*–7036; (c) C. J. Pedersen, *J. Am. Chem. Soc.*, **1970**, 92, 386–391. (d) C. J. Pedersen, *J. Am. Chem. Soc.*, **1970**, 92, 391–394.15.
16. (a) K. Kim, ed. *Cucurbiturils and related macrocycles*. Vol. 28. Royal Society of Chemistry, **2019**; (b) M.-X. Wang, *Chem. Commun.*, **2008**, 4541–4551; (c) M. Xue, Y. Yang, X. Chi, Z. Zhang and F. Huang, *Acc. Chem. Res.*, **2012**, 45, 1294–1308; (d) P. Keehn, S. M. Rosenfeld, ed. *Cyclophanes*. Elsevier, **2012**; (e) M. J. MacLachlan, *Pure Appl. Chem.*, **2006**, 78, 873–888; (f) K. Miki and K. Ohe, *Chem. Eur. J.*, **2020**, 26, 2529–2575; (g) Y. Wang, H. Wu and J. F. Stoddart, *Acc. Chem. Res.*, **2021**, 54, 2027–2039; (f) Z. Liu, S. K. M. Nalluri and J. F. Stoddart, *Chem. Soc. Rev.*, **2017**, **46**, 2459–2478; (f) F. Coutrot, *Chemistry Open*, **2015**, 4, 556–576.
17. J. S. Rowlinson, *Nature*, **1973**, 244, 414–417.
18. R. U. Lemieux and U. Spohr, *Adv. Carbohydr. Chem. Biochem.*, **1994**, 50, 1–20.
19. P. Ehrlich, Experimental researches on specific therapy, **1907**. The collected papers of Paul Ehrlich, Vol. 3, Himmelweit, F., Ed., Pergamon, London, **1956**, 106–134.
20. D. J. Cram, *J. Incl. Phenom.*, **1988**, 6, 397–413.
21. D. J. Cram, S. Karbach, Y. H. Kim, L. Baczynskyj and G. W. Kallemeyn, *J. Am. Chem. Soc.*, **1985**, 107, 2575–2576.
22. D. J. Cram, *Science*, **1983**, 219, 1177–1183.

23. Juan Xie and Nicolas Bogliotti, *Chem. Rev.*, **2014**, 114, 7678–7739.

24. R. Pereda-Miranda, D. Rosas-Ramírez and J. Castañeda-Gómez, Resin Glycosides from the Morning Glory Family, *Progress in the Chemistry of Organic Natural Products*, Vol. 92, A.D. Kinghorn et al. (eds.), Springer-Verlag, Wien, **2010.**

25. L. Pouységu, D. Deffieux, G. Malik, A. Natangelo and S. Quideau, *Nat. Prod. Rep.*, **2011**, **28**, 853–874

26. (a) J. C. López, J. Plumet, *Eur. J. Org. Chem.*, **2011**, 1803–1825; (b) K. Khanbabaee and T. van Ree, *Synthesis*, **2001**, 11, 1585–1610; (c) S. B. Adhikari, A. Chen and G. Wang, *Molecules*, **2021**, 26, 3394–3420.

27. S. Jarosz and A. Listkowsk, *Curr. Org. Chem.*, **2006**, 10, 643–662.

28. I. Orbán, P. Bakó and Z. Rapi, *Chemistry*, **2021**, 3, 550–577.

29. M. A. Potopnyk and S. Jarosz, Nitrogen-Containing Macrocycles Having a Carbohydrate Scaffold, *Advances in Carbohydrate Chemistry and Biochemistry*, Vol 71, Derek Horton (ed.), Academic Press, Washington, **2014**.

30. G. Crini, *Chem. Rev.*, **2014**, 114, 10940−10975.

31. (a) A. Villiers, *C. R. Acad. Sci.*, **1891**, CXII, 435–437; (b) A. Villiers, *C. R. Acad. Sci.*, **1891**, CXII, 536-538.

32. (a) T. Loftsson and D. Duchêne, Int. J. Pharm., **2007**, 329, 1–11; (b) A. Gonzalez Pereira, M. Carpena, P. García Oliveira, J. C. Mejuto, M. A. Prieto and J. Simal Gandara, *Int. J. Mol. Sci.*, **2021**, 22, 1339–1362

33. F. Z. Schardinger, *Unters. Nahr. U. Genussm.*, **1903**, 6, 865–880.

34. K. Freudenberg and F. Cramer, *Z. Naturforsch.*, **1948**, 3b, 464.

35. (a) D. French, *Adv. Carbohydr. Chem.*, **1957**, 12, 189–260; (b) F. Cramer, Einschlussverbindungen. Springer-Verlag, Berlin, **1954**.

36. F. Cramer, W. Saenger and H.–CH. Spatz, H., *J. Am. Chem. Soc.*, **1967**, 89, 14–20.

37. B. D. Wagner, P. J. MacDonald and M. Wagner, *J. Chem. Ed.*, **2000**, 77, 178–181.

38. B. D. Wagner, Fluorescence studies of supramolecular host-guest inclusion complexes, *Handbook of Photochemistry and Photobiology*, H. S. Nalwa Ed., Vol. 3: Supramolecular Photochemistry, American Scientific Publishers, Los Angeles, **2003**.

39. B. D. Wagner, *Curr. Anal. Chem.*, **2007**, 3, 183–195.

40. J. Szejtli, *Chem. Rev.*, **1998**, 98, 1743–1753.

41. A. Matencio, S. Navarro-Orcajada, F. García-carmona and J. M. López-Nicolás, Trends Food Sci. Technol., **2020**, 104, 132–143.

42. (a) N. Sharma, A. Baldi, *Drug Deliv.*, **2016**, 23, 729–747; (b) M. A. Rouf, I. Vural, E. Bilensoy, A. Hincal and D. D. Erol, *J. Incl. Phenom. Macrocycl. Chem.*, **2011**, 70, 167–175; (c) M. S. S. B. Monteiro, R. A. Ozzetti, A. L. Vergnanini, L. de Brito-Gitirana, N. M. Volpato, Z. M. F. de Freitas, E. Ricci-Júnior and E. P. dos Santos, *Int. J. Nanomed.* **2012**, 7, 3045–3058; (d) H.-J. Buschmann and E. Schollmeyer, *J. Cosmet. Sci.*, **2002**, 53, 185–191.

43. M. Naguib, *Anesth. Analg.*, **2007**, 104, 575–581.

44. L. Szente and J. Szemán, *Anal. Chem.*, **2013**, 85, 8024–8030.

45. E. Schneiderman and A. M. Stalcup, *J. Chromatogr. B*, **2000**, 745, 83–102.

46. T. Ogoshi and A. Harada, *Sensors,* **2008**, 8, 4961–4982.

47. (a) P. B. Savage, W. D. Thomas and N. K. Dalley, *J. Incl. Phenom.*, **1997**, 29, 335–346; (b) J. C. Morales and S. Penadés, *Angew. Chem. Int. Ed.*, **1998**, 37, 654–657; (c) J. C. Morales, D. Zurita and S. Penadés, *J. Org. Chem.*, **1998**, 63, 9212–9222.

48. R. R. Bukownik and C. S. Wilcox, *J. Org. Chem.*, **1988**, 53, 463–471.

49. F. Diederich, *Angew. Chem. Int. Ed. Engl.*, **1988**, 27, 362–386.

50. D. Doyle and P. V. Murphy, *Carbohydr. Res.*, **2008**, 343, 2535–2544.43.

51. (a) C. S. Wilcox, M. D. Cowan, *Carbohydr. Res.*, **1987**, 171, 141–160; (b) A. G. M. Barret and N. S. Maní, *Tetrahedron Lett.*, **1987**, 28, 6133–6136; (c) C. Vincent, M. Martín-Lomas and S. Penadés, *Tetrahedron*, **1989**, 45, 3605–3612; (d) S. Penadés and J. M. Coterón, *J. Chem. Soc., Chem. Commun.,* **1992**, 683–684.

52. J. M. Goterón, C. Vicent, C. Bosso and S. Penadés, *J. Am. Chem. Soc.***, 1993**, 115, 10066–10076.

53. J. Jimenez-Barbero, E. Junquera, M. Martin-Pastor, S. Sharma, C. Vicent and S. Penadés, *J. Am. Chem. Soc.*, **1995**, 117, 11198–11204.

54. T. Velasco-Torrijos and P. V. Murphy, *Tetrahedron Asymmetry*, **2005**, 16, 261–272.

55. (a) D. V. Jarikote, W. Li, T. Jiang, L. A. Eriksson and P. V. Murphy, *Bioorg. Med. Chem.*, **2011**, 19, 826–835; (b) Paul V. Murphy, S. André and H.-J. Gabius, *Molecules,* **2013**, *18*, 4026–4053.

56. J. Fritzsche. *Comptes Rendus Acad. Sci.*, Paris, **1867**, 69, 1035.

57. W. Markwald. *Z. Phys. Chem*., **1899**, 30, 140.

58. Y. Hirshberg. *Compt. Rend. Acad. Sci*., Paris, **1950**, 231, 903.

59. H. Bouas-Laurent and H. Dürr, *Pure Appl. Chem.*, **2001**, 73, 4, 639–665.

60. Heinz Durr and Henri Bouas-Laurent (Eds), *Photochromism: Molecules and systems*, Studies in Organic Chemistry 40, Elsevier, Amsterdam, **2003**.

61. R. Exelby and R. Grinter, *Chem. Rev.*, **1965**, 65, 2, 247–260.

62. P. D. Kiser, M. Golczak, A. Maeda, K. Palczewski, *Biochimica et Biophysica Acta* **2012**, 1821, 137–151.

63. G. Fuks, J. Heiser, E. Moulin, A. Perrot, X. Yao and N. Giuseppone, *Chem. Rev.*, **2020**, 120, 310–433.

64. (a) C. Brieke, F. Rohrbach, A. Gottschalk, G. Mayer, A. Heckel, *Angew. Chem. Int. Ed.*, **2012**, 51, 8446–8476; (b) G. Mayer, A. Heckel, *Angew. Chem. Int. Ed.*, **2006**, 45, 4900–4921.

65. (a) M.-M. Russew and S. Hecht, *Adv. Mater.*, **2010**, 22, 3348–3360; (b) A. Goulet-Hanssens, F. Eisenreich and S. Hecht, *Adv. Mater.*, **2020**, 32, 1905966. (c) J. Boelke and S. Hecht, *Adv. Optical Mater.*, **2019**, 7, 1900404.

66. (a) Z. L. Pianowski, *Chem. Eur. J.*, **2019**, 25, 5128–5144; (b) W. Szymański, J. M. Beierle, H. A. V. Kistemaker, W. A. Velema and B. L. Feringa, *Chem. Rev.* **2013**, 113, 6114–6178.

67. (a) T. Fehrentz, M. Schönberger, Dirk Trauner, *Angew. Chem. Int. Ed.*, **2011**, 50, 12156–12182; (b)W. A. Velema, W. Szymanski and B. L. Feringa, *J. Am. Chem. Soc.*, **2014**, 136, 2178−2191; (c) J. Broichhagen, J. A. Frank and D. Trauner, *Acc. Chem. Res.*, **2015**, 48, 1947–1960; (d) M. M. Lerch, M. J. Hansen, G. M. van Dam, W. Szymanski and B. L. Feringa, *Angew. Chem. Int. Ed.*, **2016**, 55, 10978–10999; (e) K. Hüll, J. Morstein and D. Trauner, *Chem. Rev.*, **2018**, 118, 10710−10747; (d) M. J. Fuchter, *J. Med. Chem.*, **2020**, 63, 11436−11447.

68. C. Dugave and L. Demange, *Chem. Rev.*, **2003**, 103, 2475–2532.

69. R. N. Beale and E. M. F. Roe, *J. Chem. Soc.*, **1953**, 2755–2763.

70. (a) D. H. Waldeck, *Chem. Rev.*, **1991**, 91, 415–436; (b) W.-G. Han, T. Lovell, T. Liu and L. Noodleman, *Chem. Phys. Chem.*, **2002**, 3, 167–178.

71. (a) F. B. Mallory, C. S. Wood and J. T. Gordon, *J. Am. Chem. Soc.*, **1964**, 86, 3094–3102; (b) K. B. Jørgensen, *Molecules,* **2010**, *15*, 4334–4358.

72. D. Villarón and S. J. Wezenberg, *Angew. Chem. Int. Ed.*, **2020**, 59, 13192–13202.

73. M. Irie, T. Fukaminato, K. Matsuda and S. Kobatake, *Chem. Rev.*, **2014**, 114, 12174−12277.

74. B. L. Feringa, *Acc. Chem. Res.*, **2001**, 34, 504–513.

75. J. C. Splitstoser, T. D. Dillehay, J. Wouters and A. Claro, *Sci. Adv.*, **2016**, 2, e1501623.

76. (a) A. Baeyer, *Ber. Dtsch. Chem. Ges.*, **1883**, 16, 2188– 2204; (b) H. Schmidt, *Chemie in unserer Zeit*, **1997**, 3, 121−128.

77. (a) G. M. Wyman, *J. Chem. Soc. D*, **1971**, 1332– 1334; (b) J. Pina, D. Sarmento, M. Accoto, P. L. Gentili, L. Vaccaro, A. Galvão, J. S. Seixas de Melo, *J. Phys. Chem. B*, **2017**, 121, 2308– 2318.

78. C. Petermayer and H. Dube, *Acc. Chem. Res.*, **2018**, 51, 1153–1163.

79. B. Koeppe and F. Römpp, *Chem. Eur. J.*, **2018**, 24, 14382–14386.

80. C.-Y. Huang, A. Bonasera, L. Hristov, Y. Garmshausen, B. M. Schmidt, D. Jacquemin and S. Hecht, *J. Am. Chem. Soc.*, **2017**, 139, 15205–15211.

81. S. Wiedbrauk and H. Dube, *Tetrahedron Letters*, **2015**, 56, 4266–4274.

82. M. W. H. Hoorens, M. Medved', A. D. Laurent, M. Di Donato, S. Fanetti, L. Slappendel, M. Hilbers, B. L. Feringa, W. Jan Buma and W. Szymanski, *Nature Communications*, **2019**, 10, 2390.

83. B. L. Feringa and H. Wynberg, *J. Am. Chem. Soc.*, **1977**, 99, 602–603.

84. B. L. Feringa, *J. Org. Chem.*, **2007**, 72, 6635–6652.

85. R. A. van Delden, M. K. J. ter Wiel and Ben L. Feringa, *Chem. Comm.*, **2004**, 200–201.

86. (a) J. M. Abendroth, O. S. Bushuyev, P. S. Weiss and C. J. Barrett, *ACS Nano*, **2015**, 9, 7746–7768. (b) B. L. Feringa *Acc. Chem. Res.*, **2001**, 34, 504–513.

87. S. F. Pizzolato, B. S. L. Collins, T. van Leeuwen and B. L. Feringa, *Chem. Eur. J.*, **2017**, 23, 6174–6184.

88. (a) H. Stobbe, *Ber. Dtsch. Chem. Ges.*, **1905**, 38, 3673−3682; (b) H. Stobbe, *Liebigs Ann. Chem.*, **1911**, 380, 1−129.

89. A. Santiago and R. S. Becker, *J.Am.Chem.Soc.*, **1968**, 52, 3654−3658.

90. Y. Yokoyama, *Chem. Rev.* **2000**, 100, 1717–1740.

91. Y. Yokoyama and Y. Kurita, *Mol. Cryst. Liq. Cryst.*, **1994**, 246, 87–94.

92. B. Yao, Y. Wang, N. Menke, M. Lei, Y. Zheng, L. Ren, G. Chen, Y. Chen and M. Fan, *Mol. Cryst. Liq. Cryst.*, **2005**, 430, 211–219.

93. J. Walz, K. Ulrich, H. Port, H. C. Wolf, J. Wonner and F. Effenberger, *Chem. Phys. Lett.*, **1993**, 213, 321−324.

94. I. Willner, S. Rubin, J. Wonner, F. Effenberger and P. Bäuerle, *J. Am. Chem. Soc.*, **1992**, 114, 3150−3151.

95. S. Nakamura and M. Irie, *J. Org. Chem*., **1988**, 53, 6136−6138.

96. M. Irie and M. Mohri, *J. Org. Chem.*, **1988**, 53, 803−808.

97. M. Hanazawa, R. Sumiya, Y. Horikawaa and M. lrie, *J. Chem. Soc., Chem. Commun.*, **1992**, 206−207.

98. M. Irie, *Chem. Rev.*, **2000**, 100, 1685–1716.

99. H. Tian and Y. Feng, *J. Mater. Chem.*, **2008**, 18, 1617–1622.

100. S.-Z. Pu, Q. Sun, C.-B. Fan, R.-J. Wang, and G. Liu, *J. Mater. Chem. C*, **2016**, 4, 3075– 3093.

101. E. C. Harvey, B. L. Feringa, J. G. Vos, W. R. Browne and M. T. Pryce, *Coord. Chem. Rev.*, **2015**, 282–283, 77– 86.

102. X. Yao, T. Li, J. Wang, X. Ma and H. Tian, *Adv. Opt. Mater.*, **2016**, 4, 1322–1349.

103. L. Kortekaas and W. R. Browne, *Chem. Soc. Rev.*, **2019**, 48, 3406–3424.

104. J. H. Day, *Chem. Rev.*, **1963**, 63, 65–80.

105. A. Mustafa, *Chem. Rev.*, **1948**, 43, 509–523.

106. R. Klajn, *Chem. Soc. Rev.*, **2014**, 43, 148-184.

107. J. Yan, L.-X. Zhao, C. Li, Zhe Hu, G.-F. Zhang, Z.-Q. Chen, T. Chen, Z.-L. Huang, J. Zhu and M.-Q. Zhu, *J. Am. Chem. Soc.*, **2015**, 137, 2436–2439.

108. M.-Q. Zhu, L. Zhu, J. J. Han, W. Wu, J. K. Hurst and A. D. Q. Li, *J. Am. Chem. Soc.*, **2006**, 128, 4303–4309.

109. (a) H. Xia, K. Xie and G. Zou, *Molecules,* **2017**, *22*, 2236–2252; (b) G. Berkovic, V. Krongauz, and V. Weiss, *Chem. Rev.*, **2000**, 100, 1741–1754.

110. (a) D. R. Wenz and J. Read de Alaniz, *Org. Lett.* **2013**, 15, 3250–3253; (b) S. Helmy, S. Oh, F. A. Leibfarth, C. J. Hawker and Javier Read de Alaniz, *J. Org. Chem.* **2014**, 79, 11316–11329; (c) S. Helmy, F. A. Leibfarth, S. Oh, J. E. Poelma, C. J. Hawker and J. Read de Alaniz, *J. Am. Chem. Soc.*, **2014**, 136, 8169–8172.

111. J. Stenhouse, *Justus Liebigs Ann. Chem.*, **1850**, 74, 278–297.

112. (a) C. Piutti and F. Quartieri, *Molecules*, **2013**, 18, 12290–12312; (b) O. Nieto Faza, C. Silva López, R. Álvarez and Á. R. de Lera, *Chem. Eur. J.*, **2004**, 10, 4324–4333.

113. M. M. Lerch, W. Szymański and B. L. Feringa, *Chem. Soc. Rev.*, **2018**, 47, 1910–1937.

114. R. Castagna, G. Maleeva, D. Pirovano, C. Matera and P. Gorostiza, *J. Am. Chem. Soc.*, **2022**, 144, 15595–15602.

115. M. M. Lerch, M. J. Hansen, W. A. Velema, W. Szymański and B. L. Feringa, *Nat. Commun.*, **2016**, 7, 12054–12064.

116. S. Jia, J. D. Du, A. Hawley, W.-K. Fong, B. Graham and B. J. Boyd, *Langmuir*, **2017**, 33, 2215–2221.

117. S. Singh, K. Friedel, M. Himmerlich, Y. Lei, G. Schlingloff and A. Schober, *ACS Macro Lett.*, **2015**, 4, 1273–1277.

118. S. O. Poelma, S. S. Oh, S. Helmy, A. S. Knight, G. L. Burnett, H. T. Soh, C. J. Hawker and J. Read de Alaniz, *Chem. Commun.*, **2016**, 52, 10525–10528.

119. D. Wang, L. Zhao, H. Zhao, J. Wu, M. Wagner, W. Sun, X. Liu, M. Miao and Y Zheng, *Commun. Chem.*, **2019**, 2, 1–8.

120. (a) H. M. D. Bandara and S. C. Burdette, *Chem. Soc. Rev.*, **2012**, 41, 1809–1825; (b) E. Merino, *Chem. Soc. Rev.*, **2011**, 40, 3835–3853.

121. (a) A. Nobel, *Justus Liebigs Ann. Chem.*, **1856**, 98, 253–256; (b) P. Griess, *Liebigs Ann. Chem.*, **1858**, 106, 123–125; (c) C. Martius and P. Griess, *Zeitschrift für Chemie*, **1862**, 2, 689.

122. G. S. Hartley, *Nature*, **1937**, 140, 281.

123. A. Bafana, S. S. Devi and T. Chakrabarti, *Environ. Rev.*, **2011**, 19, 350–371.

124. J. A. Bouwstra, A. Schouten and J. Kroon, *Acta Crystallogr. Sect. C*, **1983**, 39, 1121–1123.

125. A. Mostad and C. Romming, *Acta Chem. Scand.* **1971**, 25, 3561–3568.

126. (a) J. Griffiths, *Chem. Soc. Rev.*, **1972**, 1, 481–493.

127. R. Turansky, M. Konopka, N. L. Doltsinis, I. Stich and D. Marx, *Phys. Chem. Chem. Phys.*, **2010**, 12, 13922–13932.

128. (a) J. Henzl, M. Mehlhorn, H. Gawronski, K.-H. Rieder and K. Morgenstern, *Angew. Chem. Int. Ed.*, **2006**, 45, 603–606; (b) X. Tong, M. Pelletier, A. Lasia and Y. Zhao, *Angew. Chem. Int. Ed.*, **2008**, 47, 3596–3599.

129. T. Cusati, G. Granucci, M. Persico and G. Spighi, *J. Chem. Phys.*, **2008**, 128, 194311–194319.

130. (a) P. Hamm, S. M. Ohline and W. Zinth, *J. Chem. Phys.*, **1997**, 106, 519–529; (b) I. K. Lednev, T. Q. Ye, P. Matousek, M. Towrie, P. Foggi, F. V. R. Neuwahl, S. Umapathy, R. E. Hester and J. N. Moore, *Chem. Phys. Lett.*, **1998**, 290, 68–74.

131. M. Quick, A. L. Dobryakov, M. Gerecke, C. Richter, F. Berndt, I. N. Ioffe, A. A. Granovsky, R. Mahrwald, N. P. Ernsting and S. A. Kovalenko, *J. Phys. Chem. B*, **2014**, 118, 8756–8771.

132. J. L. Magee, W. Shand Jr. and H. Eyring, *J. Am. Chem. Soc.*, **1941**, 63, 677–688.

133. D. Y. Curtin, E. J. Grubbs and C. G. McCarty, *J. Am. Chem. Soc.*, **1966**, 88, 2775–2786.

134. (a) H. M. D. Bandara, T. R. Friss, M. M. Enriquez, W. Isley, C. Incarvito, H. A. Frank, J. Gascon and S. C. Burdette, *J. Org. Chem.*, **2010**, 75, 4817–4827; (b) Y.-W. Hao, H.-Y. Wang, Y.-J. Huang, B.-R. Gao, Q.-D. Chen, L.-B. Li and H.-B. Sun, *J. Mater. Chem. C*, **2013**, 1, 5244–5249.

135. (a) J. K. Yu, C. Bannwarth, R. Liang, E. G. Hohenstein and T. J. Martínez, *J. Am. Chem. Soc.*, **2020**, 142, 20680–20690; (b) E. M. M. Tan, S. Amirjalayer, S. Smolarek, A. Vdovin, F. Zerbetto and W. Jan Buma, *Nat. Commun.*, **2015**, 5860–5867.

136. (a) R. S. H. Liu and A. E. Asato, *Proc. Natl. Acad. Sci.*, **1985**, 82, 259–263; (b) R. S. H. Liu and G. S. Hammond, *Proc. Natl. Acad. Sci.*, **2000**, 97, 11153–11158; (b) R. S. H. Liu, G. S. Hammond, *Chem. Eur. J.*, **2001**, 7, 4537–4544; (c) A. Gerwien, M. Schildhauer, S. Thumser, P. Mayer and H. Dube, *Nat. Commun.*, **2018**, 9, 2510–2519.

137. F. Serra and E. M. Terentjev, *Macromolecules*, **2008**, 41, 981–986.

138. (a) C.-W. Chang, Y.-C. Lu, T.-T. Wang and E. W.-G. Diau, *J. Am. Chem. Soc.*, **2004**, 126, 10109–10118 (b) N. Biswas and S. Umapathy, *J. Chem. Phys.*, **1997**, 107, 7849–7858.

139. T. Fujino and T. Tahara, *J. Phys. Chem. A*, **2000**, 104, 4203–4210.

140. F. Aleotti, L. Soprani, A. Nenov, R. Berardi, A. Arcioni, C. Zannoni and M. Garavelli**,** *J. Chem. Theory Comput.* **2019**, 15, 6813–6823.

141. A. Nenov, R. Borrego-Varillas, A. Oriana, L. Ganzer, F. Segatta, I. Conti, J. Segarra-Marti, J. Omachi, M. Dapor, S. Taioli, C. Manzoni, S. Mukamel, G. Cerullo and M. Garavelli, *J. Phys. Chem. Lett.* **2018**, 9, 1534–1541.

142. (a) H. Rau and E. Lueddecke, *J. Am. Chem. Soc.*, **1982**, 104, 1616–1620; (b) Y.-C. Lu, E. W.-G. Diau and H. Rau, *J. Phys. Chem. A*, **2005**, 109, 2090–2099; (c) R. Siewertsen, H. Neumann, B.

Buchheim-Stehn, R. Herges, C. Näther, F. Renth and F. Temps, *J. Am. Chem. Soc.* **2009**, 131, 15594–15595; (d) W. Moormann, T. Tellkamp, E. Stadler, F. Röhricht, C. Näther, R. Puttreddy, K. Rissanen, G. Gescheidt, R. Herges, *Angew. Chem. Int. Ed.*, **2020**, 59, 15081–15086.

143. (a) C. Ciminelli, G. Granucci and M. Persico, *J. Chem. Phys.*, **2005**, 123, 174317–174327; (b) C. Nonnenberg, H. Gaub and I. Frank, *Chem. Phys. Chem.*, **2006**, 7, 1455–1461; (c) R. Siewertsen, J. Boyke Schönborn, B. Hartke, F. Renth and F. Temps, *Phys. Chem. Chem. Phys.*, **2011**, 13, 1054–1063.

144. H. Rau, in *Photochromism: Molecules and Systems*, ed. H. Duerr and H. Bouas-Laurent, Elsevier, Amsterdam, Revised edn, **2003**, pp. 165–192.

145. (a) F. A. Jerca, V. V. Jerca, D. F. Anghel, G. Stinga, G. Marton, D. S. Vasilescu and D. M. Vuluga, *J. Phys. Chem. C*, **2015**, 119, 10538–10549; (b) V. V. Jerca, F. A. Jerca, I. Rau, A. M. Manea, D. M. Vuluga, F. Kajzar, *Optical Materials*, **2015**, 48, 160–164.

146. (a) D. G. Whitten, P. D. Wildes, J. G. Pacifici and G. Irick, Jr, *J. Am. Chem. Soc.*, **1971**, 93, 2004–2008; (b) A. A. Blevins and G. J. Blanchard, *J. Phys. Chem. B*, **2004**, 108, 4962–4968.

147. (a) J. Garcia-Amorós, S. Nonell and D. Velasco, *Chem. Commun.*, **2012**, 48, 3421–3423; (b) J. García-Amorós and D. Velasco, *Beilstein J. Org. Chem.* **2012,** 8, 1003–1017; (c) J. Garcia-Amorós, M. Díaz-Lobo, S. Nonell, D. Velasco, *Angew. Chem.*, **2012**, 124, 12992–12995; (d) J. Garcia-Amorós, B. Maerz, M. Reig, A. Cuadrado, L. Blancafort, E. Samoylova and D. Velasco, *Chem.Eur.J.*, **2019**, 25, 7726–7732.

148. J. Garcia-Amorós, A. Sánchez-Ferrer, W. A. Massad, S. Nonell and D. Velasco, *Phys. Chem. Chem. Phys.*, **2010**, 12, 13238–13242.

149. (a) A. A. Beharry and G. A. Woolley, *Chem. Soc. Rev.*, **2011**, 40, 4422–4437; (b) M. Dong, A. Babalhavaeji, S. Samanta, A. A. Beharry and G. A. Woolley, *Acc. Chem. Res.*, **2015**, 48, 2662–2670.

150. O. Sadovski, A. A. Beharry, F. Zhang and G. A. Woolley, *Angew. Chem. Int. Ed.*, **2009**, 48, 1484–1486.

151. A. A. Beharry, O. Sadovski, and G. A. Woolley, *J. Am. Chem. Soc.*, **2011**, 133, 19684–19687.

152. S. Samanta, T. M. McCormick, S. K. Schmidt, D. S. Seferos and G. A. Woolley, *Chem. Commun.*, **2013**, 49, 10314–10316.

153. M. Dong, A. Babalhavaeji, C. V. Collins, K. Jarrah, O. Sadovski, Q. Dai and G. A. Woolley, *J. Am. Chem. Soc.*, **2017**, 139, 13483–13486.

154. D. Bleger, J. Schwarz, A. M. Brouwer and S. Hecht, *J. Am. Chem. Soc.*, **2012**, 134, 20597–20600.

155. C. Knie, M. Utecht, F. Zhao, H. Kulla, S. Kovalenko, A. M. Brouwer, P. Saalfrank, S. Hecht and D. Bleger, *Chem. Eur. J.*, **2014**, 20, 16492–16501.

156. (a) S. Samanta, A. A. Beharry, O. Sadovski, T. M. McCormick, A. Babalhavaeji, V. Tropepe and G. A. Woolley, *J. Am. Chem. Soc.*, **2013**, 135, 9777–9784; (b) L. N. Lameijer, S. Budzak, N. A. Simeth, M. J. Hansen, B. L. Feringa, D. Jacquemin and W. Szymanski, *Angew. Chem. Int. Ed.*, **2020**, 59, 21663–21670.

157. (a) A. Rullo, A. Reiner, A. Reiter, D. Trauner, E. Y. Isacoff and G. A. Woolley, *Chem. Commun.*, **2014**, *50*, 14613–14615; (b) D. B. Konrad, J. A. Frank and D. Trauner, *Chem. Eur. J.*, **2016**, *22*, 4364–4368; (c) M. Wegener, M. J. Hansen, A. J. M. Driessen, W. Szymanski and B. L. Feringa, *J. Am. Chem. Soc.*, **2017**, *139*, 17979–17986; (d) A. Kerckhoffs, Z. Bo, S. E. Penty, F. Duarte and Matthew J. Langton, *Org. Biomol. Chem.*, **2021**, 19, 9058–9067.

158. D. B. Konrad, G. Savasci, L. Allmendinger, D. Trauner, C. Ochsenfeld and A. M. Ali, *J. Am. Chem. Soc.*, **2020**, 142, 6538–6547.

159. (a) Z. Ahmed, A. Siiskonen, M. Virkki and A. Priimagi *Chem. Commun.*, **2017**, 53, 12520–12523; (b) K. Kuntze, J. Viljakka, E. Titov, Z. Ahmed, E. Kalenius, P. Saalfrank and A. Priimagi, *Photochem. Photobiol. Sci*., **2022**, 21, 159–173.

160. M. Hammerich, C. Schütt, C. Stähler, P. Lentes, F. Röhricht, R. Höppner and R. Herges, *J. Am. Chem. Soc.*, **2016**, 138, 13111–13114.

161. (a) P. Lentes, E. Stadler, F. Röhricht, A. Brahms, J. Gröbner, F. D. Sönnichsen, G. Gescheidt and R. Herges, *J. Am. Chem. Soc.*, **2019**, 141, 13592–13600; (b) P. Lentes, P. Frühwirt, H. Freißmuth, W. Moormann, F. Kruse, G. Gescheidt and R. Herges, *J. Org. Chem.*, **2021**, 86, 4355–4360.

162. M. Saha, S. Ghosh and S. Bandyopadhyay, *New J. Chem.*, **2018**, 42, 10784–10790.

163. M. S. Maier, K. Hüll, M. Reynders, B. S. Matsuura, P. Leippe, T. Ko, L. Schäffer and D. Trauner, *J. Am. Chem. Soc.*, **2019**, 141, 17295–17304.

164. S. Crespi, N. A. Simeth and B. König, *Nat. Rev. Chem.*, **2019**, 3, 133–146.

165. M. Endo, K. Nakayama, Y. Kaida and T. Majima, *Tetrahedron Letters*, **2003**, 44, 6903–6906.

166. (a) J. Otsuki, K. Suwa, K. Narutaki, C. Sinha, I. Yoshikawa and K. Araki, *J. Phys. Chem. A*, **2005**, 109, 8064–8069; (b) J. Otsuki, K. Suwa, K. K. Sarker and C. Sinha, *J. Phys. Chem. A*, **2007**, 111, 1403–1409.

167. J. Calbo, C. E. Weston, A. J. P. White, H. S. Rzepa, J. Contreras-García and M. J. Fuchter, *J. Am. Chem. Soc.*, **2017**, 139, 1261–1274.

168. T. Wendler, C. Schütt, C. Näther and R. Herges, *J. Org. Chem.*, **2012**, 77, 3284–3287.

169. C. E. Weston, R. D. Richardson, P. R. Haycock, A. J. P. White and M. J. Fuchter, *J. Am. Chem. Soc.*, **2014**, 136, 11878–11881.

170. J. Calbo, A. R. Thawani, R. S. L. Gibson, A. J. P. White and M. J. Fuchter, *Beilstein J. Org. Chem.*, **2019,** 15, 2753–2764.

171. (a) L. Stricker, E.-C. Fritz, M. Peterlechner, N. L. Doltsinis and B. Jan Ravoo, *J. Am. Chem. Soc.*, **2016**, 138, 4547–4554; (b) N. A. Simeth, S. Crespi, M. Fagnoni and B. König, *J. Am. Chem. Soc.*, **2018**, 140, 2940–2946; (c) C. Slavov, C. Yang, A. H. Heindl, H. A. Wegner, A. Dreuw and J. Wachtveitl, *Angew. Chem. Int. Ed.*, **2020**, 59, 380–387; (d) Z.-Y. Zhang, Y. He, Y. Zhou, C. Yu, L. Han and T. Li, *Chem. Eur. J.*, **2019**, 25, 13402–13410; (e) Y. He, Z. Shangguan, Z.-Y. Zhang, M. Xie, C. Yu and T. Li, *Angew. Chem. Int. Ed.*, **2021**, 60, 16539–16546; (f) J. Simke, T. Bösking and B. Jan Ravoo, *Org. Lett.*, **2021**, 23, 7635–7639.

172. (a) F. Hamon, F. Djedaini-Pilard, F. Barbot and C. Len, *Tetrahedron*, **2009**, 65, 10105–10123; (b) E. Merino, *Chem. Soc. Rev.*, **2011**, 40, 3835–3853.

173. M. Barbero, I. Degani, S. Dughera, R. Fochi, P. Perracino, *Synthesis*, **1998**, 1235–1237.

174. D. Y. Curtin and J. L. Tveten, *J. Org. Chem.*, **1961**, 26, 1764–1768.

175. W. P. Neumann and C. Wicenec, *Chem. Ber.*, **1991**, 124, 2297–2301.

176. M. J. Hansen, M. M. Lerch, W. Szymanski and B. L. Feringa, *Angew. Chem. Int. Ed.*, **2016**, 55, 13514–13518.

177. (a) A. Baeyer, *Chem. Ber*. **1974**, 7, 1638–1840; (b) C. Mills*, J. Chem. Soc. Trans.*, **1895***,* 67*,* 925–933*.*

178. B. G. Gowenlock and G. B. Richter-Addo, *Chem. Rev.*, **2004**, 104, 3315–3340.

179. B. Priewisch and K. Rück-Braun, *J. Org. Chem.*, **2005**, 70, 2350–2352.

180. R. F. Nystrom and W. G. Brown, *J. Am. Chem. Soc.*, **1948**, 70, 3738–3740.

181. (a) T. Tellkamp, J. Shen, Y. Okamoto and R. Herges, *Eur*. *J*. *Org*. *Chem*., **2014**, 25, 5456–5461; (b) W. Moormann, D. Langbehn and R. Herges, *Synthesis*, **2017**, 49, 3471–3475.

182. S. Ameerunisha and P. S. Zacharias, *J. Chem. Soc., Perkin Trans. 2*, **1995**, 1679–1682.

183. G. R. Srinivasa, K. Abiraj and D. Channe Gowda, *Aust. J. Chem.*, **2004**, 57, 609–610.

184. B. Ortiz, P. Villanueva and F. Walls, *J. Org. Chem.*, **1972**, 37, 2748–2750.

185. H. K. Hombrecher and K. Lüdtke, *Tetrahedron*, **1993**, 49, 9489–9494.

186. K. Orito, T. Hatakeyama, M. Takeo, S. Uchiito, M. Tokuda and H. Suginome, *Tetrahedron*, **1998**, 54, 8403–8410.

187. N. A. Noureldin and J. W. Bellegarde, *Synthesis*, **1999**, 6, 939–942.

188. J. C. Stowell and C. M. Lau, *J. Org. Chem.*, **1986**, 51, 1614–1615.

189. A. A. John and Q. Lin, *J. Org. Chem.*, **2017**, 82, 9873–9876.

190. (a) S. Schultzke, M. Walther and A. Staubitz, *Molecules*, **2021**, 26, 3916–3929; (b) J. Berry, T. K. Lindhorst and G. Despras, *Chem*. *Eur*. *J*., **2022**, 28, e202200354.

191. G. G. Furin, *Russ. Chem. Rev.*, **1987**, 56, 532–545.

192. H. M. Nanjundaswamy and M. A. Pasha, *Synth. Commun.*, **2005**, 35, 2163–2168.

193. D. Konwar, R. C. Boruah and J. S. Sandhu, *Synthesis*, **1990**, 4, 337–339.

194. A. Saini, S. Kumar and J. S. Sandhu, *Synlett.*, **2006**, 395–398.

195. J. A. Hyatt *Tetrahedron Lett.*, **1977**, 18, 141–142.

196. D. A. Blackadder and C. Hinshelwood, *J. Chem. Soc.*, **1957**, 2904–2906.

197. E. Drug and M. Gozin, *J. Am. Chem. Soc.*, **2007**, 129, 13784–13785.

198 (a) T. H. L. Nguyen, N. Gigant and D. Joseph, *ACS Catal.*, **2018**, 8, 1546–1579; (b) M. Walther, W. Kipke, S. Schultzke, S. Ghosh and A. Staubitz, *Synthesis*, **2021**, 53, 1213–1228.

199. (a) J. Li, W. Cong, Z. Gao, J. Zhang, H. Yang and G. Jiang, *Org. Biomol. Chem.*, **2018**, 16, 3479–3486; (b) D. B. Konrad, J. A. Frank and D. Trauner, *Chem*. *Eur*. *J*., **2016**, 22, 4364–4368; (c) V. Poonthiyil, F. Reise, G. Despras and T. K. Lindhorst, *Eur. J. Org. Chem.*, **2018**, 45, 6241–6248; (d) A. Müller-Deku and O. Thorn-Seshold, *J. Org. Chem.*, **2022**, 87, 16526–16531.

200. (a) G. Li, X. Ma, C. Jia, Q. Han, Y. Hang, J. Wang, L. Yu and S. Yang, *Chem. Commun.*, **2017**, 53, 1261–1264; (b) G. Li, X. Lv, K. Guo, Y. Wang, S. Yang, L. Yu, Y. Yu and J. Wang, *Org. Chem. Front.*, **2017**, 4, 1145–1148.

201. (a) Z. Mahimwalla, K. G. Yager, J.-I. Mamiya, A. Shishido, A. Priimagi and C. J. Barrett, *Polym. Bull.*, **2012**, 69, 967–1006; (b) E. Merino and M. Ribagorda, *Beilstein J. Org. Chem.*, **2012,** 8, 1071–1090; (c) S. L. Oscurato, M. Salvatore, P. Maddalena and A. Ambrosio, *Nanophotonics*, **2018**, 7, 1387–1422.

202. (a) L. Dong, Y. Feng, L. Wang and W. Feng, *Chem. Soc. Rev.*, **2018**, 47, 7339–7368; (b) B. Zhang, Y. Feng and W. Feng, *Nano-Micro Lett.*, **2022**, 14, 138–175.

203. (a) A. S. Matharu, S. Jeeva and P. S. Ramanujam, *Chem. Soc. Rev.*, **2007**, 36, 1868–1880; (b) A. R. Yuvaraj and S. Kumar, *Gen. Chem.*, **2018**, 4, 170020.

204. (a) R. Reuter and H. A. Wegner, *Chem. Commun*., **2011***,* 47*,* 12267–12276; (b) Z. Li, J. Liang, W. Xue, G. Liu, S. Hua Liu and J. Yin, *Supramol. Chem.*, **2013**, 26, 54–65; (c) E. Wagner-Wysiecka,

N. Łukasik, J. F. Biernat and E. Luboch*, J. Incl. Phenom. Macrocycl. Chem.*, **2018**, 90, 189–257; (d) J. Yu, D. Qi and J. Li, *Commun. Chem.*, **2020**, 3, 189.

205. W.-C. Geng, H. Sun and D.-S. Guo, *J. Incl. Phenom. Macrocycl. Chem.*, **2018***,* 92, 1–79.

206. U. Funke and H. F. Grützmacher, *Tetrahedron*, **1987**, 43, 3787–3795.

207. D. Röttger and H. Rau, *J. Photochem. Photobiol. A.*, **1996**, 101, 205–214.

208. (a) H. Rau and I. Walner, *Phys. Chem. Chem. Phys.*, **2002**, 4, 1776–1780; (b) Y.-C. Lu, E. W.-G. Diau and H. Rau, *J. Phys. Chem. A*, **2005**, 109, 2090–2099.

209. N. Tamaoki, K. Ogata, K. Koseki and T. Yamaoka, *Tetrahedron*, **1990**, 46, 5931–5942.

210. (a) S. A. Nagamani, Y. Norikane and N. Tamaoki, *J. Org. Chem.*, **2005**, 70, 9304–9313; (b) Y. Norikane and N. Tamaoki, *Org. Lett.*, **2004**, 6, 2595–2598.

211. N. Tamaoki, K. Koseki and T. Yamaoka, *J. Chem. Soc. Perkin Trans.*, **1992**, 2, 1107–1110.

212. (a) Y. Norikane, K. Kitamoto and N. Tamaoki, *Org. Lett.*, **2002**, 4, 3907–3910; (b) Y. Norikane, K. Kitamoto and N. Tamaoki, *J. Org. Chem.*, **2003**, 68, 8291–8304; (c) Y. Norikane and N. Tamaoki, *Eur. J. Org. Chem.*, **2006**, 5, 1296–1302.

213. Y. Norikane, R. Katoh and N. Tamaoki, *Chem. Commun.*, **2008**, 1898–1900.

214. E. Tauer and R. Machinek, *Liebigs Ann.*, **1996**, 1213–1216.

215. (a) A. H. Heindl, L. Schweighauser, C. Logemann and H. A. Wegner, *Synthesis*, **2017**, 49, 2632–2639; (b) C. Slavov, C. Yang, A. H. Heindl, T. Stauch, H. A. Wegner, A. Dreuw and J. Wachtweitl, *J. Phys. Chem. Lett.*, **2018**, 9, 4776–4781.

216. (a) R. Reuter, N. Hostettler, M. Neuburger and H. A. Wegner, *Eur. J. Org. Chem.*, **2009**, 5647–5652; (b) C. Sladov, C. Yang, L. Scweighauser, H. A. Wegner, A. Dreuw and J. Wachtweitl, *Chem. Phys. Chem.*, **2017**, 18, 2137–2141.

217. A. H. Heindl, J. Becker and H. A. Wegner, *Chem. Sci.***, 2019**, 10, 7418–7425.

218. (a) N. Eleya, S. Ghosh, E. Lork and A. Staubitz, *J. Mater. Chem. C*, **2021**, 9, 82–87; (b) S. Ghosh, C. Eschen, N. Eleya and A. Staubitz, *J. Org. Chem.*, **2022**, https://doi.org/10.1021/acs.joc.2c00549.

219. S. Shinkai, T. Minami, Y. Kusano and O. Manabe, *J. Am. Chem. Soc.*, **1983**, 105, 1851–1856.

220. S. Shinkai, A. Yoshioka, H. Nakayama and O. Manabe, *J. Chem. Soc. Perkin Trans.*, **1990**, 2, 1905–1909.

221. (a) S. T. J. Ryan, J. del Barrio, R. Suardíaz, D. F. Ryan, E. Rosta and O. A. Scherman, *Angew. Chem. Int. Ed.*, **2016**, 55, 16096–16100; (b) Z. Ye, Z. Yang, L. Wang, L. Chen, Y. Cai, P. Deng, W. Feng, X. Li and L. Yuan, *Angew. Chem. Int. Ed.*, **2019**, 58, 12519–12523; (c) X. Chi, W. Cen, J. A. Queenan, L. Long, V. M. Lynch, N. M. Khashab and J. L. Sessler, *J. Am. Chem. Soc.*, **2019**, 141, 6468–6472; (d) Y. Liu, H. Wang, P. Liu, H. Zhu, B. Shi, X. Hong and F. Huang, *Angew. Chem. Int. Ed.*, **2021**, 60, 5766 –5770.

222. Y. Liu, H. Wang, L. Shangguan, P. Liu, B. Shi, X. Hong and F. Huang, *J. Am. Chem. Soc.*, **2021**, 143, 3081–3085.

223. (a) M. S. Hossain, S. Chatterjee and S. Bandyopadhyay, *Chem. Eur. J.*, **2022**, 28, e202201902; (b) H. B. Cheng, S. Zhang, J. Qi, X.-J. Liang and J. Yoon, *Adv. Mater.*, **2021**, 33, 2007290.

224. G. Ouyang, D. Bialas and F. Würthner, *Org. Chem. Front.*, **2021**, 8, 1424–1430.

225. G. C. Kim, J. H. Ahn, J. H. Oh, S. Nam, S. Yun, J. Yu and Y. Lee, *Biomacromolecules*, **2018**, 19, 2863–2869.

226. M. R. Jafari, L. Deng, P. I. Kitov, S. Ng, W. L. Matochko, K. F. Tjhung, A. Zeberoff, A. Elias, J. S. Klassen and R. Derda, *ACS Chem. Biol.*, **2014**, 9, 443–450.

227. (a) S.-S. Sun, J. A. Anspach and A. J. Lees, *Inorg. Chem.*, **2002**, 41, 1862–1869; (b) F. Rakotondradany, M. A. Whitehead, A.-M. Lebuis and H. F. Sleiman, *Chem. Eur. J.*, **2003**, 9, 4771–4780; (c) Y. Norikane, Y. Hirai and M. Yoshida, *Chem. Commun.*, **2011**, 47, 1770-1772; (d) R. Reuter and H. A. Wegner, *Chem. Commun.*, **2013**, 49, 146–148.

228. (a) F. Vögtle, W. M. Müller, U. Müller, M. Bauer and K. Rissanen, *Angew. Chem. Int. Ed.*, **1993**, 32, 1295–1297; (b) M. Bauer, W. M. Müller, U. Müller, K. Rissanen and F. Vögtle, *Liebigs Ann.*, **1995**,649–656; (c) M. Asakawa, P. R. Ashton, V. Balzani, C. L. Brown, A. Credi, O. A. Matthews, S. P. Newton, F. M. Raymo, A. N. Shipway, N. Spencer, A. Quick, J. F. Stoddart, A. J. P. White and D. J. Williams, *Chem. Eur. J.*, **1999**, 5, 860–875.

229. (a) K. Takaishi, M. Kawamoto, K. Tsubaki and T. Wada, *J. Org. Chem.*, **2009**, 74, 5723–5726; (b) G. Haberhauer and C. Kallweit, *Angew. Chem. Int. Ed.*, **2010**, 49, 2418–2421; (c) K. Takaishi, A. Muranaka, M. Kawamoto and M. Uchiyama, *J. Org. Chem.*, **2011**, 76, 7623–7628; (d) R. Reuter and H. A. Wegner, *Org. Lett.*, **2011**, 13, 5908–5911; (e) K. Takaishi, M. Kawamoto, K. Tsubaki, T. Furuyama, A. Muranaka and M. Uchiyama, *Chem. Eur. J.*, **2011**, 17, 1778–1782; (f) G. Haberhauer, C. Kallweit, C. Wölper and D. Bläser, *Angew. Chem. Int. Ed.*, **2013**, 52, 7879–7882; (g) J. Lu, A. Xia, N. Zhou, W. Zhang, Z. Zhang, X. Pan, Y. Yang, Y. Wang and X. Zhu, *Chem. Eur. J.*, **2015**, 21, 2324–2329; (h) L. Kerner, A. Kicková, J. Filo, S. Kedžuch, and M. Putala, *J. Phys. Chem. A*, **2015**, 119, 8588–8598.

230. (a) T. Muraoka, K. Kinbara and T. Aida, *Nature*, **2006**, 440, 512–515; (b) H. Kai, S. Nara, K. Kinbara and T. Aida, *J. Am. Chem. Soc.*, **2008**, 130, 6725–6727; (c) M. C. Basheer, Y. Oka, M. Mathews and N. Tamaoki, *Chem. Eur. J.*, **2010**, 16, 3489–3496; (d) P. Commins and M. A. Garcia-Garibay, *J. Org. Chem.*, **2014**, 79, 1611–1619; (e) A. Adam and G. Haberhauer, *J. Am. Chem. Soc.*, **2017**, 139, 9708–9713.

231. E. Durgun and J. C. Grossman, *J. Phys. Chem. Lett.*, **2013**, 4, 854–860.

232. S. Vela, A. Scheidegger, R. Fabregat and C. Corminboeuf, *Chem. Eur. J.*, **2020**, 27, 419–426.

233. A. C. Rios and Y. Tor, *Isr. J. Chem.*, **2013**, 53, 469–483.

234. H. J. Cleaves II, *J. Theor. Biol.*, **2010**, 263, 490–498.

235. (a) W. R. Hargreaves, S. J. Mulvihill and D. W. Deamer, *Nature*, **1977**, 266, 78–80; (b) A. Lopez and M. Fiore, *Life*, **2019**, 9, 49–70.

236. (a) T. K. Lindhorst, *Essentials of Carbohydrate Chemistry and Biochemistry*, 2nd edition, Wiley-VCH, Weinheim, **2007**; (b) H.-J. Kim, A. Ricardo, H. I. Illangkoon, M. J. Kim, M. A. Carrigan, F. Frye and S. A. Benner, *J. Am. Chem. Soc.*, **2011**, 133, 9457–9468; (c) S. A. Benner, H.-J. Kim and M. A. Carrigan, *Acc. Chem. Res.* **2012**, 45, 2025–2034.

237. (a) For the RNA first model see: B. Alberts, A. Johnson, J. Lewis, et al. The RNA World and the Origins of Life, in *Molecular Biology of the Cell*, 4th edition, New York: Garland Science, **2002**; For the metabolism first model see: (b) G. Wächtershäuser, *Proc. Natl. Acad. Sci.*, **1990**, 87, 200–204; (c) R. T. Stubbs, M. Yadav, R. Krishnamurthy and G. Springsteen, *Nat. Chem.*, **2020**, 12, 1016–1022.

238. H. J. Cleaves II, *Evo. Edu. Outreach*, **2012**, 5, 342–360.

239. S. L. Miller, *Science*, **1953**, 117, 528–529.

240. *A. Butlerow*, *Liebigs Ann.*, **1861**, 120, 295–298.

241. W. Löb, *Chem. Ber.*, **1913**, 46, 684–697.

242. (a) J. M. de Bruijn, A. P. G. Kieboom and H. van Bekkum, *J. Carbohydr. Chem*., **1986**, 5, 561–569; (b) I. V. Delidovich, A. N. Simonov, O. P. Taran, V. N. Parmon, *Chem. Sus. Chem.*, **2014**, 7, 1833–1846.

243. A. Varki, *Glycobiology*, **2017**, 27, 3–49.

244. L. Möckl, *Front. Cell Dev. Biol.*, **2020**, 8, 253.

245. A. Varki, R. D. Cummings, J. D. Esko, et al., editors. *Essentials of Glycobiology*, 3rd edition, Cold Spring Harbor (NY): Cold Spring Harbor Laboratory Press; **2015**-**2017**.

246. N. Sharon and H. Lis, *Sci. Am.*, **1993**, 268, 82–89.

247. R. D. Cummings, *Glycoconj. J.*, **2019**, 36, 241–257.

248. N. Sharon, *Biochim. Biophys. Acta, 2006, 1760, 527*–537.

249. S. Reitsma, D. W. Slaaf, H. Vink, M. A. M. J. van Zandvoort and M. G. A. oude Egbrink, *Pflugers Arch. – Eur. J. Physiol.*, **2007**, 454, 345–359.

250. H.-J. Gabius, M. Cudic, T. Diercks, H. Kaltner, J. Kopitz, K. H. Mayo, P. V. Murphy, S. Oscarson, R. Roy, A. Schedlbauer, S. Toegel and A. Romero, *ChemBioChem*, **2022**, 23, e202100327.

251. R. Khan, F. C. Petersen and S. Shekhar, *Front. Immunol.*, **2019**, 10, 1023.

252. J. B. Kaper, J. P. Nataro and H. L. T. Mobley, *Nat. Rev. Microbiol.*, **2004**, 2, 123–140.

253. (a) U. Neu, J. Bauer and T. Stehle, *Curr. Opin. Struct. Biol*., **2011**, 21, 610–618; (b) Y.-J. Park, A. C. Walls, Z. Wang, M. M. Sauer, W. Li, M. A. Tortorici, B.-J. Bosch, F. DiMaio and D. Veesler, *Nat. Struct. Mol. Biol.*, **2019**, 26, 1151–1157; (c) M. Awasthi, S. Gulati, D. P. Sarkar, S. Tiwari, S. Kateriya, P. Ranjan and S. K. Verma, *Viruses*, **2020**, 12, 909–919.

254. D. Chappell, M. Jacob, K. Hofmann-Kiefer, M. Rehm, U. Welsch, P. Conzen and B. F. Becker, *Cardiovasc. Res.*, **2009**, 83, 388–396.

255. (a) A. Varki, R. D. Cummings, M. Aebi, N. H. Packer, P. H. Seeberger, J. D. Esko, P. Stanley, G. Hart, A. Darvill, T. Kinoshita, J. J. Prestegard, R. L. Schnaar, H. H. Freeze, J. D. Marth, C. R. Bertozzi, M. E. Etzler, M. Frank, J. F. Vliegenthart, T. Lütteke, S. Perez, E. Bolton, P. Rudd, J. Paulson, M. Kanehisa, P. Toukach, K. F. Aoki-Kinoshita, A. Dell, H. Narimatsu, W. York, N. Taniguchi, S. Kornfeld, *Glycobiology*, **2015**, 25, 1323–1324; (b) O. Jaeschke, *"Synthesis of functional glycoconjugates to explore structural aspects of carbohydrate recognition"*, Doctoral thesis, Christian Albrechts university, Kiel, **2021**.

256. T. W. Rademacher, R. B. Parekh and R. A. Dwek, *Annu. Rev. Biochem.*, **1988**, 57, 785–838.

257. M. González-Cuesta, C. Ortiz Mellet and J. M. García Fernández, *Chem. Commun.*, **2020**, 56, 5207–5222.

258. C. Müller, G. Despras and T. K. Lindhorst, *Chem. Soc. Rev.*, **2016**, 45, 3275–3302.

259. (a) S. Hakomori, *Arch. Biochem. Biophys.*, **2004**, 426, 173–181; (b) N. Stromberg, P. G. Nyholm, I. Pascher and S. Normark, *Proc. Natl. Acad. Sci.*, **1991**, 88, 9340–9344.

260. G. Despras, V. Poonthiyil and T. K. Lindhorst, Chapter 39: Photochromic carbohydrate conjugates, in *Molecular Photoswitches: Chemistry, Properties, and Applications,* Z. L. Pianowski Editor, 1st Edition, WILEY-VCH GmbH, **2022**.

261. O. Srinivas, N. Mitra, A. Surolia and N. Jayaraman, *J. Am. Chem. Soc.*, **2002**, 124, 2124–2125.

262. O. Srinivas, N. Mitra, A. Surolia and N. Jayaraman, *Glycobiology*, **2005,** 15, 861–873.

263. (a) N. Laurent, D. Lafont, F. Dumoulin, P. Boullanger, G. Mackenzie, P. H. J. Kouwer and J. W. Goodby, *J. Am. Chem. Soc.*, **2003**, 125, 15499–15506; (b) S. Abraham, S. Paul, G. Narayan, S. K. Prasad, D. S. S. Rao, N. Jayaraman and S. Das, *Adv. Funct. Mater.*, **2005**, 15, 1579–1584.

264. F. Hamon, F. Djedaini-Pilard, F. Barbot and C. Len, *Tetrahedron*, **2009**, 65, 10105–10123.

265. (a) R. Huisgen, *Proc. Chem. Soc.*, **1961**, 357–396; (b) H. C. Kolb and K. B. Sharpless**,** *Drug Discov. Today***, 2003,** 8**,** 1128–1137.

266. (a) Y. Liu, Z.X. Yang and Y. Chen, *J. Org. Chem.*, **2008**, 73, 5298–5304; (b) V. Chandrasekaran and T. K. Lindhorst, *Chem. Commun.*, **2012**, 48, 7519–7521.

267. (a) T. Fujimoto, A. Nakamura, Y. Inoue, Y. Sakata and T. Kaneda, *Tetrahedron Lett.*, **2001**, 42, 7987–7989; (b) Y. Liu, Y.L. Zhao, H.Y. Zhang, Z. Fan, G.D. Wen and F. Ding, *J. Phys. Chem. B*, **2004**, 108, 8836–8843; (c) X. Ma, Q. Wang and H. Tian, *Tetrahedron Lett.*, **2007**, 48, 7112–7116.

268. a) V. Chandrasekaran, K. Kolbe, F. Beiroth and T. K. Lindhorst, *Beilstein J. Org. Chem.* **2013,** 9, 223–233; (b) V. Chandrasekaran, E. Johannes, H. Kobarg, F. D. Sönnichsen and T. K. Lindhorst, *ChemistryOpen*, **2014**, 3, 99–108; (c) V. Chandrasekaran, H. Jacob, F. Petersen, K. Kathirvel, F. Tuczek and T. K. Lindhorst, *Chem. Eur. J.*, **2014**, 20, 8744–8752; (d) A. Müller, H. Kobarg, V. Chandrasekaran, J. Gronow, F. D. Sönnichsen and T. K. Lindhorst, *Chem. Eur. J.*, **2015**, 21, 13723–13731; (e) G. Despras, J. Hain and S. O. Jaeschke, *Chem. Eur. J.*, **2017**, 23, 10838–10847; (f) E. Fast, A. Schlimm, I. Lautenschläger, K. U. Clausen, T. Strunskus, C. Spormann, T. K. Lindhorst and F. Tuczek, *Chem. Eur. J.*, **2020**, 26, 485–501.

269. (a) J. Hain, V. Chandrasekaran and T. K. Lindhorst, *Isr. J. Chem.*, **2015**, 55, 383–386; (b) J. Hain and G. Despras, *Chem. Commun.*, **2018**, 54, 8563–8566.

270. L. Möckl, A. Müller, C. Bräuchle and T. K. Lindhorst, *Chem. Commun.*, **2016**, 52, 1254–1257.

271. T. Weber, V. Chandrasekaran, I. Stamer, M. B. Thygesen, A. Terfort and T. K. Lindhorst, *Angew. Chem. Int. Ed.*, **2014**, 53, 14583–14586.

272. G. Despras, L. Möckl, A. Heitmann, I. Stamer, C. Bräuchle and T. K. Lindhorst, *ChemBioChem*, **2019**, 20, 2373–2382.

273. (a) J. R. Kumita, O. S. Smart and G. A. Woolley, *Proc. Natl. Acad. Sci.*, **2000**, 97, 3803–3808; (b) D. G. Flint, J. R. Kumita, O. S. Smart and G. A. Woolley, *Chem. Biol.*, **2002**, 9, 391–397; (c) Z. Zhang, D. C. Burns, J. R. Kumita, O. S. Smart and G. A. Woolley, *Bioconjugate Chem.*, **2003**, 14, 824–829; (d) L. Guerrero, O. S. Smart, G. A. Woolley and R. K. Allemann, *J. Am. Chem. Soc.*, **2005**, 127, 15624–15629; (e) L. Guerrero, O. S. Smart, C. J. Weston, D. C. Burns, G. A. Woolley and R. K. Allemann, *Angew. Chem. Int. Ed.*, **2005**, 117, 7956–7960; (f) G. A. Woolley, *Acc. Chem. Res.*, **2005**, 38, 486–493; (g) S. Samanta, C. Qin, A. J. Lough and G. A. Woolley, *Angew. Chem. Int. Ed.*, **2012**, 51, 6452–6455.

274. C. E. Hoyle and C. N. Bowman, *Angew. Chem. Int. Ed.*, **2010**, 49, 1540–1573.

275. A. Müller and T. K. Lindhorst, *Eur. J. Org. Chem.*, **2016**, 1669–1672.

276. (a) M. C. Carreño, I. García, M. Ribagorda, E. Merino, S. Pieraccini and G. P. Spada, *Org. Lett.*, **2005**, 7, 2869–2872; (b) M. C. Carreño, I. García, I. Núñez, E. Merino, M. Ribagorda, S. Pieraccini and G. P. Spada, *J. Am. Chem. Soc.*, **2007**, 129, 7089–7100; (c) I. Núñez, E. Merino, M. Lecea, S. Pieraccini, G. P. Spada, C. Rosini, G. Mazzeo, M. Ribagorda, M. C. Carreño, *Chem. Eur. J.*, **2013**, 19, 3397−3406.

277. (a) B. Jousselme, P. Blanchard, M. Allain, E. Levillain, M. Dias and J. Roncali, *J. Phys. Chem. A*, **2006**, 110, 3488–3494; (b) M. Mathews and N. Tamaoki, *J. Am. Chem. Soc.*, **2008**, 130, 11409–11416.

278. J. Xie and N. Bogliotti, Chem. Rev., **2014**, 114, 7678−7739.

279. C. Lin, S. Maisonneuve, R. Métivier and J. Xie, *Chem. Eur. J.*, **2017**, 23, 14996−15001.

280. C. Lin, S. Maisonneuve, C. Theulier and J. Xie, *Eur. J. Org. Chem.*, **2019**, 1770–1777.

281. (a) C. Lin, J. Jiao, S. Maisonneuve, J. Mallétroit and J. Xie, *Chem. Commun.*, **2020**, 56, 3261–3264; (b) J. Jiao, S. Maisonneuve and J. Xie, *J. Org. Chem.*, **2022**, 87, 8534–8543.

282. Y. Kim, N. N. Mafy, S. Maisonneuve, C. Lin, N. Tamaoki and J. Xie, *ACS Appl. Mater. Interfaces*, **2020**, 12, 52146–52155.

283. P. Sokołowska, K. Dąbrowa and S. Jarosz, *Org. Lett.*, **2021**, 23, 2687–2692

284. R. Das and B. Mukhopadhyay, *ChemistryOpen*, **2016**, 5, 401–433.

285. (a) L. Bohe and D. Crich, *Carbohydr. Res.*, **2015**, 403, 48–59; (b) P. O. Adero, H. Amarasekara, P. Wen, L. Bohé and D. Crich, *Chem. Rev.*, **2018**, 118, 8242–8284.

286. (a) H. H. Jensen and M. Bols, *Acc. Chem. Res.*, **2006**, 39, 259–265; (b) M. Heuckendorff, C. M. Pedersen and M. Bols, *Chem. Eur. J.*, **2010**, 16, 13982–13994; (c) C. M. Pedersen, J. Olsen, A. B. Brka and M. Bols, *Chem. Eur. J.*, **2011** 14, 7080–7086; (d) C. M. Pedersen L. G. Marinescu and M. Bols, *C. R. Chimie*, **2011**, 14, 17–43; (e) M. Bols and C. M. Pedersen, *Beilstein J. Org. Chem.*, **2017,** 13, 93–105.

287. (a) G. Báti, J.-X. He, K. B. Pal and X.-W. Liu, *Chem. Soc. Rev.*, **2019**, 48, 4006–4018; (b) S. van der Vorm, T. Hansen, J. M. A. van Hengst, H. S. Overkleeft, G. A. van der Marel and J. D. C. Codée, *Chem. Soc. Rev.*, **2019**, 48, 4688–4706; (c) Victoria Dimakos and M. S. Taylor, *Chem. Rev.*, **2018**, 118, 11457–11517

288. (a) A. I. Tokatly, D. Z. Vinnitskiy, N. E. Ustuzhanina and N. E. Nifantiev, *Russian Journal of Bioorganic Chemistry*, **2021**, 47, 53–70; (b) M. Karak, Y. Joh, M. Suenaga, T. Oishi and K. Torikai, *Org. Lett.*, **2019**, 21, 1221–1225; (c) A. A. Hettikankanamalage, R. Lassfolk, F. S. Ekholm, R. Leino and D. Crich, *Chem. Rev.*, **2020**, 120, 7104–7151.

289. (a) V. Hamala, L. Č. Šťastná, M. Kurfiřt, P. Cuřínová, M. Dračínský and J. Karban, *Org. Biomol. Chem.*, **2020**, 18, 5427–5434; (b) A. Khanam and P. K. Mandal, *Asian J. Org. Chem.*, **2021**, 10, 296–314; (c) M. Marianski, E. Mucha, K. Greis, S. Moon, A. Pardo, C. Kirschbaum, D. A. Thomas, G. Meijer, G. von Helden, K. Gilmore, P. H. Seeberger and K. Pagel, *Angew. Chem. Int. Ed.*, **2020**, 59, 6166–6171; (d) K. Xu, Q. Man, Y. Zhang, J. Guo, Y. Liu, Z. Fu, Y. Zhu, Y. Li, M. Zheng and N. Ding, *Org. Chem. Front.*, **2020**, 7, 1606–1615.

290. H. Paulsen, *Angew. Chem. Int. Ed.*, **1982**, 21, 155–173.

291. (a) M. M. Mukherjee, R. Ghosh and J. A. Hanover, *Front. Mol. Biosci.*, **2022,** 9, 896187; (b) J. Ling and C. S. Bennett, *Asian J. Org. Chem.*, **2019**, 8, 802–813; (c) S. S. Nigudkar and A. V. Demchenko, *Chem. Sci.*, **2015**, 6, 2687–2704; (d) J.-H. Kim, H. Yang, and G.-J. Boons, *Angew. Chem. Int. Ed.*, **2005**, 44, 947–949.

292. C. D. Hurd and R. P. Zelinski, *J. Am. Chem. Soc.*, **1947**, 69, 243–246.

293. W. Koenigs, E. Knorr, *Chem. Ber.*, **1901**, 34, 957–981.

294. (a) R. R. Schmidt and J. Michel, *Angew. Chem. Int. Ed. Engl.*, **1980**, 19, 731–732; (b) Zerong Wang, *Comprehensive Organic Name Reactions and Reagents*, John Wiley & Sons, Inc., Hoboken, NJ, **2010**: Chapter 565, *Schmidt glycosylation*, pp 2498–2502.

295. (*a*) N. Kurita, S. Nebashi and M. Kojima, *Chem. Phys. Lett.*, **2005**, 408, 197—204; (*b*) G. Gabor, Y. F. Freí and E. Fischer, *J. Phys. Chem. A*, **1968**, 72, 3266–3272; (c) P. Ball and C.H. Nicholls, *Dyes Pigm.*, **1982**, 3, 5–26.

296. A. Lyčka, D. Šnobl, V. Macháček and M. Večeřa, *Org. Magn. Reson.*, **1981**, 16, 17–19.

297. J. Berry, G. Despras and T. K. Lindhorst, *RSC Adv.*, **2020**, 10, 17432-17437.

298. B. Fraser-Reid, Z. Wu, U. E. Udodong and H. Ottosson, *J. Org. Chem.*, **1990**, 55, 6068–6070.

299. a) K. P. R. Kartha and H. J. Jennings, *J. Carbohydrate Chemistry*, **1990**, 9, 777–781; b) *Carbohydr. Res.*, **2002**, 337, 1247–1259 c) R. Kakarla, R. G. Dulina, N. T. Hatzenbuhler, Y. W. Hui and M. J. Sofia, *J. Org. Chem.*, **1996,** 61*,* 8347–8349; d) B. Yu and H. Tao, *Tetrahedron Lett.*, **2001**, 42, 2405–2407.

300. B. Lal, B. N. Pramanik, M. S. Manhas and A. K. Bose, *Tetrahedron Lett.*, **1977**, 23, 1977–1980.

301. A. Bartoszewicz, M. Kalek, J. Nilsson, R. Hiresova and J. Stawinski, *Synlett*, **2008**, 1, 37–40.

302. (*a*) G. H. Vwneman, S. H. van Leeuwen and J. H. van Boom, *Tetrahedron Lett.*, **1990**, 31, 1331 –1334; (*b*) P. Konradsson, U. E. Udodong and B. Fraser-Reid, *Tetrahedron Lett.*, **1990**, 31, 4313–4316.

303. H. Lönn, *Carbohydr. Res.*, **1985**, **139**, 105–113.

304. P. Fügedi and P. J. Garegg, *Carbohydr. Res.*, **1986**, 149, 9–12.

305. J. Tatai and P. Fugedi, *Org. Lett.*, **2007**, 9, 4647–4650.

306. R.-Z. Mao, F. Guo, D.-C. Xiong, Q. L., J. Duan and X.-S. Ye, *Org. Lett.*, **2015**, 17, 5606–5609.

307. M. Nakanishi, D. Takahashi and K. Toshima, *Org. Biomol. Chem.*, **2013**, 11, 5079–5082.

308. M. D. Burkart, Z. Y. Zhang, S. C. Hung and C. H. Wong, *J. Am. Chem. Soc.*, **1997**, 119, 11743–11746.

309. D. Kahne, S. Walker, Y. Cheng and D. Van Engen, *J. Am. Chem. Soc.*, **1989**, 111, 6881–6882.

310. (a) S. Sattin, M. Panza, F. Vasile, F. Berni, G. Goti, J. Tao, E. Moroni, D. Agard, G. Colombo and A. Bernardi, *Eur. J. Org. Chem.*, **2016**, 3349–3364; (b) H.-M. Chen and S. G. Withers, *Carbohydr. Res.*, **2018**, 467, 33–44.

311. *O*-Methylated DHAB derivatives could not be isolated after glycosylation as they were always obtained as mixtures with the corresponding glycosylated products. To confirm DHAB *O*-methylation, both the mono- and di-*O*-methylated derivatives were independently prepared and their NMR and TLC characteristics analysed (*cf.* Experimental section). These data allowed us to confirm their structure as byproducts formed during the glycosylations.

312. M. C. Galan, C. Brunet and M. Fuensanta, *Tetrahedron Lett.*, **2009**, **50**, 442–445.

313. D. Crich and M. Smith, *J. Am. Chem. Soc.*, **2001**, **123**, 9015–9020.

314. K. Horita, T. Yoshioka, T. Tanaka, Y. Oikawa and O. Yonemitsu, *Tetrahedron,* **1986**, *42*, 3021–3028.

315. (a) E. Brachet*,* J. D. Brion*,* M. Alami*,* S. Messaoudi, *Adv. Synth. Catal.*, **2013***,* 355*,* 2627–2636; (b) A. Bruneau*,* M. Roche*,* A. Hamze*,* J. D. Brion*,* M. Alami*,* S. Messaoudi*, Chem. Eur. J.*, **2015***,* 21*,* 8375–8379*.*

316. H. Driguez*, ChemBioChem*, **2001***,* 2*,* 311–318*.*

317. (a) S. Iamsaard*,* E. Anger*,* S. J. Aβhoff*,* A. Depauw*,* S. P. Fletcher*,* N. Katsonis*, Angew. Chem. Int. Ed.*, **2016***,* 55*,* 9908–9912; (b) P. Pfaff*,* K. T. G. Samarasinghe*,* C. M. Crews*,* E. M. Carreira*, ACS Cent. Sci.*, **2019**, 5, 1682–1690; (c) W. Moormann*,* D. Langbehn*,* R. Herges*, Beilstein J. Org. Chem.*, **2019**, 15, 727–732.

318. A. Bruneau, M. Roche, M. Alami and S. Messaoudi, *ACS Catal.*, **2015**, 5, 1386–1396.

319. C. Lucas-Lopez*,* N. Murphy and X. Zhu*, Eur. J. Org. Chem.*, **2008***,* 26*,* 4401–4404*.*

320. X.-M. Liu*,* X.-Y. Jin*,* Z.-X. Zhang*,* J. Wang and F.-Q. Bai*, RSC Adv.*, **2018***,* 8*,* 11580–11588*.*

321. D. Wang, F. Schellenberger, J. T. Pham, H.-J. Butt and S. Wu, *Chem. Commun.*, **2018**, 54, 3403–3406.

322. (a) A.-L. Leistner, S. Kirchner, J. Karcher, T. Bantle, M. L. Schulte, P. Gödtel, C. Fengler, Z. L. Pianowski, *Chem. Eur. J.*, **2021**, 27, 8094–8099; (b) J. Volarić, J. Butter, A. M. Schulte, K.-O. van den Berg, E. Santamaría-Aranda, W. Szymanski and B. L. Feringa, *J. Org. Chem.*, **2022**, 87, 14319–14333.

323. (a) S. Fan, Y. Lam, L. He and J. H. Xin, *R. Soc. Open Sci.*, **2022**, 9, 211894; (b) S. Fan, Y. Lam, L. He and J. H. Xin, *ACS Omega*, **2022**, 7, 11082–11091.

324. E. Sawicki, *J. Org. Chem.*, **1957**, 22, 915–919.

325. H. Nishioka, X. Liang, T. Kato and H. Asanuma, *Angew. Chem. Int. Ed.*, **2012**, 51, 1165–1168.

326. H. Asanuma, T. Ishikawa, Y. Yamano, K. Murayama and X. Liang, *ChemPhotoChem*, **2019**, 3, 418–424.

327. U. A. Hrozhyk, S. V. Serak, N. V. Tabiryan, L. Hoke, D. M. Steeves, B. Kimball and G. Kedziora, *Mol. Cryst. Liq. Cryst.*, **2008**, 489, 257–272.

328. A. Ulman, C. S. Willand, W. Kohler, D. R. Robello, D. J. Williams and L. Handley, *J. Am. Chem. Soc.*, **1990**, 112, 7083–7090.

329. D. G. Hanken, R. R. Naujok, J. M. Gray and R. M. Corn, *Anal. Chem.*, **1997**, 69, 240–248.

330. D.-M. Shin, K. S. Schanze and D. G. Whitten, J. Am. Chem. Soc., **1989**, 111, 8494–8501.

331. J. Broichhagen, M. Schönberger, S. C. Cork, J. A. Frank, P. Marchetti, M. Bugliani, A. M. James Shapiro, S. Trapp, G. A. Rutter, D. J. Hodson and D. Trauner, *Nat. Commun.*, **2014**, 5, 5116–5127.

332. C. Hansch, A. Leo and R. W. Taft, *Chem. Rev.*, **1991**, 91, 165–195.

333. T. Clark, J. S. Murray, P. Lane and P. Politzer, *J. Mol. Model.*, **2008**, 14, 689–697.

334. P. Politzer, J. S. Murray, T. Clark and G. Resnati, *Phys. Chem. Chem. Phys.*, **2017**, 19, 32166–32178.

335. I. Chataigner, C. Panel, H. Gérard and S. R. Piettre, *Chem. Commun.*, **2007**, 3288–3290.

336. (a) E. J. Corey and E. T. Kaiser, *J. Am. Chem. Soc.*, **1961**, 83, 490–491; (b) D. J. Cram, D. A. Scott and W. D. Nielsen, *J. Am. Chem. Soc.*, **1961**, 83, 3696–3707; (c) H. L. Goering, D. L. Towns and B. Dittmar, *J. Org. Chem.*, **1962**, 27, 736–739; (d) D. J. Cram *Organic Chemistry, A series of monographs. The Fundamentals of Carbanion Chemistry*, Academic Press, New York–London, **1965**, pp. 71–84.

337. S. Wolfe, A. Rauk and I. G. Csizmadia, *J. Am. Chem. Soc.*, **1969**, 91, 1567–1569.

338. (a) D. Wang, F. Schellenberger, J. T. Pham, H.-J. Butt *and* S. Wu, Chem. Commun., **2018**, 54, 3403–3406; (b) M. W. Haydell, M. Centola, V. Adam, J. Valero and M. Famulok, *J. Am. Chem. Soc.*, **2018**, 140, 16868–16872.

339. F. Zhao, L. Grubert, S. Hecht and D. Bléger, *Chem. Commun.*, **2017**, 53, 3323–3326.

340. E. Marsault and M. L. Peterson, *J. Med. Chem.*, **2011**, 54, 1961–2004.

341. K. C. Nicolaou, D. Vourloumis, N. Wissinger and P. S. Baran, *Angew. Chem. Int. Ed.*, **2000**, 39, 44–122.

342. (a) A. Fürstner, *Acc. Chem. Res.*, **2021**, 54, 861–874; (b) T. Gulder and P. S. Baran, *Nat. Prod. Rep.*, **2012**, 29, 899–934.

343. (a) W. Zhang and J. S. Moore, *Angew. Chem. Int. Ed.*, **2006**, 45, 4416–4439; (b) W. Baker, J. F. W. McOmie and W. D. Ollis, *J. Chem. Soc.*, **1951**, 200–201.

344. (a) V. Martí-Centelles, M. D. Pandey, M. I. Burguette and S. V. Luis, *Chem. Rev.*, **2015**, 115, 8736−8834; (b) G. Blankenstein and J. Zhu, *Eur. J. Org. Chem.*, **2005**, 1949–1964.

345. N. V. Gerbeleu, V. B. Arion, J. Burgess, *Template Synthesis of Macrocyclic Compounds*; Wiley: Weinheim, Germany, **2007**.

346. K. Takaishi, M. Kawamoto, A. Muranaka and M. Uchiyama, *Org. Lett.*, **2012**, 14, 3252–3255.

347. K. Łęczycka-Wilk, K. Dąbrowa, P. Cmoch and S. Jarosz, *Org. Lett.*, **2017**, 19, 4596–4599.

348. (a) L. Reguera and D. G. Rivera, *Chem. Rev.*, **2019**, 119, 9836–9860; (b) L. A. Wessjohann, D. G. Rivera, and O. E. Vercillo, *Chem. Rev.*, **2009**, 109, 796–814.

349. (a) C. Bechtler and C. Lamers, *RSC Med. Chem.*, **2021**, 12, 1325–1351; (b) A. Parenty, X. Moreau, G. Niel and J.-M. Campagne, *Chem. Rev.*, **2013**, 113, PR1–PR40.

350. A. Gradillas and J. Pérez-Castells, *Angew. Chem. Int. Ed.*, **2006**, 45, 6086–6101.

351. (a) S. Sengupta and G. Mehta, *Org. Biomol. Chem.*, **2020**, 18, 1851–1876; (b) W. Zhang, *Nat. Prod. Rep.*, **2021**, 38, 1109–1135; (c) X. Yu and D. Sun, *Molecules*, **2013**, 18, 6230–6268.

352. D. C. Harrowven and S. L. Kostiuk, *Nat. Prod. Rep.*, **2012**, 29, 223–242.

353. (a) S. Lü, Z. Wang and S. Zhu, *Nat. Comm.*, **2022**, 13, 5001; (b) L. Raynal, N. C. Rose, J. R. Donald and C. D. Spicer, *Chem. Eur. J.*, **2021**, 27, 69–88; (c) D. Pasini, *Molecules*, **2013**, 18, 9512–9530.

354. K. Tanaka, S. Fukuoka, H. Miyanishi and H. Takahashi, *Tetrahedron Lett.*, **2010**, 51, 2693–2696.

355. P. Skrabal, J. Steiger and H. Zollinger, *Helv. Chim. Acta*, **1976**, 59, 2915–2918.

356. H.-M. Kang, H.-Y. Kim, J.-W. Jung and C.-G. Cho, *J. Org. Chem.*, **2007**, 72, 679–682.

357. (a) L. Santhosh, S. Durgamma, Shekharappa and Vommina V. Sureshbabu, *Org. Biomol. Chem.*, **2018**, 16, 4874–4880; (b) M. I. García-Moreno, P. Díaz-Pérez, J. M. Benito, C. Ortiz Mellet, J. Defaye and J. M. García Fernandez, *Carbohydr. Res.*, **2002**, 337, 2329–2334.

358. M. Jana and A. K. Misra, *J. Org. Chem.*, **2013**, 78, 2680–2686; Compound **34** was synthesized following the same procedure starting from the 6-tosylate.

359. J. Berry, G. Despras and M. Kurfiřt, 2,3,4-Tri-*O*-Benzoyl-6-*O*-(Tert-Butyldiphenylsilyl)-1-Thio-β-D-Glucopyranose, in P. Kosma, T. M. Wrodnigg and A. Stütz (Eds.), *Carbohydrate Chemistry: Proven Synthetic Methods*, Volume 5 (1st ed.), CRC Press, Boca Raton, Chapter 31, **2021**.

360. A. T. Khan and E. Mondal, *Synlett*., **2003**, 5, 694–698.

361. P.-C. Lin, A. K. Adak, S.-H. Ueng, L.-D. Huang, K.-T. Huang, J. A. Ho and C.-C. Lin, *J. Org. Chem.*, **2009**, 74, 4041–4048.

362. C. G. Venier, T. G. Squires, Y.-Y. Chen, G. P. Hussmann, J. C. Shei and B. F. Smith, *J. Org. Chem.*, **1982**, 47, 3773–3774.

363. L. Liu and Q.-X. Guo, *Chem. Rev.*, **2001**, 101, 673–696.

364. J. P. Henschke, P.-Y. Wu, C.-W. Lin, S.-F. Chen, P.-C. Chiang and C.-N. Hsiao, *J. Org. Chem.*, **2015**, 80, 2295–2309.

365. J. S. Brimacombe and L. C. N. Tucker, *Carbohydr. Res.*, **1975**, 40, 387–390.

366. E. I. Balmond, D. M. Coe, M. C. Galan and E. M. McGarrigle, *Angew. Chem. Int. Ed.*, **2012**, 51, 9152–9155.

367. B. Clique, A. Ironmonger, B. Whittaker, J. Colley, J. Titchmarsh, P. Stockley and A. Nelson, *Org. Biomol. Chem.*, **2005**, 3, 2776–2785.

368. B.-C. Yu, Y. Shirai and J. M. Tour, *Tetrahedron*, **2006**, 62, 10303–10310.

369. L. Johnson, B. Ringstrand and P. Kaszynski, *Liq. Cryst.*, **2009**, 36, 179–185.

370. S. Shen, L. Dong, H. Lu, Y. Dong, Q. Yang and J. Zhang, *Bioorg. Med. Chem.*, **2020**, 28, 115602.

Abbreviations

AB	azobenzene
ABGs	azobenzene glycoconjugates
ABn	derivatives of the azobenzenes class
aAB	derivatives of the aminoazobenzene class
ppAB	derivatives of the push-pull azobenzene class
ADMET	absorption, distribution, metabolism, and excretion – toxicity
1,8-ANS	8-Anilinonaphtalene-1-sulfonic acid
Boc	*tert*-butyloxycarbonyl
BSP	benzene-sulfiniyl-piperidine
cAMP	cyclic adenosine monophosphate
CDs	cyclodextrins
CD	circular dichroism
ConA	concanavalin A
DASAs	donor-acceptor Stenhouse adducts
DAST	diethylaminosulfur trifluoride
DBU	1,8-diazabicyclo[5.4.0]undec-7-ene
DDQ	2,3-dichloro-5,6-dicyano-1,4-benzoquinone
DIAD	diisopropylazodicarboxylate
DHAB	4,4´-dihydroxyazobenzene
DMA	*N*,*N*-dimethylacetamide
DMAB	4,4´-dimethylazobenzene chromophore
DMAP	dimethylaminopyridine
DMF	*N*,*N*-dimethylformamide
DMSO	dimethylsulfoxide
DMTST	dimethyl(methylthio)sulfonium trifluoromethanesulfonate
DNA	deoxyribonucleic acid
DPPA	diphenylphosphorylazide
DSAB	4,4´-dithioazobenzene chromophore
DTBMP	2,6-di-*tert*-butyl-4-methyl-pyridine
DTT	dithiothreitol
EDG	electron donating group
ESPT	excited-state proton transfer
EWG	electron withdrawing group
GC	gas chromatography
HMEC-1	human microvascular endothelial cells variant 1

HPLC	high performance liquid chromatography
IR	infrared
*m*CPBA	*meta*-chloroperbenzoic acid
MCRs	multicomponent reactions
MMTr	monomethoxytrityl
MRSA	methicillin-resistant staphylococcus aureus
MS	molecular sieves
NBS	*N*-bromosuccinimide
NCS	*N*-chlorosuccinimide
NIR	near infrared
NIS	*N*-iodosuccinimide
NMI	*N*-methylimidazole
NMR	nuclear magnetic resonance
PMB	*para*-methoxybenzyl
PNA	peanut agglutinin
PRSP	penicillin-resistant streptococcus pneumoniae
PSS	photostationary state
RDM	ring-closing metathesis
RNA	ribonucleic acid
RT	room temperature
SAMs	self-assembled monolayers
S_EAr	electrophilic aromatic substitution
S_N1	unimolecular nucleophilic substitution
S_N2	bimolecular nucleophilic substitution
TBAF	tetrabutylammonium fluoride
TBS	*tert*-butyldimethylsilyl
TBDPS	*tert*-butyldiphenylsilyl
TCCA	trichlorocyanuric acid
TFA	trifluoroacetic acid
TFAB	tetrafluoro azobenzene chromophore
THF	tetrahydrofurane
TMS	trimethylsilyl
Troc	trichloroethoxycarbonyl
TLC	thin layer chromatography
UV-Vis	ultraviolet-visible

Acknowledgements

I would like, first and foremost, to express all my gratitude to my two supervisors, Pr. Dr. Thisbe K. Lindhorst and Dr. Despras, for entrusting me with this project and allowing the fulfilment of a life´s goal.

I thank Pr. Van Gemmeren for being second assessor, and Prs. Sönnichsen and Hartke for taking part in the examination of this thesis.

I also thank all the members of the Lindhorst group that have shared their time with me during this thesis, and for the fruitful discussions and good atmosphere.

I thank also all the members of the analytical department for their help and time in measuring my samples.

Finally, I warmly thank all my friends, my family and my girlfriend for their unconditional support.